Almuhanna, Hassan Nasser B. (2024) *Elucidating BCR-mediated regulation of FOXO1 in chronic lymphocytic leukaemia: a role for deubiquitinase proteins?* PhD thesis

https://theses.gla.ac.uk/84781/

Copyright and moral rights for this work are retained by the author

A copy can be downloaded for personal non-commercial research or study, without prior permission or charge

This work cannot be reproduced or quoted extensively from without first obtaining permission in writing from the author

The content must not be changed in any way or sold commercially in any format or medium without the formal permission of the author

When referring to this work, full bibliographic details including the author, title, awarding institution and date of the thesis must be given

Enlighten: Theses
https://theses.gla.ac.uk/
research-enlighten@glasgow.ac.uk

Elucidating BCR-mediated regulation of FOXO1 in chronic lymphocytic leukaemia: a role for deubiquitinase proteins?

Hassan Almuhanna, MSc

Submitted in fulfilment of the requirements for the Degree of Doctor of Philosophy

Paul O'Gorman Leukaemia Research Centre

Institute of Cancer Sciences, School of Medicine, Veterinary and Life Sciences

University of Glasgow

September 2024

Abstract

The B-cell receptor (BCR) activity in chronic lymphocytic leukaemia (CLL) cells is vital for disease progression, driving cell survival, proliferation, and chemoresistance. Forkhead box protein O1 (FOXO1), a transcription factor widely considered as a tumour suppressor in B-cell malignancies, is inactivated downstream of BCR activation. Previously, we demonstrated that FOXO1 expression is significantly upregulated in lymph node (LN) biopsies of poor prognostic CLL patients. However, FOXO1 cytoplasmic localisation and deregulation of FOXO target genes, including cyclin-dependent kinase inhibitor 1A (*CDKN1A*), cyclin-dependent kinase inhibitor 1B (*CDKN1B*), and cyclin D1 (*CCND1*), may suggest functional inactivity of FOXO1 in these CLL patients. This finding indicates that FOXO1 possesses tumour-suppressive function in CLL cells. Aligning with previous studies, our data demonstrated that FOXO1 is an effector of BCR crosslinking *in vitro*, promoting FOXO1 inactivation and nuclear exclusion through phosphatidylinositol 3-kinase (PI3K)/ protein kinase B (AKT)-dependent phosphorylation of FOXO1. This was further confirmed using the Bruton's tyrosine kinase (BTK) inhibitor ibrutinib, which restored FOXO1 nuclear localisation and subsequently increased FOXO1 DNA binding and transcriptional activities, as indicated by the modulation of FOXO target genes, including the upregulation of Bcl-2-binding component 3 (*BBC3*) and the downregulation of cyclin D2 (*CCND2*). Furthermore, the levels of phosphorylated and total FOXO1 protein were transiently upregulated upon BCR crosslinking, peaking at 30 minutes and sustaining up to 2 hours. Therefore, we investigated FOXO1 regulation upon BCR crosslinking in relation to post-translational modifications involving the ubiquitination-proteasome system (UPS) pathway, particularly deubiquitinase (DUB) proteins.

Little is known about the role of individual DUB family members in CLL. Our analysis revealed that expression levels of DUB proteins in patient CLL cells were largely upregulated, including the expression of ubiquitin-specific protease 7 (USP7) and ubiquitin-specific protease 9, x-linked (USP9x). FOXO1 co-immunoprecipitation (co-IP) demonstrated USP7 interaction with FOXO1 in primary CLL cells and cell lines. The FOXO1-USP7 interaction was largely unaffected by BCR crosslinking, while inhibition with ibrutinib increased this interaction, suggesting that the PI3K/AKT pathway may play a role beyond modulating FOXO1 phosphorylation, potentially including modulation of FOXO1 interaction with DUB proteins. Treating CLL cells with the pan-DUB inhibitor PR-619 downregulated AKT^{S473} and

FOXO1^{T24} phosphorylation. However, USP7 inhibitors (P5091 and HBX19818) and the USP9x inhibitor (WP1130) were largely less effective at inhibiting the PI3K/AKT pathway. This suggests that DUB proteins have a regulatory role in the activity of the PI3K/AKT signalling pathway, but the inhibition of an individual DUB protein was not sufficient to exert a significant effect on PI3K/AKT activity. Additionally, the inhibitors induced the accumulation of MEC1 cells in the G0/G1 phase but did not impact cell proliferation. The combination of ibrutinib and DUB inhibitors enhanced CLL response to ibrutinib, leading to a greater reduction in cell viability, proliferation, and cell cycle accumulation at the G0/G1 phase.

DUB inhibitors or knockdown (KD) of USP7 or USP9x demonstrated no effect on total FOXO1 protein expression, while FOXO1 transcriptional activity was increased in MEC1 cells by HBX19818 or USP7/USP9x KDs, as indicated by the upregulation of FOXO target genes, including *CDKN1B* and *BBC3*. This effect was further enhanced by the combination of HBX19818 with ibrutinib. The nuclear localisation of FOXO1 while only modestly regulated by the inhibition of DUB proteins, particularly PR-619 and HBX19818 was enhanced when combined with ibrutinib. Additionally, USP7 or USP9x KD alone or in combination with ibrutinib increased FOXO1 DNA binding activity. This suggests that a reduction of USP7 interaction with FOXO1 may facilitate the promotion of FOXO1 to its DNA binding site, resulting in increased FOXO1 transcriptional activity.

Proteome and subsequent co-IP analysis of FOXO1 novel interactors revealed an interaction between FOXO1 and the E3 ligase tripartite motif containing 21 (TRIM21), with TRIM21 being predominantly cytoplasmic. TRIM21 KD resulted in a reduction of total FOXO1 and FOXO1 nuclear localisation, suggesting that FOXO1 is a substrate of TRIM21, which plays a role in regulating FOXO1 stability, localisation, and potentially its activity.

Our findings suggest that unleashing FOXO1 anti-tumour activity by simultaneously inhibiting BCR-mediated phosphorylation and USP7 deubiquitination of FOXO1 may present an alternative therapeutic strategy for CLL patients.

Table of Contents

List of Tables

List of Figures

Acknowledgement

First and foremost, I would like to express my sincere gratitude to my primary supervisor Professor Alison Michie for her outstanding mentorship and support throughout my PhD journey. Your insightful guidance, combined with your positive, loving, fun and enthusiastic personality, has been a constant source of inspiration for me. Your ability to foster a supportive research environment has created a space where I could thrive and develop as a researcher. Thank you

I am also deeply grateful to my second supervisor Dr. Heather Jørgensen for her invaluable contributions to my research. Your expertise has provided me with a strong foundation and has enriched my scientific knowledge and skills. Your encouragement and constructive feedback have been invaluable in shaping my research direction and improving the quality of my work. Thank you

A big thank you to the Michie's: Dr Jodie, Jennifer and Dr Michae for their exceptional teaching and mentorship. Your expertise has been instrumental in developing my basic laboratory skills and equipping me to conduct independent research. I am also grateful to Jamie and Jiatian for their kindness, support, and friendship, which have made my time in the lab even more memorable. Thank you

I would like to extend my gratitude to the POG-LRC family for creating such a supportive community. The enjoyable times we spent together, including our weekly flip-flop meetings and Christmas lunches, have been invaluable sources of joy and a sense of belonging. Thank you.

I am very grateful to my beloved country Saudi Arabia and the Ministry of Education for providing me with this opportunity to pursue my PhD. Their generous funding and support have enabled me to focus on my research and achieve my academic goals. Thank you

I am eternally grateful to my parents and siblings for their love, support, and belief in me. Their understanding and encouragement have been my source of strength throughout this challenging journey. I am also indebted to my friends for their support, friendship, and the countless happy memories we have shared. Thank you

Finally, I would like to thank my beloved wife, Shahad, and our little Queen Zahraa. Their love, understanding, and support have been my sources of strength. Shahad strength and

resilience during her pregnancy with Zahraa have been a constant source of inspiration for me. I am grateful for their presence in my life and for the joy they bring me. Thank you

﴿وَقُلْ رَبِّ زِدْنِي عِلْمًا﴾

‘My Lord, increase me in knowledge’

Author’s Declaration

The work presented in this thesis represents the original work carried out by the author and has not been submitted, in any form, to any other university.

Hassan Almuhanna

September 2024

List of Abbreviations

18S	18S ribosomal RNA
7-AAD	7-amino-actinomycin D
ABL	Abelson murine leukaemia viral oncogene homolog 1
ACSL4	Acyl-CoA Synthetase Long-Chain Family Member 4
AID	Activation induced cytidine deaminase
AKT	Protein kinase B
ALL	Acute lymphoblastic leukaemia
AML	Acute myeloid leukaemia
AMP	Adenosine monophosphate
AMPK	Kinases including AMP kinase
APA	Apatinib
APRIL	A proliferation-inducing ligand
ARID1A	AT-rich interactive domain 1A
ARID5B	AT-rich interactive domain 5B
ARPC5	Actin-related protein complex 5 subunit
ASXL1	Additional sex combs-like 1
ATM	Ataxiatelangiectasia-mutated
ATP	Adenosine triphosphate
B2M	Beta-2-microglobulin
BAD	BCL-2-associated death promoter
BAFF	B-cell activating factor
BAFFR	B-cell activating factor receptor
BAK	Bcl-2 homologous antagonist/killer
BAX	BCL-2-associated X protein
BAZ2A	Bromodomain containing protein 2A
BBC3 (PUMA)	BCL-2-binding component 3
BCA	Bicinchoninic acid assay
BCL-2	B-cell lymphoma-2
BCL-2A1	BCL-2-related protein A1
BCL6	B-cell lymphoma 6
BCL-XL	B-cell lymphoma-extra large
BCMA	B-cell maturation antigen
BCOR	BCL6 corepressor
BCR	B-cell receptor
BH	BCL-2 homology
BIM	BCL-2-interacting mediator of cell death
BIRC3	Baculoviral inhibitor of apoptosis repeat-containing protein 3
BL	Burkitt lymphoma
BLNK	B-cell linker
BM	Bone marrow
BMF	Bcl-2 modifying factor
BR	Bendamustine and rituximab
BRAF	B-Raf proto-oncogene, serine/threonine kinase
BRCA2	Breast cancer 2

BRCC3	BRCA1/BRCA2-containing complex subunit 3
BSA	Bovine serum albumin
BTK	Bruton's tyrosine kinase
BTLA	B-T lymphocyte attenuator
$Ca2^{+}$	Calcium
CAR	Chimeric antigen receptor
CARD11	Caspase recruitment domain family member 11
CBA	Chromosome-binding analysis
Cbl	Casitas B-lineage lymphoma
CCL17	CC chemokine ligand 17
CCL19	CC chemokine ligand 19
CCL21	CC chemokine ligand 21
CCL22	CC chemokine ligand 22
CCL3	CC chemokine ligand 3
CCL4	CC chemokine ligand 4
CCND1	Cyclin D1
CCND2	Cyclin D2
CD	Cluster of differentiation
CD4	Cluster of differentiation 4
CD5	Cluster of differentiation 5
CD8	Cluster of differentiation 8
CD19	Cluster of differentiation 19
CD20	Cluster of differentiation 20
CD23	Cluster of differentiation 23
CDC25B	Cell division cycle protein 25B
CDCA7	Cell division cycle associated protein 7
CDK1/2	Cyclin dependent kinase 1/2
CDK4/6	Cyclin-dependent kinase 4/6
CDKI	Cyclin-dependent kinase inhibitors
CDKN1A	Cyclin-dependent kinase inhibitor 1A
CDKN1B	Cyclin-dependent kinase inhibitor 1B
cDNA	Complementary DNA
CENPB	Centromere protein B
CFLAR	CASP8 and FADD-like apoptosis regulator
cFLIP	Cellular FLICE
CHD2	Chromodomain helicase DNA binding protein 2
ChIP-seq	Chromatin immunoprecipitation-sequencing
CHK1	Checkpoint kinase 1
cHL	Classical Hodgkin lymphoma
CHOP	Cyclophosphamide, Hydroxydaunorubicin, Oncovin (vincristine), Prednisone, Cyclophosphamide, Hydroxydaunorubicin, Oncovin (vincristine), Prednisone
CIB	Chlorambucil
CIT	Combination of chemotherapy with immunotherapy
CK	Complex karyotype
CK1	Casein kinase

CK1ε	Casein kinase 1 epsilon
CKI	Cyclin-dependent kinase inhibitor
cKO	Conditional knockout
CLL	Chronic lymphocytic leukaemia
CLP	Common lymphocyte progenitor
CML	Chronic myelogenous leukaemia
cMYC	Cellular MYC
CNOT3	CCR4-NOT transcription complex subunit 3
CO_2	Carbon dioxide
co-IP	Co-immunoprecipitation
COP1	Constitutive photomorphogenic 1
CpG	Cytosine-phosphate-guanine
CR	Complete response
CREB1	cAMP response element-binding protein 1
CREBBP	CREB-binding protein
CSR	Class switch recombination
C_T	Cycle threshold
CTV	CellTrace Violet
CUL9	Cullin 9
CXCL12	CXC chemokine ligand 12
CXCL13	CXC chemokine ligand 13
CXCR4	C-X-C chemokine receptor type 4
CXCR5	Chemokine receptor type 5
DAF2	Dauer formation-2
DAPI	4’,6-diamidino-2-phenylindole
DBD	DNA binding domain
DDB2	DNA binding protein 2
DDR	DNA damage response
DDX3X	DEAD-box helicase 3 X-linked
DICER1	Dicer 1
DIS3	RNase III enzyme D3
DLBCL	Diffuse large B-cell lymphoma
DMEM	Dulbecco's Modified Eagle Medium
DMSO	Dimethylsulphoxide
DNA	Deoxyribonucleic acid
DR	Death receptor
DSB	HRR-dependent double-strand break
DSMZ	Deutsche Sammlung von Mikroorganismen und Zellkulturen
DSS	Disuccinimidyl suberate
DTT	Dithiothreitol
DUB	Deubiquitinase/deubiquitinating enzymes
DYRK1A	Dual specificity tyrosine phosphorylation regulated kinase 1A
DZ	Dark zone
E1	Ubiquitin-activating enzymes
E2	Ubiquitin-conjugating enzymes
E2F1	E2F transcription factor 1

E3	Ubiquitin ligase
EBF1	Early B-cell factor 1
EC_{50}	Half maximal effective concentration
EDTA	Ethylenediamine tetra-acetic acid
EEF1A1	Eukaryotic elongation factor 1 alpha 1
EGR-1	Early growth response 1
EGR2	Early growth response 2
EIF2B1	Eukaryotic initiation factor 2B subunit 1
ELF1	E74-like factor 1
EMT	Epithelial-mesenchymal transition
ER	Estrogen receptor
ERIC	European Research Initiative on CLL
ERK	Extracellular signal-regulated kinase
ESCCA	European Society for Clinical Cell Analysis
EWSR1	Ewing sarcoma breakpoint region 1
EZH1	Enhancer of Zeste Homologue 1
$F(ab')_2$	Fragment antibody binding
FAM50A	Family with sequence similarity 50, member A
FASL	FAS-ligands
FBS	Fetal bovine serum
FBXW7	F-box and WD repeat domain containing 7
Fc	Fragment crystallisable
FC	Fludarabine and cyclophosphamide
FCR	Fludarabine, cyclophosphamide, and rituximab
FDA	Food and Drug Administration
FDC	Follicular dendritic cells
FISH	Fluorescence in situ hybridization
FL	Follicular lymphoma
FLT3	Fms-related tyrosine kinase 3
FOX	Forkhead Box
FOXO1	Forkhead box protein O1
FOXO3a	Forkhead box protein O3a
FOXO4	Forkhead box protein O4
FOXO6	Forkhead box protein O6
FR2	Framework region 2 of the heavy chain
FR3	Framework region 3 of the heavy chain
FUBP1	Far upstream element-binding protein 1
G0	Resting phase/quiescence
G1	Gap 1 phase
G2	Gap 2 phase
G6PC2	Glucose-6-phosphatase 2
GADD45A	Growth arrest and DNA-damage-inducible protein 45-alpha
GAPDH	Glyceraldehyde-3-phosphate dehydrogenase
GC	Germinal centre
GC	Gastric cancer
GCIB	Obinutuzumab and chlorambucil

GEP	Gene expression profiling
GFP	Green Fluorescent Protein
GFR	Growth factor receptor
GIST	Gastrointestinal stromal tumours
GMPS	Guanosine Monophosphate Synthetase
GNB1	Guanine nucleotide-binding protein alpha 1
GPS2	G protein pathway suppressor 2
GSK3	Glycogen synthase kinase 3
GUSB	Glucuronidase beta
Hb	Haemoglobin
HCDR3	Heavy chain complementarity-determining region 3
HDM2	Human double minute 2
HEK293FT	Human embryonic kidney 293 cell
HeLa	Human cervical cancer cell
HepG2	Human liver cancer cell
HER	Human epidermal growth factor receptor
HER-2	Human epidermal growth factor receptor 2
HHR	Homologous Recombination Repair
HIF-1α	Hypoxia-Inducible Factor 1-alpha
HL	Hodgkin lymphoma
hr	Hour(s)
HRK	Harakiri
HRP	Horseradish peroxidase
HSC	Haematopoietic stem cell
IC_{50}	Inhibitory Concentration 50%
ID1	Inhibitor of differentiation 1
Ig	Immunoglobulin
IgD	Immunoglobulin D
IGF-1	Insulin-like growth factor-1
IGFR1	Insulin-like Growth Factor 1 Receptor
IgH	Immunoglobulin heavy chain
IGHD	Immunoglobulin heavy constant delta
IGHJ	Immunoglobulin heavy joining
IGHV	Immunoglobulin heavy-chain variable
IgL	Light chain
IGLV3-21R110	Immunoglobulin variable light chain 3-21 region 110
IgM	Immunoglobulin M
IGVL	Immunoglobulin light-chain variable region
IKBKB	IκB kinase beta
IKK	IkappaB kinase
IKZF3	IKAROS family zinc finger 3
IL-10	Interleukin-10
IL-16	Interleukin-16
IL-4	Interleukin-4
IL-6	Interleukin-6

IL7R	Interleukin-7 receptor
IL-8	Interleukin-8
INK4	Inhibitor of cyclin-dependent kinase 4
INO80	Inositol requiring 1 homolog 80
INPP5D	Phosphatidylinositol 5-phosphatase 1 domain-containing protein 5
IP	Immunoprecipitation
IPI	International Prognostic Index
IRF4	Interferon regulatory factor 4
ITAM	Immunoreceptor tyrosine-based activation motifs
ITPKB	Inositol-trisphosphate 3-kinase B
iwCLL	International Workshop on CLL
IκB	Inhibitor of κB
JAMM	Metalloprotease DUBs consist solely of the zinc-dependent JAB1/MPN/MOV34 metalloprotease
JNK	c-jun terminal kinase
KD	knockdown
kg	Kilogram
KLHL6	Kelch-like protein 6
KMT2D	Lysine (K)-specific methyltransferase 2D
KO	Knockout
KRAS	Kirsten rat sarcoma virus 2 oncogene
LFA-1	Leukocyte function-associated antigen 1
LFA-3	Leukocyte function-associated antigen 3
liso-cel	Lisocabtagene maraleucel
l-MYC	lung-specific MYC
LN	Lymph node
LYN	Tyrosine-protein kinase Lyn
LZ	Light zone
M	Mitosis/mitotic phase
M	Molar
MACS	Magnetic-activated cell sorting
MAP2K1	Mitogen-activated protein kinase kinase 1
MAP2K2	Mitogen-activated protein kinase kinase 2
MAP4K5	Mitogen-activated protein kinase kinase kinase 5
MAPK	Mitogen-activated protein kinase
MAPK4	Mitogen-activated protein kinase 4
MBD1	Methyl-CpG binding domain protein 1
MCL	Mantle Cell Lymphoma
MCL1	Myeloid cell leukaemia-1
M-CLL	IGVH-mutated CLL
MDM2	Mouse double minute 2 homolog
MED1	Mediator of RNA polymerase II transcription subunit 1
MED12	Mediator of RNA polymerase II transcription subunit 12
mg	Milligrams
MGA	Myeloid zinc finger 1
min	Minute(s)

MINDY	Motif interacting with ubiquitin-containing novel DUB family
miR	microRNA
MJD	the Machado-Joseph disease protease
mLST8	Mammalian lethal scid syndrome 8
MM	Multiple myeloma
MNC	Mononuclear cells
mRNA	Messenger RNA
MS	Mass spectrometry
MSL3	Male-specific lethal 3
MST1	Mammalian sterile 20-like kinase
mTOR	Mammalian target of rapamycin
mTORC1	Mammalian target of rapamycin complex 1
mTORC2	mTOR complex-2
MYC	Myelocytomatosis oncogene
MYD88	Myeloid differentiation primary response gene 88
MZ	Marginal zone
N_2	Nitrogen
NCAPG	Non-SMC condensin I complex subunit G
NDC	No drug control
NEDD4-1	Neural precursor cell expressed developmentally down-regulated protein 4-1
NEK8	NIMA-related kinase 8
NES	Nuclear export signal
NFAT	Nuclear factor of activated T cells
NFKB1	Nuclear factor kappa B subunit 1
NFKBIB	Nuclear factor kappa B inhibitor beta
NFKBIE	Nuclear factor kappa B inhibitor epsilon
NF-κB	Nuclear Factor Kappa B
NHL	Non-Hodgkin lymphoma
NK	Natural killer
NLC	Nurse-like cells
NLS	Nuclear localisation signal
nM	Nanomolar
N-MYC	Neuroblastoma MYC
NOTCH1	Neurogenic locus notch homolog protein 1
NOXA	Phorbol-12-myristate-13-acetate-induced protein 1
NPC	Nasopharyngeal carcinoma
NRAS	Neuroblastoma RAS viral oncogene homolog 1
NSCLC	Non-small cell lung cancer
NSD1	Nuclear receptor binding SET domain protein 1
NXF1	Nuclear export factor 1
OC	Ovarian cancer
ORR	Overall response rate
OS	Overall survival
OUT	Ovarian tumour protease
Par-4	Partitioning Defective 4

PARP	Poly(ADP-ribose) polymerase
PAX5	Paired box 5
PB	Peripheral blood
PBS	Phosphate-buffered saline
PDGFRβ	Platelet-Derived Growth Factor Receptor beta
PDK1	Phosphoinositide-dependent kinase-1
Pen	Penicillin
PFS	Progression-free survival
PH	Pleckstrin homology
Ph	Philadelphia
PHB2	Prohibitin 2
PI	Propidium iodide
PI3K	Phosphatidylinositol 3-kinase
PI3Kα	PI3K isoform p110α
PI3Kβ	PI3K isoform p110β
PI3Kγ	PI3K isoform p110γ
PI3Kδ	PI3K isoform p110δ
PIK3CD	Phosphatidylinositol 3-kinase catalytic subunit delta
PIP2	Phosphorylates phosphatidylinositol biphosphate
PIP3	Phosphatidylinositol 3, 4, 5-triphosphate
PLCG2	Phospholipase C gamma 2
PLC-γ2	Phosphorylate phospholipase C gamma 2
POLR3B	Polymerase (RNA) III subunit B
POT1	Protection of telomeres 1
PP2A	Protein phosphatase 2A
PRAS40	Proline-rich Akt substrate 40
Pre-B-cell	Precursor B-cell
pro-B-cells	Progenitor B-cells
PTEN	Phosphatase and tensin homolog
PTPN11	Protein tyrosine phosphatase non-receptor type 11
PVDF	Polyvinylidene difluoride
PWWP3A	PWWP domain protein 3A
R/R	Relapsed/Refractory
RAF1	Raf proto-oncogene serine/threonine kinase
RAG	Recombination-activating gene
RAPTOR	Regulatory associated protein of target of rapamycin
RAS	Rat sarcoma
RB	Retinoblastoma protein
RCC	Renal cell carcinoma
R-CHOP	Rituximab, Cyclophosphamide, Hydroxydaunorubicin, Oncovin (vincristine), Prednisone
RCIB	Rituximab and chlorambucil
RELA	Rel proto-oncogene, NF-κB subunit 5
RICTOR	Rapamycin-insensitive companion of TOR
RNA	Ribonucleic acid
RNA-seq	RNA sequencing

ROS	Reactive oxygen species
RPMI	Roswell Park Memorial Institute
RPS15	Ribosomal protein S15
RPS16	Ribosomal protein S16
RPS23	Ribosomal protein S23
RRM1	Ribonucleotide reductase subunit M1
RT	Room temperature
RUFY1	RNA U1 small nuclear ribonucleoprotein Y component
RUNX2	Runt-related transcription factor 2
S	Synthesis phase
SALL4	Sal-like 4
SAMHD1	SAM domain and HD domain-containing protein 1
SCR	Scrambled
SEM	Standard error of mean
SENP7	Sentrin/SUMO-specific protease 7
SESN3	Sestrin 3
SETD2	SET domain containing 2
SETD7	SET Domain Containing 7
SF3B1	Splicing factor 3b subunit 1
SGK	Glucocorticoid-regulated kinase
SH2	Src-homology 2
SHIP-1/-2	SH2-domain-containing inositol 5’-phosphatase-1 and -2
SHM	Somatic hypermutation
SHP-1	Tyrosine phosphatase-1
shRNA	Short hairpin RNA
SH-SY5Y	Human neuroblastoma cell
sIgM	Surface immunoglobulin M
SIN1	Stress-induced phosphoprotein 1
SKP2	F-box protein S-phase kinases-associated protein2
SLO	Secondary lymphoid organ
SP140	Sp140 chromatin protein
SPEN	Split ends homolog (Drosophila)
STAT3	Signal transducer and activator of transcription 3
Strep	Streptomycin
SYK	Spleen tyrosine kinase
T12	Trisomy 12
TACI	Transmembrane activator of TNF family
TB	Terrific Broth
TBP	TATA-box binding protein
TCF12	Transcription factor 12
TCF3	Transcription factor 3
TEC	Tyrosine kinase expressed in T cells
TFCP2	Transcription factor CP2
TLR	Toll-like receptor
TME	Tumour microenvironment
TMT	Tandem Mass Tag

TNF	Tumour necrosis factor
TNFR	Tumour necrosis factor receptor
TP53 (p53)	Cellular tumour antigen p53
TRAF3	TNF receptor-associated factor 3
TRAIL	TNF-related apoptosis-inducing ligand
TRIM21	Tripartite motif containing 21
TRMT1	tRNA methyltransferase 1
TTFT	Time to first treatment
UBA	Ubiquitin-associated domain
UBD	Ubiquitin-binding domain
UCH	Ubiquitin carboxy-terminal hydrolase
U-CLL	IGVH-unmutated CLL
UIM	Ubiquitin-interacting motif
UK	United Kingdom
uMRD	Undetectable minimal residual disease
UPS	Ubiquitination-proteasome system
US	United States
US	Unstimulated
USP	Ubiquitin-Specific Proteases
USP1	Ubiquitin-Specific Protease 1
USP7	Ubiquitin-Specific Protease 7
USP8	Ubiquitin-Specific Protease 8
USP9x	Ubiquitin-Specific Protease 9, x-linked
USP10	Ubiquitin-Specific Protease 10
USP11	Ubiquitin-Specific Protease 11
USP14	Ubiquitin-Specific Protease 14
USP18	Ubiquitin-Specific Protease 18
USP28	Ubiquitin-Specific Protease 28
V(D)J	Variable(Diversity)Joining
VCAM-1	Vascular cell adhesion molecule 1
VEGFR	Vascular endothelial growth factor receptor
VH-CDR3	Variable heavy complementarity determining region 3
WCC	White cell count
WCL	Whole cell lysate
WES	Whole-exome sequence
WGS	Whole genome sequence
Wnt	Wingless-type MMTV integration site family
WT	Wild type
XLA	X-linked agammaglobulinemia
XPO1	Exportin 1
YAP	Yes Associated Protein
ZAP-70	Zeta chain associated protein kinase 70
ZC3H18	Zinc finger C3H domain-containing protein 18
ZMYM3	Zinc finger MYM-type 3
ZNF292	Zinc finger protein 292
ZnF-UBP	Ubiquitin-specific zinc finger protease domain

µM	Micromolar

Chapter 1. Introduction

1.1 Chronic lymphocytic leukaemia

CLL is the most common form of haematological malignancy/leukaemia of adults in the Western World, which characterises by monoclonal expansion and progressive infiltration of $CD19^{+}$ $CD23^{+}$ $CD5^{+}$ IgM^{low} IgD^{low} mature appearing B-cells in the peripheral blood (PB), bone marrow (BM) and secondary lymphoid organs (SLOs; spleen and lymph node (LN)) (1-4). Kikushige, Ishikawa (5) stated that the capacity to generate clonal B-cells is acquired at the haematopoietic stem cell (HSC) stage, suggesting that CLL leukaemogenesis might include these multipotent, self-renewing HSCs. CLL development is often initiated by chromosomal deletions or additions, followed by the acquisition of further mutations that increase the aggressiveness of CLL disease (6). The clinical progression of CLL is highly heterogenous which can be indolent or progressive. While the progressive disease may require therapy shortly after diagnosis because of aggressive and rapid progression, the indolent disease may never require treatment (2, 7-9). CLL cells are arrested in cell cycle G0/G1 stage, with a small number of the clone exhibits a proliferative activity (10). CLL and normal mature B-cells both express high levels of surface antigens including CD23, CD25, CD69 and CD71 which are upregulated following antigen encounter, while Fc gamma receptor IIb, CD22 and CD79b are downregulated after cellular activation (1, 4). Similarly, CLL cells resemble memory B-cells in the expression of marker CD27 (11). Despite the similarities between CLL cells and normal mature B-cells, CLL cells acquire clinical and biological prognostic characteristics which determine the risk of the progression of disease. The pathogenesis of CLL disease is clinically ranked by the staging systems developed by Rai (12), and Binet (commonly followed in the United Kingdom; UK) (13). Furthermore, biological markers including serum levels (β2 macroglobulin (14), thymidine kinase (14), soluble CD23 (15)), genetic factors (the immunoglobulin heavy-chain variable region gene (*IGHV*) mutational status (16), and cytogenetic alterations (deletion and addition)) (17), and expression of cellular parameters (zeta chain associated protein kinase 70 (ZAP-70) (18) and CD38 (19)), implicated in CLL pathogenesis and utilised for prognostic stratification of CLL (4). The progression of CLL disease is tightly linked to the tumour microenvironment (TME), promoting CLL cells survival and proliferation through engagement/activation of BCR signalling and interaction with non-malignant accessory cells (T cells, stromal cells, and nurse-like cells (NLCs)) in the SLOs (4). The discovery of BCR signalling inhibitors, particularly

Bruton's tyrosine kinase (BTK) and Phosphatidylinositol 3-kinase (PI3K) inhibitors have revolutionised therapy for CLL disease. Despite the improvement of CLL patients progression-free survival (PFS) and overall survival (OS) rates with BCR inhibitors, a significant number of patients acquire resistance to current therapies or discontinue the treatment due to toxicities (20). Additionally, approximately 3-8% of CLL patients treated with ibrutinib have developed Richter syndrome, an aggressive lymphoma (21). Richter syndrome is defined as the occurrence of secondary aggressive lymphomas in patients with a concomitant diagnosis of CLL, with two pathological variants: diffuse large B-cell lymphoma (DLBCL) and rarely Hodgkin lymphoma (HL) (21). Despite the effectiveness of ibrutinib, the rate of Richter transformations remains comparable to the rate observed with chemotherapy (21), highlighting the unmet clinical need for novel therapeutic strategies for CLL patients.

1.1.1 The epidemiology of CLL

With an annual incidence of 5.8/100,000 persons which account for 3,803 new cases in the UK between 2016-2018, CLL is commonly described as the most common leukaemia which accounts for 38% of new diagnosed leukaemia cases (22). CLL is known to mainly affect the elderly, with 40% of newly diagnosed cases in patients aged 75 and over (22, 23). The incidence rates of CLL diagnosis in patients under 45 years old accounts for only 9.1% of all CLL cases (24). The highest incidence of CLL is in patients aged between 85-89 years, with the highest rates between the age of 85 to 89 in females and 90+ in males (22). The overall incidence rates for both males and females increased by 9% between 2005-2007 and 2015-2017 in the UK (22). While the incidence rates for females remained stable, in males the incidence rates elevated by 7% (22). CLL incidence rates are higher in males (8.6/100,000) than females (4.3/100,000), accounting for 63% of newly diagnosed cases in males compared to 37% in females between 2016-2018 in the UK (22). Of note, several reports suggest that female CLL patients have better prognostic features, including lower levels of β2-microglobulin, ZAP-70, and CD38 expression, less cytogenetic alterations, and a better response to chemotherapy (25, 26). Conversely, male gender is correlated with a shorter OS (25, 27). In the UK, the mortality incidence rates of CLL are significantly higher in males (2.4/100,000) than females (1.1/100,000) between 2017-2019, accounting for 61% and 39%, respectively (28). Despite the increased correlation between mortality and age in CLL

cells, the mortality rates in female aged 60-64 is 3.3 times lower than males (28). However, the overtime mortality trends for males and females have decreased by 28% between 2007-2009 and 2017-2019 in the UK (28). This improvement of CLL patients survival could be contributed to the effectiveness of BCR inhibitors (20, 29). Besides male sex and increasing age which are associated with the risk of developing CLL, hereditary and genetic factors also play a role. Individuals with a first-degree relative diagnosed with CLL have an 8.5-fold increased risk of developing the disease (30). Additionally, monozygotic twins (identical twins) have a higher risk of developing leukaemia compared to dizygotic twins (non-identical twins) (31). The incidence rates of CLL are linked to ethnicity/race where Caucasian have the highest rates, followed by African, and Hispanic, with Asians having the lowest rates of CLL (32). Interestingly, Asian migrants and their descendants residing in Western countries maintain a low incidence of CLL (33), further indicating a correlation between genetic factors and CLL disease. Although geographic location appears to have no influence on CLL development, certain environmental exposures including Agent Orange and some insecticides, have been linked to increase the risk of CLL (34-36).

1.1.2 Diagnosis and staging systems of CLL

This section follows the latest version of the International Workshop on CLL (iwCLL) guidelines for clinical diagnosis and risk stratification of CLL (37, 38). Additionally, introducing the prognostic model established by the International CLL-IPI (International Prognostic Index) working group which combines biological and clinical parameters, promoting a more targeted management of CLL (39).

1.1.2.1 Diagnosis of CLL

CLL patients mostly experience asymptomatic disease at the time of diagnosis, while a minority of patients experience physical symptoms related to the disease including fatigue, unintentional weight loss, excessive night sweats, increased frequency of infections and abdominal fullness (2). Symptomatic patients might experience enlarged LNs, hepatomegaly, and splenomegaly, which can be detected during physical examination (2). However, the diagnosis of CLL is confirmed through laboratory tests, including complete blood count (CBC), blood smear and immunophenotyping (37). A definitive diagnosis of CLL

requires a persistent PB-B lymphocyte count of ≥ 5 x 10^9/L B lymphocytes for at least three months (37, 38). The absolute count and clonality of circulating B lymphocytes are confirmed by flow cytometry (37). A blood smear examination allows visualisation of CLL cell morphology (37). Characteristically, CLL cells resemble mature lymphocytes with a narrow rim of cytoplasm and a condensed, single large nucleus lacking visible nucleoli and exhibiting partially clumped chromatin (37, 38). The detection of smudge cells on blood smears is a distinctive feature related to CLL (37). A large harmonisation study conducted by European Research Initiative on CLL (ERIC) and European Society for Clinical Cell Analysis (ESCCA), classified 14 out of 35 markers by flow cytometry as 'required' or 'recommended' for CLL diagnosis (40). CLL markers required for diagnosis included $CD19^+$, $CD5^+$, $CD20^+$, $CD23^+$, kappa and lambda immunoglobulin light chains (Igκ and Igλ) (40). The recommended markers can be helpful for differential diagnosis of CLL from other lymphoid malignancies (40). These recommended markers include $CD43^+$, $CD79b^+$, $CD81^+$, $CD200^+$, $CD10^-$ and $ROR1^+$ (40). The iwCLL guidelines also described additional diagnostic tests for CLL as 'not essential' which includes interphase fluorescence in situ hybridization (FISH), conventional karyotyping and marrow examination (37).

1.1.2.2 CLL staging systems

The Rai and Binet staging systems are the two main clinical tools used to classify the risk of CLL (12, 13, 37). The Rai system historically categorised CLL patients into five stages (0 to IV) based on factors including lymphocytosis, lymphadenopathy, and splenomegaly (12, 41). Currently, a revised simplified Rai system combining the original five stages into three broader risk categories (37, 38). The Binet staging system is mainly based on the number of involved lymphoid tissue organs and whether there is anaemia and thrombocytopenia (13, 41). The Binet staging system consists of three stages A, B and C (Table 1.1) (13). The Rai system is mainly used in the United States (US), while Binet staging system is commonly employed in Europe (41). For patients in the early stages (Rai 0, Binet A) with asymptomatic CLL, studies have shown no benefit of early therapeutic intervention (42-44). In contrast, patients with advanced disease stages (Rai stage III/IV or Binet stage C) who experience symptoms associated with active CLL are considered candidates for treatment initiation (45). Although intermediate and advanced stages may indicate the requirement for

therapeutic intervention, patients who experience a stable platelet counts of >100x 10^9/L do not necessarily require treatment, unless showing active disease symptoms (37).

Stage	Clinical characteristics	Median life expectancy (years)
A	Up to 2 areas of lymphadenopathy, no anaemia (Hb ≥10 g/dL)/ thrombocytopenia (platelet count ≥100x 10^9/L)	13
B	More than 3 areas of lymphadenopathy, no anaemia (Hb ≥10 g/dL)/ thrombocytopenia (platelet count ≥100x 10^9/L)	8
C	Anaemia (Hb <10 g/dL)/ thrombocytopenia (platelet count <100x 10^9/L)	2

Table 1.1: The Binet staging system (2, 13, 37).
Haemoglobin (Hb), grams per decilitre (g/dL).

Due to the lack of precision in classifying prognostic subgroups of CLL patients with Rai and Binet clinical staging systems, CLL-IPI prognostic score systems were proposed based on multivariate analyses consists of clinical stage, patient age, mutational status of *IGHV*, serum level of β2-macroglobulin and the presence of 17p deletion (del(17p))/cellular tumour antigen p53 (*TP53*) mutation (Table 1.2) (39). CLL-IPI system has been validated in various studies and was further simplified by Delgado, Doubek (46) to only include two biomarkers (*IGHV* mutational status and FISH cytogenetic) (47-49). These prognostic scoring systems might further evolve with the advancement in CLL treatment and clinical prognosis.

Prognostic factor	Adverse factor	Risk score
Del(17p)/*TP53*	Deletion/mutation	4
IGHV mutational status	Unmutated	2
β2-macroglobulin concentration	Greater than 3.5 mg/L	2
Clinical stage	Rai (I – IV) or Binet (B and C)	1
Patient age	Older than 65 years	1
	Total risk score	0-10

Table 1.2: CLL - International Prognostic Index (CLL-IPI) scoring system (39).
The risk score was calculated for each risk category based on the regression parameters from the Cox regression analysis (39). The five risk categories/prognostic factors are assigned scores that added to a total risk score ranging between 0 to 10, with higher scores indicating increasing risk (39).

1.1.3 CLL prognostic factors

The identification of prognostic biomarkers linked to different CLL progression stages has fundamentally improved CLL management. This understanding allows clinicians to make an informed treatment decisions and effectively monitor patient response to therapy (37, 38).

1.1.3.1 Cellular origin and BCR stereotyped subsets of CLL

Normal B lymphocytes originate from HSCs and undergo a series of ordered rearrangements of the immunoglobulin heavy chain (IgH) and light chain (IgL) loci (50). These rearrangements are crucial for creating the precursor B-cell receptor (pre-BCR) (50). The B-cells maturation/development steps including progenitor 'pro-', pre-, and immature B-cell in the BM, leading to the development of mature naïve B-cells expressing both IgM and IgD isotype of BCRs (2, 50, 51). The naïve mature B-cells migrate to SLOs to continue their maturation by antigen encounter through interaction with T cells and follicular dendritic cells (FDC) (50). This antigen encounter diversifies BCR through somatic hypermutation (SHM) and class switch recombination (CSR), differentiating B-cells into plasma cells (50, 51) (Figure 1.1).

The cellular origin of CLL cells can be traced through the mutational status of *IGHV* genes which is an important prognostic key to categorising the pathogenesis and risk levels of CLL (4). The status of *IGHV* genes mutation can be subdivided into two major subsets, unmutated and mutated, with CLL carrying unmutated *IGHV* genes (U-CLL) evolved from a mature naïve $CD5^+$ pre-germinal centre (pre-GC) B-cell that did not undergo clonal expansion, whereas CLL carrying mutated *IGHV* genes (M-CLL) derived from more mature $CD5^+$ $CD27^+$ post-GC B lymphocyte that has undergone SHM and antigen selection (4, 52) (Figure 1.1). Despite similarities in morphology and phenotype between U-CLL and M-CLL, these subsets arise independently during B-cell development from distinct lineages, with no apparent conversion from U-CLL to M-CLL (51). The presence of U-CLL is associated with a poorer prognosis and often requires earlier treatment due to the increased expression of proteins including ZAP-70, CD38, and myeloid cell leukaemia 1 (MCL1), which promote cell survival and proliferation (53, 54). In contrast, the presence of M-CLL is linked with favourable outcomes (53). Interestingly, the expression of surface immunoglobulin M (sIgM) is higher, resulting in maintaining signalling capacity (55).

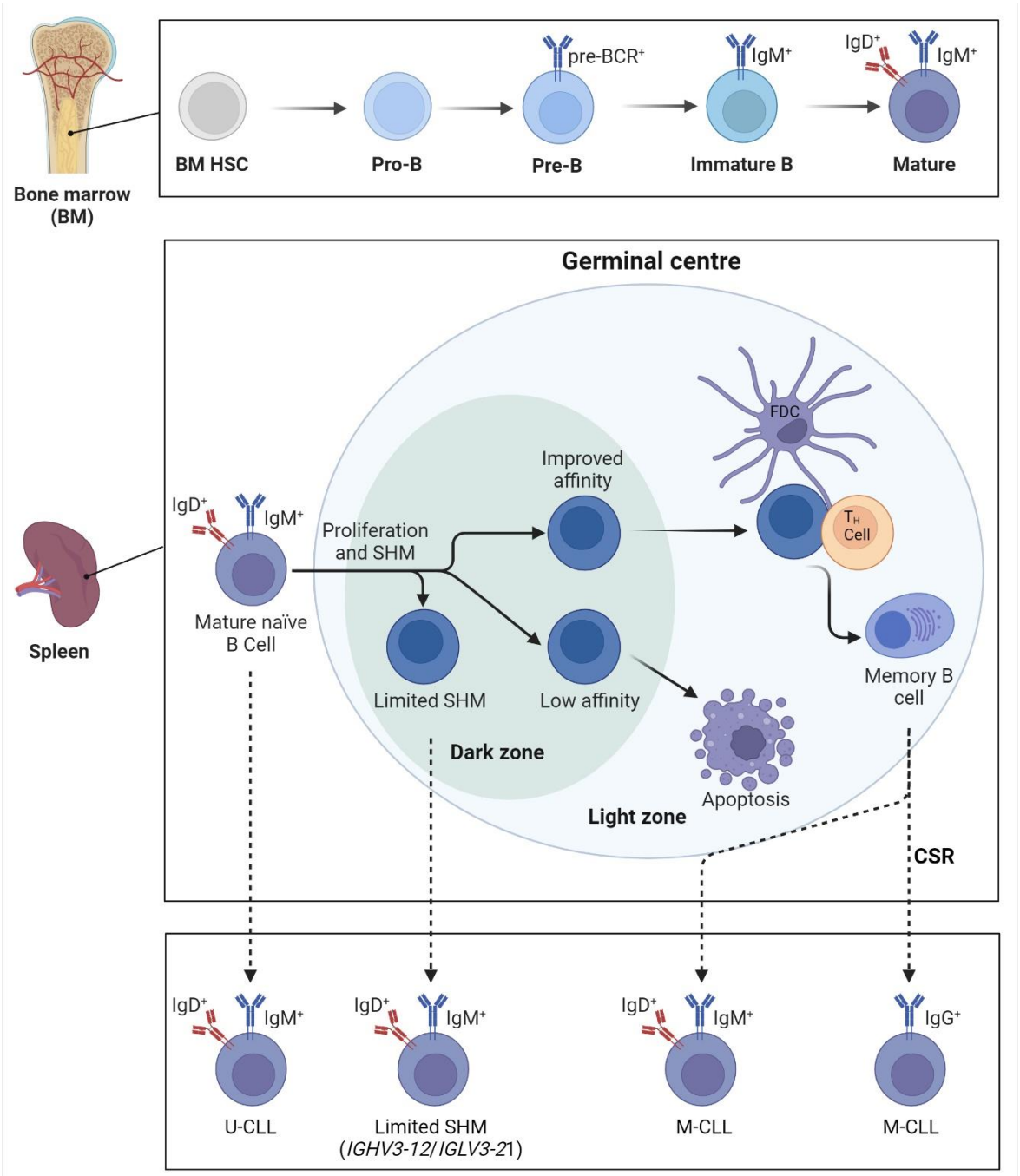

Figure 1.1: Cellular origins of CLL cells (modified from (2, 51)).
HSC: haematopoietic stem cell. FDC: follicular dendritic cell. T_H Cell: T helper cell.

With appropriate microenvironment signals, IgM signalling is greatly retained, aiding in increased survival, proliferation and disease progression in U-CLL cells, while in M-CLL, the expression of IgM is reduced leading to a more anergic and reduced ability to efficiently signal (55) (Figure 1.2). Thus, BCR signalling capacity, and the surrounding microenvironment plays an essential role in the pathogenesis and survival of CLL.

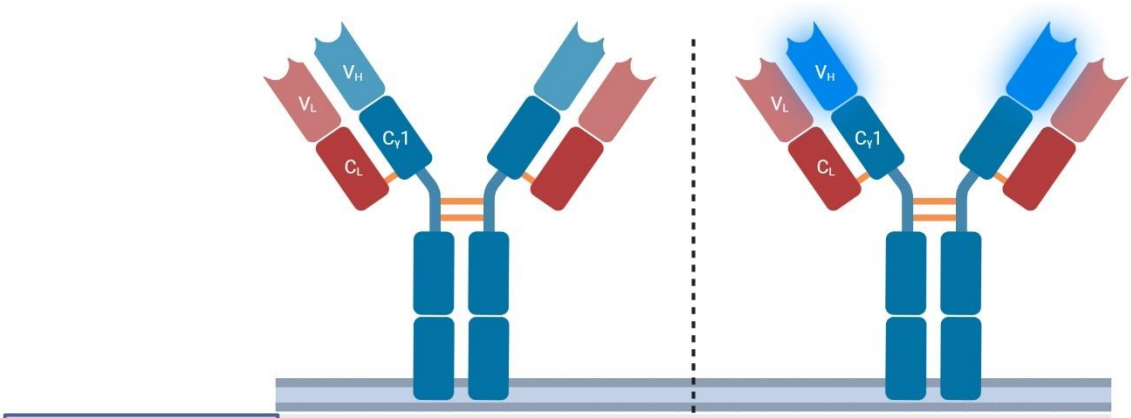

IGHV status	U-CLL	M-CLL
Frequency in CLL patient	40%	60%
Homology with germinal *IGHV*	≥98% sequence homology	<98% sequence homology
BCR reactivity	Strong	Weak, anergic
Antigen recognition	high poly-reactivity	Higher BCR specificity
Clinical outcome	Poor	Favourable

Figure 1.2: Hallmarks of U-CLL and M-CLL patients (modified from (51)).

Approximately one-third of CLL patients express stereotyped BCR, consisting of unique subsets of highly homologous variable heavy complementarity determining region 3 (VH-CDR3) sequences, which results in subsets having identical alias stereotyped BCR, with almost two thirds having U-CLL (56, 57). CLL patients with similar BCR stereotypy shares similar genetic mutations, BCR signalling properties and clinical outcomes (Table 1.3). Moreover, stereotyped subsets #1, #2 and #8 are associated with poor clinical outcome while subset #4 is linked to favourable and indolent CLL (58-65). Interestingly, subset #2 express either M-CLL (60%) or U-CLL (40%), but equally aggressive independently of *IGHV* mutational status (58). Therefore, screening for these BCR stereotypy subsets could be useful tools to estimate the course and progression of the disease.

Stereotyped subset	Subset #1	Subset #2	Subset #4	Subset #8
IGHV/IGVL gene identity	*IGHD6-19/IGHJ4/ IGKV1[D]-39*	*IGHV3-21/IGHj6/IGLV-21*	*γ-switched IGHV4-34/IGKV2-30*	*γ-switched IGHV4-39/IGHD6-13/ IGHJ5*
Frequency (approximately)	2.4%	2.8%	1%	0.5%
IGHV mutational status	Unmutated	Mutated (60%) Unmutated (40%)	Mutated	Unmutated
BCR signalling capacity	high	high	Low, anergic	high
Genetic abnormalities in treatment-naïve CLL	Del(11q) or del(17p), *NOTCH1*, *NFKBIE* mutations.	Del(13q), *SF3B1* mutations	Del(13q)	T12, *NOTCH1* mutations
Clinical outcome	Aggressive	Aggressive	indolent	Aggressive
Median TTFT*	1.6 years	1.9 years	11 years	1.5 years increased risk of Richter's

Table 1.3: The biological and clinical characteristic of the most common CLL stereotyped subsets (modified from (51)).
*Time to first treatment; TTFT.

1.1.3.2 Genetic abnormalities

CLL has a fairly stable genome when compared to other leukaemia or solid tumours (8). At diagnosis, approximately 80% of CLL patients show between none to two genetic alterations and the remaining 20% possess three or more mutations (17, 66). Moreover, biological and clinical prognostic factors have been identified to aid in defining the risk of the disease progression and to develop personalised therapeutic strategies. The most vital prognostic tools are cytogenetic aberrations including partial losses of one affected chromosome, such as deletions on 11q, 13q, and 17p, or gains of entire chromosomes, such as trisomy 12 (T12) (8). The pathogenicity of CLL and patients respond to treatment significantly correlated to chromosomal abnormalities, with the most frequent del(13q) in about 55% of CLL patients (17) (Table 1.4). This deletion is associated with low-risk disease and favourable outcomes (67). Additionally, del(13q) contains an important regulatory region that in normal $CD5^+$ B-cells highly express microRNA-15-a (miR-15-a) and microRNA-16-1 (miR-16-1), which

negatively regulate the levels of anti-apoptotic B-cell lymphoma-2 (BCL-2) (17, 68) . Another common chromosomal aberration in CLL is T12 within 17-18% of cases (17, 19). It has been shown that the presence of T12 in CLL cells facilitate the appearance of a secondary cytogenetic mutations in genes including Neurogenic locus notch homolog protein 1 (*NOTCH1*) (69, 70). Additionally, CLL cells with T12 and mutated *IGHV* genes are more susceptible to acquiring an additional trisomy such as chromosome trisomy 19 (71).

The chromosomal aberrations that signal high risks and poor clinical outcomes are del(11q) and del(17p), the site of the ataxiatelangiectasia-mutated (*ATM*) gene and *TP53*, respectively (19, 72). The del(11q) accounts for approximately 17-18% of CLL patients, and is associated with other chromosomal abnormalities, increasing the number of genetic alterations, leading to genomic instability (17, 19, 73). Patients with del(11q) characterised by the presence of large and multiple lymphadenopathies, with poor prognostic factors including unmutated *IGHV* genes (8). Additionally, *ATM* plays a key role in regulating the DNA damage response pathway (72). Acquiring both del(11q) and *ATM* mutation leads to impaired responses to purine analogs and alkylating agents, resulting in chemotherapy resistance (74). Del(17p) is another cytogenetic abnormality that identified with a very high risk and resistance to treatment and is found in about 7% of CLL patients at diagnosis (17, 19, 73). The del(17p) is highly correlated with additional *TP53* mutations resulting in an increased resistance to chemotherapies and ibrutinib to lesser extent (75-77). This deletion increased to approximately 30% in chemotherapy treated patients and undergo refractory CLL (78). The resistance to chemotherapy can be explained by the loss of *TP53* genes which leads to degradation of cell cycle (79, 80). Additionally, it has been shown that minority subclones harbouring *TP53* mutation genes became the predominant clone in CLL patients, who completed the course of chemotherapy (81), indicating the importance of *TP53* as a driver to chemoresistance. Beside the del(17p), overexpression of mouse double minute 2 homolog (MDM2), a p53-specific ubiquitin ligase which regulates the ubiquitination of proteins, also trigger the dysfunction of p53 (82). It has been found that patients with del(17p) overexpressed CD38, ZAP-70 and exhibit unmutated *IGHV*, leading to higher genetic complexity, poor prognosis, and resistance to treatments (83-85). Therefore, early screening for these abnormalities may help in selecting the appropriate therapy for CLL patients.

Aberration	Number of patients* [1, 2]	Median survival (months) [1]
Del(13q)	55-56%	133
Del(11q)	17-18%	79
T12	16-17%	114
Del(17p)	7%	32

Table 1.4: Percentage and median survival of CLL cytogenetic abnormalities. *Percentage of cytogenetic aberrations at diagnosis [1](17), [2](19).

Beside the genetic parameters including the mutational status of *IGHV* genes and cytogenetic abnormalities, recent evidence identified by using chromosome-binding analysis (CBA) suggests that complex karyotype (CK) may have significant prognostic importance for therapy decision making in CLL (86). CK is defined by the presence of ≥ 3 chromosomal abnormalities, and approximately 15% of CLL patients have CK (86). Additionally, the presence of CK was associated with poor prognostic outcome including U-CLL, del(11q), T12, *TP53* mutation and advance clinical stage (86). The clinical impact of CK shows an association between CK and shorter OS compared to non-CK (86).

Molecular mapping of whole-exome sequencing (WES) and whole genome sequencing (WGS) identified 109 new driver genes in CLL, potentially advancing the prognostic paradigm in CLL oncogenesis and prognostication (87). These driver genes of CLL were involved in BCR signalling and differentiation, Notch signalling, DNA damage and cell cycle control, nuclear factor kappa B (NF-κB) signalling, mitogen-activated protein kinase (MAPK) signalling, myelocytomatosis oncogene (MYC) signalling, Wnt signalling, RNA processing, chromatin modification, proteostasis and inflammation pathway (6, 87, 88) (Table 1.5). Interestingly, in 24% of CLL cohort, CLL patients harboured at least one gene from the newly identified CLL driver genes (Table 1.5)(87). Moreover, a mutation in the inositol-trisphosphate 3-kinase B (*ITPKB*) gene, a central inhibitor of the BCR signalling pathway (89), was found to cause abnormal activation of the rat sarcoma (RAS)/extracellular signal-regulated kinase (ERK) pathway in mice with B-cell lymphoma (90). This occurs because the *ITPKB* mutation leads to the production of IP4, which competes with RAS/GAP (90, 91). Therefore, *ITPKB* mutations could serve as a potential biomarker for increased BCR signalling (89). Mutations in the *NOTCH1* gene are important recurrent mutation which shown to have an independent prediction of poor survival CLL (92).

CLL biological pathway	Previously identified genes	Novel genes
BCR signalling and differentiation	*CARD11*, *IKZF3*, *IRF4*, *ITPKB*, *KLHL6*, *PAX5*, *IGLV3-21*^{R110}	*GPS2*
Notch signalling	*NOTCH1*, *FBXW7*, *SPEN*	-
DNA damage and cell cycle regulation	*ATM*, *BRCC3*, *CCND2*, *DYRK1A*, *POT1*, *TP53*	*ARPC5*, *CDC25B*, *CDKN1B*, *CENPB*, *CUL9*, *INO80*, *MED1*, *NCAPG*, *NEK8*, *PWWP3A*, *RRM1*, *ZC3H18*
NF-κB signalling	*NFKBIE*	*IKBKB*, *NFKB1*, *NFKBIB*, *RELA*
MAPK signalling	*BRAF*, *CREB1*, *GNB1*, *KRAS*, *MAP2K1*, *NRAS*, *PTPN11*	*MAP2K2*, *MAP4K5*, *MAPK4*, *RAF1*
MYC signalling	*FUBP1*, *MGA*	*CDCA7*
Wnt signalling	*MED12*	*TFCP2*, *USP8*
RNA processing	*CNOT3*, *DDX3X*, *EWSR1*, *FAM50A*, *FUBP1*, *NXF1*, *SF3B1*, *XPO1*, *ZC3H18*	*DICER1*, *DIS3*, *ZNF292*
Chromatin modification	*ARID1A*, *ASXL1*, *BAZ2A*, *BCOR*, *CHD2*, *CREBBP*, *IKZF3*, *KMT2D*, *SETD2*, *ZMYM3*	*ARID5B*, *INO80*, *MBD1*, *MSL3*, *NSD1*, *SP140*
Proteostasis	*RPS15*	*CUL9*, *EEF1A1*, *RPS16*, *RPS23*, *RUFY1*, *SENP7*, *TRMT1*, *USP8*
Inflammation	*BIRC3*, *DDX3X*, *EGR2*, *IRF4*, *MYD88*, *SAMHD1*, *TRAF3*	*POLR3B*

Table 1.5: CLL pathways affected by putative driver genes (modified from (87)).

Patients with *NOTCH1* mutations have a 3.77-fold increase of mortality, experience shorter treatment-free survival, and are at a higher risk of Richter transformation (92). Interestingly, Notch pathway activation is highest in CLL cells isolated from LN (93). *NOTCH1* mutation stabilises the activation of the Notch pathway, leading to resistance to pro-apoptotic stimuli and promoting CLL cell survival (92-94). *TP53* is a common mutation in CLL, particularly in advanced and high-risk patients, with high association with del(17p) (6, 95). *TP53* encodes for p53 which is a nuclear transcription factor with pro-apoptotic function in response to cellular stresses including DNA damage a protein (96), and functions as a tumour suppressor in cancer (97). *TP53* mutations impair this function (98), which often leads to resistance to chemotherapy and a shorter time to first treatment (TTFT) (6, 99). Mutations in the *ATM* gene (located on chromosome 11q22-23) are another cause of p53 dysfunction in CLL (100, 101), and it is implicated in the activation of p53 in response to cellular stress (102, 103). Clinical observation illustrates that reduced levels of ATM protein was associated

with poor response to therapy (100, 101). Beyond *TP53* and *ATM* mutations, the most common mutations linked to unfavourable disease outcomes in CLL are found in baculoviral inhibitor of apoptosis repeat-containing protein 3 (*BIRC3*), *NOTCH1* and splicing factor 3b subunit 1 (*SF3B1*) mutations (104). These mutations are found in high frequency in post-chemotherapy refractory CLL patients compared to untreated (104-106). In CLL8 trial (Table 1.6) (107), treatment with chemoimmunotherapy (CIT) led to clone selection enrichment of CLL harbouring *TP53*, *BIRC3*, dEAD-box helicase 3 X-linked (*DDX3X*) and mitogen-activated protein kinase kinase 1 (*MAP2K1*) mutations, as well as del(17p) and del(11q) (6, 108). Furthermore, *TP53* and *SF3B1* mutations were associated with shorter PFS (6). Therefore, screening for these mutations may characterise the disease and guide therapy decisions as many of these mutations are predictor of drug resistance and relapsed/refractory (R/R) CLL.

1.1.3.3 Additional prognostic factors

Immunophenotyping markers including the levels of ZAP-70 and CD38 are reliable prognostic markers in CLL, and often associated with unmutated *IGHV* and poor outcome (83, 109, 110). Moreover, ZAP-70 is one of the most well documented markers in CLL cells (18, 109, 111, 112), and it is structurally homologous to spleen tyrosine kinase (SYK), which is an important signalling pathway in BCR (113). Detecting high levels of ZAP-70 indicates a more aggressive disease course (18, 109). ZAP-70 has a role as tyrosine kinase expressed in natural killer (NK) cells and T cells as well as its ability to enhance BCR signalling in CLL cells (112, 114). CD38 is a transmembrane protein supporting the differentiation and interaction of B-cells through the ligation of CD31 (115), a cell adhesion molecule expressed by NLCs and T lymphocytes of the CLL-TME (116, 117). High levels of CD38 expression in CLL patients indicates faster disease progression and shorter survival (16). Furthermore, serum markers including the levels of soluble CD23, β2-microglobulin and thymidine kinase are associated with high risk and progressive disease (15, 118). β2-microglobulin retains independent prognostic value in several prognostic scoring systems (39, 119, 120). Additionally, Thompson, O'Brien (121) demonstrated that patients with low β2-microglobulin levels had superior PFS compared to patients who did not achieve normalised β2-microglobulin levels during treatment with ibrutinib. This suggests that β2-microglobulin may be a predictive biomarker that can help in assessing the effectiveness of CLL therapies.

1.1.4 The BCR signalling pathway

The BCR signalling pathway is the central pathway promoting the survival and proliferation of normal B-cells and CLL cells (51). Furthermore, the importance of the BCR signalling pathway in the pathogenesis of CLL is evident through its role as a key prognostic factor (38), the most modulated pathway in the TME (122), and the effectiveness of BCR-targeted therapies including BTK and PI3K inhibitors which significantly improved the PFS and OS of CLL patients compared to chemotherapies (123). Beyond CLL, the BCR is crucial for the development, differentiation, selection, antibody production, and survival of normal B-cells (124). As evidence of the BCR critical role, a study demonstrated that BCR ablation resulted in rapid cell death of mature B-cells (125), indicating a functioning BCR is vital for their survival. Furthermore, mature resting B-cells maintain low levels of BCR signalling to survive in the absence of exogenous stimulus (126), further indicating the reliance of normal B-cells on the BCR signalling pathway. This low level of signalling can occur independently of antigen ligation and is termed tonic signalling (126, 127). Together, this shows the BCR important role for normal and malignant B-cells in their survival through tonic or antigen-dependent stimulation.

1.1.4.1 V(D)J recombination

The BCR undergoes a regulated process of assembly and maturation throughout B-cell development. This begins in the BM, where the Ig heavy (H) chain variable (V), diversity (D), and joining (J) gene segments are rearranged through a process called V(D)J recombination, facilitated by recombination-activating gene (RAG) 1/2 proteins (128). This rearrangement is key and allows the transition of progenitor (pro)-B-cells to precursor (pre)-B-cells (128, 129). The V(D)J recombination generates a vast diversity of antigen-binding regions within the Ig heavy chain complementarity-determining region 3 (HCDR3) (130). This diversity is important for determining the specificity and affinity of the BCR for antigens (51). Following V(D)J recombination, the light chain (V and J segments) rearrangement occurs, leading to the formation of the pre-BCR (51). The pre-BCR promotes the development of pre-B-cells into immature B-cells expressing the IgM and IgD isotypes on their surface (131). However, not all B-cells become mature B-cells, where cells that recognise self-antigen are eliminated through a process called central tolerance in the GCs (51, 131). Immature B-cells that pass this selection process undergo further maturation in SLOs, where the cells undergo SHM

(51). These mutations are then selected for by antigen encounter, leading to the development of B-cells with high-affinity BCRs, facilitated by activation induced cytidine deaminase (AID) (128). This resulting in the BCR maturation into a highly specific and functional molecule, allowing mature B-cells to recognise and respond effectively to foreign antigens (51, 128).

1.1.4.2 BCR structure and signalling transduction

The BCR (IgM) is non-covalently bound to Igα (CD79a) and Igβ (CD79b) (4, 51, 132, 133). At the site of BCR activation, antigen binding to BCR leads to a cluster of kinases and scaffold proteins known as signalosome (134). This event of signalosome triggers the phosphorylation of immunoreceptor tyrosine-based activation motifs (ITAM) in CD79a/CD79b the C-terminal tail of BCR-correlated by the Src family kinase LYN and SYK (Figure 1.3) (133, 135, 136). Phosphorylated ITAM is a docking site for the adaptor molecule B-cell linker (BLNK) protein (134, 137, 138). Furthermore, the interaction between phosphorylated ITAM with BLNK recruits SYK and BTK, important components to couple BCR to distal signalling, dually phosphorylate phospholipase C gamma 2 (PLC-γ2) (134). Beside BCR activation, LYN mediates dephosphorylation of ITAM which contains two conserved tyrosine residues, a docking site for Src-homology 2 (SH2)-domain containing tyrosine phosphatase-1 (SHP-1) and SH2-domain-containing inositol 5'-phosphatase-1 and -2 (SHIP-1/-2), forming a negative feedback loop (137-139). Therefore, the strength of BCR transduction mediating phosphorylation and dephosphorylation is determined by LYN recruitment. LYN feedback loop regulation is controlled via upregulation of intracellular calcium ($Ca2^{+}$) signalling through SYK-mediated activation of PLC-γ2, and degradation of phosphatidylinositol 3, 4, 5-triphosphate (PIP3) mediated by SHIP-1 and phosphatase and tensin homolog (PTEN) (140). Another important arm of the BCR signalosome is class IA PI3K subunits (p110δ) protein pathway (134). Activation of PI3K phosphorylates phosphatidylinositol biphosphate (PIP2) creating a second molecule PIP3, which acts as a docking hub for effector proteins including BTK, AKT and PLC-γ (134). PI3K protein has an important function for B-cell survival by inactivating pro-apoptotic factors including BCL2-associated death promoter (BAD) and BCL-2-associated X protein (BAX) as well as Forkhead box protein O (FOXO) family of transcription factors and PTEN (140, 141). The phosphorylation of AKT also activates IkappaB kinase (IKK), inhibiting inhibitor of κB (IκB)

and subsequently positively regulates the nuclear factor NF-κB, promoting proliferation and survival of B-cell (142). PI3K plays an essential role in cell growth and cycle progression of B-cells through activation of AKT which is involved in protein expression, cell cycle and glycogen synthesis (143). BCR upon antigen binding give rise to these whole downstream signals which allow cell division, survival and prevent apoptosis (134). Therefore, signalling through BCR can directly promote survival of B-cells and prevent cell apoptosis.

1.1.4.3 BCR signalling in CLL cells

A hallmark characteristic among neoplastic B-cell malignancies is the sustained expression of BCR, and it is crucial for their development and persistence (144-146). Moreover, dysregulation of BCR signalling, often characterised by hyperactivation of BCR, is a common characteristic of B-cell malignancies, including CLL (147). Several studies have shown that CLL cells have the capacity to activate the BCR signalling pathways in an antigen-independent cell-autonomous (self-activation) manner (127, 148). Moreover, cellular activation has been associated with CLL disease progression (149). A recent study by Ziegler, Kim (149) suggested that CLL cell heterogeneity is driven by dysfunctional BCR signalling, characterised by constitutive clustering and hyperactivation of downstream BCR kinases. This proposition of existence of a tonic BCR signal in CLL cells was supported by the presence of constitutive activated and overexpressed of downstream signalling kinases including LYN, SYK, PI3K and ERK (150-153). BCR-mediated autonomous signalling in CLL is driven by an intermolecular crosslink between an oncogenic HCDR3 domain and specific motifs located within the framework region 2 of the heavy chain (FR2) and framework region 2 of the heavy chain (FR3) domains of the Ig molecule (127). Additionally, autonomous signalling leads to increased Ca^{2+} signalling and upregulates the activity of BCR downstream signalling factors including BTK, SYK and PI3K (154). An *in vivo* mouse study, showed that loss of Igα subunit in CLL cells resulted in a complete loss of the diseased cells (155), highlighting the dependency of CLL cells on BCR signalling. The autonomous signalling capacity of BCR signalling is associated with the Ig stereotypy of *IGHV* and *IGLV* genes (156, 157). GEP data revealed that *in vitro* BCR stimulation with anti-IgM strongly upregulated SYK activation and BCR target gene expression in U-CLL compared with M-CLL cells (122). This is supported by CLL stereotypy which influences the capacity of BCR activation, as indicated by subset #1, 2 and 8 (Table 1.3), where these subsets are often

associated with U-CLL (51). Furthermore, ZAP-70 expression exclusively enhanced tonic BCR signalling in U-CLL, not M-CLL (158). Conversely, CLL cells lacking ZAP-70 often exhibit an anergic BCR (loss of BCR responsiveness) (159). A study by Sadras, Martin (160) indicated that ZAP-70 competes with SYK in BCR signalling, redirecting it from $Ca2^{+}$-transcription factor nuclear factor of activated T cells (NFAT) signalling towards the activation of the PI3K signalling pathway. This redirection allows B-cell clones to escape the NFAT-induced anergic state, preventing negative selection that would eliminate self-reactive or pre-oncogenic B-cells (160). Therefore, the expression of ZAP-70 in B-cells permits sustained signalling induced by self-reactive BCRs, helping malignant BCR-mediated B-cell conversion (160, 161). These observations have shown the pivotal role of the BCR in CLL pathogenesis, with its dysfunctional signalling promoting tumour cell survival through hyperactivation of downstream kinases. Therefore, understanding the mechanisms underlying BCR activation in CLL is crucial for the development of targeted therapies.

1.1.4.3.1 The PI3K signalling pathway

This pathway regulates most the hallmarks of cancer, including cell cycle, survival, metabolism, motility, and genomic instability (162, 163). The PI3K signalling axis transduces signalling from the BCR, chemokine and adhesion receptors, promoting migration, development and survival as well as rearrangement of B-cell cytoskeletal (164, 165). Out of the four classes of PI3K protein, the four isoforms of class I are implicated in cancer, where PI3Kα (p110α) is often a genetic driver (166), and PI3Kβ (p110β) is implicated in tumorigenesis (167), while both PI3Kδ (p110δ) and PI3Kγ (p110γ) are the most expressed in lymphocytes (168). PI3Kδ is found to play a crucial role as second messenger of several cell receptors including BCR, CD40, interleukin-6 (IL-6) and chemokine receptor type 5 (CXCR5), promoting cell survival proliferation, chemokine secretion, motility and adhesion to stromal cells (169-172). In B-cells, PI3Kδ is involved in migration, proliferation, survival and differentiation, which is frequently dysregulated in CLL and non-Hodgkin lymphoma (NHL) cells (168, 173). Moreover, PI3Kγ is involved in promoting growth, survival of lymphoid malignancies, specifically in response to chemokines (174, 175). Additionally, PI3K was reported to be constitutively active in freshly isolated PB-CLL cells (153). Therefore, the PI3K pathway has become the focus for novel targeted therapies including the approved

therapies of both idelalisib and duvelisib targeting PI3Kδ and PI3Kγ, respectively (described in section 1.1.6.3.2).

PI3K is a group of plasma membrane-associated lipid kinases, acting as second messengers, recruiting cytoplasmic proteins to the cellular membrane (176, 177). In B-cells, the activation of PI3K is initiated by antigen-dependent and -independent BCR activation, enhanced by CD19, a B-cell surface co-receptor (153, 177). PI3K activation leads to phosphorylation of PIP2 into PIP3, a second messenger cytoplasmic-associated membrane that binds and recruits pleckstrin homology (PH)-domain containing effectors including phosphoinositide-dependent kinase-1 (PDK1), BTK, and AKT (142, 178). PIP3-mediated recruitment of AKT and PDK1 to the cell membrane activates cell survival and growth pathways (179, 180). This allows the dependent activation and phosphorylation of AKT by PDK1 at T308 (AKT^{T308}) (179, 180). Although the activation of AKT on T308 is enough to drive downstream protein activations, additional phosphorylation sites is required to fully activate AKT (142). This second phosphorylation comes from mTOR complex-2 (mTORC2) which phosphorylates AKT at S473 (AKT^{S473}), promoting maximal activation of AKT (181, 182). The full activation of AKT is particularly important for the activation of FOXO transcription factors (182). Negative regulation of the PI3K signalling pathway involves PTEN dephosphorylation of PIP3 to PIP2, leading to the reduction of activated downstream kinases (183).

The members of the AKT sub-family of AGC serine/threonine kinases including AKT1, AKT2, and AKT3, are considered universal downstream effectors of PI3K signalling (142). AKT phosphorylation levels often serve as a surrogate marker for PI3K activation (142, 178). Mutations in the AKT PH-domain, commonly observed in cancers, promote its membrane localisation, emphasising its critical role in PI3K-driven oncogenic signalling (184). The FOXO transcription factors are substrates of AKT, where AKT-mediated phosphorylation of FOXO suppresses their transcriptional activity, leading to nuclear export and degradation (185). Furthermore, AKT is involved in growth factor signalling including insulin receptor homolog (Dauer formation-2; DAF-2) (142, 178). In *Caenorhabditis elegans*, AKT function downstream of the insulin receptor and PI3K (AGE1) to suppress the FOXO transcription factor DAF-16 (186). Similarly, in mammalian cells, insulin-induced AKT activation suppresses FOXO activity (178). AKT regulates various cellular processes, including survival, proliferation, metabolism, and motility (142). Its role in B-cell development is highlighted

by the reduced B-cell numbers in the marginal zone (MZ) following AKT1 and AKT2 deletion (187). Conversely, Forkhead box protein O1 (FOXO1) deletion increases MZ B-cells (188), emphasising the opposing roles of AKT and FOXO. The influence of AKT extends to B-cell differentiation and development. Class switching, a process requiring AID expression, is regulated by the interplay between PI3K/AKT signalling and FOXO activity (177, 189). While PI3K/AKT activation suppresses class switching, FOXO promotes it (189, 190). Additionally, loss of PTEN leads to suppression of class switching through upregulation of PI3K signalling (190). Conversely, constitutively active FOXO1 or AID can restore class switching (189, 190). Similarly, blocking AKT or mTORC2 activation leads to class switching in a FOXO-dependent manner (191). Therefore, the balance between PI3K/AKT/mammalian target of rapamycin (mTOR) signalling is crucial for maintaining cellular homeostasis (178). In CLL cells, inhibition of AKT induces apoptosis through MCL1 degradation and p53 activation (192). Additionally, CLL cells resistant to apoptosis are associated with chemokines including CXC chemokine ligand 12 (CXCL12), CC chemokine ligand 21 (CCL21), CC chemokine ligand 19 (CCL19), and CXC chemokine ligand 13 (CXCL13), which promote cell survival by enhancing PI3K/AKT signalling and subsequently inactivating Forkhead box protein O3a (FOXO3a) proapoptotic activity (193). Interestingly, resistance to PI3K/mTOR inhibitors can occur through a "rebound" mechanism involving the upregulation of rapamycin-insensitive companion of TOR (RICTOR), a component of mTORC2, and subsequent AKT activation, leading to FOXO inactivation (178, 194). AKT, as a central effector of PI3K signalling, plays an important role in diverse cellular processes, including cell survival, proliferation, and differentiation of normal B-cells and CLL cells. Its dysregulation contributes to CLL pathogenesis, making this pathway a promising therapeutic target.

1.1.4.3.2 BTK activation downstream the BCR signalling pathway

BTK, a member of the TEC family of kinases, is an important downstream effector of PI3K in lymphocytes (178, 195). Upon BCR engagement, PI3K is activated, generating PIP3 (178). The selective PH-domain of BTK binds to PIP3, leading to its activation and subsequent activation of PLCγ_2 (178, 195). PLCγ_2 activation triggers downstream signalling pathways, including MAPK pathway and the activation of NFAT (196). The maximal signalling output within the BCR signalling pathway requires the activation of both PI3K and BTK (197, 198). The interdependence of PI3K and BTK is further supported by genetic studies. Loss of *BTK*

gene or mutations effecting the BTK PH-domain, leading to X-linked agammaglobulinemia (XLA), and deletions in the phosphatidylinositol 3-kinase catalytic subunit delta (*PIK3CD*) gene (encoding PI3Kδ) result in similar immunodeficiency phenotypes (178, 199), highlighting their joint role in B-cell development and function. Beyond BCR signalling, PI3K and BTK are also downstream effectors of CD40 and chemokine receptors (178, 200). Activation of these receptors by their respective ligands promotes PI3K and BTK activation, leading to cell migration towards survival factors such as B-cell activating factor (BAFF) and increased adhesion to supportive cells within the TME (178). Conversely, inhibiting PI3K or BTK results in rapid LN shrinkage due to impaired chemokine-dependent homing and reduced cell retention within LN niches (123, 178). These findings collectively demonstrate the promising anti-tumour effects of targeting BTK in CLL by disrupting critical signalling pathways essential for CLL cell survival and proliferation.

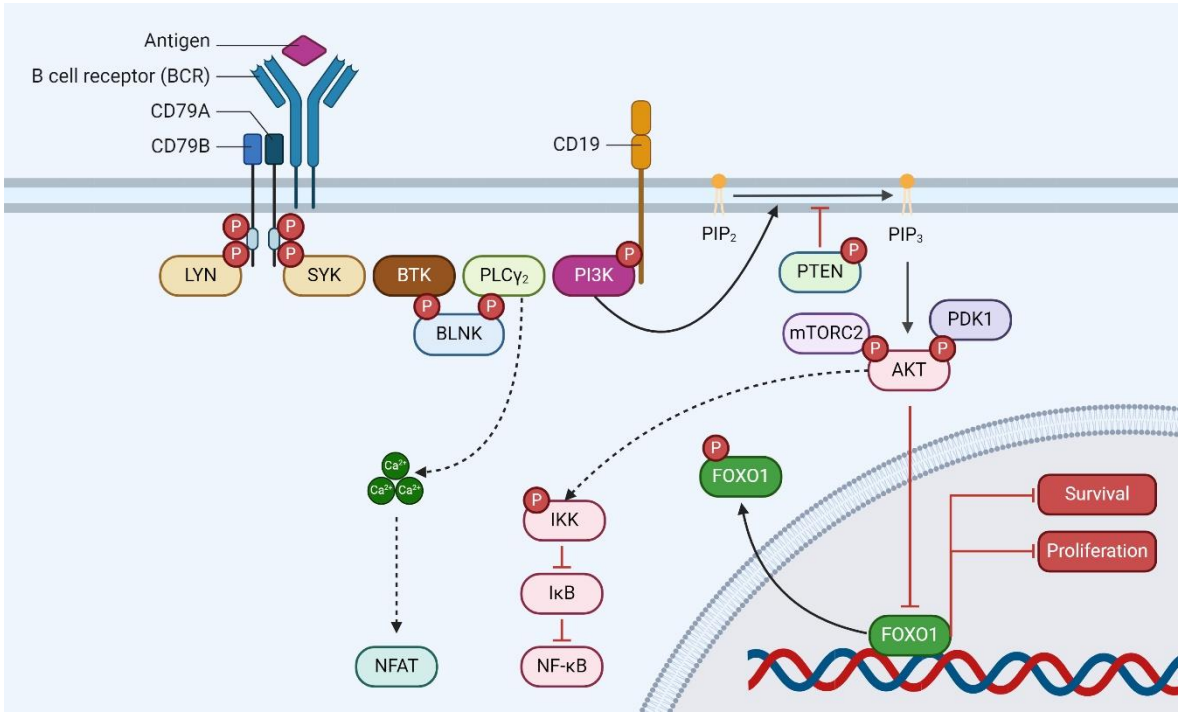

Figure 1.3: The BCR signalling pathway (modified from (51, 142, 177)).

1.1.5 CLL tumour microenvironment

The pathogenesis of CLL cells depends on survival signals provided through interaction with supportive non-neoplastic cells together with matrix factors within the so-called TME (2, 201). The proliferation of CLL cells take place in a distinct tissue area termed pseudofollicles or proliferation centres by interacting with accessory cells including NLC, mesenchymal stromal cells and T cells (202-205) (Figure 1.4), with these factors combined creating

supportive microenvironment for the survival of CLL and promoting drug resistance. Furthermore, the principal site of BCR activation of normal as well as CLL cells is the lymphatic tissues (132, 201). Once CLL cells enter the lymphoid tissue, they engage with TME accessory cells, triggering BCR signalling that promotes resistance to cytotoxic agents (2, 122, 206). Gene expression profiling (GEP) data underscores the importance of BCR signalling for CLL cells, highlighting it as the most modulated pathway (122). The GEP data also illustrated that the expression of cellular MYC (cMYC), a transcription factor involved in lymphomagenesis and G1/S transition, and E2F transcription factor 1 (E2F1) were upregulated in the LN, which together promote proliferation of CLL cells (122, 207). Interestingly, the response to this crosstalk within the TME varies depending on factors including CD38 levels, *NOTCH1* mutations, and *IGHV* mutational status (122). Of note, the study demonstrated that LN-resident U-CLL displays a stronger expression of BCR targets compared M-CLL (122), potentially due to U-CLL BCR polyreactive characteristic and its recognition of autoantigens presented in the TME (208). Several key players within the TME contribute to BCR activation and CLL survival (206). The interaction between NLCs and CLL cells leads to BCR activation (209). Furthermore, NLCs play a crucial role by interacting with CLL cells mediated by CD31 on NLCs and CD38 on CLL surfaces (210), providing survival signals through tumour necrosis factor (TNF) family members BAFF and A proliferation-inducing ligand (APRIL), which bind to corresponding receptors B-cell maturation antigen (BCMA), transmembrane activator of TNF family (TACI), and B-cell activating factor receptor (BAFFR) on CLL cells (211). This interaction leads to activation of NF-κB pathway, which enhances the activation and signalling of BCR through induction of miR-155 (212, 213). This induction downregulates the expression of phosphatidylinositol 5-phosphatase 1 domain-containing protein 5 (*INPP5D*), a gene encoding SHIP-1, a negative regulator of BCR signalling (213). Adding to this supportive TME, stromal cells and NLCs also express anti-apoptotic factors, further contributing to CLL cell survival within the TME (132, 214). *In vitro* studies have shown that CLL cells were protected from spontaneous apoptosis through stimulation with soluble CD40 and interleukin-4 (IL-4) and co-culturing with stromal cells and NLCs (209, 215, 216). T cells secrete IL-4, which upregulates surface IgM on CLL cells, facilitating their interaction with autoantigens (217). Additionally, CD40 ligand (CD40L; CD154) on T cells interact with CD40 on CLL cells, activating NF-κB, leading to the production of anti-apoptotic proteins including B-cell lymphoma-extra-large (BCL-XL) and MCL1 (201, 218). This interaction also upregulates *TP63*, promoting CLL cell migration into the

supportive TME (219). CLL trafficking between SLOs and PB is regulated by the expression of chemokines including CXCL12 and CXCL13 secreted by stromal cells as well as C-X-C chemokine receptor type 4 (CXCR4) and CXCR5 which are expressed by B-cells (220, 221). CLL cells are not passive actors in shaping their environment. They actively contribute by expressing chemokines including CC chemokine ligand 3 (CCL3) and CC chemokine ligand 4 (CCL4) upon BCR stimulation (209). Additionally, they can express CC chemokine ligand 22 (CCL22) and interleukin-8 (IL-8), leading to the mobilisation of T cells and monocytes to the site of CLL cells (132). This suggests that CLL cells seek the support of the TME by actively engaged in a complex crosstalk, leading to favourable conditions promoting disease progression and protection from cytotoxic agents.

Disrupting this supportive TME shows promise for therapeutic strategies. Pre-clinical studies have demonstrated the effectiveness of BCR inhibition in disrupting the TME by inhibiting key survival pathways including NF-κB, PI3K, and cMYC (122, 173, 222). Additionally, BCR inhibition can reduce T cell secreted cytokines including IL-6, interleukin-10 (IL-10), and TNF-α, further weakening the TME support for CLL cells (173). Moreover, inhibition of the BCR pathway by Ibrutinib treatment interferes with the TNF family members CD40L and BAFF (222), NLC-secreted survival signals (CCL3 and CCL4) (223), cytosine-phosphate-guanine (CpG)-induced CLL cell proliferation (222), and BCR-induced adhesion to the extracellular matrix component fibronectin and the vascular cell adhesion molecule 1 (VCAM-1), which is activated by integrin α4β1, leading to suppression of CLL cell migration towards CXCL12 and CXCL13 chemokines and apoptosis (223, 224). Similarly, idelalisib disrupts the TME by suppressing migration, abrogating BCR and NLC survival signals, and suppressing chemokine secretion (173, 225). The TME plays an important role in CLL pathogenesis by influencing BCR signalling and promoting CLL cell survival, proliferation, and drug resistance. Therefore, understanding the interaction mechanism of CLL-BCR with TME could potentially identify new target molecules and leads to development of novel and effective therapeutic strategies for CLL.

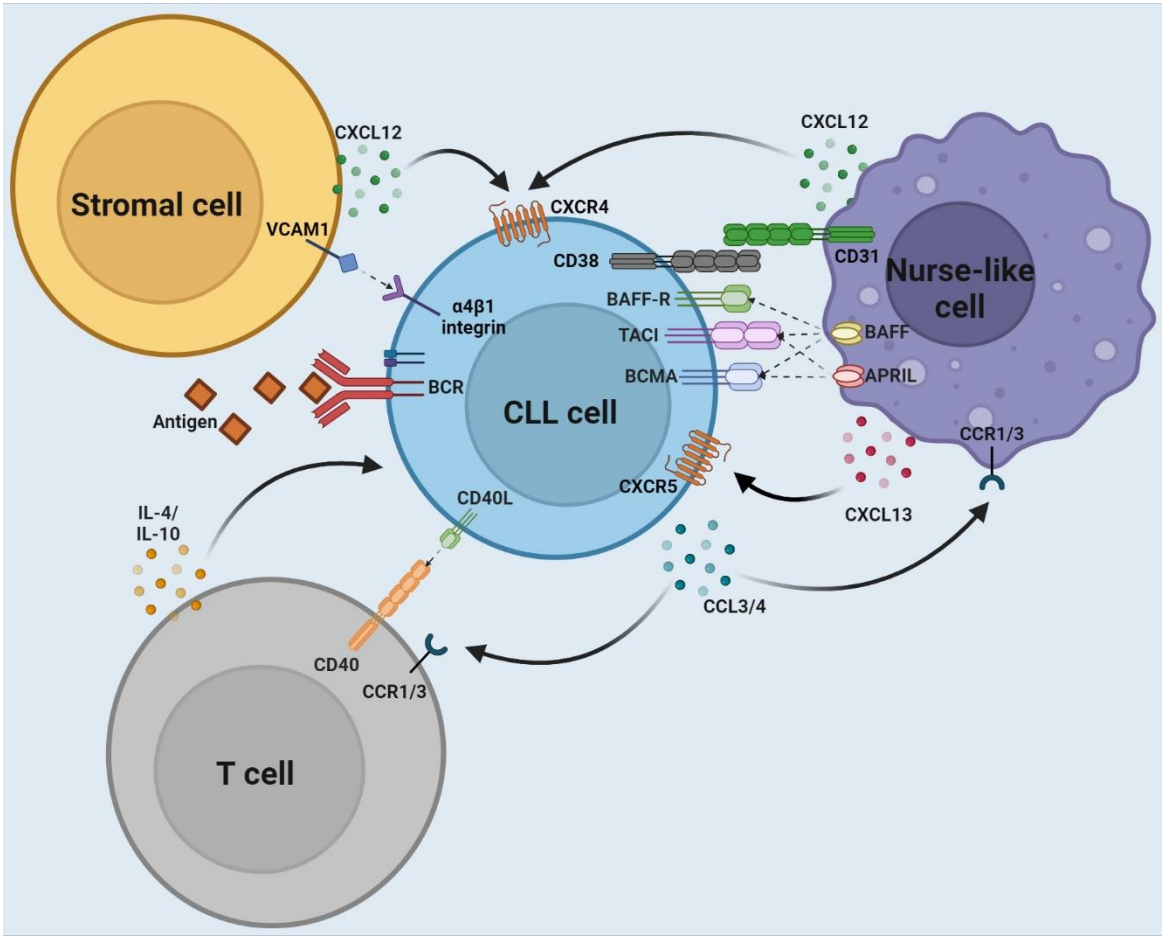

Figure 1.4: CLL interaction with accessory cells in its TME (Modified from (2)).

1.1.5.1 *In vitro* CLL-TME modelling of BCR stimulation

The mutational status of *IGHV* and ZAP-70 expression are established prognostic biomarkers in CLL (46, 54, 114, 226), which both enhance BCR signalling capacity, highlighting the BCR important role in CLL pathogenesis including cell survival, proliferation, and drug resistance (227). Therefore, mimicking BCR stimulation of CLL cells within their TME has become a valuable modelling system for studying BCR-mediated pathogenesis of CLL disease. Traditionally, anti-Ig antibodies and bacterial fragments including *Staphylococcus aureus* Cowan strain were employed to stimulate BCR signalling in B-cells (228). However, several studies have shown that the BCR pathway can be stimulated using anti-human IgG $F(ab')_2$ fragments (229, 230). This approach effectively stimulates the BCR pathway, promoting CLL cell survival by increasing the expression of key proteins: NF-κB, PI3K, anti-apoptotic proteins, and ERK1/2-MAPK (229, 230). Moreover, the GEP data further strengthens this model validity by demonstrating markers similarity between isolated CLL from LN and PB-CLL cells stimulated with anti-IgM (122). Additional, alternative models for BCR signalling

stimulation have been explored, including co-culture with NLCs and stimulation with vimentin, a stromal cell-derived factor (209, 231). Since the BCR is the most highly regulated pathway in CLL cells isolated from LN, these model systems are valuable tools for studying novel therapeutic agents. While other model systems exist to mimic the CLL-TME, including CD40/CD40L interaction, stromal cell contact, Toll-like receptor (TLR) signalling, and interleukin/chemokine interactions (extensively reviewed (232)) as well as three-dimensional co-culture model (233), they fall outside the scope of this thesis.

1.1.6 CLL treatment

Around 50% of newly CLL patients have asymptomatic and low-risk disease. This translates to only 8% of these patients requiring treatment within five years of diagnosis (123, 234). In fact, nearly 30% of CLL patients may never require treatment throughout their lifetime (123). Additionally, CLL7 and CLL12 trials demonstrated no evidence of improved survival benefit for treating asymptomatic CLL (235, 236) (Table 1.6). However, CLL patients with

Trial	Treatment	Patient cohort	Outcome
CLL4	F vs FC	Treatment naïve, Binet C or B/A, symptomatic	FC has a better ORR, PFS, and adverse effects compared to F alone, while OS was similar between the combination and monotherapy (237)
CLL7	FCR vs watch and wait	Binet A, high-risk treatment naïve	Early treatment with FCR therapy provided no evidence of survival benefit for patients (235)
CLL8	FC vs FCR	Treatment naïve	FCR induced long-term remission and improvement in OS in, particularly in patients with mutated *IGHV* (107)
CLL10	FCR vs BR	Treatment naïve	FCR therapy more suited for fit patients, while BR was associated with less toxic effects (238)
CLL11	CIB vs RCIB vs GCIB	Treatment naïve, high risk	The GCIB combination of anti-CD20 with chemotherapy demonstrated superior improvement in CLL patients with coexisting conditions compared to RCIB or CIB alone (239)
CLL12	Ibrutinib vs wait and watch	Treatment naïve, Binet A, asymptomatic	Early treatment with ibrutinib provided no justification to change the current standard of watch and wait (236)

Table 1.6: The German CLL study trials.
F; fludarabine, FCR; fludarabine, cyclophosphamide, and rituximab, FC; fludarabine and cyclophosphamide, BR; bendamustine and rituximab, CIB; chlorambucil, GCIB; obinutuzumab and

chlorambucil, RCIB; rituximab and chlorambucil, PFS; progression free survival, ORR; overall response rate.

symptoms including anaemia, cytopenia, lymphadenopathy, hepatosplenomegaly, and recurrent infections sign of progressive disease and require treatment (37). While CLL is not currently curable, there are treatment options available including chemotherapy, CIT (combining chemotherapy with immunotherapy), and more recent targeted therapies that specifically target the BCR signalling pathway or BCL-2 proteins (236).

1.1.6.1 Chemotherapy

Prior to the approval of targeted therapies for CLL, chemotherapy treatment was the gold standard for several decades (44). The chemotherapy regiments consisted of purine nucleoside analogues (fludarabine, petostatin, and cladribine), alkylating agents (chlorambucil, cyclophosphamide or bendamustine), and glucocorticoids (2, 123, 240-242). Among purine nucleoside analogues, fludarabine is the most well-studied chemotherapy drug for CLL (38). Fludarabine displays higher overall response rates (ORRs) and complete response (CR) rates compared to alkylating agents and corticosteroids (243-245). Furthermore, the CLL4 trial investigated the combination of fludarabine and cyclophosphamide (FC) for fit patients with advanced CLL (Table 1.6) (237). This study showed that FC resulted in a significantly longer PFS at 5 years (36%) compared to single agent fludarabine or chlorambucil (10%) (237). Additionally, FC was superior for older patients (>70 years old) across various prognostic groups (237). Notably, FC was associated with a lower incidence of haemolytic anaemia (5%) compared to fludarabine (11%) or chlorambucil (12%) (237). The success of FC combination therapy paved the way for new treatment strategies, leading to the development of FC combined with anti-CD20 monoclonal antibody (mAb) immunotherapy, such as rituximab (107). The CLL8 trial established this combination as standard therapy for CLL (107).

1.1.6.2 Chemoimmunotherapy

CD20 is a protein found on the surface of mature B-cells (38) (Figure 1.5). While its function is still being investigated, it is suspected to act as a calcium channel in the cell membrane

(234). The randomised phase 3 (COMPLEMENT 1) trial showed that the addition of anti-CD20 mAbs to chemotherapy has significantly prolonged the survival rates of CLL patients (246) (Figure 1.5). Treatment decisions are based on factors including age, coexisting comorbidities, and the advancement of the disease (247, 248). For fit younger patients, patients are commonly treated with intensive CIT, and receive a combination therapy of fludarabine, cyclophosphamide, and rituximab (FCR) (80, 249). However, for elderly patients, a combination of bendamustine and rituximab (BR) is used (238, 250). Additionally, for elderly patients with coexisting comorbidities (in cases where an aggressive treatment is not suitable), chlorambucil combined with obinutuzumab is an option (239, 246). The median PFS after 5 years for these regimens is 56.8 months for FCR, 41.7 months for BR and 29.2 months for chlorambucil/obinutuzumab (80, 238, 239). The duration of remission after treatment can vary depending on the patient risk profile (107, 251). Patients with lower-risk CLL found to experience longer remission with FCR (251). Conversely, patients with higher-risk disease, particularly those with specific chromosomal deletions (del(17p) or del(11q)), experience shorter PFS (107). Of note, CLL10 trial showed there is a 7% risk of developing secondary myeloid malignancies within a median follow-up of 58 months in patients receiving FCR (Table 1.6) (252). Interestingly, research suggests that patients with M-CLL without del(17p) or del(11q) deletions respond better to FCR treatment compared to patients with U-CLL and these chromosomal deletions (251). Clinical trials have confirmed the effectiveness of anti-CD20 therapy (107, 238, 246, 250). For instance, the CLL8 trial showed that patients receiving FCR achieved higher response rates and longer PFS compared to patients receiving FC alone (80, 107). Additionally, the CLL11 trial demonstrated that single-agent anti-CD20 antibodies (rituximab or obinutuzumab) offered improved response rates and longer median PFS (11.1 and 26.7 months, respectively) compared to chlorambucil alone (Table 1.6) (239). Combination of chlorambucil and ofatumumab also showed superiority in median PFS (22.2 months) compared to chlorambucil alone (13.1 months) (246). However, the lower effectiveness of both FCR and FC in treating patients with U-CLL, del(17p), and del(11q) highlights the need for novel therapies for this subgroup of CLL patients with a more aggressive disease course.

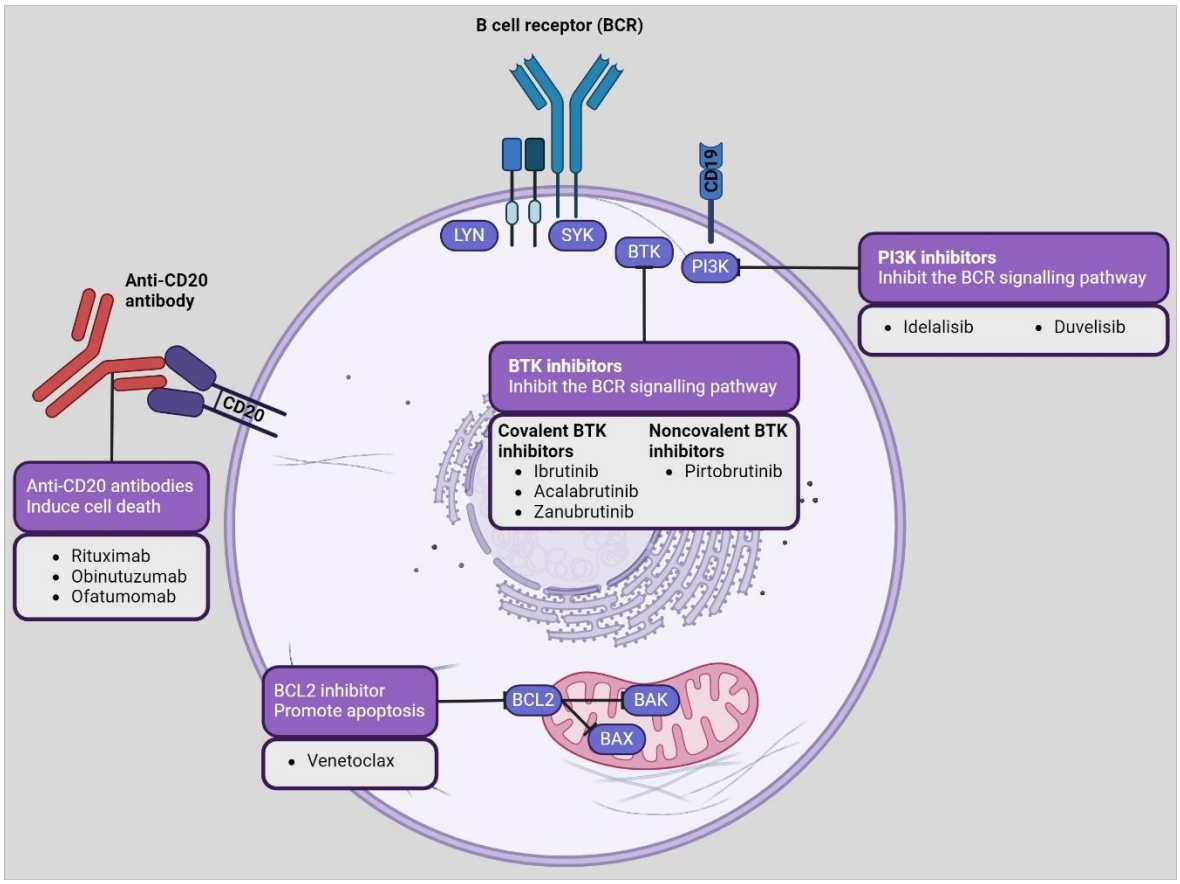

Figure 1.5: Different therapeutic strategies for CLL (Modified from (123)).

1.1.6.3 BCR inhibitors

The BCR signalling is a crucial pathogenic pathway promoting the survival and proliferation of malignant B-cells (51, 206). Since the introduction of BCR signalling inhibitors which target proteins within the BCR pathway, specifically BTK and PI3K inhibitors (253) (Figure 1.5), CIT has become less commonly used as primary therapy for CLL due to inferior efficacy (123). The effectiveness of BCR inhibitors may be linked to different aspects of the BCR pathway that are recognised as important prognostic factors in CLL including the mutation status or stereotypy of *IGHV* gene (38). The BCR pathway relies on the activity of several tyrosine kinases, including BTK, SYK, ZAP-70, Src family kinases (especially LYN), and PI3K (254). Deletion of LYN and BTK in murine CLL models indicated that these kinases may enable interaction between malignant B-cells and the TME (38, 255). Therefore, inhibiting the activity of these BCR associated kinases has revolutionised the treatment strategies for CLL by disrupting these survival mechanisms of CLL cells (38, 255, 256). This targeted approach has led to significant improvements in treatment outcomes (123). Compared to traditional CIT, BCR inhibitors have demonstrated superior response rates and more durable

remission (38, 123). Additionally, treatment with BCR inhibitors cause rapid shrinkage of enlarged LNs by increasing transient of CLL cells in PB which is known as “redistribution lymphocytosis" (38, 123).

1.1.6.3.1 BTK inhibitors

Ibrutinib (PCI-32765) is a small molecule inhibitor that targets BTK downstream the BCR signalling pathway in CLL (257, 258). It is administered orally and covalently binds to a cysteine residue at (C481) in the BTK protein (258). This binding irreversibly inhibits the enzymatic activity of BTK through high-affinity covalent binding to a cysteine residue (Cys-481) in the active site of BTK (257, 258). Inhibition of BTK by ibrutinib disrupts multiple pathways critical for CLL cell survival (259, 260). A study has shown that ibrutinib induces apoptosis in CLL cells in the presence of exogenous stimuli including factors produced by immune cells (CD40L, BAFF, IL-4, IL-6, TNF-α) and components of the TME (fibronectin, stromal cells) (222). Importantly, ibrutinib is more selective for CLL cells, inducing higher levels of apoptosis in CLL compared to normal B-cells, while sparing T cells (222). Furthermore, ibrutinib blocks downstream signalling pathways activated by BCR, including PI3K, NF-κB, and ERK1/2, which are important for CLL cell survival and proliferation (222, 260). A new *in vitro* study has shown that ibrutinib treatment reduces the ability of CLL cells to respond to chemokines (CCL19, CXCL12, and CXCL13) (259). Additionally, it reduces the levels of adhesion molecules (integrins Leukocyte function-associated antigen 1 (LFA-1), Leukocyte function-associated antigen 3 (LFA-3), B-T lymphocyte attenuator (BTLA), and CD276) on the surface of CLL cells, which are crucial for cell motility, adhesion, and migration (259). By affecting these processes, ibrutinib may disrupt the homing of CLL cells to LN and BM, where they typically reside and proliferate. Pre-clinical studies show that ibrutinib treatment sustainably downregulates BCR and NF-κB signalling pathways in CLL cells, reducing tumour burden in LN and BM (260), suppresses the expression of surface activation markers (CD69 and CD86), regardless of *IGHV* mutational status or the presence of del(17p) (260), and downregulates the production of inflammatory cytokine and signalling molecules including TNF-α/β, CCL3, CCL4, CC chemokine ligand (CCL17), and interleukin-16 (IL-16) in CLL patients (224, 260, 261). These findings suggest that ibrutinib works through multiple mechanisms to target CLL cells and their interaction with the TME.

Ibrutinib, a first-in-class BTK inhibitor (262), has revolutionised the treatment landscape for CLL. Clinical trials have consistently demonstrated its efficacy and safety across various prognostic groups. The initial trial of ibrutinib in patients with R/R CLL showed promising results (263). Treatment response was independent of traditional prognostic factors including advanced disease stage, prior treatment history, or the presence of the del(17p) (263, 264). Notably, patients who were treatment-naïve achieved a 7-year PFS rate of 83%, while those with R/R disease had a 7-year PFS rate of 34% (264). The RESONATE phase 3 trial in previously treated CLL further solidified ibrutinib role in CLL treatment, where ibrutinib monotherapy demonstrated significantly higher PFS of 40% compared to 3% with ofatumumab at a 5-year follow-up (265). The RESONATE-2 phase 3 trial established ibrutinib as a viable first-line treatment option for CLL patients aged 65 years and older (266). This study showed a significant 7-year PFS rate of 59% and improved OS compared to chlorambucil (9%) (267). The Alliance trial also explored the effectiveness of ibrutinib in previously untreated older patients, comparing ibrutinib alone or combined with rituximab to BR, where both ibrutinib regimens resulted in longer PFS compared to BR (268). Interestingly, the addition of rituximab to ibrutinib did not significantly improve PFS compared to ibrutinib alone (268). Notably, the BR arm experienced a higher rate of haematological adverse events (61%) compared to ibrutinib alone (41%) and ibrutinib plus rituximab (39%) (268). The iLLUMINATE phase 3 trial evaluated ibrutinib plus obinutuzumab in both young and older patients with previously untreated CLL, and co-existing medical conditions (269). Compared to chlorambucil plus obinutuzumab, the ibrutinib combination achieved a significantly longer median PFS (79% vs. 35%) after a median follow-up of 30 months (269). The E1912 phase 3 trial compared ibrutinib plus rituximab to the traditional FCR regimen, where ibrutinib plus rituximab offered superior PFS and OS compared to FCR (270). Notably, ibrutinib plus rituximab resulted in a higher PFS rate (90.7%) in patients with U-CLL compared to FCR (62.5%) at a 3-years follow-up (270). The SEQUOIA phase 3 trial compared zanubrutinib, a next-generation BTK inhibitor, to BR, where zanubrutinib demonstrated a superior PFS rate (85.5%) compared to BR (69.5%) at a 2-year follow-up (271). Similarly, the phase 3 ELEVATE-TN trial showed that patients treated with acalabrutinib (another next-generation BTK inhibitor) plus obinutuzumab or acalabrutinib alone achieved significantly higher PFS rates (87% and 78%, respectively) compared to chlorambucil plus obinutuzumab (25%) (272). These trials have led to the approval of ibrutinib, acalabrutinib, and zanubrutinib as the first-line treatment of CLL. Importantly,

these trials have also highlighted the benefits of BTK inhibitors for patients with adverse prognostic factors including *TP53* aberration, which is presented in 10% of untreated CLL patients and associated with a poorer prognosis (107, 123).

While ibrutinib has transformed CLL treatment, it is not without treatment complications. Approximately 23% of patients experience adverse events, including increased risk of bleeding, fatigue, diarrhoea, bruising, rash, arthralgia, myalgia, high blood pressure, and atrial fibrillation, leading to treatment discontinuation (2, 265, 267, 273). The first trial comparing acalabrutinib to ibrutinib in previously treated CLL patients harbouring del(17p) or del(11q) showed lower treatment discontinuations with acalabrutinib (14.7%) compared with ibrutinib (21.3%) (274). This infrequent occurrence of the adverse events with acalabrutinib is due to its superior selectivity to inhibit BTK (275, 276). Similarly, the ALPINE trial compared zanubrutinib to ibrutinib in patients with R/R CLL who had received at least one prior therapy (29). At a 2-year follow-up, the trial showed zanubrutinib superiority over ibrutinib with better PFS (78.4% vs. 65.9%, respectively) and OS (29). Additionally, zanubrutinib caused fewer adverse events leading to treatment discontinuation (29). These findings highlight the potential of next-generation BTK inhibitors including acalabrutinib and zanubrutinib, with improved selectivity for BTK translating into better tolerability. In progressive CLL disease, the development of resistance mechanisms under ibrutinib treatment is often associated with the acquisition of sequence variations in the BTK active site (C481S) or gain-of-function variations in the downstream gene phospholipase C gamma 2 (*PLCG2*) in approximately 66-80% of patients (123, 277, 278). Pirtobrutinib, a non-covalent, reversible, highly selective BTK inhibitor is a promising BTK inhibitor for patients who develop resistance to ibrutinib due to mutations in the BTK active site (C481S) (279, 280). Early data from phase 1/2 BRUIN study in R/R CLL patients who previously received BTK inhibitors suggest promising results with a lower incidence of known BTK inhibitors-related adverse events (280, 281).

1.1.6.3.2 PI3K inhibitor

PI3K has an important role in regulating many aspects of cellular biology and is frequently hyperactivated in cancers (163, 282). The PI3K family of proteins exhibits multifunctional roles regulating cellular growth, differentiation, metabolism, motility, and intracellular trafficking (282). With three classes of PI3K (I, II, and II), where class I is associated with

proliferation and survival of malignant B-cells (283, 284). The class I PI3K consists of four isoforms including α, β, δ, and γ (284). The constitutive activation of the PI3K pathway is dependent on class I PI3K p110 isoform (PI3Kδ) (283), leading to dysregulation of cell-cycle progression and survival (285). The PI3K pathway can be targeted by idelalisib (CAL-101), a selective inhibitor for PI3Kδ and duvelisib (IPI-145), a dual selective inhibitor for both PI3Kδ and PI3Kγ (286, 287). Pre-clinical studies showed idelalisib inhibition of PI3K promotes apoptosis, inhibits cellular migration towards signalling molecules including CXCL12 and CXCL13, reduces survival signals including BCR-induced AKT (known as PKB) phosphorylation and ERK activation in primary CLL cells (225). A phase 3 clinical trial demonstrated the effectiveness of idelalisib in combination with rituximab for patients with R/R CLL (288). This combination therapy significantly improved PFS compared to placebo plus rituximab, with a PFS rate of 93% at 24 weeks (288). The idelalisib arm also improved OS (288). Therefore, the combination of idelalisib and rituximab has been approved for the treatment of R/R CLL (289). However, patients receiving idelalisib treatment should be observed for idelalisib adverse effects including transaminitis, pneumonitis and colitis, which are often severe and require discontinuation of the therapy (290). Additionally, idelalisib is not recommended as first line therapy for CLL due to treatment association with grade 3 or higher elevations in liver enzymes (123, 291). Duvelisib shares a similar safety profile with idelalisib (292). It was approved for CLL patients who have received at least two prior therapies (38, 292). Lastly, umbralisib, a dual inhibitor, targeting both PI3Kδ and casein kinase 1 epsilon (CK1ε), represents a promising new generation of PI3K inhibitors for CLL treatment (293). A phase 1/1b study has shown encouraging results for umbralisib in combination with ibrutinib in R/R CLL (294). While umbralisib overall toxicity profile resembles idelalisib, it was associated with lower incidence of transaminitis or diarrhoea (38, 295).

1.1.6.3.3. Additional BCR inhibitors

SYK is another attractive target downstream of the BCR signalling pathway as it is involved in the initial step of signal transduction of the pathway (296). Entospletinib (GS-9073) is an adenosine triphosphate (ATP) competitive inhibitor of SYK (297). Pharmacodynamic analysis showed that entospletinib treatment rapidly reduces the phosphorylation of signal transducer and activator of transcription 3 (STAT3), a protein involved in cell proliferation

and survival, and expression of anti-apoptotic MCL1 protein (298). A phase 2 clinical trial examined entospletinib as a monotherapy for patients with R/R CLL (299). This study showed promising results, with a median PFS of 13.8 months and an ORR of 61% (299). However, 29% of patients experienced serious adverse events, including dyspnoea, pneumonia, febrile neutropenia, dehydration, and pyrexia (299). A phase 1/2 study explored the use of entospletinib in combination with obinutuzumab for R/R CLL patients (298). This study demonstrated encouraging an ORR, with a 53% rate in high-risk patients and a 62.5% rate in patients who had previously received a kinase inhibitor treatment (298). While entospletinib plus obinutuzumab shows promise results, 96% showed treatment-related adverse events including 65% grade 3 or higher and one patient discontinued the therapy (298).

1.1.6.4 BCL-2 inhibitor

BCL-2 family plays a critical role in regulating the intrinsic or mitochondrial pathway of apoptosis (300). This family consists of 18 proteins that share structural similarities known as BCL-2 homology (BH) domains (301). BCL-2 proteins are categorised based on their structure and function into three main groups, anti-apoptotic proteins (BCL-2, BCL-XL, MCL1, BCL-2-related protein A1 (BCL-2A1), and BCL-B) promote cell survival, pro-apoptotic multidomain proteins (BAX and BCL-2 antagonist killer 1 (BAK)) directly trigger apoptosis, and pro-apoptotic BH3-only proteins (BCL-2-interacting mediator of cell death (BIM), BCL-2-binding component 3 (PUMA), phorbol-12-myristate-13-acetate-induced protein 1 (NOXA), and Harakiri (HRK)) indirectly trigger apoptosis through neutralising the anti-apoptotic proteins (301). The balance between anti-apoptotic and BH3-only proteins determines the cell fate – survival or death, which is controlled through protein-protein interactions (302). Anti-apoptotic proteins possess a hydrophobic groove on their surface serves as a binding site for the α-helical BH3 domain present in pro-apoptotic proteins (303). When bound, the BH3-only proteins neutralise the anti-apoptotic proteins, permitting apoptosis to proceed (303). BH3 mimetics are small molecule drugs designed to mimic the BH3 domain of pro-apoptotic proteins (300) (Figure 1.5). These drugs directly bind to the hydrophobic groove of anti-apoptotic BCL-2 proteins, neutralising their survival-promoting function (301). Interestingly, CLL cells are characterised by high expression levels of anti-apoptotic BCL-2 proteins (304, 305). This overexpression contributes to the chronic

survival of CLL cells and their resistance to cell death signals (304, 305). Therefore, targeting the BCL-2 family with BH3 mimetics has shown promising therapeutic benefits for CLL.

Venetoclax (ABT-199) is a highly selective small molecule that acts as a BH3 mimetic to inhibit BCL-2 (306). Several clinical trials have established venetoclax as frontline therapy for CLL, particularly in R/R CLL (123). A phase 1 study evaluated the safety and efficacy of venetoclax monotherapy in R/R CLL patients (307). The study demonstrated a promising median PFS of 30.2 months (307). Notably, patients with a favourable mutational profile, no prior resistance to BCR inhibitors, and no bulky lymphadenopathy experienced the most durable benefits (307). Furthermore, the MURANO phase 3 trial compared venetoclax plus to BR in R/R CLL patients (308). Patients received venetoclax for two years, with rituximab administered for the first six months (308). The venetoclax combination arm achieved a significantly longer time to next treatment or death, with a median of 63 months compared to 24 months with BR (308). Moreover, the CLL14 phase 3 trial assessed the effectiveness of fixed-duration venetoclax plus obinutuzumab compared with chlorambucil plus obinutuzumab in treatment-naïve elderly CLL patients (309). Patients received 12 cycles of venetoclax and obinutuzumab compared to chlorambucil plus obinutuzumab (309). At three months after treatment completion, 40% of patients on the venetoclax arm achieved undetectable minimal residual disease (uMRD) compared to only 7% in the chlorambucil arm (309). Furthermore, the venetoclax combination significantly improved PFS, with a rate of 74% at the 4-year follow-up compared to 35.4% for the chlorambucil arm (309). Based on these successful trials, venetoclax combined with anti-CD20 antibodies has been approved as a first-line therapy for R/R CLL (123). Interestingly, a phase 2 trial explored the use of a fixed-duration combination of ibrutinib plus venetoclax in elderly CLL patients with poor prognostic features (310, 311). The combination achieved a high rate of BM uMRD (75%) independently of the prognostic factors, with a PFS of 93% at the 3-year follow-up (311). Despite venetoclax efficacy, resistance has been reported including mutations in BCL-2 (Gly101Val) that reduce venetoclax binding, overexpression of pro-survival proteins including BCL-XL and MCL1, and the emergence of clones with CKs (312, 313). The CLL14 and ELEVATE TN studies showed favourable PFS with BTK inhibitors for patients with *TP53* aberrations compared to venetoclax plus obinutuzumab (4-year PFS of 76% vs 3-year PFS of 60.4%, respectively) (123, 272). However, a direct comparison between BTK inhibitors as monotherapy and venetoclax combinations is lacking. The ongoing CLL17 trial, comparing ibrutinib monotherapy to fixed-duration venetoclax plus obinutuzumab or fixed-duration

ibrutinib plus venetoclax, aims to further evaluate the effectiveness of BTK inhibitors compared with venetoclax combinations in CLL patients with poor prognoses, including those with *TP53* mutations (ClinicalTrials.gov ID: NCT04608318).

1.1.6.5 Cellular therapies

Allogeneic HSC transplantation has been considered a potential curative option for younger, fit CLL patients with high-risk features including del(17p), *TP53* mutations, or CK, especially those who have relapsed after prior lines of therapy (2, 314). However, several factors limit the applicability of allogeneic HSC transplantation, including the older age of the majority of CLL patients, the need for a suitable donor, and the increased risk of infections following transplantation, all of which pose significant challenges (2).

Chimeric antigen receptor (CAR) T-cell therapy represents another cellular therapy approach for CLL. While CAR T-cell therapy has demonstrated remarkable success in other B-cell malignancies (315-317), its efficacy in CLL has been modest, with low response rates and short remissions (318, 319). However, a study combining ibrutinib with CAR T cells (at a 1:1 ratio of CD4 and CD8 cells) in patients with R/R CLL demonstrated promising outcomes (320). This study achieved a more durable remission with uMRD in BM in 61%, OS of 86% and PFS of 59% at 1-year follow-up (320). A phase 1/2 TRANSCEND CLL 004 study evaluating the lisocabtagene maraleucel (liso-cel) CD19-directed CAR T cells as monotherapy for R/R CLL patients with high-risk features who received at least two prior lines of therapy including BTK inhibitors and venetoclax based regimens (321, 322). This therapy has shown durable complete remissions, high rates of uMRD (63.3% in PB and 59.2% in BM), and a manageable safety profile (322). This trial led to the first Food and Drug Administration (FDA) approval of CD19 CAR T cells therapy for R/R CLL patients (323). The ongoing studies are delivering encouraging findings and providing alternative therapeutical strategies for the unmet need to treat high risk naïve or R/R CLL patients.

1.1.7 FOXO transcription factors

The progression of malignant cells is driven by two hallmarks of cancer: sustained proliferative signalling and the ability to evade growth suppression (324). To achieve continuous growth, these cells often manipulate components of growth factor receptor

(GFR) signalling pathways (324). The PI3K/AKT pathway, activated downstream of GFR signalling, is frequently hyperactivated in cancer, promoting cell survival and proliferation (325). FOXO transcription factors, key components downstream of the PI3K/AKT pathway, are negatively regulated to promote the survival and proliferation of malignant cells (326). FOXO transcription factors belong to the Forkhead box (FOX) family, a large group of transcription factors sharing a conserved winged-helix DNA binding domain (327). With 50 FOX proteins identified in the human genome, FOX proteins are classified by their tissue specific expression and sequence homology within the winged-helix DNA domain (327). FOXO transcription factors are consisted of four members, including FOXO1, FOXO3a, Forkhead box protein O4 (FOXO4), and Forkhead box protein O6 (FOXO6) (327). The FOXO family members shares a highly conserved transcription factors domain which binds to their target genes as monomers or heterodimers and recognises the DNA consensus sequence (5'-GTAAA(C/T)A-3') in the genome (327, 328). FOXO proteins are expressed in distinct tissues, where FOXO1 is highly expressed in adipose tissue, FOXO3 in the brain, kidney, and heart, FOXO4 in skeletal muscle, and FOXO6 in nervous tissues (329, 330). Despite tissue-specific expression, FOXO proteins share regulatory overlapping and functional redundancy (331). FOXOs activity is regulated mainly by external stimuli including growth factor signalling and cellular stress (elevated reactive oxygen species (ROS) levels, nutrient starvation and DNA damage), through post-translational modifications which affect their protein stability, protein-protein interaction, subcellular localisation and transcriptional activity (332, 333). The most studied post-translational modification of FOXOs is regulation via phosphorylation at different conserved serine and threonine amino acids residues (334). Beside phosphorylation, FOXOs are regulated in response to external stimuli by multiple layers of post-translational modifications including acetylation, methylation, ubiquitination and deubiquitination (335). FOXO proteins are important for maintaining cellular homeostasis by regulating various processes, including apoptosis, cell cycle inhibition, metabolism, stress resistance, DNA repair, inflammation, immune response, and differentiation (336). This section primarily focuses on FOXO post-translational modifications, including phosphorylation, ubiquitination, and deubiquitination. The regulation of FOXO proteins by acetylation and methylation, while important, falls outside the scope of this thesis.

1.1.7.1 AKT-mediated phosphorylation of FOXOs

The PI3K/AKT signalling pathway is often dysregulated in cancer, resulting in AKT activation and subsequently inhibition of FOXO activity by altering its nuclear-cytoplasmic subcellular localisation (337). The subcellular distribution of FOXO proteins is regulated by nuclear export signal (NES) and a nuclear localisation signal (NLS) domain, enabling the shuttling of FOXO proteins between the nucleus and cytoplasm (338). The structure of FOXO consists of an N-terminal Forkhead DNA binding domain (DBD), NES and NLS domain proximal to the C-terminal (Figure 1.6a). Upon activation of PI3K/AKT signalling, AKT phosphorylates FOXO1, FOXO3, and FOXO4 at three conserved RxRxxS/T residues, except for FOXO6, lacking one of AKT phosphorylation sites, reducing its sensitivity to AKT-mediated inactivation (336, 339, 340). Additionally, AKT triggers phosphorylation of FOXOs at three serine/threonine sites of FOXO1 (T24, S256 and S319), FOXO3 (T32, S253 and S315), and FOXO4 (T28, S193 and S258), while FOXO6 at two sites (T26 and S184) (339). AKT-mediated phosphorylation of nuclear FOXOs creates a docking site for chaperone protein 14-3-3, masking the NLS and revealing NES of nuclear FOXOs to block FOXOs nuclear entry and promote nuclear export (336) (Figure 1.6b). Furthermore, Zhang, Gan (341) reported that AKT-mediated

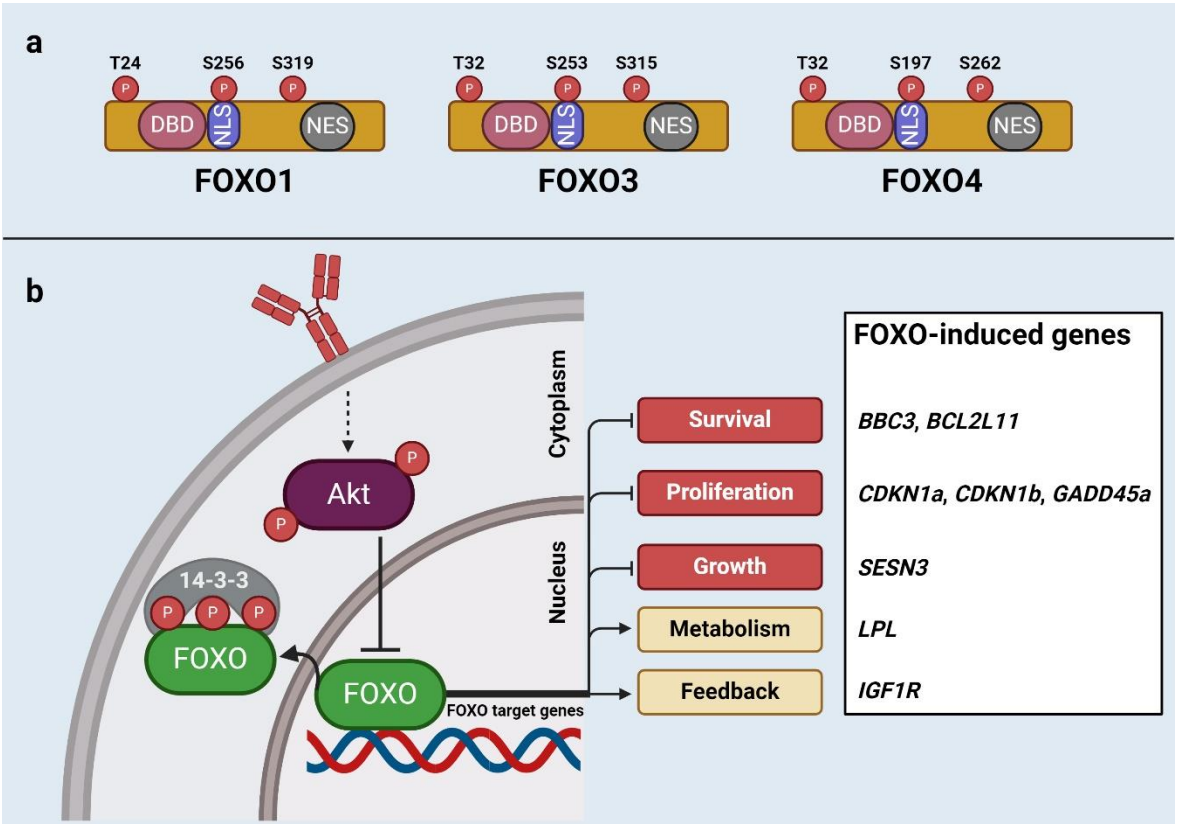

Figure 1.6: AKT-mediated regulation of FOXO family members target genes (modified from (142)).

phosphorylation of FOXO1 (S256) reduces its DNA-binding activity. Conversely, dephosphorylation of FOXOs leads to nuclear accumulation, which can occur upon loss of GFR signalling, promoting dephosphorylation of PIP3 by PTEN and subsequently reducing the activation of PI3K/AKT signalling (326, 342). Dephosphorylation of FOXOs is mediated by protein phosphatase 2A (PP2A), which generally works independently of the phosphorylation residue (343). In addition to AKT-mediated inactivation of FOXOs, serum and glucocorticoid-regulated kinase (SGK), ERK, P38, cyclin dependent kinase 1/2 (CDK1/2), casein kinase (CK1), and IKK can promote FOXOs inactivation, while kinases including AMP kinase (AMPK), c-jun terminal kinase (JNK) and mammalian sterile 20-like kinase (MST1) can promote FOXOs activity, with each kinase recognising a specific motif within FOXO proteins (336). For instance, reactive oxygen species (ROS)-mediated activation of JNK blocks FOXO-dependent inactivation by growth factor signalling through phosphorylation of the insulin adaptor IRS1/2 (342). Additionally, JNK enhances FOXO activation by phosphorylating the 14-3-3 protein, leading to release FOXO from 14-3-3 and exposure of the NLS, promoting FOXOs nuclear translocation (344). MST1 also activates FOXOs by disrupting the 14-3-3 binding to FOXO1 through phosphorylating FOXO1 (S212) (345). Furthermore, under low glucose conditions, ATP levels decrease, leading to the activation of AMPK, an ATP/adenosine monophosphate (AMP) sensor (342). Following AMPK activation, FOXOs are phosphorylated, leading to nuclear translocation and subsequently promoting the expression of target genes involved in metabolism and stress resistance (342, 346). These observations suggest a dual role for FOXOs, maintaining cellular homeostasis in response to stress signals, in addition to their role in determining cell fate through cell cycle inhibition and apoptosis, highlighting a context dependent function for FOXO proteins.

1.1.7.2 FOXO regulation by ubiquitination and deubiquitination

The activity of AKT can promote FOXO ubiquitination and subsequent proteasomal degradation (347). Ubiquitination is a reversible post-translational modification that targets proteins for degradation or coordinates signal transduction pathways (348, 349). Ubiquitination is a key post-translational modification regulating FOXOs activity and stability, highlighting the role of the ubiquitin-proteasome system (UPS) in regulating FOXOs expression levels (335). In HepG2 cells, the degradation of FOXO1 by ubiquitination required phosphorylation mediated by the PI3K/AKT pathway (350, 351). Ubiquitination of

FOXO proteins is often linked to growth factor signalling through the PI3K/AKT pathway activation (351, 352). In addition to AKT-mediated FOXOs degradation by ubiquitination, IKK and ERK were reported to have similar effect on FOXOs (353, 354). AKT-mediated phosphorylation of FOXOs (e.g. FOXO1 at S256) are recognised by the activated F-box protein S-phase kinases-associated protein2 (SKP2), an E3 ligase, in the SCF E3 ligase complex, triggering FOXOs ubiquitination and degradation (355). Therefore, SKP2 requires AKT-mediated phosphorylation to recognise FOXOs and subsequently targets them for ubiquitination and degradation. Additionally, AKT can directly phosphorylate SKP2, resulting in its activation and subsequent cytoplasmic translocation, as well as preventing SKP2 degradation (356). Loss of PTEN was shown to be associated with elevated mRNA levels of SKP2 (357), further indicative of its AKT-dependent function. In T cell lymphomas, low levels of FOXO1 were associated with elevated levels of SKP2 (351, 358). Similarly, ERK-mediated phosphorylation of FOXO1 leads to recruitment of MDM2, an E3 ligase, for FOXO ubiquitination and degradation (359). In contrast, cellular stress mediated FOXO ubiquitination, including oxidative stress and glucose availability, leads to FOXOs nuclear accumulation and activation (360, 361). Van der Horst, de Vries-Smits (360) showed that MDM2-mediated ubiquitination of FOXO4 at lysine199 (Lys199) and Lysine211 (Lys211), led to nuclear translocation and activation of FOXO4. This study also showed that FOXO4 accumulation in the nucleus was reversed by a deubiquitinase (DUB) protein ubiquitin-specific protease (USP) 7 (USP7) (360). Conversely, ERK-mediated phosphorylation of FOXO3a led to MDM2-mediated degradation (351). Constitutive photomorphogenic 1 (COP1), a ring finger E3 ubiquitin ligase, mediates FOXO1 proteasomal degradation, which requires AKT phosphorylation of FOXO1 (362). Furthermore, gene expression of FOXO1 targets was suppressed by COP1-mediated ubiquitination (362). In prostate cancer, nuclear accumulation of PTEN required Neural precursor cell expressed developmentally down-regulated protein 4-1 (NEDD4-1) ubiquitination of PTEN, while USP7 reversed PTEN nuclear accumulation, favouring cytoplasmic accumulation (363). These observations indicate a context dependent ubiquitination of FOXOs which may lead to either proteasomal degradation or nuclear accumulation and enhancement of FOXOs activity.

1.1.7.3 FOXOs tumour suppressive function

In PTEN deficient cell lines, FOXO1 and FOXO3 are inactivated by sequestration in the cytoplasm, while re-expression of PTEN induces cell cycle arrest in G1 phase and apoptosis, which can be attained by hyperactivation of FOXOs in these cells (364, 365). Histopathology studies focusing on FOXOs localisation and their association with cancer outcome, further emphasises on FOXOs role as tumour suppressors, where elevated levels of FOXO1 (T24) phosphorylated form by PI3K/AKT pathways are associated with inferior OS and disease-free survival in several solid and leukaemic cancers including soft tissue sarcoma (366), prostate (367), and acute myeloid leukaemia (AML) (342, 368). In contrast, elevated expression of FOXO3 is associated with favourable disease outcomes in colorectal (369), urothelial (370), and neuroblastoma cancer (371). Interestingly, in MCF7 breast cancer cells with positive estrogen receptor (ER+), a nuclear receptor for estrogen hormone, overexpression of nuclear FOXO3 was associated with inhibition of motility, invasiveness and anchorage-dependent growth, while in cells with negative estrogen (ER-), FOXO3 was associated with aggressive metastatic breast cancer (372). Therefore, the tumour suppressive activity of FOXOs is multifaceted and largely depends on physiological conditions and cell/tissue types. This section is focused on the mechanism of FOXOs tumour suppressive activity which results in cell cycle arrest and apoptosis.

1.1.7.3.1 FOXOs regulation of the cell cycle

FOXO activation by pharmacological inhibition of PI3K/AKT pathways or overexpression of FOXO, led to a robust cell cycle arrest in cancer cell lines derived from acute T cell leukaemia, glioblastoma, and colon carcinoma (373-376). The cell cycle progression starts from G0 ‘quiescent state’ and progress from G1 to S phase (342). Early G1 phase requires inhibition of the retinoblastoma family of protein (retinoblastoma protein (RB), p107 and p130) through GFR signalling which upregulates the expression of cyclin D proteins (*CCND1*, *2* and *3*), and subsequently promoting the upregulation of cyclin-dependent kinase 4/6 (CDK4/6) complexes (342). The inhibition of retinoblastoma family proteins promotes the release of E2F, stimulators of proliferation, which induces transcription of S phase proteins (342). The S phase requires the expression of cyclin E-CDK2 complexes for DNA replications and cellular growth before entering mitosis, which requires cyclin B/CDK1 complexes to be initiated (342). FOXOs function as master regulators of cell cycle progression, through the

upregulation of cyclin-dependent kinase inhibitors (CDKIs) *CDKN1A* ($p21^{Waf1/Cip1}$) and *CDKN1B* ($p27^{Kip1}$) (375, 377), inhibiting cyclin E-CDK2 and cyclin D-CDK4/6 complexes responsible for progression through the cell cycle G1/S phase. FOXOs also mediate transcriptional repression of *CCND1* and *CCND2*, inducing cell cycle arrest independent of $p27^{Kip1}$ activity (378). Additionally, FOXOs regulate the inhibitor of cyclin-dependent kinase 4 (INK4) family members of cyclin-dependent kinase inhibitors (CKIs) including $p15^{INK4b}$ (*CDKN2B*), $p16^{INK4a}$ (*CDKN2A*), $P18^{INK4c}$ (*CDKN2C*) and $p19^{INK4d}$ (*CDKN2D*), which inhibit the cell cycle progression in G1 phase by bocking CDK4/6 and cyclin D (375, 379-381). The expression of p130 is also regulated by FOXOs, blocking progression to S phase and inducing quiescence state (376, 382). Therefore, FOXOs can mediate cell cycle arrest at different phases (G0/G1, S, G2 and M) through regulating the expression of CKIs and retinoblastoma proteins.

1.1.7.3.2 FOXOs regulation of apoptosis

FOXO family members have been reported in several different cell types to function as inducers of apoptosis through both intrinsic and extrinsic pathways (330, 342). The intrinsic pathway, also known as the mitochondrial pathway, is regulated by the activity of BAK and BAX proteins (342, 383). The activation of BAK and BAX proteins is determined by the balance between pro-apoptotic (BIM, BAD, BH3-interacting domain death agonist (BID), PUMA, NOXA, BCL-2 related ovarian killer (BOK), and BCL-2 modifying factor (BMF)) and anti-apoptotic (BCL-2, BCL-XL, and MCL1) factors, leading to mitochondrial outer membrane permeabilization and apoptosis (383). FOXO proteins regulate apoptosis through the intrinsic pathways by upregulation of pro-apoptotic BIM (*BCL2-L11*) and PUMA (*BBC3*) proteins, while repressing anti-apoptotic BCL-XL (*BCL2-L1*) protein (382, 384), promoting mitochondrial-mediated apoptosis. Furthermore, cells can trigger apoptosis through the extrinsic pathway by engagement of extracellular ligands including TNF, FAS-ligands (FASL), and TNF-related apoptosis-inducing ligand (TRAIL) to the extracellular domain of tumour necrosis factor receptor (TNFR) and the death receptors (DRs), respectively (342, 385-387). Activation of the intrinsic and extrinsic pathways leads to the activation of caspase-3 and caspase-7 cascade, the irreversible executioner enzymes of apoptosis (342, 385-387). FOXOs proteins promote apoptosis through the extrinsic pathway by increasing the expression of DR cognate ligands, including FASL (330, 382).

1.1.7.4 The role of FOXOs in normal and malignant B-cells

1.1.7.4.1 The role FOXO proteins in normal B-cells

FOXO proteins, particularly FOXO1, play a crucial role in the development of normal B-cells (388). In early B-cell differentiation, FOXO1 is suggested to be the dominant family member expressed at this stage (189), and is induced by transcription factor 3 (TCF3), transcription factor 12 (TCF12), and early B-cell factor 1 (EBF1) (389, 390), driving the differentiation commitment of the common lymphocyte progenitor (CLP) into the pro-B-cell (388). Furthermore, the progression of B-cell differentiation from pro- to pre-B-cell stages requires FOXO1 and EBF1 positive feedback loop, activating PAX5 (391). Of note, successful V(D)J recombination, regulated by RAG proteins, is important for the progression of B-cell between pro- and pre-B stages (128). At the pro-B stage, knockout of *FOXO1*, but not *FOXO3A* or *FOXO4*, downregulates the recombination activating genes *RAG1* and *RAG2*, resulting in blocking the differentiation of B-cell beyond this stage (392). Furthermore, FOXO1 depletion in early pro- and pre-B-cell stages impairs the differentiation of B-cell through downregulation of the expression of interleukin 7 receptor (IL7R), a receptor involved in B-cell survival and development (392). Notably, contrary to reported FOXOs role in cell cycle arrest and apoptosis in malignant cells (373-376), FOXO1 is involved in the proliferation and survival of pro- and pre- B-cells (388). Depletion of *FOXO1* at pro-B-cell stage causes repression of proliferation and induction of apoptosis, accompanied by upregulation of BIM and downregulation of BCL-XL (189). Furthermore, FOXO1 plays a temporal-specific role in pre-B-cell stage (393, 394). For instance, depleting AKT phosphorylation sites T308 and S473 increases FOXO1 levels and accelerates pre-B-cell proliferation through upregulation of cyclin D3 levels (388, 395), while BLNK-dependent inactivation of PI3K induces FOXO1 transcriptional activity, leading to the induction of FOXO1 target gene B-cell lymphoma 6 (BCL6) and subsequently inhibition of proliferation (388, 396).

In mature B-cells, FOXO1 is the most abundant protein member of the FOXO family followed by FOXO3a (388, 397). While FOXO1 phosphorylation is consistently observed in resting B-cells, FOXO1 phosphorylation further increases in stimulated B-cells (396). BCR-mediated phosphorylation of FOXO1 leads to nuclear exclusion and later protein degradation in mature B-cells (396). Additionally, BCR signalling via PI3K pathway triggers downregulation of *FOXO1* transcription levels in mature B-cells (398). Interestingly, overexpression of wild-

type FOXO1, but not FOXO3a, leads to increase in cell apoptosis (397). Conversely, overexpression of wild-type FOXO3a delays cell cycle progression (397). Expression of constitutively active form with mutation of 3 serine and threonine residues on FOXO1 (A3) and FOXO3A(A3) increases cell cycle arrest and apoptosis in activated mature B-cells (397). In BCR-ablated B-cells, FOXO target genes including BCL-2-like protein 11 (*BCL2L11*) and *CDKN1B* are upregulated (399), an upregulation that is reversed by the expression of constitutively active from of PI3K (P110*) (400), indicating that FOXOs transcriptional activity is regulated through the PI3K pathway in mature B-cells. Interestingly, conditional deletion of FOXO1 in transitional B-cells affects homing of PB-B-cells and reduces the number of B-cells in the LN (189). Additionally, FOXO1 deletion blocks CSR through downregulation of L-selectin (CD62L) and *AICDA* (AID) (189). In B-cells within GCs, FOXO1 expression is the most abundant compared to other FOXOs and plays a crucial role in GC formation and function (401). Upon antigen encounter, the formation of GC is created by follicular cells in SLOs where mature B-cells undergo a series of events including activation, proliferation, SHM, affinity mutation and CSR to subsequently differentiate into memory or plasma cells (128, 388, 402). The structure of GC is subdivided into a dark zone (DZ), harbouring highly proliferative B-cells undergoing SHM, and a light zone (LZ), harbouring B-cells undergoing activation, CSR and selection (388, 403). In the DZ, the transcriptional activity of FOXO1 mediates the expression of CXCR4 and BCL6, favouring B-cells homing of DZ and represses genes including *TP53*, respectively (401). In the LZ, FOXO1 mediates the expression of *AICDA*, essential for SHM and CSR (388, 401). FOXO1-null GC B-cells exhibit impaired DZ formation (losing architectural polarity), affinity selection and CSR, while maintaining SHM normal function (388, 401). Therefore, FOXO1 high expression is a key component to maintain CSR and proliferation of B-cells within the DZ (388). FOXO1 is also involved in the generation of plasma cells (189). *FOXO1* knockout leads to increased plasma cell formation, while its constitutive activation downregulates antibody-secreting cells generation, likely through the induction of BCL6 (189, 388). Thus, maturation and survival of B-cells requires the precise modulation of FOXO1 expression and transcriptional activity within a narrow range.

1.1.7.4.2 The role FOXO proteins in malignant B-cells

FOXO transcription factors are generally considered as tumour suppressors by virtue of their established ability to inducing cell cycle arrest and apoptosis (361). The Mx-Cre-inducible conditional FOXO (*FOXO1/3/4*$^{-/-}$*)* triple knockout of adult mice led to the development of thymic lymphomas and haemangiomas, accompanied by a loss of cellular proliferation and survival restrictions, further confirming the tumour suppressor role of FOXO proteins (404). Additionally, the triple-FOXO1/3/4-deficient mice highlighted the overlapping and redundant function of FOXO isoforms, as evidence by the mild tumour phenotypes observed in dual knockouts (*FOXO1/FOXO3*$^{-/-}$ or *FOXO1/FOXO4*$^{-/-}$) (404). Despite their classic tumour suppressor function, several B-cell malignancies demonstrated that FOXOs have the ability to promote tumorigenesis and drug resistance (405, 406).

In classical Hodgkin lymphoma (cHL), FOXO1 is downregulated via constitutive activation of AKT/PKB and MAPK/ERK kinases as well as upregulation of miR-183, miR-96, and miR-182 cluster (407). Expression of FOXO1(A3) in cHL cell lines led to cell cycle arrest in G0/G1 phase and apoptosis, associated with increased expression of FOXO target genes *BCL2L11* and *CDKN1B* (407). This study suggests that the downregulation of FOXO1 expression may contribute to the progression of cHL, and that FOXO1 transcriptional activity plays a tumour suppressive role in this disease. In tonic BCR signalling-dependent DLBCL, FOXO1 expression was observed in 80% of tumours and was associated with longer OS (408). Additionally, inhibiting tonic BCR signalling with R406, a SYK inhibitor, downregulated AKT-dependent phosphorylation of FOXO1, triggering the upregulation of FOXO target genes involved in cell cycle arrest and apoptosis, including *CDKN1B*, *TNFSFR10* (TRAIL) and growth arrest and DNA-damage-inducible protein 45-alpha (*GADD45A*) (408). Expression of FOXO1(A3) promoted cell cycle arrest and apoptosis, while knockdown (KD) of FOXO1 conferred resistance to SYK inhibitor R406 (408). This study indicates that the inhibition of FOXO1 transcriptional activity by tonic BCR signalling is required for SYK and AKT to promote survival of DLBCL disease.

In precursor B-cell acute lymphoblastic leukaemia (ALL), inhibition of pre-BCR^{+} ALL cells with PRT318, a SYK inhibitor, caused downregulation of FOXO1 phosphorylation, increased total FOXO1 levels, and accompanied by FOXO1 nuclear accumulation and increased expression of FOXO1 targets, including p27^{Kip1} and BLNK proteins (409). Expression of FOXO1(A3) reduced cell proliferation, accompanied by the upregulation of p27^{Kip1} and BLNK

and the reduction of MYC protein expression, indicating that FOXO1 inactivation through constitutive activation of pre-BCR signalling contributes to the oncogenesis of pre-B ALL (409). In multiple myeloma (MM), abrogating AKT signalling activity promoted cell cycle arrest and apoptosis through the activation of FOXO1 and glycogen synthase kinase 3 (GSK3) (410). Furthermore, abrogating AKT signalling activity sensitised MM cells to BH3-mimetics, achieved through FOXO1- and GSK3-mediated downregulation of MCL1 (410). Inhibition of AKT kinase activity in FOXO1-deficient cells had no effect on cell apoptosis induced by AKT inhibition (410). Similarly, pharmacological inhibition of FOXO1 activity with AS1842856 rescued MM cell lines from apoptosis induced by AKT kinase inhibition (410). This study indicates that the activity of FOXO1 is required to induce cell cycle arrest and apoptosis through the inhibition of the AKT pathway and that FOXO1 functions as a tumour suppressor in MM cells.

Contrary to FOXO1 tumour suppressive role in tonic BCR signalling-dependent DLBCL, FOXO1 mutations were reported in approximately 8.6% of DLBCL cases, with 46.2% of recurrent mutations affecting the N-terminal region and diminishing the FOXO1 T24 phosphorylation site (405). This mutation prevented the binding of FOXO1 to the 14-3-3 protein, promoting FOXO1 nuclear localisation (405). However, FOXO1 nuclear accumulation was associated with a poor prognosis in these patients (405). Similarly, in Burkitt lymphoma (BL), FOXO1 mutation blocked AKT-mediation of FOXO1 T24 phosphorylation, locking FOXO1 in the nucleus (406). This mutation promoted proliferation and survival, while FOXO1 depletion impaired tumour growth, indicating that mutated nuclear FOXO1 is a tumour promotor in BL (406). In CLL, several studies have demonstrated a tumour suppressive role for FOXO1 (193, 411, 412). In proliferating CLL cells, the gene levels of *FOXO1*, *PTEN* and *CDKN1B* ($p27^{Kip1}$) were low (411). Subcellular localisation analysis revealed that FOXO1 was predominantly resided in the nucleus in quiescent CLL cells, while in the cytoplasm in the proliferative CLL cells (411). Proliferation of CLL cells required the overexpression of miR-22, which suppressed the expression of PTEN, subsequently enhancing the activation of PI3K/AKT signalling pathway, and inhibiting FOXO1 transcriptional activity (411). This inactivation of FOXO1 was associated with downregulation of FOXO target gene *CDKN1B* (411). Ticchioni, Essafi (193) demonstrated that CLL survival was associated with inactivation of FOXO3a by the PI3K/AKT pathway, which was activated by homeostatic chemokines including CXCL12, CCL21, CCL19 and CXCL13. The expression of FOXO3A(A3) promoted cell apoptosis in CLL (193). We

demonstrated that FOXO1 is overexpressed in CLL cells within LN biopsies of poor prognostic patients, PB-CLL cells, and mouse-derived CLL-like cells (412). However, FOXO1 was predominantly localised in the cytoplasm and inactive (412). AZD8055 treatment, a dual mTOR inhibitor, inhibited mTORC2/AKT-dependent phosphorylation of $FOXO1^{T24}$, promoting FOXO1 nuclear localisation and activity (412). Additionally, the CLL tumour load in mice was reduced by AZD8055, potentially driven by FOXO1 nuclear accumulation and subsequent activity (412). Interestingly, FOXO1 has been reported to induce the activity of Grb2-associated binder 1 (*GAB1*) and its accumulation outside immune niches in CLL cells (413). The accumulation of *GAB1* helps maintain the survival of CLL cells through sustained tonic BCR signalling and subsequent maintenance of basal AKT phosphorylation (413). This study suggests that sustaining low levels of FOXO1 activity promotes the accumulation of *GAB1*, subsequently inducing tonic BCR signalling and sustaining CLL cell survival in PB (413). Conversely, strong inhibition of the BCR-mediated activation of the PI3K/AKT pathway leads to FOXO1 activation and subsequent cell apoptosis (413). These studies suggest that FOXO proteins have a dual-faceted function, acting as either tumour suppressors or promoters in a tissue- and context-dependent manner. Additionally, somatic point mutations of FOXO1 have been reported in BL, follicular lymphoma (FL), and DLBCL, with a frequency of 11%, 6% and 5%, respectively (414). in CLL, FOXO1 mutations are even less frequent, occurring in approximately 2% of cases (414). Therefore, the transcriptional activity of FOXO1, mediated by the inactivation of the PI3K/AKT pathway, potentially possesses a suppressive role in CLL cells.

1.1.8 The ubiquitin-proteasome system (UPS)

Ubiquitination is a versatile post-translational modification that regulates proteolytic and non-proteolytic processes, including proteasomal/lysosomal degradation, protein activity, interaction, localisation, and quality control (415, 416). Furthermore, ubiquitination regulates vital cellular functions, including the cell cycle, apoptosis, differentiation, gene expression, DNA repair, and signal transduction (416). With a high rate of protein turnover, approximately 30% of newly synthesised proteins are rapidly degraded with a half-life of less than 10 minutes (min) (417). UPS plays a crucial role in regulating protein function and stability (417). The UPS pathway has been implicated in the pathogenesis of many diseases, including cancer (417). Additionally, the UPS regulates several signalling pathways involved

in CLL pathogenesis including NF-κB (418), PI3K/AKT/mTOR (419), MYC (420), and NOTCH (421).

The UPS consists of the 26S proteasome, a large protein complex that acts as a regulator of protein levels by breaking down damaged, misfolded proteins and ubiquitinated proteins tagged for degradation (422). The 26S proteasome consists of a 20S core particle capped by two 19S regulatory particles on each end (Figure 1.7). The ligation of a mono- or poly-ubiquitin chain to a protein is achieved through the covalent attachment of a highly conserved 76 amino acid protein called ubiquitin, to a substrate/protein (422). This attachment of ubiquitin requires the sequential activation of three distinct enzymes: ubiquitin-activating enzymes (E1), ubiquitin-conjugating enzymes (E2), and ubiquitin-ligating enzymes (E3) (Figure 1.7). The process begins with E1 creating a thioester bond

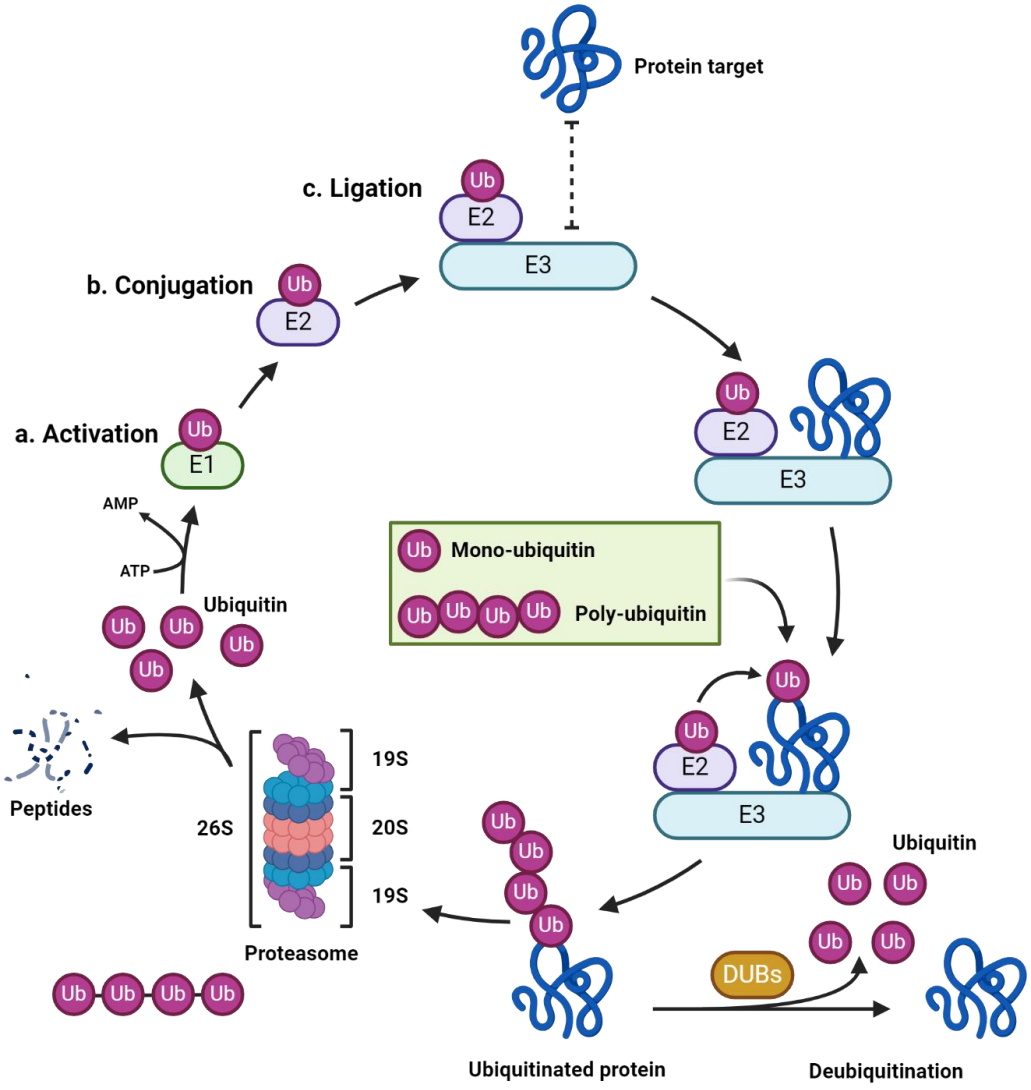

Figure 1.7: Overview of the ubiquitin-proteasomal system (UPS) (modified from (423)). E1, ubiquitin-activating enzymes; E2, ubiquitin-conjugating enzymes; E3 ligase; ATP, adenosine triphosphate; AMP, adenosine monophosphate; DUBs, Deubiquitinases; Ub, ubiquitin.

between the carboxy-terminal glycine residue of ubiquitin and the active site cysteine of E1, which requires ATP (422). The ubiquitin is then transferred to the carrier protein E2, forming a stronger thioester bond (422). Lastly, a substrate-specific E3 ligase transfers ubiquitin to a lysine residue on the target protein, forming mono- or poly-ubiquitin chains with different lengths, topologies, and functional outcomes (422, 424). The fate of most ubiquitinated proteins is proteasomal degradation, which is triggered by polyubiquitin chains including Lys6 (K6), K11, K27, K29, K33, K48, and K63 (425). However, not all polyubiquitinated proteins are tagged for proteasomal degradation. For instance, K63 ubiquitination is involved in regulating signal transduction, protein kinase activation, DNA repair, and vesicle trafficking (426, 427). In contrast to polyubiquitination, monoubiquitination does not always trigger protein degradation, instead, it contributes to the regulation of protein function, including determining protein subcellular localisation and protein-protein interactions (427, 428). Mono- or poly-ubiquitinated proteins are then transported to the multimeric 26S proteasome complex, which shreds the protein into oligopeptides and releases the ubiquitin for recycling by the UPS (429). Of note, ubiquitination of a protein can be influenced by phosphorylation, which can lead to polyubiquitination of a protein and subsequently proteasomal degradation (430). Additionally, the activation of E3 ligases can be triggered through phosphorylation of E3 ligases, signalling for their activation (430). Dysfunction of UPS has been implicated in the pathogenesis of many diseases, including MM, neuroblastoma, cervical cancer, liver cancer, breast cancer, and prostate cancer (431-433), indicating that inhibition of the UPS could be a therapeutic strategy for these diseases. Inhibition of the UPS pathway activity can be targeted at the proteasomal level and the ubiquitination E3 ligases levels (434). For instance, bortezomib, an inhibitor of 20S proteasome, has been approved for the treatment of MM and mantle cell Lymphoma (MCL) (434, 435), demonstrating the validity of targeting the UPS in cancer therapies.

On the other hand, the reversal of protein ubiquitination is regulated by DUB enzymes, cleaving C-terminus isopeptide bond of ubiquitin (422) (Figure 1.7), protecting proteins from degradation and preventing ubiquitin-mediated protein activation or subcellular localisation (436). DUB proteins consist of approximately 100 DUB family members encoded by the human genome (434). The DUB family of proteins consists of two groups: cystine-based or metalloprotease DUBs (436). The cystine-based DUBs consist of six families, including ubiquitin-specific proteases (USPs), ovarian tumour proteases (OUTs), ubiquitin

carboxy-terminal hydrolases (UCHs), the Machado-Joseph disease proteases (MJDs), the motif interacting with ubiquitin-containing novel DUB family (MINDY), and ZUP1, while the metalloprotease DUBs consist solely of the zinc-dependent JAB1/MPN/MOV34 metalloproteases (JAMMs) family (436). DUB proteins are highly selective and specific to individual proteins or structural motifs (434). The structure of DUBs is characterised by a key domain, the ubiquitin-binding domain (UBD) (422). This domain consists of a ubiquitin-specific zinc finger protease domain (ZnF-UBP), a ubiquitin-interacting motif (UIM), and a ubiquitin-associated domain (UBA) (430). It has been suggested that the selectivity and specificity of DUBs targeting individual proteins/structural motifs are defined by the ZNF-UBP domains (422, 434). Therefore, the main function of DUBs is to regulate ubiquitination by balancing conjugation and deconjugation of substrates, subsequently regulating protein abundance and cellular pathways.

1.1.8.1 DUB proteins in the hallmarks of cancer

DUBs have been implicated in the six hallmarks of cancer (sustaining proliferative signalling, evading growth suppressors, resisting cell death, enabling replicative immortality, and activating invasion and metastasis) (162), with multifaceted functions that can be associated with either cancer-promotion or cancer-suppression, depending on the context and tumour type (425). The regulation of DUB proteins on their specific target proteins can occur directly or indirectly (425). Direct regulation involves the direct binding and deubiquitination of the proteins, while indirect regulation occurs through the regulation of a substrate which causes an imbalance in ubiquitinated proteins, potentially affecting various ubiquitinated proteins rather than a single specific target (425). These methods of DUB regulation can lead to the stabilisation of the target protein by removing degradative ubiquitin signals or altering the target conformation, interactions and activity in the case of non-degradative ubiquitin signals (425). In cancer, it has been suggested that the most common mode of DUB regulation is indirect, involving the promotion or suppression of proteins (425). For instance, USP11 indirectly downregulate the expression of the tumour suppressor protein breast cancer 2 (BRCA2) by stabilising the E3 ligase SKP2, resulting in prostate cancer cell proliferation (437). Additionally, DUBs can influence translation and transcription through the dysregulation of epigenetic mechanisms or the transcriptional activation of oncogenes (425, 438). While mutations in DUB proteins are relatively rare,

many cancers exhibit dysregulated expression of DUBs mRNA and protein levels, which have been associated with disease progression (439, 440). This suggests that dysregulated expression of DUBs may provide a survival advantage for cancer cells through their post-translational modification of proteins.

DUBs have been reported to sustain proliferative signalling in leukaemic cells including chronic myelogenous leukaemia (CML) and AML (441, 442). The chromosomal translocation of the Philadelphia (Ph) chromosome (9 and 22) produces the BCR-ABL fusion gene, a key feature of CML (443). While the ABL kinase can exhibit both suppressive and promotive function in cell proliferation and survival depending on its subcellular localisation and the context signals, the BCR-ABL fusion protein is primarily localised in the cytoplasm and exhibits constitutive tyrosine kinase activation, leading to the activation of several oncogenic pathways including PI3K/AKT pathway, promoting cell proliferation and survival of CML (444). Overexpression of USP7 resulted in the upregulation of BCR-ABL protein but not its mRNA, while USP7 KD increased K48-linked polyubiquitination of BCR-ABL and subsequently proteasomal degradation (441). Of note, ubiquitin-specific protease 9, x-linked (USP9x) was suggested to act as a DUB of BCR-ABL by cleaving K63-linked polyubiquitination, leading to formation of BCR-ABL aggresomes but not degradation, and subsequently inactivation of its oncogenic activity (441). P5091, a USP7-selective inhibitor, activate poly(ADP-ribose) polymerase (PARP) and caspase-3 cleavage, inducing CML cell apoptosis (441). The expression of checkpoint kinase 1 (CHK1) in AML is associated with high clonogenic ability, short OS and relapse (445). CHK1 functions as a checkpoint response in cell cycle progression and DNA damage response (446). The expression of USP7 was reported to be enriched in AML patients and was associated with relapse and resistance to therapy (442). The USP7 inhibitor (P22077) reduced the cell viability and proliferation of AML cells *in vitro* and *in vivo*, without affecting normal haematopoietic cell survival, independently of p53 mutational status (442). USP7 co-immunoprecipitated with CHK1 protein, and the USP7-CHK1 interaction stabilised CHK1 protein through the deubiquitination of K48-linked polyubiquitination, leading to impaired survival (442). Additionally, inhibition of USP7 resulted in the downregulation of CHK1 protein without affecting its subcellular localisation (442). Schauer, Liu (447) demonstrated that XL177A, an irreversible inhibitor of USP7, inhibited the growth of many cancer cell lines primarily through a p53-dependent mechanism. XL177A treatment of MCF7 cells, that express wild-type *TP53*, led to a rapid degradation of the E3 ligase human double minute 2 (HDM2),

followed by upregulation of p53 and $p21^{Waf1/Cip1}$ proteins (447). The upregulation of p53 stimulated the transcription cell cycle arrest genes *CDKN1A* and *GADD45A*, as well as the apoptosis-related genes *BAX* and damage specific DNA binding protein 2 (*DDB2*) (447). The high expression of USP14 was associated with abnormal proliferation in breast cancer (448). This abnormal proliferation was driven by USP14-CDK1 interaction, which stabilised CDK1 by cleaving K48-linked ubiquitination (448). *USP14* KD was associated with the downregulation of CDK1 levels and caused cell cycle arrest at G2/M phase (448). In contrast, overexpression of USP14 was associated with increased levels of CDK1 (448). The MYC family are important oncogenic proteins involved in the regulation of cell growth and proliferation (449). This family consists of three members: cMYC, lung-specific MYC (l-MYC), and neuroblastoma MYC (N-MYC), which are often found to be upregulated in human cancer (449). Interestingly, both cMYC and N-MYC are substrates of USP7, where overexpression of USP7 promotes the stability of cMYC and N-MYC (449). In contrast, inhibition of USP7 with P5091 blocked tumour development through the downregulation of N-MYC expression in neuroblastoma (449). Additionally, USP9x depletion was reported to destabilise the expression of the cMYC protein, resulting in the downregulation of cMYC levels (450). Similarly, depletion of USP14 was associated with decreased protein expression levels of cyclin D1 and cMYC in oesophageal squamous cell carcinoma (451). Collectively, these studies indicate that DUBs are involved in regulating proliferation in cancer through the stabilisation of oncogenic proteins, while inhibition of DUBs activity blocks proliferation and induces cells death.

Activation of the PI3K signalling pathway is often associated with cancer. (178). DUB proteins can regulate the PI3K signalling pathway by suppressing PTEN, enhancing the activity of the PI3K signalling pathway (363). In prostate cancer, the expression of USP7 was upregulated and associated with PTEN, predominantly residing in the cytoplasm (363). This cytoplasmic localisation of PTEN was mediated by the interaction of USP7 with PTEN, resulting in the removal of monoubiquitination, a key regulator of PTEN nuclear access. This study suggested that cytoplasmic PTEN lacked full tumour suppressive function, and nuclear PTEN is essential for PTEN to exert its full tumour suppressive activity (363). The mTOR signalling pathway is often highly activated in tumour cells, leading to tumour progression, metastasis, and invasion (452, 453). This pathway is positively regulated through growth factors such as insulin-like growth factor-1 (IGF-1) and its cognate receptor IGF-1R, human epidermal growth factor receptor (HER) family and their associated ligands,

and vascular endothelial growth factor receptors (VEGFRs) and their associated ligands, which transmit signals to the mTOR pathway through the PI3K/AKT signalling axis (454). Conversely, the mTOR pathway is negatively regulated through PTEN, which inhibits the PI3K/AKT signalling pathway, blocking the transmission of growth factor signalling to mTOR (454). mTOR consists of two complexes: the mammalian target of rapamycin complex 1 (mTORC1) and mTORC2 (453). mTORC1 is composed of mTOR, regulatory associated protein of target of rapamycin (RAPTOR), mammalian lethal scid syndrome 8 (mLST8), and proline-rich AKT substrate 40 (PRAS40), while mTORC2 is composed of mTOR, RICTOR, stress-induced phosphoprotein 1 (SIN1), and mLST8 (454). Additionally, mTORC1 is more sensitive to rapamycin and is responsible for protein translation and cell growth, while mTORC2 is less sensitive to rapamycin and is responsible for the full activation of AKT, promoting cell proliferation and survival (454). The activity of the mTOR pathway has been reported to be regulated by ubiquitination, through the stabilisation of mTORC2 expression from proteolytic degradation as well as the modulation of its activity through non-proteolytic ubiquitination (455). Wrobel, Siddiqi (455) demonstrated that USP9x KD in human cervical cancer (HeLa) cells, human neuroblastoma (SH-SY5Y) cells, human liver cancer (HepG2) cells, and human embryonic kidney 293 (HEK293FT) cells downregulated the phosphorylation levels of mTORC2 target proteins, including AKT^{S473}, FOXO3a and PKCα. Notably, USP9x-depletion only downregulated the levels of RICTOR from the mTORC2 components without affecting the mTORC1 component RAPTOR. Furthermore, in USP9x-depleted cells, stimulating the mTOR pathway with growth factors, including serum and insulin had no effect on the expression levels of phosphorylated AKT^{S473}, indicating that USP9x is required to modulate the activity of mTORC2 (455). The impact of USP9x-depletion on RICTOR was observed through increased total ubiquitination and K63-linked polyubiquitination of RICTOR, suggesting that USP9x-mediated deubiquitination of RICTOR in these cells has a non-proteolytic function with respect to mTORC2 activity (455). Additionally, the downregulation of K63-linked polyubiquitination of RICTOR mediated by USP9x-depletion altered the component interactions of the mTORC1 and mTORC2 complexes, reducing the interaction between mTOR and RICTOR while increasing the interaction between mTOR and RAPTOR (455). Conversely, overexpression of USP9x downregulated the ubiquitination of RICTOR, which subsequently upregulated the phosphorylation of AKT^{S473} through RICTOR activation and upregulated the interaction between RICTOR and mTOR (455), suggesting that USP9x-mediated deubiquitination of

RICTOR promoted mTORC2 assembly. Furthermore, inhibition of IGFR-1 or serum starving resulted in the downregulation of USP9x expression (455), indicating that USP9x expression is regulated by growth factors. This was confirmed with addition of serum upregulating the expression of *USP9x* mRNA levels, and upregulation of both USP9x and RICTOR proteins (455). Collectively, these studies indicate that DUBs positively enhance the activation of the PI3K/AKT signalling pathway by inhibition of PTEN or enhancing mTORC2 activation.

DUBs have been implicated in replicative immortality, evasion of growth suppression, immune evasion, angiogenesis, cellular energetics, and invasion and metastasis, as recently reviewed by Dewson, Eichhorn (425). These areas are beyond the scope of this thesis.

1.1.8.2 DUB inhibitors in B-cell malignancies

The approval of bortezomib for the treatment of MM and MCL highlighted the importance of the UPS as a target for B-cell malignancies (434). Considering the roles of DUBs in the UPS pathway and their involvement in the hallmarks of cancer (425), there has been growing interest in exploiting DUBs as therapeutic targets. Despite the lack of successful clinical trials for DUB inhibitors, numerous pre-clinical studies have been published with promising indications for potential therapeutic success (Table 1.7). Currently, both pan-DUBs inhibitors and specific/selective inhibitors of individual DUB proteins have been

Deubiquitinase protein	Compound name	Clinical stage	Cancer models targeted studies
USP1	• SJB3-019A	Pre-clinical	B-ALL (456), MM (457)
USP2	• ML364	Pre-clinical	MCL (458)
USP7	• HBX19818 • P5091 • Compound 4 • XL188 • FT671 • FT827	Pre-clinical Pre-clinical Pre-clinical Pre-clinical Pre-clinical Pre-clinical	CLL (459, 460), B-cell leukaemia mouse models and MM (461, 462), leukaemia (463)
USP9x	• WP1130	Pre-clinical	MM (464), MCL (465)
USP14	• b-AP15 • VLX1570	Pre-clinical Phase 1 (terminated)	MM (466, 467), DLBCL (468), MCL (469)

Table 1.7: Small-molecule inhibitors of the DUB proteins in B-cell malignancies (modified from (423, 470, 471)).

B-ALL, B-cell acute lymphoblastic leukaemia; MM, multiple myeloma; MCL, mantle cell lymphoma; CLL, chronic lymphocytic leukaemia; DLBCL, diffuse large B-cell lymphoma.

identified (472), with many inhibitors demonstrating efficacy in inducing apoptosis in B-cell malignancies (Table 1.7). However, the development of DUB inhibitors is still in its early stages, and further research is required to improve their safety, specificity and efficacy. This section is focused on specific/selective DUB inhibitors and their effects on B-cell malignancies USP1 is reported to play an oncogenic role in regulating various cellular processes including DNA repair, cell proliferation, differentiation, and apoptosis (456). USP1 was upregulated in BM-derived B-ALL patients and was associated with progression of B-ALL through the upregulation of ID1 expression and activity (456). Overexpression of ID1, an oncogenic protein essential for proliferation, migration and stem cell renewal, was linked to poor outcomes (456). This upregulation of inhibitor of differentiation 1 (ID1) was associated with increased activation of PI3K/AKT signalling pathway (456). USP1 KD or inhibition with SJB-019A, a specific inhibitor of USP1, downregulated the expression of ID1 and subsequently the phosphorylation of AKT, leading to the repression of cell proliferation and induction of cell apoptosis in B-ALL cells (456). USP1 was also upregulated in MM and associated with worse OS. SJB3-019A induced caspase dependent apoptosis of MM cells, induced cell cycle arrest at the G1 phase, and overcame bortezomib resistance (457). Similarly, USP1 KD downregulated MM cell viability (457). Furthermore, SJB3-019A blocked ID1 signalling, leading to the downregulation of NOTCH1 and NOTCH2 proteins, which are associated with MM stem cell renewal and survival (457). These studies demonstrate that USP1 plays a pathogenic role in these B-cell malignancies, an effect that can be blocked by the SJB3-019A inhibitor.

MDM2 is a RING-finger type E3 ubiquitin ligase that can destabilise p53 expression and activity through proteasomal degradation, halting p53 pro-apoptotic and tumour suppressive functions (473). In MCL, USP2 has been associated with the stabilisation of oncogenic proteins, including MDM2 and cyclin D1 (458). ML364, a specific USP2 inhibitor, destabilised the expression of cyclin D1 through increasing its proteasomal degradation, leading to cell cycle arrest in Mino and HCT116 cell lines (458). Additionally, ML364 downregulated homologous recombination-mediated DNA repair (HRR) (458). This study demonstrated that USP2 is a tumour promoter through its stabilisation of cyclin D1, indicating that it is a potential therapeutic target in B-cell malignancies.

The pathogenesis of CLL disease is highlighted by genomic aberrations, particularly the del(11q) and del(17p), which are the sites of the DNA repair genes *ATM* and *TP53*,

respectively (459). DDR genes manage DNA repair and apoptosis, and the loss of these genes drives tumour progression by allowing mutations and chromosomal modifications to persist and accumulate, elevating genomic instability and resistance to conventional and targeted CLL therapies (459). DNA damage response pathway (DDR) proteins are post-translationally modified by ubiquitination/deubiquitination (474). In CLL cells, *in vitro* treatment with HBX19818, an irreversible USP7 inhibitor, demonstrated selective inhibition of USP7, which resulted in a reduction in the viability of primary CLL cells, regardless of their quiescent or proliferative status (459). This reduction in the viability of CLL cells was independent of ATM/p53-defective status, and sensitised ATM/p53-defective CLL cells to chemotherapy (459). *In vivo* treatment of CLL murine models with HBX19818 or USP7 KD led to a reduction in tumour load, observed through the reduction in splenic weight (459). Interestingly, overexpression of USP7 in CLL cells was independent of ATM/p53-defective status and was associated with the stabilisation of RAD18, an E3 ubiquitin ligase involved in promoting post-replication repair (459). RAD18 helps in the relocation of proteins necessary for Homologous Recombination Repair (HRR) to the site of DNA damage (459). HRR-dependent double-strand break (DSB) repair was downregulated by HBX19818 or USP7 depletion (459). Another study by Carrà, Panuzzo (460) demonstrated that USP7 mRNA and protein levels were upregulated in primary CLL patient samples. P5091, a USP7-selective inhibitor, induced cell apoptosis, and inhibited the cell cycle of both *TP53*-mutated MEC1 and *TP53* wild-type EHEB cells, suggesting that the tumour-suppressive effect of P5091 is independent of *TP53* mutation in CLL cells (460). Interestingly, the combination of P5091 and idelalisib synergistically inhibited cell proliferation and induced cell apoptosis in CLL cell lines, suggesting a role for USP7 in regulating the PI3K/AKT pathway (460). Of note, USP7 mediated PTEN nuclear exclusion through the cleavage of endogenous ubiquitination of PTEN, with P5091 treatment of MEC1 cells leading to the restoration of PTEN endogenous ubiquitination levels and subsequent promotion of PTEN nuclear localisation and activity (460). He, Wang (461) demonstrated that USP7 expression was upregulated in MM and was associated with poor prognosis and survival of MM cells. Inhibition of USP7 with P5091 induced cell apoptosis (461), and overcome bortezomib resistance in MM cells (462). Collectively, these studies identify USP7 as a tumour promotor in CLL and MM. Targeting USP7 with its selective inhibitors, in combination with BCR inhibitors enhance the induction of cell apoptosis and cell cycle arrest.

The expression of USP9x was upregulated in MM and was associated with a shorter PFS (464). USP9x stabilised MCL1, an antiapoptotic protein, preventing its proteasomal degradation in MM (464). Treatment of primary tumour cells from newly diagnosed or drug-refractory myeloma patients with WP1130, a partial selective USP9x inhibitor, promoted MCL1 downregulation and cell apoptosis (464). Additionally, USP9x KD resulted in the induction of cell apoptosis (464). Pham, Tamayo (465) demonstrated that WP1130 treatment of typical and blastoid-variant MCL cells resulted in the inhibition of cell growth and the induction of apoptosis. Furthermore, WP1130 treatment inhibited NF-κB activity in MCL (465). The combination of WP1130 with bortezomib synergistically enhanced the inhibition of NF-κB, concurrently downregulating the protein and mRNA levels of NF-κB target genes cMYC and cyclin D1, as well as downregulating BCL-2 protein expression while upregulating BAX protein expression (465). These studies indicate that USP9x is a potential tumour promoter in B-cell malignancies.

USP14 was reported to be highly expressed in MM compared to B-cells from healthy donors (467). b-AP15 is a selective inhibitor of the enzymatic activity of USP14, without inhibiting proteasome activity (467). Treatment of primary MM cells and cell lines with b-AP15 reduced cell viability and proliferation, even in co-culture with BM stroma cells, and overcame bortezomib resistance (467). b-AP15 mediated growth arrest and cell apoptosis of MM cells were associated with the downregulation of cyclin B1 and the activation of intrinsic and extrinsic apoptotic signalling pathways, including caspase-8, -9, and subsequently caspase-3 (467). *In vivo* studies using MM mouse models demonstrated that treatment with b-AP15 inhibited tumour progression and prolonged their survival (467). Additionally, b-AP15 has been reported to induce cell apoptosis in DLBCL and MCL cells (468, 469). Wang, Mazurkiewicz (466) showed that USP14 KD resulted in the reduction in cell viability of MM cells. Furthermore, *in vivo* studies treating mouse models of MM with VLX1570, an analogue of b-AP15 with higher potency and improved solubility, showed extended survival with treatment of USP14 inhibitor (466). The promising potential of the USP14 inhibitor VLX1570 in pre-clinical studies led to the first clinical trial of DUB inhibitors in B-cell malignancies (475). The phase 1 single-arm trial investigated the safety, tolerability, and efficacy of VLX1570 in combination with low-dose dexamethasone, an anti-inflammatory treatment, in patients with relapsed or R/R MM (475). Patients were treated with escalating doses of VLX1570 ranging from 0.05 to 1.2 mg/kg in a 28-day cycle (on days 1, 2, 8, 9, 15, and 16) (475). The anti-tumour effect of VLX1570 was observed at doses equal

to or greater than 0.6 mg/kg (475). However, at a dose of 1.2 mg/kg, two patients experienced severe progressive respiratory insufficiency associated with diffuse pulmonary infiltrates, culminating in their death (475). The severe lung toxicity led to the discontinuation of the trial (NCT02372240).

1.1.8.3 The role of DUBs in regulating FOXO transcription factors

FOXO family members are post-translationally modified by ubiquitination and deubiquitination (415, 416), resulting in proteasomal degradation, subcellular localisation, and inactivation (332, 333). BCR-mediated activation of the PI3K/AKT/mTORC2 axis leads to the phosphorylation of FOXO1 and its association with 14-3-3 protein (336). This association results in the cytoplasmic sequestration of FOXO1 and subsequent proteasomal degradation, potentially mediated by the E3 ligase SKP2 through K48-linked polyubiquitination (355, 360). In addition to its proteolytic function, the UPS pathway is also involved in non-proteolytic ubiquitination, including K63-linked polyubiquitination and monoubiquitination (425). In CLL cells, DUB enzymes, particularly USP7, play a crucial role in oncogenesis through the inactivation of two key tumour suppressors: PTEN and p53 proteins (460). Several studies have shown that USP7 interacts with FOXO family members, including FOXO1 (476, 477), FOXO3a and FOXO4 (360). Hall, Tabata (477) demonstrated that monoubiquitination of FOXO1 promoted its transcriptional activity, while the removal of monoubiquitin from FOXO1 by USP7 reduced FOXO1 occupancy on the promoter sites of its target genes. Interestingly, the expression and localisation of FOXO1 were not impacted by the overexpression or USP7 KD (477). However, overexpression of USP7 suppressed the expression of FOXO targets involved in cell cycle inhibition, including $p27^{Kip1}$ and p130 (360, 376). Similarly, monoubiquitination of FOXO4 upregulated its transcriptional activity, and USP7 KD resulted in FOXO4 nuclear accumulation and activation (360), suggesting that USP7 is involved in the suppression of FOXO activity. Gao, Zhu (478) demonstrated through proteome analysis of USP7 KD melanoma cell lines that PI3K/AKT pathway and FOXO are targets of USP7 deubiquitination activity. Furthermore, knockout of USP7 in B16 melanoma cell lines resulted in the downregulation of AKT phosphorylation, suggesting that USP7 may indirectly mediate its suppression of FOXOs through the enhancement of PI3K/AKT signalling activity (478). USP9x can also regulate the PI3K/AKT signalling pathway in neural progenitors and myoblasts (455, 479, 480). USP9x depletion reduced mTORC1 assembly

and activity, while restoring RICTOR expression levels in USP9x-depleted cells led to increased phosphorylation of mTORC2 targets, including AKT and FOXO3a (479). In B-cells, BCR-dependent upregulation and activation of PKCβ, a leukaemogenic protein upstream activator of IKK and NF-κB (481), required USP9x enzymatic activity (482). USP9x knockout in B-cells resulted in a delay in ERK1/2 activation, which was associated with a reduction in PKCβ (482). In T cells, the activation of ZAP-70, required multiple phosphorylation events as well as the removal of monoubiquitin by USP9x, enhancing ZAP-70 catalytic activity (482). Taken together, these studies suggest that USP9x may indirectly affect the transcriptional activity of FOXOs through modulating proteins involved downstream of the BCR signalling pathway.

1.2 Project aims

Despite the accumulated knowledge about FOXO1 post-translational modification through phosphorylation and its subsequent inactivation through nuclear exclusion, the role deubiquitination/DUB proteins in regulating FOXO1 expression, subcellular localisation, and transcriptional activity upon dependent-BCR activation has not yet been explored in CLL. Additionally, the potential role of DUB enzymes in modulating the PI3K/AKT signalling pathway remains poorly understood in CLL cells. Therefore, this thesis aims were to:

I. Profile the expression levels of FOXO family members and DUB enzymes in primary CLL cells and examine their regulation via BCR signalling pathway.
II. Address DUB protein modulation of FOXO1 expression, subcellular localisation, and transcriptional activity in CLL cells via BCR signalling pathway.
III. Explore novel FOXO1 interactors and examine their role in modulating FOXO1 activity.

Chapter 2. Materials and Methods

2.1 Product Supplies and addresses

The suppliers' information and addresses of the materials and reagents used in this project are listed (Table 2.1). Of note, the general supplies of plastic ware used were purchased from Greiner Bio-One Ltd or Fisher Scientific UK, unless otherwise specified.

Company	Distributor	Address
Abcam	Abcam Plc	Cambridge, CB2 0AX, UK
Active Motif	Active Motif, Inc.	Waterloo Atrium Drève Richelle 167 – boîte 4 BE-1410 Waterloo, Belgium
BD Biosciences	BD Biosciences	Berkshire, RG41 5TS, UK
Bioline	Bioline Reagents Ltd.	London, NW2 6EW, UK
Cell Signalling Technology	Cell Signaling Technology, Inc.	London, WC1H 9BB, UK
Eppendorf	Eppendorf UK Ltd.	Stevenage, SG1 2FP, UK
Fisher Scientific Whatman plc	Fisher Scientific UK Ltd.	LE11 5RG, Loughborough, UK
GraphPad Prism (v9.4.1)	GraphPad Software Inc	2365 Northside Dr #560, San Diego, CA 92108, United States
Greiner Bio-One	Greiner Bio-One Ltd.	Gloucestershire, GL10 3SX, UK
Gibco Invitrogen	ThermoFisher Scientific – UK	Renfrew, PA4 9RF, UK
Hawksley	Hawksley & Sons Ltd.	Sussex, BN15 8TN, UK
Labtech	Labtech Ltd.	East Sussex, TN21 8DB, UK
Li-Cor Odyssey Fc	Li-Cor Biotechnology UK Ltd.	Cambridge, CB4 0WS, UK
Miltenyi Biotec	Miltenyi Biotec Ltd.	Surrey, GU24 9DR, UK
QIAGEN	QIAGEN Ltd.	Manchester, M13 0BH, UK
Sartorius	Sartorius UK Ltd.	Epsom, KT19 9QQ, UK
Scientific Laboratory Supplies	Scientific Laboratory Supplies Ltd.	Nottingham, NG11 7EP, UK
Selleckchem	Stratech Scientific Ltd.	Ely, CB7 4EX, UK
Sigma-Aldrich	Merck Life Sciences UK Limited	Glasgow, G20 0XA, Scotland
STEMCELL Technologies	STEMCELL Technologies UK Ltd.	Cambridge, CB25 9TL, UK
ZEISS Axio Observer	Carl Zeiss NTS Ltd.	Cambridge, CB23 6DW

Table 2.1: Suppliers and distributors addresses.

2.2 Cell tissue culture

All cell culture work were carried out using sterile technique in a class II microbiological safety cabinet. The cells were incubated in humidified incubator at 37 °C and 5% of carbon dioxide (CO_2).

2.2.1 Primary CLL cells

PB was collected from patients with confirmed diagnosis of CLL that were treatment-naïve or had received treatment but not in the preceding 3 months, and after informed consent. The usage of primary CLL cells were approved by the West of Scotland Research Ethics Service, NHS Greater Glasgow and Clyde (UK) and all work was conducted in alignment with approved guidelines (REC Ref: 20/WS/0066) (483). Further approval was obtained with project number 2021-003 from the Cell Bank Approval Committee of Paul O'Gorman Leukaemia Research Centre, The University of Glasgow. A database of anonymised patient samples contained linked clinical information including treatment status, patient gender, clinical stage (Binet), and the presence and type of cytogenetic abnormality identified by FISH, where available. A list of the patient samples used in this project is listed in Table 2.2.

Primary CLL Sample	Gender	Binet Stage*	Treatment	FISH
CLL8	F	A	UT	del(11q)
CLL9	F	A	T	-
CLL57	M	C	UT	-
CLL78	M	-	T	del(17p)
CLL93	M	C	T	del(17p)
CLL102	F	C	T	del(11q)
CLL109	M	B	-	del(17p)
CLL116	M	A	UT	Normal
CLL122	M	-	T	del(17p)
CLL132	F	B	UT	del(17p)
CLL138	F	A	T	-
CLL140	F	C	UT	T12
CLL151	M	B	UT	del(11q)
CLL162	M	-	-	-
CLL163	M	-	-	-
CLL168	M	B	UT	T12 / del(13q)
CLL169	F	C	UT	del(11q)
CLL170	F	-	T	-
CLL171	M	C	UT	-
CLL172	M	-	-	Normal
CLL173	M	B	T	del(11q)
CLL175	M	C	T	-
CLL176	M	A	UT	-
CLL177	M	B	UT	-
CLL179	M	B	T	-
CLL180	F	B	T	-
CLL184	M	-	T	-
CLL185	M	C	-	-
CLL186	M	C	UT	-
CLL187	M	B	UT	-
CLL189	M	B	T	-
CLL190	M	C	UT	-
CLL191	M	A	UT	del(11q) / del(17p)
CLL193	F	A	UT	-
CLL194	M	C	UT	-
CLL195	M	C	UT	No del(11q) / del(17p) / p53 mut
CLL196	F	B	UT	-
CLL198	M	-	T	-
CLL200	M	C	-	-

Table 2.2: List of patients CLL sample characteristics.

M = Male, F = Female, POS = positive, NEG = Negative, T = Treated, UT = Untreated, - = not determines. Normal = no cytogenetic abnormality detected by FISH. * Staging chronic lymphocytic leukaemia with Binet: Stage A = mild, B = intermediate, C = advanced.

2.2.1.1 Enrichment of CLL cells from PB

The isolation of CLL cells from whole blood was performed according to the Hay, Moles (484) protocol. Briefly, we routinely receive consented CLL patient cells from the clinic in ethylenediamine tetra-acetic acid (EDTA) blood collection tubes, accompanied by the white cell count (WCC). The purification method was proceeded for PB-CLL samples depending on the WCC.

CLL blood samples with WCC < 40 x 10^6 cell/mL required an extra step call the RosetteSep step, where the CLL blood samples were incubated at room temperature (RT) for 20 min in 50 µL of RosetteSep Human B-cell Enrichment Cocktail (STEMCELL Technologies) per 1 mL blood.

If the WCC ≥ 40 x 10^6/mL, the RosetteSep step was skipped and the CLL blood samples were diluted 1:1 at RT with CLL wash buffer (phosphate-buffered saline (PBS), 0.5% Fetal bovine serum (FBS), 2 mM ethylenediamine tetraacetic acid (EDTA)) in a 50 mL Falcon tube. The diluted blood was then carefully layered onto density separation medium Histopaque®-1077 Hybri-MaxTM (Sigma) at RT. For instance, a 30 mL of diluted blood sample is layered into 10 mL of Histopaque in 50 mL tube, or 4 mL of Histopaque for a sample of 10 mL into 15 mL tube. The layered samples were carefully centrifuged at RT for 30 min at 400x*g* with no brake. Slowly and carefully the white buffy layer was harvested into a fresh 50 mL conical centrifuge tube by utilising a Pasteur pipette and wash twice in 40 mL of CLL wash buffer by RT centrifugation for 10 min at 300x*g*. The cells were then counted using trypan blue as describe in (Section 2.2.1.2). The purity of isolated CLL cells were assessed by flow cytometry as described by our group publication (484). If the cells were needed immediately for an experiment after CLL isolation, they were seeded at a concentration of 10 x 10^6 cell/ml in Roswell Park Memorial Institute 1640 (RPMI) (Gibco, ThermoFisher Scientific) supplemented with 2 mM L-glutamine (1% L-glutamine), 50 U/mL penicillin and 50 µg/mL streptomycin (1% Pen/ Strep), and FBS, heat inactivated (10% FBS) (Gibco, ThermoFisher Scientific) referred to as 'complete RPMI'. This complete RPMI medium was used to incubate the cells into T25 or T75 flasks for at least 4 hours (hr) before setting up the experiment. If the cells were not immediately required for experimentation, they were cryopreserved in the cell bank as describe in (Section 2.2.1.3). Additionally, CLL cell pellets were gathered at this stage for protein (40 x 10^6) and RNA (20 x 10^6) samples, representative of *ex-vivo* PB-CLL samples.

2.2.1.2 Cell counting using Trypan Blue

An aliquot of the cell suspension was diluted as required in PBS and transferred into an Eppendorf and further diluted by 1:1 in 1X pre-filtered trypan blue solution (0.4%) (Gibco, ThermoFisher Scientific). The cell counting was performed by using a haemocytometer counting chamber (Hawksley) by pipetting 10 µL diluted cells under the coverslip and viewed by a compound microscope (Nikon) at 40X magnification. The following formula was used to determine cell counts:

$$\frac{Cell}{mL} = \left(\frac{Cell\ Count}{Number\ of\ Chambers}\right) \times Dilution\ Factor \times 10^4$$

Viable cells were determined by the colour, with live cells remaining white due to intact membrane excluding trypan blue, while dead cells stained blue. By counting the cells in the four corner squares (including cells touching the left and top corners and excluding the right and bottom corners of the large squares) the cell count was obtained.

2.2.1.3 Cryopreservation of primary CLL cells

Isolated CLL cells (Section 2.2.1.1) were cryopreserved by resuspending the cell pellet in CLL 'freezing media' (90% FBS, 10% dimethylsulphoxide (DMSO)), and 1 mL cells at a density of (5-10 x 10^7/mL) was transferred to 2 mL cryovials. The cryovials were frozen slowly at 1 °C/min by placing them in Mr. Frosty freezing container filled with 250 mL isopropanol. The container was then transferred to -80 °C freezer. Subsequently, cryovials were transferred to liquid N_2 tanks for long-term storage.

2.2.1.4 Thawing cryopreserved primary CLL cells

Cryovials of cells were removed from liquid (Nitrogen) N_2 and immediately placed into dry ice to be processed. The vial was quickly thawed for 1 min in the 37 °C water bath until the ice is almost completely melted. Inside the laminar flow hood, the thawed CLL suspension was gently transferred into a 15 mL conical tube and 10 mL DAMP solution (DNAseI 5000U, 20% Human Serum Albumin, 1M $MgCl_2$, 0.155M Trisodium citrate, PBS) was slowly added dropwise over 10 min to maximise the recovery of CLL. The cells were then centrifuged at RT for 5 min at 250x*g*, and the pellet was resuspended in complete RPMI medium and then recentrifuged. CLL cells were transferred to T25 or T75 flasks in complete RPMI medium at

a minimum concentration of 5-10 x 10^6 cells/ml and incubated in preparation for experiments in a humidified atmosphere containing 5% CO_2 at 37 °C. The recovery of CLL cells was determined the following day by performing a cell count as describe in (Section 2.2.1.2).

2.2.2 Enrichment of healthy B-cells from buffy coat samples

Buffy coat samples offer a rich source of white blood cells/leukocytes, allowing the enrichment of sizable numbers of B lymphocytes. Buffy coats were obtained from the Scottish National Blood Transfusion Service, (UK; Ref 17 ~ 10), following a fresh blood donation of healthy donors. To enrich for healthy B lymphocytes from buffy coat, we used two different approaches; positive selection of cells expressing CD20 antigen using human CD20 MicroBeads (Miltenyi) for gene expression comparison, and negative selection containing cocktail of biotin-conjugated monoclonal antibodies selecting for human leukocytes except for B-cells using human Pan B-cell Isolation (Miltenyi) for protein expression comparisons.

The process for isolating primary CLL cells with > 40 x 10^6 cells (as described in section 2.2.1.1) was followed to isolate leukocytes from buffy coat. The cells then were counted to adjust the number of cells to meet the protocol requirements, and 5 x 10^5 cells were removed as a pre-enrichment control (Figure 2.6a). The enrichment process of B lymphocytes used magnetic-activated cell sorting (MACS) separation technology following the manufacturer's instructions. Of note, all solutions were pre-cooled, and cells were kept on ice throughout the procedure. the cell suspension was pelleted by centrifugation at 300x*g* for 10 min, and the supernatant was removed. 'MACS wash' buffer was prepared containing (pH 7.2 PBS, 0.5% bovine serum albumin (BSA) (Sigma), 2 mM EDTA).

CD20 MicroBeads magnetic labelling for positive selection was performed by resuspending the pellet in 80 µL of buffer per 10^7 total cells, followed by the addition of 20 µL of CD20 MicroBeads per 10^7 total cells. Following Magnetic labelling, the cells were incubated for 15 min on ice. After the incubation, the cells were washed by adding 1 mL of buffer per 10^7 total cells. followed by 10 min of centrifugation at 300x*g*. The supernatant was completely removed, and the pallet was resuspended in 500 µL of buffer per 10^8 total cells.

Pan B-cell Isolation magnetic labelling for negative selection was employed by resuspending the pellet in 40 µL of buffer per 10^7 total cells, followed by the addition of 10 µL of Pan B-cell biotin-antibody cocktail per 10^7 total cells. Following Magnetic labelling, the cells were incubated for 5 min on ice. After the incubation, 30 µL of buffer per 10^7 total cells was added, followed by the addition of 20 µL of anti-Biotin Microbeads per 10^7 total cells and an additional 10 min incubation on ice. Following the second incubation, the volume was adjusted to a minimum of 500 µL of buffer.

Magnetic separation was performed using 'LS' MACS columns. Up to 1 x 10^9 cells were resuspended in 3 mL MACS wash buffer and transferred onto the LS columns, which were then placed in magnetic field of suitable MACS separator. For enriched B lymphocytes, the plunged cells in the positively selected samples were collected, whereas the flow-through was collected in the negatively selected samples. To ensure efficiency of the procedures, flow-through from positive selection or flushed cells from the negative selection were also collected (Figure 2.6b & c). Following B-cell enrichment, the cells were immediately seeded into T25 or T75 flasks for at least 4 hr at a concentration of 10 x 10^6/mL in complete RPMI, followed by plating the cells at a concentration of 1-2 x $10x^6$/condition for Annexin V/7-AAD apoptosis assay. Additionally, purified B lymphocytes pellets were gathered at this stage for protein (2-5 x 10^6) and RNA (2-5 x 10^6) samples, employed to compare the expression of healthy vs CLL cells. The samples were analysed by flow cytometry (Section 2.6.2).

2.2.3 Cell lines.

The guidelines of Leibniz Institute DSMZ (Deutsche Sammlung von Mikroorganismen und Zellkulturen) were employed to passage and optimise cell culture conditions for cell lines (Table 2.3). Cells that reached 20 passages were replaced with fresh vial of cells, which were frozen in an early passage.

Cell line	Description	Cell culture	Source/References
MEC1 (Suspension cells)	Generated in 1993 from PB of a 61-year-old man with CLL. Expressing CD24, CD23, CD27, CD38 and CXCR4, which are expressed in progressive CLL cells. MEC1 cells are known to retain non-favourable characteristics with the presence of del(p17) and *TP53* mutation.	Cells were maintained in complete DMEM media at 37 °C in a humidified atmosphere containing 5% CO_2; maintained at 0.5–2 x10^6 cell/mL; split at ratio of 1:3 every 3 days, with doubling time of 40 hr.	A kind gift from Prof. Joseph Slupsky, University of Liverpool, UK (485-487)
HG-3 (Suspension cells)	Generated in 1998 from 70-year-old man with CLL Rai Stage II. It is a lymphoblastoid cell line with B1 cell characteristics, derived from *IGHV1-2* unmutated CLL patient clone, characterised by the presence of del(13q) which resemble favourable prognostic factor in CLL.	Cells were maintained in complete RPMI media at 37 °C in a humidified atmosphere containing 5% CO_2; maintained at 0.5–1 x10^6; passage at a ratio of 1:3 every 3 days, with doubling time of 50-60 hr.	A kind gift from Dr Mark Catherwood, Queen's University Belfast, UK (488, 489)
HEK293T (293T) (Adherent cells)	Selected for their high transfection efficiency, derived from embryonal human kidney 293 cell.	Cells were maintained in complete DMEM media at 37 °C in a humidified atmosphere containing 5% CO_2; maintained at 70% cell confluence; split at a ratio 1:5 every 3 days by trypsinisation (Section 2.2.3.2), with doubling time of 24-30 hr.	(490)

Table 2.3: Cell line information.

2.2.3.1 Cell line culture media and maintenance

The cell culture media contained supplements to sustain the survival and growth of CLL cell lines (MEC1 and HG-3) and adherent cells HEK293T. MEC1 and HEK293T cell lines were cultured in Dulbecco's Modified Eagle Medium (DMEM), (Gibco, ThermoFisher Scientific)

supplemented with 2 mM L-glutamine (1% L-glutamine), 50 U/mL penicillin and 50 µg/mL streptomycin (1% Pen/ Strep), and Fetal Bovine Serum, heat inactivated (10% FBS), (Gibco, ThermoFisher Scientific). The HG-3 cell line were cultured in complete RPMI medium. Of note, cell culture media containing supplements is referred in this project as 'complete DMEM' or 'complete RPMI' cell culture media. Unless otherwise stated.

MEC1 cells were passaged every 3 days in fresh complete DMEM medium, maintaining a concentration of 0.5-2 x 10^6 cell/mL. Similarly, HG-3 cells were passaged in fresh complete RPMI medium every 3 days, maintaining a cell density of 0.5-1 x 10^6 cell/mL. Adherent HEK293T cells were passaged in fresh RPMI medium when they reached a confluency greater than 80%. If these cell lines were required for experiments, they were passaged overnight to ensure that the suspension cells were at their maximum growth rate and adherent cells were at their optimal confluency (80%).

2.2.3.2 Trypsinisation of adherent cell lines

To detached confluent HEK293T cells from the T75 flasks, first the media was completely removed as it deactivates trypsin. The cells were then washed with 10 mL PBS before 3 mL pre-warm trypsin-EDTA (0.25%), phenol red (Gibco, ThermoFisher Scientific) was added to the cells and incubated for 2 mins at 37 °C. The flask was gently tapping to detach the remaining adherent cells and checked under the microscope to ensure 90% detachment of cells. Following trypsin treatment, an equivalent volume of complete DMEM was added before RT centrifugation at 300x*g* for 5 min. A second wash with complete DMEM was applied before seeding the cells at the appropriate concentration in a plate/flask.

2.2.3.3 Stock maintenance and cryopreservation of cell lines

Maintenance of the cell lines was achieved by expanding a master stock, creating multiple early passaged stocks at a concentration of 2-5 x 10^6 cells/cryovial. Prior to cryopreservation, cell lines were passaged to ensure that the suspension cells were at their maximum growth rate and the adherent cells were at their optimal confluency. Importantly, the cells were examined for cell viability via trypan blue prior to freezing stocks to guarantee healthy stock of cells. The cryopreservation procedure of cell lines followed the same method as primary CLL cells (Section 2.2.1.3).

To thaw fresh stocks of cell lines, vials were removed from liquid N_2 and immediately thawed in 37 °C water bath as described for primary CLL cells (Section 2.2.1.4). Slowly, 10 mL pre-warmed complete DMEM/RPMI medium was added to the cells, then the cells were centrifuged at 300x*g* for 5 min at RT. The previous step was repeated twice to guarantee the removal of freezing buffer. The cells then were transferred into appropriate flask and maintained with accordance to the DSMZ guidelines (Table 2.3).

2.2.4 Inhibitor treatments and cell stimulations

2.2.4.1 Inhibitors

As this project focused on the BCR signalling pathway, more specifically PI3K/AKT signalling pathway regulation of FOXO1 protein, ibrutinib (IBR; BTK inhibitor) a first line therapy for CLL patient was used either alone or in combination with a number of DUB inhibitors including selective USP7 inhibitors (P5091, HBX19818), and less selective DUB inhibitors (PR-619, WP1130). Further details of individual inhibitors proprieties are described below:

Ibrutinib (formerly known as PCI-32765) is a potent, irreversible inhibitor that covalently binds to BTK at cysteine 481 binding site, blocking BCR downstream signalling which is critical for CLL cell survival and proliferation (262). It was approved by the FDA in 2014 and was initially administrated for R/R CLL patients, and it is now widely used as first line therapy for patients with del(17p) (263, 491).

P5091 exhibits potent, selective, and specific deubiquitylating activity inhibiting USP7. The inhibition of USP7, leads to HDM2/MDM2 degradation and upregulation of p53 and $p21^{Waf1/Cip1}$ levels (not dependent on p53 status) in a time- and dose-dependent manner (460). The IC_{50} was 8.2 µM for USP7 in MEC1 cells (460). P5091 is shown to inhibit USP7 without blocking proteasome activity in cells, leading to overcoming the resistance of conventional therapies such as dexamethasone, doxorubicin as well as bortezomib in MM (462).

HBX19818 is a selective USP7 inhibitor covalently binds to cysteine 223 in USP7 active site, leading to inactivation of USP7 (492). HBX19818 inhibition of USP7 resulted in destabilisation of MDM2 by increasing its polyubiquitination, leading to a strong induction of functional activation of p53 (492).

PR-619 is a reversible, non-selective inhibitor of the DUB family (493). This inhibitor is a cell permeable pyridinamine class with a broad spectrum of targets including USP 2, 4, 5, 7, 8, 9X, 10, 14, 15, 16, 19 ,20, 22, 28, 47, 48 (493). PR-619 is reported to increase polyubiquitination of proteins in a dose and time-dependent manner and a half maximal effective concentration (EC_{50}) of 6.86 µM for USP7 (493).

WP1130 is a partially selective DUB inhibitor able to directly inhibit USP9x, USP5 and USP14 activities, and has been reported to rapidly induce the accumulation of polyubiquitinated K48 and K63 linked proteins without effecting 20S proteasome activity (494).

The inhibitors (purchased from Selleckchem, Stratech Scientific Ltd), were dissolved in DMSO as instructed by the manufacturer. Aliquoted inhibitors were stored at -80 °C for a maximum of 2 years. Of note, the inhibitors were freshly prepared, and the concentration was adjusted to obtain the appropriate working concentration by diluting the aliquoted inhibitors in complete RPMI/DMEM medium (Table 2.4). An adjusted concentration of DMSO was also included as a vehicle control or no drug control (NDC) for drug treatment.

Inhibitor	Stock Concentration	M.Wt*	Diluent	Working Concentration for primary CLL cells+	Working concentration for CLL cell lines+
Ibrutinib	10 mM	440.5	DMSO	1 µM	1 µM
P5091	10 mM	348.22	DMSO	2 µM	10 µM
HBX19818	10 mM	421.96	DMSO	8 µM	10 µM
PR-619	50 mM	223.28	DMSO	2 µM	3 µM
WP1130	10 mM	384.27	DMSO	1 µM	2 µM

Table 2.4: Information about inhibitor preparation.
*Molecular Weight. + Treatment concentration of inhibitors used in the experiments, unless otherwise stated.

2.2.4.2 BCR stimulation with αIgM F(ab')$_2$ Fragments

Soluble αIgM F(ab')$_2$ fragments (Stratech Scientific Ltd) were used at a concentration of 10 µg/mL to continuously stimulate BCR by mimicking soluble antigen exposure of primary CLL cells for series of durations ranging from 30 min to 48 hr, incubated at 37 °C. Primary CLL cells (0.7-1 x 10^7/condition) were incubated in 1 mL of complete RPMI medium, pre-treating

with drug inhibitors (Ibrutinib, PR-619, P5091, or WP1130) or DMSO/vehicle control for 30 min prior to BCR stimulation with $F(ab')_2$ or left unstimulated (US/control).

2.3 SDS-PAGE and Western blotting

2.3.1 Preparation of cell lysate

Following drug treatment (Table 2.4) and/or cell stimulation (Section 2.2.4.2), at a cell density of 7-10 x 10^6/condition for primary CLL cells or 1 - 2 x 10^6/condition for cell lines, the cells were transferred from tissue culture plates to 1.5 mL Eppendorf tubes to be washed twice in 1 mL of ice-cold PBS by centrifugation for 5 min at 4^o C and 300x*g*. The pellets were then resuspended in 30 – 50 µL of cell lysis buffer (20 mM Tris (pH 7.4), 2 mM EDTA, 1% Triton, 1 mM dithiothreitol (DTT)), accompanied with 1:10 dilution of stock of protease inhibitor (tablet/1 mL) and phosphatase inhibitor (tablet/1 mL) (Roche). The pellet then was mixed by vortexing the tubes for 30 seconds (sec) and incubated on ice for 20 min with periodic vortexing, and a 30 sec final vortex. Following protein lysate incubation, the tubes were centrifuged at 14000x*g* for 20 min at 4 °C. The supernatants were then transferred into new tube and stored at -20 °C freezer. For the purpose of protein quantification, a 5 µL was taken from each lysate and transferred into 0.5 mL Eppendorf tubes, to minimise freeze thaw cycle.

2.3.2 Protein quantification

The concentration of protein lysates was determined using bicinchoninic acid assay (BCA) protein assay kit (Pierce, ThermoFisher Scientific), following the manufacturer instructions for microplate procedure. The absorbance was read using Spectramax M5 plate reader (MDS Analytical Technologies). A standard curve was generating to calculate protein concentrations using Microsoft Excel, with BSA standard curve concentration range from 125-2000 µg/mL.

2.3.3 Sodium dodecyl sulphate-polyacrylamide gel electrophoresis (SDS-PAGE)

Protein electrophoresis was performed using NuPAGE® Novex® pre-cast 4-12% Bis-Tris gels with Invitrogen Xcell SureLockTM Mini cell system and all the buffers used were purchased from Invitrogen, TheromFisher Scientific. Protein lysates were mixed in a ratio of 1:4 of 4x NuPAGE LDS sample buffer (106 mM Tris HCl, 141 mM Tris Base, 2% LDS, 10% Glycerol, 0.51 mM EDTA, 0.22 mM SERVA Blue G250, 0.175 mM Phenol Red (pH8.5)), and 1:10 10X NuPAGE reducing agent with distilled water to reach an equal final volume. The samples were denatured using a heated plate at 70 °C for 10 min, then briefly centrifuged for 5 sec. The samples were then loaded alongside a protein leader (HyperPAGE, Bioline) and protein electrophoresis ran using 120 voltages for 105 min with 1x NuPAGE MOPS running buffer (50 mM 3-(N-morpholino) propane sulfonic acid (MOPS), 50 mM Tris-Base, 305 mM SDS, 1 mM EDTA (pH7.7)) until the dye front reached the bottom of gel. Gels were then placed on 'activated' polyvinylidene difluoride (PVDF) transfer membranes, 0.45 µM (ThermoFisher Scientific), which was previously incubated in 100% methanol (Sigma) for 30 sec. 20X NuPAGE transfer buffer (25 mM bicine, 25 mM Bis-Tris, 1.0 mM EDTA, 50 µM Chlorobutanol (pH7.2)) was diluted to 1x in distilled water and 10% methanol. Protein transfer was performed using the gel/membrane sandwich method, which consisted of 1.0 mm gel blotting paper (Whatman PLC) and sponges. Invitrogen XCell IITM Blot Module was used to perform membrane transfer running at 30 voltages for 90 min.

2.3.4 Western blotting

PVDF membranes were washed for 5 min in Tris-buffered saline with 0.1% Tween ® 20 detergent (TBST) (10 mM Tris-HCl, 50 mM NaCl, 0.1% Tween 20 (pH7.4)) then blocked with 5% non-fat milk in TBST for 1 hr, unless otherwise stated. The membranes were washed four times, 5 min/wash with TBST, and were incubated overnight at 4 °C on a roller with primary antibodies (Table 2.5). Primary antibodies were prepared following manufacturer's instructions, unless otherwise stated. Following incubation, membranes were washed four times with TBST for 5 min/wash, and then incubated at RT on a roller for 1 hr with the appropriates species of horseradish peroxidase (HRP)-conjugated secondary antibodies (Cell Signalling Technology) or fluorescent secondary antibodies (Li-Cor). Secondary antibodies were prepared following the manufacturer's datasheets (Table 2.5). Following

Specificity	Species	Dilution	Dilutant	Cat.	Manufacturer
AKT	Rabbit	1:2000	5% BSA	9272	CST ®
p-AKT (Ser473)	Rabbit	1:2000	5% BSA	4060	CST ®
β-Actin*	Rabbit	1:1000	5% BSA	3700	CST ®
BIM	Rabbit	1:1000	5% BSA	2933	CST ®
cMYC	Rabbit	1:1000	5% BSA	ab32072	Abcam ®
FOXO1#	Rabbit	1:1000	5% BSA	2880	CST ®
p-FOXO1 (Thr24)	Rabbit	1:1000	5% BSA	9464	CST ®
FOXO3a	Rabbit	1:1000	5% BSA	2497	CST ®
p-FOXO3a (Thr32)	Rabbit	1:1000	5% BSA	9464	CST ®
FOXO4	Rabbit	1:1000	5% BSA	9472	CST ®
GAPDH*	Rabbit	1:1000	5% Milk	5174	CST ®
HAUSP/USP7#	Rabbit	1:1000	5% BSA	4833	CST ®
Lamin A/C*	Rabbit	1:1000	5% BSA	2032	CST ®
MCL1	Rabbit	1:1000	5% BSA	5453	CST ®
p-p44/42 MAPK (Erk1/2)	Rabbit	1:2000	5% BSA	4370	CST ®
$p21^{Waf1/Cip1}$	Rabbit	1:1000	5% BSA	2947	CST ®
$p27^{Kip1}$	Rabbit	1:1000	5% BSA	3686	CST ®
p53	Mouse	1:500	5% Milk	Sc-126	Santa Cruz ®
PTEN	Rabbit	1:1000	5% BSA	9559	CST ®
TRIM21#	Rabbit	1:1000	5% BSA	92043	CST ®
β-Tubulin*	Rabbit	1:1000	5% BSA	2128	CST ®
USP1	Rabbit	1:1000	5% BSA	8033	CST ®
USP8	Rabbit	1:1000	5% BSA	8728	CST ®
USP9x#	Rabbit	1:1000	5% Milk	14898	CST ®
USP10	Rabbit	1:1000	5% Milk	5553	CST ®
USP14	Rabbit	1:1000	5% BSA	11931	CST ®
USP18	Rabbit	1:1000	5% BSA	4813	CST ®
USP28	Rabbit	1:1000	5% BSA	4217	CST ®
ZAP-70	Mouse	1:2000	5% Milk	610239	BD Biosciences ®
Rabbit IgG control+	Rabbit	-	IP lysis buffer	Ab37415	Abcam ®
Anti-rabbit goat IgG, HRP-linked	Rabbit	1:1000	5% Milk	7074	CST ®
Anti-mouse horse IgG, HRP-linked	Mouse	1:1000	5% Milk	7076	CST ®
IRDye®680RD Goat-anti Rabbit IgG	Rabbit	1:15000	TBST	926-68071	Li-Cor ®
IRDye®800CW Goat-anti Mouse IgG	Rabbit	1:15000	TBST	827-08364	Li-Cor ®

Table 2.5: Western blot and co-immunoprecipitation (co-IP) antibodies information.
*Protein loading controls. #These antibodies used for immunoblotting and co-immunoprecipitation (co-IP). +This antibody was used in co-IP as a rabbit IgG control.

the incubation with secondary antibodies, membranes were washed in TBST four times for 5 min/wash, and immunodetection was carried out using the Immobilon® Forte Western HRP Substrate (Sigma) by Li-Cor Odyssey® which was connected to Image StudioTM Lite v5.2 software.

2.3.5 Densitometry analysis

Images generated by the Li-Cor System (Section 2.3.4) were further analysed in Image Studio™ Lite v5.2 software with densitometry carried out following the manufacturer instructions. Quantification of protein expression was performed by adjusting the background noise using the software to remove saturated pixels from analysis, then selecting the band of interest using a rectangle shape tool for quantification. The densitometry was determined by signal values (total pixel intensity for the rectangle shape minus the background and area values). Signal values of protein then normalised to signal values of loading control band as described previously (484).

2.4 FOXO1 regulation assays

2.4.1 Co-Immunoprecipitation (co-IP)

To pull down protein, immunoprecipitation Pierce Crosslink IP kit (ThermoFisher Scientific) was used according to the manufacturer's instructions. In brief, following drug treatment (Table 2.4) and/or cell stimulation (Section 2.2.4.2), at a cell density of 10-15 x 10^6/condition for primary CLL cells or 2-4 x 10^6/condition for cell lines, the cells were transferred from tissue culture plates to 1.5 mL Eppendorf tubes to be washed twice in ice-cold PBS by centrifugation for 5 min at 4 °C and 300x*g*. The mass of cell pallets was measured to determine the volume of the immunoprecipitation (IP) lysis buffer (10:1 volume/weight). Notably, we routinely obtain pallet weights of about 50 mg that require 500 mL of IP lysis buffer. The pellets were then resuspended in 500 mL ice-cold IP lysis buffer (2 × 50 mL, 0.025M Tris, 0.15M NaCl, 0.001M EDTA, 1% NP-40, 5% glycerol; pH 7.4), supplemented with 1:10 dilution of stock of protease inhibitor (tablet/1 mL) and phosphatase inhibitor (tablet/1 mL), followed by 10 min incubation on ice and periodically vortexed during incubation. Following the incubation, the cell lysates were centrifuged at 13000x*g* for 10 mins in pre-cold 4 °C centrifuge. The supernatant was transferred into a fresh 1.5 Eppendorf

tube, and 2-3% of the whole cell lysate (WCL) was transferred into a fresh 0.5 Eppendorf tube to serve as a control for WCL/condition.

To reduce the non-specific binding of proteins, the cell lysates were pre-cleared with 80 µL of agarose resin slurry for 1 hr with gentle end-over-end mixing at 4 °C. After pre-clearing, the concentration of the lysate was measured as described in (Section 2.3.2). Of note, the concentration of antibody or IgG control used in these co-IP experiments were optimised to 1 µg for a total protein centration of 500 µg/condition.

The binding of antibody to protein A/G plus agarose was incubated on a rotator at RT for 1 hr, followed by crosslinking with disuccinimidyl suberate (DSS) for 1 hr at RT. The crosslinking step was employed to minimise eluted antibodies as well as minimising the heavy and light chain in the immunoblots. The antibodies used in the co-IP experiments are listed in (Table 2.5).

The pre-cleared lysate was added to the antibody-crosslinked resin and incubated overnight with gentle end-over-end mixing. Following the overnight incubation, the supernatant of unbound proteins was removed from the resin by centrifugation for 1 min at 1000x*g*, and 2-3% was transferred into a fresh 0.5 mL Eppendorf tube to serve as a control ensuring the efficacy of the co-IP.

To elute co-IP proteins, the bound proteins were incubated with 10 µL of elution buffer (50 mL, pH 2.8, contains primary amine), and incubated at RT for 10 min before centrifugation. A second elution was performed using 30 µL of elution buffer, followed by an additional 10 mins incubation before centrifugation. The eluted proteins were neutralised with 3 µL 1M Tris (pH=9.5) and prepared for SDS-PAGE according to the manufacture protocol (Figure 2.1).

Lastly, Since the antibodies were crosslinked to the resin, the agarose beads were stored in 1x coupling buffer (25 mL, when diluted results in 0.01M sodium phosphate, 0.15M NaCl; pH 7.2) at 4 °C and reused for a maximum of three co-IP experiments.

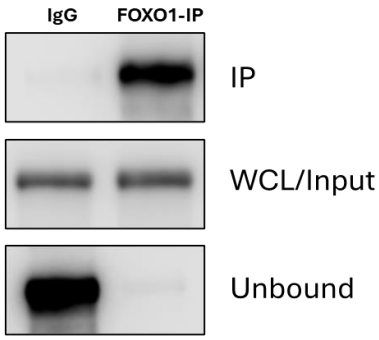

Figure 2.1: FOXO1 co-IP controls.
FOXO1 and IgG control co-immunoprecipitation (co-IP) in MEC1 cells were accompanied by blots of whole cell lysate (WCL) or Input and unbound proteins to ensure the efficacy of the co-IP.

2.4.2 Mass spectrometry

To identify specific FOXO1 interaction partners, mass spectrometry (MS) was performed on co-IP of FOXO1 from unstimulated and $F(ab')_2$-stimulated primary CLL cells. Primary CLL cells were thawed (Section 2.2.1.4) and incubated overnight in RPMI, followed by cell counting (Section 2.2.1.2) and plating at a concentration of (10-15 x 10^6/condition) for treatment. Cells were either unstimulated or stimulated with $F(ab')_2$ for 0.5 hr before harvesting and performing co-IPs (Section 2.4.1) with FOXO1 or IgG control antibodies (Table 2.5). Eluted FOXO1 co-IP and IgG control (40 µL/condition) were sent to Glasgow Polymics to perform Nanoflow HPLC Electrospray Tandem Mass Spectrometry (nLC-ESI-MS/MS) using two 6plex Tandem Mass Tag (TMT) systems (ThermoFisher Scientific).

Here is a brief description of the methodology which was used by Glasgow Polymics to process the samples for MS. Prior to starting Filter Aided Sample Preparation (FASP) step, the samples were reduced. Briefly, FASP was performed by mixing 30 µL of protein extract with 200 µL of UA (8M urea (Sigma, U5128) in 0.1M Tris/HCL pH 8.5) in a filter unit and centrifuge at 14,000x*g* for 15 min. The filter unit was washed again with 200 µL of UA and the flow-through was discarded. 100 µL IAA (0.05M iodoacetamide in UA prepare 0.1ml per sample) solution was added to the filter unit and incubated for 20 min, followed by centrifugation for 10 min. The filter unit was washed twice with 100 µL of UA and then twice with 100 µL of 50 mM of ammonium bicarbonate. 120 µL of ABC (0.05 M NH4HCO3 in water) with trypsin (ratio of 1:100) were added to the filter unit and incubate at 37°C for 4 hr or overnight. The filter unit then was transferred to new collection tubes and centrifuge, followed by washing with 50 µL of ACN (10% Acetonitrile in water) and acidification of the sample with trifluoroacetic acid (CF3COOH) before drying in a vacuum centrifuge.

The second step was peptide TMT labelling, briefly, TMT Label reagents were equilibrated to RT and dissolved in anhydrous acetonitrile. 8 µL of TMT label reagent was added to 9 µg of reduced and alkylated protein digest, ensuring that no more than 100 µg of protein is labelled per reaction. The reaction was incubated for 1 hr at RT and then quenched for 45 min with 5% hydroxylamine. labelled samples were combined at equal amount and store at -80 °C, followed by drying down 6 µg of the labelled samples on a 96-well plate for MS analysis.

The TMT-labelled samples were analysed by nLC-ESI-MS/MS, and protein identification and quantification were performed using Proteome Discoverer 2.4 (ThermoFisher Scientific) software (Figure 2.2). The Sequest search engine was used to interrogate identified protein sequences in the Swissprot database using Homo sapiens taxonomy, with a mass tolerance of 10 ppm allowed for the precursor and 0.6 Da for MS/MS matching.

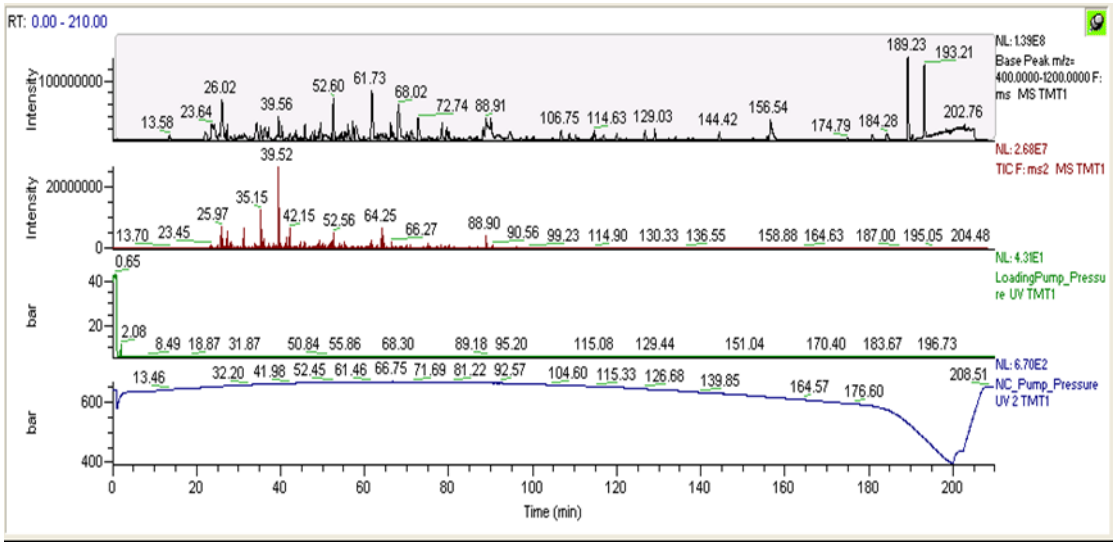

Figure 2.2: Mass spectrometry view of raw data.
The top trace in black represents the full mass spectrometry (MS) spectrum, where peptides are detected. Peptides with a minimum amino acid charge of 2+ to 4+ were considered acceptable and selected for fragmentation, while those with a single charge were considered contamination (e.g., detergents or polymers) and excluded. The second trace in red shows the signals from the fragmentation spectrum. The abundance of signals indicates a successful protein identification, while a missing signal may suggest interference from iron or contamination. The third trace in green represents the pressure of the loaded sample, with a dip at the beginning indicating an unsuccessful sample injection. The bottom trace in blue shows the pump pressure, where a deviation or jump in pressure indicates a problem with the sample separation.

2.4.3 Cellular fractionation

The translocation of FOXO1 protein was examined by subcellular fractionation to understand how cells respond to drug inhibition of BCR signalling and DUB enzymes in $F(ab')_2$ stimulated and unstimulated primary CLL cells. Following drug treatment (Table 2.4) and/or cell stimulation (Section 2.2.4.2), at a cell density of 7-10 x 10^6/condition for primary CLL cells or 1-2 x 10^6/condition for cell lines, primary CLL cells were pre-treaded for 30 min with inhibitors, followed by 30 min $F(ab')_2$ stimulation, whereas cell lines received 1 hr treatment with the inhibitors alone. The nuclear and cytoplasmic protein were generated by using Nuclear Extraction Kit (Active Motif), and WCL was obtained as a positive control.

The cellular fractionation was generated accordance to 'preparation of subcellular fractions' protocol (484). Briefly, during the treatment time of the cells, the reagents were prepared and kept on ice. The cells were mildly lysed with 50 µL of 1x hypotonic buffer for 15 min on ice, followed by the addition of 2.5 µL of detergent and vortex for 10 sec to generate the cytoplasmic fraction. The nuclear fraction was then generated by adding 50 µL of complete lysis buffer (add 0.5 µL of protease inhibitor cocktail, 5 µL of 10 mM DTT, and 2.5 µL of detergent to 42 µL of lysis buffer), and incubated for 30 on ice. To quantify the protein lysates, 5 µL lysate was transferred into 0.5 mL reaction tube to perform a BCA assay (Section 2.3.2) and prepared for running on SDS-PAGE (Section 2.3.3) or stored at -80 °C until required.

2.4.4 FOXO1 activity

FOXO1 transcription factor activity was examined using a DNA-binding ELISA 96 plate TransAM® FKHR (FOXO1) Transcription Factor ELISA Kit (Active Motif).

The TransAM protocol requires a nuclear fraction to study FOXO1 activity, therefore, cellular fractionation was followed to obtain nuclear fraction (Section 2.4.3). The protocol for FOXO1 activity kit was followed according to the manual provided by the manufacturer. In brief, the protein content of the nuclear fraction was quantified and an equal concentration of 10-15 µg of total protein was used for all samples. To monitor the specificity of the assay, controls were used including, positive control 'Raji nuclear extract', negative control 'blank', competitive binding using wild type (WT) and mutated consensus oligonucleotides as competitor for FKHR binding (Figure 2.3). The plate was incubated with 100 µL developing solution for 10 min and the reaction was stopped by adding 100 µL stop solution. The

absorbance was read at 450 nm using SpectraMax M5 microplate reader (Molecular Devices), within a maximum of 5 min of adding the stop solution. The data were analysed using Microsoft Excel and GraphPad Prism software v9.4.1.

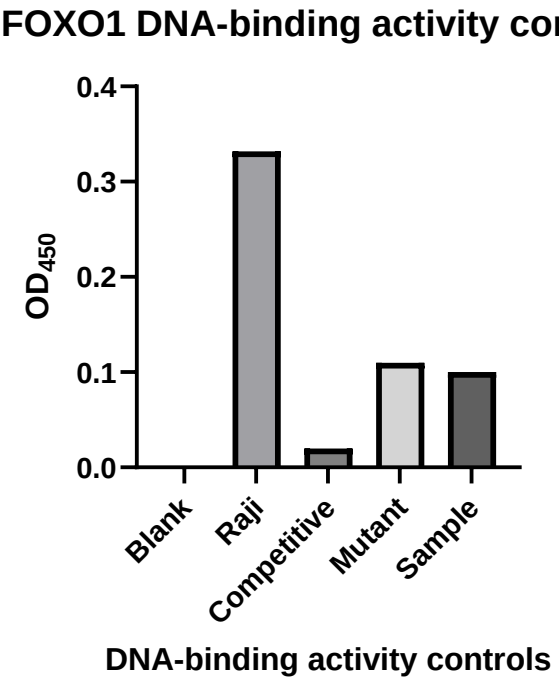

Figure 2.3: FOXO1 DNA binding activity controls.
To monitor the specificity of the assay, controls were used including, positive control 'Raji nuclear extract', negative control 'blank', competitive binding using wild type (WT) and mutated consensus oligonucleotides as competitor for FKHR binding**.** The absorbance was read at 450 nm using SpectraMax M5 microplate reader.

2.5 Quantitative PCR

2.5.1 RNA extraction

RNA was extracted from cell lines (HG3 and MEC1; 1-2 x 10^6/mL) or primary CLL samples (0.5-1 x 10^7/mL) by washing the cells in sterile ice-cooled PBS and pelleting by centrifugation for 5 min at 300x*g*. The extraction of RNA was performed using the RNA-Easy mini kit following the manufacturer instructions (QIAGEN). The concentration of RNA was determined using a NanoDrop spectrophotometer (ThermoFisher Scientific). Of note, RNA concentration measuring unit (ng/µL), and the ratios of 260/280 and 260/230 were considered to determine the quality of the extracted RNA. RNA samples were stored in -80 °C freezer.

2.5.2 Reverse transcription PCR

Following RNA extraction, cDNA synthesis was prepared with the SuperScriptTM III Reverse Transcriptase kit (Invitrogen, ThermoFisher Scientific), using 500 ng/condition of RNA in 20 µL reaction volume. The reaction of cDNA synthesis was generated using ProFlex PCR system (ThermoFisher Scientific), and the manufacturer's instructions were followed to syntheses cDNA. To monitor contamination and quality of the reaction, reverse transcriptase negative was used as control. Briefly, in a nuclease-free microcentrifuge tube the following components were mix (Table 2.6). Of note, RT-PCR grade water (ThermoFisher Scientific) was used in the reaction mix and to dilute the synthesised cDNA in a ratio of 1:50. The diluted cDNA was then stored at -20 °C until required.

Volume	Components
1 µL	Oligo $(dT)_{12-18}$
1 µL	10mM dNTP Mix
500ng	RNA
Final volume of 13 µL	RT-PCR grade water
Heat mixture to 65 °C for 5 min, then incubate on ice for 1 min.	
4 µL	5x first-strand buffer
1 µL	0.1 M DTT
1 µL	RNaseOUT Recombinant RNase Inhibitor
1 µL	SuperScript ™ III RT
Incubate at 50 °C for 60 min and then inactivate the reaction by heating at 70 °C for 15 min.	

Table 2.6: cDNA synthesis mix.
The 10 mM dNTP Mix contained (10 mM each dATP, dGTP, dCTP and dTTP at neutral pH)

2.5.3 TaqMan® Real-Time qPCR

Quantitative PCR was carried out using a TaqMan® 2X Universal PCR Master Mix (ThermoFisher Scientific). The TaqMan® Gene Expression Assay (FAM) probes detected human gene expression changes (Table 2.7). A total volume of 10 µl/reaction was prepared in a MicroAmp™ Optical 384 or 96 reaction plate (ThermoFisher Scientific), consisting of 5 µL TaqMan® 2X Universal PCR Master Mix, 0.5 µL appropriate TaqMan® Gene Expression Assay, 2 µL cDNA, 2.5 µL nuclease-free water. Each sample was assayed in triplicate, with the presence of two negative controls: nuclease-free water and negative reverse transcriptase control. Wells were sealed with MicroAmp™ Optical Adhesive Film (ThermoFisher Scientific) and centrifuged for 5 min at 300x*g*. The plates then were inserted into an Applied Biosystems 7900 Fast Real-Time PCR System thermal cycler, which was programmed to complete 40 cycles. Each cycle consisted of 50 °C for 2 min, 95 °C for 10 min, 95 °C for 15 sec, and 60 °C for 1 min. The results were analysed using Sequence Detection Systems software v 2.3 (Applied Biosystems). The cycle threshold (C_T) was calculated for reference gene and target gene. The results were calculated by $\Delta\Delta C_T$ method and generated by Microsoft Excel and GraphPad Prism software v9.4.1 (GraphPad Software, Inc.).

Gene Name	Species	Chromosome Location	Assay ID	Manufacturer
18S	Human	N/A	Hs99999901_s1	ThermoFisher Scientific ®
B2M	Human	Chr.15: 44711487 - 44718159	Hs00984230_m1	ThermoFisher Scientific ®
BBC3	Human	Chr.19: 47220822 - 47232998	Hs00248075_m1	ThermoFisher Scientific ®
BCL2L1	Human	Chr.20: 31664452 - 31723999	Hs00236329_m1	ThermoFisher Scientific ®
BCL2L11	Human	Chr.2: 111120914 - 111168445	Hs00153408_m1	ThermoFisher Scientific ®
CCND2	Human	Chr.12: 4273736 - 4305356	Hs00153380_m1	ThermoFisher Scientific ®
CCNG2	Human	Chr.4: 77157204 - 77170060	Hs00171119_m1	ThermoFisher Scientific ®
CFLAR	Human	Chr.2: 201116015 - 201172688	Hs01116280_m1	ThermoFisher Scientific ®
FOXO1	Human	Chr.13: 40555664 - 40666597	Hs01054576_m1	ThermoFisher Scientific ®
FOXO3	Human	Chr.6: 108559823 - 108684769	Hs00818121_m1	ThermoFisher Scientific ®
FOXO4	Human	Chr.X: 71096149 - 71103534	Hs00936217_g1	ThermoFisher Scientific ®
GADD45A	Human	Chr.1: 67685177 - 67688338	Hs00169255_m1	ThermoFisher Scientific ®
GAPDH	Human	Chr.12: 6534405 - 6538375	Hs99999905_m1	ThermoFisher Scientific ®
IGF1R	Human	Chr.15: 98648539 - 98964530	Hs00609566_m1	ThermoFisher Scientific ®
MCL1	Human	Chr.1: 150574551 - 150579738	Hs01050896_m1	ThermoFisher Scientific ®
MYC	Human	Chr.8: 127736069 - 127741434	Hs00153408_m1	ThermoFisher Scientific ®
SESN3	Human	Chr.11: 95165513 - 95232541	Hs00914870_m1	ThermoFisher Scientific ®
TRIM21	Human	Chr.11: 4384897 - 4393696	Hs00172616_m1	ThermoFisher Scientific ®
USP7	Human	Chr.16: 8892094 - 8963912	Hs00931763_m1	ThermoFisher Scientific ®
USP8	Human	Chr.15: 50424359 - 50501083	Hs00987105_g1	ThermoFisher Scientific ®
USP9x	Human	Chr.X: 41085420 - 41236579	Hs00245009_m1	ThermoFisher Scientific ®
USP14	Human	Chr.18: 158483 - 213739	Hs00193036_m1	ThermoFisher Scientific ®
ZAP-70	Human	Chr.2: 97712030 - 97744327	Hs00277148_m1	ThermoFisher Scientific ®

Table 2.7: TaqMan Probes for RT-qPCR.

2.5.4 Optimisation and selection of RT-qPCR housekeeping genes

Known housekeeping genes, including Glucuronidase beta (*GUSB*), TATA-box binding protein (*TBP*), Beta-2-microglobulin (*B2M*), 18S ribosomal RNA (*18S*), E74-like factor 1 (*ELF1*), and Eukaryotic initiation factor 2B subunit 1 (*EIF2B1*). were tested in primary CLL cells and cell lines MEC1 and HG-3. The C_T value was used to determine the optimum housekeeping control for our quantitative PCR analysis. The data indicated that the TaqMan primer *B2M* was the optimum housekeeping control for primary and cell lines cells (Figure 2.4).

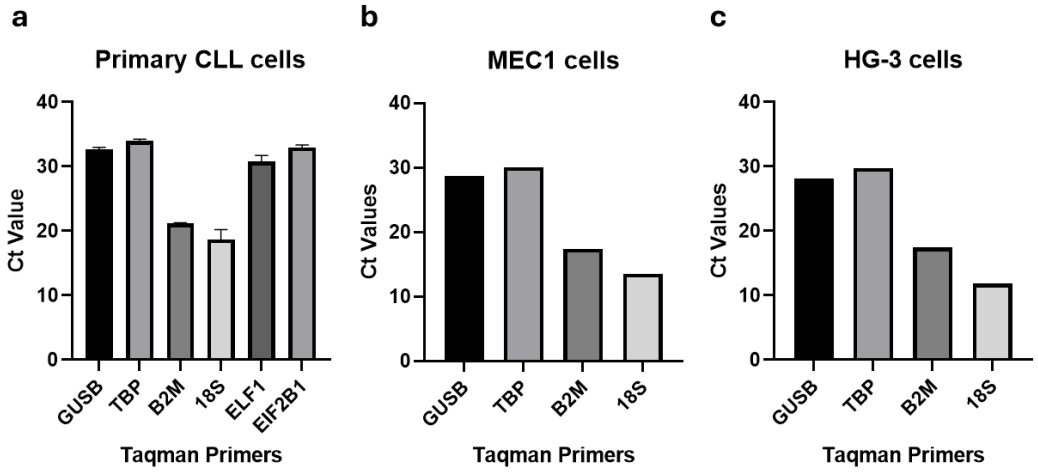

Figure 2.4: Optimisation of housekeeping genes for primary CLL cells and cell lines.
RT-qPCR to assess transcription levels of *GUSB*, *TBP*, *B2M*, *18S*, *ELF1*, and *EIF2B1*, in (a) primary CLL cells, (b) MEC1 cells, and (c) HG-3 cells. The C_T value was used to produce these figures. Data expressed as the mean with SD.

2.6 Flow Cytometry

Antibodies/flow cytometry reagents were purchased from (BD Biosciences), unless otherwise stated (Table 2.8).

Description	Reactivity	Format	Dilution Ratio*	Manufacturer
7-AAD	Human	PerCP-Cy5-5-A	1:40	BD Biosciences ®
Annexin V	Human	FITC	1:40	BD Biosciences ®
Annexin V	Human	APC	1:40	BD Biosciences ®
CD4	Human	PE	1:40	BD Biosciences ®
CD5	Human	FITC	1:40	BD Biosciences ®
CD19	Human	APC-Cy7	1:40	BD Biosciences ®
DAPI	Human	Pacific Blue	1:1000	BD Biosciences ®

Table 2.8: Antibodies for Flow Cytometry.
*The stains and antibodies were diluted in Hank's Balanced Salt Solution (1xHBSS), or PBS.

2.6.1 Cell viability staining and apoptosis analysis

The viability of cells in the presence and absence of drug treatments (Table 2.4) were assessed by flow cytometry using Annexin V and 7-amino-actinomycin D (7-AAD) staining (495). Cells (0.5-1 x 10^6 cells/condition) were harvested into round bottomed polystyrene tubes (FACS tubes) and washed once with diluted pre-cooled Hank's Balanced Salt Solution (10x HBSS; 12.6 mM $CaCl_2$, 4.9 mM $MgCl_2$, 4.1 mM $MgSO_4$, 53.3 mM KCl, 4.4 mM, KH_2PO_4, 1379 mM NaCl, 3.36 mM Na_2HPO_4-$7H_2O$, 55.6 mM Dextrose), (ThermoFisher Scientific) diluted 1:10 in distilled water) by centrifugation at 250x*g* for 5 min at 4 °C, and then discarding the supernatant. Following washing, the cell pellet was resuspended in 2.5 µL each Annexin V and 7-AAD and mixed in 95 µL HBBS and incubated in the dark at RT for 15 min to allow staining. The reaction was then quenched with 200 µL 1x HBSS in preparation for analysis. A representative FACS plot for Annexin V-FITC and 7-AAD cell staining is shown (Figure 2.5). Appropriate controls were included in all experiments: unstained cells and single colour controls of dead and live cells. Of note, dead cells controls were prepared by adding 70% ethanol to the cells, then centrifuging and discarding the supernatant, followed by performing two washes with 1x HBSS buffer. The data were generated by flow cytometry

FACSCanto II analyser (BD Biosciences), linked to a FACSDiva software (BD Biosciences). The data analysis was generated by FlowJo v10 (Tree Star, Inc.) and GraphPad Prism v9.4.1.

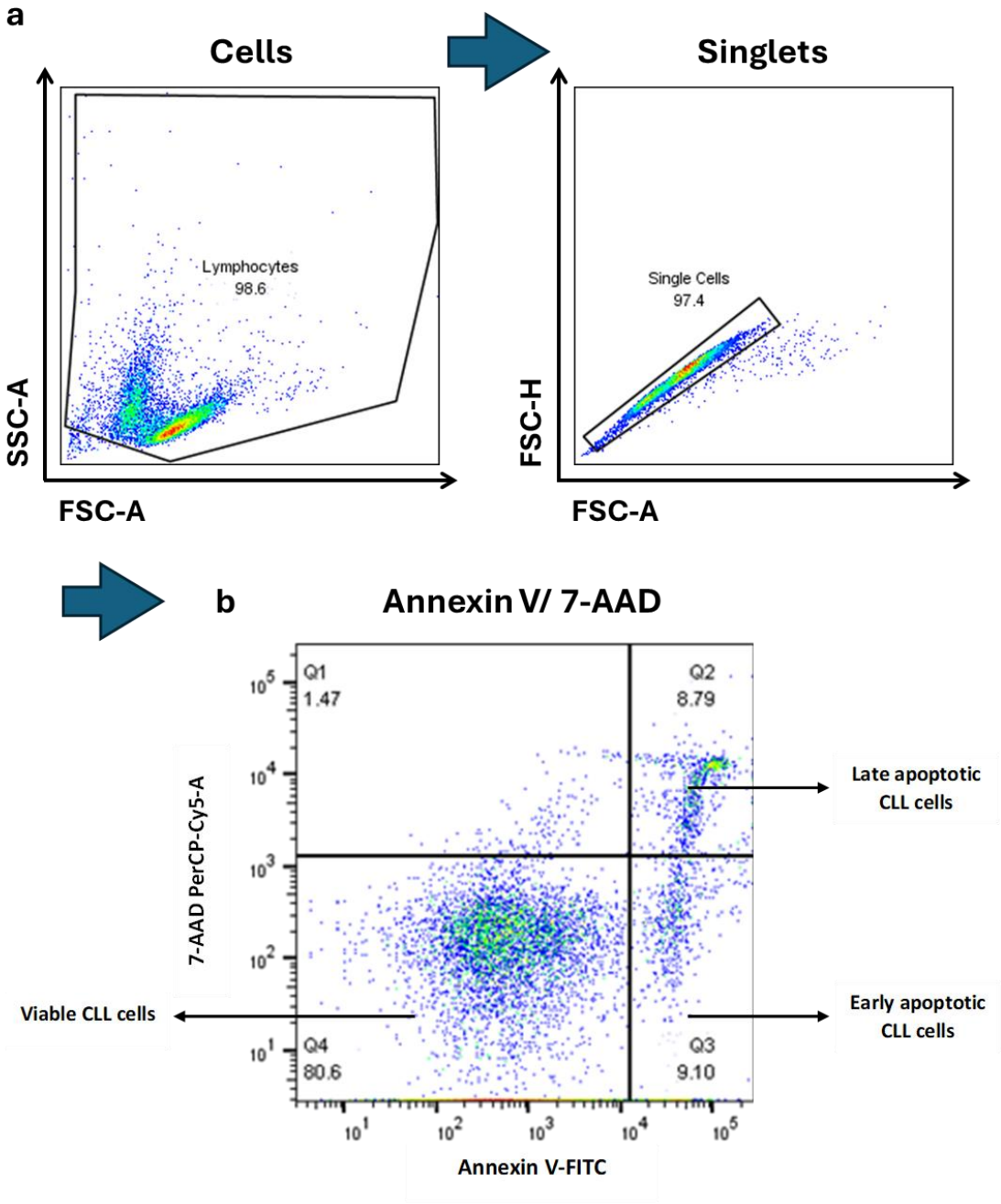

Figure 2.5: Gating strategy for cell viability and apoptosis by Annexin V/7-AAD staining. To evaluate cell viability primary CLL cells or cell lines following drug treatment, cells were stained with Annexin V/7-AAD staining to differentiate between viable and non-viable cells by flow cytometry. (a) Forward scatter (FSC) and side scatter (SSC) were employed to gate viable and non-viable cells (left panel) and selected for singlets (right panel). (b) A bivariate histogram was then selected to detect viable cells (Annexin V^-/7-AAD^-), early apoptotic (Annexin V^+/7-AAD^-) and late apoptotic cells (Annexin V^+/7-AAD^+). The percentages of the populations were observed using a quadrant gate.

2.6.2 Buffy coat purity check

Following B-cell enrichment (Section 2.2.2), 1 x 10^6/cells were transferred to a FACS tube under sterile conditions and stained with anti-CD4, anti-CD5, anti-CD19 for 15 min at 4 °C, in dark. Following staining with the antibodies, cells were washed with 1 mL 1x HBSS and centrifuged 300x*g* for 5 min at 4 °C, the cell pellet was resuspended in 200 µL PBS and kept protected from light. Unstained and single stained controls were run alongside the test samples. The percentage of $CD19^+$, $CD4^+$ and $CD5^+$ cells in samples were determined by flow cytometry. B-cell purity was > 90% as determined by flow cytometry (Figure 2.6).

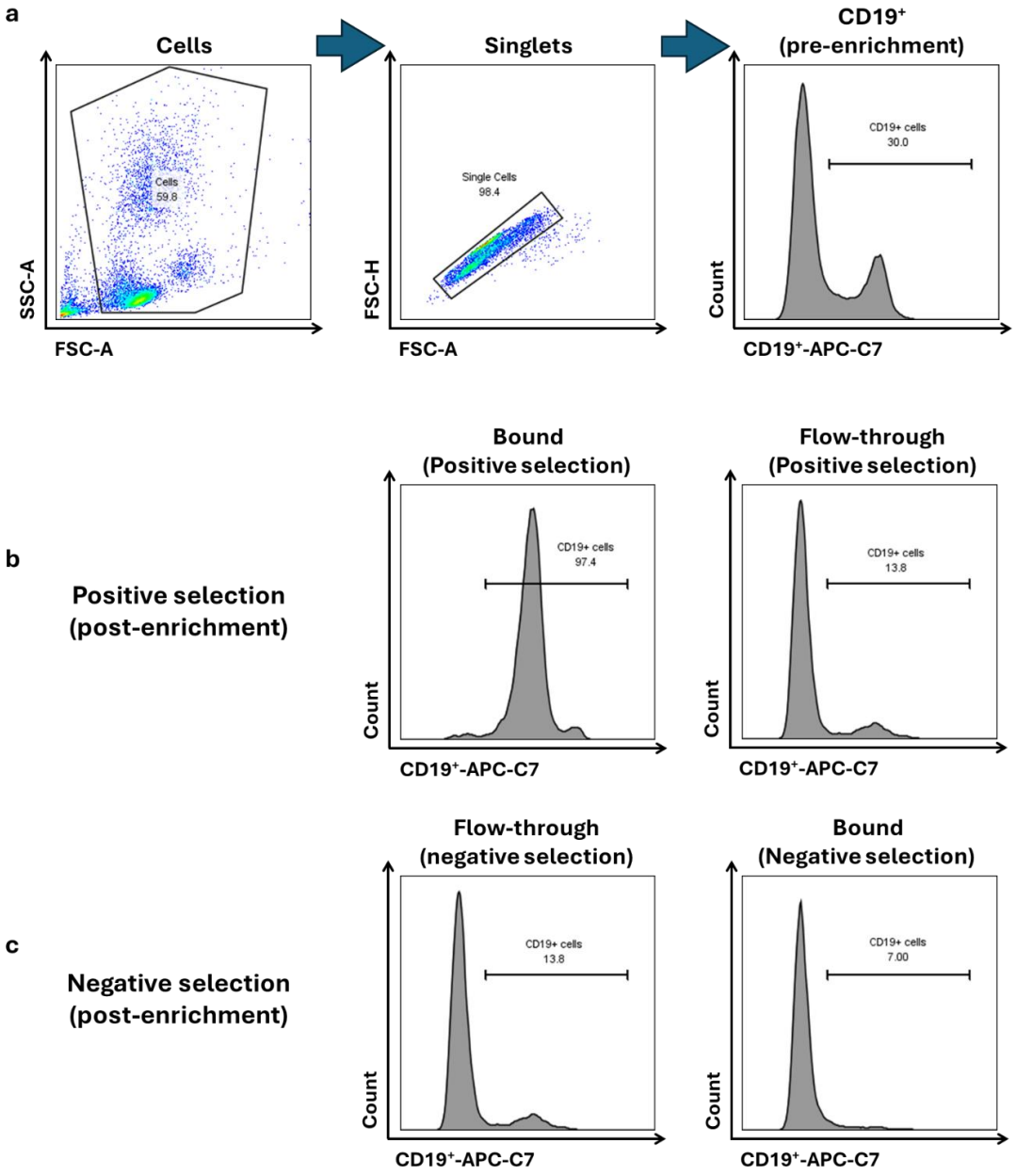

Figure 2.6: Gating strategy for isolation of buffy coat samples.
$CD19^+$ B-cells were positively or negatively selected from buffy coat samples with CD20 MicroBeads or Pan B-cell Isolation cocktail, respectively. The following gating strategy were performed to detect

$CD19^+$ B-cells isolated using CD20 MicroBeads or Pan B-cell Isolation cocktails by flow cytometry. (a) forward scatter (FSC) and side scatter (SSC) were used to gate lymphocytes (left panel), and subsequently gate for singlets (middle panel). Prior to $CD19^+$ B-cells enrichment, 0.3-0.5 x 10^6 cells were removed to assess the percentage of $CD19^+$ B-cells pre-enrichment (right panel). (b) Positive selection post-enrichment using CD20 MicroBeads, the percentage of $CD19^+$ B-cells were identified using (bound; left panel), while (flow-through; left panel) were used to ensure efficacy of positive enrichment. (c) Negative selection post-enrichment using Pan B-cell Isolation cocktails, the percentage of $CD19^+$ B-cells were identified using (flow-through; left panel), while (bound; left panel) were used to ensure efficacy of negative enrichment. The percentage of $CD19^+$ B-cells post-enrichment by positive or negative selection was typically around 90% $CD19^+$ B-cells.

2.6.3 Cell proliferation analysis by Cell trace violet (CTV)

CTV (ThermoFisher Scientific) was used to trace multiple cell divisions using a dye dilution by flow cytometry (496, 497). The MEC1 or HG-3 cells were passaged overnight and then seeded into appropriate plate at (1 x 10^6/ condition). The CTV stain was prepared by dissolved the CTV powder in DMSO as instructed by the manufacturer, followed by 1:1000 dilution ratio in pre-warmed PBS at 37 °C. Prior to CTV staining, the cells were transferred into 50 mL falcon tubes and centrifuge at 300x*g* for 5 min to remove the medium. The cell pellet was resuspended in 5 mL in the prepared CTV stain and the cells were incubated in dark at 37 °C for 20 min. Following incubation, the stained cells were centrifuge at 300x*g* for 5 min and resuspended after removing the stain in 1:5 (25 mL) of pre-warmed complete medium to quench the CTV reaction and stop cell death. The cells were incubated at RT for 5 mins, then centrifuge at 300x*g* for 5 min. After removing the complete medium, the cell pellet was resuspended in an appropriate volume of medium and seeded into plate ready for treatment. At this point, 0.5 mL of cell suspension was transferred to a FACS tube to serve as a positive control of day zero and ran on the flow cytometry machine. Of note, during the time course (24 hr, 48 hr, 72 hr) of the treatment, the cells were incubated with the drugs and 300 µL of cell suspension was used for each time point to examine cell proliferation. Additionally, viability stains including Annexin V and 7-AAD were used in the analysis (Section 2.6.1) to gate on viable cells as well as including negative and positive controls (Figure 2.7). Data were generated by FACS machine and analysed by FlowJo v10 and GraphPad Prism v9.4.1.

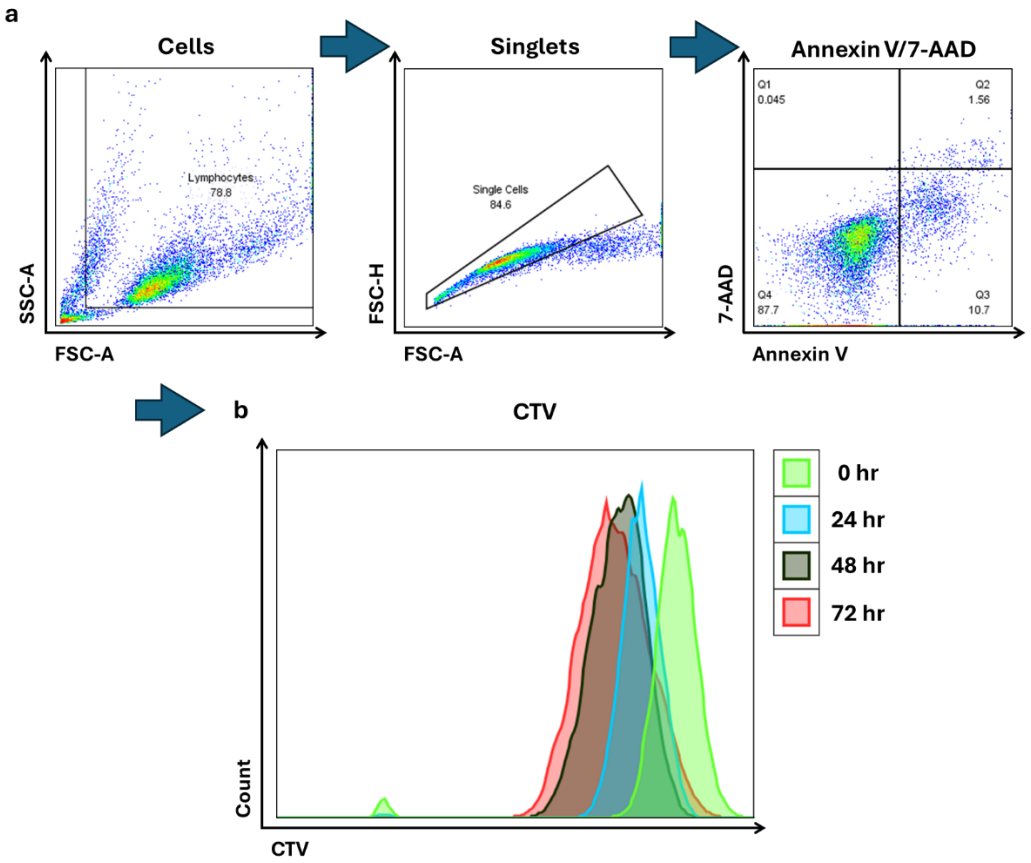

Figure 2.7: Gating strategies for CTV staining over three days.
Tracing Cell division/proliferation of MEC-1 cells upon drug treatment was assessed by celltrace violet (CTV) labelling of the cells. (a) Forward scatter (FSC) and side scatter (SSC) were used to gate cells (left panel) and select for singlets (middle panel), and Annexin V/7-AAD staining was used to select for viable cells (right panel). (b) The viable cells gated in Q4 (Annexin V^-/7-AAD^-) were used to create histogram indicative of the fluorescent intensity of CTV-labelled MEC1 cells across 4 timepoints: 0 hr (green), 24 hr (blue), 48 hr (black) and 72 hr (red).

2.6.4 Assessment of cell cycle by propidium Iodide (PI) staining

To observe the effect of drug treatment on the cell cycle of MEC1 cells, PI stain was used to quantify the DNA content at different stages of the cell cycle, including G0/G1, S, and G2/M by flow cytometry. A day prior to the experiment, MEC1 cells were passaged overnight and then seeded at a concentration of 1 x 10^6/condition for treatment (Table 2.4). Following drug treatment, the cells were collected and transferred into FACS tubes and washed twice in 1 mL of pre-cooled PBS, where each wash was followed by 4 °C centrifugation at 200x*g* for 5 mins to remove PBS. The fixation and permeabilization of the cells were performed by adding 1 mL of ice-cold 80% ethanol (Sigma) dropwise while voretexing the FACS tube, to minimise clumping and ensure thorough fixation of the cells. The cells were fixed overnight in -20 °C and can be stored for up to 2-3 weeks. To prepare the cells for staining after

fixation, the cells were washed twice by 1 mL of pre-cold PBS, then centrifuged for 5 min at 850x*g*. The cells were stained for 15 min in the dark at RT with 400 µL of PI/RNase staining buffer (BD biosciences). This stain containing RNase to remove RNA as PI stain both DNA and RNA. Following the incubation with the stain, the cell cycle assay was observed by flow cytometry (Figure 2.8). The data then were analysed using FlowJo v10 and GraphPad Prism.

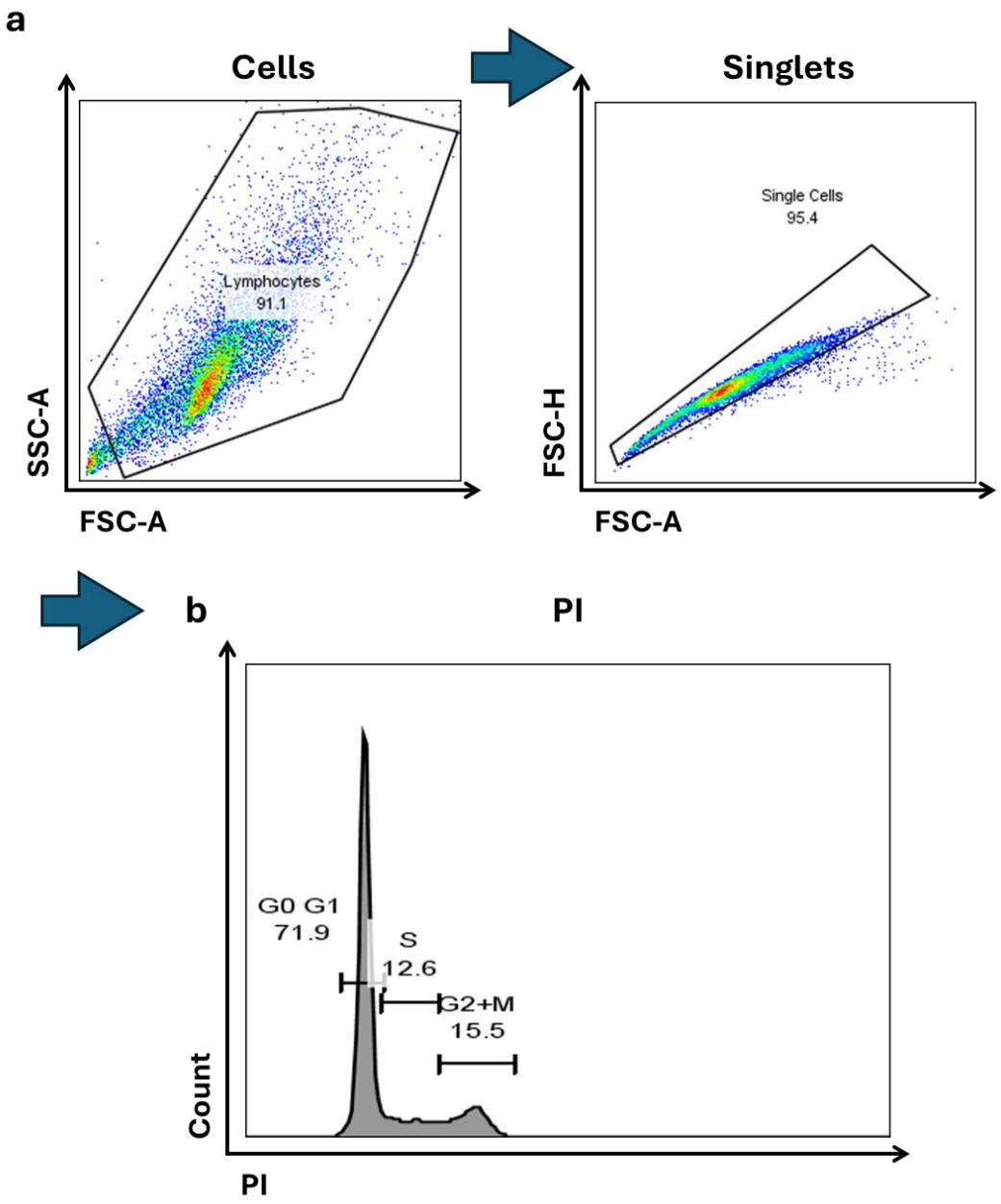

Figure 2.8: Gating strategies for cell cycle analysis PI staining.
Cell cycle analysis was performed by propidium iodide (PI) staining to quantify the fraction of cells in each phase of the cell cycle (G1/0, S and G2) in response to cell drug treatment. (a) Forward scatter (FSC) and side scatter (SSC) were used to gate cells (left panel) and select for singlets (right panel). (b) DNA content was examined by PI staining using a histogram. The histogram was used to identify the DNA content by PI staining for G0/G1, S and G2/M phases of the cell cycle.

2.7 short hairpin RNA (shRNA) KD and transfection of MEC1 cells

2.7.1 Glycerol stocks of shRNA constructs

The USP7, USP9x and TRIM21 shRNA constructs were obtained from a bacterial glycerol stock (Terrific Broth (TB), 100 µg/mL carbenicillin, 15 % glycerol) library (MISSION shRNA; Sigma) (Table 2.9). The glycerol stocks of shRNA construct were stored in -80 °C.

Symbol	Clone ID	Target sequence	Vector ID	Region
USP7	TRCN0000004058	CCTGGATTTGTGGTTACGTTA	TRC1	CDS
USP7	TRCN0000004059	TGTATCTATTGACTGCCCTTT	TRC1	3UTR
USP7	TRCN0000010845	CGTGGTGTCAAGGTGTACTAA	TRC1	CDS
USP7	TRCN0000318521	CCTGGATTTGTGGTTACGTTA	TRC2	CDS
USP7	TRCN0000318578	CCAGCTAAGTATCAAAGGAAA	TRC2	CDS
USP7	TRCN0000349562	CGTGGTGTCAAGGTGTACTAA	TRC2	CDS
USP7	TRCN0000349627	TGTATCTATTGACTGCCCTTT	TRC2	3UTR
USP9x	TRCN0000007361	GAGAGTTTATTCACTGTCTTA	TRC1	3UTR
USP9x	TRCN0000007362	CGATTCTTCAAAGCTGTGAAT	TRC1	CDS
USP9x	TRCN0000007363	CGACCCTAAACGTAGACATTA	TRC1	CDS
USP9x	TRCN0000007364	CGCCTGATTCTTCCAATGAAA	TRC1	CDS
USP9x	TRCN0000011091	CCACCTCAAACCAAGGATCAA	TRC1	CDS
TRIM21	TRCN0000003986	TGGCATGGTCTCCTTCTACAA	TRC1	CDS
TRIM21	TRCN0000234748	GAAGAGAGATTTGATAGTTAT	TRC2	CDS
TRIM21	TRCN0000234745	TGGAAGTGGAAATTGCAATAA	TRC2	CDS

Table 2.9: shRNA constructs. The shRNA constructs were all purchased from Sigma.

2.7.2 shRNA construct

RNA interference (RNAi) is a biological process that utilises RNA molecules to inhibit gene expression and study gene function. shRNA is a sequence of RNA that can integrate into DNA and consists of two complementary 19-22 base pair (bp) RNA sequences connected by a short loop of 4-11 nucleotides, resembling the hairpin structure found naturally in microRNA. The shRNA sequence is transported to the cytoplasm and recognised by Dicer, which processes the shRNA into siRNA duplexes. The derived siRNA binds to the target mRNA and is incorporated into the RNA-induced silencing complex (RISC), targeting specific mRNA degradation. The transduction of shRNA into mammalian cells through viral vectors allows for permanent KD of the targeted gene and stable integration of shRNA. The stability of this KD offers advantages, including reducing the need for several rounds of transfection and increasing reproducibility of results (498). Fluorescent markers such as Green Fluorescent Protein (GFP) were included to track cells expressing of shRNAs and assess the efficiency of the transfection and transduction processes.

shRNA mediated KD of USP7, USP9x and TRIM21, expression was performed via lentiviral delivery of shRNA plasmid. The following method illustrates the processes of delivering and expanding shRNA constructs, generating stably transduced MEC1 cells to evaluate the role of USP7, USP9x and TRIM21 on FOXO1 regulation. In addition, the shRNA technique required additional plasmids, including VSV-G (envelope vector), HIV-1 (packaging vector), GFP and scrambled (SCR) shRNA control. These constructs were generated into *Escherichia coli,* then prepared into glycerol stock by the suppliers Sigma. The pLKO.1-puro and TRC2-pLKO-puro construct includes ampicillin and puromycin antibiotic resistance genes used for the selection of bacterial and mammalian cells, respectively. The TRC1 and TRC2 pLKO backbone maps are presented in Figure 2.9 (499).

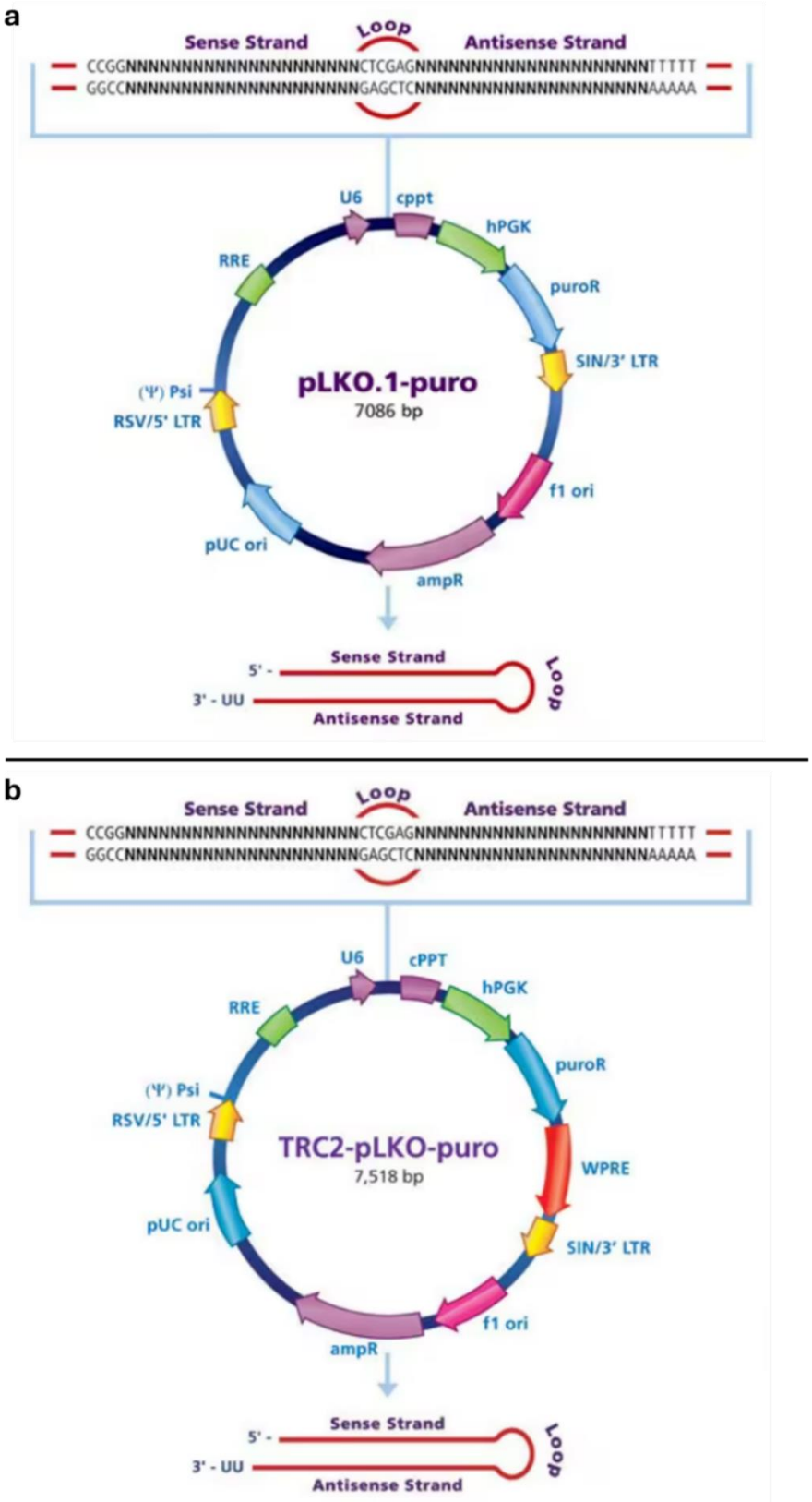

Figure 2.9: TRC1 and TRC2 pLKO backbone vector maps (499).
Schematic of backbone vectors maps for TRC1 and TRC2 with shRNA inserts. (a) The TRC1-pLKO.1-puro plasmid is 7,086 bp long and contains an ampicillin resistance (ampR; purple) gene for bacterial selection and a puromycin resistance (puroR; blue) gene for mammalian selection. (b) The TRC2-pLKO-puro plasmid is slightly larger than TRC1, measuring 7,518 bp in length due to the addition of the Woodchuck Hepatitis Post-Transcriptional Regulatory Element (WPRE; red), which enhances the expression of transgenes delivered by lentivirus (499).

2.7.3 Selection of bacterial clones and inoculation of liquid cultures

Glycerol stocks were used to isolate plasmid DNA (Table 2.9). To isolate a single bacterial clone (*Escherichia coli*) and acquire purified DNA, the bacterial glycerol stock was opened under the flame and a sterile loop was dipped in the glycerol stock then diluted into 500 µL of antibiotic-free terrific broth (TB) in a 1.5 mL Eppendorf tube. The culture was incubated for 30 min in a shaking heat block at 37 °C. A sample of the culture (50 µL) was plated on LB agar plates (InvivoGen) supplemented with 100 µg/mL ampicillin. The LB agar was prepared by following the manufacturer's instructions (InvivoGen; Fast-Media LB Agar Base), including autoclaving of the mix prior to the addition of ampicillin. Streaking the LB agar was performed near a flame to maintain sterility, and the loop was discarded after each streak to maximise the separation of bacterial colonies and reduce the risk of obtaining a contaminated plasmid. A quality control was prepared by streaking the LB agar plate under the flame with a clean loop. The plates were incubated in a humidified incubator overnight at 37 °C (Figure 2.10). The next day, four individual bacterial colonies were picked and transferred into a 15 mL Falcon tube (Fisher Scientific) containing 5 mL of TB supplemented with 100 µg/mL ampicillin or a control containing only TB with 100 µg/mL ampicillin. The tubes were then incubated overnight in a shaker at 37 °C (Figure 2.10).

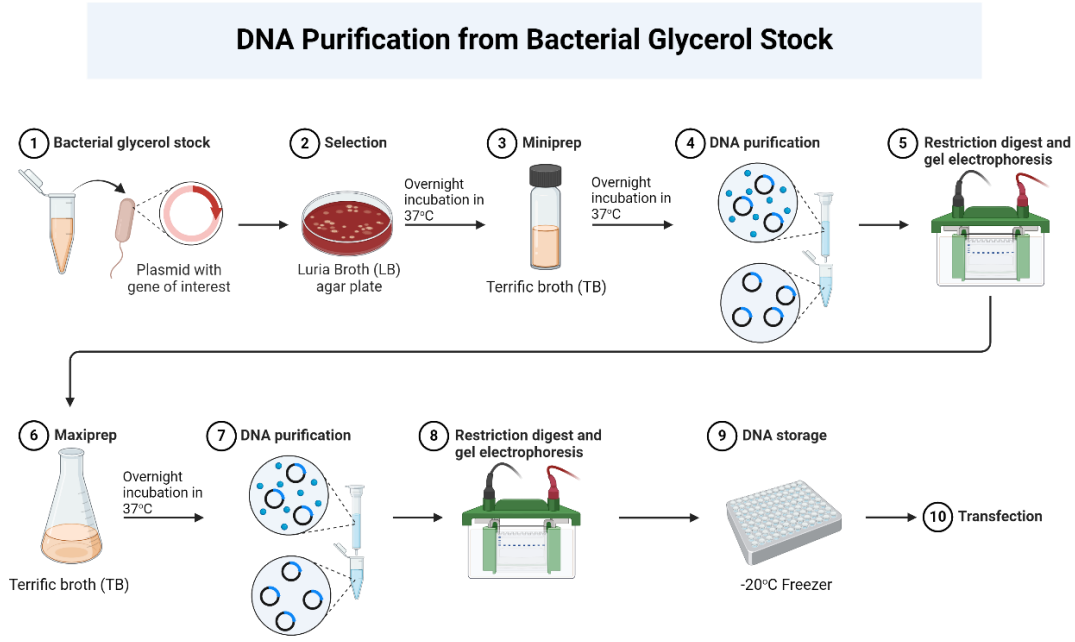

Figure 2.10: DNA purification from bacterial glycerol stock.
The diagram provides a summary of the purification process for plasmids containing shRNA from bacterial glycerol stock. ①Bacterial glycerol stocks containing shRNA were purchased from Sigma shRNA MISSION. ②The bacteria were streaked onto LB agar plates, and four single colonies were selected for miniprep. ③Miniprep was performed to expand the selected single colonies and

determine DNA purity. ④DNA purification was performed using a miniprep kit to purify DNA from the bacterial broth. ⑤DNA restriction digest was performed with NcoI-HF and BamHI-HF enzymes to determine the presence of the shRNA sequence insert in the purified DNA. At this step, glycerol stocks were also generated. ⑥Maxiprep was performed following shRNA validation by restriction digest. ⑦ & ⑧ Repeat steps ④ and ⑤, respectively. ⑨The concentration of DNA was determined by NanoDrop after verification of plasmid presence by restriction digest and stored at -20 °C until required. ⑩The purified DNA was used for lentiviral transfection.

2.7.4 Minipreparation 'Miniprep'

To prepare plasmid DNA from bacteria, QIAprep Spin Miniprep Kit (QIAGEN) was used according to the manufacturer's instructions. The purified plasmid DNA isolated from the miniprep, eluted in 20-30 µL of elution buffer (10 mM Tris·Cl, pH 8.5), was employed to verify the presence of a shRNA sequence within the TRC1-pLKO.1-puro and TRC2-pLKO-puro cloning vector by restriction digests (Section 2.7.5). Of the 5 mL culture, 4 mL was used for miniprep, and the remaining 1 mL was used, after verifying by restriction digests, for generating glycerol stocks and maxiprep. Of note, glycerol stocks were generated by mixing bacterial broth with 25% glycerol. NanoDrop spectrophotometer was used to determine the concentration and purity of the plasmid.

2.7.5 Restriction digests

The restriction digests were performed to verify the presence of the shRNA sequence insert in the purified DNA. The protocol for restriction digests were generated using NEBcloner v1.13.0 software (New England Biolabs) and followed according to the manufacturer's protocol. Briefly, 200 ng of purified plasmid, using either the miniprep or maxiprep protocol (Section 2.7.4 or 2.7.7), was digested with 1 µL of NcoI-HF (New England Biolabs) and 1 µL of BamHI-HF (New England Biolabs) restriction enzymes. 1x CutSmart Buffer (New England Biolabs) was added to the reaction and incubated for 30 min at 37 °C. Of note, NcoI-HF and BamHI-HF single digests were included, as well as no enzyme control. The restriction digests were performed using DNA gel electrophoresis to run the digested DNA samples (Section 2.7.6). The digestion of TRC1-pKLO.1-puro produced ~1,247 base pairs (bp) insert and ~5,793 backbone fragments, while the digestion of TRC2-pKLO-puro produced ~1,801 base pairs (bp) insert and ~5,671 backbone fragments (Figure 2.9).

2.7.6 DNA gel electrophoresis preparation

1 % agarose gel was prepared by dissolving 1 g agarose powder (Sigma) into 100 mL 1x TAE buffer (40 mM Tris, 20 mM acetate, 1 mM EDTA, pH 8.2) into conical flask. The mix was gently heated in the microwave to dissolve agarose. The liquid was cooled before adding 10 µL 10,000X SYBR Safe DNA gel Stain concentrate (ThermoFisher Scientific). The mix was subsequently poured into a gel tray and allowed to set.

Before loading the samples into the wall, 1X TriTrack DNA Loading Dye (ThermoFisher Scientific) was added to DNA digest generated in section 2.7.5. The gel then placed inside gel box and filled with 1X TAE buffer. A 1kb DNA ladder GeneRuler (ThermoFisher Scientific) was used and undigested, single-digestion were used as controls beside the digested DNA samples (double-digest). The gel was run at 100 V until reaching 70 % of the gel total length. The DNA gel was viewed using the Odyssey Fc Imaging System linked to Image Studio Lite v5.2 using the 600 nm channel.

2.7.7 Maxipreparation 'Maxiprep'

Following miniprep and verification of the plasmid DNA, 200 µL of bacterial liquid culture from the miniprep was transferred to autoclaved conical flasks containing 100 mL TB with 100 µg/mL ampicillin or control containing only TB with 100 µg/mL ampicillin. The flasks then incubated overnight in a shaker at 37 °C.

The next day, maxiprep was performed using PureLink™ Fast Low-Endotoxin Maxi Plasmid Purification Kit (ThermoFisher Scientific) according to the manufacturer's instructions. DNA was eluted in 75-150 µL of elution buffer (10 mM Tris-HCl, pH 8.5, 0.1 mM EDTA). NanoDrop spectrophotometer was used to determine the concentration and purity of the plasmid. The plasmid DNA was then verified by restriction digests (Section 2.7.5 & 2.7.6), then stored at -20 °C until needed.

2.7.8 Transfection of HEK293T cells and generation of lentiviral particles

The calcium phosphate method was adapted for transfection of HEK293T (500), a highly transfectable version of human embryonic kidney 293 cell line, to produce a supernatant containing lentiviral shRNA particles that are harvested to transduce MEC1 cells (Figure

2.11). The transfection was performed using SCR, GFP positive constructs, target shRNA constructs, and medium-only as negative control. Prior to transfection, adherent HEK293T cells were seeded with 10 mL complete DMEM medium in 6 cm tissue culture plates (Greiner Bio-One) and incubated at 37 °C, 5% CO_2. The desired confluency of HEK293T cells was between 70-80 %. The media was replaced with 5 mL fresh complete DMEM medium before transfection. Two solutions were prepared for each transfection, solution A containing (5 µg shRNA construct, 2.5 µg VSV.G envelope vector, 2.5 µg HIV-1 packaging vector, 50 µL 2.5 M $CaCl_2$, topped up to 150 µL with sterile distilled water) and solution B containing (150 µL 2X HEPES buffered saline (Sigma)). Each solution was prepared separately in a 1.5 mL Eppendorf tube, where solution A was vortexed then added dropwise to solution B, followed by vigorous bubbling using 1000 µL tip and incubated at RT for 30 min.

After incubation, the mixture was introduced dropwise to the plate containing HEK293T cells and then swirled and incubated overnight at 37 °C, 5% CO_2. The next day, the media was discarded and replaced with fresh complete DMEM media/plate of HEK293T cells, and incubated for 48 hr at 37 °C, 5% CO_2. Following the 2 days incubation, the efficiency of HEK293T cell transfection was checked by examining cells transfected with GFP-expressing construct using a fluorescence microscope Axio Observer (ZEISS), or flow cytometry. The supernatant of HEK293T cells, containing lentiviral particles or only media from the control, were collected and filtered through a 0.45 µm filter (Sartorius) to remove any cell debris. Each plate of HEK293T cells were then replenished with 5 mL fresh complete DMEM for a further incubation of 24 hr at 37 °C, 5% CO_2. The media was again collected, filtered and freshly introduced to MEC1 cells. The remaining lentiviral was stored in 4 °C for a maximum of 3 days.

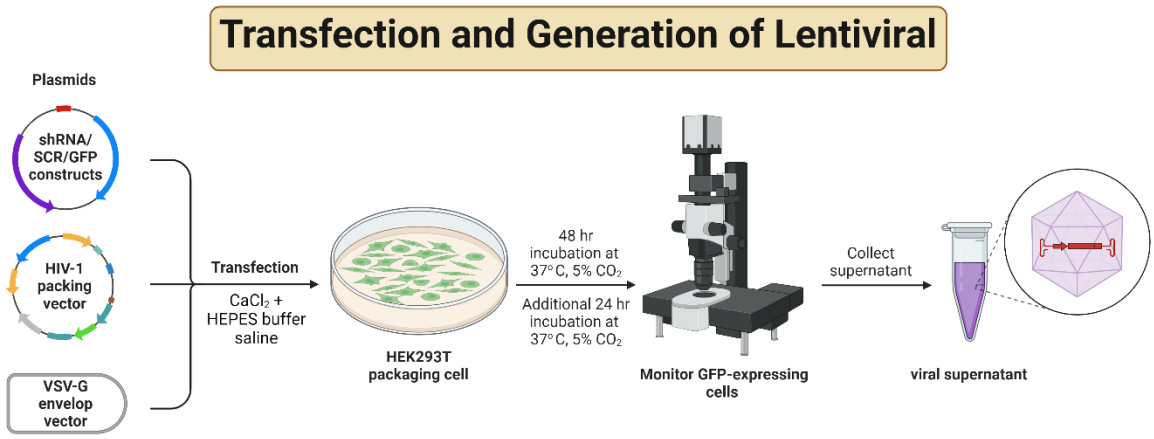

Figure 2.11: Transfection of HEK293T cells and generation of lentiviral.
HEK293T cells were transfected with shRNA/GFP/SCR constructs, an HIV-1 vector, and a VSV-G vector, mixed with calcium chloride and HEPES buffer saline. The media was removed the next day, and fresh media was added to the HEK293T cells, followed by incubation for 48 hr. Prior to collecting the lentiviral particles, GFP-transfected cells were monitored for transfection efficiency using a fluorescence microscope or flow cytometry. After 48 hr of incubation, the supernatant containing lentiviral particles was filtered and collected. Fresh media was added to the cells, and they were incubated for an additional 24 hr, followed by the collection of the supernatant containing lentiviral particles for immediate use in transduction.

2.7.9 Transduction of CLL cell lines

A day prior to transduction, 2 x 10^6 cells/condition of early-passaged MEC1 cells were seeded in a 6-well plate in 2 mL of fresh complete DMEM medium and incubated overnight at 37 °C, 5% CO_2. On the first day of transduction, 2 mL of filtered viral supernatant containing 10 µg/mL polybrene (Sigma) was added. In parallel, MEC1 cells were transduced with GFP, SCR, or with non-transduced MEC1 cells serving as a control to monitor cell viability. The cells were incubated for 24 hr at 37 °C, 5% CO_2. Following incubation, MEC1 cells were harvested, centrifuged at 300x*g* for 5 min, and resuspended in 2 mL of fresh complete DMEM medium. The cells were then seeded into a new 6-well plate. An additional 2 mL of fresh viral supernatant containing 10 µg/mL polybrene (Sigma) was added. The plate was incubated for 48-72 hr at 37 °C, 5% CO_2. GFP-expressing cells were then examined under a fluorescence microscope or by flow cytometry to monitor the efficacy of the transduction.

Prior to puromycin selection, the transduced cells were incubated for 24 hr at 37 °C, 5% CO_2 in fresh complete DMEM media. The next day, 2 µg/mL of puromycin was added to all cells GFP control (non-puromycin resistant), SCR, and KD, except for non-transduced control. The puromycin-selection of transduced cells was monitored by examining the viability with

trypan blue or Annexin V/7-AAD compared to the viability of GFP control. The transduced cells were supplied with fresh complete DMEM media supplemented with 2 µg/mL of puromycin every 3 days. At 7 and 14 days of puromycin selection, the efficacy of KDs were examined by RT-qPCR and Western blotting compared to the SCR control (Figure 2.12). The most efficient KDs were further expanded in the presence of 1 µg/mL of puromycin to maintain selection pressure. KDs statu were monitored every 14 days at both the gene and protein levels and the transduced MEC1 cells passaged up to a maximum of 20 passages.

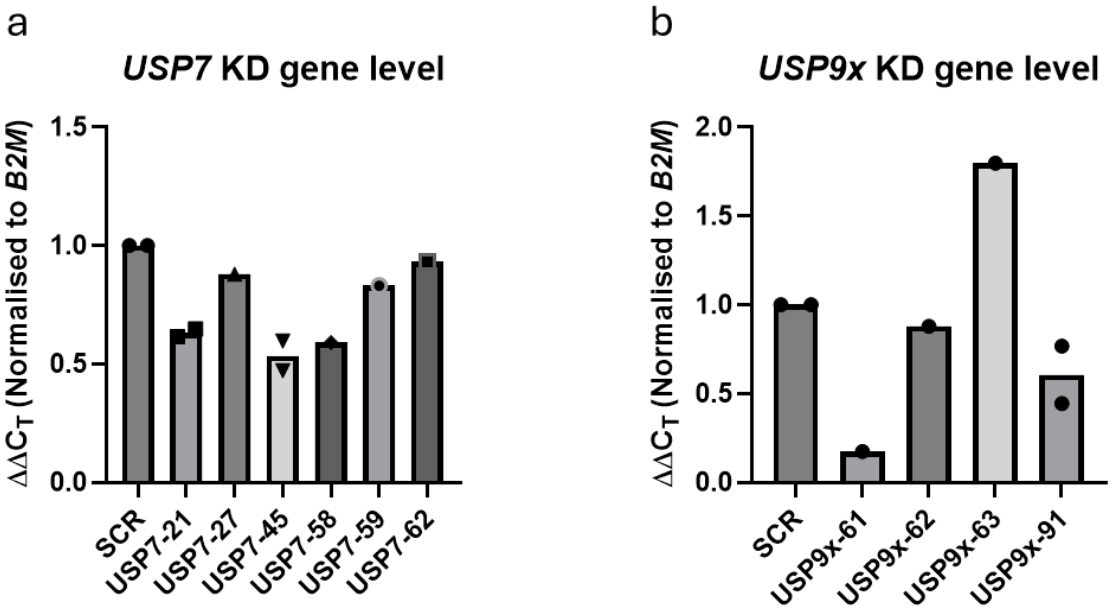

Figure 2.12: The efficiency of USP7 and USP9x shRNA constructs at knocking down the mRNA levels.

The transcription levels of *USP7* and *USP9x* knockdowns (KDs) in MEC1 cells were assessed by RT-qPCR in comparison to scrambled (SCR) control. (a) *USP7* mRNA levels of shRNA KDs in MEC1 cells (Table 2.9). (b) *USP9x* mRNA levels of shRNA KDs in MEC1 cells (Table 2.9). The $\Delta\Delta C_T$ method was used to calculate expression levels, where samples were normalised to housekeeping gene *B2M*. Each dot represented an individual datapoint.

2.8 Statistical analyses

The data were analysed using GraphPad prism v9.4.1 software to create a range of tests including One-way ANOVA and paired t-tests. Microsoft Excel was used to determine the concentration of proteins and normalisation of data generated from densitometry analysis. Flow cytometry data were analysed using FlowJo v10 and GraphPad prism v9.4.1 software. P-values were calculated by One-way ANOVA as well as unpaired and paired t-test on a minimum of at least 3 biological replicates. Additionally, Normality test (Shapiro Wilk test) was applied due to t-test and ANOVA test assumption of samples normality. Treated values of drug were compared with US or NDC. Mean ± standard error of mean (SEM). * = $p \leq 0.05$; ** = $p \leq 0.01$; *** = $p \leq 0.001$; **** = $p \leq 0.0001$.

Chapter 3. Profiling the expression levels of FOXO family members in primary CLL cells and examining FOXO1 regulation via the BCR signalling pathway.

3.1 Introduction:

FOXO transcription factors, widely regarded as tumour suppressors, regulate transcription of many genes involved in cell cycle arrest, apoptosis, metabolism, and stress resistance (399, 412, 501). The development of therapies targeting components downstream of BCR signalling, including ibrutinib (BTK inhibitor) (502) and idelalisib (PI3K inhibitor) (503) has transformed management strategies for CLL patients. Indeed, the treatment of relapsed CLL or patients harbouring poor prognostic characteristics has significantly improved in the past years with the approval of ibrutinib and idelalisib (263, 491, 503, 504). Although durable remission has been reported in large number of patients treated with these agents (505), CLL remains largely incurable, with drug resistance and relapse a frequent occurrence (506). This highlights the necessity to develop novel therapies.

Previous studies from our group revealed that FOXO1 protein level is overexpressed in CLL cells and more distinct in poor prognostic patients (2). The data presented in the paper indicated that short-term stimulation of primary CLL cells with $F(ab')_2$ fragments promoted upregulation of FOXO1 protein expression. Given the prognostic importance of BCR signalling in CLL, we hypothesised that BCR-mediated signalling promoted rapid upregulation of total FOXO1 protein expression and $FOXO1^{T24}$ phosphorylation through mTORC2/AKT signalling pathway. FOXO1 has been reported to be regulated by phosphorylation, methylation and deubiquitylation (360), and these findings have prompted us to investigate a role for DUB enzymes in CLL cells. Although FOXOs has been extensively studied in normal and malignant B-cells, little is known about the regulatory roles of ubiquitination and deubiquitination of FOXO1 following BCR-mediated signalling or its inhibition.

This chapter investigates mRNA expression of FOXO family members (*FOXO1*, *FOXO3* and *FOXO4*) and number of DUB genes including *USP7*/*9x*/*14*. Moreover, we examined FOXO1 and DUB proteins expression *ex-vivo* in CLL patient samples with a wide range of diagnostic

characterisations including Binet stages, chromosomal aberration, and treatment status. Furthermore, we examined the impact of BCR-mediated signalling and its inhibition with ibrutinib as well as DUB inhibitors on CLL cell apoptosis and protein expression.

3.2 Specific Aims

I. Establish the gene and protein expression of FOXO family members *ex-vivo* in patient CLL samples and B-cells from healthy donors.
II. Examine the effect of BCR ligation on regulating FOXO1 gene and protein expression in CLL patient cells and cell lines.
III. Investigate the effect of BTK inhibitor in regulating FOXO1 protein expression.
IV. Establish the gene and protein expression of DUBs *ex-vivo* in patient CLL samples and B-cells from healthy donors.
V. Determine the effect of DUB inhibitors in initiating CLL cell apoptosis.
VI. Examine the effect of DUB inhibitor in regulation FOXO1 protein expression.

3.3 Results

3.3.1 *FOXO1* is overexpressed at transcription level in CLL cells compared to healthy CD19$^+$ cells

In a prior study, we demonstrated differential gene expression patterns of FOXO family members within a cohort of CLL patient samples, with a significant upregulation in the transcription levels of *FOXO1* and *FOXO4*, while *FOXO3* exhibited a significant downregulation in CLL patient samples (412). To confirm our previous published findings regarding the transcriptional profiles of FOXO family members, a new cohort of CLL patient samples was selected and the expression of *FOXO1*, *FOXO3* and *FOXO4* were investigated by RT-qPCR to validate our published observations.

The gene expression level of FOXO family members *FOXO1*, *FOXO3* and *FOXO4* were examined *ex-vivo* in PB-derived CLL cells compared to CD19$^+$ B-cells from healthy donors (healthy control). The gene expression levels of FOXO family members in CLL patient cells and healthy control were normalised to glyceraldehyde-3-phosphate dehydrogenase (*GAPDH*) (housekeeping gene). The relative gene expression levels of CLL cells and healthy control CD19$^+$ cells were calculated using the gene expression mean derived from the cohort of healthy controls. These data demonstrated that the transcription levels of FOXO family members were differentially expressed in CLL cells (Figure 3.1a-c). While *FOXO1* and *FOXO4* transcription levels were significantly upregulated in CLL cells compared to healthy CD19$^+$ B-cells, *FOXO3* gene expression levels in CLL patient cells were the same as healthy CD19$^+$ cells (Figure 3.1a-c). Within the cohort of CLL patient samples, stratification of the expression of *FOXO1* based upon cytogenetic aberration (no del(11q) or del(17p), del(11q), del(17p)) revealed no significant differences in the levels of *FOXO1* between patient samples harbouring cytogenetic abnormalities and those without such aberrations (Figure 3.1d). Similarly, stratification of *FOXO3* levels based on cytogenetic abnormalities revealed no changes in *FOXO3* levels (Figure 3.1e). However, *FOXO4* stratification based on cytogenetic abnormalities showed a downregulation of *FOXO4* levels in patients harbouring del(17p) compared to no del(11q)/del(17p) (p = 0.10) and del(11q) with (p = 0.18) (Figure 3.1f). Further stratification of *FOXO1*, *FOXO3* and *FOXO4* levels based on Binet stages (A, B, C), gender (male, female), and treatment status (pre-treatment, post-treatment) indicated no significant difference in FOXOs transcription levels (data not shown).

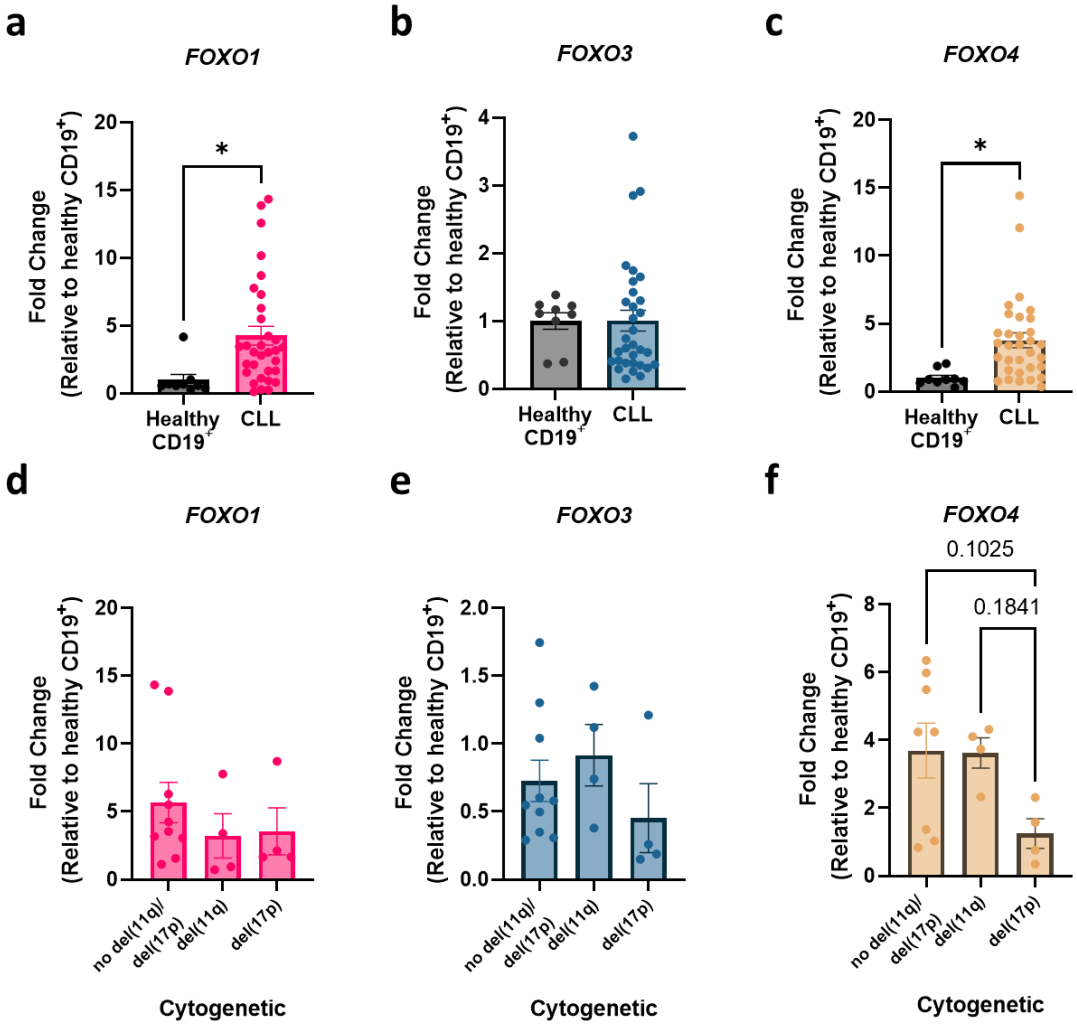

Figure 3.1: mRNA expression levels of FOXO family members in PB-derived CLL cells and healthy B-cells *ex-vivo*.

(a - c) RT-qPCR to assess expression levels of *FOXO1*, *FOXO3* and *FOXO4* in B-cells from healthy donors (Healthy CD19$^+$; black bars; n = 9) and PB-CLL patient samples (CLL; *FOXO1* = pink bar, *FOXO3* = blue bar, *FOXO4* = light brown bar; n = 32). RT-qPCR to assess expression levels of (d) *FOXO1* (pink bar), (e) *FOXO3* (blue bar), and (f) *FOXO4* (light brown bar) in CLL patient samples stratified by cytogenetic abnormalities as indicated. The ΔC_T method was used to calculate expression levels, where samples were normalised to housekeeping gene *GAPDH*. The mean gene expression levels of FOXO family members in healthy CD19$^+$ were used to calculate the relative gene expression levels of healthy B-cells and CLL cells. Each dot represented an individual datapoint. Data expressed as the mean ± SEM, and statistics calculated by unpaired t-test (a – c) or unpaired One-way ANOVA, Tukey test (d - f); * $p \leq 0.05$.

It was of interest to examine the transcriptional levels of *ZAP-70* due to its role in enhancing BCR signalling, which plays a central role in the survival of CLL cells (226). BCR signalling enhances CLL survival by regulating a number of genes including *MCL1*, which was of interest due to its anti-apoptotic activity (285), and could serve as an indicator of CLL disease burden. Moreover, PTEN has been reported to act as tumour suppressor in CLL cells and its activity is compromised by the BCR signalling pathway (460, 507). This observation

resonates with findings suggested by Cosimo, Tarafdar (412) regarding FOXO1 regulation in CLL cells (2). Therefore, the transcriptional levels of these gene could be used as makers of CLL disease burden. The basal transcriptional levels of *MCL1*, *PTEN* and *ZAP-70* were examined *ex-vivo* in PB-derived CLL samples in comparison to healthy $CD19^+$ cells using RT-qPCR, and expressed as described above. Contrary to expectations, the transcript levels of *MCL1* showed a decrease in CLL patient samples compared to healthy $CD19^+$ cells, although this did not reach significance (Figure 3.2a; $p = 0.08$). *PTEN* mRNA levels in CLL patient cells and healthy B-cells demonstrated no significant difference in expression levels (Figure 3.2b). As expected, the expression of *ZAP-70* was significantly upregulated in CLL patient cells compared to healthy controls (Figure 3.2c). Stratification of *MCL1* transcription levels in regard to cytogenetic abnormalities illustrated no significant differences between patients with no cytogenetic abnormalities compared to patient harbouring del(11q) or del(17p) (Figure 3.2d). Interestingly, *PTEN* stratification based on cytogenetic aberration revealed a significant upregulation in transcription levels in patients harbouring del(17p) compared to patients with no cytogenetic aberration, while patients with del(11q) showed no significant changes in transcriptional levels between those with no del(11q)/del(17p) and samples with del(11q) (Figure 3.2e). Stratification of *ZAP-70* mRNA levels demonstrated a significant increase of *ZAP-70* in CLL cells with del(11q) compared to no del(11q)/del(17p) (Figure 3.2f). Additional stratification of *MCL1*, *PTEN* and *ZAP-70* transcriptional levels based on Binet stages, gender, and treatment status revealed no significant difference in their transcript levels (data not shown).

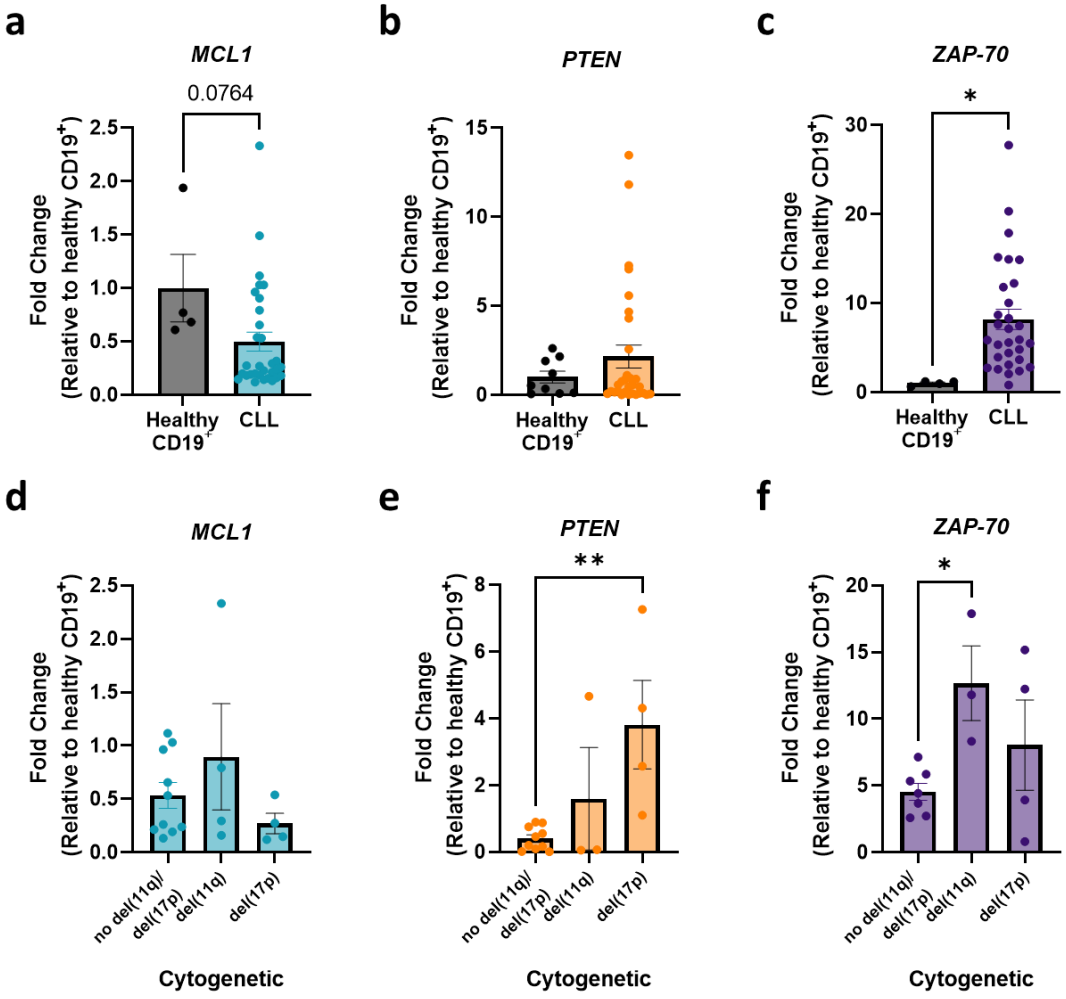

Figure 3.2: *ZAP-70* was significantly upregulated in primary PB-derived CLL cells compared to healthy B-cells.
(a-c) RT-qPCR to assess expression levels of *MCL1*, *PTEN* and *ZAP-70* in B-cell from healthy donor (Healthy $CD19^+$; black bars; n ≥ 4) and *ex-vivo* PB-CLL patient samples (CLL; *MCL1* = blue bar, *PTEN* = orange bar, *ZAP-70* = purple bar; n = 30). RT-qPCR to assess expression levels of (d) *MCL1* (blue bar), (e) *PTEN* (orange bar), and (f) *ZAP-70* (purple bar) in CLL patient samples stratified by cytogenetic abnormalities as indicated. The ΔC_T method was used to calculate expression levels, where samples were normalised to housekeeping gene *GAPDH*. The mean gene expression levels in healthy $CD19^+$ were used to calculate the relative gene expression levels of healthy B-cells and CLL cells. Each dot represented an individual datapoint. Data expressed as the mean ± SEM. Statistics calculated by unpaired t-test (a-c) or unpaired One-way ANOVA, Tukey test (d-f); * $p \leq 0.05$, ** $p \leq 0.01$.

3.3.2 The protein expression of FOXO1 is significantly upregulated in CLL cells compared to B-cells from healthy donors

Overexpression of FOXO1 protein has been reported in LN biopsies of CLL patients with an unfavourable prognosis (412). In addition, ligand-independent 'tonic' and ligand-dependent BCR signalling can induce proliferation and maintain CLL cell survival (508, 509). Since AKT is regulated by BCR signalling which in return negatively regulates FOXO1 transcription

activity through phosphorylation at conserved RxRxxS/T residues (FOXO1^{T24}, FOXO1^{S256}, FOXO1^{S319}) (408), we investigated the phosphorylation (FOXO1^{T24}) and expression status of FOXO1 in PB-derived CLL samples compared to CD19^{+} B-cells from healthy donors (Figure 3.3).

The data revealed a heterogeneity in the basal levels of AKT^{S473} phosphorylation, FOXO1^{T24} phosphorylation and total FOXO1 expression (Figure 3.3a). The data showed that AKT^{S473} phosphorylation demonstrated a trend toward downregulation (p = 0.16) in CLL samples compared to healthy control (Figure 3.3b), while AKT expression levels were similar between CLL cells and healthy CD19^{+} cells (Figure 3.3c). Further stratification of AKT^{S473} phosphorylation protein levels based on cytogenetic aberrations (no del(11q)/del(17p) or with one/both del(11q)/del(17p)) indicated a slight decrease of AKT^{S473} phosphorylation level (p = 0.3) in patients with poorer prognostic characteristics (Figure 3.3d). In contrast, stratification of AKT protein levels based on cytogenetic abnormalities showed a modest increase level (p = 0.2) in CLL cells with poor prognostic characteristics compared to undetectable cytogenetic changes (Figure 3.3e). While FOXO1^{T24} phosphorylation was significantly downregulated in CLL cells compared to healthy CD19^{+} cells, FOXO1 protein level was significantly upregulated in CLL cells compared to healthy controls (Figure 3.3f & g). Additionally, stratification of FOXO1^{T24} phosphorylation level based on cytogenetic abnormalities revealed a significant upregulation of FOXO1^{T24} phosphorylation in CLL cells with poor prognostic characteristics compared to undetectable cytogenetic (Figure 3.3h), while FOXO1 expression showed no statistically significant difference (Figure 3.3i). Further stratification of AKT^{S473}, AKT, FOXO1^{T24} and FOXO1 levels based on Binet stages, gender, and treatment status displayed no significance difference in expression levels between CLL cells and healthy CD19^{+} cells (data not shown).

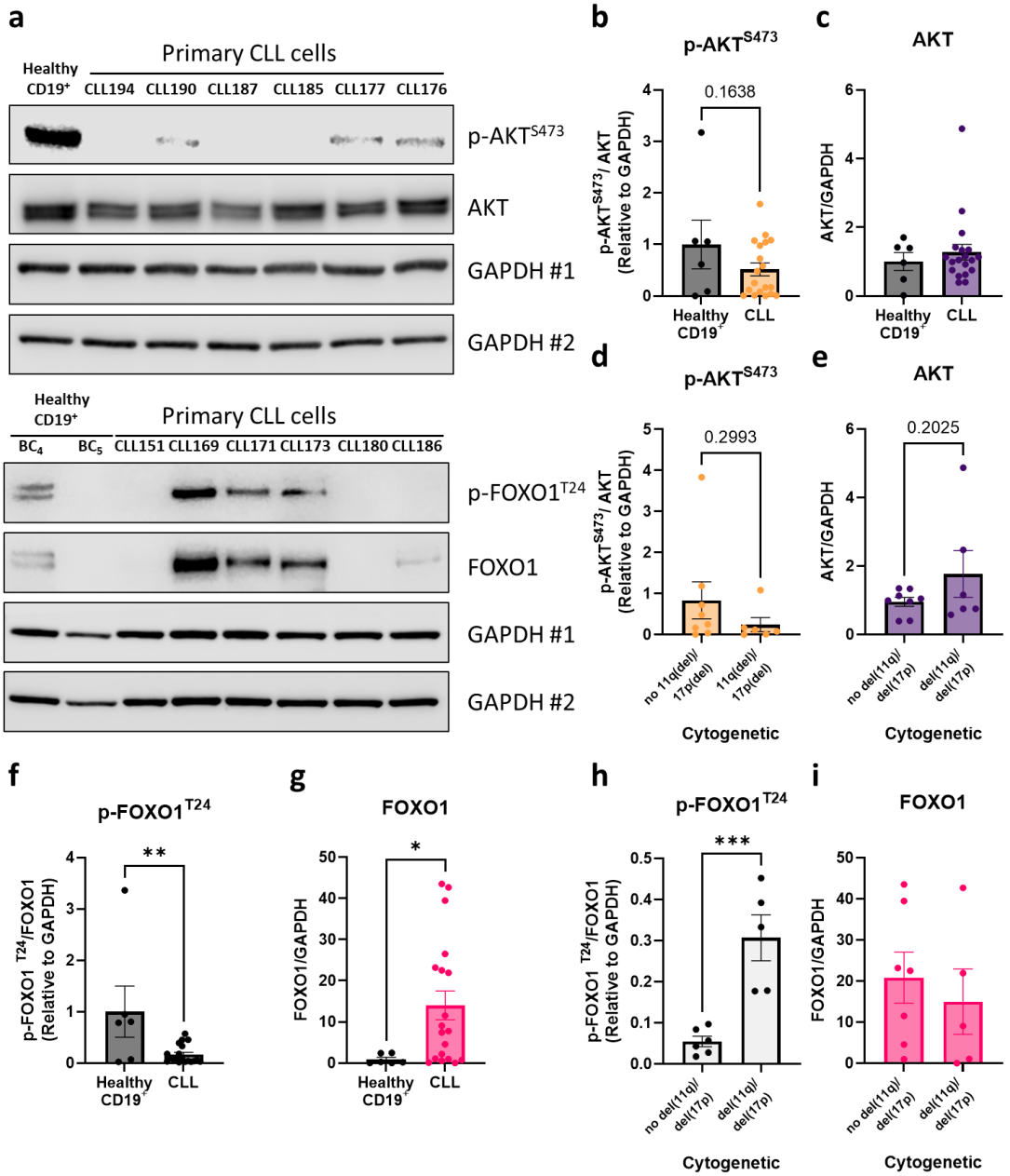

Figure 3.3: FOXO1 protein expression was significantly upregulated in primary CLL cells compared to B-cells from healthy donors.

(a) Representative Western blot to assess protein expression of *ex-vivo* PB-CLL cells compared with healthy CD19^{+} cells from healthy donor's buffy coats (BC), probed for AKT^{S473} phosphorylation, AKT, FOXO1^{T24} phosphorylation, FOXO1, and GAPDH (loading control; #1 and #2 representing mirror blots). (b, c) Relative protein expression of AKT^{S473} phosphorylation and AKT between B-cell from healthy donors (Healthy CD19^{+}; black bars; n = 6) and CLL patient samples (CLL; p-AKT^{S473}= beige bar, AKT = purple bar; n = 19). Assessing protein expression levels of (d) p-AKT^{S473} (beige bar), (e) AKT (purple bar) in CLL patient samples stratified by cytogenetic abnormalities (no del(11q)/ del(17p); undetectable cytogenetic abnormalities, del(11q)/ del(17p); either one or both cytogenetics abnormalities were detected). (f, g) Relative protein expression of FOXO1^{T24} phosphorylation and FOXO1 between B-cell from healthy donors (Healthy CD19^{+}; black bars; n = 6) and CLL patient samples (CLL; p-FOXO1^{T24} = white bar, FOXO1 = pink bar; n = 19). Assessing protein expression levels of (h) p-FOXO1^{T24} (white bar), (i) FOXO1 (pink bar) in CLL patient samples stratified by cytogenetic abnormalities (no del(11q)/ del(17p); undetectable cytogenetic abnormalities, del(11q)/ del(17p)). Samples were normalised to loading control GAPDH. The mean expression

levels of proteins in healthy $CD19^+$ cells were used to calculate relative protein expression levels of healthy B-cells and CLL cells. Each dot represented an individual datapoint. Data expressed as the mean ± SEM. Statistics calculated by unpaired t-test (b-i); * $p \leq 0.05$, ** $p \leq 0.01$, *** $p \leq 0.001$.

In section 3.3.1, we explored the transcription expression of *MCL1*, *ZAP-70* and *PTEN* due to their involvement in the BCR pathway. In this section, we extended our investigation to examine the protein levels, to establish their baseline levels in *ex-vivo* PB-derived CLL cells compared to healthy $CD19^+$ cells. The data revealed a heterogeneity in the protein expression of MEC1, PTEN and ZAP-70 in *ex-vivo* PB-derived CLL cells and healthy controls (Figure 3.4a). The data demonstrated that MCL1 protein level was not different in CLL cells compared to healthy $CD19^+$ cells, as some healthy $CD19^+$ cells showed high expression of MCL1 protein, others expressed little to undetectable levels of MCL1 (Figure 3.4b). Stratification of MCL1 expression level based on the presence of cytogenetic abnormalities, indicated a modest elevation ($p = 0.13$) in CLL cells with del(11q)/del(17p) compared to no del(11q)/del(17p) (Figure 3.4c). As expected, ZAP-70 protein level was significantly upregulated in CLL cells compared to healthy controls (Figure 3.4d). Further stratification of ZAP-70 expression level indicated that patient CLL cells harbouring poor prognostic cytogenetic indicator (del(11q)/del(17p)) exhibited an increase ($p = 0.09$) in ZAP-70 levels compared to undetectable aberration (Figure 3.4e). Expression of PTEN was significantly downregulated in CLL cells compared to healthy $CD19^+$ cells (Figure 3.4f). Upon stratification of PTEN expression level based on cytogenetic abnormalities, the data revealed that PTEN expression level is visibly elevated ($p = 0.14$) in poor prognostic cytogenetic compared to undetectable (Figure 3.4g). Furthermore, subdivision of samples by Binet stages revealed that PTEN was significantly downregulated in stage B and C compared to stage A (Figure 3.4h). Further stratification of MCL1 and ZAP-70 expression levels based on Binet stages, displayed no significance difference in expression levels between CLL cells and healthy $CD19^+$ cells (data not shown).

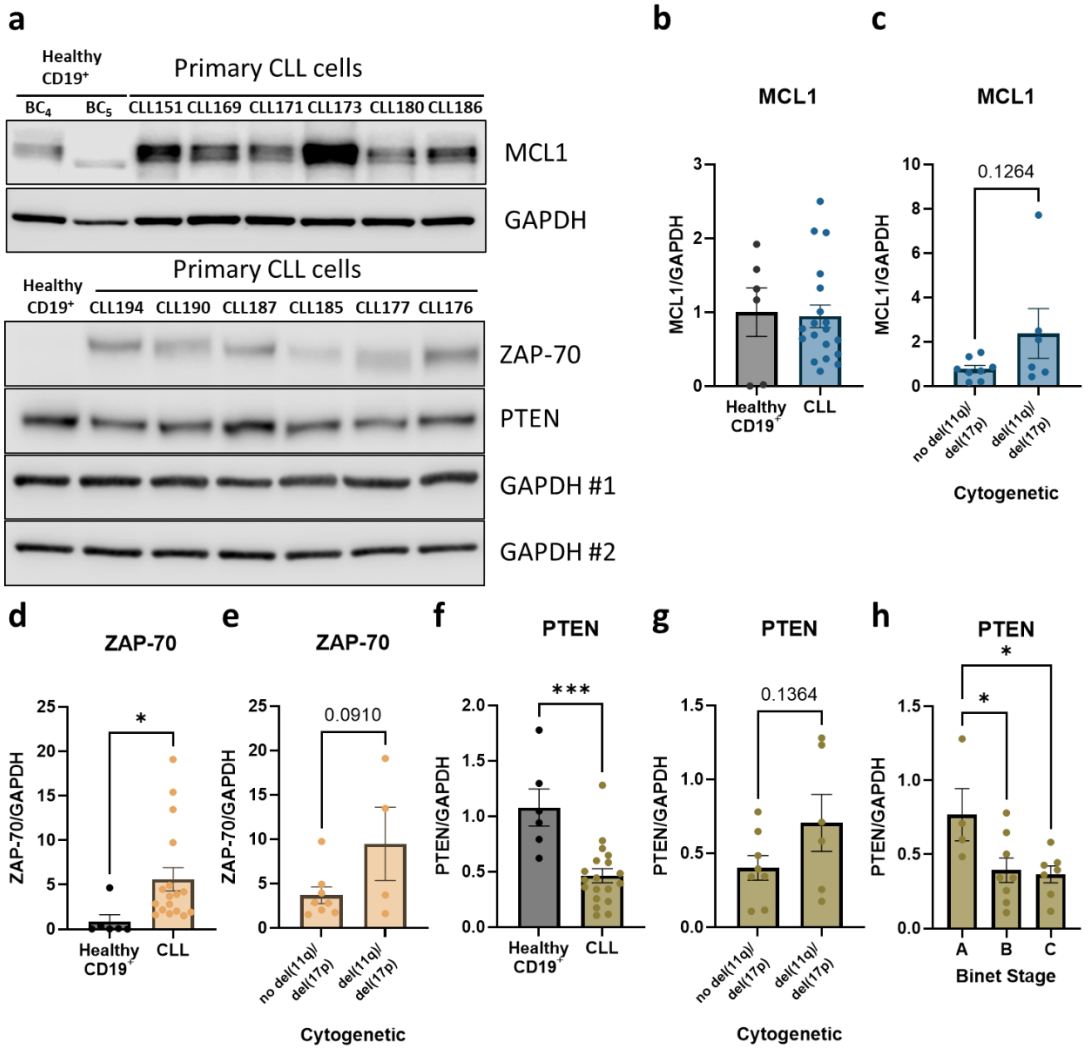

Figure 3.4: PTEN protein expression was significantly downregulated in *ex-vivo* CLL cells compared to B-cells from healthy donors.

(a) Representative Western blot to assess protein expression of *ex-vivo* PB-CLL cells compared with healthy CD19$^+$ cells from healthy donor's buffy coats (BC), probed for MCL1, ZAP-70, PTEN, and GAPDH (loading control; #1 and #2 representing mirror blots; extension of Figure 3.3). (b) Relative protein expression of MCL1 between B-cell from healthy donors (Healthy CD19$^+$; black bars; n = 6) and CLL patient samples (CLL; MCL1 = blue bar; n = 19). Assessing protein expression levels of (d) MCL1 (blue bar) in CLL patient samples stratified by cytogenetic abnormalities (no del(11q)/ del(17p); undetectable cytogenetic abnormalities, del(11q)/ del(17p); either one or both cytogenetics abnormalities were detected). (d) Relative protein expression of ZAP-70 (Healthy CD19$^+$; black bars; n = 6) and (CLL; ZAP-70 = beige bar; n = 19). (e) Stratification of ZAP-70 (beige bar) protein expression levels by cytogenetic abnormalities as described in (c). (f) Relative protein expression of PTEN (Healthy CD19$^+$; black bars; n = 6) and (CLL; PTEN = oil green bar; n = 19). (g) Stratification of PTEN (oil green bar) protein expression levels by cytogenetic abnormalities as described above. (h) Stratification of PTEN (oil green bar) protein expression levels by Binet stages (A, B, C). Samples were normalised to loading control GAPDH. The mean expression levels of proteins in healthy CD19$^+$ cells were used to calculate the relative protein expression levels of healthy B-cells and CLL cells. Each dot represented an individual datapoint. Data expressed as the mean ± SEM. Statistics calculated by unpaired t-test (b-g) or unpaired One-way ANOVA, Tukey test (h); * $p \leq 0.05$, *** $p \leq 0.001$.

3.3.3 MEC1 highly express FOXO1 at transcription level compared to HG-3 cells

As MEC1 and HG-3 cells are well established CLL cell lines, with MEC1 cells resembling poor risk genetics (*TP53* mutation and del(17p)) (460, 487), and HG-3 resembling favourable prognostic (del(13q)) (489), we profiled the mRNA expression of *FOXO1* and known poor prognostic biomarkers including *MCL1*, *MYC* and *ZAP-70*. Gene expression in HG-3 and MEC1 cells was expressed relative to the mean gene expression of HG-3 cells (Figure 3.5). The data demonstrated a significant increase of *FOXO1* and *MCL1* mRNA levels in MEC1 cells compared to HG-3 cells (Figure 3.5a & b). Surprisingly, the transcriptional levels of both *MYC* and *ZAP-70* were significantly upregulated in favourable prognostic HG-3 cells compared to MEC1 cells (Figure 3.5c & d).

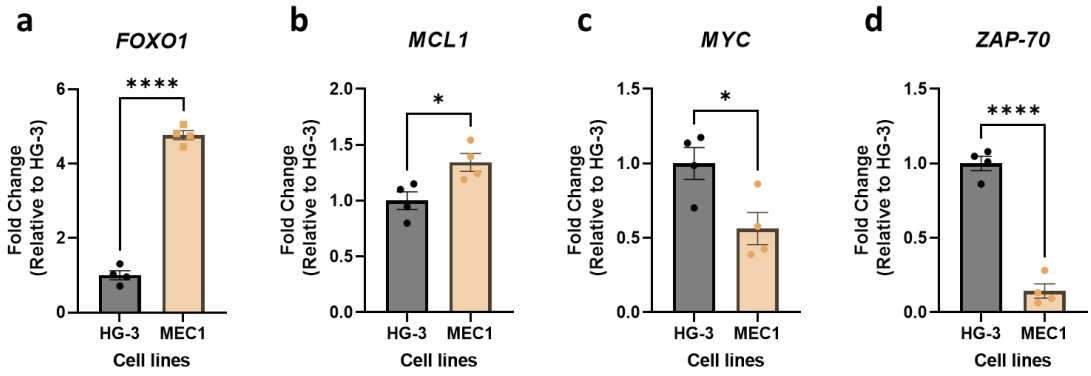

Figure 3.5: The transcriptional level of *FOXO1* was significantly upregulated in MEC1 compared to HG-3 cells.

(a-d) RT-qPCR to assess gene expression levels of *FOXO1, MCL1, MYC* and *ZAP-70* in HG-3 cells (black bar; n = 4) and MEC1 cells (beige bar; n = 4). The ΔC_T method was used to generate expression levels, where samples were normalised to the reference gene (*GUSB*) and scattered dots indicate the mean fold change in gene expression relative to HG-3 ± SEM. Individual samples are symbolised by dots. Statistics calculated by unpaired t-test, * $p \leq 0.05$, **** $p \leq 0.0001$.

3.3.4 FOXO1 protein is highly expressed in the MEC1 compared to the HG-3 cells

It has been suggested that FOXO1 could serve as a marker of poor prognosis in CLL cells, as FOXO1 was found to be overexpressed in LN biopsies from patients with poor prognosis (412). Comparing the protein expression of HG-3 and MEC1 cell lines, we demonstrate that MEC1 cells highly expressed $FOXO1^{T24}$ phosphorylation and total FOXO1 compared to HG-3 cells (Figure 3.6a-c). In alignment with transcription level of *MYC*, the protein expression of cMYC was significantly upregulated in HG-3 cells compared to MEC1 cells (Figure 3.6a&d). MCL1 protein level in MEC1 cells was higher (p = 0.17) compared to HG-3 (Figure 3.6e), following similar pattern as the transcription levels of *MCL1* in section 3.3.3. Furthermore, PTEN expression level was significantly higher in HG-3 cells compared to MEC1 cells (Figure 3.6f). FOXOs regulate several genes involved in cell death and cell cycle arrest. FOXO1 target genes included *BCL2L11*, *CDKN1A* and *CDKN1B*, which encode the pro-apoptotic BCL-2 family member BIM, $p21^{Waf1/Cip1}$ and $p27^{Kip1}$ (400, 510), respectively. Given the important role of FOXO1 in controlling the activity of these genes, we assessed their expression as an indicator of FOXO1 regulation. The expression of $p21^{Waf1/Cip1}$ was slightly lower (p = 0.11) in HG-3 cells compared to MEC1 cells (Figure 3.6g). Notably, the expression of the FOXO1 targets $p27^{Kip1}$ was significantly lower in HG-3 cells compared to MEC1 cells (Figure 3.6h). Also, expression of BIM isoforms (BIM_{EL}, BIM_L, BIM_S) was significantly lower in MEC1 compared to HG-3 cells (Figure 3.6i).

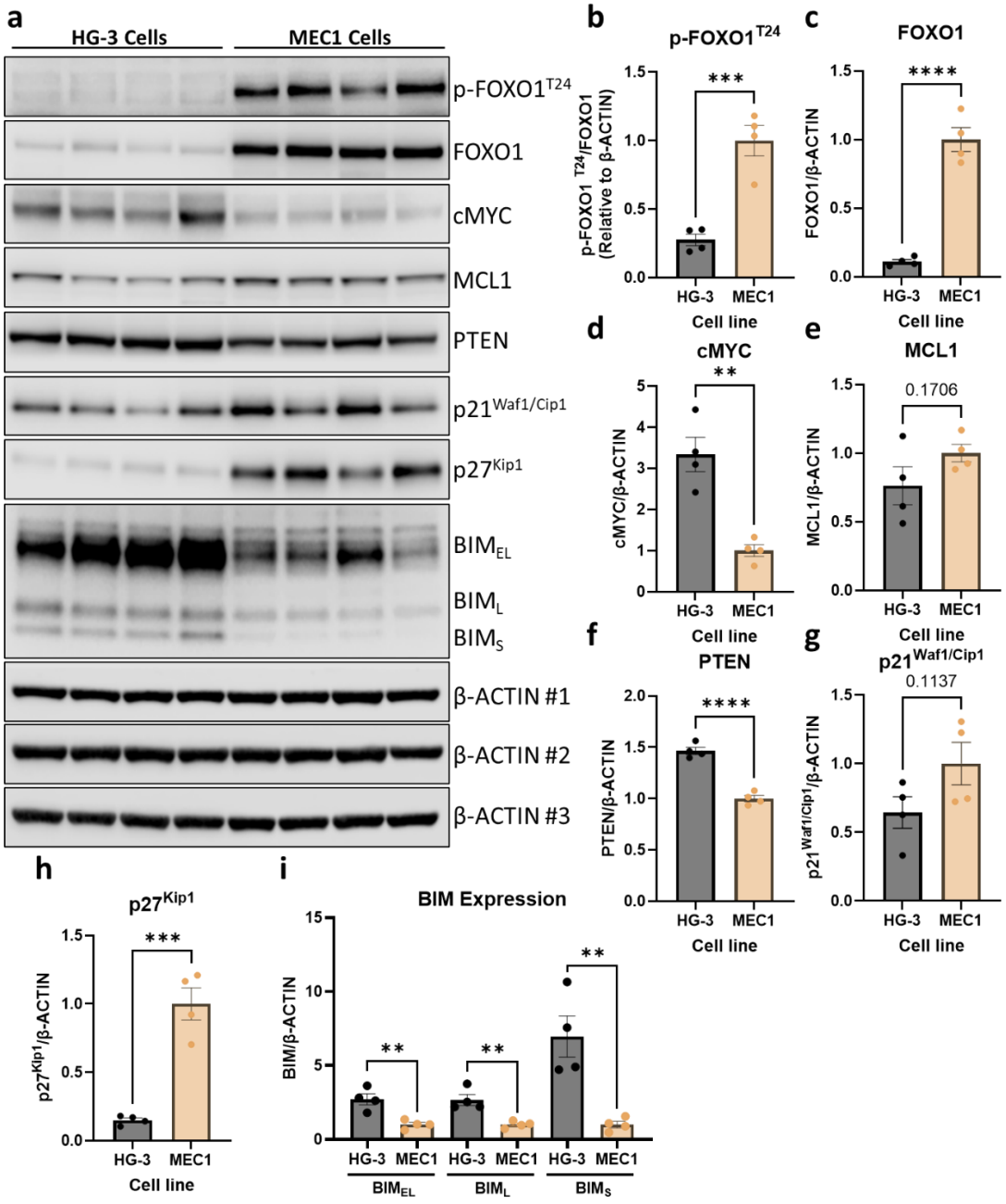

Figure 3.6: CLL cell lines indicated a variability in FOXO1^{T24} phosphorylation and total FOXO1 expression.

(a) Representative Western blot to assess protein expression of HG-3 cells (n = 4) compared with MEC1 cells (n = 4), probed for p-FOXO1^{T24}, FOXO1, cMYC, MCL1, PTEN, p21$^{Waf1/Cip1}$, p27^{Kip1}, BIM and β-ACTIN (loading control; #1, #2, and #3 representing mirror blots). Relative protein expression of (b) p-FOXO1^{T24}, (c) FOXO1, (d) cMYC, (e) MCL1, (f) PTEN, (g) p21$^{Waf1/Cip1}$, (h) p27^{Kip1}, and (i) BIM isoforms (EL, L, S) between HG-3 cells (HG-3; black bars; n = 4) and MEC1 cells (MEC1 = beige bar; n = 4). Samples were normalised to loading control β-ACTIN. The mean expression levels of proteins in MEC1 cells were used to calculate the relative protein expression levels of MEC1 cells and HG-3 cells. Each dot represented an individual datapoint. Data expressed as the mean ± SEM. Statistics calculated by unpaired t-test (b-i); ** $p \leq 0.01$, *** $p \leq 0.001$, **** $p \leq 0.0001$.

3.3.5 F(ab')$_2$ stimulation rapidly upregulates FOXO1 in primary CLL cells

To demonstrate the signalling capacity of the BCR in primary CLL cells, we examined the phosphorylation status of AKT^{S473} and FOXO1^{T24} upon BCR stimulation in comparison with unstimulated CLL cells (Figure 3.7a). These data indicated that the level of phosphorylation of AKT^{S473} was significantly upregulated at 0.5 hr up to 1 hr in F(ab')$_2$ stimulated CLL cells compared to unstimulated cells, while between 2 hr and 24 hr, AKT^{S473} phosphorylation reduced to basal levels (Figure 3.7b). Total AKT expression displayed steady levels across all BCR stimulation time points (Figure 3.7c). The phosphorylation of FOXO1^{T24} and Total FOXO1 levels followed a similar trend as AKT^{S473} phosphorylation, with both FOXO1^{T24} phosphorylation and total FOXO1 significantly upregulated at 0.5 hr up to 1 hr in F(ab')$_2$ stimulated CLL cells compared to unstimulated (Figure 3.7d). This upregulation in FOXO1^{T24} phosphorylation and total FOXO1 was sustained up to 2 hr, followed by reduction to basal level beyond 2 hr up to 24 hr of F(ab')$_2$ stimulation (Figure 3.7d & e).

MCL1 protein levels in F(ab')$_2$ stimulated CLL cells were significantly increased compared to unstimulated cells (Figure 3.7f). This increase was sustained up to 4 hr of F(ab')$_2$ stimulation, followed by non-significant elevation up to 24 hr (Figure 3.7f). While the expression of PTEN was unaffected by F(ab')$_2$ stimulation in the early timepoint (0.5 hr to 4 hr), the protein level of PTEN was significantly increased at 24 hr of stimulation (Figure 3.7g).

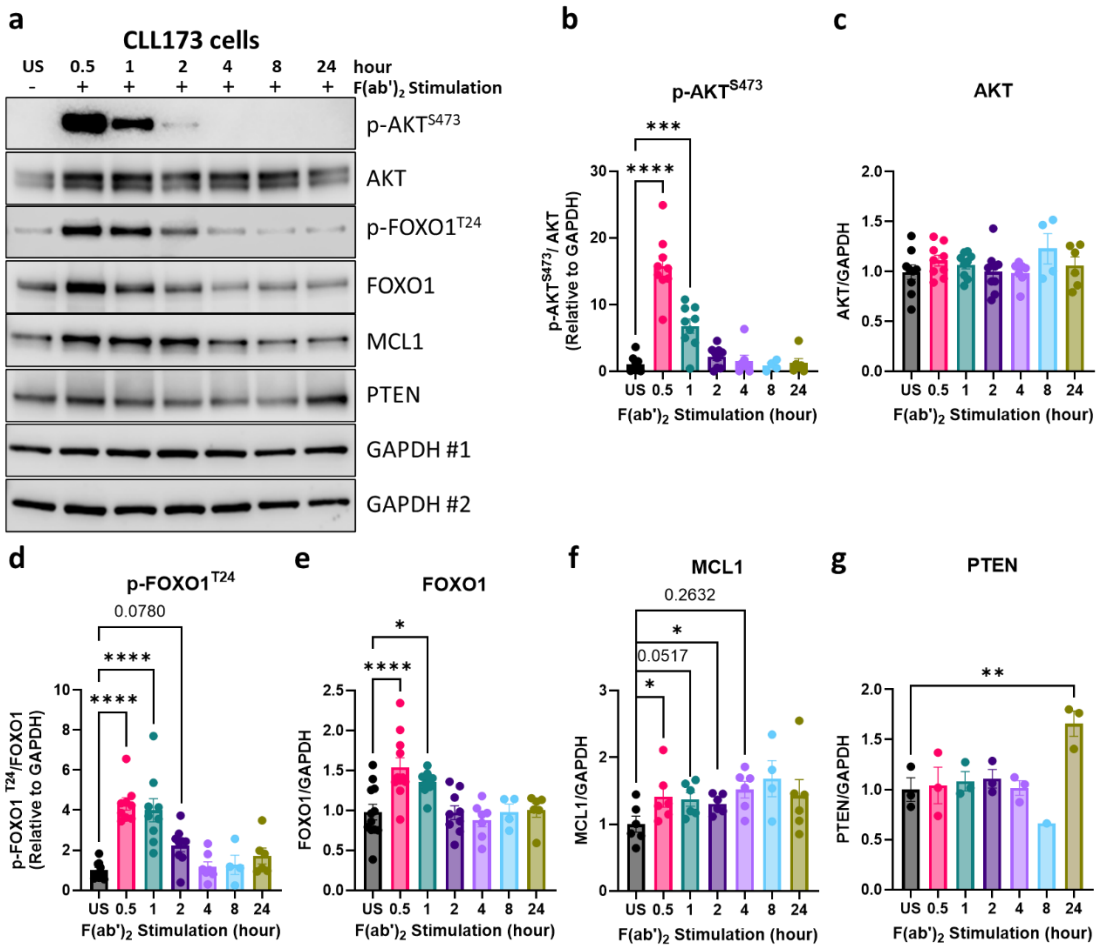

Figure 3.7:**Time-course of FOXO1 expression upon BCR crosslinking.**
(a) Representative Western blot of primary CLL sample (CLL173 patient sample), unstimulated (US; -) or stimulated (+) with F(ab')$_2$ fragments (10 ng/mL) for the indicated timepoints (hour; hr), (0.5 – 24 hr). The blot was probed for antibodies for AKT^{S473}, AKT, FOXO1^{T24}, FOXO1, MCL1, PTEN and GAPDH (loading control; #1 and #2 representing mirror blots). Relative protein expression of (b) p-AKT^{S473}, (c) AKT, (d) p-FOXO1^{T24}, (e) FOXO1, (f) MCL1, and (g) PTEN between unstimulated (US = black bar; n ≥ 3) and F(ab')$_2$ stimulated for (0.5 hr = pink bar; n ≥ 3), (1 hr = navy bar; n ≥ 3), (2 hr = purple bar; n ≥ 3), (4 hr = light purple bar; n ≥ 3), (8 hr = blue bar; n ≥ 1), (24 hr = oil green bar; n ≥ 3). Samples were normalised to loading control GAPDH. The mean expression levels of proteins in unstimulated were used to calculate the relative protein expression levels of unstimulated and F(ab')$_2$ stimulated timepoints. Each dot represented an individual datapoint. Data expressed as the mean ± SEM. Statistics calculated by One-way ANOVA, Dunnett test (b-g); * p ≤ 0.05, ** p ≤ 0.01, *** p ≤ 0.001, **** p ≤ 0.0001.

The expression of p21$^{Waf1/Cip1}$ was modestly increased in 1 hr to 2 hr of F(ab')$_2$ stimulation, followed by reduction to basal level in timepoints after 2 hr up to 24 hr (Figure 3.8a & b). However, p27^{Kip1} expression was unaffected by F(ab')$_2$ stimulation, indicating no changes in expression in all timepoints (Figure 3.8c). Lastly, ZAP-70 protein levels in F(ab')$_2$ stimulated CLL cells were significantly increased compared to unstimulated (Figure 3.8d). This increase

in protein levels was sustained up to 4 hr of F(ab')$_2$ stimulation, followed by non-significant elevation up to 24 hr (Figure 3.8d).

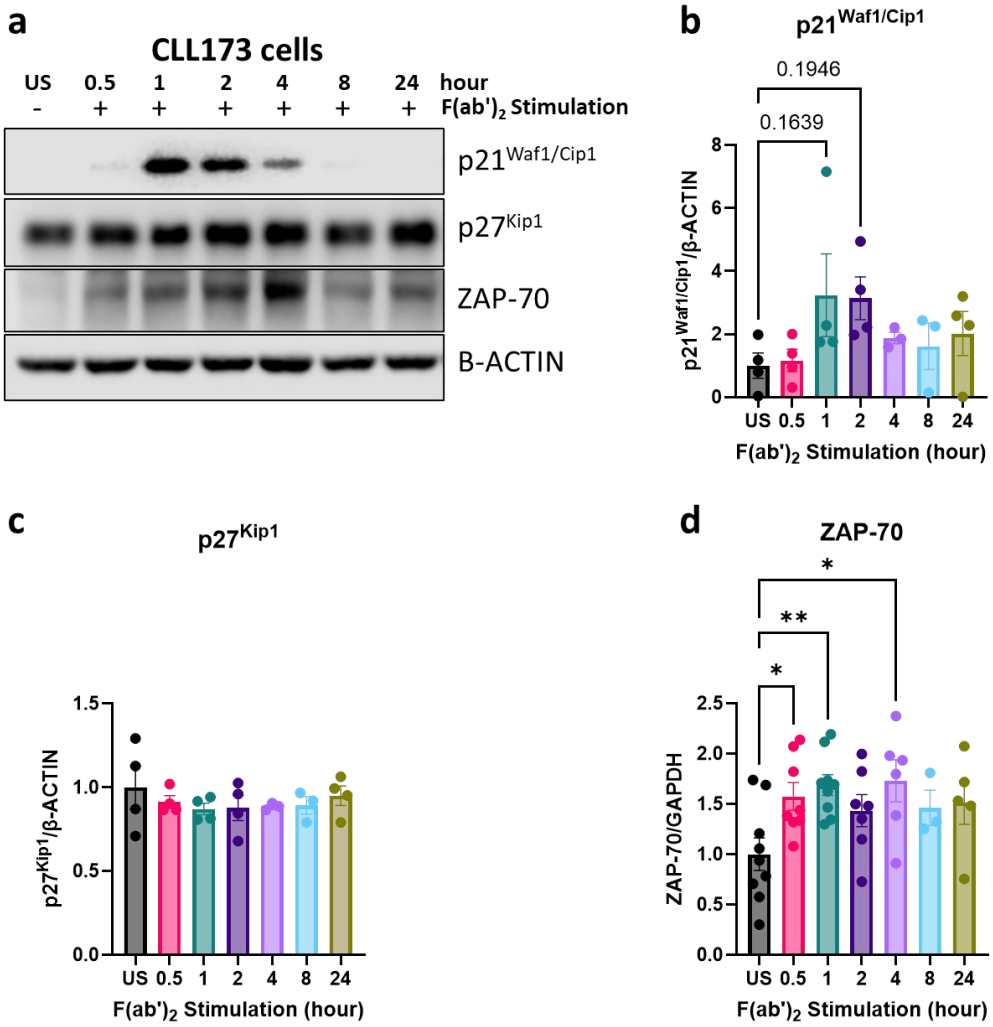

Figure 3.8:ZAP-70 protein expression was stabilised upon BCR crosslinking with F(ab')$_2$. (a) Representative Western blot of primary CLL sample (CLL173 patient sample), unstimulated (US; -) or stimulated (+) with F(ab')$_2$ fragments (10 ng/mL) for the indicated timepoints (hour; hr), (0.5 – 24 hr). The blot was probed for p21$^{Waf1/Cip1}$, p27^{Kip1}, ZAP-70, and β-ACTIN (loading control). Relative protein expression of (b) p21$^{Waf1/Cip1}$, (c) p27^{Kip1}, and (d) ZAP-70 between unstimulated (US = black bar; n ≥ 4) and F(ab')$_2$ stimulated for (0.5 hr = pink bar; n ≥ 4), (1 hr = navy bar; n ≥ 4), (2 hr = purple bar; n ≥ 4), (4 hr = light purple bar; n ≥ 3), (8 hr = blue bar; n ≥ 3), (24 hr = oil green bar; n ≥ 4). Samples were normalised to loading control β-ACTIN. The mean expression levels of proteins in unstimulated were used to calculate the relative protein expression levels of unstimulated and F(ab')$_2$ stimulated timepoints. Each dot represented an individual datapoint. Data expressed as the mean ± SEM. Statistics calculated by One-way ANOVA, Dunnett test (b-d); * p ≤ 0.05, ** p ≤ 0.01.

Building on this data, F(ab')$_2$-induced BCR signalling led to rapid upregulation of FOXO1^{T24} phosphorylation expression within 0.5 hr (Figure 3.9a & b). Consistent with earlier observations (Figure 3.7d & e), FOXO1 expression was rapidly and significantly upregulated in all CLL patient cells assessed following F(ab')$_2$ stimulation (Figure 3.9c).

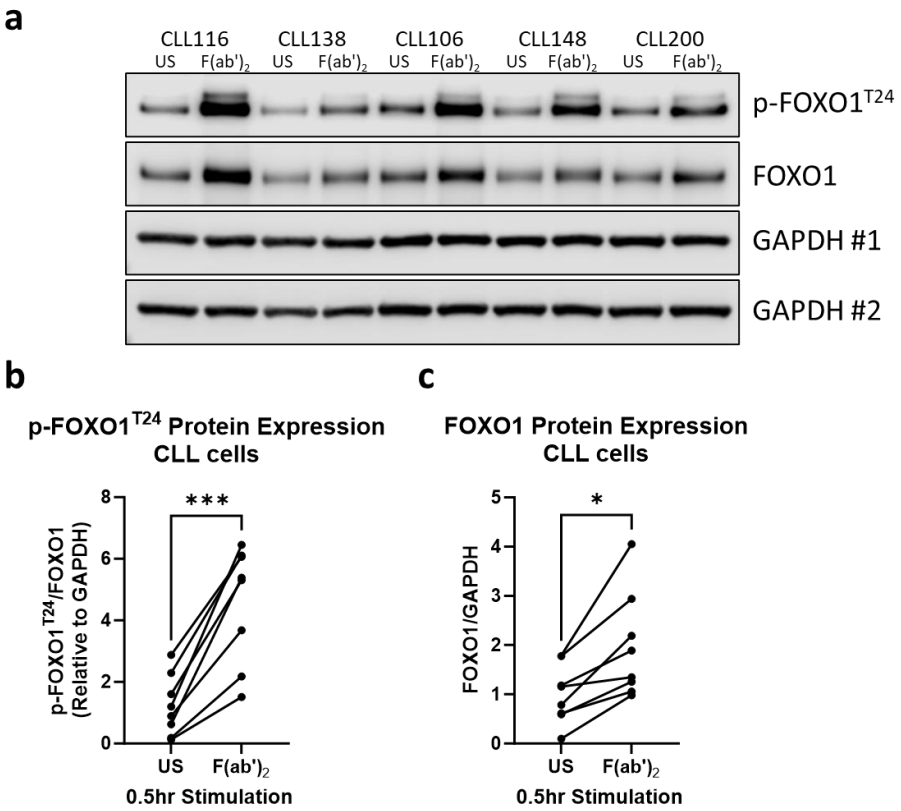

Figure 3.9: Short-term F(ab')$_2$ stimulation promotes FOXO1 upregulation and phosphorylation downstream of BCR.

(a) Representative Western blot of primary CLL samples (CLL116, CLL138, CLL106, CLL148, CLL200), unstimulated (US) or stimulated with F(ab')$_2$ fragments (10 ng/mL) for (0.5 hr). The blot was probed for p-FOXO1^{T24}, FOXO1, and GAPDH (loading control; #1 and #2 representing mirror blots). Relative protein expression of (b) p-FOXO1^{T24} (n = 8) and (c) FOXO1 (n = 8) between unstimulated (US) and F(ab')$_2$ stimulated, which were represented by dots connected by individual black line for each datapoint. Samples were normalised to loading control GAPDH. Data expressed as the mean ± SEM. Statistics calculated by paired t-test (b & c); * $p \leq 0.05$, *** $p \leq 0.001$.

3.3.6 The phosphorylation of FOXO1^{T24} and total FOXO1 were reduced by ibrutinib treatment in MEC1 cells

To further investigate the role of BCR signalling in regulating the expression of p-FOXO1^{T24} and total FOXO1, MEC1 cells were treated with the BTK inhibitor ibrutinib for 1 hr and 24 hr (Figure 3.10a). The data revealed that inhibition of BCR signalling by ibrutinib induced a significant downregulation of AKT^{S473} phosphorylation at 1 hr and 24 hr of treatment compared to untreated in MEC1 cells (Figure 3.10b). Notably, this downregulation was significantly greater at 1 hr compared to 24 hr (Figure 3.10b). The expression levels of AKT protein were unaffected by ibrutinib treatment at both 1 hr and 24 hr compared to

untreated (Figure 3.10c). Ibrutinib induced downregulation of FOXO1^{T24} phosphorylation mirroring its effects on AKT^{S473} phosphorylation (Figure 3.10d). This reduction of FOXO1^{T24} phosphorylation at 1 hr of ibrutinib treatment was significantly greater than 24 hr treatment (Figure 3.10d). Interestingly, the protein expression levels of FOXO1 were significantly downregulated at 1 hr of ibrutinib treatment compared to untreated MEC1 cells (Figure 3.10e). However, the expression levels of FOXO1 at 24 hr were unaffected by ibrutinib treatment compared to untreated (Figure 3.10e).

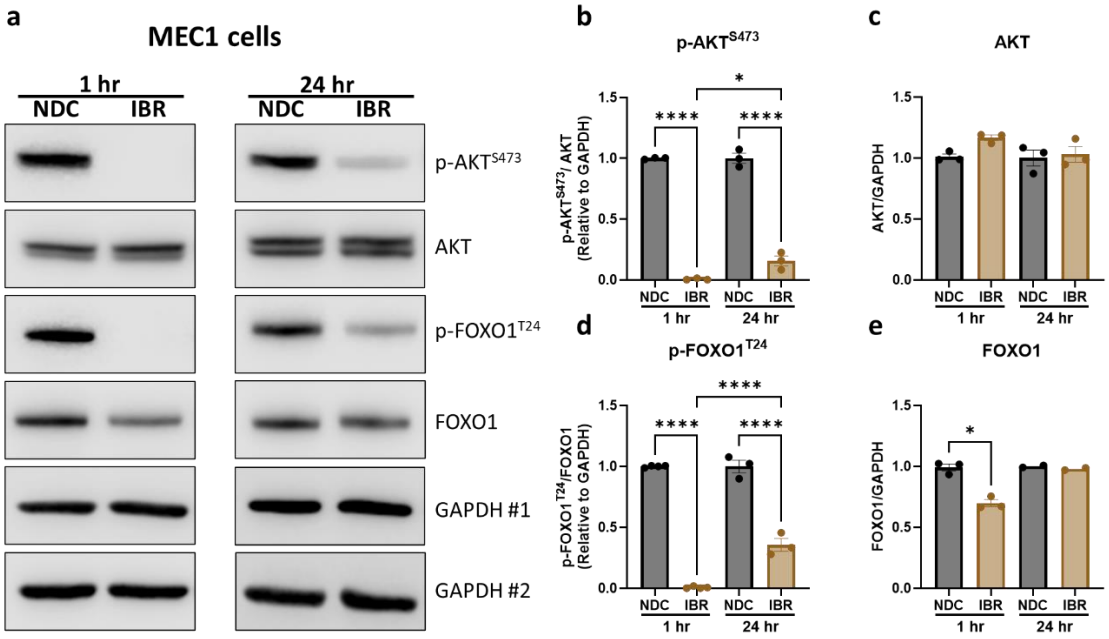

Figure 3.10: The protein expression of FOXO1 was significantly downregulated by short-term inhibition with ibrutinib in MEC1 cells.

(a) Representative Western blot of MEC1 cells, treated with ibrutinib (IBR; 1 µM) for the indicated timepoints (1 hr and 24 hr; hour) or no drug control (NDC; DMSO). The blots were probed for AKT^{S473} phosphorylation, AKT, FOXO1^{T24} phosphorylation, FOXO1, and GAPDH (loading control; #1 and #2 representing mirror blots). Relative protein expression of (b) p-AKT^{S473} (c) AKT, (d) p-FOXO1^{T24}, and (e) FOXO1 between no drug control (NDC/DMSO = black bar; n ≥ 2) and ibrutinib (IBR = brown bar; n ≥ 2) at 1 µM for (1 hr and 24 hr) timepoints. Samples were normalised to loading control GAPDH. The mean expression levels of proteins in NDC were used to calculate the relative protein expression levels of NDC and ibrutinib treatment at the indicated timepoints. Each dot represented an individual datapoint. Data expressed as the mean ± SEM. Statistics calculated by One-way ANOVA, Tukey test (b-e); * $p \leq 0.05$, **** $p \leq 0.0001$.

3.3.7 Phosphorylation of FOXO1^{T24} and total FOXO1 were reduced to baseline levels by ibrutinib in F(ab')$_2$ stimulated CLL patient cells

To explore the role of BCR signalling in regulating the expression of FOXO1, CLL patient samples were pre-treated for 1 hr with ibrutinib followed by BCR crosslinking with F(ab')$_2$

for 0.5 hr (Figure 3.11a). The data showed a significant increase in AKT^{S473} phosphorylation levels upon BCR crosslinking with F(ab')$_2$ compared to unstimulated CLL patient cells (Figure 3.11b). This elevation in AKT^{S473} phosphorylation levels were reversed by ibrutinib treatment, restoring AKT^{S473} phosphorylation levels to baseline (Figure 3.11b). No changes in AKT levels were noted by F(ab')$_2$ simulation or ibrutinib treatment (Figure 3.11c), similar to MEC1 cells (Figure 3.10). Further, the expression levels of FOXO1^{T24} phosphorylation significantly increased in stimulated CLL cells compared to unstimulated controls (Figure 3.11d). This upregulation of FOXO1^{T24} phosphorylation was significantly reduced by ibrutinib treatment, restoring FOXO1^{T24} phosphorylation to baseline levels (Figure 3.11d), mirroring the effect of ibrutinib on AKT^{S473} phosphorylation. Similarly, FOXO1 protein levels were significantly upregulated upon BCR stimulation with F(ab')$_2$ and were significantly downregulated by ibrutinib, restoring FOXO1 expression to unstimulated levels (Figure 3.11e).

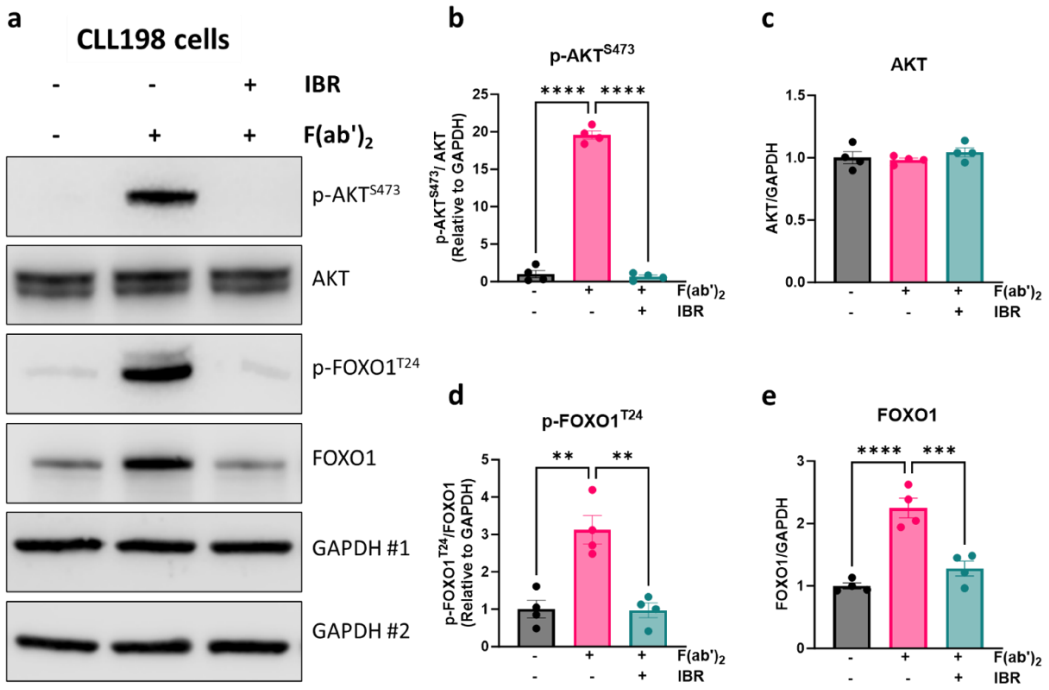

Figure 3.11: Upregulation of FOXO1 expression upon BCR crosslinking was significantly downregulated by ibrutinib treatment in CLL patient cells.

(a) Representative Western blot of CLL patient cells (CLL198), the cells were pre-treated for 1 hr with ibrutinib (IBR (+); 1 µM) for 1 hr or untreated (DMSO (-)), followed by 0.5 hr stimulation (+) or no stimulation (DMSO (-)) by F(ab')$_2$ fragment (10 ng/mL). The blots were probed for p-AKT^{S473}, AKT, p-FOXO1^{T24}, FOXO1, and GAPDH (loading control; #1 and #2 representing mirror blots). Relative protein expression of (b) p-AKT^{S473} (c) AKT, (d) p-FOXO1^{T24}, and (e) FOXO1 between unstimulated/untreated (F(ab')$_2$/IBR$^{-/-}$ = black bar; n = 4), stimulated/untreated (F(ab')$_2$/IBR$^{+/-}$ = pink bar; n = 4), and stimulated/ibrutinib treated (F(ab')$_2$/IBR$^{+/+}$ = blue bar; n = 4). Samples were normalised to loading control GAPDH. The mean expression levels of proteins in F(ab')$_2$/IBR$^{-/-}$ were used to calculate the relative protein expression levels. Each dot represented an individual

datapoint. Data expressed as the mean ± SEM. Statistics calculated by One-way ANOVA, Tukey test (b-e); ** $p \leq 0.01$, **** $p \leq 0.0001$.

3.3.8 FOXO1 was slightly upregulated in three-month post-ibrutinib *ex-vivo* CLL cells

It has been reported that ibrutinib treatment reduces BCR-mediated stimulation of $S6^{S235/236}$, AKT^{S473} and $FOXO^{T24}$ phosphorylation to baseline level in CLL cells *in vitro* (412). We were interested in examining BCR signalling activity by looking at the phosphorylation of AKT and FOXO1 expression in early post-ibrutinib treated patient samples. The samples were obtained from *ex-vivo* PB-derived CLL cells before treatment and after up to three-months of ibrutinib treatment, and phosphorylation levels of AKT^{S473} and $FOXO1^{T24}$ as well as FOXO1 expression were determined (Figure 3.12a). AKT^{S473} phosphorylation did not significantly differ between pre- and post-ibrutinib CLL cells (Figure 3.12b). Downstream of AKT, phosphorylation of $FOXO1^{T24}$ was downregulated ($p = 0.19$) in three out of four patient samples in post-ibrutinib treatment compared to pre-treatment (Figure 3.12c). In contrast to phosphorylation of $FOXO1^{T24}$, total FOXO1 expression was upregulated in all post- compared to pre-ibrutinib with a variation in FOXO1 expression between CLL patient samples (Figure 3.12d). Furthermore, the expression of PTEN levels were demonstrably elevated ($p = 0.06$) in post- compared to pre-treatment samples (Figure 3.12e). To a lesser extent, $p21^{Waf1/Cip1}$ was increased ($p = 0.26$) in post- compared to pre-ibrutinib treatment samples (Figure 3.12f). Notably, $p27^{Kip1}$ protein levels were significantly upregulated in post- compared to pre-treatment (Figure 3.12g), which aligns with elevated expression of FOXO1 in these patient samples. The protein levels of BIM isoforms indicated an increase level of BIMs (BIM_{EL}, BIM_L, BIM_S), while BIM_{EL} and BIM_S only showed a trend toward increased expression in post- compared to pre-ibrutinib samples, BIM_L exhibited a statistically significant increase in post- compared to pre-ibrutinib (Figure 3.12h). These findings suggest that FOXO1 activity is upregulated in ibrutinib-treated patients.

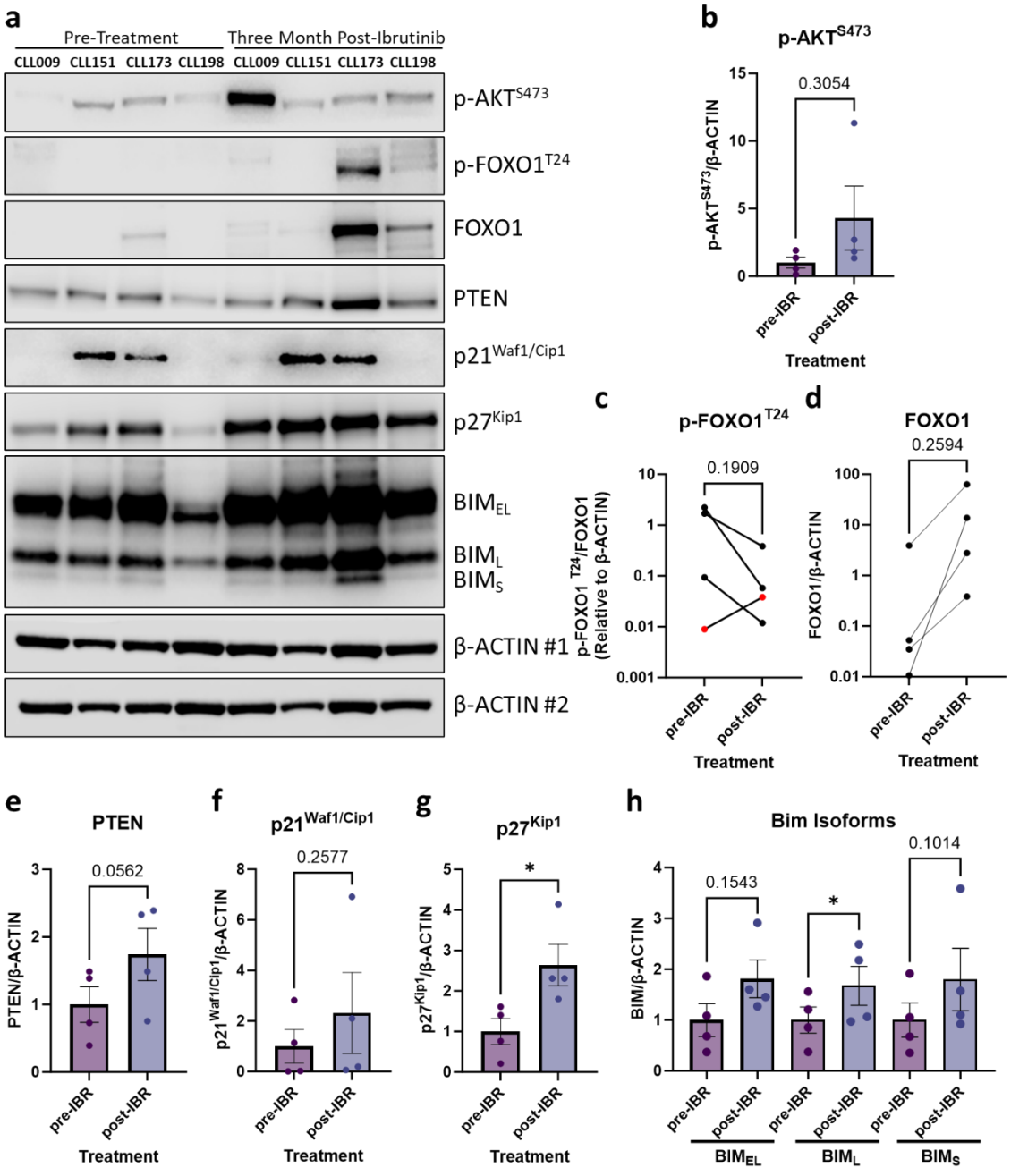

Figure 3.12: p27^{Kip1} expression was upregulated in three-month post-ibrutinib *ex-vivo* CLL cells.

(a) Representative Western blot of *ex-vivo* PB-derived CLL patient samples to assess protein expression of pre-ibrutinib treatment (pre-treatment) compared with three months post-ibrutinib patient samples (CLL009, CLL151, CLL173, CLL198), probed for p-AKT^{S473}, p-FOXO1^{T24}, FOXO1, PTEN, p21$^{Waf1/Cip1}$, p27^{Kip1}, BIM, and β-ACTIN (loading control; #1 and #2 representing mirror blots). Relative protein expression of (b) p-AKT^{S473}, (c) p-FOXO1^{T24}, (d) FOXO1 in pre-IBR and post-IBR samples are shown, with CLL173 sample shown as red dot. (e) PTEN, (f) p21$^{Waf1/Cip1}$, (g) p27^{Kip1}, and (h) BIM isoforms (EL, L, S) between pre-ibrutinib (pre-IBR = purple bar; n = 4) and three months post-ibrutinib (post-IBR = blue bar; n =4). Samples were normalised to loading control β-ACTIN. The mean expression levels of proteins in pre-IBR were used to calculate the relative protein expression levels of pre-IBR and post-IBR. Each dot represented an individual datapoint. Data expressed as the mean ± SEM. Statistics calculated by unpaired t-test (b-h); * $p \leq 0.05$.

3.3.9 FOXO family members were unaffected by F(ab')$_2$ stimulation at the transcriptional level

To address whether the noted upregulation of FOXO1 was post-translational, we initially investigated the transcriptional levels of FOXO family members in F(ab')$_2$ stimulated CLL cells. The CLL cells were stimulated from 0.5 to 24 hr with F(ab')$_2$ fragment (Figure 3.13). The data showed that *FOXO1*, *FOXO3* and *FOXO4* did not statistically change in transcriptional levels with stimulation (Figure 3.13a, b, c). However, the data indicated a slight decrease in expression at 2 hr of stimulation for *FOXO1* and *FOXO3*, although this was not significant. *FOXO1* target genes including *BCL2L11* and *CCND2* also showed no significant differences between F(ab')$_2$ stimulated CLL cells and unstimulated (Figure 3.13d & e), which aligned with transcription levels of *FOXO1*. The mRNA level of early growth response 1 (*EGR-1*) was used as a positive indicator of F(ab')$_2$ stimulation (511, 512), which demonstrated a transient upregulation of *EGR-1* at 0.5 hr and 1 hr in F(ab')$_2$ stimulated compared to unstimulated (Figure 3.13f). The transcription levels of CASP8 and FADD-like apoptosis regulator (*cFLAR*), encoding for cellular FLICE (cFLIP) and regulated by the NF-κB pathway (513), were investigated as another pathway regulated by BCR activity. *cFLAR* mRNA levels were differentially expressed between CLL patient samples across the indicated timepoints, although showing no significant difference in expression between F(ab')$_2$ stimulated and unstimulated CLL cells (Figure 3.13g). The transcription levels of *MCL1* were unaffected by the crosslinking of BCR with F(ab')$_2$ fragment across the time-course between stimulated and unstimulated CLL patient cells (Figure 3.13h). The transcription levels of *MYC* were slightly but not significantly upregulated in stimulated CLL patient cells during the early timepoints (2 hr to 4 hr), then the levels were reduced later (6 hr to 24 hr) (Figure 3.13i).

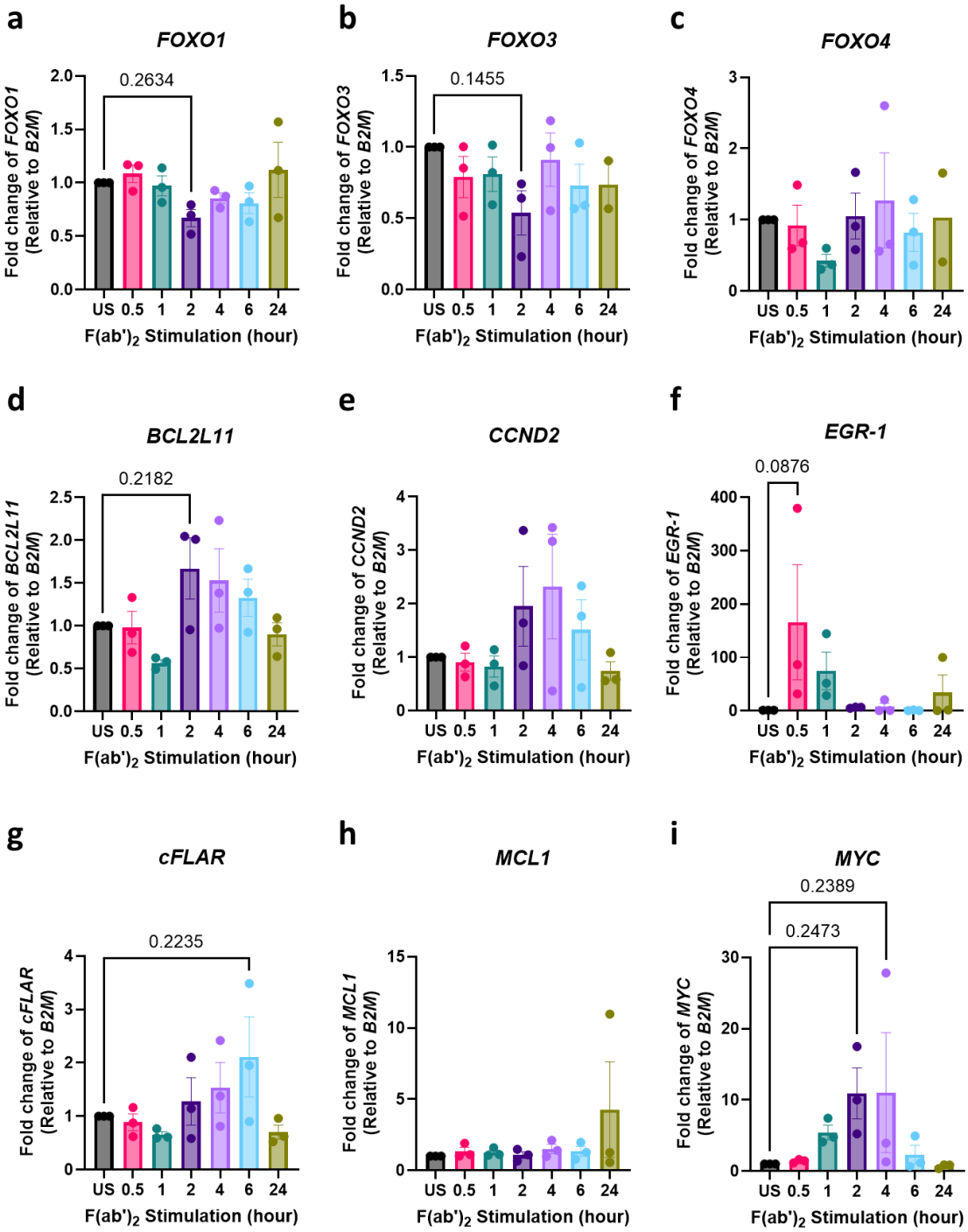

Figure 3.13: The mRNA levels of FOXO family members were unaffected upon BCR crosslinking with F(ab')$_2$ in primary CLL cells.

RT-qPCR to assess expression of *FOXO1*, *FOXO3*, *FOXO4*, *BCL2L11*, *CCND2*, *EGR-1*, *cFLAR*, *MCL1*, and *MYC* in unstimulated (US = black bar; n = 3) and F(ab')$_2$ (10 ng/mL) stimulated for (hour; hr), (0.5 hr = pink bar; n = 3), (1 hr = navy bar; n = 3), (2 hr = purple bar; n = 3), (4 hr = light purple bar; n = 3), (6 hr = blue bar; n = 3), (24 hr = oil green bar; n ≥ 2) primary CLL cell samples. The $\Delta\Delta C_T$ method was used to calculate expression levels, where samples were normalised to housekeeping gene *B2M*. Each dot represented an individual datapoint. Data expressed as the mean ± SEM. Statistics calculated by One-way ANOVA, Dunnett test.

3.3.10 Gene expression levels of DUB enzymes in *ex-vivo* CLL cells compared to B-cells from healthy donor

In section 3.3.9, the transcriptional levels of *FOXO1* were unaffected by BCR crosslinking with $F(ab')_2$, suggesting that the rapid upregulation of FOXO1 occurs post-translationally. As it has been reported, FOXO family members are post-translationally modified by phosphorylation, ubiquitination/deubiquitylation, acetylation/deacetylation, and methylation (326, 514), we investigated DUB enzyme regulation of FOXO1 protein. USP7 was reported to have a regulatory role with FOXOs family in CLL cells (360, 460). BCR ligation has also been shown to upregulate the expression of ZAP-70 and MCL1 which can be stabilised by deubiquitylation (466, 482). Therefore, it was of interest to examine the gene expression levels of individual DUB enzymes (*USP7*, *USP9x* and *USP14*) in *ex-vivo* primary CLL cells. The data revealed no significant difference in *USP7* mRNA levels between CLL cells and $CD19^+$ B-cells derived from healthy donors (Figure 3.14a). Interestingly, *USP9x* was significantly reduced in *ex-vivo* primary CLL cells, compared to B-cells from healthy donors (Figure 3.14b). Similar to *USP7*, the expression of *USP14* did not differ between CLL cells and heathy controls (Figure 3.14c). Stratification of DUB gene expression based on cytogenetic abnormalities (Figure 3.12d - f), Binet stages, treatment status and gender indicated that the transcript levels of *USP7*, *USP9x* and *USP14* were not significantly different (data not shown).

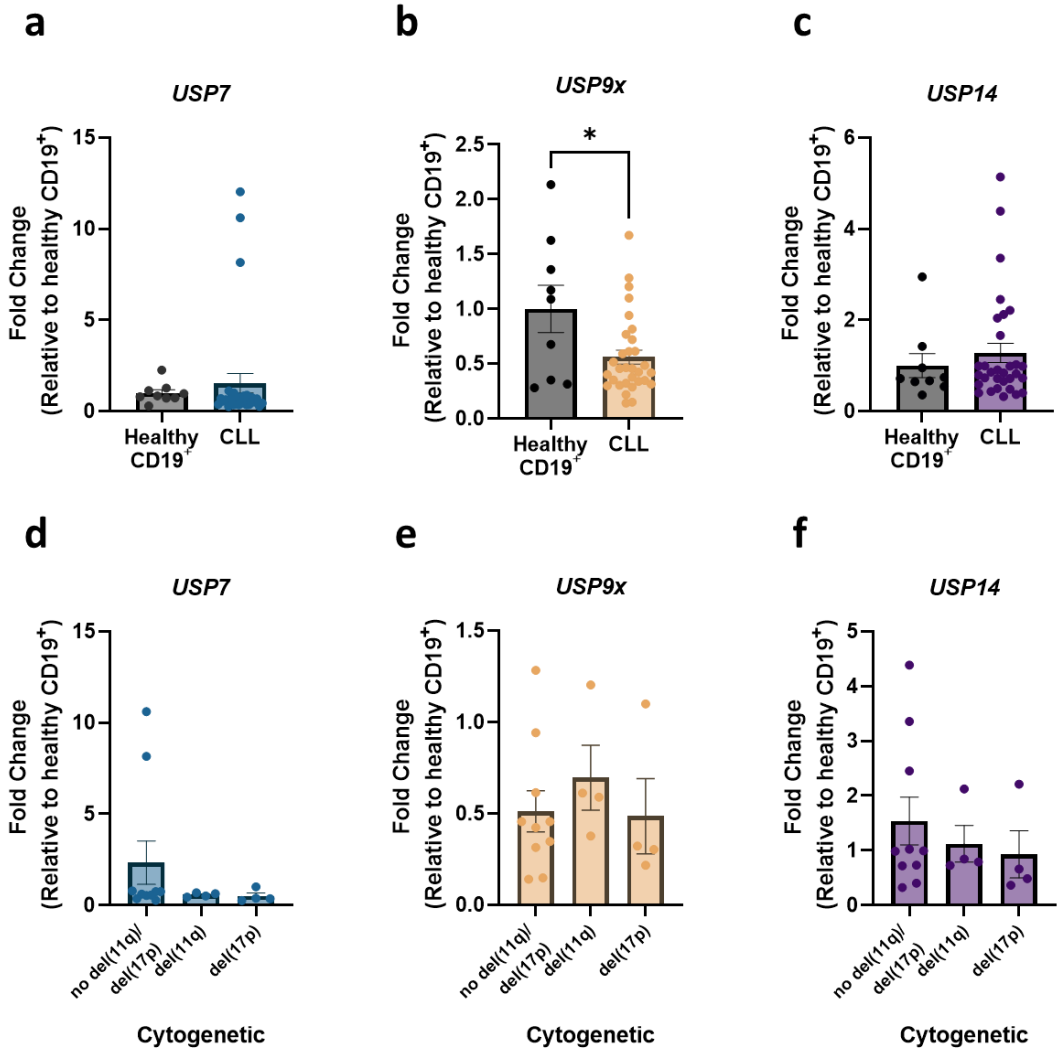

Figure 3.14: DUB expression in *ex-vivo* CLL patient cells compared to healthy B-cells.
(a-c) RT-qPCR to assess expression levels of *USP7, USP9x,* and *USP14* in B-cell from healthy donor (Healthy $CD19^+$; black bars; n = 9) and *ex-vivo* PB-CLL patient samples (CLL; *USP7* = blue bar, *USP9x* = beige bar, *USP14* = purple bar; n = 32). RT-qPCR to assess expression levels of (d) *USP7* (blue bar), (e) *USP9x* (orange bar), and (f) *USP14* (purple bar) in CLL patient samples stratified by cytogenetic abnormalities as indicated. The ΔC_T method was used to calculate expression levels, where samples were normalised to housekeeping gene *GAPDH*. The mean gene expression levels of DUB family members in $CD19^+$ were used to calculate the relative gene expression levels of healthy B-cells and CLL cells. Each dot represented an individual datapoint. Data expressed as the mean ± SEM. Statistics calculated by unpaired t-test (a-c) or One-way ANOVA, Tukey test (d-f); * $p \leq 0.05$.

3.3.11 Protein expression levels of DUB enzymes in *ex-vivo* CLL cells compared to B-cells from healthy donors

Intriguingly, the STRING database indicated that FOXO1 expression is associated with USP7, which in turn is linked by co-expression with USP8, USP10, USP14 and USP28, all of which are reported to be linked with haematological malignancies (467, 515-517) (Figure 3.15).

As those DUB proteins were associated with the expression of USP7 protein, we examine their protein expression in CLL cells compared to healthy $CD19^+$ B-cells (Figure 3.16a & d). Protein expression of USP7 was significantly upregulated in CLL cells, compared with healthy controls (Figure 3.16a & b). Stratification of USP7 expression levels based on cytogenetic abnormalities indicated an upregulation of USP7 (p = 0.07) in patient CLL cells harbouring either one or both del(11q)/del(17p) compared to CLL cells with undetectable cytogenetic aberration (Figure 3.16b). Similarly, significant upregulation of USP9x expression levels were observed in CLL cells, compared to healthy B-cells, with a trend toward upregulation (p = 0.07) in patient harbouring poorer cytogenetic abnormalities compared to patients with no cytogenetic abnormalities (Figure 3.16c). The expression levels of USP1 were examined and the data indicated a trend toward upregulation (p = 0.09) of USP1 in CLL patient samples compared to healthy controls (Figure 3.16d & e). Stratification of USP1 based on cytogenetic abnormalities revealed a demonstrable upregulation in CLL patient cells with poorer cytogenetic aberrations compared to normal cytogenetic CLL cells (Figure 3.16e). The expression levels of USP8 (Figure 3.16f), USP10 (Figure 3.16g), and USP14 (Figure 3.16h) were significantly elevated in CLL patient cells compared to healthy $CD19^+$ B-cells. Stratification of these proteins in regard to the present or absence of cytogenetic abnormalities revealed no significant differences between patients harbouring poorer cytogenetics aberration and normal cytogenetic CLL patient cells (Figure 3.16f, g, h). The expression of USP18 and USP28 were examined, and their levels were slightly elevated (p = 0.22) and (p =0.16), respectively, in CLL patient cells compared to healthy controls (Figure 3.16i, j). Stratification of these proteins according to cytogenetic abnormalities indicated no changes in the expression of USP18 and USP28 in CLL patient cells harbouring poorer cytogenetic abnormalities and undetectable cytogenetic (Figure 3.16i, j). Additionally, further stratification of the DUB protein expression levels in CLL patient samples according to Binet staging, patients' gender and treatment status showed that the protein expression of USP1, 7, 10, 14 and 18 were similar across Binet stages, whereas USP8, 9x, 28 demonstrated a trend towards upregulation in poorer prognostic CLL subsets according to Binet stages (data not shown).

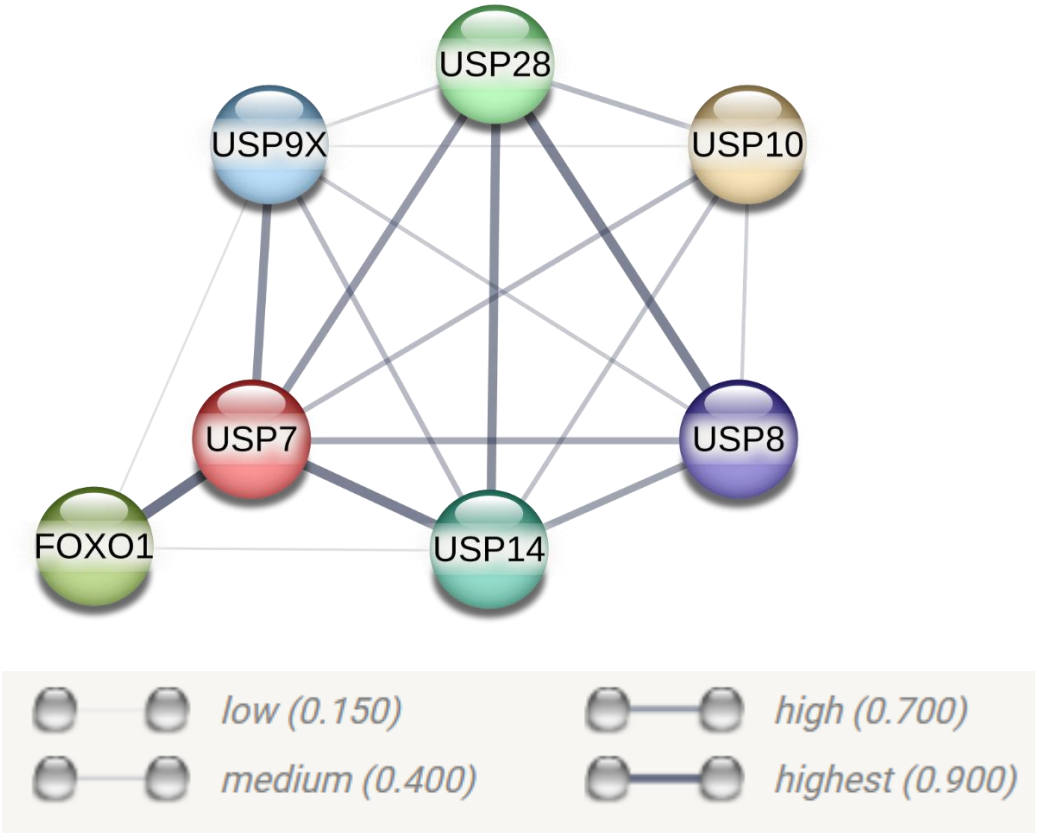

Figure 3.15: FOXO1 is linked to USP7 which is linked to other DUB proteins.
This protein-protein network interaction map was generated and downloaded from STRING database website (2021) (518). Proteins within this network were joined on multiple lines of evidence, including co-expression, co-occurrence, databases annotations, gene fusion events, experimental data, gene neighbourhood, and text-mining of scientific literature. The strength of evidence supporting each protein-protein association is represented by the thickness of the connecting lines. The confidence scores ranging from highest to lowest (0.900, 0.700, 0.400, 0.150) as indicated in the figure. These scores reflect the potential of a true interaction between the proteins.

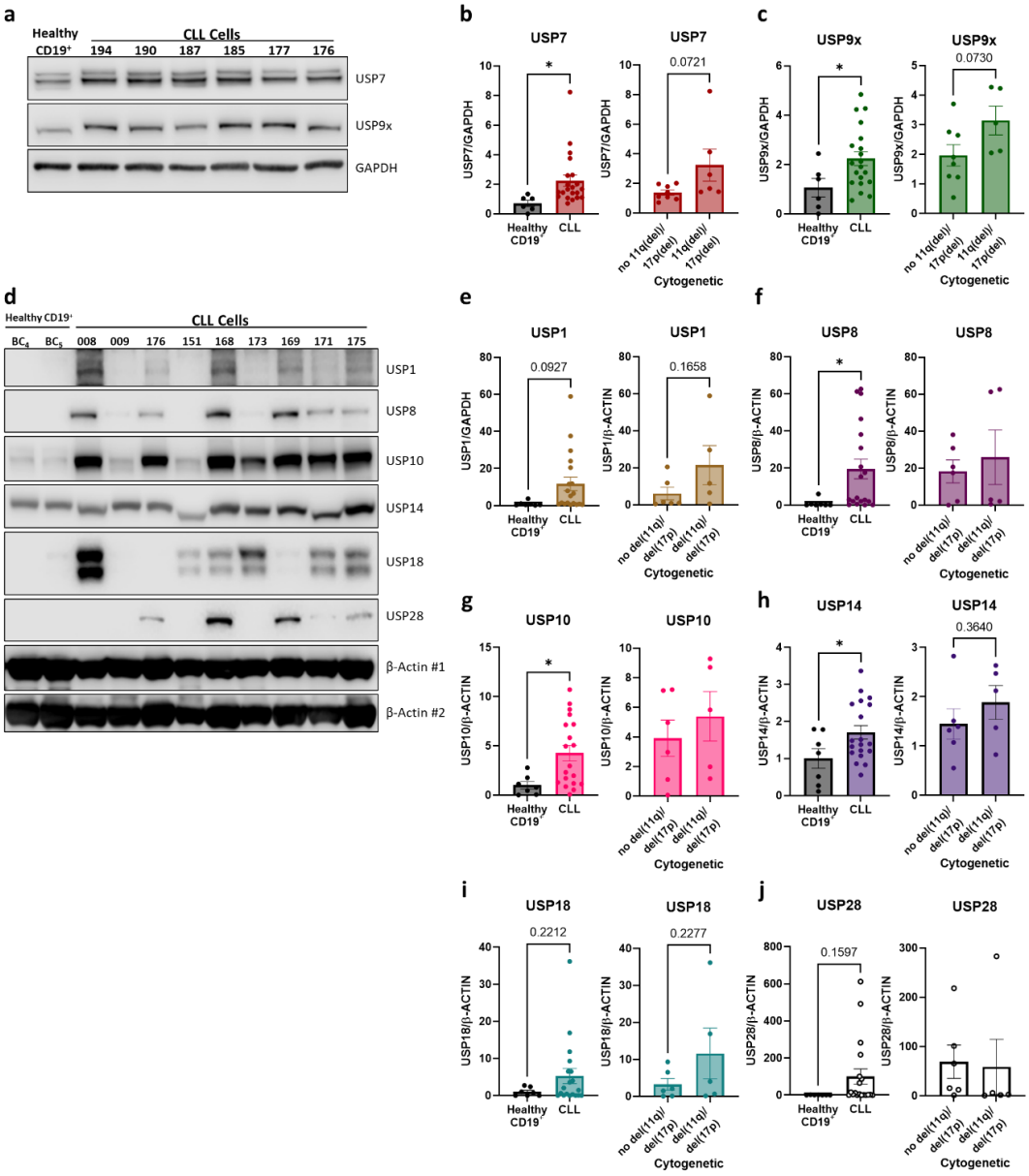

Figure 3.16: DUB family members are differentially expressed in *ex-vivo* CLL patient cells. (a) Representative Western blot to assess protein expression of *ex-vivo* PB-CLL patient cells compared with healthy CD19$^+$ cells from healthy donors, probed for USP7, USP9x, and GAPDH (loading control). (b, c) Relative protein expression of USP7 and USP9x between B-cell from healthy donors (Healthy CD19$^+$; black bars; n = 6) and CLL patient samples (CLL; USP7 = red bar, USP9x = green bar; n = 20). Assessing protein expression levels of (b) USP7 (red bar), (c) USP9x (green bar) in CLL patient samples stratified by cytogenetic abnormalities (no del(11q)/ del(17p); undetectable cytogenetic abnormalities, del(11q)/ del(17p); either one or both cytogenetics abnormalities were detected). (d) Representative Western blot to assess protein expression of *ex-vivo* PB-CLL patient cells compared with healthy CD19$^+$ cells from healthy donors (buffy coat; BC_4, BC_5), probed for USP1, USP8, USP10, USP14, USP18, USP28, and β-ACTIN (loading control; #1 and #2 representing mirror blots). (e - j) Relative protein expression of USP1, 8, 10, 14, 18, 28 between B-cell from healthy donors (Healthy CD19$^+$; black bars; n = 7) and CLL patient samples (CLL; USP1 = brown bar, USP8 = purple bar, USP10 = pink bar, USP14 = blue bar, USP18 = navy blue bar, USP28 = white bar; n = 19). Assessing protein expression levels of USP1, 8, 10, 14, 18 and 28 in CLL patient samples stratified by cytogenetic abnormalities presence or absence of del(11q)/del(17p) alone or together as described above. Samples were normalised to loading control β-ACTIN. The mean expression of proteins in healthy CD19$^+$ cells were used to calculate the relative protein expression levels of healthy B-cells

and CLL cells. Each dot represented an individual datapoint. Data expressed as the mean ± SEM. Statistics calculated by unpaired t-test (b, c, e-j); * p ≤ 0.05.

3.3.12 mRNA transcription levels of USP7 were significantly higher in MEC1 compared to HG-3 cells

We examined the transcription levels of DUBs in CLL cell lines; MEC1 (poor prognosis) and HG-3 (favourable prognosis) cells to determine *USP7*, *USP9x* and *USP14* levels (Figure 3.17). The data revealed that the transcription levels of *USP7* was significantly higher in MEC1 cells compared to HG-3 cells (Figure 3.17a). However, the transcription levels of *USP9x* were similar in both MEC1 and HG-3 cells (Figure 3.17b). Similarly, the data hinted that *USP14* transcription levels was similar in both cell lines (Figure 3.17c).

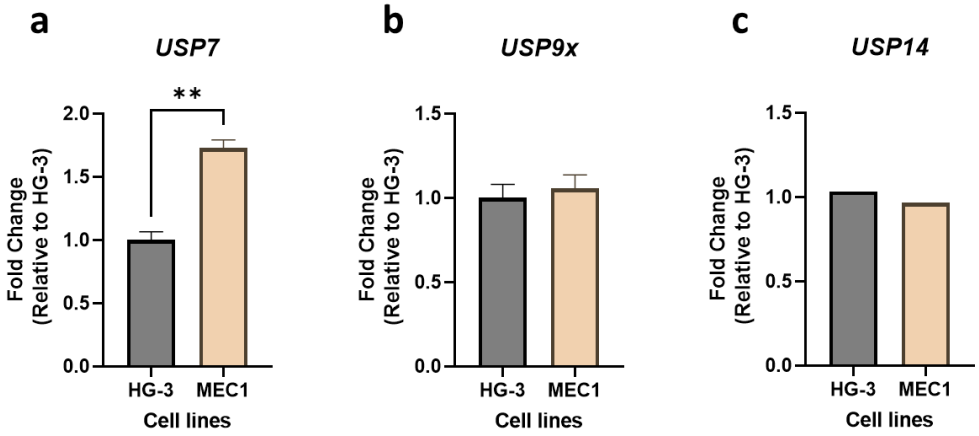

Figure 3.17: The transcriptional level of *USP7* was significantly upregulated in MEC1 compared with HG-3 cells.
(a, b) RT-qPCR to assess gene expression levels of *USP7* and *USP9x* in HG-3 cells (black bar; n = 3) and MEC1 cells (beige bar; n = 3). (c) RT-qPCR to assess gene expression levels of *USP14* in HG-3 cells (black bar; n = 1) and MEC1 cells (beige bar; n = 1). The ΔC_T method was used to generate expression levels, where samples were normalised to the reference gene (*GUSB*) and the mean fold change of gene expression relative to HG-3 ± SEM. Statistics calculated by unpaired t-test, ** p ≤ 0.01.

3.3.13 Protein expression levels of DUB enzymes in CLL cell lines MEC1 compared to HG-3 cells

To further investigate the expression of DUB enzymes in CLL cell lines, we examined the expression of DUB enzymes in MEC1 and HG-3 cells. The data illustrated differential expression levels of USP7, 8, 9x and 10 in MEC1 cells compared to HG-3 cells (Figure 3.18a).

The expression levels of USP7 were slightly but consistently higher (p = 0.052) in MEC1 cells compared to HG-3 (Figure 3.18a & b). While USP8 protein levels were significantly higher in MEC1 cells compared to HG-3 cells (Figure 3.18c), USP9x expression levels were similar in both cell lines (Figure 3.18d). However, the protein expression of USP10 was consistently and significantly lower in MEC1 cells compared to HG-3 cells (Figure 3.18e).

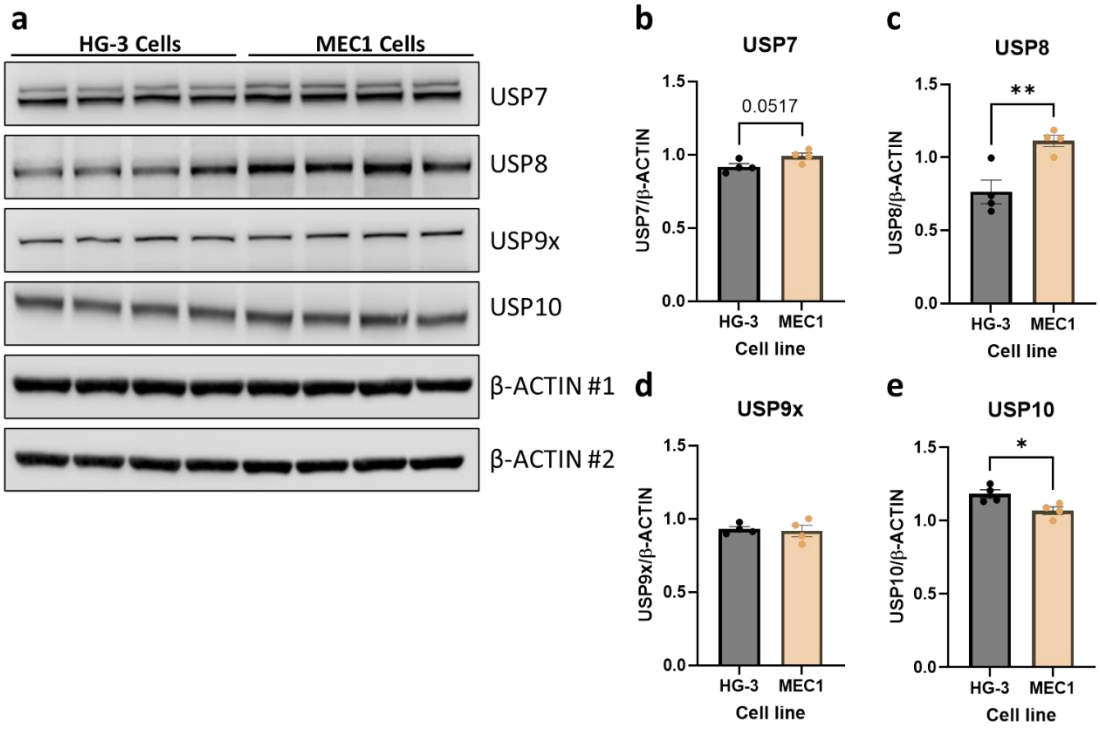

Figure 3.18: CLL cell lines indicated variability in DUB protein expression.
(a) Representative Western blot to assess protein expression of HG-3 cells (n = 4) compared with MEC1 cells (n = 4), probed for USP7, USP8, USP9x, USP10 and β-ACTIN (loading control; #1, #2, and #3 representing mirror blots). Relative protein expression of (b) USP7, (c) USP8, (d) USP9x and (e) USP10 between HG-3 cells (HG-3; black bars; n = 4) and MEC1 cells (MEC1 = beige bar; n = 4). Samples were normalised to loading control β-ACTIN. The mean expression levels of proteins in MEC1 cells were used to calculate the relative protein expression levels of MEC1 cells and HG-3 cells. Each dot represented an individual datapoint. Data expressed as the mean ± SEM. Statistics calculated by unpaired t-test (b-e); * $p \leq 0.05$, ** $p \leq 0.01$.

3.3.14 DUB inhibitors induced CLL cell death *in vitro*

To investigate the role of DUB enzymes in BCR mediated FOXO1 regulation, we first assessed the selectivity of several DUB inhibitors towards CLL cells and determined the IC_{50} for each inhibitor. We focused on a broad range pan-DUB inhibitor (PR-619), a USP7 selective inhibitor (P5091), a selective USP9x and USP14 inhibitor (WP1130), and a selective USP7, 8, and 10 inhibitors (HBX19818).

To evaluate the selectivity of DUB inhibitors PR-619, P5091 and WP1130 to CLL cells, we isolated mononuclear cells (MNCs) from buffy coats obtained from healthy individuals, and assessed the effect of the inhibitors on MNCs, $CD19^+$ B-cell, activated $CD4^+$ T cell and CLL patient cells viability. The isolated cells were treated with increasing concentrations of PR-619/P5091/WP1130 in the range of 0.1 to 100 μM, or DMSO vehicle control (NDC) (Figure 3.19). To assess these inhibitors on CLL cell lines, we treated MEC1 and HG-3 cells. Following a 48 hr treatment, apoptosis was measured by flow cytometry using Annexin V FITC/7-AAD staining.

PR-619 inhibitor reduced the percentage of viable cells in a concentration-dependent manner. The calculated IC_{50} for CLL cells was significantly lower than MNCs, T cells and B-cells (Figure 3.19a & b). Furthermore, B-cells IC_{50} was significantly lower than T cell and MNCs, while T cell IC_{50} was similar to MNCs (Figure 3.19a, b & k). CLL cell lines MEC1 and HG-3 showed similar IC_{50} to each other (Figure 3.19c & k). These data indicated that PR-619 selectively targeted CLL cells for apoptosis as indicated by the lower IC_{50} concentrations.

P5091 inhibitor reduced the percentage of viable cells in a dose-dependent manner. The calculated IC_{50} for CLL cells was significantly lower than MNCs, while visibly lower than T cells and B-cells with no statistical difference (Figure 3.19d, e & k). Furthermore, B-cells IC_{50} was significantly lower than MNCs, and exhibited lower IC_{50} compared to T cells, but not statistically significant (Figure 3.19d, e & k). Additionally, T cell IC_{50} was significantly lower than MNCs (Figure 3.19d, e & k). CLL cell lines MEC1 and HG-3 showed similar IC_{50} to each other (Figure 3.19f & k). These data indicated that P5091 selectively targeted CLL cells for apoptosis as indicated by the lower concentrations of IC_{50}.

WP1130, a selective inhibitor of USP5, 9x, 14 and UCH37 (494), reduced the percentage of viable cells in a concentration-dependent manner. The calculated IC_{50} for CLL cells was significantly lower than MNCs, while only visibly lower than T cells. On the other hand, CLL cells IC_{50} was similar to B-cells (Figure 3.19g, h & k). WP1130 IC_{50} with B-cells was significantly lower than MNCs (Figure 3.19g, h & k). Furthermore, while WP1130 IC_{50} in B-cell was lower compared to T cells, it was not statistically significant (Figure 3.19g, h & k). Additionally, T cells IC_{50} showed no statistical difference compared to MNCs, but were visibly lower (Figure 3.19g, h & k). WP1130 showed similar IC_{50} in CLL cell lines MEC1 and HG-3 (Figure 3.19i & k). These data indicated that WP1130 was selective to CLL cells compared with T lymphocytes.

HBX19181 inhibitor reduced the percentage of MEC1 cell viability in a concentration-dependent manner; the IC_{50} was 13 µM in MEC1 cells (Figure 3.19j & k). Overall, these findings suggest that CLL cells generally exhibit a susceptibility to DUB inhibitors compared to healthy cell types.

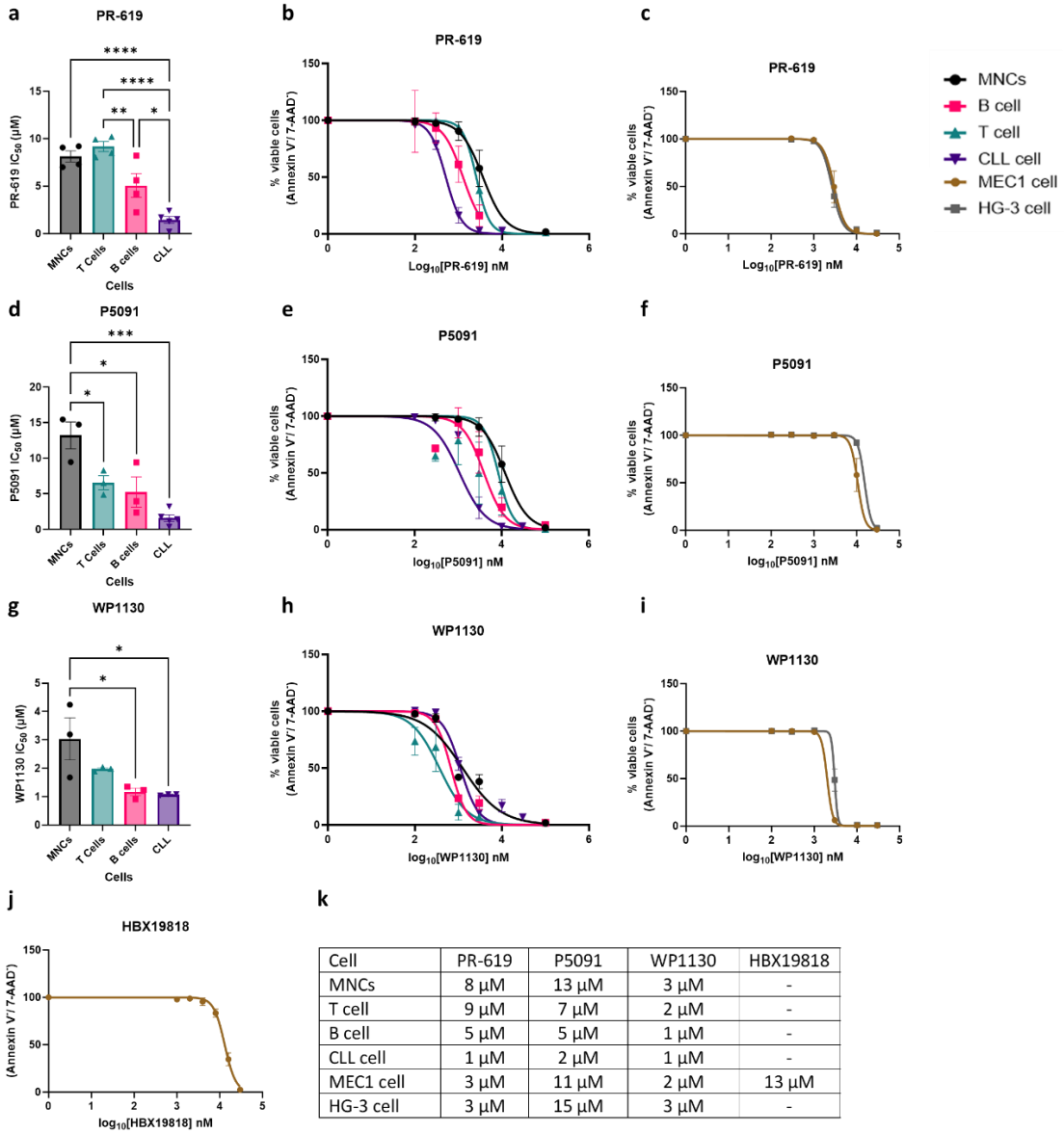

Cell	PR-619	P5091	WP1130	HBX19818
MNCs	8 µM	13 µM	3 µM	-
T cell	9 µM	7 µM	2 µM	-
B cell	5 µM	5 µM	1 µM	-
CLL cell	1 µM	2 µM	1 µM	-
MEC1 cell	3 µM	11 µM	2 µM	13 µM
HG-3 cell	3 µM	15 µM	3 µM	-

Figure 3.19: DUB inhibitors reduced the viability of cells after 48 hr in a concentration-dependent manner.

FACS data of cell (n>3) viability as determined by Annexin V/7-AAD staining. The cells were treated for 48 hr with increased concentrations of DUB inhibitors or vehicle (DMSO) control. MNCs were stained with anti-CD19, anti-CD4 and anti-CD5 antibodies, then the viability was measured by FACS using Annexin V FITC/7-AAD staining. The IC_{50} was measured for MNCs (black line), healthy B (pink line) and T (oil green line) cells by gating on positive CD19 APC-Cy7 and CD4 FITC cells (a, b, d, e, g, h). The IC_{50} was measured for CLL (blue line; a, b, d, e, g, h), MEC1 (brown line; c, f, i, j, l), and HG-3 (grey line; c, f, i) cells. (k) Table of determined IC_{50} values with inhibitors and cell types as indicated,

measured by µM. Data expressed as the mean ± SEM. Statistics calculated by One-way ANOVA, Tukey test (a, d, g); * $p \leq 0.05$, ** $p \leq 0.01$, *** $p \leq 0.001$, **** $p \leq 0.0001$.

3.3.15 Pan-deubiquitinase inhibitor (PR-619) induced rapid downregulation of FOXO^{T24} phosphorylation in a concentration dependent manner

To investigate a role for DUB enzymes in regulating FOXO1 expression, we treated MEC1 cells with PR-619, pan-DUB inhibitor, with increasing concentrations of drug (3 µM, 6 µM, 9 µM) for the following times: 1 hr, 2 hr, 4 hr for each timepoint (Figure 3.20a). FOXO^{T24} phosphorylation was reduced in PR-619 treated cells compared to NDC in a concentration dependent manner (Figure 3.20a, b). The downregulation of FOXO^{T24} phosphorylation was consistent across all timepoints, peaking at 1 hr of PR-619 treatment (Figure 3.20b). At 1 hr of PR-619 treatment, FOXO1 expression was slightly reduced in a concentration dependent manner compared to NDC (Figure 3.20c). However, at 2 hr and 4 hr of treatment, the expression of FOXO1 was unaffected by the increased concentration of PR-619 (Figure 3.20c). While the expression of MCL1 increased slightly with drug, MCL1 levels were reduced with the highest dose at 4 hr of treatment (Figure 3.20d). Although, the level of p21$^{Waf1/Cip1}$ expression mostly was unaffected by the drug at low and higher concentrations, p21$^{Waf1/Cip1}$ expression levels were modestly reduced at 4 hr with the highest dose of PR-619 (Figure 3.20e). Despite the visible increase in MDM2 expression level with low dosage of PR-619 (3 µM) at 1 hr and 4 hr, MDM2 levels were depleted with the highest dose after 4 hr of treatment (Figure 3.20f).

As expected, PR-619 inhibitor increased overall ubiquitination of proteins in a concentration manner (Figure 3.20g & h). Densitometry analysis of ubiquitination showed an elevation of levels of ubiquitinated proteins at 1 hr and 2 hr compared to NDC. Notably, the most significant increase in ubiquitinated protein levels occurred at 2 hr with the highest concentration and at 4 hr with lower concentrations (3 µM, 6 µM) compared to NDC. These data indicate that short time incubation PR-619 may induce downregulation of FOXO1^{T24} phosphorylation in a concentration-dependent manner.

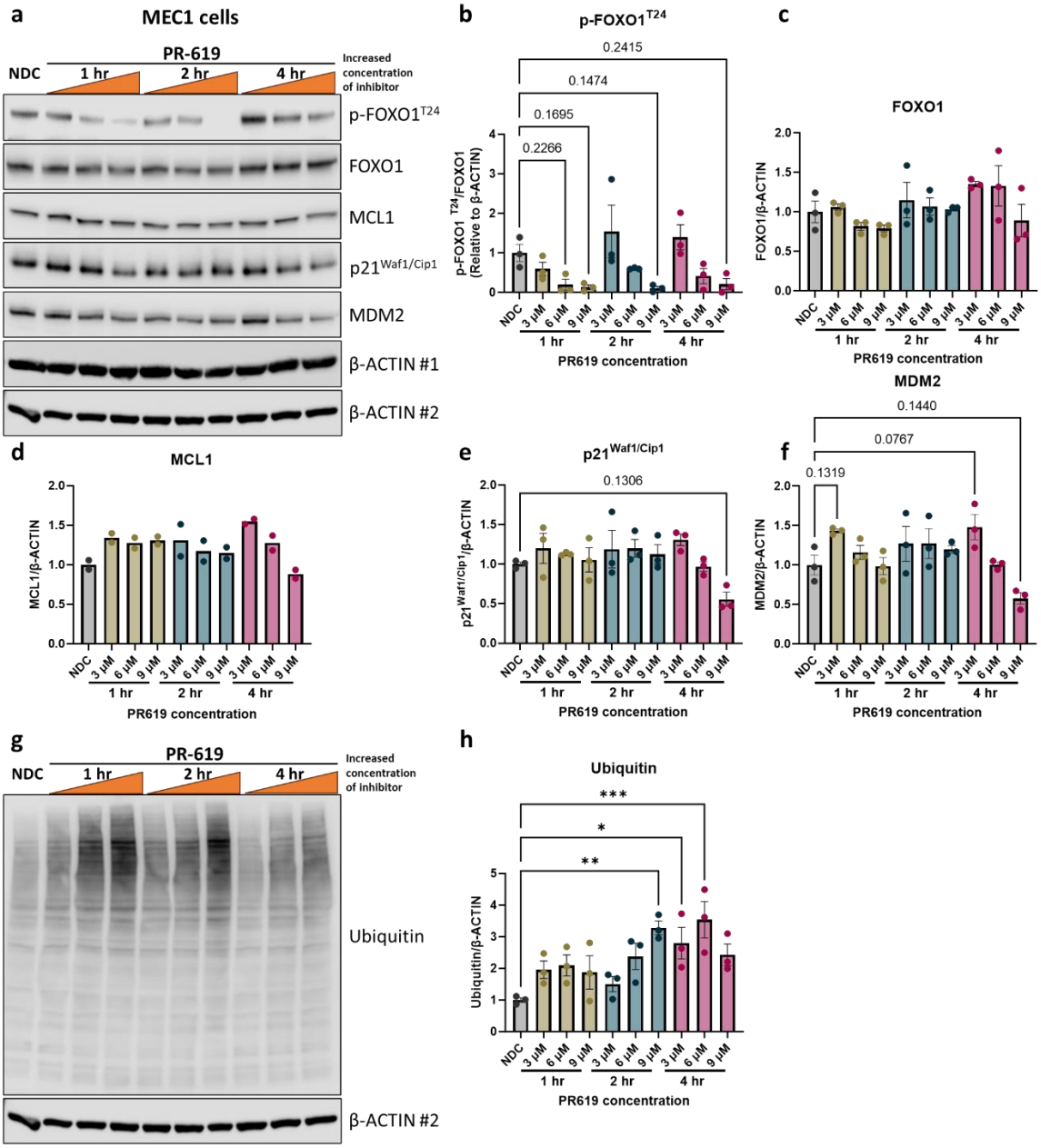

Figure 3.20: Increasing concentrations of PR-619 demonstrably reduced FOXO^{T24} phosphorylation in a concentration dependent manner.

(a, g) Representative Western blot of MEC1 cells, treated with increased concentration of PR-619 (3 µM, 6 µM, 9 µM) for the indicated timepoints (1 hr, 2 hr, 4 hr; hour) or no drug control (NDC; DMSO). The blots were probed for FOXO1^{T24} phosphorylation, FOXO1, MCL1, p21$^{Waf1/Cip1}$, MDM2, Ubiquitin and β-ACTIN (loading control; #1 and #2 representing mirror blots). Relative protein expression of (b) p-FOXO1^{T24} , (c) FOXO1, (d) MCL1, (e) p21$^{Waf1/Cip1}$, (f) MDM2, and (h) Ubiquitin between no drug control (NDC/DMSO = black bar; n ≥ 2) and increased concentration of PR-619 (3 µM, 6 µM, 9 µM) treatment for (1 hr = oil green bar; n ≥ 2), (2 hr = blue bar; n ≥ 2), and (4 hr = red bar; n ≥ 3). Samples were normalised to loading control β-ACTIN. The mean expression levels of proteins in NDC were used to calculate the relative protein expression levels of NDC and PR-619 increased concentration at the indicated timepoints. Each dot represented an Individual datapoint. Data expressed as the mean ± SEM. Statistics calculated by One-way ANOVA, Dunnett test (b-f, h); * $p \leq 0.05$, ** $p \leq 0.01$, *** $p \leq 0.001$.

3.3.16 WP1130 induced rapid downregulation of FOXO^{T24} phosphorylation and total FOXO1 expression in a concentration dependent manner

To further explore the effects of DUB proteins in regulating the expression levels of total FOXO1 and FOXO1^{T24} phosphorylation, MEC1 cells were treated with WP1130 in increasing concentrations and incubation time as indicated (Figure 3.21a & g). FOXO1^{T24} phosphorylation was significantly reduced in MEC1 cells in a dose-dependent manner compared to untreated controls (Figure 3.21b). This downregulation was sustained across all investigated timepoints for the highest concentrations (4 µM and 6 µM) (Figure 3.21b). For the lower concentrations (2 µM and 4 µM), the most significant effect peaked at 1 hr of treatment, demonstrating a more significant downregulation of FOXO1^{T24} phosphorylation levels compared to 2 hr and 4 hr treatment (Figure 3.21b). Interestingly, the highest concentration (6 µM) maintained consistently reduced levels of FOXO1^{T24} phosphorylation across all timepoints (Figure 3.21b). The effect of WP1130 treatment on FOXO1 protein levels revealed a concentration-dependent effect of WP1130 on FOXO1 levels, as visualised in the Western blot (Figure 3.21a & c). The data indicated that the lowest concentration (2 µM) exhibited a transient downregulation at 1 hr, followed by upregulation at 2 hr which was restored to baseline levels at 4 hr compared to untreated MEC1 cells (Figure 3.21c). The higher concentration (4 µM) illustrated a consistent downregulation of FOXO1 levels across all timepoints, peaking at 1 hr and maintained across the observed timepoints (Figure 3.20c). The highest concentration (6 µM) demonstrated the most potent effect on FOXO1 expression, reducing its levels throughout the timepoints, peaking at 1 hr and a further reduction at 4 hr compared to 2 hr treatment (Figure 3.21c).

The protein levels of MCL1 were unaffected by increased concentration of the treatment at 1 hr, 2 hr and 4 hr compared to untreated MEC1 cells (Figure 3.21d). However, at 4 hr, the lowest concentration (2 µM) illustrated a significant increased, while the highest concentration (6 µM) demonstrated a significant downregulation of MCL1 levels compared to untreated cells (Figure 3.21d). Notably, the expression levels of MDM2 and p21$^{Waf1/Cip1}$ indicated that WP1130 treatment affects their expression levels in a time- and concentration- dependent manner (Figure 3.21e & f). The downregulation of MDM2 and p21$^{Waf1/Cip1}$ was visible at 4 hr with the higher concentrations (4 µM and 6 µM), while the lowest concentration (2 µM) had little to no effect on their expression levels across the timepoints (1 hr, 2 hr and 4 hr) (Figure 3.21a, e, f).

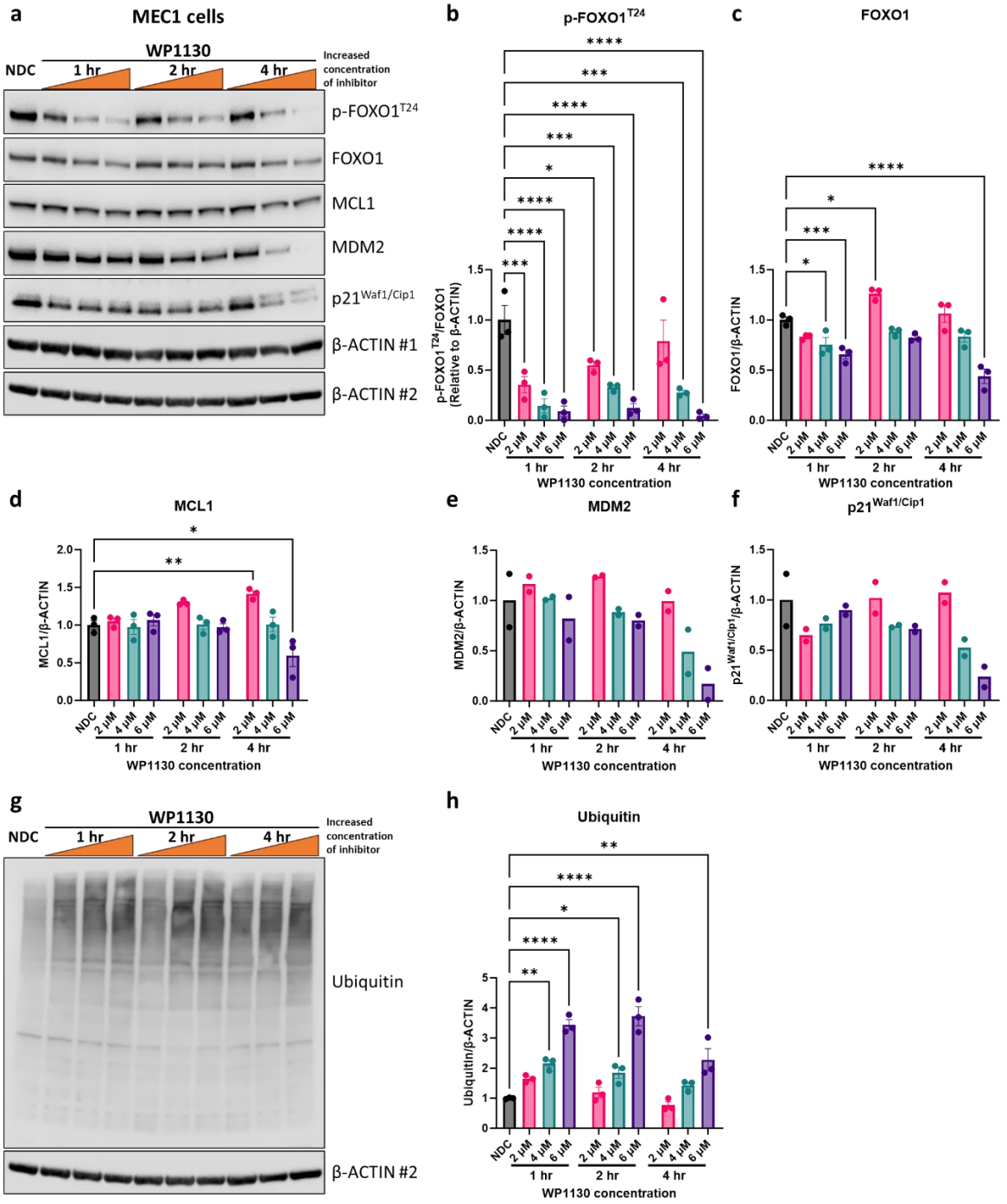

Figure 3.21: Increasing concentrations of WP1130 significantly reduced FOXO^{T24} phosphorylation in a concentration dependent manner.

(a, g) Representative Western blot of MEC1 cells, treated with increased concentration of WP1130 (2 μM, 4 μM, 6 μM) for the indicated timepoints (1 hr, 2 hr, 4 hr) or NDC (DMSO). The blots were probed for FOXO1^{T24} phosphorylation, FOXO1, MCL1, MDM2, p21$^{Waf1/Cip1}$, Ubiquitin and β-ACTIN (loading control; #1 and #2 representing mirror blots). Relative protein expression of (b) p-FOXO1^{T24}, (c) FOXO1, (d) MCL1, (e) MDM2, (f) p21$^{Waf1/Cip1}$, and (h) Ubiquitin between NDC = black bar; n ≥ 2), and WP1130 treated cells (2 μM = pink bar; n ≥ 2), (4 μM = oil green bar; n ≥ 2), and (6 μM = purple bar; n ≥ 2) as indicated. Samples were normalised to loading control β-ACTIN. Each dot represents an individual datapoint. Data expressed as the mean ± SEM. Statistics calculated by One-way ANOVA, Dunnett test (b-f, h); * p ≤ 0.05, ** p ≤ 0.01, *** p ≤ 0.001, **** p ≤ 0.0001.

Consistent with expectations, treatment with WP1130 induced a dose-dependent increase in protein ubiquitination (Figure 3.21g & h). Densitometric analysis of the blots confirmed this observation, revealing a significant upregulation of ubiquitinated proteins at the higher concentrations (4 µM and 6 µM) after 1 hr and 2 hr compared to NDC (Figure 3.21h). Interestingly, at 4 hr timepoint, only the highest drug concentration maintained a significantly upregulated level of ubiquitination compared to NDC (Figure 3.21h). Unexpectedly, at this latest timepoint, all drug concentrations showed slightly lower levels of ubiquitination compared to the 1 hr and 2 hr timepoints (Figure 3.21h).

These data indicated that short term incubation WP1130 may induce downregulation of $FOXO1^{T24}$ phosphorylation and FOXO1 in a concentration-dependent manner.

3.4 Discussion

This chapter provided an insight into the expression profile of FOXO1, which revealed an upregulation of FOXO1 at both mRNA and protein levels in CLL cells compared to healthy $CD19^+$ B-cells. The BCR crosslinking with $F(ab')_2$ fragment resulted in a rapid and transient increase in $FOXO^{T24}$ phosphorylation and FOXO1 in primary CLL cells, which was blocked by ibrutinib, confirming the role of BCR signalling in FOXO1 modulation. Interestingly, this rapid and transient modulation was specific to protein levels, suggesting a mechanistic role for ubiquitination and deubiquitination in sustaining these transient upregulating levels of $FOXO^{T24}$ phosphorylation and FOXO1. Further investigation using STRING database, a search tool for protein-protein interaction, identified potential DUB enzymes which may interact with FOXO1, including USP7, which could further interact with other DUB enzymes. Notably, protein expression levels of DUB enzymes were largely upregulated in CLL patient cells, suggesting a role for DUB enzymes in CLL disease progression. Treatment of MEC1 cells with increased doses of pan-DUB inhibitor (PR-619) and selective DUB inhibitor (WP1130) reduced the expression levels of $FOXO^{T24}$ phosphorylation and FOXO1, which peaked at the earliest timepoint, revealing a potential role in sustaining the rapid transient upregulation of $FOXO^{T24}$ phosphorylation and FOXO1 by BCR crosslinking with anti-IgM $F(ab')_2$ fragment.

3.4.1 FOXO family members are differentially regulated in CLL cells compared to healthy B-cells

The transcription levels of FOXO family members were in alignment with Cosimo, Tarafdar (412) reported transcription levels, observing significant upregulation of *FOXO1* and *FOXO4*, while *FOXO3* levels did not differ between CLL patient samples and healthy B-cells. Furthermore, Cosimo, Tarafdar (412) reported an association between poorer prognostic features in CLL cells and the upregulation of *FOXO1* expression levels, with factors including cytogenetic abnormalities, Binet stage, and patient treatment status. However, stratification within our CLL cohort based on these prognostic factors indicated no statistical differences in *FOXO1* mRNA levels. This discrepancy may occur due to CLL heterogeneity and sample prognostic subset differences. However, *FOXO1* regulation appears context specific. The mRNA levels of *FOXO1* were elevated in CLL cells with del(17p), aligning with findings in CLL cell lines which demonstrated significantly higher *FOXO1* mRNA levels in MEC1 (del(17p); poor prognostic) compared to HG-3 (del(13q); favourable prognostic) cells.

The expression levels of FOXO family members could be regulated by microRNA including miR-21, miR-27a, miR- 96 and miR-128 which were showed to downregulate FOXO family members in MCF-7 breast cancer cells (519). MicroRNAs, a vast family of short non-coding RNAs, have emerged as post-transcriptional regulators of gene expression (520). Interestingly, inhibiting of these microRNAs restored *FOXO1* levels and promoted cell death (519). While our data demonstrated upregulation levels of *FOXO4*, a downregulation trend of *FOXO4* was observed in CLL patient cells harbouring del(17p). This reduction in *FOXO4* levels might be contributed to upregulation of a number of microRNAs in CLL with del(17p) (521), which may target and regulate *FOXO4* expression. Additionally, p53, located on chromosome 17p, has been reported to interact with FOXO4 in senescent cancer cells (522). Therefore, in the absence of p53 due to del(17p), this interaction was disrupted and may contribute to the observed downregulation of *FOXO4* levels in CLL with del(17p).

Intriguingly, our data revealed an unexpected pattern in *MCL1* expression, a BCL-2 family member closely associated with adverse prognostic outcomes in CLL. *MCL1* mRNA levels in CLL cells demonstrated a trend toward downregulation compared to healthy B-cells. This observation suggested a potential association with *IGVH* mutational status, as unmutated *IGVH* reported to display significant upregulation of *MCL1* transcription levels compared to mutated *IGVH*. However, limitations in the availability of data regarding the *IGVH* mutation status in our CLL cohort, restricted our ability to stratify *MCL1* levels based on *IGVH* mutation status. Therefore, this unexpected trend in *MCL1* levels in CLL cells may occur due to higher proportion of *IGVH* mutated CLL cells (523), skewing the overall *MCL1* levels downwards. Additionally, MEC1 cells have CK and did not have somatic mutation (487), exhibited a significantly higher *MCL1* levels compared to HG-3 cells, supporting the role of unmutated *IGVH* in upregulating *MCL1* expression levels. Since our CLL cells were derived from PB, their quiescent state may have contributed to lower *MCL1* mRNA levels. However, it has been reported that *MCL1* transcription levels in CLL cells demonstrated similar expression levels between PB and LN samples (524), suggesting this explanation might be less likely.

PTEN, a well-established tumour suppressor gene, plays crucial role in CLL pathogenesis (460, 507). PTEN-deficient CLL B-cells led to constitutive active PI3K/AKT signalling, promoting CLL cells development and survival (155). Given the known inactivation of both

PTEN and FOXO1 by BCR signalling pathway and their documented roles as tumour suppressors in CLL cells (155, 355, 412, 460), we investigated PTEN expression in CLL as another potential target regulated in a similar manner as FOXO1. The mRNA expression levels of *PTEN* in CLL cells were surprisingly similar to the levels of healthy B-cells. This finding contradicted our initial expectation of a significant downregulation in CLL based on its tumour suppressive function. Notably, one previous study reported a significant upregulation of *PTEN* mRNA in CLL cells compared to healthy B-cells (155). This study concluded that *PTEN* mRNA levels did not reflect the significant downregulation in protein levels which could suggest a role for post-translational regulators such as miR-21 affecting *PTEN* expression levels (155). Notably, it has been reported that in CLL with del(17p), PTEN protein was predominantly localised in the cytoplasm compared to the healthy B-cells which showed a balanced presence of PTEN in the nucleus and cytoplasm (460). This unbalanced in PTEN localisation may trigger compensatory upregulation of *PTEN* mRNA as a mechanism to maintain PTEN reduced activity. Additionally, another study linked *PTEN* mRNA upregulation with unmutated *IGVH*, suggesting a potential association of *PTEN* mRNA levels with poor prognosis (155). Further investigation using larger CLL cohort of patients harbouring del(17p) and mutated/unmutated *IGVH* would illuminate the relationship between *PTEN* mRNA expression and poor prognostic features.

ZAP-70 is a tyrosine kinase predominantly expressed in T cells and NK cells (112). Increased expression of ZAP-70 in CLL cells is associated with enhanced BCR signalling, promoting cell proliferation and survival, and linked to poor prognosis (112). Our analysis revealed a significant upregulation of *ZAP-70* mRNA levels in CLL cells compared to healthy B-cells, suggesting that our CLL cohort might harbour underlying features associated with poor prognosis. Notably, the upregulation was even more pronounced in CLL samples with del(11q) and to a lesser extent with del(17p) compared to normal cytogenetic, further consolidating ZAP-70 as an indicator of aggressive disease. Interestingly, we observed higher *ZAP-70* mRNA levels in HG-3 cells, representing favourable prognosis, compared to MEC1 cells. This pattern was repeated with *MYC* expression, with HG-3 cells showing significantly higher levels of mRNA compared to MEC1 cells. these findings suggested that HG-3 cells might possess more active NF-κB pathway compared to MEC1 cells, making them an attractive model for studying this important signalling pathway in CLL cells.

To comprehensively assess FOXO family members activity in CLL cells compared to healthy B-cells, examining additional established FOXO target genes including *CCND1-3*, *CDKN1A* and *CDKN1B* would be desirable (412). This would provide a broader picture of FOXOs regulation and may reveal additional targets. Moreover, using techniques including RNA-seq or ChIP-seq specifically focused on *FOXO1* would provide valuable insights into *FOXO1* regulation, shed light on the complex roles of microRNAs, and its contribution to CLL progression.

3.4.2 FOXO1^{T24} phosphorylation was downregulated, while FOXO1 was upregulated in CLL patient samples, highlighting the role of tonic signalling in CLL cells' survival.

Our data revealed a trend towards downregulation of both AKT^{S473} and FOXO1^{T24} phosphorylation in CLL cells compared to healthy B-cells. This downregulation may be due to CLL cells residing in PB, where the cells might exhibit a quiescent state and lower phosphorylation levels. The lymphatic tissues serve as the primary site for BCR activation in both healthy and malignant B-cells (206). BCR activation, triggered by antigen binding (dependent ligation) or antigen independent inducing a cascade of signalling events that promote proliferation, differentiation, and antibody production in healthy B-cells (525). Additionally, in malignant B-cells, BCR signalling also plays an important role in disease pathogenesis (206, 526). BCR mutations leading to independent activation occur in some lymphomas like DLBCL (527) as well as CLL cells (528). Furthermore, in healthy B-cells, tonic signalling has been shown to promote survival primarily through the PI3K/AKT signalling pathway (400), although other pathways might also contribute to B-cells survival. This tonic signal which may trigger low-level phosphorylation compared to antigen-dependent BCR signalling (529), has been reported to be closely linked to ZAP-70 (160), which is strongly associated with unmutated *IGVH* (111, 530). Together, these findings suggested a level of activation in CLL cells, as evidenced by the detectable low levels of phosphorylation of AKT^{S473} and FOXO1^{T24} in our CLL cohort compared to healthy B-cells. This may also suggest that our CLL cohort primarily composed of cells with mutated *IGVH*, resulting in lower level of tonic signalling. Furthermore, stratification of AKT^{S473} and FOXO1^{T24} phosphorylation levels based on the presence/absence of unfavourable cytogenetic abnormalities showed significantly higher FOXO1^{T24} phosphorylation, while AKT^{S473} phosphorylation trended

toward lower levels compared to patient with normal cytogenetics. This increase in FOXO1^{T24} phosphorylation levels may be linked to unmutated *IGVH* and ZAP-70, leading to enhanced tonic signal and resulting in higher phosphorylation compared to normal cytogenetic. CLL cells demonstrated significantly higher levels of FOXO1 protein expression compared to healthy B-cells, aligning with Cosimo, Tarafdar (412) findings which indicated overexpression of FOXO1 in LN of poorer prognostic CLL patients. This pattern was further substantiated by MEC1 cells (poor prognosis) expressing significantly higher phosphorylation of FOXO1^{T24} and total FOXO1 compared to HG-3 cells (favourable prognosis), suggesting FOXO1 as a potential indicator of CLL pathogenesis. This upregulation of FOXO1 in MEC1 further supported by the concordant upregulation of *FOXO1* mRNA levels in CLL cells. However, despite this upregulation, FOXO1 remains largely inactive in CLL cells through PI3K/mTOR/AKT signalling pathway (412, 414). This pathway phosphorylates FOXO1, promoting FOXO1 translocation from the nucleus, where it exerts its tumour-suppressive effects, to the cytoplasm, effectively silencing its anti-tumorigenic activity (344, 412). This intricate interplay between BCR signalling and FOXO1 activity highlighted the potential of targeting FOXO1 for CLL therapy.

Although Smit, Hallaert (524) reported higher MCL1 levels in LN and upon CD40L co-culture, our PB-derived CLL samples showed levels similar to healthy B-cells. However, MCL1 tended to be upregulated in CLL patients with unfavourable cytogenetic abnormalities, supporting its association with poor prognosis and potentially influenced by unmutated *IGVH* status. Together, this suggested that the upregulation in MCL1 expression may be more prominent in LN microenvironment. As expected, our CLL cohort had significantly higher ZAP-70 protein levels compared to healthy B-cells. This, along with the observed trend towards elevation in patients with unfavourable cytogenetics, further suggested features of poor prognosis within our cohort. ZAP-70 is known to be associated with both unmutated *IGVH* and poor prognosis (18, 111, 530), further strengthening this interpretation. CLL cells exhibited significantly lower PTEN protein levels compared to healthy B-cells, with a further downregulation in Binet stages B and C in compared to stage A, aligning with Schmid, Khadour (155) and indicating an association between low PTEN expression and poor prognosis in both mutated and unmutated CLL. Notably, the downregulation was more pronounced in unmutated CLL (81% vs. 63% for mutated) (155). However, our mRNA data showed similar *PTEN* levels, with significantly higher levels in CLL cells with del(17p).

Interestingly, our protein data hinted at a trend towards upregulation in the subset with unfavourable cytogenetics, despite the overall lower levels compared to healthy B-cells. This concordant trend in both protein and mRNA specifically within unfavourable cytogenetic abnormalities suggested a potential compensatory mechanism for PTEN inactivation due to its increased cytoplasmic presence in these high-risk subgroup of CLL cells (460).

We aimed to profile the protein expression of FOXO1^{T24} phosphorylation and total FOXO1 in CLL cell lines, MEC1 and HG-3. Our data revealed that MEC1 cells exhibited higher levels of both FOXO1^{T24} phosphorylation and total FOXO1, as well as P21$^{Waf1/Cip1}$, P27^{Kip1}, and a trend towards upregulation of MCL1 levels compared to HG-3 cells. Conversely, HG-3 showed higher levels of PTEN, cMYC, and BIM ($_{EL}$, $_{L}$, $_{S}$). These findings strengthen the association between MEC1 cells and poor prognosis, while HG-3 cells align more closely with favourable prognosis. Furthermore, MEC1 cells resemblance to poor prognosis and its overexpression of FOXO1, which aligned with observations of CLL cells in LN by Cosimo, Tarafdar (412), made MEC1 cells a more suitable model for studying FOXO1 expression and regulation. Additionally, the higher cMYC expression and lower FOXO1^{T24} phosphorylation in HG-3 cells suggested a lower dependence on the PI3K/AKT pathway and potentially a greater reliance on alternative pathways including NF-κB, as indicated by cMYC expression. Based on these findings, we will focus on MEC1 and primary CLL cells to investigate FOXO1 regulation and its activity downstream the BCR signalling pathway.

3.4.3 BCR signalling rapidly regulates the expression of FOXO1 in CLL cells.

BCR signalling plays a fundamental role in B-cells survival through tonic signalling in quiescent cells and antigen-dependent signalling in LN (126, 525). This dependence on BCR signalling extends to CLL cells, dictating survival, disease progression, and treatment resistance (4). Importantly, the BCR serves as a key platform for integrating signals from different stimuli (402). PI3K, a key pathway downstream of the BCR, exhibited hyperactivity in CLL cells and correlated with poor prognosis in BL and DLBCL (531, 532). PI3K recruitment to the plasma membrane generates PIP_3, essential for optimal BTK activation and subsequently AKT activation (52). It has been demonstrated that higher levels of PI3K-signalling were implicated in CLL development and maintenance (400). Furthermore, constitutive PI3K activation, as seen in PTEN deficient mouse cells, accelerated CLL

development in young mice and promoted efficient engraftment and maintenance of CLL-like B-cells *in vivo* and *in vitro* (155). Notably, in BCR-deficient B-cells, PI3K, but not NF-κB signalling pathway, was able to rescue mature B-cells from cell death, suggesting PI3K mediation of negative regulation of FOXO1 as central driver of B-cell survival (400). Together, these findings highlighted the crucial role of BCR signalling in CLL cell survival primarily though PI3K activation, with FOXO1 as a central target negatively regulated by phosphorylation and cytoplasmic translocation. Relating to our data, we observed rapid and transient upregulation of AKT^{S473}, $FOXO1^{T24}$ phosphorylation and FOXO1 upon BCR crosslinking with soluble $F(ab')_2$ fragment, aligning with Cosimo, Tarafdar (412). However, the levels of AKT^{S473}, $FOXO^{T24}$ phosphorylation and FOXO1 upregulation in $F(ab')_2$ stimulated CLL cells were heterogenous among our CLL samples. This heterogeneity may be associated to *IGVH* status and ZAP-70 expression in CLL cells (51, 112, 226). We speculated that the TME may enhance the durability of BCR signalling, which our monoculture model lacks. Additionally, FOXO1 is known to be negatively regulated by BCR signalling (400, 412), which may suggest that despite FOXO1 increased protein levels, FOXO1 was inactive in both LN and $F(ab')_2$ stimulated CLL cells. Therefore, investigation of FOXO1 activity status in LN and PB-derived CLL cells would further enhance our understanding of FOXO1 role in CLL pathogenesis. It has been reported that FOXO family transcription factors play an important role in regulating genes involved in various cellular processes, including growth factor signalling, cell cycle arrest and apoptosis (342).

Notably, cell division progression critically relies on CDKs to induce cell cycle progression towards S phase and initiate mitosis (533). This is tightly regulated by $p21^{Waf1/Cip1}$ and $P27^{Kip1}$ which bind and inhibit CDK complexes and induce cell-cycle arrest (534). FOXOs influence this process by regulating the expression of cyclin-CDK inhibitors including $p21^{Waf1/Cip1}$ (*CDKN1A*) and $P27^{Kip1}$ (*CDKN1B*), influencing cell cycle progression (535). However, the specific relationship between FOXO1 and its gene in the context of BCR signalling in CLL cells remains unclear. Our analysis of protein levels in CLL cells revealed no significant differences in $p21^{Waf1/Cip1}$ and $P27^{Kip1}$ expression upon BCR stimulation with $F(ab')_2$ fragment. While a slight upregulation of $p21^{Waf1/Cip1}$ was observed in some patient samples, its potential functional significance remains questionable due to reported cytoplasmic localisation through PI3K/AKT signalling pathway (536). Intriguingly, previous studies have demonstrated differential regulation of $p21^{Waf1/Cip1}$ and $P27^{Kip1}$ upon BCR crosslinking with

anti-IgM (537, 538). Upregulation of $p21^{Waf1/Cip1}$ has been observed in immature B-cells stimulated with anti-IgM, associated with p53 expression (537). On the other hand, $p27^{Kip1}$ levels were unaffected by $F(ab')_2$ stimulation up to 24 hr, while longer incubation with anti-IgM (48-72 hr) had been shown to induce downregulation in mature B-cells (538). These findings highlighted the complex interplay between BCR signalling, FOXO1 regulation/expression, and target proteins including $p21^{Waf1/Cip1}$ and $P27^{Kip1}$ in unstimulated and stimulated CLL cells. To further elucidate the role of FOXO1, $p21^{Waf1/Cip1}$ and $P27^{Kip1}$, investigation of protein localisation using assays including nuclear fractionation or immunofluorescence may reveal their functional state as well as potential role associating FOXO1 with $p21^{Waf1/Cip1}$ and $P27^{Kip1}$ upon BCR stimulation in CLL cells.

The PI3K/AKT signalling pathway is negatively regulated by PTEN, which dephosphorylation PIP_3 into PIP_2 (539). Notably, our data revealed a significant upregulation of PTEN protein levels in CLL cells after 24 hr of $F(ab')_2$ stimulation compared to unstimulated CLL cells. This observed increase may be attributed to the absence of the supportive TME in our *in vitro* experiments. This lack of TME may trigger a negative feedback loop, leading to increase PTEN expression as a compensatory mechanism. Additionally, prolonged exposure to soluble $F(ab')_2$ fragment could induce this increase in PTEN expression, leading to PI3K/AKT pathway inhibition. It has been reported that BCR plays an important role in mediating the regulation of MCL1 in CLL cells (197). Notably, a previous study demonstrated that BCR stimulation with immobilised anti-IgM upregulated MCL1 levels, subsequently providing protection against BCL-2 inhibitor (venetoclax), while siRNA KD of MCL1 restored drug sensitivity (197). Our findings aligned with these observations, revealing a significant upregulation of MCL1 protein in $F(ab')_2$ stimulated compared to unstimulated CLL cells. This increase in MCL1 expression further showed its potential involvement in BCR driving CLL progression. Interestingly, ZAP-70 expression, associated with enhanced BCR signalling (112), displayed heterogeneity in our CLL samples following $F(ab')_2$ stimulated. While all stimulated CLL cells demonstrated consistent ZAP-70 upregulation levels at early timepoints (0.5-1 hr), ZAP-70 levels diverged at later timepoints (8-24 hr), decreasing in some CLL cells, and remaining upregulated in other samples. This observed heterogeneity may be attributed to patient specific *IGVH* mutation status, as previous studies have documented correlation between ZAP-70 expression and *IGHV* status (18, 111, 112, 226, 530). Furthermore, ZAP-70 data suggested a subtle effect of prolonged $F(ab')_2$ stimulated on BCR

signalling depending on individual CLL patient characteristics, with distinct prognostic subsets. This indicated a potential difference within our CLL cohort in durability and signal strength in response to BCR crosslinked with $F(ab')_2$.

3.4.4 $FOXO1^{T24}$ phosphorylation and FOXO1 were significantly reduced by ibrutinib in $F(ab')_2$ stimulated CLL cells.

As previously discussed, BCR signalling plays a crucial role in CLL survival and proliferation by regulating key pathways including PI3K/mTOR/AKT and NF-κB. Due to this centrality, targeted therapies including BTK and PI3K inhibitors have been developed (502, 503). This project focused on Ibrutinib, a first line BTK inhibitor for CLL patients with unmutated/mutated *TP53* in the UK (540). This FDA-approved agent inhibits CLL proliferation, disrupts cytokine and chemokine signalling, reduces interactions with LN stromal cells, and induces direct cytotoxicity (263, 502, 541). Our data revealed that within 1 hr of ibrutinib treatment, both MEC1 and $F(ab')_2$ stimulated CLL cells exhibited blocking of AKT^{S473} and $FOXO1^{T24}$ phosphorylation, and reduction in FOXO1 protein levels. While MEC1 cells maintained reduced AKT^{S473} and $FOXO1^{T24}$ phosphorylation to a lesser extent at 24 hr of ibrutinib treatment, FOXO1 levels returned to basal levels. This partial restoration of phosphorylation mirrors findings from a study which showed steady increases in AKT and FOXO1 phosphorylation by day 5 of ibrutinib treatment (413), potentially due to tonic signalling through the PI3K pathway (400). Our *ex-vivo* pre- and post-ibrutinib data supported this, showing trending downregulation of AKT^{S473} and $FOXO1^{T24}$ phosphorylation, potentially maintained by PI3K tonic signalling. Interestingly, FOXO1 protein levels in MEC1 cells increased after 24 hr of Ibrutinib treatment, which could be due to blocked FOXO1 phosphorylation leading to protein accumulation. Two separate studies further support this observation, reporting FOXO1 (413) and FOXO3 (542) upregulation and accumulation in MEC1 cells after 24 hr of Ibrutinib treatment. Consistent with these findings, our *ex-vivo* data show a trend towards FOXO1 upregulation in post-ibrutinib CLL samples compared to pre-ibrutinib. Furthermore, *ex-vivo* analysis revealed higher expression of $p21^{Waf1/Cip1}$, $p27^{Kip1}$ and BIM in post-ibrutinib CLL samples compared to pre-ibrutinib. This may suggest that FOXO1 accumulation translates to functional activity, further supported by the significant upregulation of PTEN, a known FOXO1 effector (543), in post-ibrutinib CLL cells compared to pre-ibrutinib. While these observations suggested potential FOXO1 activation and nuclear localisation in post-ibrutinib CLL samples, further studies are needed to confirm

its activity and subcellular distribution. This investigation would highlight a potential tumour suppressive role for FOXO1 in post-ibrutinib-treated CLL cells.

3.4.5 Transient upregulation of FOXO1 protein upon BCR crosslinking are caused by a post-translational mechanism.

Rapid and transient changes in FOXO1 phosphorylation and protein levels observed in $F(ab')_2$-stimulated CLL cells prompted us to investigate whether these alterations extended to the gene level. While *EGR-1* gene expression confirmed effective BCR stimulation, mRNA levels of FOXO family members and their target genes (*BCL2L11*, *CCND2*) remained unchanged between stimulated and unstimulated CLL cells. This suggested that the observed FOXO1 upregulation at protein levels might be specific to the protein level, potentially mediated by post-translational mechanisms. This finding suggested that FOXO1 protein is post-translationally regulated by DUBs and ubiquinitation including mono/polyubiquitination chains which are linked by Lys48- or K48- ubiquitin (360, 460). Of note, ubiquitination of a protein is reversed by DUBs enzymes which remove ubiquitin chains and prevent both lysosomal and proteasomal degradation, enhancing protein stability (544). In CLL cells, DUB enzymes and particularly USP7, are shown to play an important role in oncogenesis through inactivation of three key tumour suppressors including PTEN, FOXOs and p53 proteins (460). USP9x and USP14 play a major role in tumorigenesis of DLBCL (545), MM (466) and prostate cancer (546). Little is known about the molecular mechanism of FOXO1 association with DUB enzymes in CLL cells, however USP7, has been reported to regulate FOXO family members in various diseases including melanoma (478), HEK293T cells (360), hepatic gluconeogenesis (477) and lung cancer (547). Importantly, USP7 cleavage of monoubiquitinated FOXOs leads to cytoplasmic localisation and decreased activity (360, 477). Collectively, given the lack of mRNA level changes and the established role of DUBs in FOXOs regulation, we hypothesised that the transient FOXO1 upregulation in $F(ab')_2$ stimulated CLL cells is primarily driven by post-translational mechanisms, particularly associated with DUB proteins. Therefore, our study focused on investigating the association between DUB proteins and FOXO1 upon BCR stimulation and inhibition, as well as exploring the potential therapeutic implications of selective DUB inhibitors.

3.4.6 Analysis of DUB family gene expression in *ex-vivo* CLL cells revealed high heterogeneity in their transcription levels.

The STRING protein-protein interaction database revealed a high confidence score for association between FOXO1 and USP7, with USP7 further connecting to USP9x and USP14 with similar confidence. Building on this, we investigated the mRNA expression levels of these DUBs in *ex-vivo* PB-derived CLL cells and healthy B-cells. While our data showed no significant difference in *USP7* mRNA levels between CLL and healthy B-cells, this contrasted with a study that showed upregulation of *USP7* in CLL (460). This discrepancy may arise from CLL heterogeneity, differences in prognostic subsets between our CLL cohort and the mentioned study, or limitations in obtaining age-matched B-cells from healthy donors. Notably, USP7 overexpression has been associated with poor prognosis features including del(17p), *TP53* mutations, and ibrutinib resistance (459), and our data aligned with this by demonstrating higher mRNA levels of *USP7* in MEC1 compared to HG-3 cells. However, the limited availability of patient information in our CLL cohort restricted further investigation into association between *USP7* mRNA levels and poor prognostic features in CLL cells. *USP9x* was significantly lower in CLL cells compared to healthy B-cells. This downregulation was unexpected, and it may be because USP9x protein levels were higher in B-cells compared to monocytes and granulocytes (548). This study also showed that the protein levels of USP9x were high in the LN which may indicate that expression of USP9x is LN specific, while our CLL cohort was PB-derived cells (548). In B-cells, USP9x is essential for PKCβ kinase activation after BCR activation (482), further supporting its potential LN expression specificity. Interestingly, *USP9x* mRNA levels were similar in MEC1 and HG-3 cells, suggesting its expression was unaffected by cytogenetic abnormalities, consistent with *ex-vivo* CLL cells analysis.

Like *USP7*, *USP14* levels were similar in CLL and healthy B-cells, as well as in MEC1 and HG-3 cells. This suggested that USP14 mRNA levels might be unaffected by CLL prognosis features including cytogenetic abnormalities. Contrary to our data, in NHL, the mRNA levels of *USP14* were upregulated compared to PBMCs from healthy donors (549). However, our analysis was limited by the lack of complete prognosis information in our CLL cohort and the absence of age-matched B-cells from healthy donors, prevented us from associating *USP14* levels with specific prognostic features including *IGVH* mutation status and CD38 expression. Further studies with larger, well-annotated CLL cohorts and age-matched B-cell

from healthy donors are desirable to validate these findings and address the limitations previously mentioned. Additionally, investigating protein levels and activities of these DUBs, along with their functional interactions with FOXO1, could provide an insight into their roles in CLL pathogenesis and potential therapeutic target.

3.4.7 *ex-vivo* CLL cells have upregulated DUB protein levels, suggesting a potential association between DUB expression and CLL prognosis.

STRING database predictions indicated that USP7 might act as a central hub connecting several DUB enzymes and interacts with FOXO1 (34), potentially altering FOXO1 function and fate. Compared to healthy B-cells, CLL cells, particularly those with poor cytogenetic abnormalities, exhibited overexpression of USP7, 8, 9x, 10, and 14. This suggested potential interactions between these DUBs, as their coordinated overexpression aligned with their predicted association with USP7. Further analysis in MEC1 and HG-3 cell lines revealed a slight but consistent upregulation of USP7, mirroring the trend observed in CLL cells with unfavourable cytogenetics. This aligns with reports linking USP7 expression to del(17p) and *TP53* mutation (459), both present in MEC1 cells and associated with poor prognosis in CLL. Although, USP8 was not significantly different between CLL cells with normal and unfavourable cytogenetics, USP8 levels were higher in MEC1 cells compared to HG-3 cells, hinting at a potential association with poor prognosis. This was consistent with reported USP8 involvement in MLL leukaemogenesis and its potential role as driver gene of poor prognosis in CLL (87, 515). USP9x showed a trend towards upregulation in CLL patient cells with poor cytogenetics, whereas MEC1 and HG-3 cells, despite differing in prognostic features, displayed similar USP9x levels. Interestingly, despite USP9x reported role in stabilising MCL1 and the correlation between their expression in other models, our data suggested no such link in CLL. This aligned with report of MCL1 levels being independent of USP9x KD in ovarian cancer cells (545). USP10 levels followed a similar pattern, being higher in MEC1 cells and showing no significant differences based on CLL cytogenetics, mirroring USP8 expression. This aligned with USP10 reported role in stabilising SYK in AML and its association with poor prognosis (550). USP14 and USP9x, known to be overexpressed and associated with poor prognosis in MM (545, 551). Finally, USP1, 18, and 28 also showed trends towards upregulation in CLL samples, particularly those with poor cytogenetic abnormalities. While USP1 and USP18 were not connected to FOXO1 in the STRING

database, their reported roles in cancer development justify further investigation (552, 553). Our data supported the STRING database prediction of USP7 as a central hub connecting multiple DUBs, with their coordinated overexpression observed in CLL, particularly those with poor cytogenetic features.

Interestingly, our data revealed a dissociation between mRNA and protein levels for USP7 and USP14 in CLL cells compared to healthy B-cells. While their mRNA levels were similar in both CLL cells and healthy B-cells, protein levels for both DUBs were significantly upregulated in CLL cells. Conversely, USP9x exhibited a significant decrease in mRNA, yet the protein levels showed significant upregulation in CLL cells compared to healthy B-cells. This discrepancy between the mRNA levels and protein levels may arise from several factors including the efficiency of ribosomes translation of mRNA into protein, competition for tRNA availability, protein stability and half-life, folding secondary structure, elongation modulation and quality control checkpoints may all contribute to the mRNA protein level variations (554-556).

3.4.8 CLL cells possess a higher sensitivity to DUB inhibitors, suggesting a potential therapeutic window for targeting DUBs in CLL treatment.

Our *in vitro* studies demonstrated that DUB inhibitors selectively targeted and reduced the viability of CLL cell subsets while sparing healthy T and B-cells. Broad-range inhibitor PR-619 and selective USP7 inhibitor P5091 achieved this selectivity, while the dual USP9x/14 inhibitor WP1130 reduced both CLL and B-cell viability. This differential sensitivity suggests a reliance of CLL cells on specific DUB activities for their survival (557). The importance of DUBs in CLL is supported by their documented role in regulating crucial pathways including PI3K (460). As reported recently, PR-619 downregulated AKT and ERK phosphorylation and upregulated $p21^{Waf1/Cip1}$, thereby inhibiting cell proliferation and cell cycle progression in cancer cell lines JJ012 and SW1353 cells (558). Similarly, treatment with P5091 in MEC1 cells enriched the nuclear fraction of PTEN, potentially activating it and suppressing the PI3K pathway (460). While WP1130 inhibited USP9x activity, leading to reduced MCL1 levels and cell growth inhibition in T-ALL cells in *vivo* (557). HBX19818 induces apoptosis in CLL cells with similar efficacy in both mono- and co-culture settings, further supporting the sensitivity of CLL cells to DUB inhibition (84). Collectively, the selective targeting and effectiveness of DUB inhibitors against CLL cells, coupled with their documented roles in

cancer relevant pathways, suggested a promising therapeutic window for DUB inhibitors in CLL cells.

3.4.9 Both PR-619 and WP1130 induced a concentration-dependent decrease in FOXO1^{T24} phosphorylation, suggesting that DUBs may play a role in regulating FOXO1 activity.

Our findings revealed that PR-619 reduced FOXO1^{T24} phosphorylation in a dose-dependent manner, with the strongest effect observed at earlier time points. This aligned with expectations, as PR-619 was reported to inhibit AKT phosphorylation (558), and we previously demonstrated that FOXO1 was phosphorylated downstream of AKT in CLL cells. Interestingly, PR-619 did not affect FOXO1 protein expression, unlike ibrutinib which previously showed to downregulate FOXO1 upon BCR inactivation. This suggested alternative regulatory mechanisms for FOXO1, possibly involving direct protein interactions or BCR-mediated transient modifications. While PR-619 displayed a dose- and time-dependent reduction in p21$^{Waf1/Cip1}$ levels, this finding initially appeared contradictory to reported p21$^{Waf1/Cip1}$ upregulation upon PR-619 inhibition. However, MDM2 expression also decreased in a similar manner, aligning with reported USP7 stabilising of MDM2, an E3 ligase targeting p53 for degradation (459). Notably, PR-619 mediated apoptosis has been shown to occur independently of *ATM* and *TP53* status, even sensitising p53-defective cells to chemotherapeutic agents (459). Additionally, PR-619 induced ubiquitination and protein accumulation, suggesting potential partial proteasomal inhibition alongside DUB enzymes inhibition.

WP1130 exhibited similar effects to PR-619, including reducing in FOXO1^{T24} phosphorylation and MDM2 expression, as well as increasing ubiquitination. However, unlike PR-619, WP1130 also downregulated FOXO1, and both p21$^{Waf1/Cip1}$ and MCL1 levels. These observations suggest distinct target profiles for these inhibitors within the DUB family. While both PR-619 and WP1130 effectively reduced FOXO1^{T24} phosphorylation and increased ubiquitination, the unexpected decrease in p21$^{Waf1/Cip1}$ with PR-619 justified further investigation. Cellular fractionation or immunofluorescence techniques could reveal the subcellular localisation of p21$^{Waf1/Cip1}$ and FOXO1, providing insights into their potential activity.

Chapter 4. Exploring DUB protein modulation of FOXO1 expression, subcellular localisation and activity in CLL cells via BCR signalling pathway.

4.1 Introduction

Ibrutinib and other BTK-targeting treatments are now a leading first-line therapy for CLL patients (559-563), indicating the significance of BCR signalling in driving CLL development and survival (51). Our previous data demonstrated a rapid and transient upregulation of p-FOXO1^{T24} and total FOXO1 expression upon BCR crosslinking with F(ab')$_2$ fragment and this upregulation was specific to FOXO1 protein levels. This rapid upregulation was suspected to be regulated by ubiquitination and deubiquitylation which has been suggested in several studies (326, 360, 477, 564). A number of DUB proteins have been shown to regulate key tumour suppressors including FOXO1, PTEN and p53, of which USP7 particularly affects their stability and controls their activity and expression (460, 477, 565). This suggested a role for DUB proteins, and particularly USP7, USP9x and USP10, in regulating FOXO1 directly or indirectly through regulating key proteins in the BCR signalling pathway including mTORC2 and ZAP-70 (477, 479, 480, 482, 566). Therefore, we investigated the regulation of DUB proteins following BCR crosslinking, as BCR signalling is an effector of FOXO1 expression (412).

Using the pan-DUB inhibitor PR-619 and selective USP5, 9x, and 14 inhibitor WP1130, we demonstrated an effective reduction in p-FOXO1^{T24} after 1 hr of treatment. FOXO1 phosphorylation is reported to delocalise FOXO1 from the nucleus to the cytoplasm, resulting in its inactivation (412, 567, 568). These data indicated a role for DUB inhibitors in regulating FOXO1 expression and potentially activity. Furthermore, it has been reported that USP9x stabilises the protein expression of MCL1 in MM cells (545). Additionally, PTEN, a negative regulator of the PI3K/AKT pathway (569), is inhibited by BCR activation (570), and USP7 has been reported to supress PTEN in CLL cells (460). We investigated their regulation in the context of BCR signalling and examined DUB inhibitors effect to understand the potential role of DUBs in regulating the BCR pathway.

4.2 Specific aims

Our data indicate that FOXO1 is an effector of the BCR signalling pathway, where BCR crosslinking results in a transient upregulation of $FOXO1^{T24}$ phosphorylation and total FOXO1, and this is reversed by the BTK inhibitor ibrutinib. FOXOs are post-translationally regulated by phosphorylation, methylation, ubiquitination and deubiquitination (360). Since FOXO1 expression was transiently upregulated by BCR crosslinking, the role of DUB proteins in regulating FOXO1 expression, localisation, target genes, and activity are investigated in this chapter.

I. Investigate BCR crosslinking with $F(ab')_2$ fragment time-course on the expression of DUB protein in primary CLL cells.
II. Examine the impact of ibrutinib alone or in combination with DUB inhibitors on AKT/FOXO1 axis in MEC1 and primary CLL cells, analysing cell viability, proliferation, cell cycle progression and FOXO regulation - transcription levels of FOXO1 target genes, subcellular localisation and FOXO1 DNA binding activity - in MEC1 cells and primary CLL cells.
III. Determine the interaction between FOXO1 and DUB proteins in MEC1 and CLL cells.
IV. Investigate the role of USP7 and USP9x through shRNA KD alone or in combination with ibrutinib on regulating FOXO1 expression, subcellular localisation, activity, and cell viability and proliferation in MEC1 cells.

4.3 Results

4.3.1 The expression of DUB proteins in primary CLL cells were unaffected by BCR crosslinking with F(ab')$_2$ fragment.

To investigate DUB protein family expression following BCR crosslinking, we stimulated primary CLL cells with F(ab')$_2$ fragment from 0.5 - 24 hr (Figure 4.1a). The data showed no significant difference in USP7 protein expression between unstimulated and stimulated CLL cells at the examined time points (Figure 4.1a & b). The protein levels of USP9x did not change between unstimulated and up to 8 hr of F(ab')$_2$ stimulation, however a significant upregulation of USP9x was noted compared to unstimulated CLL cells at 24 hr (Figure 4.1a & c). The expression levels of USP10 showed some variation between different CLL patients, with a slightly increased expression at the later timepoints compared to unstimulated CLL cells (Figure 4.1a & d).

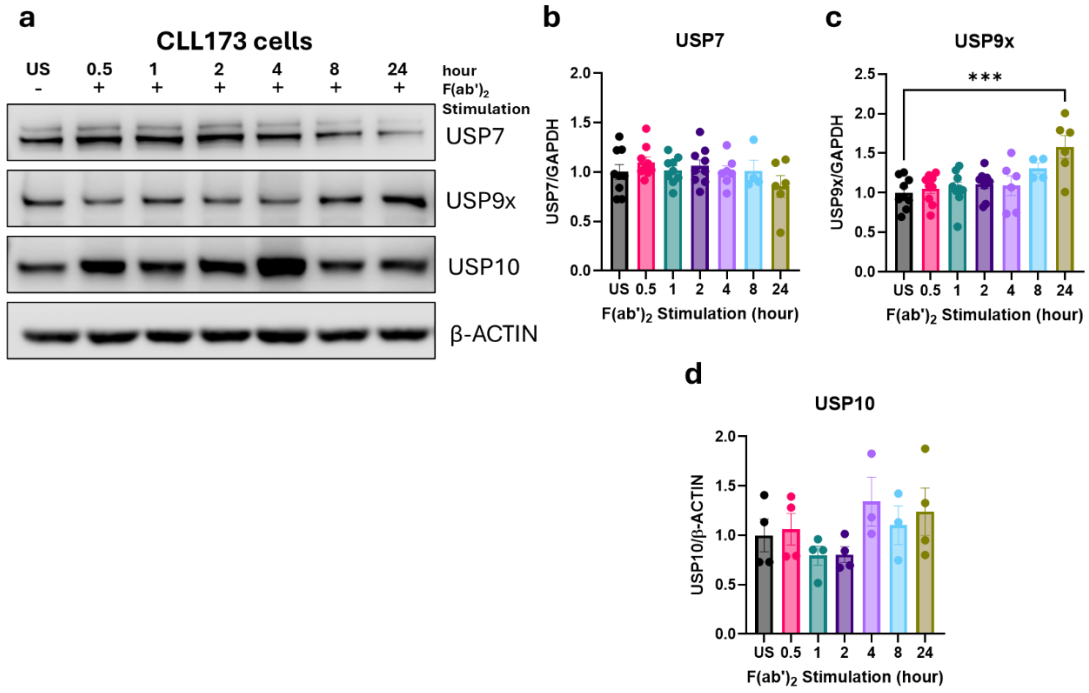

Figure 4.1: The protein expression of USP7, 9x and 10 in primary CLL cells stimulated with F(ab')$_2$ fragment.

(a) Representative Western blot of primary CLL sample (CLL173), unstimulated (US; -) or stimulated (+) with F(ab')$_2$ fragments (10 ng/mL) for the indicated timepoints (hour; hr), (0.5 – 24 hr). The blot was probed for USP7, USP9x, USP10 and β-ACTIN (loading control). Relative protein expression of (b) USP7, (c) USP9x, and (d) USP10 between unstimulated (US = black bar; n ≥ 4) and F(ab')$_2$ stimulated for (0.5 hr = pink bar; n ≥ 4), (1 hr = navy bar; n ≥ 4), (2 hr = purple bar; n ≥ 4), (4 hr = light purple bar; n ≥ 3), (8 hr = blue bar; n ≥ 3), (24 hr = oil green bar; n ≥ 4). Samples were expressed relative to loading control β-ACTIN. The mean expression levels of proteins in US were used to calculate the relative protein expression levels of US and F(ab')$_2$ stimulated timepoints. Each dot represents an individual datapoint. Data expressed as the mean ± SEM. Statistics calculated by One-way ANOVA, Dunnett test (b-d); *** p ≤ 0.001.

4.3.2 DUB inhibitors PR-619, P5091 and WP1130 rapidly reduce p-FOXO^{T24} levels in MEC1 cells in a concentration dependent manner.

Building on our previous findings that PR-619 and WP1130 reduce p-FOXO1^{T24} after 1 hr of treatment (Figure 3.20 & 3.21), which could impact on FOXO1 activity, MEC1 cells were treated with increasing concentrations of PR-619, P5091 or WP1130 according to their IC_{50} by FACS, p-AKT^{S473} and p-FOXO1^{T24} levels were assessed (Figure 4.2a). The data indicated that PR-619 significantly reduced the p-AKT^{S473} in a concentration dependent manner (Figure 4.2a & b). While the downregulation of p-AKT^{S473} was observed at the lowest concentration (3 µM) of PR-619, it was significant at the higher concentrations (6 µM and 9 µM) compared to untreated MEC1 cells (Figure 4.2a & b). The expression of AKT was unaffected by PR-619 treatment (Figure 4.2a & c). While the effect of PR-619 on p-FOXO1^{T24} followed a similar pattern as p-AKT^{S473}, the expression levels of FOXO1 were similar to untreated levels at the lower concentrations, with a trend towards downregulation (p= 0.06) in the highest concentration (9 µM) (Figure 4.2a, d, e).

P5091 did not significantly affect p-AKT^{S473} or AKT levels in a concentration dependent manner in MEC1 cells (Figure 4.2a, f, g). However, p-FOXO1^{T24} levels were significantly reduced at higher concentrations in response to increasing concentrations of P5091 (Figure 4.2a & h). Unlike pan-DUB inhibitor PR-619, the expression of FOXO1 was unaffected by the increased concentrations of P5091 treatment (Figure 4.2a & i).

Interestingly, WP1130 treatment induced a significant upregulation of p-AKT^{S473} with increased concentration, while AKT expression was significantly reduced compared with untreated MEC1 cells (Figure 4.2a, j, k). The p-FOXO1^{T24} and total FOXO1 levels were reduced in a dose-dependent manner compared to untreated MEC1 cells (Figure 4.2a, l, m). While the reduction of p-FOXO1^{T24} was significant with all the investigated concentrations, the reduction in total FOXO1 was statistically significant in the higher concentrations (4 µM and 6 µM) (Figure 4.2l & m). Collectively, DUB inhibitors reduce p-FOXO1^{T24} and total FOXO1 expression in a dose-dependent manner.

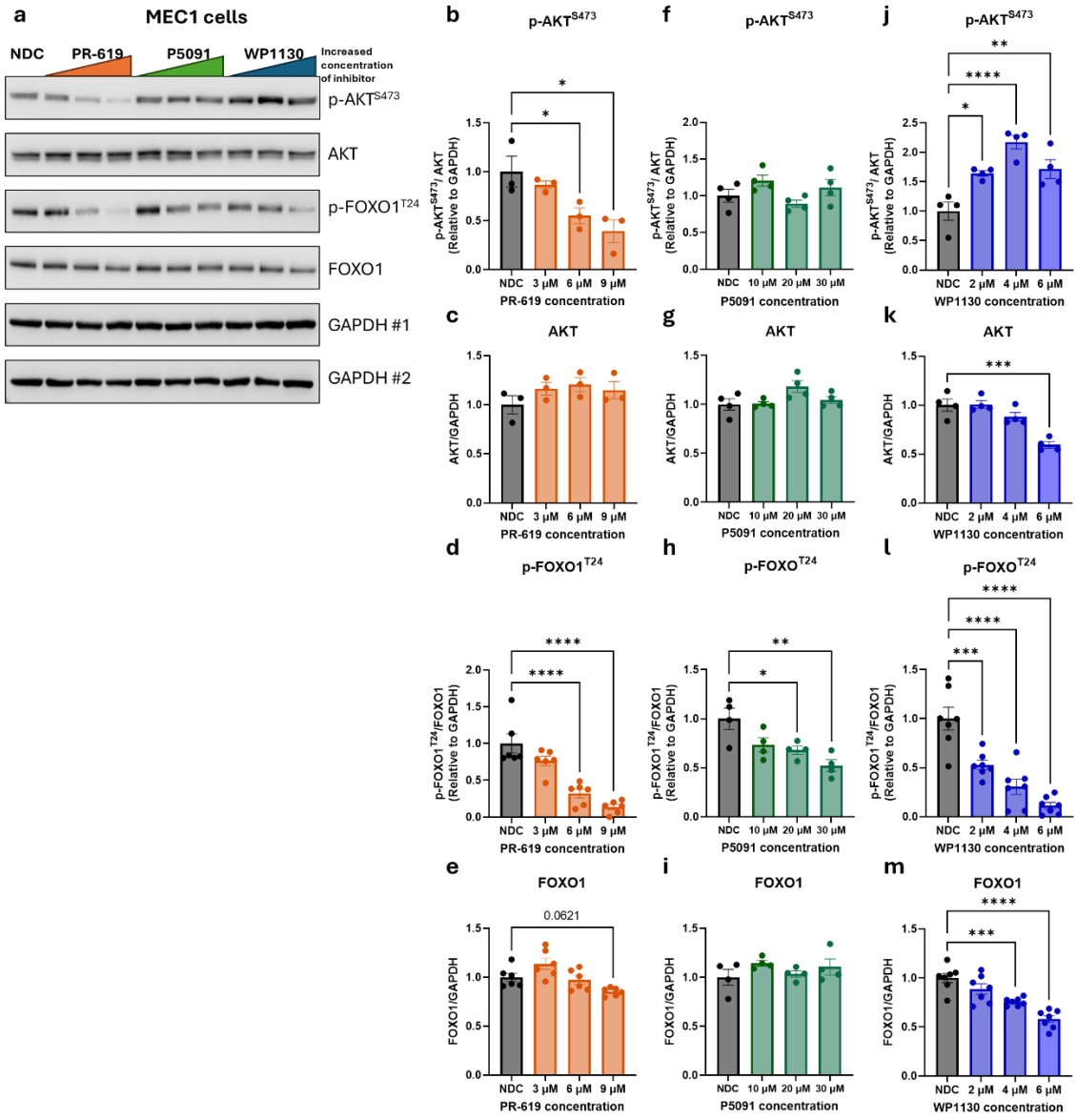

Figure 4.2: DUB inhibitors PR-619, P5091 and WP1130 reduced p-FOXO1^{T24} in MEC1 cells in a concentration dependent manner.

(a) Representative Western blot of MEC1 cells, treated with increased concentration of PR-619 (3 µM, 6 µM, 9 µM; orange bar), P5091 (10 µM, 20 µM, 30 µM; oil green bar), and WP11300 (2 µM, 4 µM, 6 µM; blue bar) for 1 hr or no drug control (NDC; DMSO). The blots were probed for p-AKT^{S473}, AKT, p-FOXO1^{T24}, FOXO1, and GAPDH (loading control; #1 and #2 representing mirror blots). Relative protein expression of (b, f, j) p-AKT^{S473}, (c, g, k) AKT, (d, h, i) p-FOXO1^{T24}, and (e, j, m) FOXO1, between NDC (black bar) and increased concentrations of PR-619 (n ≥ 3; orange bar), P5091 (n = 4; oil green bar), and WP1130 (n ≥ 4; blue bar) treatments. Samples are expressed relative to loading control GAPDH. The mean expression levels of proteins in NDC were used to calculate the relative protein expression levels of NDC and PR-619, P5091, WP1130 treatments. Each dot represented an individual datapoint. Data expressed as the mean ± SEM. Statistics calculated by One-way ANOVA, Dunnett test (b-m); * p ≤ 0.05, ** p ≤ 0.01, *** p ≤ 0.001, **** p ≤ 0.0001.

The expression levels of MCL1 were significantly increased in MEC1 cells treated with the lowest concentration of PR-619 treatment, while higher concentrations did not significantly

change MCL1 expression compared with untreated MEC1 cells (Figure 4.3a & b). The expression of PTEN was slightly elevated with PR-619 treatment at the lowest concentration (3 µM) (p = 0.18), while the higher concentrations (6 µM and 9 µM) demonstrated similar levels of PTEN as untreated MEC1 cells (Figure 4.3a & c). We also examined the impact of PR-619 treatment on the expression DUB protein family members which has been reported to be involved in haematological malignancies including USP7, 9x and 14 (467, 515-517). The data indicated that the expression levels of both USP7 and USP9x were unaffected by the increase concentration of PR-619 in compared to untreated MEC1 cells (Figure 4.3a, d, e). However, the expression levels of USP14 were slightly but significantly elevated in MEC1 cells treated with increased concentrations of PR-619 (Figure 4.3a & f).

P5091 treatment resulted in a significant decrease in the expression levels of MCL1 at the highest concentration (30 µM) of the inhibitor compared to untreated MEC1 cells (Figure 4.3a & g). PTEN levels were unaffected by the increased concentrations of P5091 compared to untreated MEC1 cells (Figure 4.3a & h). Similarly, USP7, 9x and 14 levels were unaffected by increased concentration of P5091 compared to untreated MEC1 cells (Figure 4.3a, i-k).

WP1130 treatment resulted in a significant decrease in MCL1 expression in a concentration dependent manner compared to untreated MEC1 cells (Figure 4.3a & l). The expression levels of PTEN were significantly reduced with the highest concentration of WP1130, while the lower concentration of the inhibitor showed no effect on PTEN expression levels compared to untreated MEC1 cells (Figure 4.3a & m). Similar to PTEN, USP7 and USP14 were significantly downregulated at the highest concentration of inhibitor, while USP9x expression levels were unaffected by the increased concentration of WP1130 compared to MEC1 cells (Figure 4.3a, n-p).

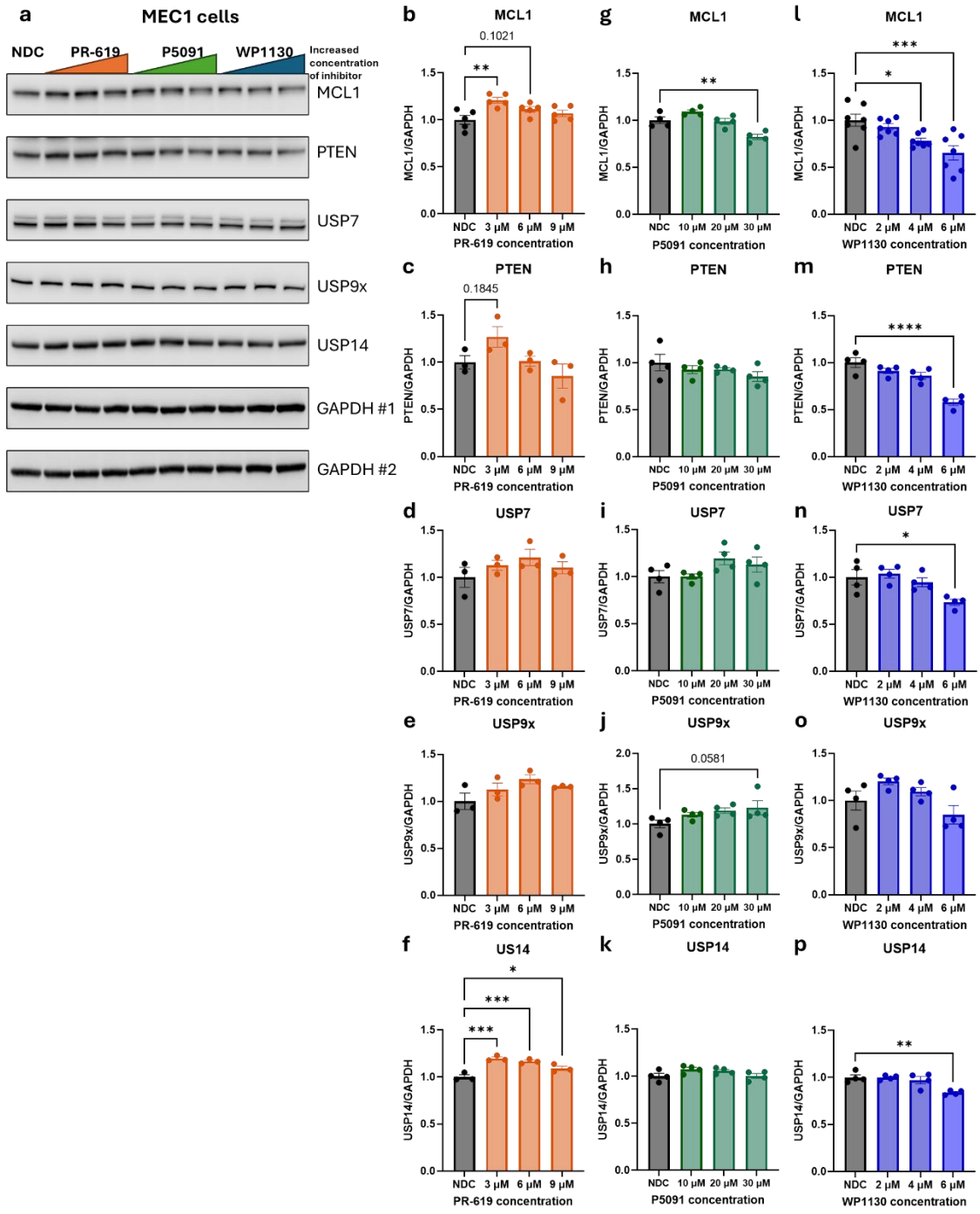

Figure 4.3: DUB inhibitors differentially impact MCL1 and PTEN expression in MEC1 cells. (a) Representative Western blot of MEC1 cells, treated with increased concentration of PR-619 (3 µM, 6 µM, 9 µM; orange bar), P5091 (10 µM, 20 µM, 30 µM; oil green bar), and WP11300 (2 µM, 4 µM, 6 µM; blue bar) for 1 hr or no drug control (NDC; DMSO). The blots were probed for MCL1, PTEN, USP7, USP9x, USP14, and GAPDH (loading control; #1 and #2 representing mirror blots). Relative protein expression of (b, g, l) MCL1, (c, h, m) PTEN, (d, i, n) USP7, (e, j, o) USP9x, and (f, k, p) USP14 between NDC (black bar) and increased concentration of PR-619 ($n \geq 3$; orange bar), P5091 ($n = 4$; oil green bar), and WP1130 ($n \geq 4$; blue bar). Samples were normalised to loading control GAPDH. The mean expression levels of proteins in NDC were used to calculate the relative protein expression levels of NDC and PR-619, P5091, WP1130 treatments. Each dot represented an individual datapoint. Data expressed as the mean ± SEM. Statistics calculated by One-way ANOVA, Dunnett test (b-p); * $p \leq 0.05$, ** $p \leq 0.01$, *** $p \leq 0.001$.

4.3.3 Combination of Ibrutinib treatment with DUB inhibitors enhanced apoptosis in MEC1 and primary CLL cells.

To investigate the combination potential of ibrutinib with DUB inhibitors in MEC1 and primary CLL cells, we treated MEC1 cells with PR-619, WP1130 and P5091 for 48 hr alone or in combination with ibrutinib, while primary CLL cells were treated with HBX19818 for 24 hr alone or in combination with ibrutinib. Cell viability was determined using Annexin V and 7-AAD staining and analysed by FACS (Figure 4.4). The data illustrate that ibrutinib reduced the viability of MEC1 cells by 9% compared to untreated cells, while the combination of ibrutinib with PR-619 resulted in significant reduction of 57% in the viability of MEC1 cells compared to ibrutinib alone (Figure 4.4a). Furthermore, the combination reduced MEC1 viability by 10% compared to PR-619 single treatment (Figure 4.4a). Similarly, the combination of ibrutinib with WP1130 significantly decreased the viability of MEC1 cells by 46% compared to ibrutinib single treatment, enhancing the reduction in MEC1 viability by 20% compared to WP1130 alone (Figure 4.4b). The combination of ibrutinib with P5091 demonstrated a significant decrease of 43% in viability of MEC1 cells compared to ibrutinib treatment. This combination enhanced the reduction in MEC1 viability by 19% compared to P5091 single treatment (Figure 4.4c).

The effect of ibrutinib in the viability of primary CLL cells was similar to MEC1 cells, showing a reduction of 9% compared to the viability of untreated cells. The combination of ibrutinib with HBX19818 demonstrated a significant reduction in the viability of CLL cells by 55% compared to ibrutinib treatment alone. The combination reduced viability of CLL cells by a further 23% compared to HBX19818 alone (Figure 4.4d).

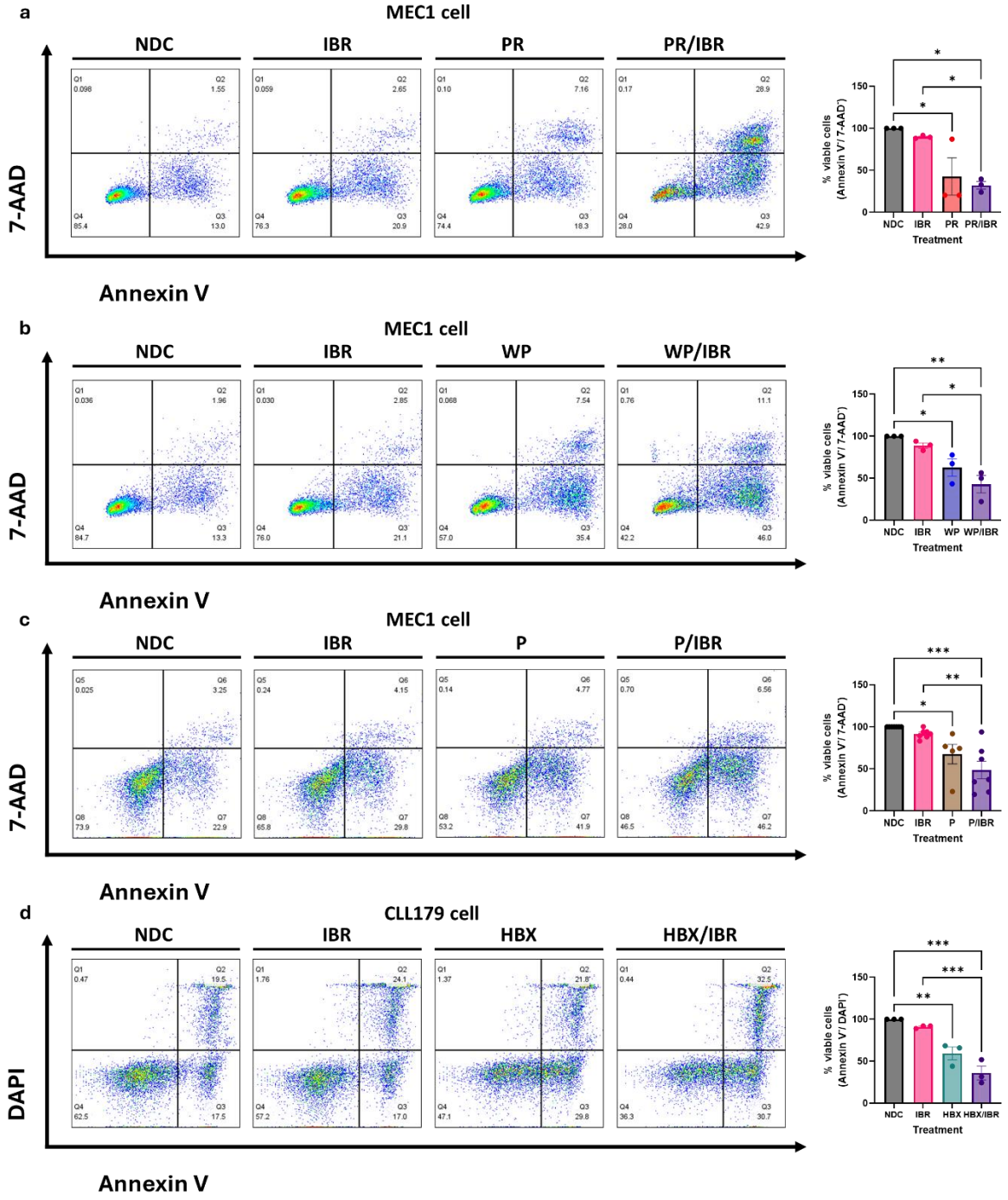

Figure 4.4: Combination of ibrutinib with PR-619, WP1130, P5091 or HBX19818 enhanced their apoptotic effectiveness in MEC1 and primary CLL cells.

Representative FACS dot plots are shown of MEC1 cells (a-c) or primary CLL cells (d) stained with Annexin V and 7-AAD to evaluate cell viability following no drug control (NDC/DMSO = black bar), and treatment with ibrutinib (IBR) ± DUB inhibitors, as indicated. (a) Treatment with IBR (pink bar; 1 µM), PR-619 (PR = red bar; 3 µM), and combination (PR/IBR = purple bar) for 48 hr (n = 3). (b) Treatment with IBR (pink bar; 1 µM), WP1130 (WP = blue bar; 2 µM), and combination (WP/IBR = purple bar) for 48 hr (n = 3). (c) Treatment with IBR (pink bar; 1 µM), P5091 (P = brown bar; 10 µM), and combination (P/IBR = purple bar) for 48 hr (n = 3). (d) Treatment with IBR (pink bar; 1 µM), HBX19818 (HBX = oil green bar; 4 µM), and combination (HBX/IBR = purple bar) for 24 hr (n = 3). Viability is defined as Annexin V negative and 7-AAD/DAPI negative. Percentage viable cells for each condition are relative to NDC for MEC1 cells or primary CLL cells. Each dot represented an individual

datapoint. Data expressed as the mean ± SEM. Statistics calculated by One-way ANOVA, Tukey test (a-d); * $p \leq 0.05$, ** $p \leq 0.01$, *** $p \leq 0.001$.

4.3.4 The combination of Ibrutinib with DUB inhibitors maintained the downregulation of AKT^{S473} and FOXO1^{T24} phosphorylation in MEC1 cells

Building on the potential of combining ibrutinib with DUB inhibitors suggested in section 4.3.3, we investigated the effects of this combination on the BCR signalling pathway, particularly FOXO1^{T24} phosphorylation and total FOXO1 levels. As expected, MEC1 cells treated with ibrutinib significantly reduced the p-AKT^{S473} compared to untreated (Figure 4.5 & 4.6a). PR-619 treatment also significantly reduced p-AKT^{S473}, which was further enhanced by the combination with ibrutinib (Figure 4.5 & 4.6a). The expression of AKT was unaffected by drug treatments (Figure 4.5 & 4.6b). Similar to AKT^{S473} phosphorylation, p-FOXO1^{T24} levels were significantly reduced by ibrutinib treatment in compared to controls (Figure 4.5 & 4.6c). MEC1 cells treated with PR-619 significantly decreased p-FOXO1^{T24}, with the combination exhibiting a further reduction compared to PR-619 single treatment and untreated controls (Figure 4.5 & 4.6c). FOXO1 expression levels were significantly decreased with both ibrutinib and PR-619 treatments alone, and further reduced by the combination compared to untreated controls (Figure 4.5 & 4.6d). However, in all cases the combination of ibrutinib with PR-619 did not further enhance the inhibitors effect on p-AKT^{S473}, p-FOXO1^{T24} and total FOXO1 levels over ibrutinib alone.

Treatment of MEC1 cells with either P5091 or HBX19818 alone or in combination with ibrutinib gave similar results in that both drugs significantly reduced the levels p-AKT^{S473} when in combination with ibrutinib, compared to the DUB inhibitor alone, while expression of AKT was unaffected by the treatments (Figure 4.5, 4.6e, f, I, j). Additionally, these DUB inhibitors alone did not affect p-FOXO1^{T24} or total FOXO1 levels, and the combination had little or no effect in addition to the effect of ibrutinib treatment (Figure 4.5, 4.6g, h, k, l).

Finally, WP1130 treatment of MEC1 cells in combination with ibrutinib significantly reduced p-AKT^{S473} levels in MEC1 cells compared to WP1130 alone which had no effect (Figure 4.5 & 4.6m). AKT levels remained unchanged with drug treatments although there was a trend towards slight reduction in AKT expression with the combination of WP1130 and ibrutinib compared to ibrutinib ($p = 0.23$) and WP1130 ($p = 0.18$) alone (Figure 4.5 & 4.6n). WP1130 treatment alone induced a noticeable reduction in p-FOXO1^{T24} ($p = 0.25$) or total FOXO1

levels compared with NDC (Figure 4.5 & 4.6o, p). The combination of WP1130 with ibrutinib induced a significant reduction in both p-FOXO1^{T24} and total FOXO1 compared to WP1130 alone (Figure 4.5 & 4.6o, p). Indeed, the combination of WP1130 with ibrutinib reduced FOXO1 levels (p = 0.12) compared to ibrutinib alone (Figure 4.5 & 4.6p). Collectively, PR-619 treatment alone demonstrated the largest reduction in p-FOXO1^{T24} or FOXO1 levels compared with the other DUB inhibitors including P5091, HBX19818 or WP1130 treatments alone.

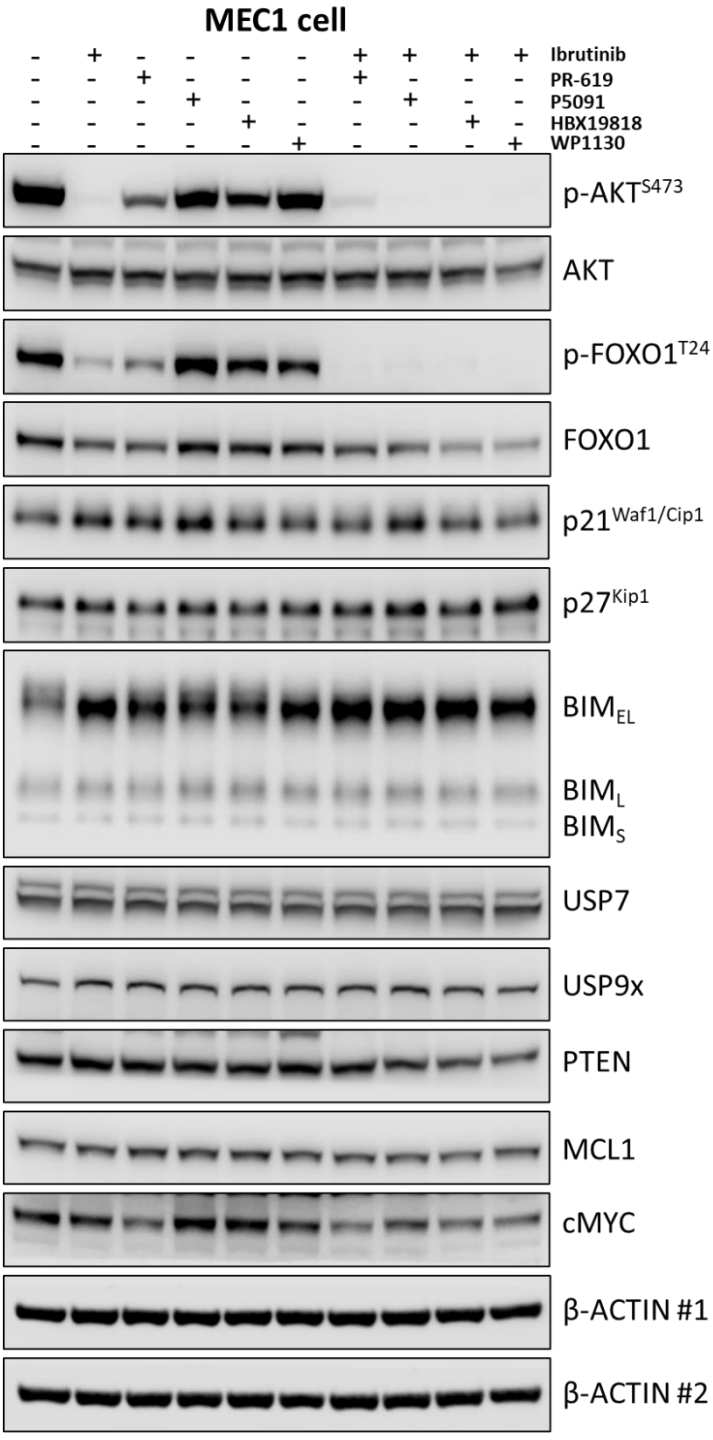

Figure 4.5: Combination of ibrutinib with PR-619, P5091, HBX19818 and WP1130 maintained the downregulation of FOXO1^{T24} phosphorylation in MEC1 cells.
Representative Western blot of MEC1 cells, treated with ibrutinib (1 µM), PR-619 (3 µM), P5091 (10 µM), HBX19818 (10 µM), or WP11300 (2 µM) for (1 hr; hour) alone or in combination with ibrutinib (1 µM), or no drug control (DMSO). The blots were probed for p-AKT^{S473}, AKT, p-FOXO1^{T24}, FOXO1, p21$^{Waf1/Cip1}$, p27^{Kip1}, BIM (EL, L, S), USP7, USP9x, PTEN, MCL1, cMYC, and β-ACTIN (loading control; #1 and #2 representing mirror blots). Added treatment (+), no treatment (-).

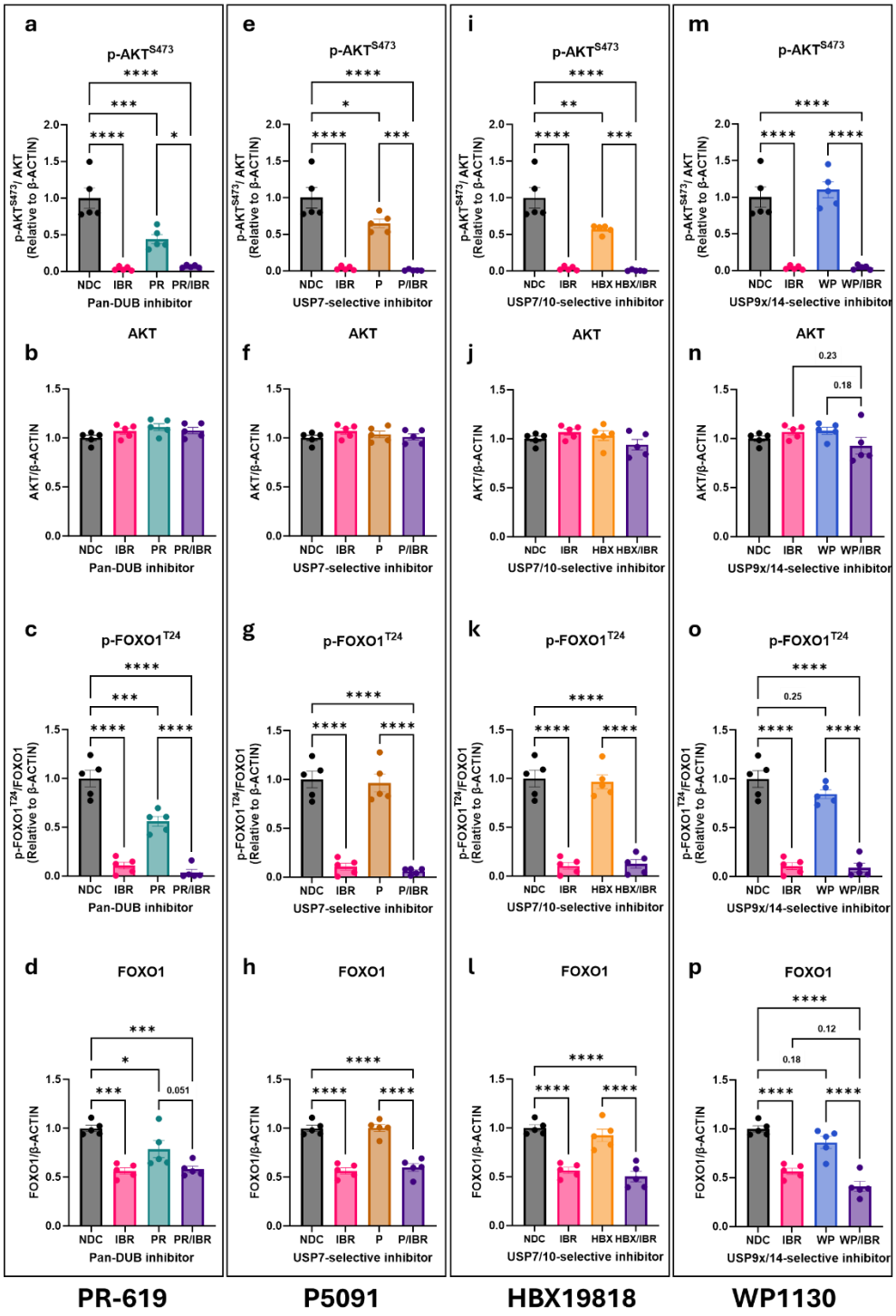

Figure 4.6: The combination of ibrutinib with PR-619, P5091, HBX19818 and WP1130 maintained the downregulation of PI3K/AKT/FOXO1 pathway in MEC1 cells.

A representative Western blot of MEC1 cells, treated with ibrutinib (IBR; 1 µM), PR-619 (PR; 3 µM), P5091 (P; 10 µM), HBX19818 (HBX; 10 µM), or WP11300 (WP; 2 µM) for (1 hr) alone or in combination with IBR, or no drug control (NDC; DMSO) in shown in Figure 4.5. Relative protein expression of (a) p-AKT^{S473}, (b) AKT, (c) p-FOXO1^{T24}, and (d) FOXO1 between NDC (black bar; n = 5), IBR (pink bar; n = 5), PR-619 (PR = oil green bar; n = 5), and combination (PR/IBR = purple bar; n = 5) treatments. Relative protein expression of (e) p-AKT^{S473}, (f) AKT, (g) p-FOXO1^{T24}, and (h) FOXO1 between NDC (black bar; n = 5), IBR (pink bar; n = 5), P5091 (P = brown bar; n = 5), and combination (P/IBR = purple bar; n = 5) treatments. Relative protein expression of (i) p-AKT^{S473}, (j) AKT, (k) p-FOXO1^{T24}, and (l) FOXO1 between NDC (black bar; n = 5), IBR (pink bar; n = 5), HBX19818 (HBX =

orange bar; n = 5), and combination (HBX/IBR = purple bar; n = 5) treatments. Relative protein expression of (m) p-AKT^{S473}, (n) AKT, (o) p-FOXO1^{T24}, and (p) FOXO1 between NDC (black bar; n = 5), IBR (pink bar; n = 5), WP1130 (WP = blue bar; n = 5), and combination (WP/IBR = purple bar; n = 5) treatments. Samples were normalised to loading control β-ACTIN. The mean expression levels of proteins in NDC were used to calculate the relative protein expression levels of NDC and IBR, PR-619, P5091, HBX19818, WP1130, combination treatments. Each dot represented an individual datapoint. Data expressed as the mean ± SEM. Statistics calculated by One-way ANOVA, Tukey test (a-p); * $p \leq 0.05$, ** $p \leq 0.01$, *** $p \leq 0.001$, **** $p \leq 0.0001$.

As FOXO1 is reported to regulate the gene transcription levels of p21$^{Waf1/Cip1}$ (*CDKN1A*), p27^{Kip1} (*CDKN1B*) and BIM (*BCL2L11*) (400, 510, 571), we investigated the protein expression levels of these genes in MEC1 cells treated with DUB inhibitors alone and in combination treatment with ibrutinib. While the drug treatments had no significant effect on the expression levels of p21$^{Waf1/Cip1}$, p27^{Kip1}, BIM$_L$ and BIM$_S$ (Figure 4.5 & 4.7a-t), each inhibitor had a similar impact on BIM$_{EL}$, resulting in a significant, or near significant, increase in expression (Figure 4.7c, h, m, r). Therefore, while ibrutinib treatment elevated the expression levels of BIM$_{EL}$, the upregulation was not statistically significantly compared to untreated controls (Figure 4.5 & 4.7c). Interestingly, PR-619 treatment alone significantly increased the expression levels of BIM$_{EL}$, and this effect was further enhanced by the combination treatment compared to PR-619 and ibrutinib alone (Figure 4.5 & 4.7c).

P5091 treatment increased the expression levels (p = 0.054) of BIM$_{EL}$, and this was further enhanced by the combination treatment compared to P5091 and ibrutinib alone (Figure 4.5 & 4.7h). This upregulation of BIM$_{EL}$ levels were significantly higher than untreated MEC1 cells. HBX19818 treatment increased the expression levels (p = 0.22) of BIM$_{EL}$, which was further enhanced by the combination treatment compared to HBX19818 (p = 0.063) and ibrutinib (p = 0.19) alone (Figure 4.5 & 4.7m). The upregulation of BIM$_{EL}$ levels were significantly higher than untreated MEC1 cells.

While WP1130 treatment alone significantly increased the expression of BIM$_{EL}$ compared to untreated, the combination with ibrutinib did not further enhance this upregulation (Figure 4.5 & 4.7r).

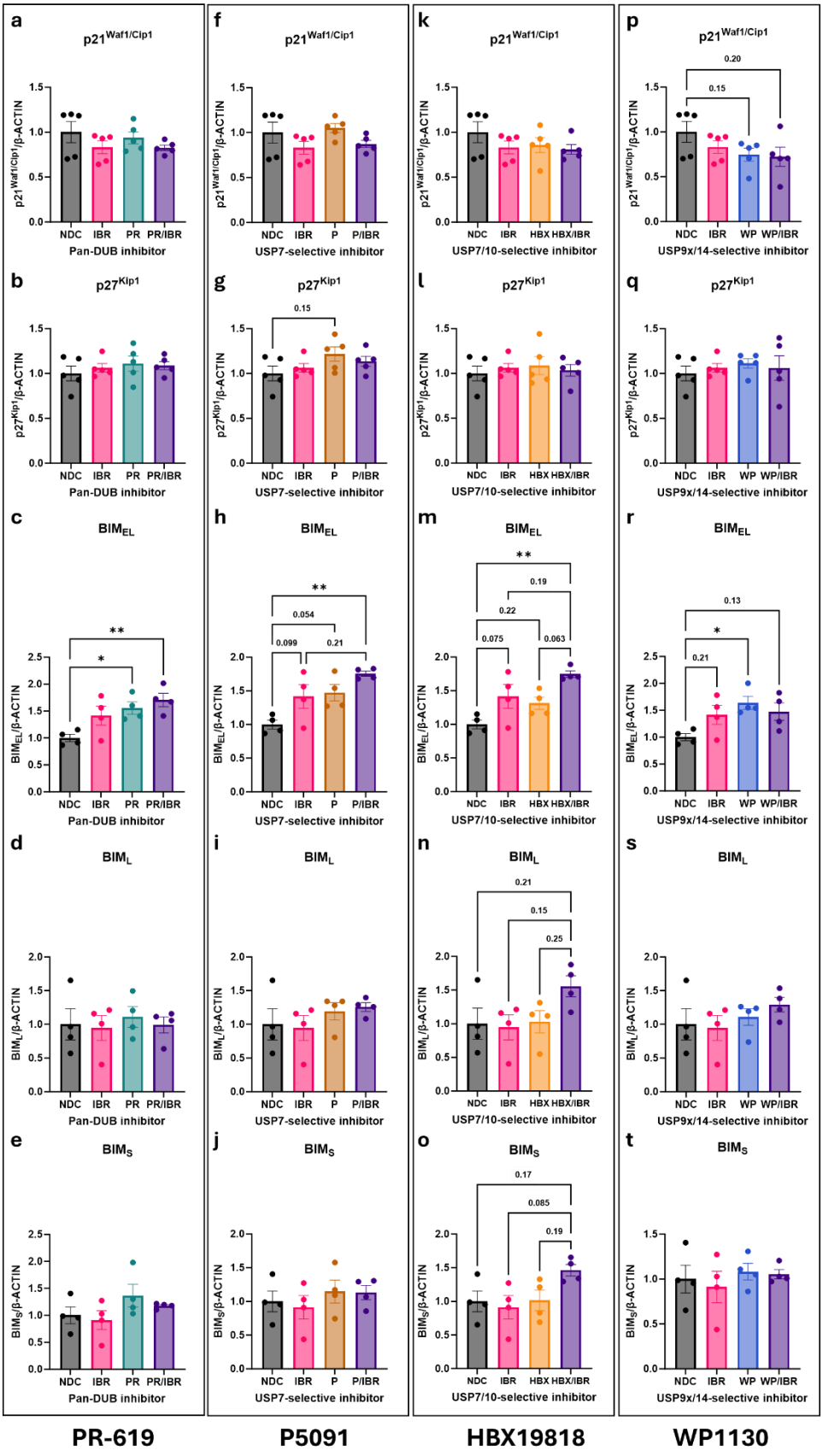

Figure 4.7: Ibrutinib treatment in combination with USP7 selective inhibitors P5091 and HBX19818 enhanced the upregulation of BIM_{EL} in MEC1 cells.

A representative Western blot of MEC1 cells, treated with ibrutinib (IBR; 1 µM), PR-619 (PR; 3 µM), P5091 (P; 10 µM), HBX19818 (HBX; 10 µM), or WP11300 (WP; 2 µM) for (1 hr) alone or in

combination with IBR, or no drug control (NDC; DMSO) in shown in Figure 4.5. Relative protein expression of (a) $p21^{Waf1/Cip1}$, (b) $p27^{Kip1}$, (c) BIM_{EL}, (d) BIM_L, and (e) BIM_S between NDC (black bar; n ≥ 4), IBR (pink bar; n ≥ 4), PR-619 (PR = oil green bar; n ≥ 4), and combination (PR/IBR = purple bar; n ≥ 4) treatments. Relative protein expression of (f) $p21^{Waf1/Cip1}$, (g) $p27^{Kip1}$, (h) BIM_{EL}, (i) BIM_L, and (g) BIM_S between NDC (black bar; n ≥ 4), IBR (pink bar; n ≥ 4), P5091 (P = brown bar; n ≥ 4), and combination (P/IBR = purple bar; n ≥ 4) treatments. Relative protein expression of (k) $p21^{Waf1/Cip1}$, (l) $p27^{Kip1}$, (m) BIM_{EL}, (n) BIM_L, and (o) BIM_S between NDC (black bar; n ≥ 4), IBR (pink bar; n ≥ 4), HBX19818 (HBX = orange bar; n ≥ 4), and combination (HBX/IBR = purple bar; n ≥ 4) treatments. Relative protein expression of (p) $p21^{Waf1/Cip1}$, (q) $p27^{Kip1}$, (r) BIM_{EL}, (s) BIM_L, and (t) BIM_S between NDC (black bar; n ≥ 4), IBR (pink bar; n ≥ 4), WP1130 (WP = blue bar; n ≥ 4), and combination (WP/IBR = purple bar; n ≥ 4) treatments. Samples were normalised to loading control β-ACTIN. The mean expression levels of proteins in NDC were used to calculate the relative protein expression levels of NDC and IBR, PR-619, P5091, HBX19818, WP1130, combination treatments. Each dot represented an individual datapoint. Data expressed as the mean ± SEM. Statistics calculated by One-way ANOVA, Tukey test (a-t); * $p \leq 0.05$, ** $p \leq 0.01$.

Analysis of USP7 and USP9x expression after treatment of MEC1 cells with each of the DUB inhibitors, either alone or in combination revealed no significant change in their expression levels (Figure 4.5 & 4.8). Further to this, PR-619-containing treatments did not alter the expression of PTEN, MCL1 or cMYC, although ibrutinib treatment alone did significantly reduce MCL1 expression compared to untreated cells (Figure 4.5 & 4.8c, d, e). P5091 or ibrutinib treatments alone did not alter PTEN levels, however the combination with ibrutinib downregulated PTEN levels (Figure 4.5 & 4.8h). In addition, P5091 alone did not affect MCL1 or cMYC expression levels compared to untreated controls, however combination with ibrutinib sightly lowered the expression of both MCL1 and cMYC compared to P5091 alone and untreated controls, although this did not reach significance (Figure 4.5 & 4.8i, j). Interestingly, the HBX19818 treatments supported the findings with P5091 treatments, as the combination treatments significantly downregulated PTEN and MCL1 in MEC1 cells, compared with untreated cells (Figure 4.5 & 4.8m, n). These studies support the role for USP7 regulating PTEN and MCL1 in MEC1 cells. Similar to the effect of PR-619 on cMYC levels, HBX19818 treatment alone and the combination reduced cMYC expression, compared to untreated controls although this did not reach significance (Figure 4.5 & 4.8o).

WP1130-containing treatments did not significantly alter the expression of PTEN and MCL1 in MEC1 cells compared to untreated controls (Figure 4.5 & 4.8r, s). However, the expression of cMYC was reduced by WP1130 alone compared to untreated, and this downregulation was significantly reduced in combination with ibrutinib (Figure 4.5 & 4.8t).

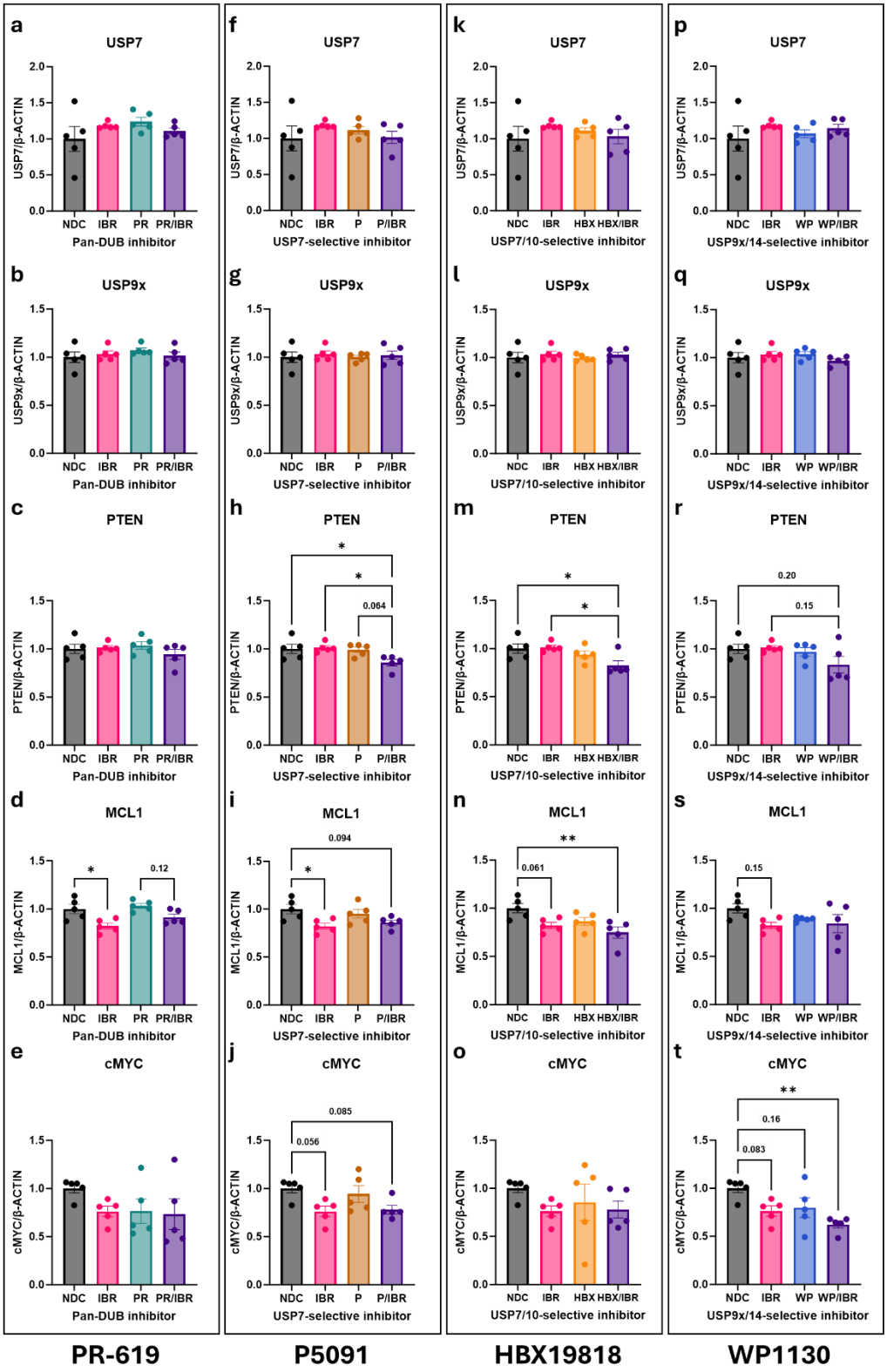

Figure 4.8: Combination of ibrutinib with P5091 or HBX19818 significantly reduced the expression levels of PTEN in MEC1 cells.

A representative Western blot of MEC1 cells, treated with ibrutinib (IBR; 1 µM), PR-619 (PR; 3 µM), P5091 (P; 10 µM), HBX19818 (HBX; 10 µM), or WP11300 (WP; 2 µM) for (1 hr) alone or in combination with IBR, or no drug control (NDC; DMSO) is shown in Figure 4.5. Relative protein expression of (a) USP7, (b) USP9x, (c) PTEN, (d) MCL1, and (e) cMYC between NDC (black bar; n = 5), IBR (pink bar; n = 5), PR-619 (PR = oil green bar; n = 5), and combination (PR/IBR = purple bar; n = 5) treatments. Relative protein expression of (f) USP7, (g) USP9x, (h) PTEN, (i) MCL1, and (g) cMYC

between NDC (black bar; n = 5), IBR (pink bar; n = 5), P5091 (P = brown bar; n = 5), and combination (P/IBR = purple bar; n = 5) treatments. Relative protein expression of (k) USP7, (l) USP9x, (m) PTEN, (n) MCL1, and (o) cMYC between NDC (black bar; n = 5), IBR (pink bar; n = 5), HBX19818 (HBX = orange bar; n = 5), and combination (HBX/IBR = purple bar; n = 5) treatments. Relative protein expression of (p) USP7, (q) USP9x, (r) PTEN, (s) MCL1, and (t) cMYC between NDC (black bar; n = 5), IBR (pink bar; n = 5), WP1130 (WP = blue bar; n = 5), and combination (WP/IBR = purple bar; n = 5) treatments. Samples were normalised to loading control β-ACTIN. The mean expression levels of proteins in NDC were used to calculate the relative protein expression levels of NDC and IBR, PR-619, P5091, HBX19818, WP1130, combination treatments. Each dot represented an individual datapoint. Data expressed as the mean ± SEM. Statistics calculated by One-way ANOVA, Tukey test (a-t); * $p \leq 0.05$, ** $p \leq 0.01$.

4.3.5 Ibrutinib treatment in combination with DUB inhibitors enhanced the inhibition of BCR signalling in primary CLL cells.

In section 3.3.7, we demonstrated that BCR crosslinking induced a rapid and transient upregulation of p-AKT^{S473} and p-FOXO1^{T24}, as well as total FOXO1. This upregulation was reversed by ibrutinib treatment in primary CLL cells. Additionally, in section 4.3.4 combining ibrutinib with DUB inhibitors maintained ibrutinib ability to block the BCR signalling pathway in MEC1 cells. Building upon these findings, we investigated the effects of DUB inhibitors, PR-619 and HBX19818, alone and in combination with ibrutinib, on unstimulated and BCR-stimulated patient CLL cells.

In unstimulated CLL cells, the levels of both p-AKT^{S473} and p-FOXO1^{T24} were unchanged by ibrutinib, PR-619 and HBX19818 treatments compared to unstimulated controls (Figure 4.9 & 4.10a, c, e, g), while BCR crosslinking significantly upregulated the levels of p-AKT^{S473} and p-FOXO1^{T24} compared to unstimulated CLL cells (Figure 4.9 & 4.10a, c), as expected. While Ibrutinib significantly inhibited BCR-mediated p-AKT^{S473} and p-FOXO1^{T24} levels, PR-619 and HBX19818 treatments reduced the BCR-mediated phosphorylation events although not significantly. Notably, combining ibrutinib with either DUB inhibitor further inhibited AKT^{S473} and FOXO1^{T24} phosphorylation to basal levels (Figure 4.9 & 4.10a, c, e, g). As expected, neither BCR crosslinking or drug treatments affected the expression of AKT compared to the control cells (Figure 4.9 & 4.10b, f). Interestingly, while the levels of total FOXO1 were not affected by ibrutinib or DUB inhibitor treatments compared to unstimulated CLL controls (Figure 4.9 & 4.10d, h), BCR crosslinking significantly increased FOXO1 expression compared to unstimulated CLL cells (Figure 4.9 & 4.10d, h). Ibrutinib significantly reduced the expression of total FOXO1, suggesting that FOXO1 upregulation is a BCR-mediated event. Additionally, FOXO1 levels were trending toward downregulation

with PR-619 or HBX19818 alone in BCR crosslinked cells, compared to stimulated control cells (p = 0.13 and 0.24 respectively). Combining ibrutinib with DUB inhibitors further enhanced the inhibitory effect on total FOXO1 expression (Figure 4.9 & 4.10d, h). These studies suggest that the BCR-mediated upregulation of FOXO1 may be partially regulated by DUB proteins.

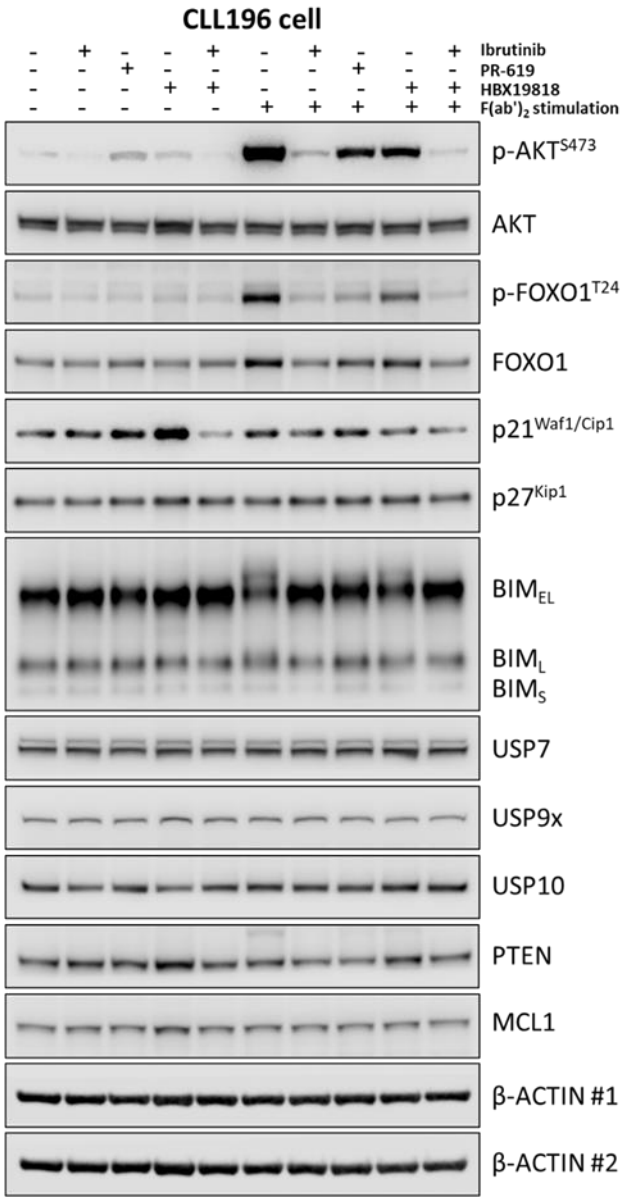

Figure 4.9: BCR crosslinking induced a significant and rapid upregulation of FOXO1^{T24} phosphorylation and total FOXO1, which was reversed by ibrutinib and DUB inhibitors.
Representative Western blot of a primary CLL sample (CLL196), unstimulated or stimulated with F(ab')$_2$ fragments (10 ng/mL) for 0.5 hr. Cells were pre-treated with ibrutinib (IBR; 1 µM), PR-619 (PR; 1.5 µM), or HBX19818 (HBX; 8 µM), or DMSO control for 1 hr alone or in combination with IBR. The blots were probed for p-AKT^{S473}, AKT, p-FOXO1^{T24}, FOXO1, p21$^{Waf1/Cip1}$, p27^{Kip1}, BIM (EL, L, S), USP7, USP9x, USP10, PTEN, MCL1, and β-ACTIN (loading control; #1 and #2 representing mirror blots). Added treatment (+), no treatment (-).

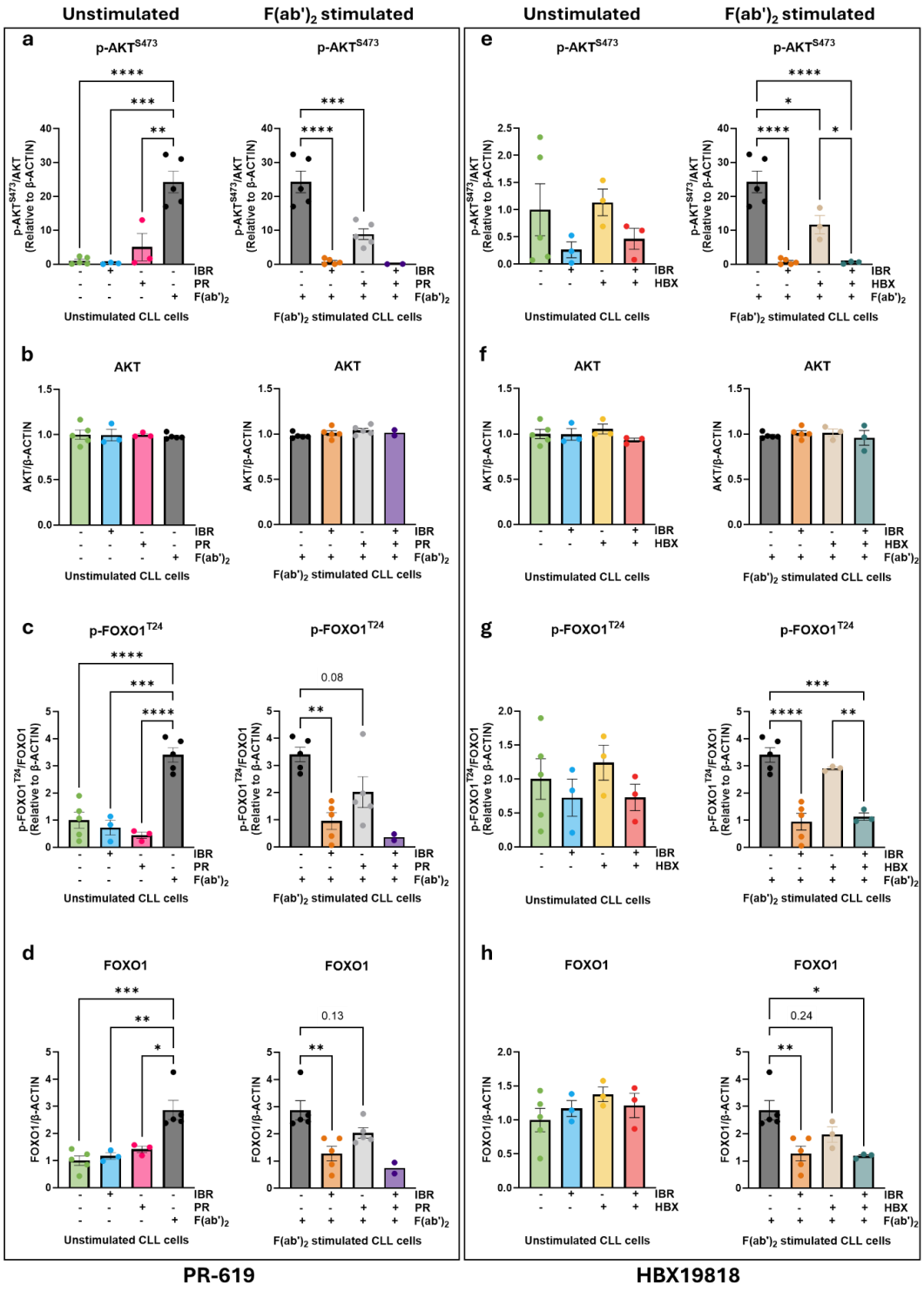

Figure 4.10: Combination of ibrutinib with PR-619 or HBX19818 maintained the inhibition of BCR-mediated phosphorylation of AKT^{S473} and FOXO1^{T24} in primary CLL cells.

Primary CLL cells were left unstimulated or stimulated with F(ab')$_2$ fragments (10 ng/mL) for 0.5 hr, following pre-treatment with ibrutinib (IBR; 1 μM), PR-619 (PR; 1.5 μM), or HBX19818 (HBX; 8 μM), for 1 hr alone or in combination. A representative Western blot is shown in Figure 4.9. Unstimulated and F(ab')$_2$ stimulated vehicle were treated with DMSO. Relative protein expression of (a) p-AKT^{S473}, (b) AKT, (c) p-FOXO1^{T24}, and (d) FOXO1, between unstimulated followed by treatment ((US/DMSO = green bar; n = 5) and IBR (turquoise bar; n = 3), PR (pink bar; n = 3), F(ab')$_2$ stimulated (F(ab')$_2$/DMSO = black bar; n = 5), IBR (orange bar; n = 5), PR (white bar; n = 5) and PR/IBR (purple bar; n = 2). Relative protein expression of (e) p-AKT^{S473}, (f) AKT, (g) p-FOXO1^{T24}, and (h) FOXO1, between US/DMSO (green bar; n = 5) and IBR (turquoise bar; n = 3), HBX (yellow bar; n = 3), and HBX/IBR (red

bar; n = 3)), F(ab')$_2$ stimulation (F(ab')$_2$/DMSO = black bar; n = 5), IBR (orange bar; n =5), HBX (beige bar; n = 3) and HBX/IBR (baby blue bar; n = 3). Samples were normalised to loading control β-ACTIN. The mean expression levels of proteins in vehicle were used to calculate the relative protein expression. Added treatment (+), no treatment (-). Each dot represented an individual datapoint. Data expressed as the mean ± SEM. Statistics calculated by One-way ANOVA, Tukey test (a-h); * $p \leq 0.05$, ** $p \leq 0.01$, *** $p \leq 0.001$, **** $p \leq 0.0001$.

Next, the expression levels of $p21^{Waf1/Cip1}$, $p27^{Kip1}$ and BIM were investigated in unstimulated, and F(ab')$_2$ stimulated primary CLL cells treated with ibrutinib, PR-619 or HBX19818 alone or in combination with ibrutinib. While the drug treatments had little if any effect on the expression of these proteins, either in the presence or absence of BCR stimulation, there was a significant upregulation in $p27^{Kip1}$ with BCR crosslinking compared to unstimulated controls (Figure 4.9 & 4.11b). Interestingly, BCR crosslinking with F(ab')$_2$ fragment demonstrated a trend toward downregulation of BIM_{EL} expression levels compared to unstimulated CLL cells (p = 0.09). This downregulation was reversed by ibrutinib treatment (p = 0.0505), but not PR-619 treatment in compared to stimulated controls (Figure 4.9 & 4.11c). While in unstimulated CLL cells the levels of BIM_{EL} were not affected by ibrutinib and HBX19818 alone, the combination treatment showed a trend toward upregulation (p = 0.17) of BIM_{EL} compared to unstimulated controls (Figure 4.9 & 4.11h). As expected, ibrutinib treatment increased the levels of BIM_{EL}, and this effect was further enhanced by the combination (p = 0.06) compared to stimulated controls. Similar to the data shown with PR-619, HBX19818 alone demonstrated no impact on the levels of BIM_{EL} compared to stimulated controls (Figure 4.9 & 4.11h).

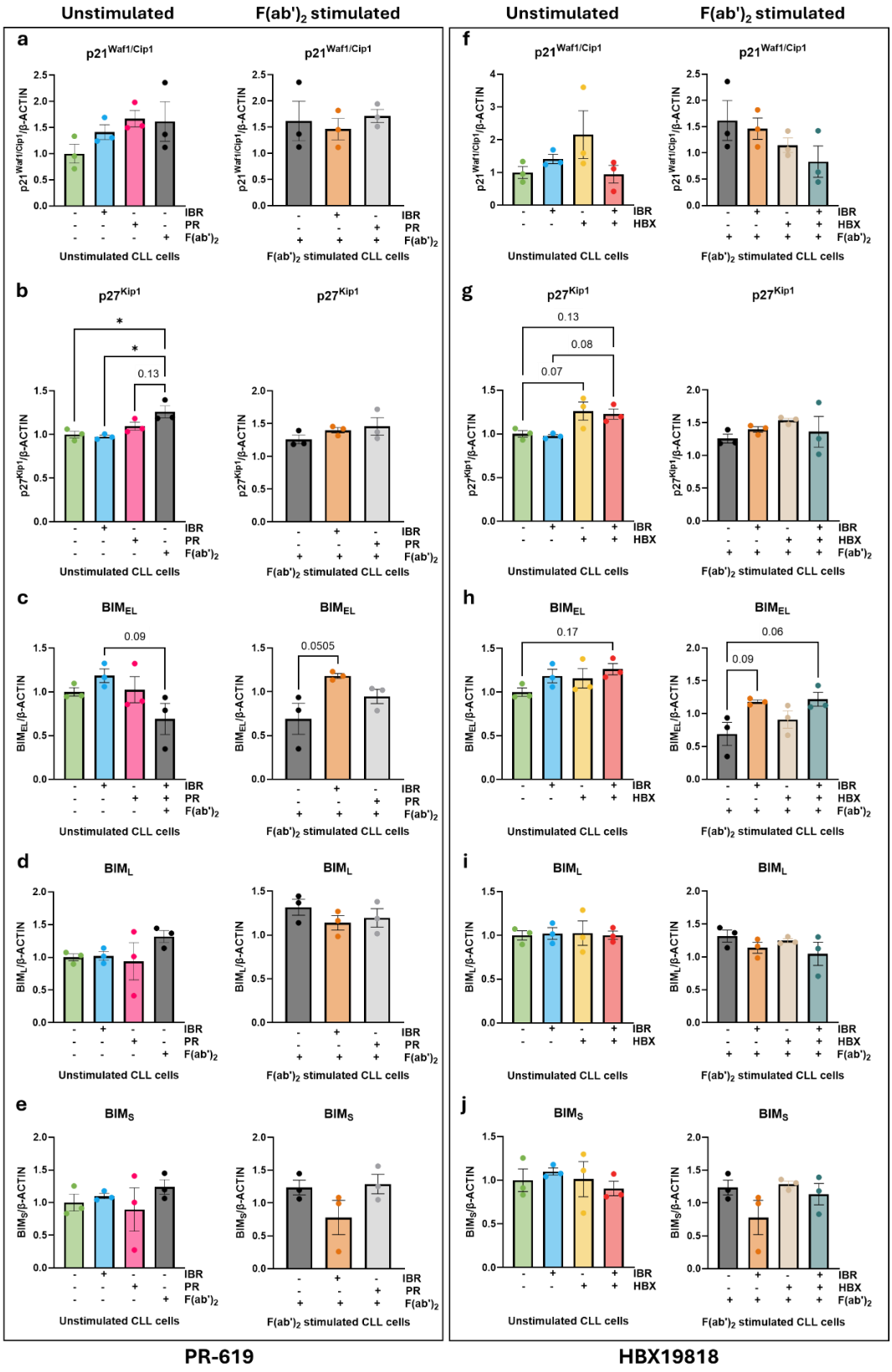

Figure 4.11: Combination of ibrutinib and the selective USP7 inhibitor HBX19818 modestly increased the expression levels of BIM_{EL} in unstimulated and $F(ab')_2$ stimulated primary CLL cells.

Primary CLL cells were left unstimulated or stimulated with $F(ab')_2$ fragments (10 ng/mL) for 0.5 hr, following pre-treatment with ibrutinib (IBR; 1 μM), PR-619 (PR; 1.5 μM), or HBX19818 (HBX; 8 μM), for 1 hr alone or in combination. A representative Western blot is shown in Figure 4.9. Unstimulated and $F(ab')_2$ stimulated vehicle were treated with DMSO. Relative protein expression of (a)

$p21^{Waf1/Cip1}$, (b) $p27^{Kip1}$, (c) BIM_{EL}, (d) BIM_L, (e) BIM_S, between unstimulated followed by treatment (US/DMSO = green bar; n = 3) and IBR (turquoise bar; n = 3), PR (pink bar; n = 3), $F(ab')_2$ stimulated ($F(ab')_2$/DMSO = black bar; n = 3), IBR (orange bar; n = 3), and PR (white bar; n = 3). Relative protein expression of (f) $p21^{Waf1/Cip1}$, (g) $p27^{Kip1}$, (h) BIM_{EL}, (i) BIM_L, and (j) BIM_S, between US/DMSO (green bar; n = 3) and IBR (turquoise bar; n = 3), HBX (yellow bar; n = 3), and HBX/IBR (red bar; n = 3) and $F(ab')_2$/DMSO (black bar; n = 3), IBR (orange bar; n =3), HBX (beige bar; n = 3) and HBX/IBR (baby blue bar; n = 3). Samples were normalised to loading control β-ACTIN. The mean expression levels of proteins in vehicle were used to calculate the relative protein expression. Added treatment (+), no treatment (-). Each dot represented an individual datapoint. Data expressed as the mean ± SEM. Statistics calculated by One-way ANOVA, Tukey test (a-j); * $p \leq 0.05$.

Analysing the expression of USP7, USP9x, USP10, MCL1 and PTEN in response to short-term BCR crosslinking in primary CLL cells, in the presence of ibrutinib and/or DUB inhibitors PR-619 or HBX19818, we found no changes in the expression of USP10 and PTEN (Figure 4.9 & 4.12c, e, h, j). Of note, BCR crosslinking induced a significant upregulation of USP7 expression in CLL cells (Figure 4.9 & 4.12a), which supports our findings in *ex-vivo* CLL samples which have an upregulation of USP7 compared with normal healthy samples (Figure 3.16). This upregulation in expression was not affected by drug treatments.

BCR crosslinking in the presence/absence of ibrutinib and/or PR-619 treatment did not affect the expression levels of both USP9x compared to the control cells (Figure 4.9 & 4.12b, c). In the unstimulated CLL cells, MCL1 expression levels were not affected by ibrutinib and PR-619, however, there was an upregulation of MCL1 by $F(ab')_2$ stimulation (p = 0.14) compared to unstimulated cells. PR-619 significant reduced MCL1 expression levels compared stimulated controls, while ibrutinib only slightly reduced its expression. This slight reduction in MCL1 expression levels by ibrutinib was further enhanced by the combination with PR-619 (Figure 4.9 & 4.12d).

In unstimulated CLL cells, the USP7 levels were upregulated by HBX19818 treatment alone compared to the control (Figure 4.9 & 4.12f). While the expression of USP9x was not affected by ibrutinib and HBX19818 alone and in combination in unstimulated CLL cells, in $F(ab')_2$ stimulated cells the combination of ibrutinib and HBX19818 significantly downregulated USP9x compared to ibrutinib alone and stimulated controls (Figure 4.9 & 4.12g). A similar pattern was noted with MCL1, with a significant downregulation in MCL1 in BCR crosslinked CLL cells when treated with ibrutinib and HBX19818 in combination (Figure 4.9 & 4.12i).

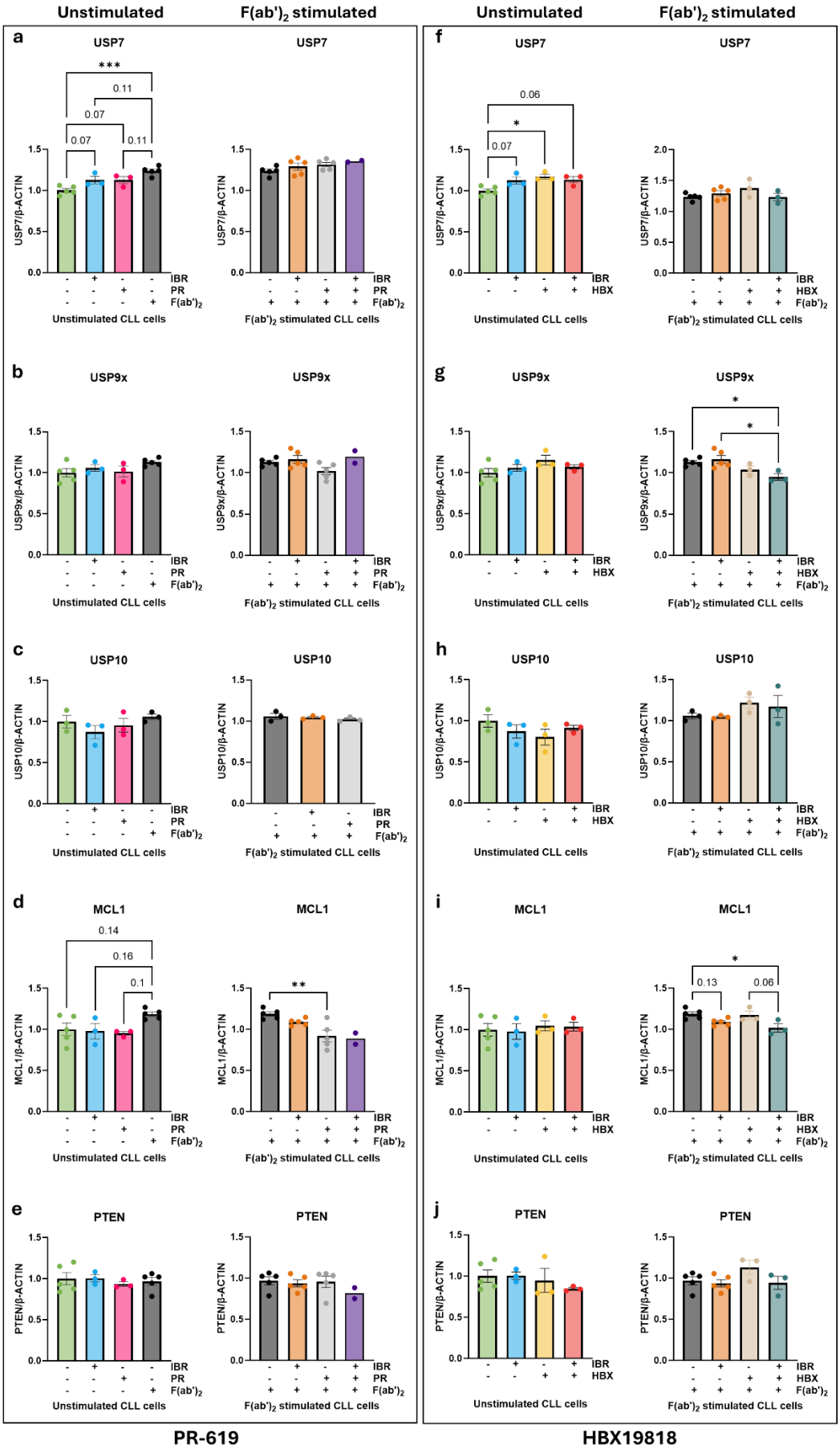

Figure 4.12: Combination of ibrutinib and HBX19818 reduced the expression levels of MCL1 in F(ab')$_2$ stimulated primary CLL cells.

Primary CLL cells were left unstimulated or stimulated with F(ab')$_2$ fragments (10 ng/mL) for 0.5 hr, following pre-treatment with ibrutinib (IBR; 1 µM), PR-619 (PR; 1.5 µM), or HBX19818 (HBX; 8 µM), for 1 hr alone or in combination. A representative Western blot is shown in Figure 4.9. Unstimulated and F(ab')$_2$ stimulated vehicle were treated with DMSO. Relative protein expression of (a) USP7, (b) USP9x, (c) USP10, (d) MCL1, and (e) PTEN between US/DMSO (green bar; n ≥ 3) and ibrutinib (IBR = turquoise bar; n = 3), PR-619 (PR = pink bar; n = 3), F(ab')$_2$ stimulated (F(ab')$_2$/DMSO = black bar; n ≥ 3), IBR (orange bar; n ≥ 3), PR (white bar; n = 3) and combination (PR/IBR = purple bar; n = 2)). Relative protein expression of (f) USP7, (g) USP9x, (h) USP10, (i) MCL1, and (j) PTEN, between US/DMSO (green bar; n ≥ 3) and IBR (turquoise bar; n ≥ 3), HBX19818 (HBX = yellow bar; n = 3), and HBX/IBR (red bar; n = 3), F(ab')$_2$ stimulated (F(ab')$_2$/DMSO = black bar; n ≥ 3), IBR (orange bar; n ≥ 3), HBX (beige bar; n = 3) and HBX/IBR (baby blue bar; n = 3). Samples were normalised to loading control β-ACTIN. The mean expression levels of proteins in vehicle were used to calculate the relative protein expression. Added treatment (+), no treatment (-). Each dot represented an individual datapoint. Data expressed as the mean ± SEM. Statistics calculated by One-way ANOVA, Tukey test (a-j); * p ≤ 0.05, ** p ≤ 0.01, *** p ≤ 0.001.

4.3.6 The expression of DUB proteins USP7, 9x and 10 in pre- and post-ibrutinib *ex-vivo* CLL patient samples.

Our data in section 3.3.11 demonstrated that the expression levels of DUB enzymes including USP7, USP9x and USP10 were upregulated in CLL cells compared to B-cells from heathy donors. Therefore, we were interested to examine their expression levels in *ex-vivo* patient CLL samples that were undergoing ibrutinib treatment. These samples were obtained from PB-derived CLL cells before treatment and after up to three-months of ibrutinib treatment. The data showed that the expression levels of USP7 were similar in pre- and post- ibrutinib treatment (Figure 4.13a & b). Furthermore, the data indicated that USP9x and USP10 expression levels were slightly but not significantly increased in post- compared to pre-ibrutinib CLL samples (p = 0.25 and 0.16), respectively (Figure 4.13a, c, d).

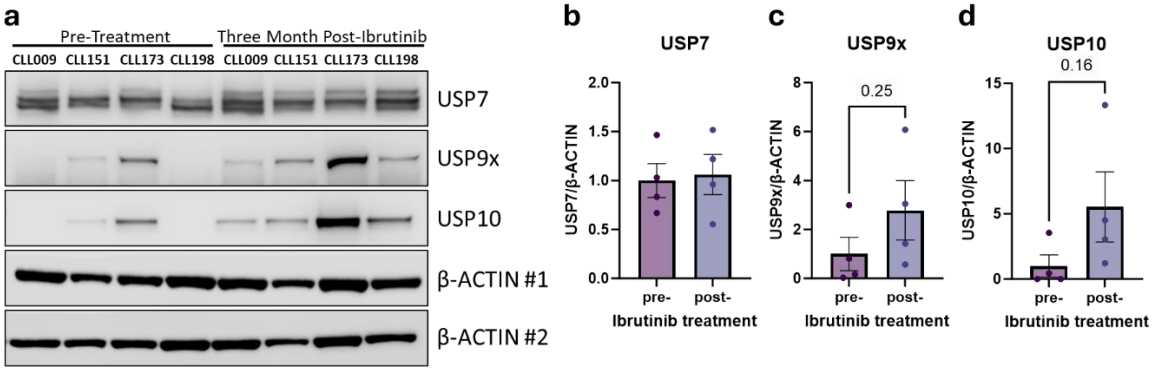

Figure 4.13: DUB proteins USP7, 9x and 10 in pre- and post-ibrutinib *ex-vivo* CLL cells.
(a) Representative Western blot of *ex-vivo* PB-derived CLL patient samples to assess protein expression of pre-ibrutinib treatment (pre-treatment) compared with three months post-ibrutinib patient samples (CLL009, CLL151, CLL173, CLL198), probed for USP7, USP9x, USP10, and β-ACTIN (loading control; #1 and #2 representing mirror blots). Relative protein expression of (b) USP7, (c)

USP9x, and (d) USP10 between pre-ibrutinib (pre-IBR = purple bar; n = 4) and three months post-ibrutinib (post-IBR = blue bar; n =4). Samples were normalised to loading control β-ACTIN. The mean expression levels of proteins in pre-IBR were used to calculate the relative protein expression levels of pre-IBR and post-IBR. Each dot represented an individual datapoint. Data expressed as the mean ± SEM. Statistics calculated by unpaired t-test (b-d).

4.3.7 The combination of ibrutinib and DUB inhibitors enhanced FOXO1 nuclear localisation in MEC1 cells

It has been reported that AKT-mediated phosphorylation of FOXO1 triggers its association with 14-3-3 protein, resulting in shuttling FOXO1 from the nucleus to the cytoplasm (344, 567). Therefore, we assessed FOXO1 subcellular localisation in MEC1 cells treated with ibrutinib, PR-619 or combination of both inhibitors, followed by cellular fractionation. The data suggested that FOXO1 was predominantly localised in the cytoplasm of MEC1 cells compared to the nuclear fraction (Figure 4.14a). Furthermore, MEC1 cells demonstrated higher cytoplasmic levels of USP7 and USP9x compared to the nuclear fractions (Figure 4.14a), with USP9x being localised primarily in the cytoplasm. Ibrutinib treatment significantly increased nuclear FOXO1 levels compared to untreated controls. Moreover, PR-619 alone demonstrated a trend towards nuclear FOXO1 upregulation, which was further enhanced by the combination with ibrutinib. This combination significantly increased nuclear FOXO1 localisation compared to ibrutinib, PR-619 alone, and untreated controls (Figure 4.14a, b). The elevation of FOXO1 in the nucleus was mirrored by a concomitant reduction of FOXO1 from the cytoplasm (Figure 4.14a, c). Similar findings were observed with FOXO1 re-localisation when MEC1 cells were treated with P5091 in the presence and absence of ibrutinib (Figure 4.15a-c). Conversely, treatment of MEC1 cells with WP1130 alone or in combination with ibrutinib did not affect nuclear or cytoplasmic FOXO1 levels compared to untreated controls (Figure 4.16a-c). Ibrutinib treatment decreased cytoplasmic FOXO1 levels compared to untreated controls (p = 0.06), as expected. The combination of ibrutinib and WP1130 showed a modest additional reduction compared to WP1130 alone, but not compared to ibrutinib alone (Figure 4.16a, c).

While the cytoplasmic levels of USP7 and USP9x were not affected by drug treatments, the combination treatment increased the nuclear levels of USP7 and USP9x compared to single and untreated controls (Figure 4.14a, d, e-g). Of note, when cells were treated with P5091, the nuclear and cytoplasmic levels of USP7 and USP9x were not affected by the inhibitors alone and combination treatment compared to untreated controls (Figure 4.15a, d-g). This

may reflect the broader spectrum DUB inhibition of PR-619. Nuclear and cytoplasmic levels of USP7, and nuclear levels of USP9x were not affected by WP1130 alone or combination compared to untreated controls (Figure 4.16a, d-f). While nuclear USP9x levels remained unaffected by the inhibitors, the combination treatment significantly increased cytoplasmic USP9x levels compared to controls and single treatments (Figure 4.16a, g).

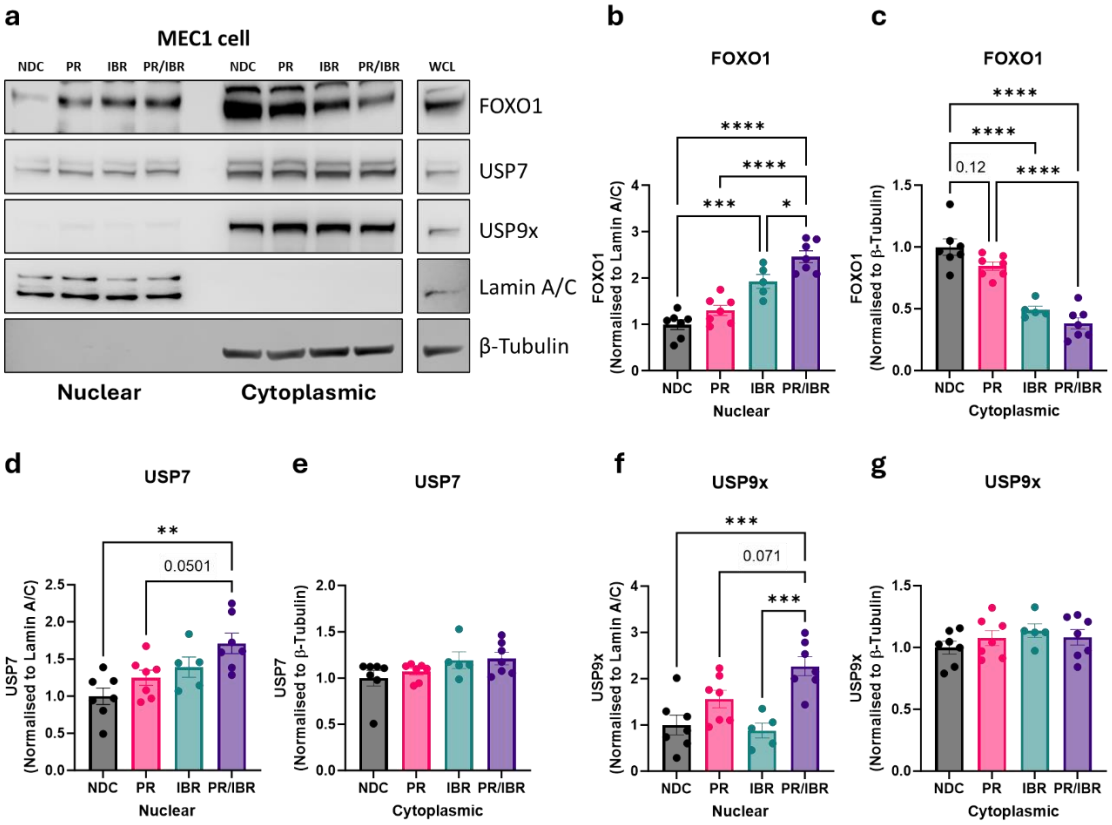

Figure 4.14: Combination of ibrutinib with PR-619 significantly increased nuclear FOXO1 levels in MEC1 cells.

(a) Representative Western blot of subcellular fractionation of MEC1 cells treated with PR-619 (PR; 3 µM), ibrutinib (IBR; 1 µM), and combination (PR/IBR), or no drug control (NDC/DMSO). Following 1 hr treatment, MEC1 cells (n ≥ 5) were fractionated into cytoplasmic, nuclear, and whole cell lysate (WCL). The blots were probed for FOXO1, USP7, USP9x, Lamin A/C (nuclear loading control), and β-Tubulin (cytoplasmic loading control). Relative protein expression of (b) nuclear FOXO1, (c) cytoplasmic FOXO1, (d) nuclear USP7, (e) cytoplasmic USP7, (f) nuclear USP9x, and (g) cytoplasmic USP9x between NDC (black bar), PR (pink bar), IBR (oil green bar), and PR/IBR (purple bar). Nuclear and cytoplasmic fractions were normalised to loading controls (Lamin A/C and β-Tubulin, respectively). The mean expression levels of proteins in NDC were used to calculate the relative protein expression levels. Each dot represented an individual datapoint. Data expressed as the mean ± SEM. Statistics calculated by One-way ANOVA, Tukey test (b-g); * $p \leq 0.05$, ** $p \leq 0.01$, *** $p \leq 0.001$, **** $p \leq 0.0001$.

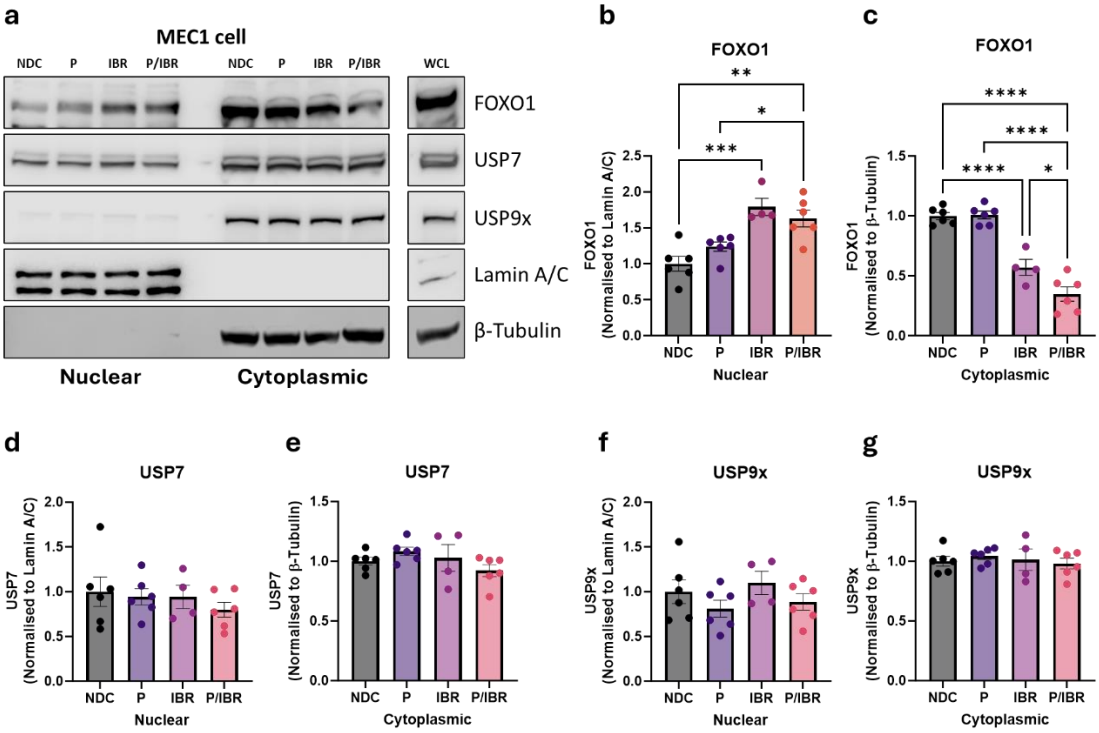

Figure 4.15: Combination of ibrutinib with P5091 significantly increased nuclear FOXO1 levels in MEC1 cells.

(a) Representative Western blot of subcellular fractionation of MEC1 cells treated with P5091 (P; 10 µM), ibrutinib (IBR; 1 µM), and combination (P/IBR), or no drug control (NDC/DMSO). Following 1 hr treatment MEC1 cells (n = 5) were fractionated into cytoplasmic, nuclear, and whole cell lysate (WCL). The blots were probed for FOXO1, USP7, USP9x, Lamin A/C (nuclear loading control), and β-Tubulin (cytoplasmic loading control). Relative protein expression of (b) nuclear FOXO1, (c) cytoplasmic FOXO1, (d) nuclear USP7, (e) cytoplasmic USP7, (f) nuclear USP9x, and (g) cytoplasmic USP9x between NDC (black bar), P (violet bar), IBR (purple bar), and P/IBR (fuchsia bar). Nuclear and cytoplasmic fractions were normalised to loading controls (Lamin A/C and β-Tubulin, respectively). The mean expression levels of proteins in NDC were used to calculate the relative protein expression levels. Each dot represented an individual datapoint. Data expressed as the mean ± SEM. Statistics calculated by One-way ANOVA, Tukey test (b-g); * $p \leq 0.05$, ** $p \leq 0.01$, *** $p \leq 0.001$, **** $p \leq 0.0001$.

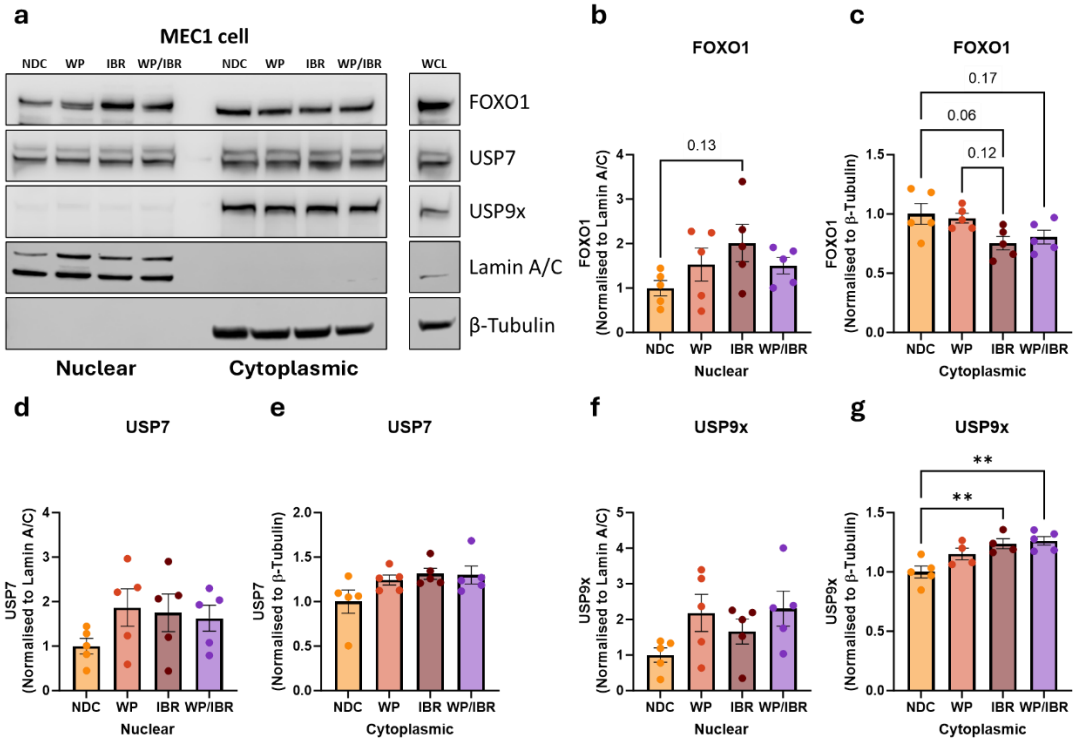

Figure 4.16: Combination of ibrutinib and WP1130 increased cytoplasmic USP9x in MEC1 cells.

(a) Representative Western blot of subcellular fractionation of MEC1 cells treated with WP1130 (WP; 2 µM), ibrutinib (IBR; 1 µM), and combination (WP/IBR), or no drug control (NDC/DMSO). MEC1 cells (n = 5) were fractionated into cytoplasmic, nuclear, and whole cell lysate (WCL). The blots were probed for FOXO1, USP7, USP9x, Lamin A/C (nuclear loading control), and β-Tubulin (cytoplasmic loading control). Relative protein expression of (b) nuclear FOXO1, (c) cytoplasmic FOXO1, (d) nuclear USP7, (e) cytoplasmic USP7, (f) nuclear USP9x, and (g) cytoplasmic USP9x between NDC (light orange bar), WP (dark orange bar), IBR (dark red bar), and WP/IBR (violet bar). Nuclear and cytoplasmic fractions were normalised to loading controls (Lamin A/C and β-Tubulin, respectively). The mean expression levels of proteins in NDC were used to calculate the relative protein expression levels. Each dot represented an individual datapoint. Data expressed as the mean ± SEM. Statistics calculated by One-way ANOVA, Tukey test (b-g); ** $p \leq 0.01$.

4.3.8 The combination of ibrutinib with PR-619 or HBX19818 enhanced the reduction of cytoplasmic FOXO1 levels in F(ab')$_2$ stimulated primary CLL cells.

Building upon our findings in MEC1 cells, where ibrutinib, in combination with PR-619 or the selective USP7 inhibitor P5091, promoted nuclear FOXO1 localisation, we investigated FOXO1 localisation in F(ab')$_2$ stimulated primary CLL cells. We aimed to elucidate the roles of ibrutinib, PR-619, and the selective USP7 inhibitor HBX19818, alone or in combination, in regulating FOXO1 localisation in CLL patient cells.

Western blotting data revealed that FOXO1 was predominantly localised in the nuclear fraction of unstimulated CLL cells, while $F(ab')_2$ simulation led to its depletion from the nuclear fraction and accumulation in the cytoplasmic fraction (Figure 4.17a, b). Unstimulated CLL cells displayed no significant changes in nuclear FOXO1 levels with ibrutinib, PR-619, or HBX19818 treatment compared to untreated controls (Figure 4.17a, b). Similar to MEC1 cells, $F(ab')_2$ stimulated CLL cells exhibited a significant upregulation of nuclear FOXO1 with ibrutinib treatment compared to stimulated controls. PR-619 alone did not alter nuclear FOXO1 levels, whereas the combination of ibrutinib with PR-619 significantly upregulated nuclear FOXO1 levels in stimulated CLL cells, with an effect comparable to ibrutinib alone (Figure 4.17a, c). Similar to PR-619, HBX19818 had no effect on nuclear FOXO1 levels in stimulated CLL cells compared to stimulated controls. While the combination of HBX19818 and ibrutinib slightly increased nuclear FOXO1 levels compared to HBX19818 alone, it reduced the effect of ibrutinib-mediated nuclear FOXO1 upregulation observed in stimulated CLL cells compared to ibrutinib alone (Figure 4.17a, d). The changes of FOXO1 location in the nucleus with BCR crosslinking and drug treatments were mirrored by opposing changes in FOXO1 levels from the cytoplasm (Figure 4.17a, e-g).

Cellular fractionation revealed comparable USP7 and USP9x levels in the nuclear and cytoplasmic fractions of primary CLL cells (Fig. 4.17a). Analysis of USP7 and USP9x in primary CLL cells showed that nuclear and cytoplasmic localisation of these proteins was not significantly affected by BCR crosslinking alone or in the presence and absence of drugs (Figure 4.17 & 4.18).

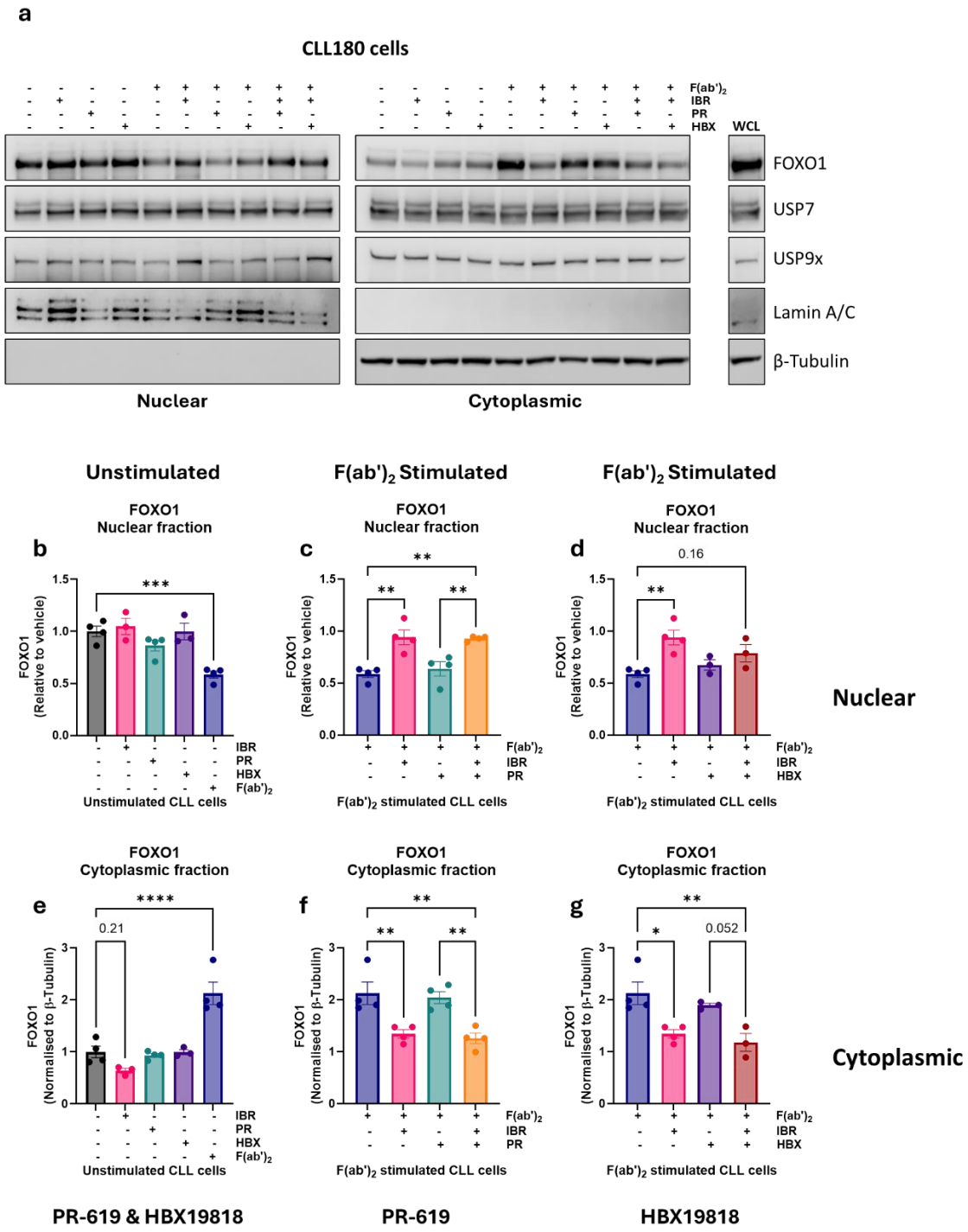

Figure 4.17: Combination of ibrutinib with PR-619 or HBX19818 slightly enhanced the effect of ibrutinib in downregulating cytoplasmic FOXO1 levels in F(ab')$_2$ stimulated primary CLL cells.

(a) Representative Western blot of subcellular fractionation of primary CLL cells (CLL180) unstimulated or stimulated with F(ab')$_2$ fragments (10 ng/mL) for 0.5 hr, following pre-treatment with ibrutinib (IBR; 1 µM), PR-619 (PR; 1.5 µM), or HBX19818 (HBX; 8 µM), for 1 hr alone or in combination with IBR (1 µM). Unstimulated vehicle and F(ab')$_2$ stimulated vehicle were treated with DMSO. CLL cells ($n \geq 3$) were fractionated into cytoplasmic, nuclear, and whole cell lysate (WCL). The blots were probed for FOXO1, USP7, USP9x, Lamin A/C (nuclear loading control), and β-Tubulin (cytoplasmic loading control). Relative protein expression of (b) nuclear FOXO1 levels in unstimulated CLL cells treated with IBR (pink bar), PR (oil green bar), HBX (purple bar), and F(ab')$_2$ stimulation (blue bar), or NDC/DMSO (black bar). (c) Nuclear FOXO1 levels in F(ab')$_2$/DMSO (blue

bar), IBR (pink bar), PR (oil green bar), and PR/IBR (light orange bar). (d) Nuclear FOXO1 levels in F(ab')$_2$/DMSO (blue bar), IBR (pink bar), HBX (purple bar), and HBX/IBR (red bar). Cytoplasmic FOXO1 levels in (e) unstimulated and (f & g) F(ab')$_2$ stimulated CLL cells treated as described in (b-d, respectively). Nuclear and cytoplasmic fractions were normalised to loading controls (Lamin A/C and β-Tubulin, respectively). The mean expression levels of proteins in NDC were used to calculate the relative protein expression levels. Added treatment (+), no treatment (-). Each dot represented an individual datapoint. Data expressed as the mean ± SEM. Statistics calculated by One-way ANOVA, Tukey test (b-g); * $p \leq 0.05$, ** $p \leq 0.01$, *** $p \leq 0.001$, **** $p \leq 0.0001$.

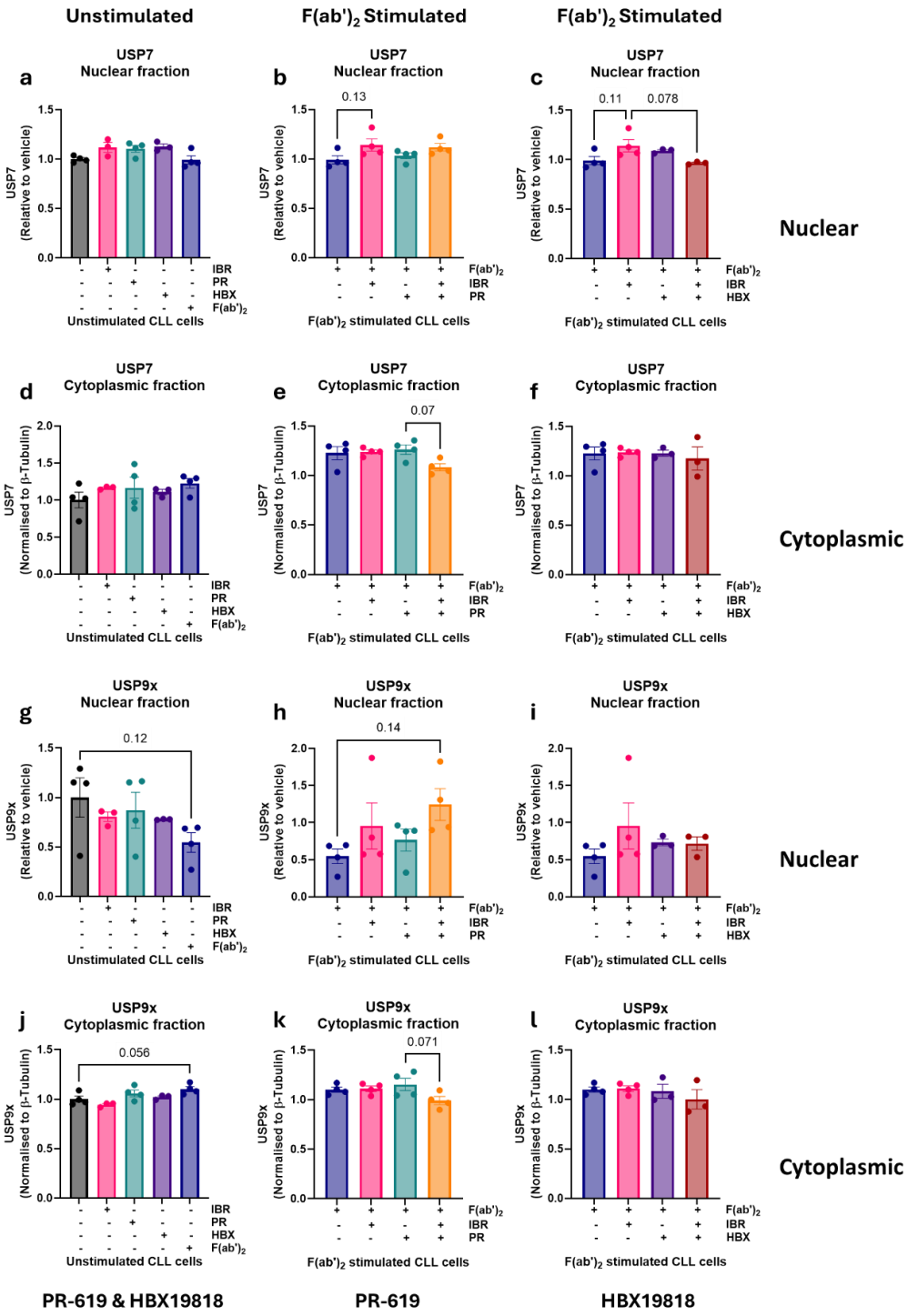

Figure 4.18: The nuclear and cytoplasmic levels of USP7 and USP9x were not affected by ibrutinib, PR-619 and HBX19818 treatments in primary CLL cells.

Primary CLL cells (CLL180) unstimulated or stimulated with $F(ab')_2$ fragments (10 ng/mL) for 0.5 hr, following pre-treatment with ibrutinib (IBR; 1 µM), PR-619 (PR; 1.5 µM), or HBX19818 (HBX; 8 µM), for (1 hr) alone or in combination with IBR. Unstimulated vehicle and $F(ab')_2$ stimulated vehicle were treated with DMSO. Following treatments, CLL cells (n ≥ 3) were fractionated into cytoplasmic, nuclear, and whole cell lysate (WCL). Relative protein expression of (a) nuclear USP7 levels in unstimulated CLL cells treated with IBR (pink bar), PR (oil green bar), HBX (purple bar), and $F(ab')_2$ (blue bar), or unstimulated (NDC/DMSO = black bar). (b) Nuclear USP7 levels in $F(ab')_2$ stimulated CLL cells (blue bar), IBR (pink bar), PR (oil green bar), and PR/IBR (light orange bar). (c) Nuclear USP7 levels in $F(ab')_2$/DMSO (blue bar), IBR (pink bar), HBX (purple bar), and HBX/IBR (red bar). (d) Cytoplasmic USP7 levels in (d) unstimulated and (e & f) $F(ab')_2$ stimulated CLL cells treated as described in (a-c, respectively). Nuclear USP9x levels in (g) unstimulated and (h & i) $F(ab')_2$ stimulated CLL cells treated as described in (a-c, respectively). Cytoplasmic USP9x levels in (j) unstimulated and (k & l) $F(ab')_2$ stimulated CLL cells treated as described in (a-c, respectively). Nuclear and cytoplasmic fractions were normalised to loading controls (Lamin A/C and β-Tubulin, respectively). The mean expression levels of proteins in NDC were used to calculate the relative protein expression levels. Added treatment (+), no treatment (-). Each dot represented an individual datapoint. Data expressed as the mean ± SEM. Statistics calculated by One-way ANOVA, Tukey test (a-l).

4.3.9 Combination of Ibrutinib with DUB inhibitors enhanced their anti-proliferative effects in MEC1 cells.

Our data indicated that the combination of ibrutinib and DUB inhibitors (PR-619, WP1130, P5091 and HBX19818) enhanced ibrutinib effects in MEC1 and CLL cells. This combination treatment resulted in increased apoptosis, reduced BCR activity through downregulation of AKT and FOXO1 phosphorylation, and upregulation of nuclear FOXO1 levels in MEC1 and CLL cells. Therefore, we investigated whether DUB inhibitors, alone and in combination with ibrutinib, could further suppress MEC1 cell proliferation compared to ibrutinib alone. To assess this, we employed CTV for proliferation analysis in MEC1 cells. The cells were treated for 48 hr with ibrutinib, PR-619, P5091 or HBX19818 alone or in combination with ibrutinib. The CTV data demonstrated that ibrutinib treatment had no significant effect on the proliferation of MEC1 cells after 48 hr of treatment compared to untreated controls (Figure 4.19). Furthermore, treatment with PR-619 showed a trend toward increased CTV, indicating reduction in MEC1 cells proliferation compared to untreated controls (p = 0.07). The combination of PR-619 with ibrutinib modestly increased the effect of ibrutinib in reducing MEC1 proliferation, although this did not reach significance (p = 0.09; Figure 4.19a). While WP1130 alone had no significant effects on proliferation, the combination with ibrutinib significantly reduced MEC1 cells proliferation compared to single treatments and untreated controls (Figure 4.19b). Similar to ibrutinib alone, the selective USP7

inhibitors P5091 and HBX19818 alone or combined with ibrutinib had minimal effects on MEC1 cells proliferation (Figure 4.19c & d).

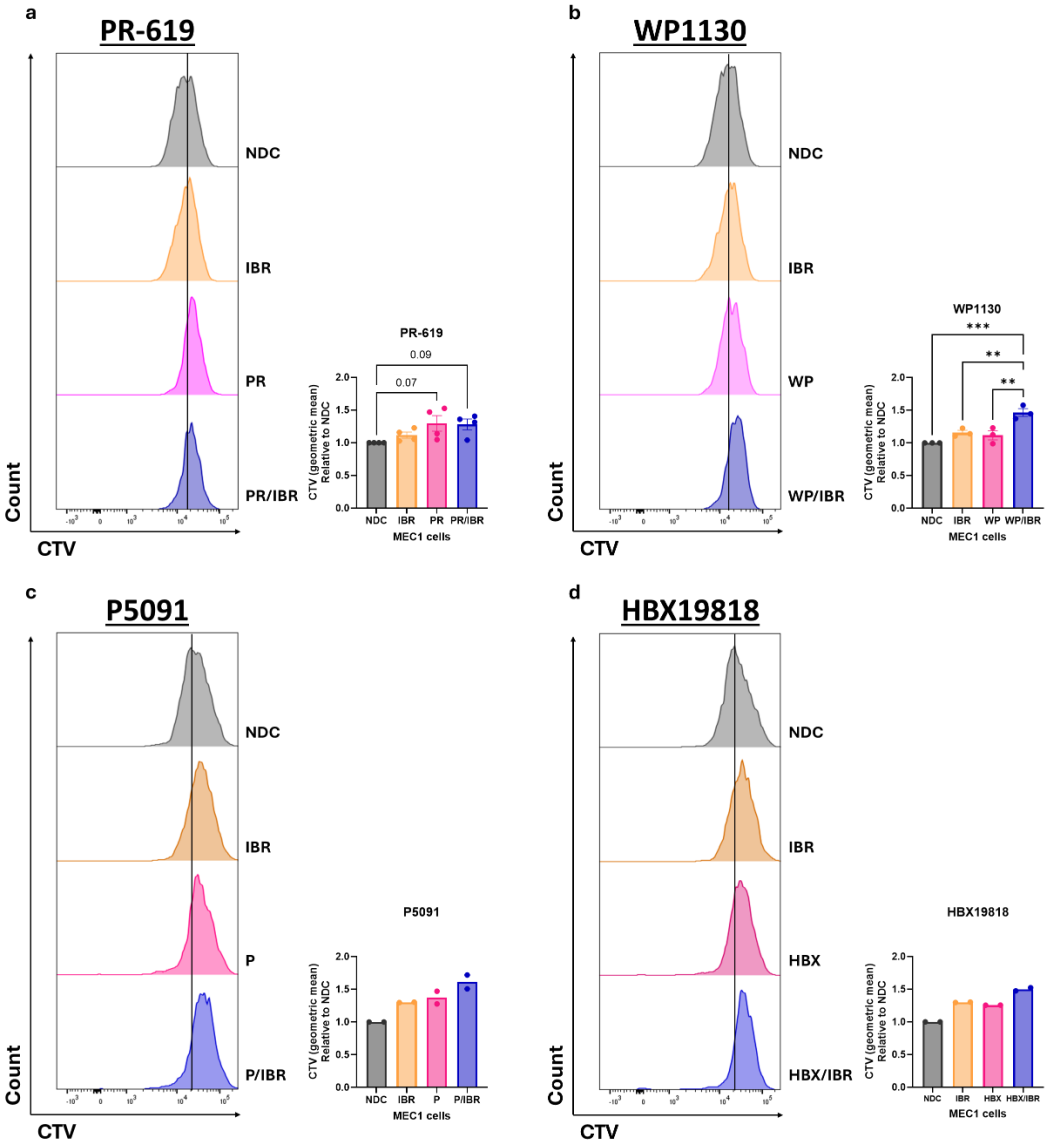

Figure 4.19: Combination of ibrutinib with WP1130 reduced proliferation in MEC1 cells. (a-d) Representative FACS histogram presenting fluorescence of CTV in MEC1 cells. (a) MEC1 cells (n = 5) were treated with ibrutinib (IBR = orange bar; 1 µM), PR-619 (PR = pink bar; 3 µM), combination (PR/IBR = blue bar), or no drug control (NDC/DMSO = black bar) for 48 hr. (b) MEC1 cells (n = 3) treated with IBR (orange bar), WP1130 (WP = pink bar; 2 µM), WP/IBR (blue bar), or /DMSO = black bar) for 48 hr. (c) MEC1 cells (n = 2) treated with IBR (orange bar; 1 µM), P5091 (P = pink bar; 10 µM), P/IBR (blue bar), or NDC/DMSO (black bar). (d) MEC1 cells (n = 2) treated with IBR (orange bar), HBX19818 (HBX = pink bar; 10 µM), WP/IBR (blue bar), or NDC/DMSO (black bar) for 48 hr. A vertical line denotes the peak of the NDC histogram. Geometric means for each condition are relative to NDC for MEC1 cells. Each dot represented an individual datapoint. Data expressed as the mean ± SEM. Statistics calculated by One-way ANOVA, Tukey test (a & b); ** $p \leq 0.01$, *** $p \leq 0.001$.

4.3.10 FOXO1 activity was significantly reduced by short-term BCR crosslinking with F(ab')$_2$ in primary CLL cells.

To determine whether the changes in FOXO1 subcellular localisation upon drug treatments resulted in modulation of FOXO1 activity, we investigated the impact of PR-619 or HBX19818 treatments, using the TransAM transcription factor activation assay. The data demonstrated that CLL cells treated with ibrutinib, PR-619 and HBX19818 had no effect on FOXO1 transcriptional activity compared to unstimulated controls (Figure 4.20a). In contrast, F(ab')$_2$ stimulation significantly decreased FOXO1 transcriptional activity compared to unstimulated controls (Figure 4.20a). Notably, ibrutinib treatment in stimulated CLL cells significantly increased FOXO1 DNA binding activity compared to stimulated controls (Figure 4.20b). While PR-619 and HBX19818 treatments in stimulated CLL cells had no significant effect on FOXO1 activity, the combination of ibrutinib with PR-619, but not HBX19818, slightly enhanced FOXO1 activity compared to either inhibitor alone or unstimulated controls (Figure 4.20b & c).

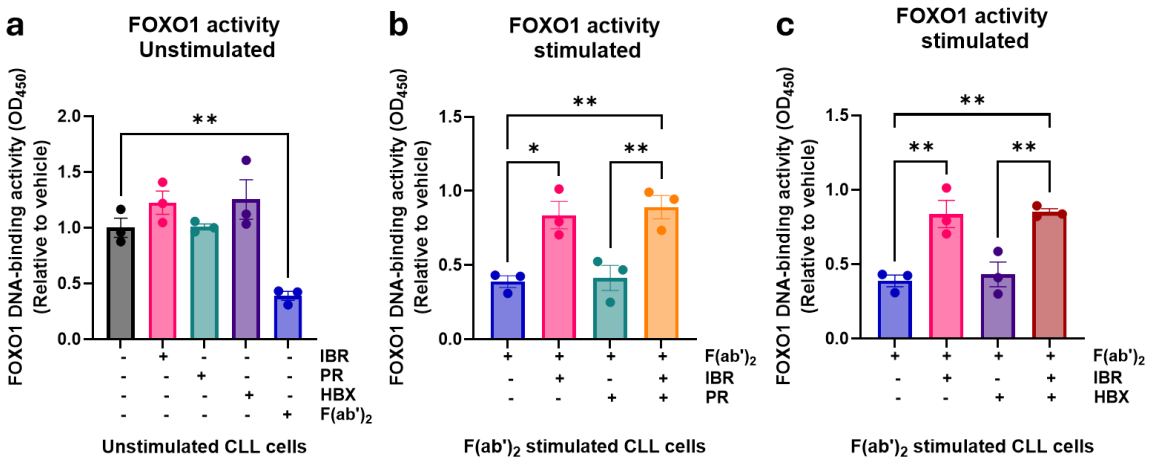

Figure 4.20: F(ab')$_2$ stimulation supressed FOXO1 transcriptional activity, which was restored by treatment with ibrutinib alone or in combination with DUB inhibitors in primary CLL cells.

Nuclear fractions were generated and TransAM FOXO1 activity assay were used to determine FOXO1 DNA-binding activity (OD_{450}). Primary CLL cells (n = 3) were unstimulated or stimulated with F(ab')$_2$ fragments (10 ng/mL) for 0.5 hr, following pre-treatment with ibrutinib (IBR; 1 µM), PR-619 (PR; 1.5 µM), or HBX19818 (HBX; 8 µM), for (1 hr) alone or in combination with IBR. FOXO1 DNA binding activity in (a) unstimulated primary CLL cells treated with NDC/DMSO (black bar), IBR (pink bar), PR (oil green bar), HBX (purple bar), or F(ab')$_2$ (blue bar). (b) FOXO1 DNA binding activity in CLL cells stimulated with F(ab')$_2$ F(ab')$_2$/DMSO (blue bar), IBR (pink bar), PR (oil green bar), and PR/IBR (light orange bar). (c) FOXO1 DNA binding activity in CLL cells stimulated with F(ab')$_2$/DMSO (blue bar), IBR (pink bar), HBX (purple bar), and HBX/IBR (red bar). The mean of FOXO1 DNA-binding activity in NDC were used to calculate the FOXO1 relative activity levels. Each dot represented an individual datapoint. Data expressed as the mean ± SEM. Statistics calculated by One-way ANOVA, Tukey test (a-c); * $p \leq 0.05$, ** $p \leq 0.01$.

4.3.11 Ibrutinib and HBX19818 in combination significantly modulated the transcription levels of FOXO1 target genes in MEC1 cells.

To determine whether the changes in FOXO1 activity upon drug treatments resulted in modulation of established FOXO1 transcriptional targets, we investigated whether the combination of ibrutinib with HBX19818 could enhance the effect on FOXO1 target genes compared to single-agent treatments initially in MEC1 cells. MEC1 cells were treated with inhibitors alone or in combination for 24 hr. The transcription levels of the genes were measured by RT-qPCR and the data were analysed using the $\Delta\Delta C_T$ method. Initially analysing the changes in FOXO family members (*FOXO1*, *FOXO3*, *FOXO4*), ibrutinib treatment did not alter the expression of any FOXO family members analysed compared to untreated controls (Figure 4.21a-c). Interestingly, HBX19818 treatment alone significantly increased the mRNA levels of *FOXO1*, *FOXO3* and *FOXO4,* which were maintained in combination with ibrutinib (Figure 4.21a-c).

The transcription levels of *USP7* were not affected by ibrutinib treatment, however HBX19818 alone and the combination significantly increased *USP7* expression compared to ibrutinib alone and untreated controls (Figure 4.21d). Interestingly, while HBX19818 demonstrated no effect on its levels compared to untreated controls, ibrutinib treatment significantly reduced *USP9x* expression, which was maintained in combination with HBX19818 (Figure 4.21e).

Analysing cell cycle related genes *CDKN1B* and *CCND2,* it was clear that ibrutinib alone, while having no effect on *CDKN1B* expression, significantly reduced *CCND2* expression (Figure 4.21f, j). Interestingly, HBX19818 alone significantly increased the expression of both *CDKN1B* and *CCND2* compared to untreated controls. The upregulation of *CDKN1B* was further enhanced by the combination treatment compared to single agents and untreated controls (Figure 4.21f). The combination treatment resulted in a downregulation of *CCND2* to a similar level as with ibrutinib alone (Figure 2.21j). Overall, these findings suggest that the combination supports an anti-proliferative effect on MEC1 cells.

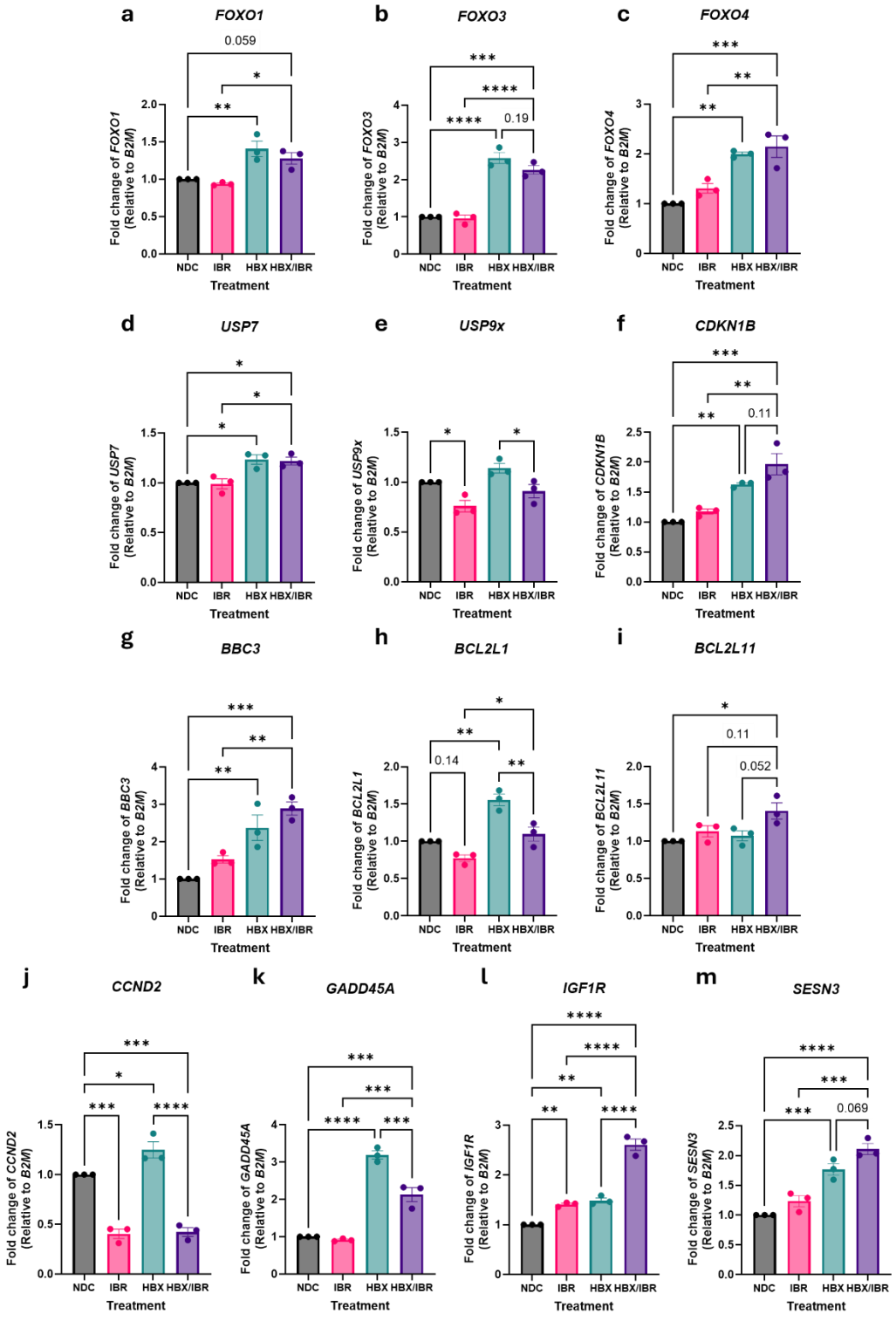

Figure 4.21: The transcription levels of FOXO1 gene targets were significantly altered by the combination of ibrutinib and HBX19818 in MEC1 cells.

RT-qPCR to assess transcription levels of (a) *FOXO1*, (b) *FOXO3*, (c) *FOXO4*, (d) *USP7*, (e) *USP9x*, (f) *CDKN1B*, (g) *BBC3*, (h) *BCL2L1*, (i) *BCL2L11*, (j) *CCND2*, (k) *GADD45A*, (l) *IGF1R*, (m) *SESN3* in MEC1 cells (n = 3) treated for 24 hr with ibrutinib (IBR = pink bar; 1 µM), HBX19818 (HBX = oil green bar; 10 µM), and combination (HBX/IBR = purple bar), or no drug control (NDC/DMSO = black bar). The $\Delta\Delta C_T$ method was used to calculate transcription levels, where samples were normalised to housekeeping gene *B2M*. Each dot represented an individual datapoint. Data expressed as the mean ± SEM. Statistics calculated by One-way ANOVA, Tukey test (a-m); * $p \leq 0.05$, ** $p \leq 0.01$, *** $p \leq 0.001$, **** $p \leq 0.0001$.

Analysis of apoptosis-related genes *BBC3, BCL2L1* and *BCL2L11*, it was clear that none of these genes were significantly regulated by ibrutinib treatment alone (Figure 4.21g-i). HBX19818 alone significantly upregulated the mRNA levels of *BBC3* and *BCL2L1* levels, encoding PUMA and BCL-XL respectively, while *BCL2L11*, encoding BIM was not affected. The combination of drugs appeared to favour a pro-apoptotic balance with a significant upregulation of *BBC3* and *BCL2L11* and basal levels of *BCL2L1*, compared to untreated cells (Figure 4.21g-i). Indeed, the combination of ibrutinib and HBX19818 significantly reduced *BCL2L1* compared to HBX19818 alone. Despite this reduction, *BCL2L1* mRNA levels with the combination treatment remained significantly higher than ibrutinib alone (Figure 4.21h).

Finally, to address the impact on additional FOXO1 targets, *GADD45A*, insulin-like growth factor 1 receptor (*IGFR1*) and sestrin 3 (*SESN3*) were analysed. HBX19818 treatment alone significantly increased the levels of all three of these FOXO1 targets, while ibrutinib only increased expression of *GADD45A* compared to untreated controls. The combination treatment resulted in a significant upregulation of *GADD45A*, *IGFR1* and *SESN3* compared with untreated cells, which is in the case of *IGFR1* and *SESN3* expression represented a further enhancement compared to both single treatments. However, the combination of ibrutinib and HBX19818 significantly reduced *GADD45A* transcription levels compared to HBX19818 alone (Figure 4.21k-m).

4.3.12 Selective USP7 inhibitors P5091 and HBX19818 in combination with ibrutinib promoted enhanced G0/G1 cell cycle arrest in MEC1 cells.

Our data showed that HBX19818 treatment alone significantly increased *CDKN1B* mRNA levels, with a further increase observed under the combination treatment. To assess the impact of selective USP7 inhibitors, alone or in combination with ibrutinib, on cell cycle progression, MEC1 cells were treated with ibrutinib, P5091 or HBX19818 alone or in combination with ibrutinib, for 72 hr. PI analysis revealed that all drugs alone reduced cell cycling, with ibrutinib and HBX19818 significantly modulating the G0/G1 and S phases of the cell cycle, while P5091 treatment caused a significant reduction in S phase only. Combination treatments caused an enhanced reduction in S phase and M phase, particularly with the HBX19818 containing combinations (Figure 4.22). Together, these data indicate that combination of DUB inhibitors with ibrutinib causes an enhanced reduction in transit through the cell cycle.

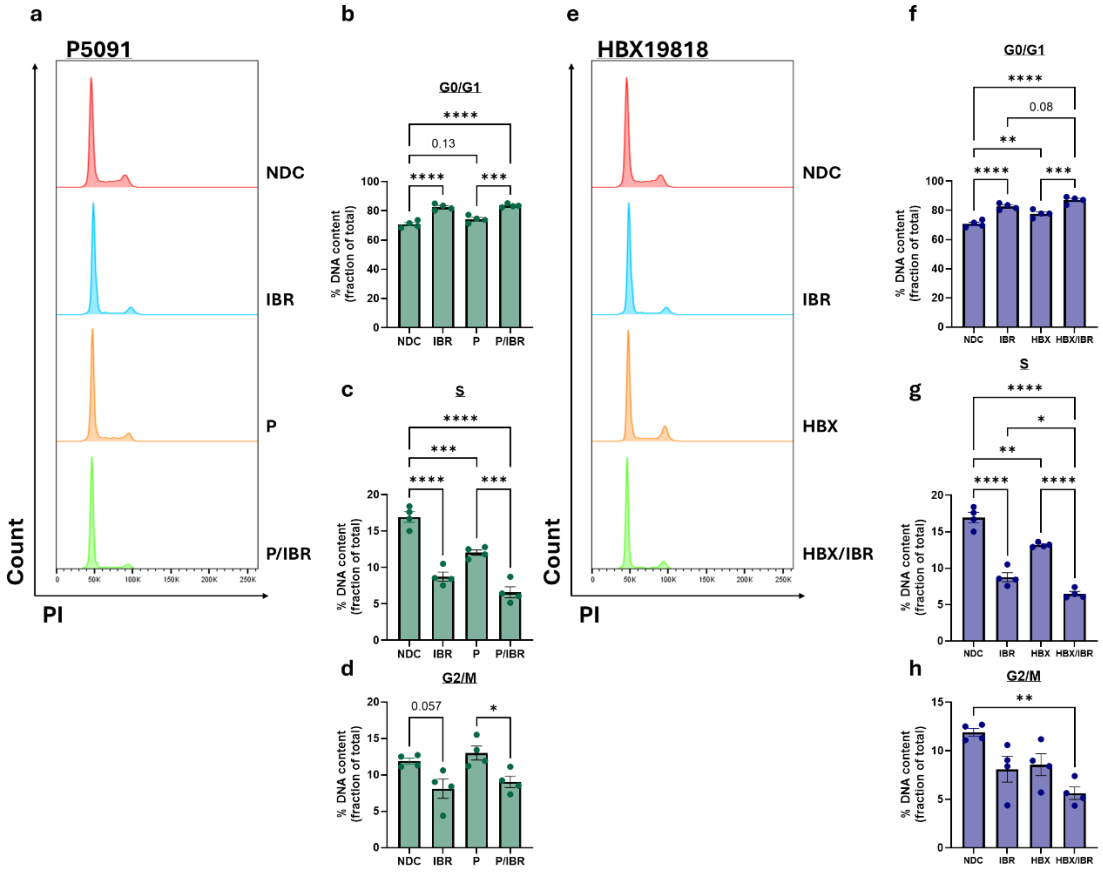

Figure 4.22: The combination of ibrutinib with selective USP7 inhibitors elevated ibrutinib effectiveness at promoting G0/G1 cell cycle arrest in MEC1 cells.
(a) Representative FACS histogram of MEC1 cells stained with PI for cell cycle analysis by quantitation of DNA content following treatment with ibrutinib (IBR; 1 µM), P5091 (P; 10 µM), and P/IBR, or no drug control (NDC/DMSO) for 72 hr. Quantification of DNA content in percentage (%) for cell cycle phase (b) G0/G1, (c) S, and (d) G2/M treated with P5091 and combination (oil green bars) as described in (a). (e) Representative FACS histogram of MEC1 cells stained with PI for cell cycle analysis treated with IBR, HBX19818 (HBX; 10 µM), and HBX/IBR, or NDC/DMSO for 72 hr. Quantification of DNA content (%) for cell cycle phase (f) G0/G1, (g) S, and (h) G2/M treated with HBX19818 and combination (oil green bars) as described in (e). Data expressed as the mean ± SEM. Statistics calculated by One-way ANOVA, Tukey test (b-d, f-h); * $p \leq 0.05$, ** $p \leq 0.01$, *** $p \leq 0.001$, **** $p \leq 0.0001$.

4.3.13 FOXO1 directly interacted with USP7 in MEC1 and primary CLL cells.

Based on our previous findings indicating that DUB proteins can modulate FOXO1 activity, we sought to investigate the potential interaction of FOXO1 with DUB proteins USP7, USP8, USP9x, USP10, USP14 and USP28 in MEC1 cells using co-IP. FOXO1, USP7 and USP9x were co-IP from cell lysates, with IgG as a control. USP7 co-IP revealed significant interaction of both USP9x and FOXO1 with USP7 compared to IgG controls (Figure 4.23a-c), while USP8, USP10, USP14, and USP28 were not detected in USP7 co-IP (data not shown). Given the

USP7 interaction with USP9x and FOXO1 in MEC1 cells, we examined the reciprocal interactions. As such, USP9x co-IP did not pull-down significant amounts of USP7 compared to IgG controls (Figure 4.23d & e). Conversely, FOXO1 co-IP showed significantly higher interaction with USP7 compared to IgG controls (Figure 4.23f & g). Additional experiments did not detect interaction between FOXO1 and USP8, USP9x, USP10, USP14, and USP28 using FOXO1 co-IP (data not shown). These findings suggested an interaction between endogenous USP7 and FOXO1 in MEC1 cells. To determine if this interaction also occurs in primary CLL cells, we performed FOXO1 co-IP in primary CLL samples. Similar to MEC1 cells, USP7 interaction with FOXO1 was significantly higher compared to IgG controls (Figure 4.23h & i). These data suggested an interaction between FOXO1 and USP7 in MEC1 and primary CLL cells.

Next, we investigated how HBX19818 and ibrutinib, alone or in combination, affected this interaction in MEC1 cells. The data showed that ibrutinib treatment slightly increased USP7 interaction with FOXO1 co-IP compared to untreated controls (p = 0.2). Conversely, HBX19818 treatment visibly reduced USP7 interaction with FOXO1 co-IP. Interestingly, the combination treatment slightly increased USP7 interaction with FOXO1 co-IP compared to HBX19818 alone, but remained lower than ibrutinib alone (p = 0.13) (4.23j & k). In BCR stimulated primary CLL cells, USP7 interaction with FOXO1 co-IP was slightly increased compared to unstimulated cells. This marginal increased in USP7 interaction with FOXO1 co-IP was observed in some patient samples, while others demonstrated similar levels of interaction as seen in unstimulated controls. Ibrutinib treatment further enhanced the increase in USP7-FOXO1 interaction compared to unstimulated cells and, to a lesser extent, $F(ab')_2$ stimulated CLL cells (Figure 4.23l & m). Furthermore, there was an interaction with USP9x and FOXO1 co-IP in some patient samples, while there was no detectable interaction in other samples (Figure 4.23l). These studies suggest a heterogeneity exists between CLL patient modulation of FOXO1-DUB protein interactions.

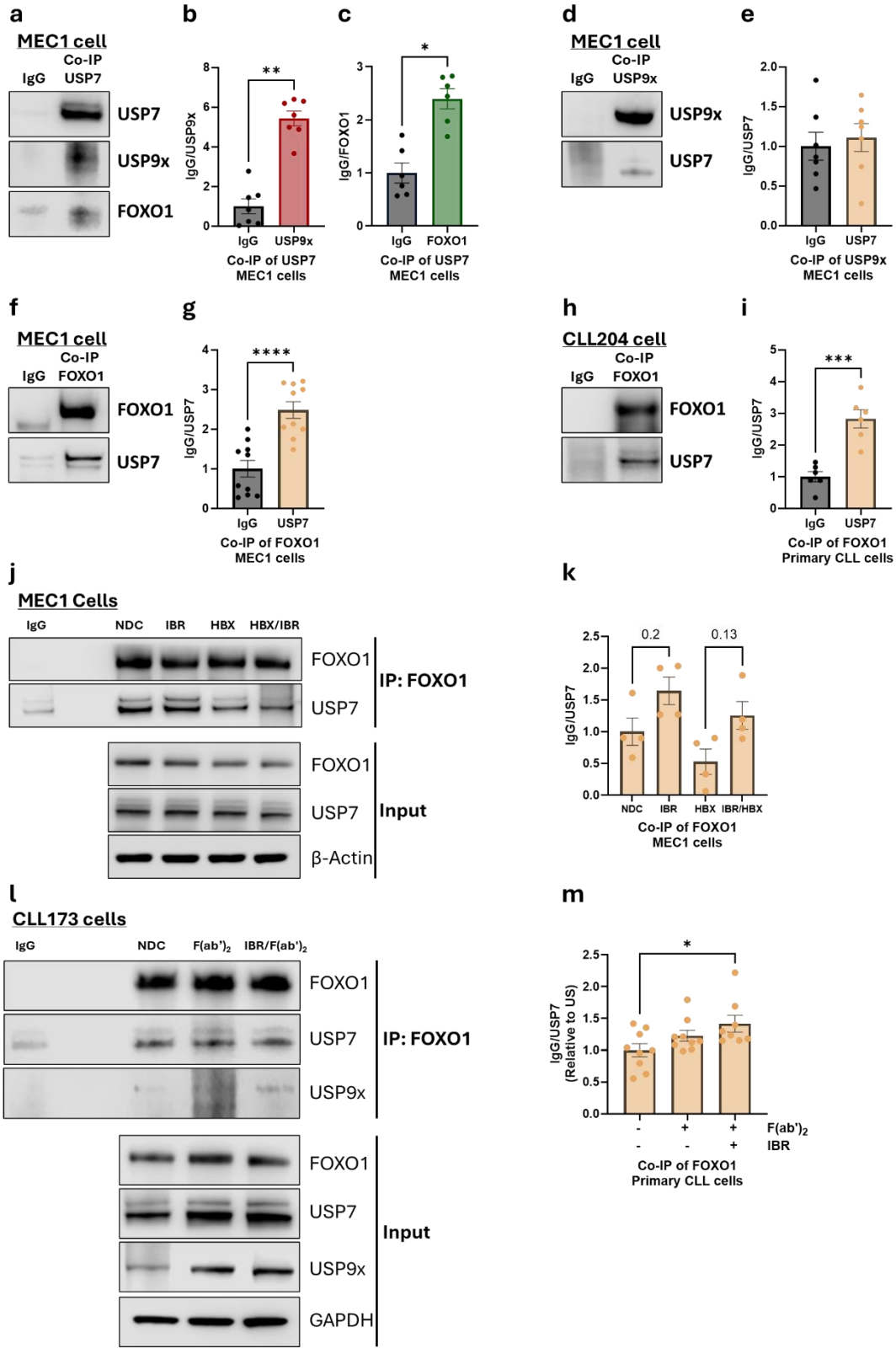

Figure 4.23: USP7 co-immunoprecipitated with FOXO1 in MEC1 and primary CLL cells.
(a) Representative Western blot of USP7 co-immunoprecipitation (co-IP) in MEC1 cells probed for USP7, USP9x and FOXO1. The relative levels of proteins pulled down in USP7 co-IP compared to IgG control (black bar) for (b) USP9x (red bar; n = 7) and (c) FOXO1 (green bar; n = 6). (d) Representative Western blot of USP9x co-IP in MEC1 cells probed for FOXO1, USP9x and USP7. The relative levels of proteins pulled down in USP9x co-IP compared to IgG control (black bar) for (e) USP7 (beige bar; n = 7). (f) Representative Western blot of FOXO1 co-IP in MEC1 cells probed for FOXO1 and USP7.

The relative levels of proteins pulled down in FOXO1 co-IP compared to IgG control (black bar) for (g) USP7 (beige bar; n = 10). (h) Representative Western blot of FOXO1 co-IP in primary CLL cells (CLL204) probed for FOXO1 and USP7. The relative levels of proteins pulled down in FOXO1 co-IP compared to IgG control (black bar) for (i) USP7 (beige bar; n = 6). (j) Representative Western blot of FOXO1 co-IP in MEC1 cells treated with ibrutinib (IBR; 1 μM), HBX19818 (HBX; 10 μM), and HBX/IBR, or no drug control (NDC/DMSO) for 1 hr. The co-IP and whole cell lysate (Input) were probed for FOXO1, USP7, and β-ACTIN (loading control for input). (K) USP7 (beige bars; n = 4) levels pulled down with FOXO1 co-IP normalised to IgG, treated as described in (j). (l) Representative Western blot of FOXO1 co-IP in primary CLL cells (CLL173) unstimulated or stimulated with $F(ab')_2$ fragments (10 ng/mL) for 0.5 hr, following 1 hr pre-treatment with IBR. co-IP and whole cell lysate (Input) samples were probed for FOXO1, USP7, USP9x, and β-ACTIN (loading control for input). (m) USP7 (beige bars; n = 8) levels pulled down with FOXO1 co-IP normalised to IgG, treated as described in (l). The mean expression levels of proteins in vehicle were used to calculate the relative protein expression levels. Each dot represented an individual datapoint. Data expressed as the mean ± SEM. Statistics calculated by paired t-test (b, c, e, g. i), and One-way ANOVA, Tukey test (k & m); * $p \leq 0.05$, ** $p \leq 0.01$, *** $p \leq 0.001$, **** $p \leq 0.0001$.

4.3.14 shRNA mediated USP7 KD and USP9x KD upregulated the expression of AKT^{S473} and $FOXO1^{T24}$ phosphorylation in MEC1 cells.

Data using DUB inhibitors in combination with ibrutinib indicated that FOXO1 nuclear translocation was induced and enhanced ibrutinib effects on apoptosis, proliferation, and cell cycle in CLL cells. Additionally, USP7 and FOXO1 directly interact in MEC1 and primary CLL cells, and USP7 may act as a hub for other DUBs including USP9x. We therefore assessed the importance of USP7 and USP9x by transducing MEC1 cells with shRNA lentiviral vectors against these targets (Figure 4.24). shRNA constructs targeting distinct regions of the USP7 and USP9x transcript were evaluated, alongside SCR shRNA control. USP7 KD and USP9x KD were established by examining transcript abundance and protein levels by RT-qPCR and Western blotting, respectively. The gene expression levels of USP7 and USP9x were repressed by constructs USP7-78 (0.41) and USP9x-64 (0.36) compared to SCR controls (Figure 4.24a & b). Similarly, the protein expression levels were reduced by constructs USP7-78 (0.58) and USP9x-64 (0.32) compared to SCR controls (Figure 4.24c-f).

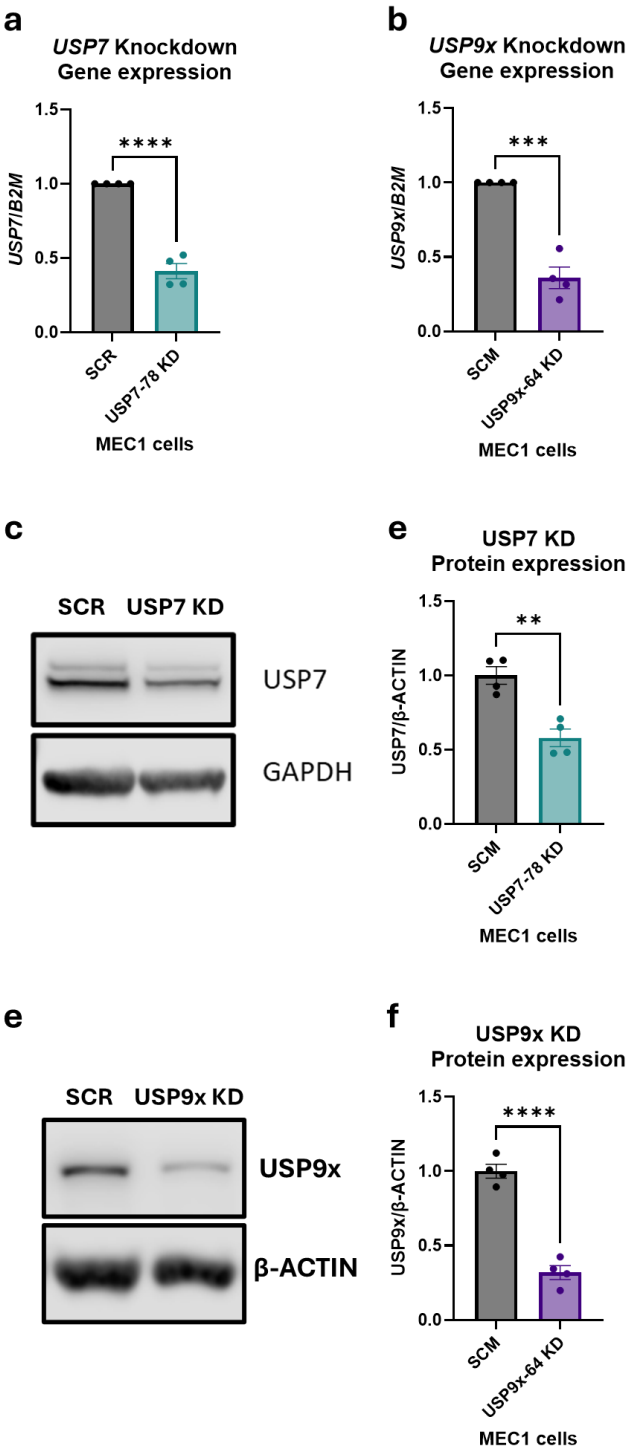

Figure 4.24: The gene and protein levels of USP7 and USP9x in shRNA KD MEC1 cells.

RT-qPCR to assess transcription levels of (a) *USP7* (USP7-78 KD = oil green bar; n = 4) and (b) *USP9x* (USP9x-64 KD = purple bar; n = 4) shRNA-mediated knockdown (KD) of MEC1 cells transduced with shRNA constructs compared to scrambled (SCR = black bar; n = 4) control. The $\Delta\Delta C_T$ method was used to calculate transcription levels: samples were normalised to the housekeeping gene *B2M* and made relative to SCR control. (c) Representative Western blot of MEC1 transduced with shRNA-USP7-78 and SCR control. The blots were probed with USP7 and GAPDH (loading control). (d) Relative protein levels of USP7 (oil green bar; n = 4) and SCR (black bar; n = 4) between USP7 KD MEC1 cells and SCR MEC1 cells. (e) Representative Western blot of MEC1 transduced with shRNA-USP9x-64 and SCR control. The blots were probed with USP9x and GAPDH (loading control). (f) Relative protein levels of USP9x-64 KD (purple bar; n = 4) and SCR (black bar; n = 4) between USP9x KD MEC1 cells and SCR MEC1 cells. The mean expression levels of proteins in SCR were used to calculate the relative protein expression levels. Each dot represented an individual datapoint. Data expressed as the mean ± SEM. Statistics calculated by paired t-test; ** $p \leq 0.01$, *** $p \leq 0.001$, **** $p \leq 0.0001$.

Our data demonstrated that selective USP7 inhibitors P5091 and HBX19818 had no significant effect on the p-FOXO1^{T24} levels and total FOXO1 in MEC1 and primary CLL cells (Figure 4.6 & 4.10). However, the combination with ibrutinib increased FOXO1 nuclear localisation, promoted G0/G1 cell cycle arrest, and upregulated key FOXO1 target genes, including *CDKN1B* (p27^{Kip1}) and *BCL2L11* (BIM) (Figure 4.21). Given the observed interaction between USP7 and FOXO1 (Figure 4.23), we investigated whether USP7 depletion could

impact the AKT-FOXO1 signalling axis and the expression of known FOXO1 targets ($p21^{Waf1/Cip1}$, $p27^{Kip1}$, and BIM) (377, 571). USP7 KD significantly upregulated p-AKT^{S473} in USP7 KD MEC1 cells compared to SCR controls. Additionally, ibrutinib treatment of SCR and USP7 KD cells inhibited p-AKT^{S473} levels completely (Figure 4.25a, b). As expected, USP7 KD and ibrutinib treatment did not affect total AKT protein levels in USP7 KD cells and SCR controls (Figure 4.25a, c). Similar to p-AKT^{S473}, p-$FOXO1^{T24}$ was significantly upregulated in USP7 KD cells compared to SCR controls, and ibrutinib treatment reduced p-$FOXO1^{T24}$ with comparable effectiveness in both USP7 KD and SCR controls (Figure 4.25a, d). The expression levels of FOXO1 were similar in USP7 KD and SCR and were similarly reduced with ibrutinib treatment in USP7 KD cells and SCR controls (Figure 4.25a, e).

As expected, USP7 expression was reduced in USP7 KD compared to SCR controls, and levels were not affected by ibrutinib treatment (Figure 4.25a, f), and expression levels of USP9x were not affected by USP7 KD and/or ibrutinib treatment (Figure 4.25a, g). The expression of $p21^{Waf1/Cip1}$ was surprisingly reduced in USP7 KD compared to SCR, and further reduced with Ibrutinib treatment (Figure 4.25a, h). In contrast to USP7 inhibitors, USP7 KD in the presence and absence of ibrutinib had no effect on $p27^{Kip1}$ expression compared to SCR control (Figure 4.25a, i). BIM isoforms (BIM_{EL}, BIM_L and BIM_S) were relatively increased in USP7 KD compared to SCR controls, but ibrutinib had little effect on their levels (Figure 4.25a, j-l). Interestingly, USP7 KD led to a relative increase in PTEN expression compared to SCR controls, which was maintained with ibrutinib treatment (Figure 4.25a, m). The expression of MCL1 was not significantly altered by USP7 KD and ibrutinib treatment in both groups (Figure 4.25a, n).

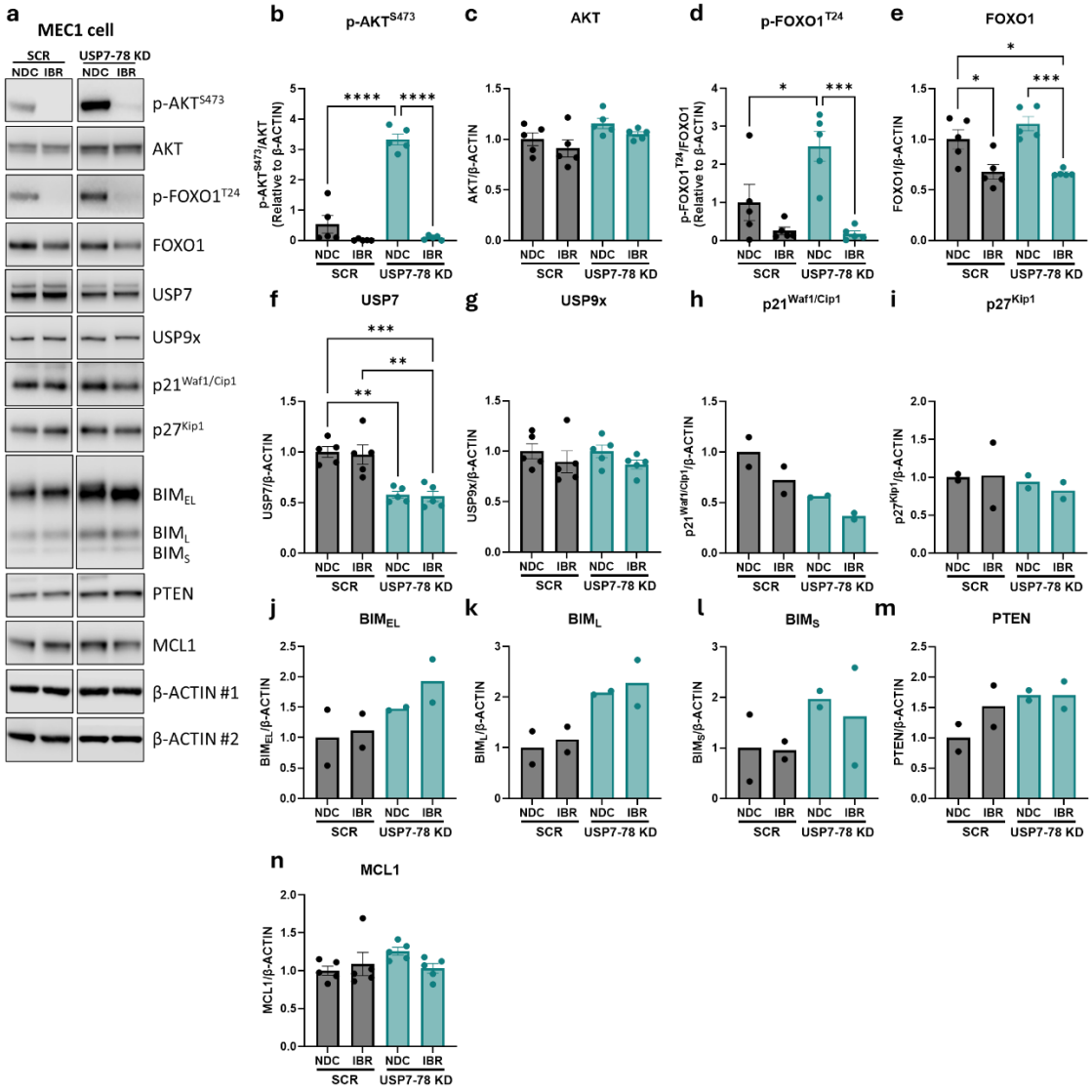

Figure 4.25: shRNA mediated USP7 KD increased the p-AKT^{S473} and p-FOXO1^{T24} in MEC1 cells.

(a) Representative Western blot of MEC1 transduced with shRNA construct USP7-78 or scrambled (SCR) control. The blots were probed with p-AKT^{S473}, AKT, p-FOXO1^{T24}, FOXO1, USP7, USP9x, p21$^{Waf1/Cip1}$, p27^{Kip1}, BIM (EL, L, S), PTEN, MCL1, and β-ACTIN (loading control; #1 and #2 representing mirror blots). The MEC1 transduced with shRNA construct USP7-78 and SCR control were treated with ibrutinib (IBR; 1 µM) for 1 hr or no drug control (NDC/DMSO). Relative proteins expression of (b) p-AKT^{S473} (n = 5), (c) AKT (n = 5), (d) p-FOXO1^{T24} (n = 5), (e) FOXO1 (n = 5), (f) USP7 (n = 5), (g) USP9x (n = 5), (h) p21$^{Waf1/Cip1}$ (n = 2), (i) p27^{Kip1} (n = 2), (g) BIM$_{EL}$ (n = 2), (k) BIM$_L$ (n = 2), (l) BIM$_S$ (n = 2), (m) PTEN (n = 2), and (n) MCL1 (n = 5) transduced with USP7-78 shRNA (oil green bars) or SCR control (black bars), and treated as described in (a). The mean expression levels of proteins in SCR vehicle were used to calculate the relative protein expression levels. Each dot represented an individual datapoint. Data expressed as the mean ± SEM. Statistics calculated One-way ANOVA, Tukey test (a-g, n); * p ≤ 0.05, ** p ≤ 0.01, *** p ≤ 0.001, **** p ≤ 0.0001.

Given the observed co-IP of USP9x with USP7 and FOXO1 in a number of primary CLL cells (Figure 4.23), we investigated whether USP9x depletion could impact the AKT-FOXO1

signalling axis and the expression of known FOXO1 targets ($p21^{Waf1/Cip1}$, $p27^{Kip1}$, and BIM) (375, 377, 571) as well as MCL1 which was shown to be stabilised by USP9x (545). Similar to the USP7 KD data, USP9x KD significantly upregulated p-AKT^{S473} and p-$FOXO1^{T24}$ in USP9x KD MEC1 cells compared to SCR controls, which was completely inhibited with ibrutinib treatment (Figure 4.26a, b, d). Similar to WP1130 treatment, USP9x KD significantly increased AKT expression compared to SCR controls, in a manner that was unaffected by ibrutinib treatment (Figure 4.26a, c). FOXO1 levels were slightly increased in USP9x KD (p = 0.17), and ibrutinib treatment decreased FOXO1 expression in both USP9x KD and SCR cells (Figure 4.26a, e).

USP7 levels were not affected by USP9x KD and ibrutinib treatment, while as expected USP9x expression were reduced in the KD cells (Figure 4.26a, f, g). USP9x KD had no effect on $p21^{Waf1/Cip1}$, $p27^{Kip1}$ PTEN or MCL1 expression compared to SCR control, and ibrutinib treatment did not change their expression in USP9x KD and SCR controls (Figure 4.26a, h, I, m, n). BIM isoforms (BIM_{EL}, BIM_L, and BIM_S) were slightly elevated in USP9x cells compared to SCR, while ibrutinib treatment largely had no effect on BIM isoforms in treated SCR, except for BIM_S, which was downregulated (Figure 4.26a & j-l).

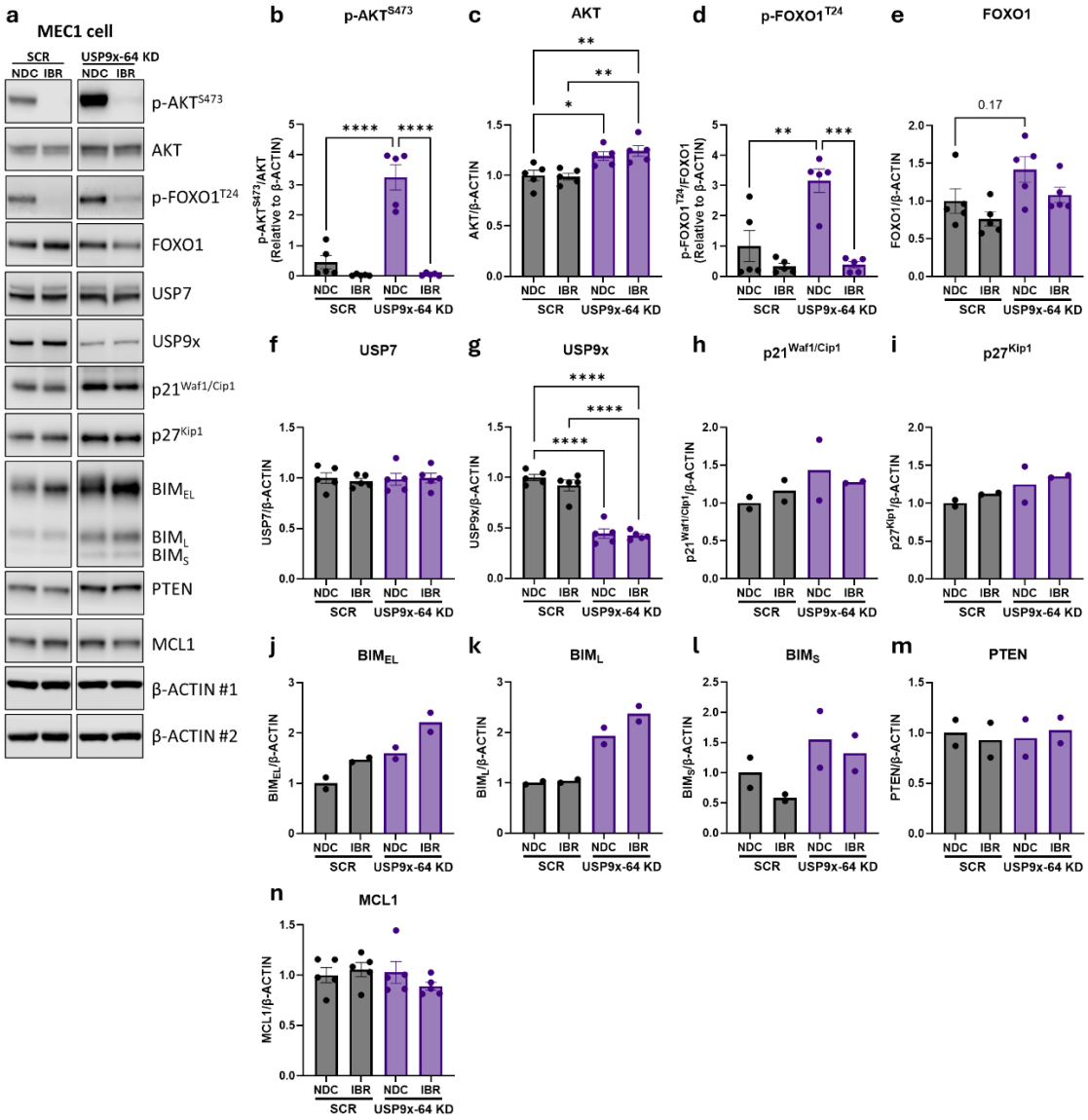

Figure 4.26: shRNA mediated USP9x KD increased the p- AKT^{S473} and total AKT in MEC1 cells.

(a) Representative Western blot of MEC1 transduced with shRNA construct USP9x-64 knockdown (KD) or scrambled (SCR) control. The blots were probed with p-AKT^{S473}, AKT, p-FOXO1^{T24}, FOXO1, USP7, USP9x, p21$^{Waf1/Cip1}$, p27^{Kip1}, BIM (EL, L, S), PTEN, MCL1, and β-ACTIN (loading control; #1 and #2 representing mirror blots). The MEC1 transduced with shRNA USP9x-64 KD and SCR control were treated with ibrutinib (IBR; 1 µM) for 1 hr or no drug control (NDC/DMSO). Relative proteins expression of (b) p-AKT^{S473} (n = 5), (c) AKT (n = 5), (d) p-FOXO1^{T24} (n = 5), (e) FOXO1 (n = 5), (f) USP7 (n = 5), (g) USP9x (n = 5), (h) p21$^{Waf1/Cip1}$ (n = 2), (i) p27^{Kip1} (n = 2), (g) BIM$_{EL}$ (n = 2), (k) BIM$_L$ (n = 2), (l) BIM$_S$ (n = 2), (m) PTEN (n = 2), and (n) MCL1 (n = 5) transduced with USP9x-64 shRNA (purple bars) KD or SCR control (black bars) cells, and treated as described in (a).The mean expression levels of proteins in SCR vehicle were used to calculate the relative protein expression levels. Each dot represented an individual datapoint. Data expressed as the mean ± SEM. Statistics calculated One-way ANOVA, Tukey test (a-g, n); * p ≤ 0.05, ** p ≤ 0.01, *** p ≤ 0.001, **** p ≤ 0.0001.

4.3.15 USP7 KD and USP9x KD had no significant impact on MEC1 viability and proliferation.

We investigated whether shRNA-mediated KD of USP7 and USP9x in MEC1 cells could sensitise them to ibrutinib treatment, enhancing apoptosis and potentially affecting proliferation. MEC1 cells with shRNA KD or control (SCR) were treated with ibrutinib for 48 hr or DMSO control. Cells were then stained with Annexin V and 7-AAD for apoptosis analysis or with CTV and apoptosis stains for proliferation analysis. Our results demonstrated that USP7 and USP9x KD had no significant effect on MEC1 cell viability compared to SCR controls. Ibrutinib treatment showed a trend towards reduced viability in USP7 KD cells (p = 0.23) compared to untreated SCR control cells, while USP9x KD had no effect on viability (Figure 4.27a, b). Similarly, the proliferation rates of USP7 and USP9x KD cells were not statistically different from control cells. However, KD cells became more sensitive to ibrutinib treatment, significantly reducing proliferation of USP7 and USP9x KD cells compared to untreated KD cells (Figure 4.27c, d).

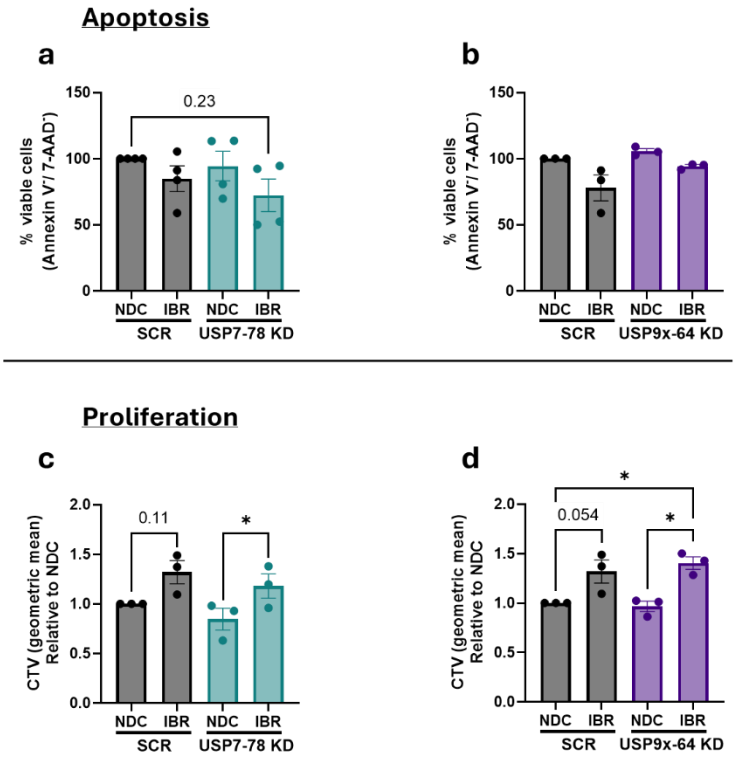

Figure 4.27: USP7 and USP9x KD had no effect on MEC1 cell viability and proliferation. MEC1 cells were transduced with shRNA construct (a&c) USP7-78 knockdown (KD) (oil green bars; n = 4), (b&d) USP9x-64 KD (purple bars; n = 3) or scrambled (SCR) control (black bars). (a&b) Cells were stained with Annexin V and 7-AAD to assess cell viability following treatment with ibrutinib (IBR; 1 µM) for 48 hr, or no drug control (NDC/DMSO). Viability is defined as Annexin V negative and 7-AAD/DAPI negative. Percentage viable cells for each condition are relative to SCR vehicle for MEC1 USP7-78 and USP9x-64 KDs. (c & d) Cells were stained with CTV to evaluate cell proliferation, following treatment with IBR for 48 hr, or NDC/DMSO. Geometric means for each condition are relative to SCR vehicle for MEC1 USP7-78 and USP9x-64 KDs. Each dot represented an individual datapoint. Data expressed as the mean ± SEM. Statistics calculated by One-way ANOVA, Tukey test (a-d); * $p \leq 0.05$.

4.3.16 USP7 KD with the ibrutinib or PR-619 combination, enhanced FOXO1 nuclear translocation in MEC1 cells.

Our data demonstrated that ibrutinib treatment alone increased nuclear FOXO1 levels while reducing cytoplasmic FOXO1 levels. Furthermore, combining ibrutinib with the broad-spectrum DUB inhibitor PR-619 or USP7 inhibitors (P5091 and HBX19818) further enhanced nuclear FOXO1 in MEC1 and primary CLL cells (Sections 4.3.7 and 4.3.8). Based on these findings, we investigated the effects of USP7 KD on FOXO1 subcellular localisation in MEC1 cells. Additionally, we were interested in whether USP7 KD combined with ibrutinib and/or PR-619 treatment would further enhance FOXO1 nuclear localisation. Therefore, SCR control and USP7 KD MEC1 cells were treated with ibrutinib, PR-619 alone, or the combination of both inhibitors for 1 hr.

USP7 KD did not significantly affect nuclear or cytoplasmic FOXO1 levels compared to SCR control cells. Similarly, PR-619 treatment had no effect on nuclear or cytoplasmic FOXO1 levels in USP7 KD and SCR control cells. However, USP7 KD appeared to sensitise FOXO1 nuclear localisation to ibrutinib treatment as USP7 KD led to a significant increase in nuclear FOXO1, exceeding the levels observed in ibrutinib treated SCR cells. The combination treatment further enhanced FOXO1 nuclear translocation, with the combination treatment in USP7 KD cells leading to a more pronounced increase in nuclear FOXO1 compared to the combination treatment in SCR cells (Figure 4.28a, b). These effects were mirrored in a decrease in FOXO1 expression in the cytoplasm (Figure 4.28a, c).

USP7 KD significantly depleted the expression of USP7 in the nuclear and cytoplasmic fraction compared to SCR control cells. Furthermore, the nuclear and cytoplasmic levels of USP7 were not affected by ibrutinib, PR-619 and the combination treatments in both USP7 KD and SCR cells (Figure 4.28a, d, e).

In SCR cells, ibrutinib, PR-619, and the combination treatment did not affect nuclear USP9x expression. Similarly, USP7 KD itself had minimal impact on nuclear USP9x. Interestingly, the combination treatment significantly increased nuclear USP9x levels in USP7 KD cells compared to cells treated with ibrutinib, PR-619, or left untreated (Figure 4.28a, f). This upregulation of nuclear USP9x was also significantly higher compared to the combination treatment of SCR control cells. The cytoplasmic levels of USP9x were not affected by ibrutinib, PR-619 and the combination treatments in both USP7 KD and SCR cells (Figure 4.28a, g).

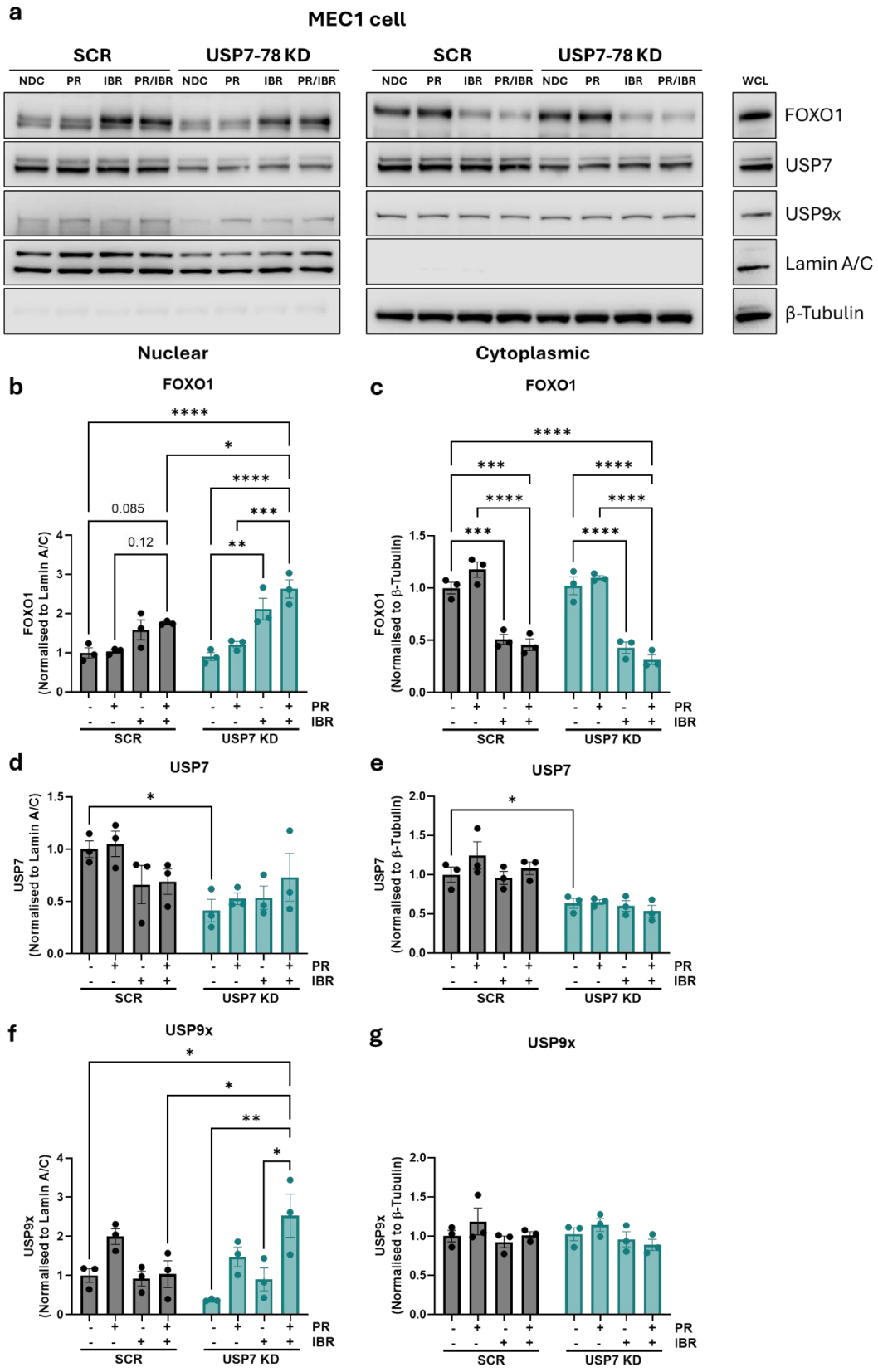

Figure 4.28: **USP7 KD MEC1 cells are sensitised to ibrutinib or PR-619 combination, enhancing FOXO1 nuclear translocation.**

(a) Representative Western blot of subcellular fractionation of MEC1 transduced with shRNA USP7-78 or scrambled (SCR) control cells, both treated with PR-619 (PR; 3 µM), ibrutinib (IBR; 1 µM), and combination (PR/IBR), or no drug control (NDC/DMSO). Following 1 hr treatment as describe in (a), shRNA USP7-78 knockdown (KD) MEC1 and SCR cells (n = 3) were fractionated into cytoplasmic,

nuclear, and whole cell lysate (WCL). The blots were probed for FOXO1, USP7, USP9x, Lamin A/C (nuclear loading control), and β-Tubulin (cytoplasmic loading control). Relative protein expression of (b) nuclear FOXO1, (c) cytoplasmic FOXO1, (d) nuclear USP7, (e) cytoplasmic USP7, (f) nuclear USP9x, and (g) cytoplasmic USP9x between USP7-78 KD MEC1 cells (oil green bars) and SCR control (black bars), treated as described in (a). Added treatment (+), no treatment (-). Nuclear and cytoplasmic fractions were normalised to loading controls (Lamin A/C and β-Tubulin, respectively). The mean expression levels of proteins in SCR vehicle were used to calculate the relative protein expression levels for USP7-78 KD and SCR MEC1 cells. Each dot represented an individual datapoint. Data expressed as the mean ± SEM. Statistics calculated by One-way ANOVA, Tukey test (b-g); *0.05, ** $p \leq 0.01$, *** $p \leq 0.001$, **** $p \leq 0.0001$.

4.3.17 USP9x KD with the ibrutinib or PR-619 combination, enhanced FOXO1 nuclear translocation in MEC1 cells.

Our data showed that WP1130 alone and in combination with ibrutinib had no effect on FOXO1 nuclear translocation in MEC1 cells (Section 4.3.7). However, the STRING database (Section 3.3.11) and co-IP (Section 4.3.13) both suggested a possible interaction between USP9x and USP7, which is known to regulate FOXO1. Based on these findings, we investigated the effects of USP9x KD on FOXO1 subcellular localisation in MEC1 cells. SCR and USP9x KD MEC1 cells with ibrutinib, PR-619 alone, or the combination of both inhibitors for 1 hr.

USP9x KD did not significantly affect nuclear or cytoplasmic FOXO1 levels compared to SCR control cells. Similarly, PR-619 treatment had no effect on nuclear or cytoplasmic FOXO1 levels in USP9x KD and SCR control cells. However, as seen above with USP7 KD, USP9x KD sensitised FOXO1 nuclear localisation to ibrutinib treatment, exceeding the levels observed in ibrutinib treated SCR control cells, and the combination treatment further enhanced FOXO1 nuclear translocation in SCR control. The combination treatment also further increased nuclear FOXO1 in USP9x KD cells compared to the inhibitors alone (Figure 4.29a, b). These effects were mirrored in a decrease in FOXO1 expression in the cytoplasm (Figure 4.29a, c).

USP9x KD significantly depleted the expression of USP9x in the cytoplasm and to a lesser extent in the nucleus ($p = 0.3$) compared to SCR cells, and were not affected by ibrutinib, PR-619 and the combination treatments in both USP9x KD and SCR cells (Figure 4.29a, d, e). The nuclear and cytoplasmic levels of USP7 were not affected by ibrutinib, PR-619 and the combination treatments in both USP9x KD and SCR cells (Figure 4.29a, f, g).

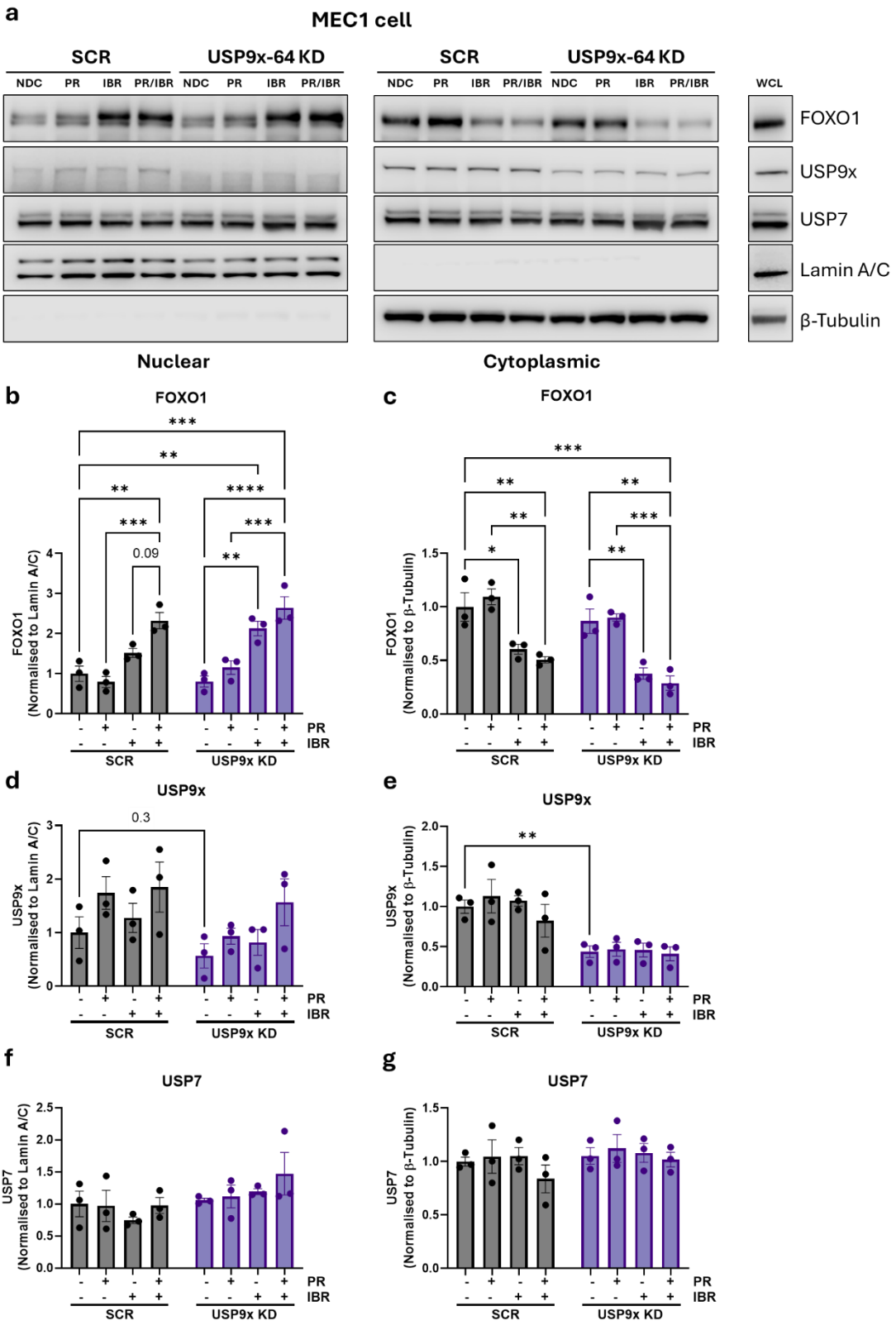

Figure 4.29: USP9x KD in MEC1 cells sensitised FOXO1 nuclear localisation to ibrutinib treatment.

(a) Representative Western blot of subcellular fractionation of MEC1 transduced with shRNA USP9x-64 or scrambled (SCR) control cells, both treated with PR-619 (PR; 3 µM), ibrutinib (IBR; 1 µM), and combination (PR/IBR), or no drug control (NDC/DMSO). Following 1 hr treatment, shRNA USP9x-64 knockdown (KD) MEC1 and SCR cells (n = 3) were fractionated into cytoplasmic, nuclear, and whole cell lysate (WCL). The blots were probed for FOXO1, USP9x, USP7, Lamin A/C (nuclear loading

control), and β-Tubulin (cytoplasmic loading control). Relative protein expression of (b) nuclear FOXO1, (c) cytoplasmic FOXO1, (d) nuclear USP9x, (e) cytoplasmic USP9x, (f) nuclear USP7, and (g) cytoplasmic USP7 between shRNA USP9x-64 KD (purple bars) and SCR (black bars) MEC1 cells, treated as described in (a). Added treatment (+), no treatment (-). Nuclear and cytoplasmic fractions were normalised to loading controls (Lamin A/C and β-Tubulin, respectively). The mean expression levels of proteins in SCR vehicle were used to calculate the relative protein expression levels for shRNA USP9x-64 KD MEC1 cells and SCR control. Each dot represented an individual datapoint. Data expressed as the mean ± SEM. Statistics calculated by One-way ANOVA, Tukey test (b-g); * $p \leq 0.05$, ** $p \leq 0.01$, *** $p \leq 0.001$, **** $p \leq 0.0001$.

4.3.18 FOXO1 DNA binding activity was increased by USP7 KD and USP9x KD in MEC1 cells.

To assess the effects of USP7 and USP9x KD on FOXO1 DNA binding activity, we performed subcellular fractionations. MEC1 cells with shRNA-mediated KD of USP7 or USP9x, and SCR control cells, were treated with ibrutinib for 1 hr, or left untreated. Subsequently, nuclear fractions were isolated and the TransAM transcription factor activation assay was used. The data revealed that USP7 or USP9x depletion alone in MEC1 cells modestly increased FOXO1 DNA binding activity compared to control cells (p = 0.16 and 0.19, respectively). As expected, ibrutinib treatment significantly enhanced FOXO1 activity in both the SCR and KD MEC1 cells. Notably, FOXO1 DNA binding activity increased in the USP7 or USP9x KD in the presence of ibrutinib, indicating that the presence of USP7 or USP9x muted the FOXO1 activity response to ibrutinib (Figure 4.30a, b).

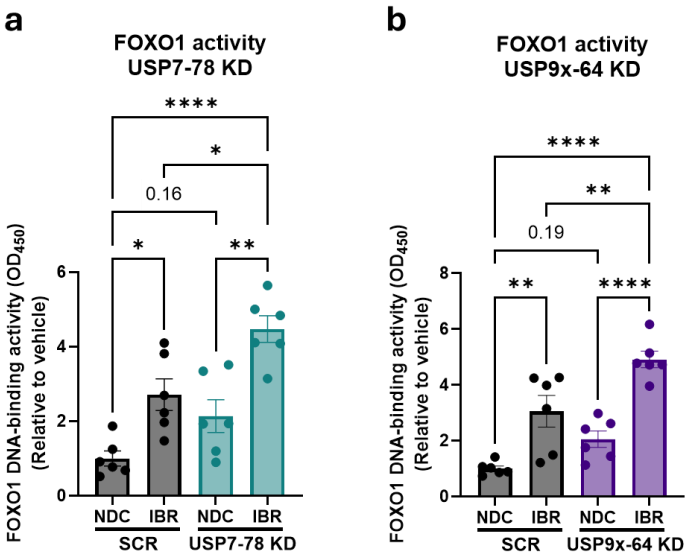

Figure 4.30: USP7 and USP9x KD upregulated FOXO1 DNA binding activity in MEC1 cells. Nuclear fractions were generated by subcellular fractionation and the TransAM FOXO1 activity assay was used to determine FOXO1 DNA-binding activity. FOXO1 activity in MEC1 transduced with shRNA construct (a) USP7-78 knockdown (KD) (oil green bars; n = 6), (b) USP9x-64 KD (purple bars; n = 6)

or scrambled (SCR = black bars) cells, treated with ibrutinib (IBR; 1 μM), or no drug control (NDC/DMSO) for 1 hr. The mean of FOXO1 activity in SCR vehicle were used to calculate USP7-78 and USP9x-64 KD relative activity levels. Each dot represented an individual datapoint. Data expressed as the mean ± SEM. Statistics calculated by One-way ANOVA, Tukey test (a & b); * $p \leq 0.05$, ** $p \leq 0.01$, **** $p \leq 0.0001$.

4.3.19 USP7 KD in MEC1 cells significantly increased FOXO1 target genes.

Given the role of FOXO1 activity in upregulating *BCL2L11* (BIM), *CDKN1A* ($p21^{Waf1/Cip1}$), and *CDKN1B* ($p27^{Kip1}$) , and downregulating *CCND2* (cyclin D) (571, 572), we investigated whether USP7 KD modulated the expression of these established FOXO1 targets. We employed RT-qPCR to measure the mRNA levels of these genes in USP7 KD MEC1 cells compared to SCR control cells. The data revealed that *FOXO1* and *FOXO4* were significantly upregulated in USP7 KD cells, while *FOXO3* expression did not change compared to SCR controls (Figure 4.31a-c). While *BCL2L1* and *BBC3* were similar in USP7 KD and SCR cells, *BCL2L11* was significantly upregulated in USP7 KD cells indicated a bias towards a pro-apoptotic cell fate (Figure 4.31d-f). Considering cell cycle regulation, *CDKN1A* mRNA levels were significantly upregulated and *CDKN1B* was slightly upregulated in USP7 KD, while *CCND2* was significantly downregulated compared with SCR controls (Figure 4.31g-i), suggesting a reduction in proliferation in USP7 KD cells. Notably, while the transcription levels of *GADD45A*, *SESN3* were significantly downregulated in USP7 KD, *IGF1R* was significantly upregulated in the KD cells compared to SCR controls (Figure 4.31j-l).

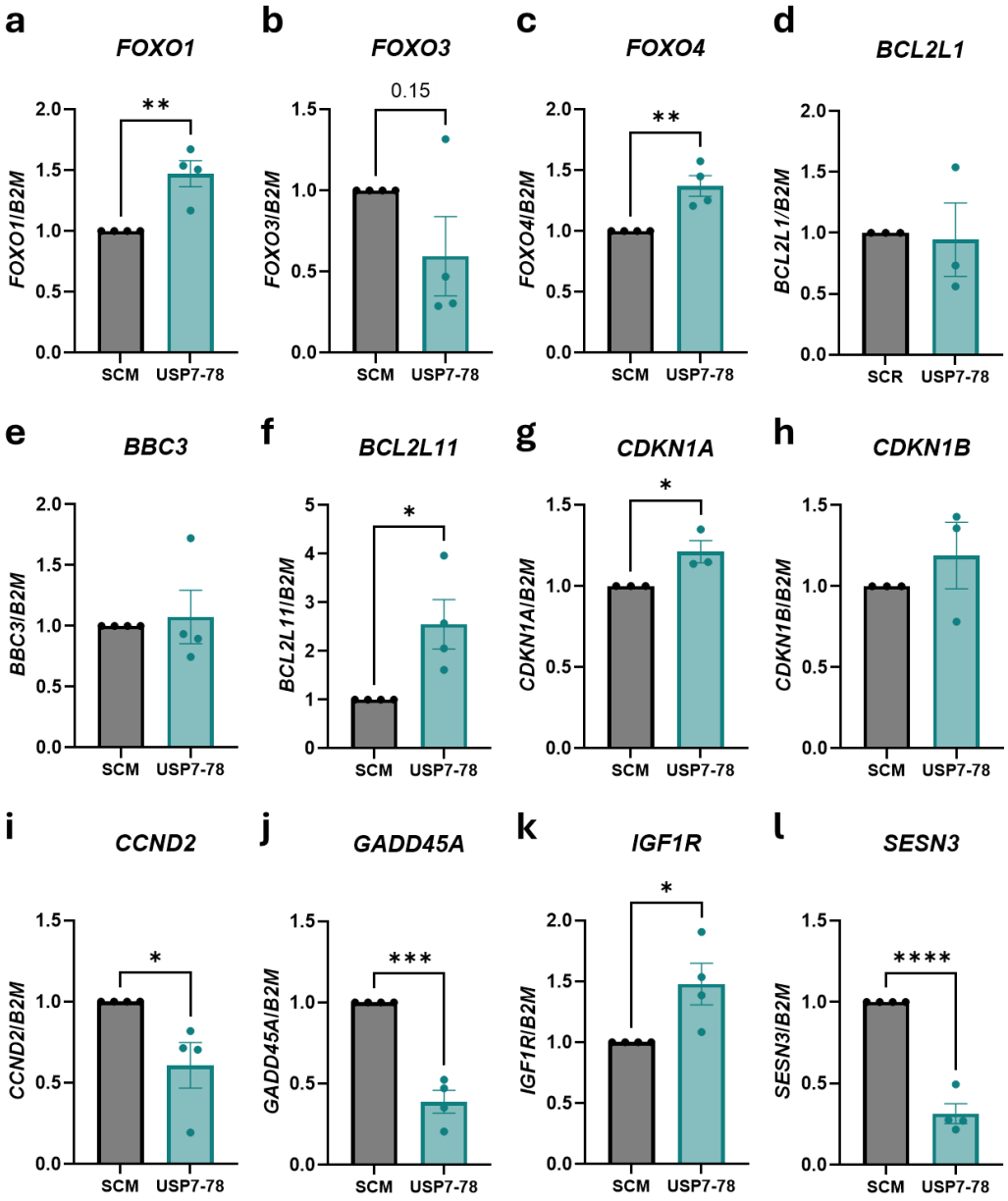

Figure 4.31: The transcription levels of FOXO1 target genes were altered by USP7 KD in MEC1 cells.

RT-qPCR to assess transcription levels of (a) *FOXO1*, (b) *FOXO3*, (c) *FOXO4*, (d) *BCL2L1*, (e) *BBC3*, (f) *BCL2L11*, (g) *CDKN1A*, (h) *CDKN1B*, (i) *CCND2*, (j) *GADD45A*, (k) *IGF1R*, and (l) *SESN3*, in MEC1 transduced with shRNA construct USP7-78 knockdown (USP7-78 KD = oil green bar; n = 4), or scrambled (SCR = black bars; n =4). The $\Delta\Delta C_T$ method was used to calculate transcription levels, where samples were normalised to housekeeping gene *B2M*, and then made relative to SCR control. Each dot represented an individual datapoint. Data expressed as the mean ± SEM. Statistics calculated by paired t-test (a-l); * $p \leq 0.05$, ** $p \leq 0.01$, *** $p \leq 0.001$, **** $p \leq 0.0001$.

4.3.20 USP9x KD in MEC1 cells upregulated FOXO1 target genes *BCL2L11* and *CDKN1B*.

To assess the mRNA levels of FOXO1 target genes in USP9x KD MEC1 cells, we preformed RT-qPCR. Interestingly the same gene modulation noted for USP7 KD cells was seen for USP9x KD cells when analysing the FOXO1 family members, *FOXO1*, *FOXO3* and *FOXO4* (Figure 4.32a-c). While *BCL2L1* did not change between USP9x KD and SCR controls, the transcription levels of *BBC3*, *BCL2L11, CDKN1A*, *CDKN1B*, and *CCND2* were significantly upregulated by USP9x depletion in MEC1 cells compared to SCR controls (Figure 4.32d-i). *GADD45A* expression was significantly reduced in USP9x KD cells compared to SCR controls (Figure 4.32j). Depletion of USP9x in MEC1 cells resulted in significant increase in both *IGF1R* and *SESN3* expression compared to SCR controls (Figure 4.32k & l). Of note, the changes in both *CCND2* and *SESN3* were the opposite to the changes in expression seen in USP7 KD cells.

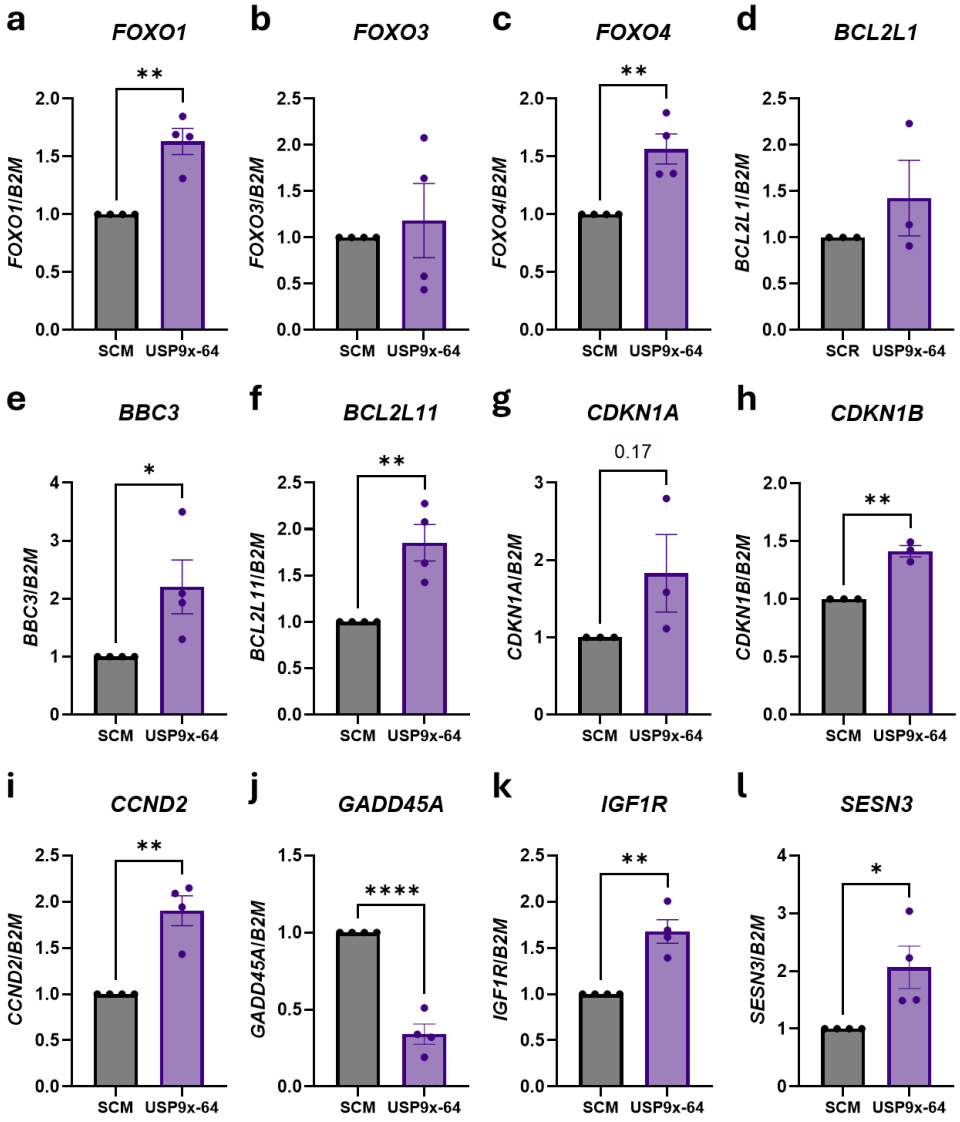

Figure 4.32: FOXO1 target genes *BCL2L11* and *CDKN1B* are significantly upregulated in USP9x KD MEC1 cells.

RT-qPCR to assess transcription levels of (a) *FOXO1*, (b) *FOXO3*, (c) *FOXO4*, (d) *BCL2L1*, (e) *BBC3*, (f) *BCL2L11*, (g) *CDKN1A*, (h) *CDKN1B*, (i) *CCND2*, (j) *GADD45A*, (k) *IGF1R*, and (l) *SESN3*, in MEC1 transduced with shRNA USP9x-64 knockdown (USP9x-64 KD; purple bar; n = 4), or SCR (black bars; n =4). The $\Delta\Delta C_T$ method was used to calculate transcription levels, where samples were normalised to housekeeping gene *B2M*, and then made relative to SCR control. Each dot represented an individual datapoint. Data expressed as the mean ± SEM. Statistics calculated by paired t-test (a-l); * $p \leq 0.05$, ** $p \leq 0.01$, **** $p \leq 0.0001$.

4.4 Discussion

This chapter investigated the regulation of FOXO1 in MEC1 and primary CLL cells focusing on the effects of ibrutinib and DUB inhibitors alone or in combination, assessing the regulation of FOXO1 phosphorylation/expression, subcellular localisation, activity, and modulation of FOXO1 target genes. We used co-IP to explore the interaction between FOXO1 and DUB proteins. shRNA-mediated KD of USP7 or USP9x was employed to determine their role, both alone and in combination with ibrutinib, in regulating FOXO1. FOXO1 co-IP demonstrated a direct interaction between FOXO1 and USP7. While this interaction was unaffected by $F(ab')_2$ stimulation, ibrutinib treatment increased the FOXO1-USP7 interaction, suggesting that the PI3K/AKT pathway may play a role in modulating this interaction. Additionally, USP7 reverse co-IP validated the USP7-FOXO1 interaction in MEC1 cells. Although knocking down USP7 had no significant effect on total FOXO1 expression, or its subcellular localisation, USP7 KD increased FOXO1 DNA binding activity and FOXO1 modulation of its target genes, including an increase in *CDKN1A* transcription and a reduction in *CCND2* transcription levels. Despite the lack of interaction between FOXO1 and USP9x, USP9x KD increased FOXO1 DNA binding activity and subsequently FOXO1 modulation of its target genes, while showing no effect on FOXO1 expression or subcellular localisation, similar to USP7 KD. Interestingly, combining ibrutinib with USP7 or USP9x KDs significantly enhanced FOXO1 nuclear localisation and DNA binding activity. Although the combination of ibrutinib with PR-619, P5091, HBX19818, or WP1130 had no additive effect on downregulating AKT^{S473} and $FOXO1^{T24}$ phosphorylation levels, the combination enhanced ibrutinib influence on cell apoptosis, proliferation, and cell cycle arrest at the G0/G1 phase. Of note, the protein expression of BIM_{EL} was increased by DUB inhibitors and further enhanced by the combination treatments. Subcellular fractionation of FOXO1 demonstrated that DUB inhibitors, including PR-619, P5091, HBX19818, and WP1130, alone had no impact on FOXO1 nuclear localisation, while ibrutinib alone or in combination with DUB inhibitors demonstrated enhanced FOXO1 nuclear accumulation and reduced cytoplasmic translocation. While the TransAM FOXO1 DNA binding activity data showed that the combination of ibrutinib with PR-619 or HBX19818 had no further enhancement on FOXO1 DNA binding activity compared to ibrutinib alone, HBX19818 treatment alone modulated FOXO1 target genes, inducing increased transcription levels of *CDKN1B*, *SESN3*, and *BBC3*, indicative of an elevation in FOXO1 activity. Furthermore, the combination of

HBX19818 with ibrutinib further enhanced the upregulation of these genes, suggesting that HBX19818 treatment sensitises the cells for ibrutinib treatment. These data suggested that the enzymatic activity of DUB proteins, particularly USP7 and USP9x, regulates FOXO1 activity through reducing FOXO1 occupation at its DNA binding site, resulting in the downregulation of FOXO1 modulation of its target genes, while having no effect on FOXO1 total expression and subcellular localisation. Therefore, simultaneously inhibiting DUB proteins, particularly USP7 deubiquitination of FOXO1 and its PI3K/AKT-mediated phosphorylation by the combination of ibrutinib and HBX19818, enhanced FOXO1 modulation of its target genes, as well as FOXO1 nuclear accumulation.

4.4.1 DUB proteins regulated BCR signalling in MEC1 and primary CLL cells.

Several DUB proteins have been identified to regulate key tumour suppressor proteins, including FOXO1, PTEN, and p53, with USP7 particularly shown to affect their stability and control their activity and expression (460, 477, 565). Our data using DUB inhibitors illustrated a downregulation in AKT^{S473} and $FOXO1^{T24}$ phosphorylation as well as total FOXO1 protein expression in MEC1 and $F(ab')_2$ stimulated patient CLL cells. These data indicate that DUB proteins potentially regulate the activity of FOXO1 through downregulation of BCR activity through AKT^{S473} and $FOXO1^{T24}$ phosphorylation. This downregulation of p-$FOXO1^{T24}$ by DUB inhibitors may act through direct interaction with FOXO family member by preventing DUB proteins from removal of monoubiquitination of FOXO1, leading to enrichment of FOXO1 in the nucleus which may result in FOXO1 activation. Indeed, our data support the movement of FOXO1 into the nucleus in the presence of DUB inhibitors, as indicated by the modulation of FOXO target genes, which indicates an increase in FOXO1 transcriptional activity. However, DUB regulatory role in FOXO1 subcellular localisation may require the inhibition of BCR-mediated inactivation of FOXO1, as has been suggested (477). Furthermore, the inhibition of DUB protein activity may modulate p-$FOXO1^{T24}$ indirectly through preventing DUB protein from stabilisation of E3 ligase including MDM2 and SKP2 (478, 573), which has been reported to induce FOXO1 proteasomal degradation.

USP9x has been reported to regulate downstream BCR proteins including mTORC2 (455, 479, 480) and ZAP-70 (482) which both play a key role in BCR activity, and may therefore, influence downregulation of p-$FOXO1^{T24}$ through inhibition of USP9x. Since *BCL2L11* expression is regulated by FOXO1 (574), we analysed protein expression of BIM isoforms

(BIM_{EL}, BIM_L and BIM_S), where BIM_{EL} levels were upregulated in MEC1 and $F(ab')_2$ stimulated CLL cells treated with DUB inhibitors (PR-619, P5091, HBX19818, WP1130). This upregulation of BIM_{EL}, which is released with BIM_L during cell apoptosis (574), potentially increased due to suppression of p-$FOXO1^{T24}$, and accumulation of FOXO1 in the nucleus (575). However, the protein expression of BIM_L and BIM_S were not affected by the DUB inhibitors.

In alignment with Carrà, Panuzzo (460), DUB inhibitors demonstrated no effect on PTEN protein expression. However, contrary to reported increased protein expression of $p21^{Waf1/Cip1}$ in MEC1 cells treated with P5091 (460), our data showed that DUB inhibitors did not influence the protein levels of both $p21^{Waf1/Cip1}$ and $p27^{Kip1}$. This discrepancy might be due to our short incubation of 1 hr with P5091 treatment and that extended incubation may be needed to further investigate DUB inhibitors regulation on the protein expression of $p21^{Waf1/Cip1}$ and $p27^{Kip1}$ in CLL cells. Of note, while the protein levels of $p27^{Kip1}$ did not increase by DUB inhibitors, the transcript levels of *CDKN1B* were upregulated upon 24 hr HBX19818 treatment in MEC1 cells indicative of elevation of FOXO1 activity. Overexpression of USP9x has been reported to upregulate the protein expression of cMYC (576), while USP14 has been suggested to impact the activity of cMYC through stabilisation of NAP1L1 (577), which is also involved in the activation of PI3K/mTOR/AKT signalling pathway (578). Additionally, in naïve B-cells, activation of BCR or CD40 signalling pathways leads to upregulation of cMYC (579). Our data showed that WP1130 inhibitor which inhibits USP5/9x/14 DUB proteins, led to downregulation of cMYC in MEC1 cells, which could be influenced by USP9x mediation of mTORC2 activity, by promoting mTORC2 via removing the Lys-63 ubiquitin linkage from RICTOR (455). Therefore, inhibition of USP9x could mediate downregulation of BCR signalling, leading to FOXO1 activation, inducing cell cycle arrest and apoptosis.

Our data demonstrated that inhibition of DUBs activity resulted in downregulation of BCR activation and dephosphorylation of FOXO1 in a concentration dependent manner, which may lead to FOXO1 nuclear translocation, inducing the expression of target genes that regulate metabolism (580), cell cycle arrest and apoptosis (581). Subcellular localisation of FOXO1 showed that inhibition of DUB proteins had no significant impact on FOXO1 nuclear and cytoplasmic localisation. Treatment with DUB inhibitor PR-619 and HBX19818 had no significant effect on FOXO1 DNA binding activity in CLL cells. This might be due to the short

1 hr treatment of the cells and longer incubation with DUB inhibitors may be required. In chapter 3, we explored the impact of PR-619 and WP1130 on the established USP7 target protein MDM2 (478) up to 4 hr of incubation, and the data showed a trend towards downregulation in a time-dependent manner, which may indicate that longer incubation with DUB inhibitors might be required to observe changes in FOXO1 subcellular localisation. In alignment with longer incubation with DUB inhibitors, it has been reported that 48 hr incubation with P5091, resulted in the upregulation of nuclear PTEN levels in MEC1 cells (460). The subcellular localisation and FOXO1 DNA binding activity data indicated that FOXO1 activity were not influenced by the short-term treatment with DUB inhibitions. The finding that FOXO1 target genes including *BBC3*, *CDKN1B*, *GADD45A*, *SESN3*, *CCND2*, and *BCL2L1* were modulated by HBX19818 inhibition (339, 382, 510, 534, 582) indicates that DUB inhibitors regulate FOXO1 activity. Indeed, DUB inhibitors reduced MEC1 and primary CLL cells viability, proliferation, and increased cells at G0/G1 phase. Aligning with our cell cycle data, USP7 KD in A375 cells induced cell cycle arrest at G0/G1 (478), indicating that USP7 promotes cell growth. However, whether FOXO1 is the main driver for the detected inhibition in cell cycle progression remains to be investigated. Our findings suggest that DUB proteins, may play a critical role in CLL cell survival by regulating FOXO1 activity through modulating FOXO1 target genes. FOXO1 is a key transcription factor downstream of BCR-mediated PI3K signalling (397), a pathway known to be crucial for CLL pathogenesis and progression (51). By potentially modulating FOXO1 activity, DUB proteins could influence this critical pathway and contribute to CLL survival.

4.4.2 The combination of Ibrutinib with DUB inhibitors enhanced ibrutinib modulation of FOXO1 activity, leading to cell cycle arrest and apoptosis in CLL cells.

Calnan and Brunet (339) suggested that FOXOs subcellular localisation is regulated by multiple layers of post-translational modifications, of which FOXOs phosphorylation and monoubiquitination are the main key regulators. Furthermore, it has been reported that DUB proteins, particularly USP7, interaction with FOXO4 resulted in deubiquitination and removal of ubiquitin from the protein (360, 478). This process led to FOXO4 cytoplasmic exclusion and inactivation (360). Here we investigated the impact of ibrutinib, alone and in combination with DUB inhibitors, on BCR-mediated FOXO1 phosphorylation in MEC1 and

short-term $F(ab')_2$ stimulated primary CLL cells. Interestingly, the data demonstrated that both ibrutinib alone and the combination treatment resulted in similar reductions in FOXO1 phosphorylation. This lack of additional effect from the combination treatment might be due to the high effectiveness of ibrutinib treatment in reducing FOXO1 phosphorylation. Furthermore, as we showed in Chapter 3, shorter (1 hr) ibrutinib treatment resulted in slightly lower FOXO1 phosphorylation compared to a longer (24 hr) incubation. Therefore, we speculate that the combination of ibrutinib and DUB inhibitors might have a more durable impact on downregulating FOXO1 phosphorylation with extended treatment durations. Of note, the combination treatment enhanced the upregulation of pro-apoptotic protein BIM_{EL} (*BCL2L11*) at both protein and mRNA levels as well as reduction of anti-apoptotic proteins cMYC and MCL1 in CLL cells. Ibrutinib treatment effectively increased FOXO1 nuclear translocation and reduced cytoplasmic FOXO1 levels in both MEC1 and primary CLL cells. Of note, the combination of ibrutinib with most DUB inhibitors (P5091, HBX19818, and WP1130) did not further enhance this effect. However, the exception was the combination of ibrutinib with PR-619 in MEC1 cells, which showed an additive effect on increasing FOXO1 nuclear localisation and cytoplasmic reduction. This enhancement was only observed in MEC1 cells but not in primary CLL cells, which could be due to CLL heterogeneity of patient samples. Despite the lack of an overall additive effect with other DUB inhibitors, a notable observation was the reduced FOXO1 cytoplasmic levels with the combination treatment. They may suggest that the simultaneous inhibition of phosphorylation and deubiquitination of FOXO1 with the combination treatment may trigger the activation of an E3 ligase target FOXO1 for monoubiquitination, and subsequently facilitate FOXO1 translocation from the cytoplasm to the nuclear, as has been suggested (360). While the combination treatment of ibrutinib and DUB inhibitors did not further enhance FOXO1 DNA binding compared to ibrutinib alone, possibly due to the short incubation time and ibrutinib high effectiveness at 1 hr of treatment, it significantly modulated FOXO1 target genes. HBX19818 increased the transcription levels of established FOXO1 target genes *CDKN1B* and *BBC3*, more effectively than ibrutinib alone. The combination further enhanced this upregulation, suggesting compatibility in targeting the two key mechanisms driving FOXO1 cytoplasmic exclusion: phosphorylation and deubiquitination. Additionally, the combination reduced the transcription of oncogenic *BCL2L1* and *CCND2* gene expression, which HBX19818 alone increased. This highlights the potential benefit of the combination in balancing the effects of these inhibitors. Notably,

ibrutinib treatment had minimal impact on CLL cell viability. However, the combination enhanced ibrutinib potency, leading to increased cell death, reduced proliferation, and augmented cell cycle arrest compared to ibrutinib alone. These data suggest that FOXO1 inactivation through BCR activation plays a critical role in CLL development and survival, and ibrutinib treatment promoted FOXO1 DNA binding activity, nuclear localisation, and cell cycle accumulation at G0/G1. These findings indicate that targeting both BCR-mediated phosphorylation and DUB-mediated regulation of FOXO1 may represent a promising therapeutic strategy for CLL patients, simultaneously inhibiting these two aspects of FOXO1 post-translational modifications.

4.4.3 USP7 interaction with FOXO1 protein, led to FOXO1 inactivation in CLL cells.

In previous chapter, the STRING database identified potential interactions between FOXO1 and DUB proteins. USP7 was predicted to co-express with USP8, 9x, 10, 14, and 28. While FOXO1 co-IP confirmed the interaction between FOXO1 and USP7, we did not find evidence of other predicted DUB proteins binding to FOXO1. Interestingly, our data also showed USP7 interaction with USP9x. To investigate this interaction further, we used shRNA mediated KD of USP7 or USP9x in MEC1 cells. Surprisingly, the shRNA mediated KD of USP7 or USP9x increased the phosphorylation of both AKT^{S473} and $FOXO1^{T24}$, while total FOXO1 protein levels remained unchanged. This suggested that USP7 and USP9x KD might activate the PI3K/AKT signalling pathway, which negatively regulates FOXO1 activity. This finding contrasts with our observation that USP7 inhibitors P5091 and HBX19818 reduced FOXO1 phosphorylation in a concentration-dependent manner. Studies in melanoma cell line A375 showed that USP7 KD had no effect on total FOXO4 levels (478). These observations suggest that a complex dose-dependent regulation of FOXO1 by USP7/USP9x may exist, where complete removal might have a different outcome compared to partial removal. Despite the unexpected increase in FOXO1 phosphorylation with the KDs, ibrutinib downregulated AKT and FOXO1 phosphorylation. Notably, BIM (*BCL2L11*) showed increased protein and mRNA expression upon KD, further enhanced by ibrutinib treatment. This aligns with the observed BIM upregulation with the combination of ibrutinib and DUB inhibitors. These findings indicated that USP7 KD and USP9x KD might influence FOXO1 activity through modulating FOXO1 DNA binding occupancy or stabilisation of regulatory proteins such as

E3 ligases MDM2 and SKP2. Additionally, our data demonstrated that PTEN protein levels were not affected by the KD which was observed by Carrà, Panuzzo (460) in MEC1 cells. Furthermore, It has been reported that USP9x stabilised the protein expression of MCL1 in MM cells by removing K48 polyubiquitination chains which tag MCL1 for proteasomal degradation (545). Our data showed that WP1130 reduced the protein expression of MCL1 in a dose-dependent manner, while USP9x KD had no effect on MCL1 protein levels. Furthermore, USP7 and USP9x KD, while not affecting FOXO1 subcellular localisation on their own, enhanced ibrutinib treatment effect on promoting FOXO1 nuclear accumulation and reduced FOXO1 cytoplasmic exclusion. This suggests that a potential cooperative role between USP7/USP9x activity and ibrutinib-mediated inhibition of p-FOXO1^{T24} in regulating FOXO1 localisation. Strikingly, FOXO1 DNA binding activity increased upon USP7 or USP9x KD and was further enhanced by ibrutinib, an effect that was not observed with DUB inhibitors. The elevation in FOXO1 activity in KD cells was supported by enhanced transcription of FOXO1 target genes including *CDKN1A*, *CDKN1B*, *BBC3*, and *BCL2L11*. However, this did not translate to a measurable increase in cell death or proliferation effects in our study.

The observed discrepancies between the effects of USP7/USP9x KD and DUB inhibitors on FOXO1 phosphorylation warrant further investigation. Using CRISPR-Cas9 technique to knockout (KO) USP7 and USP9x could allow us to compare the complete absence of these DUBs to partial downregulation, or inhibition and their impact on FOXO1 regulation (583). The potential role of other DUB family members beyond USP7 and USP9x in FOXO1 regulation requires investigation. A broader screen targeting various DUBs may identify additional DUB proteins involved in the regulation of FOXO1 activity. It is important to explore the possibility of indirect regulation by DUBs, which could involve stabilising E3 ligases including MDM2 and SKP2, which can then target FOXO1 for ubiquitination and degradation. This study highlighted the intricate interplay between FOXO1, USP7, and USP9x in CLL. While the complex regulatory mechanisms require further investigation, our findings provide evidence for the potential of targeting these DUB proteins as a therapeutic strategy in CLL, with inhibition of FOXO1 phosphorylation and USP7/USP9x activity achieving a more robust FOXO1 activation and may lead to durable therapeutic effect.

Chapter 5. TRIM21 modulation of FOXO1 expression, subcellular localisation and activity in CLL cells.

5.1 TRIM protein family

The tripartite motif (TRIM) protein family is one of the largest subfamilies of Really Interesting New Gene (RING) E3 ubiquitin ligases (584, 585). This family contains more than 70 members which are involved in regulating cellular processes including apoptosis, cell cycle progression, innate immune response, and activation or suppression of carcinogenesis (585, 586). TRIM family proteins are composed of a highly conserved order of domains in the N-terminal region also called TRIM domain, consisting of the RING domain, followed by one or two B-box domains, a long coiled-coil region, and a C-terminus. This C-terminus allows categorisation of TRIM family members into subgroups (Figure 5.1) (586, 587).

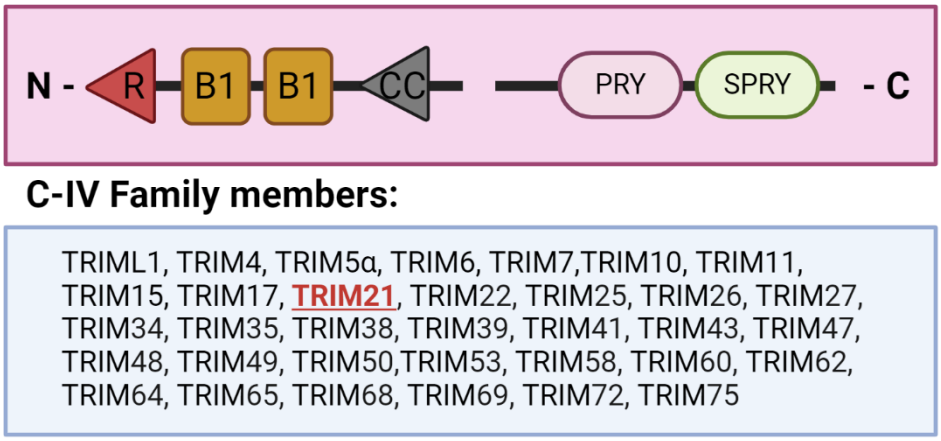

Figure 5.1: Structure of C-IV TRIM family members (modified from (586)).
The human TRIM family of proteins consists of 9 families, classified from C-I to C-XI according to the composition of the carboxy-terminal domain. TRIM21 is a member of the C-IV family with carboxy-terminal PRY SPRY domain. R; Ring finger, B; box, CC; coiled-coil.

Several TRIM family members, including TRIM5α, TRIM8, TRIM11, TRIM21, TRIM22 and TRIM25, possess RING domains that function as E3 ubiquitin ligases (588, 589). Therefore, these RING domain-containing TRIM proteins play a role in regulating cellular processes by modifying proteins through ubiquitination.

TRIM21 (also known as Ro52) has been reported to function as a ubiquitin E3 ligase, IgG receptor, and an autoantigen in autoimmune diseases including systemic lupus erythematosus and Sjögren's syndrome (590, 591). Indeed, TRIM21 binds to the Fc region of IgG through two distinct binding pockets, the PRY domain, and the SPRY domain (592). Furthermore, TRIM21 has been reported to have the highest affinity for the Fc region of IgG compared to IgA and IgM in the human body (593). TRIM21 binds simultaneously to Fc heavy chains of IgG, mediating of intracellular antibody neutralisation of viral infection (593). TRIM21 has been shown to negatively regulate the production of IRF3, 5, and 7, through its E3 ubiquitin ligase activity leading to degradation and blocking the transcription of IFN (594-597). Furthermore, through the monoubiquitination of IKKβ, TRIM21 downregulated Tax-induced NF-κB activation, which subsequently could inhibit NF-κB mediated responses in chronic inflammatory diseases and tumorigenesis (598). Overexpression of TRIM21 reduced the transcription levels of c-FLIP(L), an important downstream anti-apoptotic gene of NF-κB, potentially through suppression of NF-κB activity, leading to apoptosis mediated by TRIM21 in a aspase-8-dependent manner (599). TRIM21 KD in HeLa cells, increased BCL-2, inducing apoptosis independently of p53 expression (590). Collectively these studies indicate that TRIM21 appear to have a tumour suppressor effect. However, TRIM21 has been reported to play a dual role in cancers, exhibiting tumour-suppressive properties in DLBCL, renal cell carcinoma (RCC), ovarian cancer (OC), gastric cancer (GC), and breast cancer (600-606), while studies revealed that TRIM21 was a tumour promotor in colon, pancreatic, gliomas and thyroid cancers (607-609).

5.1.1 TRIM21 acts as tumour suppressor

In DLBCL, high levels of TRIM21 in tissue correlated with better OS and PFS, regardless of treatment regimen (CHOP or R-CHOP) or disease status (600). Furthermore, proliferating cells exhibited significantly lower TRIM21 levels, suggesting that downregulation of TRIM21 may contribute to aggressive tumour growth (600). In RCC, TRIM21 expression in primary RCC tissue was lower compared to normal tissue (601). This low expression correlated with shorter OS (601). Mechanistically, TRIM21 inhibited RCC cell glycolysis by ubiquitinating hypoxia-inducible factor 1-alpha (HIF-1α), leading to its degradation and suppressing proliferation, migration, and metastasis of RCC cells *in vitro* and *in vivo* (601). Similarly, in

OC, the tissues show reduced TRIM21 expression compared to normal tissue (602). This low level of TRIM21 was associated with shorter OS (602). Furthermore, overexpression of TRIM21 inhibited migration, invasion, proliferation, and cell cycle progression in OC cells (602). In GC, the tissues show lower TRIM21 levels compared to normal tissue (603). These low levels linked to higher recurrence rates and lower OS (603). TRIM21 KD reduced the sensitivity of GC cells to apatinib (APA), a tyrosine kinase inhibitor specific for ATP binding site in vascular endothelial growth factor receptor 2 (VEGFR-2), while overexpressing TRIM21 enhanced the effect of APA on reducing colony formation and inducing apoptosis (603). TRIM21 has been shown to interact with the enhancer of zeste homologue 1 (EZH1) protein, and its expression enhanced the effectiveness of APA by suppressing EZH1 stability, which promotes tumour growth (603). In breast cancer, high TRIM21 expression was associated with better survival in patients (604). TRIM21 was found to interact with SET domain containing 7 (SET7/9), a protein associated with promoting cell migration, invasion, and proliferation through activation of Runt-related transcription factor 2 (RUNX2) (605). TRIM21 negatively regulates SET7/9 through ubiquitination, leading to its proteasomal degradation (605). Additionally, TRIM21 was shown to interact with Snail, a regulator of epithelial-mesenchymal transition (EMT) (604). Depletion of TRIM21 expression decreases Snail ubiquitination, promoting migration and invasion of MCF7 and T47D cells (604). TRIM21 interacted with and acted as an E3 ligase for Sal-like 4 (SALL4), a pro-cancerous transcription factor, leading to its degradation and suppressing breast cancer cell proliferation and migration (606).

5.1.2 TRIM21 behaves as tumour promotor

In colon and pancreatic cancers, TRIM21 is reported to act as a tumour promoter, through its interaction with partitioning defective 4 (Par-4), a protein known to induce apoptosis (607). TRIM21 interaction with Par-4, lead to decreased sensitivity to cisplatin treatment, a commonly used chemotherapy drug, suggesting that TRIM21 might contribute to cisplatin resistance in these cancers (607). Similarly, in gliomas, TRIM21 expression was elevated, and this correlated with poorer patient outcomes (608). Mechanistically, TRIM21 promoted tumour cell proliferation by suppressing the p53- $p21^{Waf1/Cip1}$ pathway, a key pathway involved in cell cycle arrest and DNA repair (608). Additionally, it increased drug resistance in glioma cells (608). Bioinformatics analysis of thyroid cancer showed that TRIM21

overexpression correlated with LN metastasis and promotes cancer cell migration and invasion (609).

5.1.3 TRIM21-mediated ubiquitination regulates protein stability, localisation, and activity in cancer.

TRIM21 may directly or indirectly regulate proteins stability through ubiquitination. A new study showed that Yes Associated Protein (YAP), a tumour promoter protein in liver cancer, was indirectly regulated by TRIM21 (610). Furthermore, TRIM21 promoted the ubiquitination and degradation of MST1 protein, a component of the Hippo pathway, where MST1 phosphorylated YAP, leading to cytoplasmic translocation and inactivation (610). Degradation of MST1 by TRIM21 resulted in YAP dephosphorylation and translocation to the nucleus, which induced cell proliferation and contributed to hepatocellular carcinoma (HCC) development (610). In nasopharyngeal carcinoma (NPC), TRIM21 promoted p53 destabilisation through its interaction with SERPINB5 (611). SERPINB5 recruited TRIM21 to interact with GMPS, a protein that stabilises p53 after entering the nucleus (611). However, the recruitment of TRIM21 targeted guanosine monophosphate synthetase (GMPS) ubiquitination, leading to GMPS degradation and subsequent p53 destabilisation (611).

In addition to directly or indirectly regulating protein degradation, TRIM21 may influence protein stability and activity through a co-regulatory network, which could involve the interplay between TRIM21, E3 ligases (612), and DUB proteins (613). TRIM21 was reported to coregulate platelet-derived growth factor receptor beta (PDGFRβ) expression in cooperation with casitas B-lineage lymphoma (Cbl) family ubiquitin E3 ligases (612). In gastrointestinal stromal tumours (GIST), TRIM21 was shown to interact with ACSL4, a protein that promotes ferroptosis (613). Low levels of Acyl-CoA synthetase long-chain family member 4 (ACSL4) were associated with increase resistance to imatinib treatment (613). TRIM21 promoted the K48-linked ubiquitination of ACSL4, leading to its degradation by the proteasome (613). USP15, a DUB protein, counteracted this effect by removing K48-linked ubiquitin from ACSL4 (613), highlighting the interplay between E3 ligases and DUB proteins in regulating protein stability.

TRIM21 could also regulate protein activity and localisation through K63-linked ubiquitination (614, 615), beside its ability to mediate degradation via K48 linkage (615).

TRIM21 was reported to colocalise with p65, promoting K63-linked ubiquitination, which induced p65 interaction with IκB kinase (614). This interaction resulted in the phosphorylation and nuclear translocation, activating the NF-κB pathway and promoting inflammation in psoriatic epidermis (614). Similarly, TRIM21 promoted the nuclear translocation of β-catenin through K63-linked ubiquitination (615). Additionally, TRIM21 targets T1F1γ, an upstream regulator of β-catenin, for K48-linked ubiquitination, further enhancing β-catenin nuclear presence in glioblastoma with hyperactive β-catenin signalling (615). These demonstrated TRIM21 as a versatile regulator that could influence protein expression, localisation, and activity through different types of ubiquitin linkages.

5.1.4 The interaction of TRIM21 with FOXO1 in primary CLL cells

Our MS data revealed TRIM21 as a novel interactor of FOXO1 in primary CLL cells. Since we were interested in FOXO1 post-translational modification via ubiquitination and deubiquitination, we investigated whether depletion of TRIM21 expression would modulate FOXO1^{T24} phosphorylation mediated by BCR activation, total FOXO1 expression, subcellular localisation, FOXO1 activity, and its impact on CLL survival. Furthermore, given the role of TRIM21 as a tumour suppressor or promotor in various cancers, we explored the impact of TRIM21 KD using shRNA on the expression of known tumour suppressor proteins including p27^{Kip1} and PTEN.

5.2 Specific aims

I. Validate the interaction between TRIM21 and FOXO1 by co-IP assay.
II. Explore a potential interaction between TRIM21 and DUB proteins, particularly USP7 and USP9x.
III. Investigate the expression levels of TRIM21 in primary CLL cells and cell lines.
IV. Examine the role of shRNA depleted TRIM21 expression on modulating FOXO1 expression, subcellular localisation, and activity.
V. Investigate whether TRIM21 poses as a tumour suppressor or promotor in CLL cells.

5.3 Results

5.3.1 Global profiling of FOXO1 protein interaction in unstimulated and F(ab')$_2$ stimulated CLL patient samples

Co-IP identified USP7 as a protein directly interacting with FOXO1 in MEC1 and primary CLL cells. In this chapter, we employed MS for a global analysis of FOXO1 interacting proteins comparing unstimulated with BCR stimulation in primary CLL cells. Therefore, following stimulation, FOXO1 was co-immunoprecipitated, and the isolated FOXO1 complexes were then processed using Nanoflow HPLC Electrospray Tandem MS (nLC-ESI-MS/MS) with a TMT system (Figure 5.2a). The proteomics data were analysed using the Swissport database to identify peptide sequences. While USP7 was not identified among the proteins co-immunoprecipitating with FOXO1 in these experiments, the data revealed a significant increase in the interaction between FOXO1 and signalling transduction proteins 14-3-3γ and 14-3-3ζ upon BCR stimulation (Figure 5.2b & c). The increased interaction between 14-3-3 and FOXO1 proteins, served as a positive indicator of BCR activation (344, 567). Similarly, the interaction with prohibitin 1 (PHB1), involved in mitochondrial function and cell cycle regulation (616, 617), showed a trend towards an increase upon BCR stimulation (p = 0.054), while prohibitin 2 (PHB2) interaction remained largely unchanged (Figure 5.2b & c). Conversely, the data showed a significant reduction in the interaction between FOXO1 and interleukin-16 (IL-16) upon BCR stimulation (Figure 5.2b & c). The interaction with ribosomal protein L28 (RPL28), a component of the large ribosomal subunit (618), also showed a trend towards downregulation (p = 0.059; Figure 5.2b & c). Notably, the majority of identified FOXO1 interactors, including the E3 ligase TRIM21, remained relatively stable regardless of BCR stimulation (Figure 5.2b & d) and (Table S5.1). The top ten functional enrichments of the identified FOXO1 interactors were analysed using the g: Profiler database. This analysis demonstrated that the enriched categories included cellular components (particularly cytoplasmic), biological processes (including cytoplasmic translation), and molecular functions (including RNA binding) (Figure 5.2e).

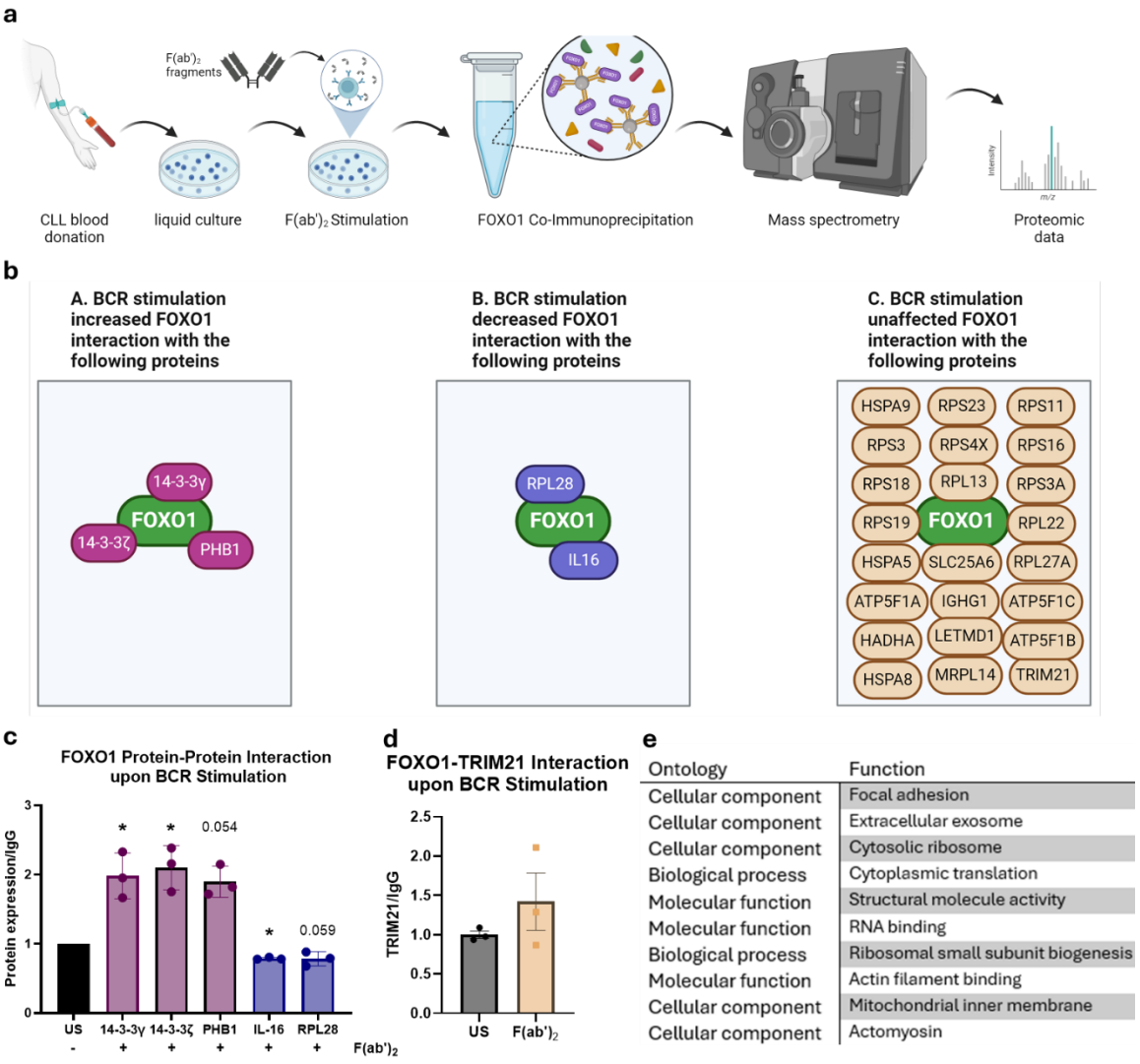

Figure 5.2: Global analysis of FOXO1 protein interaction upon BCR stimulation with F(ab')$_2$ fragment in primary CLL samples.

(a) An illustration of CLL sample preparation for MS analysis. The CLL patient samples (CLL151, CLL173 and CLL196; n = 3) were cultured overnight on RPMI complete media, then stimulated with F(ab')$_2$ fragments (10 ng/mL) for 0.5 hr or unstimulated. FOXO1 co-IP were performed to isolate FOXO1 protein including IgG control. The samples were processed by Nanoflow HPLC Electrospray Tandem MS (nLC-ESI-MS/MS) with a Tandem Mass Tag (TMT) system and 70 proteins were identified as interactor of FOXO1 co-IP. (b) The proteomics data were analysed using the Swissport database to identify peptide sequences and sorted according to the highest peptide spectrum match (PSM). BCR crosslinking with F(ab')$_2$ increased proteins (purple) interaction with FOXO1 protein (green), B. BCR crosslinking with F(ab')$_2$ reduced proteins (blue) interaction with FOXO1 protein (green), and C. BCR crosslinking with F(ab')$_2$ unaffected proteins (beige) interaction with FOXO1 protein (green). (c) Statistical analysis of BCR crosslinking increased (purple bar) or reduced (blue bar) protein interaction with FOXO1 protein, compared with unstimulated (US; black bar). (d) Statistical analysis of FOXO1-TRIM21 interaction upon BCR crosslinking, where unstimulated (US; black bar) and F(ab')$_2$ stimulated (beige bar). The interaction levels of proteins in vehicle were used to calculate the relative interactor levels for (c) & (d). Each dot represented an individual datapoint. Data expressed as the mean ± SD. Statistics calculated by paired t-test; * $p \leq 0.05$. (e) The top ten functional enrichment of FOXO1 protein-protein interactors (619).

5.3.2 TRIM21 co-immunoprecipitated with FOXO1 and USP7 in MEC1 and primary CLL cells

It has been reported that FOXO1 is post-translationally modified by ubiquitination through E3 ligases including MDM2 and SKP2, which induce FOXO1 proteasomal degradation (478, 573). Therefore, we became interested in exploring potential interaction between TRIM21 and FOXO1 protein. To validate the potential interaction between FOXO1 and TRIM21 suggested by our MS data (Table S5.1), we performed a FOXO1 IP on MEC1 and primary CLL cell lysates, with IgG as a control (Figure 5.3a-d). While TRIM21 co-IP with FOXO1 was observed in MEC1 cells, this interaction was not statistical significance compared to the IgG control (Figure 5.3a & b). Of note, TRIM21 co-immunoprecipitated with FOXO1 in primary CLL cells, with a statistically significant difference compared to the IgG control (Figure 5.3c & d). These findings validated the MS data and suggested an interaction between FOXO1 and TRIM21 in primary CLL cells.

Our co-IP experiments suggested an interaction between FOXO1 and USP7. However, this interaction was not observed in our subsequent MS analysis. Since USP7 is known to stabilise the E3 ligase MDM2 (620), we asked whether DUB proteins, particularly USP7 and USP9x, might interact with TRIM21 in MEC1 cells. USP7 and USP9x co-immunoprecipitated from MEC1 cell lysate, with IgG as a control (Figure 5.3 e-h). The data demonstrated that TRIM21 significantly co-immunoprecipitated with USP7 but not USP9x in MEC1 cells compared to the IgG control ($p=0.2$; Figure 5.3e-h). These findings suggested a particular interaction between the DUB protein USP7 and TRIM21 in MEC1 cells, but not with USP9x. It is important to note that the USP7-TRIM21 or USP9x-TRIM21 interactions were not assessed in primary CLL cells.

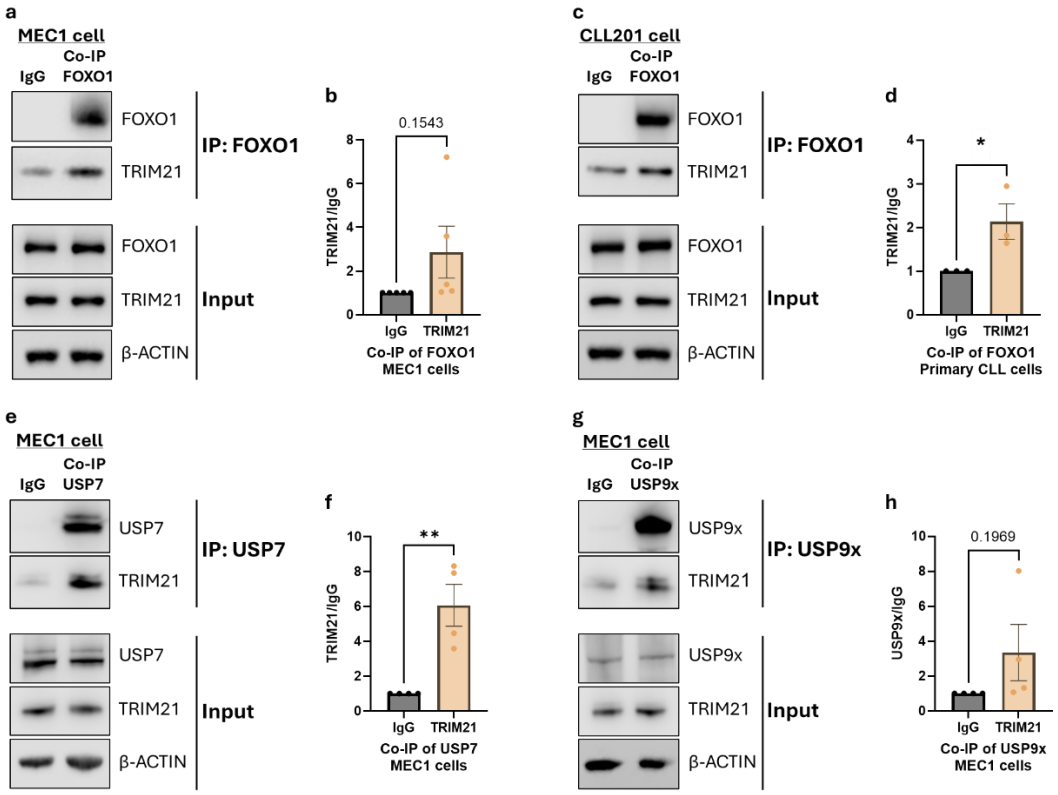

Figure 5.3: TRIM21 interaction with FOXO1 in MEC1 and primary CLL cells.
(a) Representative Western blot of FOXO1 co-IP in MEC1 cells probed for FOXO1 and TRIM21. The relative levels of proteins pulled down in FOXO1 co-IP compared to (b) IgG control (black bar) for TRIM21 (beige bar; n = 5). (c) Representative Western blot of FOXO1 co-IP in primary CLL201 cells probed FOXO1 and TRIM21. The relative levels of proteins pulled down in FOXO1 Co-IP compared to (d) IgG control (black bar) for TRIM21 (beige bar; n = 3). (e) Representative Western blot of USP7 co-IP in MEC1 cells probed for USP7 and TRIM21. The relative levels of proteins pulled down in USP7 co-IP compared to (f) IgG control (black bar) for TRIM21 (beige bar; n = 4). (g) Representative Western blot of USP9x co-IP in MEC1 cells probed for USP9x and TRIM21. The relative levels of proteins pulled down in USP9x co-IP compared to (h) IgG control (black bar) for TRIM21 (beige bar; n = 4). co-IP and whole cell lysate (Input) samples were probed for FOXO1, USP7, USP9x, TRIM21 and β-ACTIN (loading control for input). The expression levels of proteins in vehicle were used to calculate the relative protein expression levels. Each dot represented an individual datapoint. Data expressed as the mean ± SEM. Statistics calculated by paired t-test; * $p \leq 0.05$, ** $p \leq 0.01$.

5.3.3 TRIM21 protein expression was independent of BCR activity in primary CLL cells

Our MS data in section 5.3.1 revealed that BCR crosslinking with $F(ab')_2$ fragments did not affect the interaction between TRIM21 and FOXO1. Furthermore, it has been reported that PI3K/AKT/mTORC2 axis negatively regulate the transcription and protein levels of TRIM21 in prostate cancer PC3 cells (621). This prompted us to investigate whether BCR stimulation regulates TRIM21 expression. We stimulated primary CLL cells with $F(ab')_2$ fragments from 0.5 – 24 hr and analysed the protein expression (Figure 5.4a). The data showed that TRIM21

protein levels remained unchanged compared to the unstimulated control throughout the different time points (Figure 5.4b). This finding may indicate that BCR stimulation does not significantly alter TRIM21 expression (Figure 5.2b & d).

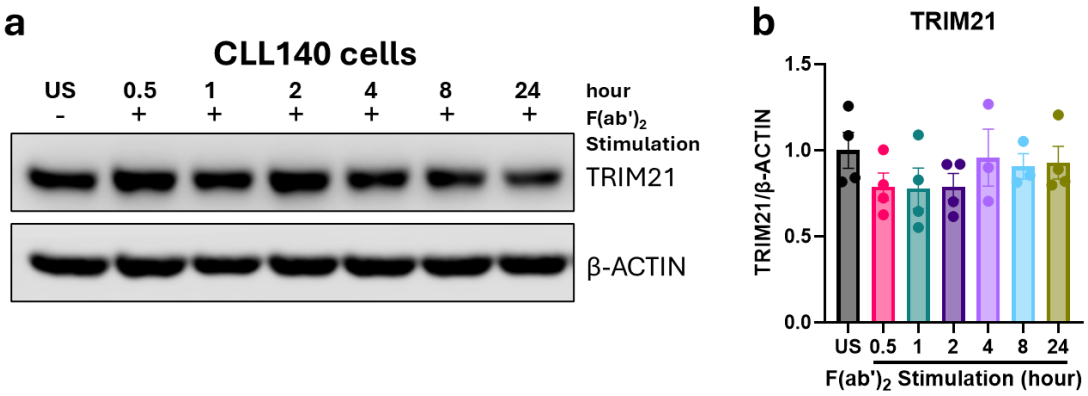

Figure 5.4: TRIM21 expression is not regulated by BCR activity in primary CLL cells.
(a) Representative Western blot of primary CLL sample (CLL140), unstimulated (US; -) or stimulated (+) with F(ab')$_2$ fragments (10 ng/mL) for the indicated timepoints (hour; hr), (0.5 – 24 hr). The blot was probed for TRIM21 and β-ACTIN (loading control). Relative protein expression of (b) TRIM21, between unstimulated (US = black bar; n = 4) and F(ab')$_2$ stimulated for (0.5 hr = pink bar; n = 4), (1 hr = navy bar; n = 4), (2 hr = purple bar; n = 4), (4 hr = light purple bar; n = 3), (8 hr = blue bar; n = 3), (24 hr = oil green bar; n = 4). TRIM21 expression is expressed relative to loading control β-ACTIN. The mean expression level of TRIM21 in US is used to calculate the relative protein expression levels of US and F(ab')$_2$ stimulated timepoints. Each dot represents an individual datapoint. Data expressed as the mean ± SEM. Statistics calculated by One-way ANOVA, Dunnett test (b).

5.3.4 TRIM21 expression levels are similar in *ex-vivo* PB-derived CLL cells and CD19$^+$ B-cells from healthy donors

Studies have revealed a complex role for the TRIM21 protein in cancer. In DLBCL patients, low TRIM21 expression correlated with poor prognosis and survival, regardless of the disease subtype or treatment regimen (600). Similarly, in ovarian cancer, TRIM21 expression is higher in healthy tissues, and overexpression of TRIM21 restricted migration, inhibited apoptosis, and cell cycle progression (602), suggesting a tumour suppressor function for TRIM21. Conversely, in glioma, high levels of TRIM21 protein were associated with a worse clinical outcome, including lower survival rates and increased resistance to temozolomide treatment (608), suggesting a tumour promotor function for TRIM21.

To investigate TRIM21 function in CLL, we initially examined its expression in CLL cells. The Western blot analysis revealed similar levels of TRIM21 protein in *ex-vivo* PB-derived CLL cells compared to CD19$^+$ B-cells from healthy donors (Figure 5.5a & b). Furthermore,

stratifying CLL patients based on cytogenetic abnormalities between patients with undetectable abnormalities and patients harbouring 11q/17p alone or together, did not reveal significant differences in TRIM21 expression (Figure 5.5a & c). Interestingly, TRIM21 protein levels were higher in the HG-3 cell line, which resembles a favourable prognosis, compared to the MEC1 cells (Figure 5.5d & e). We further investigated whether ibrutinib treatment of CLL patients affects TRIM21 expression. Our data revealed a slight but significant increase in TRIM21 protein levels in CLL patients following ibrutinib treatment (Figure 5.5f & g). These findings may suggest a potential tumour suppressor role for TRIM21 in CLL.

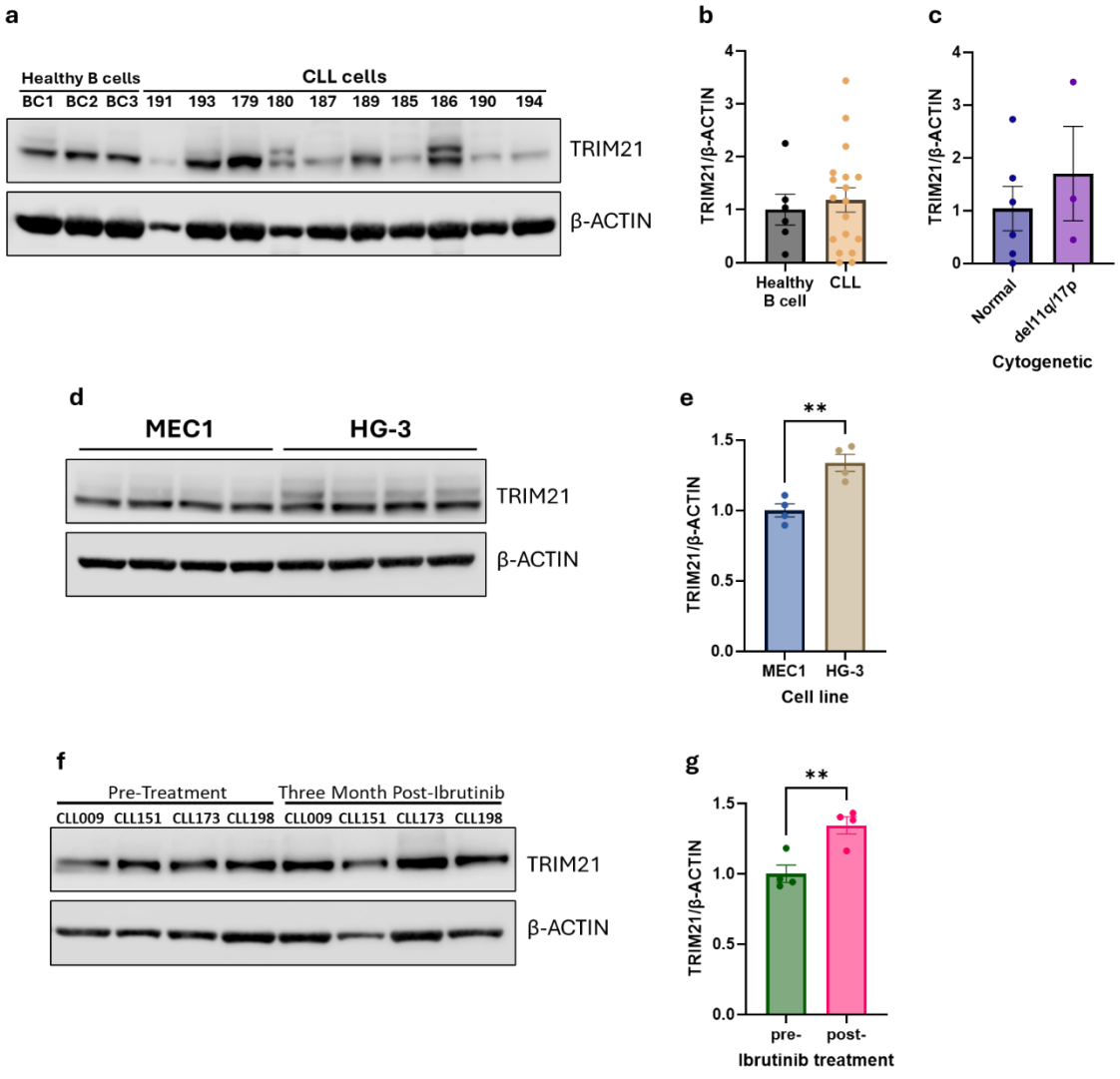

Figure 5.5: Similar expression levels of TRIM21 in *ex-vivo* CLL cells and CD19⁺ B-cells from healthy donors.

(a) Representative Western blot to assess protein expression of *ex-vivo* PB-CLL cells compared with healthy CD19⁺ cells from healthy donors, probed for TRIM21 and β-ACTIN (loading control). (b) Relative protein expression of TRIM21 between B-cell from healthy donors (Healthy CD19⁺; black bars; n = 6) and CLL patient samples (CLL; beige bar; n = 19). Assessing protein expression levels of

(c) TRIM21 expression in CLL patient samples stratified by cytogenetic abnormalities (normal; no 11q(del)/ 17p(del) = blue bar), and (11q(del)/ 17p(del) = purple bar); either one or both cytogenetics abnormalities were detected. (d) Representative Western blot to assess protein expression of MEC1 cells (n = 4) compared with HG-3 cells (n = 4), probed for TRIM21 and β-ACTIN (loading control). Relative protein expression of (e) TRIM21, between MEC1 cells (MEC1; blue bars; n = 4) and HG-3 cells (HG-3 = beige bar; n = 4). (f) Representative Western blot of *ex-vivo* PB-derived CLL patient samples to assess protein expression of pre-ibrutinib treatment (pre-treatment) compared with three months post-ibrutinib patient samples (CLL009, CLL151, CLL173, CLL198), probed for TRIM21 and β-ACTIN (loading control). Relative protein expression of (g) TRIM21, between pre-ibrutinib (pre-IBR = green bar; n = 4) and three months post-ibrutinib (post-IBR = pink bar; n =4). Samples were normalised to loading control. The mean expression levels of proteins were used to calculate relative to protein expression vehicle control. Each dot represented an individual datapoint. Data expressed as the mean ± SEM. Statistics calculated by unpaired t-test (b, c, e, g); ** $p \leq 0.01$.

5.3.5 shRNA mediated KD of TRIM21 in MEC1 cells

To investigate the functional relationship between TRIM21 and FOXO1, we aimed to knockdown TRIM21 expression and assess its impact on FOXO1 protein levels, subcellular localisation, and activity in MEC1 cells. We evaluated three different shRNA constructs targeting different regions of the TRIM21 transcript alongside a SCR shRNA control. TRIM21 KD was confirmed by evaluating both transcript abundance and protein levels. All constructs effectively reduced TRIM21 mRNA levels compared to SCR control (TRIM21-45 (0.5%), TRIM21-48 (0.48%), TRIM21-3986 (0.48%); Figure 5.6a). Western blot analysis revealed that the TRIM21-48 construct (0.38%) most efficiently reduced protein expression, followed by TRIM21-3986 (0.78%). TRIM21-45 did not reduce protein levels compared to SCR control (Figure 5.6b & c). Therefore, we selected the TRIM21-48 construct for further experiments due to its KD efficiency at both the mRNA and protein levels.

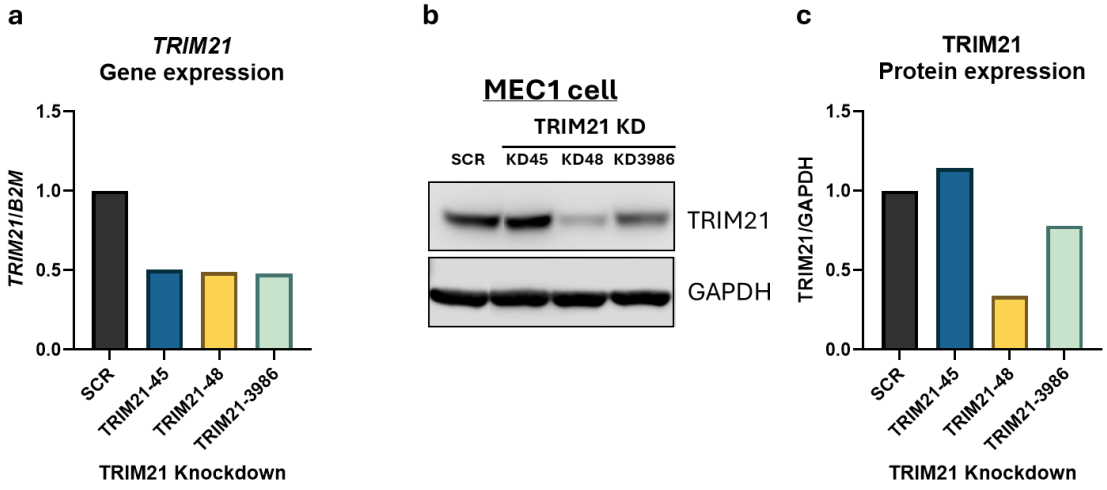

Figure 5.6: TRIM21 shRNA KD in MEC1 cells.

(a) RT-qPCR to assess transcription levels of *TRIM21* (TRIM21-45 knockdown; KD = blue bar; n = 1), (TRIM21-48 = orange bar; n = 1), and (TRIM21-3986 = light green bar; n = 1) shRNA-mediated KD of MEC1 cells transduced with shRNA constructs compared to SCR (black bar; n = 1) control. The $\Delta\Delta C_T$ method was used to calculate transcription levels: samples were normalised to the housekeeping gene *B2M* and made relative to SCR control. (b) Representative Western blot of MEC1 transduced with shRNA-TRIM21-45, 48, 3986 and SCR control. The blots were probed with TRIM21 and GAPDH (loading control). (c) Relative protein levels of TRIM21 (TRIM21-45 KD = blue bar; n = 1), (TRIM21-48 = orange bar; n = 1), and (TRIM21-3986 = light green bar; n = 1) between TRIM21 KD MEC1 cells and SCR MEC1 cells. The mean expression levels of proteins in SCR were used to calculate the relative protein expression levels.

5.3.6 TRIM21 KD reduced total FOXO1 expression in MEC1 cells.

We investigated the functional relationship between TRIM21 and FOXO1 in MEC1 cells using TRIM21-48 shRNA KD. While the AKT/FOXO1 signalling axis was not affected by TRIM21 KD, as evidenced by unchanged levels of p-AKT^{S473}, total AKT, and p-FOXO1^{T24} in both KD and SCR control cells (Figure 5.7a-d), total FOXO1 protein levels were significantly reduced in TRIM21 KD cells compared to the control (Figure 5.7a & e).

Since our previous results (Section 5.3.2) suggested a potential interaction between TRIM21 and USP7, we examined DUB proteins expression levels following TRIM21 KD. The data showed a significant upregulation of USP7 and USP9x in TRIM21 KD cells compared to the SCR control, while USP8 and USP10 expression remained unaffected (Figure 5.7a, f-i). Notably, all BIM isoforms (BIM_{EL}, BIM_L, and BIM_S) exhibited a significant increase in protein expression upon TRIM21 KD (Figure 5.7a, g-l), whereas MCL1 protein levels remained unchanged (Figure 5.7a, m). p21$^{Waf1/Cip1}$ protein expression was not affected by TRIM21 KD in MEC1 cells, unlike what has been reported in ovarian cancer cell lines (602) (Figure 5.7a, n). Conversely, p27^{Kip1} and PTEN protein levels were significantly increased upon TRIM21 KD compared to SCR control (Figure 5.7a, o, p).

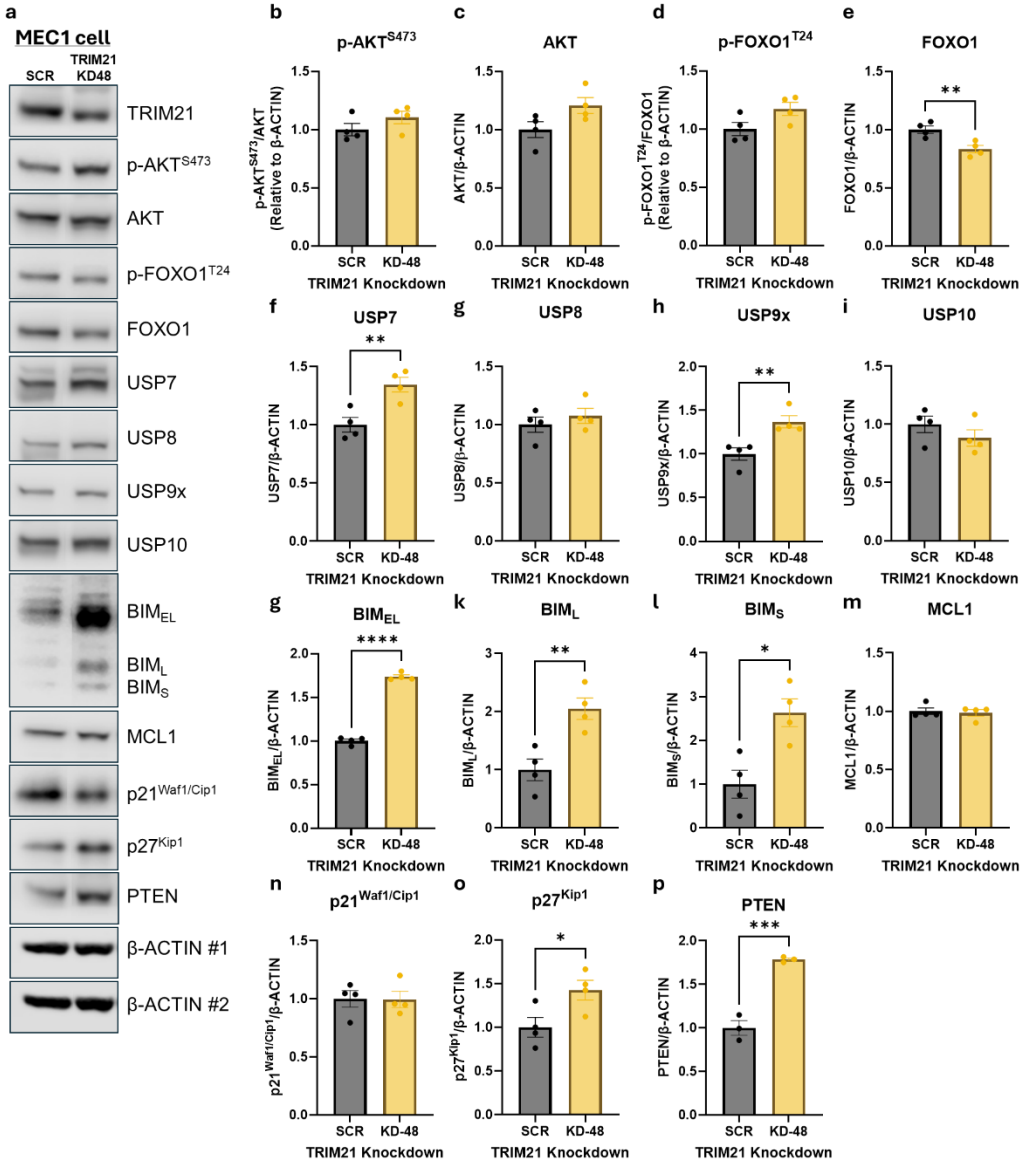

Figure 5.7: TRIM21 KD significantly reduced total FOXO1 expression in MEC1 cells.
(a) Representative Western blot of MEC1 transduced with shRNA construct of TRIM21-48 knockdown (KD) or scrambled (SCR) control. The blots were probed with p-AKT^{S473}, AKT, p-FOXO1^{T24}, FOXO1, USP7, USP8, USP9x, USP10, BIM (EL, L, S), MCL1, p21$^{Waf1/Cip1}$, p27^{Kip1}, PTEN, and β-ACTIN (loading control; #1 and #2 representing mirror blots). Relative proteins expression of (b) p-AKT^{S473}, (c) AKT, (d) p-FOXO1^{T24}, (e) FOXO1, (f) USP7, (g) USP8, (h) USP9x, (i) USP10, (g) BIM$_{EL}$, (k) BIM$_L$, (l) BIM$_S$, (m) MCL1, (n) p21$^{Waf1/Cip1}$, (o) p27^{Kip1}, and (p) PTEN, transduced with TRIM21 shRNA (orange bars) or SCR control (black bars). The mean expression levels of proteins in SCR vehicle were used to calculate the relative protein expression levels. Each dot represented an individual datapoint. Data expressed as the mean ± SEM. Statistics calculated by paired t-test; * $p \leq 0.05$, ** $p \leq 0.01$, *** $p \leq 0.001$, **** $p \leq 0.0001$.

5.3.7 TRIM21 KD visibly reduced nuclear FOXO1 localisation in MEC1 cells

Our previous findings showed that TRIM21 KD reduced total FOXO1 protein levels without affecting AKT-mediated phosphorylation of FOXO1 (Section 5.3.6). Since FOXO1 activity is regulated by its subcellular localisation, we investigated whether TRIM21 KD alters FOXO1 subcellular localisation in MEC1 cells. The data revealed that TRIM21 is primarily located in the cytoplasm (Figure 5.8a). Interestingly, there was a visible trend towards reduced nuclear FOXO1 levels in TRIM21 KD cells compared to SCR control, although this difference did not reach statistical significance (Figure 5.8a & b). Ibrutinib treatment, which promoted nuclear translocation of FOXO1 in SCR control, appeared to be less effective in upregulating nuclear FOXO1 in TRIM21 KD cells. Cytoplasmic FOXO1 levels were similar between TRIM21 KD and SCR control cells. However, ibrutinib treatment visibly less effective in reducing cytoplasmic FOXO1 in TRIM21 KD cells compared to SCR control (Figure 5.8a, c). Despite the slight but significant increase in USP7 and USP9x protein expression upon TRIM21 KD (Section 5.3.6), their subcellular localisations were similar to SCR control (Figure 5.8a, d-g).

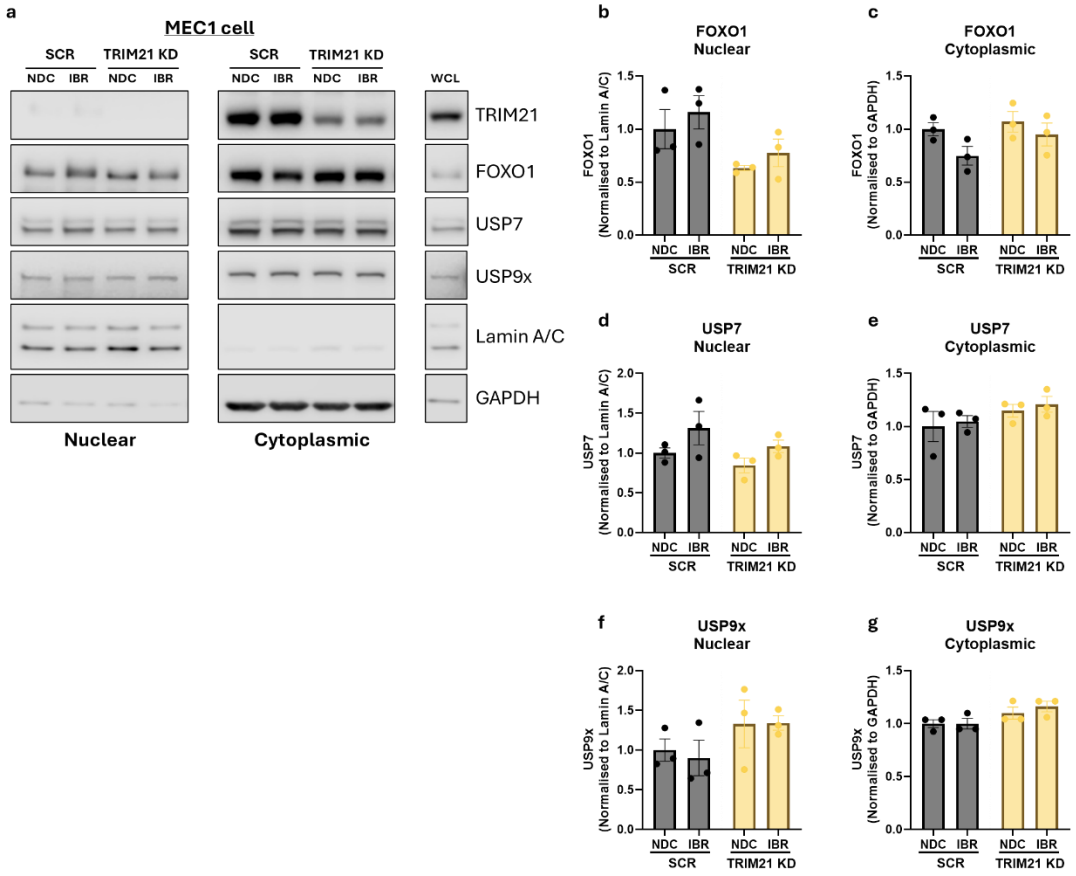

Figure 5.8: TRIM21 KD reduces FOXO1 nuclear localisation in MEC1 cells.
(a) Representative Western blot of subcellular fractionation of MEC1 transduced with shRNA TRIM21-48 or SCR control cells, both treated with ibrutinib (IBR; 1 µM), or no drug control (NDC/DMSO). Following 1 hr treatment as describe in (a), shRNA TRIM21-48 Knockdown (KD) MEC1

and scrambled (SCR) cells (n = 3) were fractionated into cytoplasmic, nuclear, and whole cell lysate (WCL). The blots were probed for TRIM21, FOXO1, USP7, USP9x, Lamin A/C (nuclear loading control), and GAPDH (cytoplasmic loading control). Relative protein expression of (b) nuclear FOXO1, (c) cytoplasmic FOXO1, (d) nuclear USP7, (e) cytoplasmic USP7, (f) nuclear USP9x, and (g) cytoplasmic USP9x between TRIM21 KD MEC1 cells (orange bars) and SCR control (black bars), treated as described in (a). Nuclear and cytoplasmic fractions were normalised to loading controls (Lamin A/C and GAPDH, respectively). The mean expression levels of proteins in SCR vehicle were used to calculate the relative protein expression levels for TRIM21-48 KD and SCR MEC1 cells. Each dot represented an individual datapoint. Data expressed as the mean ± SEM. Statistics calculated by One-way ANOVA, Tukey test.

5.3.8 FOXO1 activity was reduced by TRIM21 KD

Our previous findings showed that TRIM21 KD in MEC1 cells reduced total FOXO1 protein and its nuclear localisation (Section 5.3.7). To investigate whether this reduction affects FOXO1 activity, we assessed FOXO1 DNA binding activity using nuclear fractions and the TransAM transcription factor activation assay. The data revealed that TRIM21 KD decreased FOXO1 DNA binding activity compared to the SCR control ($p = 0.0503$; Figure 5.9a).

Since TRIM21 interaction with FOXO1 led to a reduction in FOXO1 activity, we asked whether this might impact cell viability and proliferation in MEC1 cells. We cultured SCR control and TRIM21 KD MEC1 cells for 72 hr, followed by staining with Annexin V/7-AAD for apoptosis analysis and with CTV/apoptosis stains for proliferation analysis. Our results demonstrated a slight but consistent trend towards increased cell viability in TRIM21 KD cells compared to SCR control (Figure 5.9b). Interestingly, the proliferation rate of TRIM21 KD cells exhibited a visible increase compared to the control (Figure 5.9c). These findings suggest that TRIM21 KD might promote cell survival and proliferation in MEC1 cells, potentially by reducing FOXO1 tumour suppressive activity.

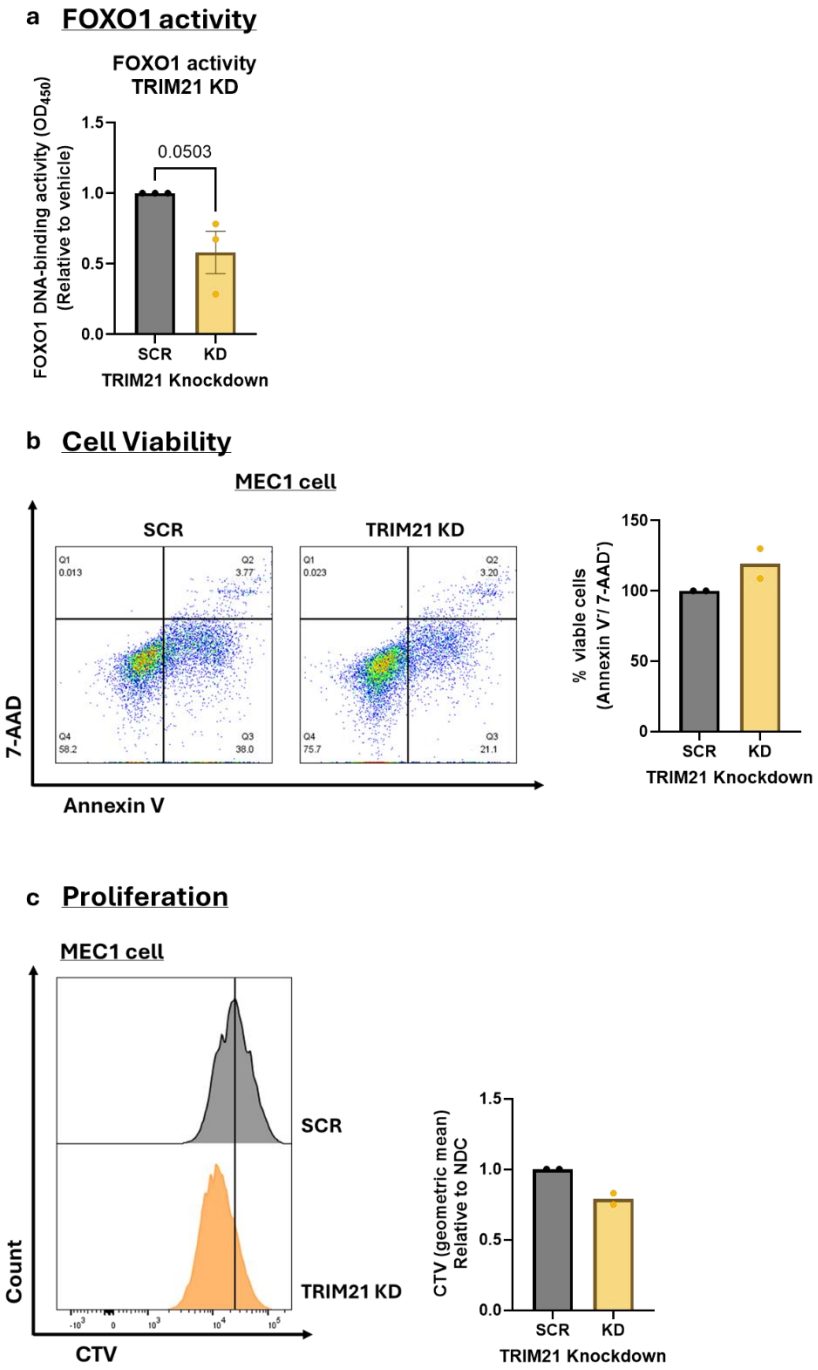

Figure 5.9: Reduced FOXO1 activity mediated by TRIM21 KD may promote MEC1 cell survival.

(a) Nuclear fractions were generated by subcellular fractionation and the TransAM FOXO1 activity assay was used to determine FOXO1 DNA-binding activity. FOXO1 activity in MEC1 transduced with shRNA construct TRIM21-48 (orange bar; n = 3) or SCR (black bars) cells. (b) Representative FACS dot plots are shown MEC1 cells stained with Annexin V and 7-AAD to evaluate cell viability of TRIM21-48 knockdown (KD) and scrambled (SCR) following 72 hr incubation in liquid culture. MEC1 cells were transduced with shRNA construct TRIM21-48 (oil orange bars; n = 2) or SCR control (black bars). Viability is defined as Annexin V negative and 7-AAD/DAPI negative. Percentage viable cells for each condition are relative to SCR. (c) Representative FACS histogram presenting fluorescence of CTV. Cells were stained with CTV to evaluate cell proliferation of TRIM21-48 KD and SCR, following 72 hr incubation in liquid culture. A vertical line denotes the peak of the NDC histogram. Geometric means for each condition are relative to SCR vehicle. Each dot represented an individual datapoint. Data expressed as the mean ± SEM. Statistics calculated by paired t-test (a).

5.4 Discussion

Our study explored the post-translational regulation of FOXO1. We observed that BCR crosslinking rapidly upregulated p-FOXO1^{T24}, and total FOXO1 via mTORC2/AKT axis in primary CLL cells. This upregulation was transient, sustaining for 2 hr upon stimulation, and was specific to protein levels, with no impact on FOXO1 transcription levels. These findings suggested a potential role for protein ubiquitination and deubiquitination in regulating FOXO1 upon BCR activation. While our data demonstrated an interaction between FOXO1 and USP7, it was not identified in our subsequent MS analysis. However, the MS data identified TRIM21 as a novel protein interactor of FOXO1 protein in primary CLL cells. Interestingly, while TRIM21 expression levels were similar in primary CLL cells and CD19^{+} B-cells from healthy donors, TRIM21 levels were higher in post-ibrutinib treated patient CLL samples. We further investigated the functional role of TRIM21 interaction with FOXO1 protein in CLL cells by generating a TRIM21 KD in MEC1. This reduced total FOXO1 protein expression without affecting its phosphorylation levels. Additionally, TRIM21 KD led to a reduction in nuclear FOXO1, and a downregulation of FOXO1 DNA binding activity. This reduction in FOXO1 activity through TRIM21 depletion resulted in a trend towards increased MEC1 cell viability and proliferation in MEC1 cells. These results suggest that the interaction between TRIM21 and FOXO1 stabilises total FOXO1 expression, mediates FOXO1 nuclear localisation, and subsequently increases FOXO1 activity, leading to cell cycle arrest and apoptosis.

5.4.1 TRIM21 interaction with FOXO1 and DUB proteins in primary CLL and MEC1 cells.

TRIM21, an intracellular Fc receptor, binds IgG antibodies with high affinity (622). Hsu and Yu (623) suggested that TRIM21 high affinity to IgG antibodies may lead to potential false-positive co-precipitation during co-IP experiments. In our study, TRIM21 co-IP demonstrated the interaction of FOXO1 and USP9x with TRIM21 co-IP in MEC1 cells were not statistically significant compared to IgG controls. This potentially reflects TRIM21 non-specific binding to IgG control. Interestingly, TRIM21 KD reduced FOXO1 protein levels and significantly increased USP9x expression, suggesting a potential role for TRIM21 in regulating these proteins, either directly or indirectly (610). This observed regulation of

FOXO1 and USP9x further strengthened the possibility of interactions between TRIM21 and these proteins. However, in primary CLL cells, our data revealed significant co-IP of TRIM21 with FOXO1. This discrepancy between MEC1 and CLL cells could be due to CLL-prognostic factors, as higher TRIM21 levels have been associated with favourable prognosis and lower proliferation in DLBCL cells (600). This aligned with our findings of higher TRIM21 expression in HG-3 cells and post-ibrutinib treated CLL patient samples. Additionally, TRIM21 KD led to slight upregulation of USP7 protein expression, and clear co-precipitation of TRIM21 with USP7 compared to IgG control, supporting a potential interaction. This may indicate a role for TRIM21 in regulating USP7 stability and its interplay with USP7 in modulating FOXO1 activity in CLL cells.

To address the limitations of TRIM21 IgG binding in co-IP experiments, future studies could utilise TRIM21 with a mutated PRY/SPRY domain with lower IgG affinity (624). Alternatively, performing a reverse co-IP by immunoprecipitating TRIM21 and verifying co-precipitation of FOXO1, USP7, and USP9x, could further strengthen the evidence for these interactions.

5.4.2 TRIM21 KD downregulated FOXO1 expression, nuclear translocation, and activity in MEC1 cells

Cheng, Huang (621) reported that overexpression of AKT and its constitutively activated forms (T308/S473) suppressed TRIM21 expression at the mRNA and protein levels in HEK293T cells. Furthermore, treating PTEN-deficient prostate cancer PC3 cells with dual PI3K/mTOR inhibitors (PKI-587 and GDC-0980), or PI3Kα/β/δ inhibitor (BAY1082439) increased the expression of TRIM21 at both mRNA and protein levels, while mTORC1 inhibitor (rapamycin) demonstrated no impact on the expression TRIM21 (586). This suggests that PI3K/AKT/mTORC2 signalling supresses TRIM21 expression. Our data demonstrated that $F(ab')_2$ stimulation largely did not affect TRIM21 expression levels in most patient samples. However, a number of patient samples exhibited a transient decrease in TRIM21 levels, mirroring our previous observation of transient FOXO1 phosphorylation, cytoplasmic translocation, and inactivation upon BCR activity. Interestingly, TRIM21 KD led to decreased FOXO1 protein levels, with a depletion of nuclear FOXO1 and reduced activity. This suggests the PI3K/AKT pathway might inactivate FOXO1 by phosphorylation along with regulation of TRIM21 expression in CLL cells. We speculated that TRIM21, acting as an E3 ligase with its RING domain, promotes FOXO1 nuclear

translocation through monoubiquitination (597, 613, 615), a ubiquitination that facilitates functional modification of proteins rather than degradation (625). Supporting this, ibrutinib treatment increased the nuclear FOXO1 pool in SCR control, but this effect was reduced in TRIM21 KD cells. This suggests that TRIM21 KD impaired FOXO1 nuclear translocation, contributing to the observed reduction in FOXO1 activity. Furthermore, TRIM21 depletion increased USP7 expression, which may stabilise E3 ligases like MDM2 and SKP2 (478, 573). These E3 ligases could target cytoplasmic FOXO1 for degradation, preventing its nuclear entry and reducing its ability to bind DNA and regulate its target genes. However, further experiments are required to validate our speculations including a co-IP experiment to pull down FOXO1 protein from TRIM21 KD cells and SCR control. This experiment would determine if TRIM21 interaction with FOXO1 leads to ubiquitination involving K48 or K63 linkages. Furthermore, examining FOXO1 target genes by RT-qPCR would strengthen the evidence of reduced FOXO1 activity due to TRIM21 KD in MEC1 cells. Overexpression of TRIM21 would also determine if FOXO1-TRIM21 interaction directly affects FOXO1 activity. Immunohistochemistry experiments could validate changes in FOXO1 subcellular localisation upon TRIM21 KD. Furthermore, FOXO1 KD or transfection with constitutively activated FOXO1 form (FOXO1-AAA) could clarify if the observed effects on cell viability and proliferation are indeed driven by reduced FOXO1 activity (626). The $F(ab')_2$ stimulation time course was based on a small number of patient samples showing transient TRIM21 decrease upon BCR stimulation. Since CLL is a heterogenous disease (627), a larger sample number would be required to determine whether PI3K/AKT signalling pathway negatively regulate TRIM21 transcription and protein levels in CLL cells. Considering the doubling time of MEC1 cells (40 hr) and the possibility of delayed effects (485), extending the cell viability and proliferation experiments to 120 hr might be beneficial for observing a clearer impact of TRIM21 KD.

5.4.3 TRIM21 exhibited a dual role as tumour suppressor/promotor in CLL cells.

TRIM21 has been implicated in various cancers, exhibiting both tumour-suppressive and tumour-promoting properties. Studies have shown its tumour-suppressive function in DLBCL, RCC, OC, GC, and breast Cancer (600-606). However, other studies suggested a

tumour-promoting role in colon cancer, pancreatic cancer, gliomas, and thyroid cancer (607-609).

Our data added to this complexity. We observed higher TRIM21 expression in the favourable prognosis HG-3 cell line and in CLL patient samples treated with ibrutinib, suggesting a potential tumour-suppressive role. Furthermore, TRIM21 KD in MEC1 cells resulted in decreased expression and activity of FOXO1, an established tumour suppressor (399, 412, 501). Additionally, TRIM21 KD led to increase cell viability and proliferation, further supporting a tumour-suppressive function. However, our findings also revealed a potential tumour-promoting aspect of TRIM21. TRIM21 KD upregulated expression of known tumour suppressor proteins including BIM, PTEN, and $p27^{Kip1}$ (400, 507, 510). This was consistent with previous reported study showing TRIM21 formation of complexes with SKP1, SKP2, and Cul1 to promote ubiquitination and degradation of phosphorylated $p27^{Kip1}$ (588). Therefore, TRIM21 modulation of FOXO1 through ubiquitination may further enhance FOXO1 anti-tumour activity and triggering cell cycle arrest and apoptosis of CLL cells.

Chapter 6. General Discussion and Conclusions

Although much is known about FOXO1 post-translational modification through phosphorylation, particularly mediated by the PI3K/AKT axis downstream of the BCR in CLL cells, the role of DUB proteins in modulating FOXO1 activity downstream of the PI3K/AKT pathway has not been fully investigated in CLL. Given the reported multifaceted role of FOXO1 in a context- and tissue-dependent manner and the fact that inhibition of the PI3K/AKT pathway induces FOXO1 tumour-suppressor activity, it was anticipated that the regulation of FOXO1 downstream of the PI3K/AKT pathway is the context in which FOXO1 acts as a tumour suppressor in CLL cells. Therefore, this thesis investigated the role of BCR-dependent phosphorylation and inactivation of FOXO1, as well as the role of DUB proteins in modulating FOXO1 expression, transcriptional activity, and subcellular localisation.

The presented data demonstrated that FOXO1 expression was upregulated at both the mRNA and protein levels, without a clear association with poor prognostic factors in CLL, including cytogenetic aberrations del(11q) and del(17p) or advanced Binet stages. Interestingly, the activity of the BCR signalling pathway was lower in PB-derived CLL cells compared to healthy B-cells, as indicated by the low phosphorylation of AKT^{S473} and $FOXO1^{T24}$. This further confirms the importance of BCR signalling for CLL cells and their high reliance on BCR activity for their survival. In agreement with previously published studies, we showed that FOXO1 is an effector of BCR crosslinking *in vitro*, promoting FOXO1 inactivation and nuclear exclusion through PI3K/AKT-dependent phosphorylation of FOXO1 (412, 543). This was further confirmed using the BTK inhibitor ibrutinib, which restored FOXO1 nuclear localisation, and subsequently increased FOXO1 DNA binding and transcriptional activities, as indicated by the modulation of FOXO target genes, including the upregulation of *BBC3* and the downregulation of *CCND2*. These findings suggest that FOXO1 tumour-suppressive activity is indeed inhibited by BCR-mediated phosphorylation and that FOXO1 acts as a tumour suppressor in CLL cells in this context. Furthermore, the levels of both phosphorylated and total FOXO1 protein were transiently upregulated upon BCR crosslinking, peaking at 0.5 hr and sustaining up to 2 hr. This transient upregulation of total FOXO1 was specific to the protein level, as *FOXO1* mRNA level did not change. Given that PI3K/AKT-mediated phosphorylation of FOXO1 has been reported to promote FOXO1 nuclear exclusion and subsequent proteasomal degradation (347) we hypothesised that

this transient upregulation of total FOXO1 upon BCR crosslinking might be regulated by post-translational modifications involving the UPS pathway, particularly DUB proteins.

The STRING database revealed a direct co-expression between USP7 and FOXO1, as well as identifying several other DUBs, including USP9x, that may indirectly modulate FOXO1. In agreement with previously published data (425, 459, 460), DUB protein expression in patient CLL cells were largely upregulated, including the expression of USP7 and USP9x. FOXO1 interacted with USP7 in primary CLL cells and cell lines. While FOXO1-USP7 interaction was largely unaffected by BCR crosslinking, inhibition with ibrutinib increased this interaction. This suggests that the PI3K/AKT pathway may play a role beyond modulating FOXO1 phosphorylation, potentially include modulation of FOXO1 interaction with DUB proteins. Interestingly, our data showed that BCR signalling had no impact on the expression or subcellular localisation of USP7 and USP9x, raising the question of whether inhibiting DUB enzymatic activity would affect the PI3K/AKT signalling pathway and its mediated phosphorylation of FOXO1. Treating CLL cells with the pan-DUB inhibitor PR-619 downregulated AKT^{S473} and $FOXO1^{T24}$ phosphorylation. However, USP7 inhibitors (P5091 and HBX19818) and the USP9x inhibitor (WP1130) demonstrated varying results and were largely less effective at inhibiting the PI3K/AKT pathway and subsequently $FOXO1^{T24}$ phosphorylation. These findings indicate that DUB proteins have a regulatory role in the activity of the PI3K/AKT signalling pathway, but the inhibition or KD of an individual DUB protein, including USP7 or USP9x, was not sufficient to exert a significant effect on PI3K/AKT activity. These DUB inhibitors reduced CLL cell viability while largely sparing healthy B-cells, suggesting a stronger reliance on DUB protein activity for CLL survival, which is in agreement with previously published data (459). Additionally, the inhibitors induced the accumulation of MEC1 cells in the G0/G1 phase but did not have a major effect on cell proliferation, in agreement with published data (459). The combination of ibrutinib and DUB inhibitors (PR-619, P5091, HBX19818, and WP1130) enhanced CLL cell response to ibrutinib, leading to a greater reduction in cell viability, proliferation, and cell cycle accumulation at the G0/G1 phase.

Despite the lack of regulation of DUB inhibitors or DUB KDs on FOXO1 expression, FOXO1 transcriptional activity was increased in MEC1 cells by the USP7 inhibitor HBX19818 or USP7/USP9x KDs, as indicated by the upregulation of FOXO target genes, including *CDKN1B* and *BBC3*. This effect was further enhanced by the combination of HBX19818 with ibrutinib,

aligning with previously published data (477). Furthermore, USP7 or USP9x KD alone or in combination with ibrutinib increased FOXO1 DNA binding activity. The nuclear localisation of FOXO1 while only modestly regulated by the inhibition of DUB proteins, particularly PR-619 and HBX19818 was enhanced when combined with ibrutinib, which may explain the enhanced regulation of FOXO1 target genes observed with the combination. These observations suggest that the reduction of USP7 interaction with FOXO1 through KD may facilitate the promotion of FOXO1 to its DNA binding site, resulting in increased FOXO1 transcriptional activity, which aligns with previously published data (477).

Our proteome and subsequent co-IP analysis of FOXO1 novel interactors revealed an interaction between FOXO1 and the E3 ligase TRIM21, with TRIM21 being predominantly cytoplasmic. TRIM21 KD resulted in a reduction of total FOXO1 and FOXO1 nuclear localisation. This regulation of FOXO1 might be promoted by TRIM21 monoubiquitination of FOXO1, resulting in its nuclear accumulation and promoting FOXO1 DNA binding activity, which agrees with previously published studies (360, 477, 628). Furthermore, our data hinted that TRIM21 KD increased MEC1 cell viability and proliferation. These findings suggest that FOXO1 is a substrate of TRIM21, which plays a role in regulating FOXO1 stability, localisation, and activity. Based on the data generated in this thesis, we propose a model where phosphorylation of FOXO1 by PI3K/AKT activity and deubiquitination of FOXO1 by USP7 lead to nuclear exclusion and reduced FOXO1 DNA binding activity (Figure 6.1). In contrast, the combination of ibrutinib and HBX19818 treatments enhance TRIM21-mediated monoubiquitination of FOXO1 by simultaneously blocking BCR- and USP7-mediated phosphorylation and deubiquitination of FOXO1, leading to FOXO1 nuclear accumulation and increase its transcriptional activity.

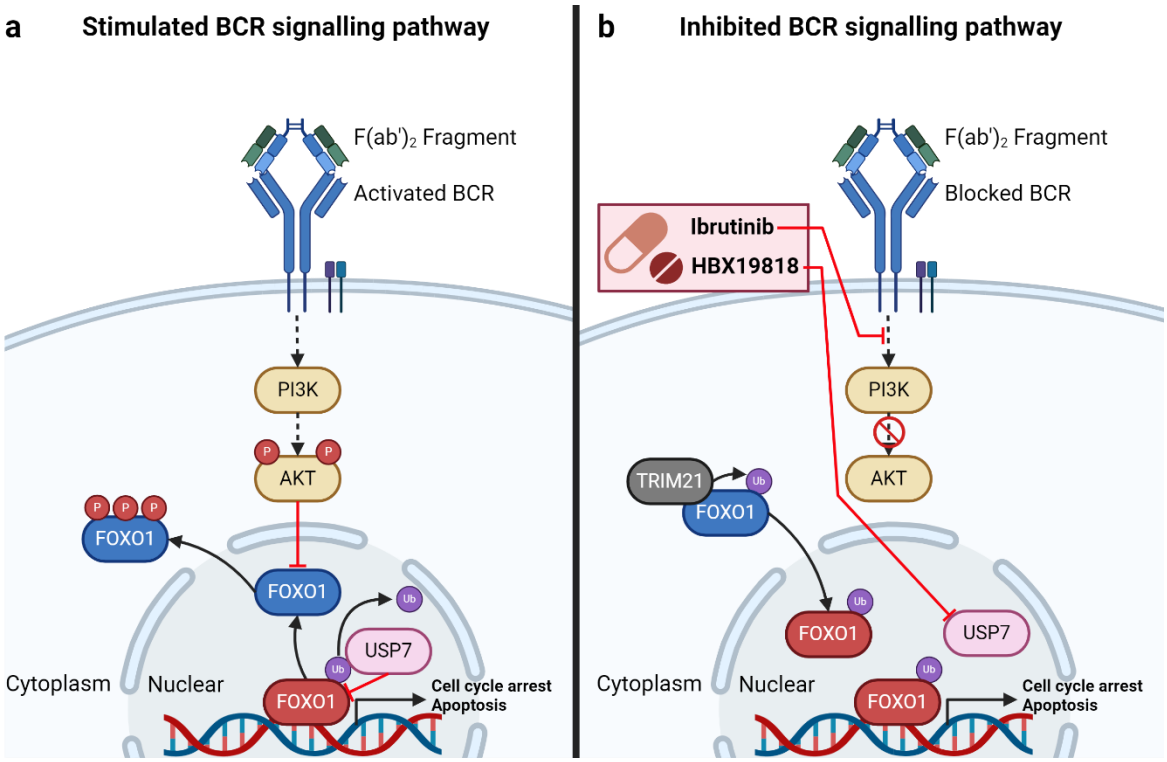

Figure 6.1: A model illustrating FOXO1 post-translational modification by phosphorylation via BCR-crosslinking and ubiquitination/deubiquitination via the UPS E3 ligase TRIM21 and DUB protein USP7.

(a) BCR crosslinking activates the PI3K pathway, leading to the phosphorylation of FOXO1 (blue; inactive), resulting in nuclear exclusion and a reduction in FOXO1 (red; active) occupancy at its DNA binding site. USP7 inhibits FOXO1 (red; active) by removing monoubiquitination, leading to reduced FOXO1 (blue; inactive) transcriptional activity. (b) Treatment with the combination of ibrutinib and HBX19818 inhibits the BCR activation by reducing the activity of the PI3K pathway leading to FOXO1 dephosphorylation (blue; inactive). The interaction of TRIM21 in the cytoplasm induces FOXO1 (blue; inactive) monoubiquitination and subsequently FOXO1 (red; active) nuclear accumulation. Inhibition of USP7 with HBX19818 prevents USP7 deubiquitination of monoubiquitinated FOXO1 (red; active), leading to increased FOXO1 transcriptional activity.

6.1 USP8 potential regulator of PI3K/AKT pathway

Our data demonstrated that the protein levels of USP8 was overexpressed in CLL cells. However, USP8 overexpression was not clearly linked to poor prognostic factors in CLL, including del(11q) and del(17p). In a recent combined genomic, transcriptomic, and epigenomic analysis of 1,148 CLL patients, USP8 was identified as a novel driver of CLL among 109 new candidate genetic drivers (87). Interestingly, USP8 was one of the few driver genes (12.3%) that were present in a large majority of U-CLL cells (87). Overexpression of USP8 has been reported to be associated with poor prognosis in GC patients by stabilising human epidermal growth factor receptor 2 (HER-2), a proto-oncogene, which can both directly and indirectly activate the PI3K/AKT pathway (629, 630). Inhibition of USP8 with

the USP8 inhibitor (MB7295) resulted in the downregulation of phosphorylated PI3K and AKT (629), further indication of USP8 involvement in the regulation of PI3K/AKT activity. In non-small cell lung cancer (NSCLC), USP8 inhibition induced cell apoptosis in gefitinib-resistant cells by suppressing the phosphorylation of STAT3, AKT, and ERK downstream of the receptor tyrosine kinase signalling pathway (631). Gefitinib is an FDA-approved treatment for NSCLC that reversibly inhibits the tyrosine kinase activity of the epidermal GFR (632). In cholangiocarcinoma, the AKT signalling pathway is involved in tumour progression, and USP8 KD inhibited cell proliferation and invasion, downregulated the phosphorylation of AKT, and upregulated the expression of p53. Conversely, overexpression of USP8 increased the activation of the AKT signalling pathway (633). These studies demonstrate that USP8 is involved in cell proliferation and invasion in various cancers and is a driver of poor prognosis in U-CLL cells, with part of its pro-tumour activity driven by USP8 regulation of the PI3K/AKT pathway. To further elucidate the role of USP8 in CLL cells, future research could investigate the effects of USP8 inhibition on CLL cell survival and proliferation through its potential involvement in the regulation of the PI3K/AKT/FOXO1 pathway.

6.2 USP10 multifaceted regulation of the PI3K/AKT activity in cancer

Our data demonstrated that the protein expression of USP10 was overexpressed in CLL cells compared to healthy B-cells, independent of cytogenetic abnormalities, including del(11q) and del(17p). Interestingly, several studies have indicated a dual role for USP10 as a tumour promoter and suppressor in various cancers (634). For instance, USP10 expression was reported to be downregulated in NSCLC cell lines and primary tissues, and its re-expression was associated with reduced cell viability, proliferation, and migration. This anti-tumour activity of USP10 was driven by USP10 deubiquitination of K63-linked polyubiquitinated PTEN in the cytoplasm, resulting in PTEN activation and subsequent inhibition of the PI3K/AKT signalling pathway (635). Similarly, low levels of USP10 expression were observed in hepatocellular carcinoma, and overexpressing USP10 led to inhibition of cell growth by stabilising PTEN and subsequently inhibiting the PI3K/AKT/mTOR activity (566). These studies indicate that USP10 anti-tumour activity is driven by modulating the activity of the PI3K/AKT pathway via PTEN stabilisation. On the other hand, USP10 stabilisation of SKP2 led to enhanced SKP2 activation of the oncogenic tyrosine kinase BCR::ABL1 fusion, a

primary driver of CML, through the degradation of CDK inhibitor $p27^{Kip1}$ and the removal of non-proteolytic K63-linked polyubiquitination of BCR::ABL1 fusion (636). In AML, USP10 inhibition with Wu-5, a novel USP10 inhibitor, overcame Fms-related tyrosine kinase 3 (FLT3) inhibitor resistance, inducing cell death by the proteasomal degradation of FLT3 (516, 637). Mutations in FLT3 are found in 15-35% of AML cases, causing the constitutive activation of FLT3, which is involved in the activation of the PI3K/AKT pathway (516). Yang, Meng (550) demonstrated that USP10 inhibition with HBX19818 and P22077, an analogue of P5091 USP7 inhibitor, or USP10 KD led to the degradation of SYK and subsequently apoptosis of SYK-driven AML cell lines (MV4-11 and Ba/F3-FLT3-ITD) (22). SYK depletion in AML suppressed PI3K/AKT activation, indicating its role in the positive regulation of the PI3K/AKT pathway (638). These studies suggest a multifaceted function for USP10 in a tissue-dependent manner. Furthermore, the suppressive function of USP10 was reported in cancers characterised by low expression of USP10, while our data showed USP10 was overexpressed in CLL cells. Additionally, the involvement of USP10 in stabilisation the E3 ligase SKP2, which has been reported to target FOXO1 for proteasomal degradation (355), suggests a potential role for USP10 in modulating FOXO1 stability. Similarly, USP10 role in regulating PTEN and SYK, both of which negatively and positively regulate the PI3K/AKT signalling pathway, further indicates the involvement of USP10 in the regulation of FOXO1.

Regarding HBX19818, the original research paper demonstrated its high selectivity for USP7 in HCT116 cells and specifically examined its effect on USP10 (492). While no effect on USP10 activity was observed at a concentration of 25 µM (492), it is worth noting that in AML Ba/F3-FLT3-ITD cell lines, HBX19818 potently inhibited the activity of USP10 at a concentration of 10 µM, as reported in a separate study (637). This suggests that HBX19818 may have tissue-specific effects, as it has been reported that HBX19818 in CLL cells was selective to USP7 inhibition (459). Therefore, further investigation into the role of USP10 in CLL cells could reveal its role in regulating the PI3K/AKT/FOXO1 pathway and whether it acts as a tumour suppressor or promoter in CLL cells.

6.3 The combination of USP7 inhibitors with approved treatments in B-cell malignancies

USP7 targeting by selective inhibitors is emerging as a promising therapy in cancer (470). Several studies have demonstrated that high levels of USP7 are directly associated with

tumour progression in CLL (459, 460), MM (461), breast cancer (639), cervical cancer (640), colorectal cancer (640), OC (641), and prostate cancer (363). To date, no USP7 inhibitors have entered clinical trials, which could be attributed to the challenges in developing selective USP7 inhibitors (642). These challenges include preventing cross-inhibition due to the highly conserved structural features of the catalytic domain of DUB proteins (643), and the weak micromolar potency of most USP7 inhibitors (642). For instance, the first trial of a DUB inhibitor in MM was discontinued due to severe lung toxicity caused by increasing the dose of VLX1570 to 1.2 mg/kg, while the anti-tumour effect was observed at a dose equal to or greater than 0.6 mg/kg (475). This suggests the need for more selective inhibitors with achievable nanomolar potency. A new study demonstrated the efficacy and selectivity of FX1-5303, a highly selective USP7 inhibitor, which inhibited USP7 activity with an IC_{50} of 0.29 nM (644). The selectivity of FX1-5303 was confirmed in a panel of 44 DUBs, where only USP7 was inhibited at a concentration of 10 µM (644). FX1-5303 also increased the levels of p53 and $p21^{Waf1/Cip1}$ and inhibited cell viability in the MM.1S MM cell line with nanomolar potency (644). Additionally, FX1-5303 showed efficacy in inhibiting proliferation in *TP53* wild-type AML cell lines, although it was less effective in *TP53* mutant AML cell lines (644). The combination of FX1-5303 and venetoclax, a BCL-2 inhibitor, demonstrated strong anti-proliferative effects in AML cell lines resistant to venetoclax (644). This combination also resulted in strong inhibition of tumour progression in *ex-vivo* AML patient samples and *in vivo* mouse models of AML and MM (644). This study demonstrated that FX1-5303 is a highly selective USP7 inhibitor with nanomolar potency, and the combination of FX1-5303 and venetoclax has demonstrated synergistic anti-tumour effects in preclinical models of AML and MM. Agathanggelou, Smith (459) tested the anti-tumour effects of HBX19818 *in vivo* using a MEC1 CLL murine xenograft model. Therapeutic doses of HBX19818 were well-tolerated in mice and resulted in a reduction of tumour load (459). Similarly, USP7 KD in mice led to a reduction in MEC1 tumour load (459). Notably, the MEC1 CLL cell line harbours del(17p)/*TP53* mutation/deletion, indicating that the inhibition of USP7 in CLL cells with HBX19818 has p53-independent activity (459). Histological assessment of HBX19818 in mice indicated no systemic inflammation in their kidney and liver tissues (459). The study also examined *in vivo* the efficacy of single or combination treatment with HBX19818 and cyclophosphamide or rituximab (459). The data indicated that HBX19818 in combination with cyclophosphamide had a stronger effect than cyclophosphamide alone or the combination of HBX19818 with rituximab (459). These findings suggest that HBX19818,

both alone and in combination with chemotherapy, induced strong anti-tumour effects independently of p53 expression, indicating its therapeutic potential for poor prognostic CLL patients with cytogenetic aberrations such as del(11q) and del(17p). While clinical practice is now moving away from chemotherapeutic options for CLL patients, our data showed the combination of HBX19818 with ibrutinib enhanced the anti-tumour potency of ibrutinib and modulated FOXO1 anti-tumour activities. This suggests that the combination of HBX19818 and ibrutinib may have therapeutic potential through the modulation of FOXO1 activity and the unleashing of its tumour-suppressive function in CLL cells.

6.4 Future directions

Our group developed a poor prognostic CLL mouse model by retrovirally transducing dominant-negative PKCα (PKCαKR) in haematopoietic progenitor cells from wild-type mice (645). This model resembles an aggressive CLL-like disease phenotype, characterised by $CD19^{+}CD5^{+}CD23^{+}IgM^{low}$ expression, upregulation of ZAP-70, and increased activation of the mTOR signalling pathway (483, 645). Future directions include examining the mRNA and protein expression levels of DUBs *in vivo*, particularly USP7, USP8, USP9x, and USP10, in the PKCαKR mouse model compared to the empty vector control (MIEV). Additionally, investigating the effect of DUB inhibitors, particularly HBX19818 alone or in combination with ibrutinib, would provide insights into monotherapies and combination effects on tumour load and OS. Furthermore, using transgenic conditional knockout (cKO) of DUBs, particularly USP7, in the MIEV and PKCαKR mouse models would offer a clearer understanding of the role of these DUBs in regulating the PI3K/AKT/FOXO1 pathway, as well as FOXO1 expression, subcellular localisation, and transcriptional activity. This experimental approach would strengthen our understanding of the role of DUB proteins in the regulation of FOXO1 and whether functional redundancy exists within the DUB family. Examining TRIM21 cKO and its effect on FOXO1 total ubiquitination, subcellular localisation, expression, and transcriptional activity would further enhance our current understanding of the role of TRIM21 in regulating FOXO1 activity.

Co-IP of FOXO1 protein from whole cell lysates of CLL patient cells and MEC1 cells demonstrated FOXO1-USP7 interaction. However, analysis of the subcellular localisation of both FOXO1 and USP7 proteins revealed their expression in both the cytoplasmic and

nuclear fractions. To determine where this interaction occurs, and considering that USP7 modulation of FOXO1 activity may be nuclear-independent (477), co-IP of FOXO1 from the nuclear and cytoplasmic fractions should be examined for FOXO1-USP7 interactions. Furthermore, immunofluorescence studies of FOXO1 subcellular localisation upon USP7 KD or overexpression could validate our cellular fractionation data and confirm whether USP7 modulates FOXO1 subcellular localisation via deubiquitination. To examine the type of ubiquitination targeted by USP7 and validate our suggestion that USP7 interacts with FOXO1 to mediate FOXO1 inactivation, deubiquitination assays following Van der Horst, de Vries-Smits (360) protocol could be performed.

Knocking down USP9x in MEC1 cells increased FOXO1 DNA binding and transcriptional activities. However, FOXO1 co-IP demonstrated no interaction between FOXO1 and USP9x. Additionally, USP9x KD and inhibition with WP1130 had no significant impact on FOXO1 expression or subcellular localisation. Therefore, we propose immunofluorescence studies of FOXO1 subcellular localisation upon USP9x KD or overexpression could further validate our cellular fractionation data and confirm whether USP9x modulates FOXO1 subcellular localisation via deubiquitination.

Our proteome analysis of FOXO1 interactors identified TRIM21 as a novel interactor of FOXO1. TRIM21 KD in MEC1 cells suggested a role for TRIM21 in regulating FOXO1 expression, subcellular localisation, and DNA binding activity. Investigation of the effect of TRIM21 overexpression on FOXO1 activity could further validate the effects of TRIM21 KD. Additionally, examining the transcriptional levels of FOXO1 target genes upon TRIM21 KD and overexpression could provide insights into the role of TRIM21 in FOXO1 transcriptional activity. Furthermore, the type of ubiquitination mediated by TRIM21 on FOXO1 was not investigated. While we strongly suspect it to be monoubiquitination (360), as TRIM21 KD depleted the FOXO1 nuclear fraction, other ubiquitination linkages could also alter FOXO1 activity, such as K63-linked ubiquitination, which has been reported to inhibit the activity of PTEN (635).

Collectively, our data highlighted the role of BCR activity in regulating CLL cell survival and evading apoptosis through signalling transduction activation of the PI3K/AKT pathway, which mediated FOXO1 inactivation and nuclear exclusion. Additionally, we demonstrated a role for the UPS pathway in modulating the activity of FOXO1 via ubiquitination by TRIM21

and DUB proteins, particularly USP7 and USP9x. DUB inhibitors, particularly the USP7 inhibitor HBX19818, alone reduced CLL cell viability and upregulated CLL cell cycle accumulation at the G0/G1 phase. This effect was further enhanced by the combination of HBX19818 with ibrutinib. Although HBX19818 or USP7/USP9x KDs, alone upregulated FOXO1 transcriptional activity without impacting FOXO1 expression or localisation, the combination with ibrutinib enhanced modulation of FOXO1, resulting in stronger activation, as indicated by increased nuclear accumulation and upregulation of FOXO1 DNA binding activity. To conclude, we consider that unleashing FOXO1 anti-tumour activity by simultaneously inhibiting BCR-mediated phosphorylation and USP7 deubiquitination of FOXO1 may present an alternative therapeutic strategy for CLL patients, independent of their prognosis.

Appendix

Protein	Accession	IgG	151_US	151_FAB	173_US	173_FAB	196_US	196_FAB
MYH9	P35579-1	241.2	130	129.7	71.7	84.3	53.7	36.7
PHB1	P35232	60.2	48.1	98.7	49.7	130.1	98.9	135.4
HSPA9	P38646	45.6	84.8	90.7	121.5	99	134.1	126.3
RPS3	P23396-1	42.3	91.6	102.4	119.6	79.1	141.9	96.3
IGHM	P01871	350.3	157.3	117.1	43.5	57.1	30.8	84.5
YWHAG	P61981	39.6	50.7	93.2	78.1	143	104.3	236.6
YWHAZ	P63104-1	31.6	44.2	88.3	77.5	155.1	106.6	243.6
RPS18	P62269	43.2	85.5	76.2	100	103.7	153.9	112.4
RPS19	P39019	50.5	83.4	91.7	101	100.1	140.4	90.7
HSPA5	P11021	106.7	117.5	112.8	71.4	86.5	118.4	97.9
ATP5F1A	P25705-1	64.4	89.8	121.9	97.1	90.3	144.8	104
MX2	P20592	87.4	65.3	66.2	125.1	155.7	50.4	41.3
PPP1R12A	O14974-4	180.9	93.6	72.8	131.7	128	32.2	24.2
NCL	P19338	105.7	95.8	97.9	111	105.8	87.2	70.3
HADHA	P40939	56.8	87.4	63.6	110.9	154.9	140.8	93.2
VIM	P08670	67.4	49.8	48.9	213	131	46.7	39.4
HSPA8	P11142-1	39.7	72.4	87.3	124.2	109.8	147.7	130
IGHD	P01880	507.4	214.9	196.5	11.6	13.1	19.4	18.2
TPM3	P06753-2	160.7	99.9	111.8	82.4	93.1	97.5	50.1
MYL6	P60660	132.1	87.6	140.3	96.9	82.7	90	47.3
NONO	Q15233	37.5	54.6	76.5	140	94.7	123.8	75.1
SFPQ	P23246-1	41.2	55.8	75.5	157.4	99.3	125.5	78.1
MYO18A	Q92614-1	244.2	132.9	100.6	86.1	102.4	34.5	31.2
RPS23	P62266	40.3	125.1	124.7	62.5	66	139.3	120.4
RPS4X	P62701	38	110.2	100.3	67.1	96.5	148.2	125.5
RPS5	P46782	40.3	127	54.2	149	100	68.8	113.2
RPL13	P26373-1	96.7	121.2	119.9	77.1	73.2	143.5	97.3
ARPC4	P59998	154.8	119.7	118.5	86.1	85.4	97.3	41.1
SLC25A6	P12236	93	95.9	194.1	39.2	58.4	154.3	85.6
ACTN1	P12814-1	138.8	97.7	87.8	143.2	116	39.8	31.8
CaM	P62158	146.8	85.5	103.2	122.8	106.9	53.5	34.2
EFHD2	Q96C19	247.1	146.3	91.5	96.6	88.6	18.1	15.5
HSPA1B	P0DMV8	85.3	85.6	83.3	122.3	106.1	101.8	97.9
H1-10	Q92522	113.3	88.3	81.7	124.3	124.6	91.2	66.7
IGHG1	P01857	29.8	88.5	52.1	92.9	114.4	162.4	92.4
IGKC	P01834	366.7	161.4	118.1	32	67.2	25.3	94
IGKV4-1	P06312	379.2	235	122.2	21.9	29.1	62.4	29.1
LETMD1	Q6P1Q0	20.5	99.4	117.2	70.8	89.7	216.6	137.1
MYL12A	O14950	139.8	96.2	105.6	66.8	68.4	73.5	66.6
IL16	Q14005-1	135.5	110.3	82.1	111.3	89.3	77.6	64
SELENOH	Q8IZQ5	92.1	104.6	85.8	110.3	107.3	75.1	56.5
TPM4	P67936	163.1	101.7	96.2	91.9	93.8	93.9	51.7
MRPL14	Q6P1L8	48.8	75.6	124.1	74.9	108.7	152.3	100.1

RPS10	P46783	47.8	61.9	78.8	121.9	111.7	137.7	91.8
RPS11	P62280	56.6	75.6	71.2	107.4	111.8	136.7	73.1
RPS14	P62263	51.5	85.2	87.4	114.6	117.6	160.4	103.2
RPS16	P62249	62.3	64.4	109.9	84.1	119.4	154.5	99.9
RPS3A	P61247	65	96.7	79.2	114.7	132.3	121.7	88.1
RPL22	P35268	91.1	103.4	56.7	97.7	203.4	122.7	70.7
RPL27A	P46776	38.4	126.8	131.9	54.6	61.8	133.9	116
RPL28	P46779	110.7	105.9	92.9	114.9	90.3	100.7	70.1
ARPC2	O15144	159	108.8	119.2	61.7	75.8	101.7	44.8
ATP5F1B	P06576	36.4	65.5	129.6	95.5	98.4	136.7	150.4
ATP5F1C	P36542-1	34.9	102.9	113.5	86.4	77.3	150.3	123.2
TRIM21	P19474	49.1	47.6	103	82.3	113.4	134.3	106.6
FOXO1	Q12778	3	73.8	74.4	114.5	92.5	185.6	197.1
HSPB1	P04792	119.4	105.2	123.4	90.1	66	96.6	77.2
HMGA1	P17096-1	28.8	56.7	41.7	141.5	166.5	146.7	79.1
H2AZ2	Q71UI9-1	50.4	71.7	88.9	95	150.2	145.4	89.5
LPXN	O60711-1	44.8	97.1	133.4	96.2	78.1	160.2	119.6
PRDX4	Q13162	89.2	111.1	129.3	74.8	84.8	106.1	106
PHB2	Q99623	62	60.5	100.7	53.7	122	116	119.3
GOLM2	Q6P4E1	217.1	132.9	129.4	27.8	73.3	16.3	168.6
SCCPDH	Q8NBX0	158.1	153.6	72.5	62	90.8	109.2	116.7
PPP1CB	P62140	135.5	84.4	110.8	103	113.5	30.2	31.5
SPTAN1	Q13813	220.7	149.2	140.8	52.9	50	42.9	96.6
MYO1C	O00159-1	184.1	95.6	99.7	100.6	114.9	64.8	40.8
MYO5A	Q9Y4I1-1	192.8	112.4	121.2	102.2	91.3	49.6	33.3
HACD3	Q9P035	356.7	135.1	121.9	29.9	80.5	34.8	79.9
ZYX	Q15942	50.6	95.4	95.5	114.1	80	129.1	110.5

Table S5. 1: FOXO1 interactive proteins in primary CLL samples.

Proteomics data were analysed using the PEDRo method for FOXO1 co-immunoprecipitation (co-IP) to identify proteins interacting with FOXO1 in three different CLL patients (646). The CLL patient samples (CLL151, CLL173 and CLL196) were cultured overnight on RPMI complete media, then stimulated with $F(ab')_2$ fragments (10 ng/mL) for 0.5 hr or unstimulated. FOXO1 co-IP were performed to isolate FOXO1 protein including IgG control. The samples were processed by Nanoflow HPLC Electrospray Tandem MS (nLC-ESI-MS/MS) with a Tandem Mass Tag (TMT) system and 70 proteins were identified as interactor of FOXO1 co-IP. US; unstimulated/control, Fab; $F(ab)'_2$ stimulated samples.

Bibliography

1. Chiorazzi N, Rai KR, Ferrarini M. Chronic lymphocytic leukemia. New England Journal of Medicine. 2005;352(8):804-15.
2. Kipps TJ, Stevenson FK, Wu CJ, Croce CM, Packham G, Wierda WG, et al. Chronic lymphocytic leukaemia. Nature reviews Disease primers. 2017;3(1):1-22.
3. Darwiche W, Gubler B, Marolleau J-P, Ghamlouch H. Chronic lymphocytic leukemia B-cell normal cellular counterpart: clues from a functional perspective. Frontiers in immunology. 2018;9:683.
4. Ten Hacken E, Burger JA. Microenvironment interactions and B-cell receptor signaling in Chronic Lymphocytic Leukemia: Implications for disease pathogenesis and treatment. Biochimica et Biophysica Acta (BBA)-Molecular Cell Research. 2016;1863(3):401-13.
5. Kikushige Y, Ishikawa F, Miyamoto T, Shima T, Urata S, Yoshimoto G, et al. Self-renewing hematopoietic stem cell is the primary target in pathogenesis of human chronic lymphocytic leukemia. Cancer cell. 2011;20(2):246-59.
6. Landau DA, Tausch E, Taylor-Weiner AN, Stewart C, Reiter JG, Bahlo J, et al. Mutations driving CLL and their evolution in progression and relapse. Nature. 2015;526(7574):525-30.
7. Jacque N, Leblond V. Chronic lymphocytic leukemia. Presse Medicale (Paris, France: 1983). 2019;48(7-8 Pt 1):807-15.
8. Puiggros A, Blanco G, Espinet B. Genetic abnormalities in chronic lymphocytic leukemia: where we are and where we go. BioMed research international. 2014;2014.
9. Zhang S, Kipps TJ. The pathogenesis of chronic lymphocytic leukemia. Annual Review of Pathology: Mechanisms of Disease. 2014;9:103-18.
10. Chiorazzi N. Cell proliferation and death: forgotten features of chronic lymphocytic leukemia B cells. Best practice & research Clinical haematology. 2007;20(3):399-413.
11. Damle RN, Ghiotto F, Valetto A, Albesiano E, Fais F, Yan X-J, et al. B-cell chronic lymphocytic leukemia cells express a surface membrane phenotype of activated, antigen-experienced B lymphocytes: Presented in part at the 42nd Annual Meeting of the American Society of Hematology, December 1-5, 2000, San Francisco, CA. Blood, The Journal of the American Society of Hematology. 2002;99(11):4087-93.
12. Rai KR, Sawitsky A, Cronkite EP, Chanana AD, Levy RN, Pasternack BS. Clinical staging of chronic lymphocytic leukemia. 1975.
13. Binet J, Auquier A, Dighiero G, Chastang C, Piguet H, Goasguen J, et al. A new prognostic classification of chronic lymphocytic leukemia derived from a multivariate survival analysis. Cancer. 1981;48(1):198-206.
14. Hallek M, Wanders L, Ostwald M, Busch R, Senekowitsch R, Stern S, et al. Serum β2-microglobulin and serum thymidine kinase are independent predictors of progression-free survival in chronic lymphocytic leukemia and immunocytoma. Leukemia & lymphoma. 1996;22(5-6):439-47.
15. Sarfati M, Chevret S, Chastang C, Biron G, Stryckmans P, Delespesse G, et al. Prognostic importance of serum soluble CD23 level in chronic lymphocytic leukemia. 1996.
16. Damle RN, Wasil T, Fais F, Ghiotto F, Valetto A, Allen SL, et al. Ig V Gene Mutation Status and CD38 Expression As Novel Prognostic Indicators in Chronic Lymphocytic Leukemia: Presented in part at the 40th Annual Meeting of The American Society of Hematology, held in Miami Beach, FL, December 4-8, 1998. Blood, The Journal of the American Society of Hematology. 1999;94(6):1840-7.
17. Döhner H, Stilgenbauer S, Benner A, Leupolt E, Kröber A, Bullinger L, et al. Genomic aberrations and survival in chronic lymphocytic leukemia. New England Journal of Medicine. 2000;343(26):1910-6.
18. Wiestner A, Rosenwald A, Barry TS, Wright G, Davis RE, Henrickson SE, et al. ZAP-70 expression identifies a chronic lymphocytic leukemia subtype with unmutated immunoglobulin genes, inferior clinical outcome, and distinct gene expression profile. Blood. 2003;101(12):4944-51.

19. Kröber A, Seiler T, Benner A, Bullinger L, Brückle E, Lichter P, et al. VH mutation status, CD38 expression level, genomic aberrations, and survival in chronic lymphocytic leukemia. Blood, The Journal of the American Society of Hematology. 2002;100(4):1410-6.
20. Ondrisova L, Mraz M. Genetic and non-genetic mechanisms of resistance to BCR signaling inhibitors in B cell malignancies. Frontiers in oncology. 2020;10:591577.
21. Rossi D, Spina V, Gaidano G. Biology and treatment of Richter syndrome. Blood, The Journal of the American Society of Hematology. 2018;131(25):2761-72.
22. Cancer Research UK. Chronic lymphocytic leukaemia (CLL) incidence statistics 2024 [Available from: https://www.cancerresearchuk.org/health-professional/cancer-statistics/statistics-by-cancer-type/leukaemia-cll/incidence#heading-Zero.
23. Leukaemia UK. Chronic lymphocytic leukaemia 2024 [Available from: https://www.leukaemiauk.org.uk/about-leukaemia/types-of-leukaemia/chronic-lymphocytic-leukaemia-cll/.
24. Cronin KA, Ries LA, Edwards BK. The surveillance, epidemiology, and end results (SEER) program of the National Cancer Institute. Cancer. 2014;120:3755-7.
25. Catovsky D, Wade R, Else M. The clinical significance of patients' sex in chronic lymphocytic leukemia. Haematologica. 2014;99(6):1088.
26. Seftel M, Demers A, Banerji V, Gibson S, Morales C, Musto G, et al. High incidence of chronic lymphocytic leukemia (CLL) diagnosed by immunophenotyping: a population-based Canadian cohort. Leukemia research. 2009;33(11):1463-8.
27. Pfeil AM, Imfeld P, Pettengell R, Jick SS, Szucs TD, Meier CR, et al. Trends in incidence and medical resource utilisation in patients with chronic lymphocytic leukaemia: insights from the UK Clinical Practice Research Datalink (CPRD). Annals of hematology. 2015;94:421-9.
28. Cancer Research UK. Chronic lymphocytic leukaemia (CLL) mortality statistics 2024 [Available from: https://www.cancerresearchuk.org/health-professional/cancer-statistics/statistics-by-cancer-type/leukaemia-cll/mortality.
29. Brown JR, Eichhorst B, Hillmen P, Jurczak W, Kaźmierczak M, Lamanna N, et al. Zanubrutinib or ibrutinib in relapsed or refractory chronic lymphocytic leukemia. New England Journal of Medicine. 2023;388(4):319-32.
30. Cerhan JR, Slager SL. Familial predisposition and genetic risk factors for lymphoma. Blood, The Journal of the American Society of Hematology. 2015;126(20):2265-73.
31. Lichtenstein P, Holm NV, Verkasalo PK, Iliadou A, Kaprio J, Koskenvuo M, et al. Environmental and heritable factors in the causation of cancer—analyses of cohorts of twins from Sweden, Denmark, and Finland. New England journal of medicine. 2000;343(2):78-85.
32. Li Y, Wang Y, Wang Z, Yi D, Ma S. Racial differences in three major NHL subtypes: descriptive epidemiology. Cancer epidemiology. 2015;39(1):8-13.
33. Tejaswi V, Lad DP, Jindal N, Prakash G, Malhotra P, Khadwal A, et al. Chronic lymphocytic leukemia: real-world data from India. JCO Global Oncology. 2020;6:866-72.
34. Baumann Kreuziger LM, Tarchand G, Morrison VA. The impact of Agent Orange exposure on presentation and prognosis of patients with chronic lymphocytic leukemia. Leukemia & lymphoma. 2014;55(1):63-6.
35. Hsu W-L, Preston DL, Soda M, Sugiyama H, Funamoto S, Kodama K, et al. The incidence of leukemia, lymphoma and multiple myeloma among atomic bomb survivors: 1950–2001. Radiation research. 2013;179(3):361-82.
36. Navarrete-Meneses M, Salas-Labadía C, Sanabrais-Jiménez M, Santana-Hernández J, Serrano-Cuevas A, Juárez-Velázquez R, et al. Exposure to the insecticides permethrin and malathion induces leukemia and lymphoma-associated gene aberrations in vitro. Toxicology in Vitro. 2017;44:17-26.
37. Hallek M, Cheson BD, Catovsky D, Caligaris-Cappio F, Dighiero G, Döhner H, et al. iwCLL guidelines for diagnosis, indications for treatment, response assessment, and supportive management of CLL. Blood, The Journal of the American Society of Hematology. 2018;131(25):2745-60.
38. Hallek M. Chronic lymphocytic leukemia: 2020 update on diagnosis, risk stratification and treatment. American journal of hematology. 2019;94(11):1266-87.

39. International CLL-IPI Working Group. An international prognostic index for patients with chronic lymphocytic leukaemia (CLL-IPI): a meta-analysis of individual patient data. The Lancet Oncology. 2016;17(6):779-90.
40. Rawstron AC, Kreuzer KA, Soosapilla A, Spacek M, Stehlikova O, Gambell P, et al. Reproducible diagnosis of chronic lymphocytic leukemia by flow cytometry: An European Research Initiative on CLL (ERIC) & European Society for Clinical Cell Analysis (ESCCA) Harmonisation project. Cytometry Part B: Clinical Cytometry. 2018;94(1):121-8.
41. American Cancer Society. How Is Chronic Lymphocytic Leukemia Staged? 2024 [Available from: https://www.cancer.org/cancer/types/chronic-lymphocytic-leukemia/detection-diagnosis-staging/staging.html.
42. Dighiero G, Maloum K, Desablens B, Cazin B, Navarro M, Leblay R, et al. Chlorambucil in indolent chronic lymphocytic leukemia. New England Journal of Medicine. 1998;338(21):1506-14.
43. Shustik C, Mick R, Silver R, Sawitsky A, Rai K, Shapiro L. Treatment of early chronic lymphocytic leukemia: intermittent chlorambucil versus observation. Hematological oncology. 1988;6(1):7-12.
44. CollaborativeGroup CT. Chemotherapeutic options in chronic lymphocytic leukemia: a meta-analysis of the randomized trials. Journal of the National Cancer Institute. 1999;91(10):861-8.
45. Hallek M, Cheson BD, Catovsky D, Caligaris-Cappio F, Dighiero G, Döhner H, et al. Guidelines for the diagnosis and treatment of chronic lymphocytic leukemia: a report from the International Workshop on Chronic Lymphocytic Leukemia updating the National Cancer Institute–Working Group 1996 guidelines. Blood, The Journal of the American Society of Hematology. 2008;111(12):5446-56.
46. Delgado J, Doubek M, Baumann T, Kotaskova J, Molica S, Mozas P, et al. Chronic lymphocytic leukemia: a prognostic model comprising only two biomarkers (IGHV mutational status and FISH cytogenetics) separates patients with different outcome and simplifies the CLL-IPI. American journal of hematology. 2017;92(4):375-80.
47. Gentile M, Shanafelt TD, Rossi D, Laurenti L, Mauro FR, Molica S, et al. Validation of the CLL-IPI and comparison with the MDACC prognostic index in newly diagnosed patients. Blood, The Journal of the American Society of Hematology. 2016;128(16):2093-5.
48. da Cunha-Bang C, Christiansen I, Niemann CU. The CLL-IPI applied in a population-based cohort. Blood, The Journal of the American Society of Hematology. 2016;128(17):2181-3.
49. Gentile M, Shanafelt TD, Mauro FR, Laurenti L, Rossi D, Molica S, et al. Comparison between the CLL-IPI and the Barcelona-Brno prognostic model: analysis of 1299 newly diagnosed cases. Am J Hematol. 2018;93(2):E35-E7.
50. Alt FW, Blackwell TK, Depinho RA, Reth MG, Yancopoulos GD. Regulation of genome rearrangement events during lymphocyte differentiation. Immunological reviews. 1986;89:5-30.
51. Ten Hacken E, Gounari M, Ghia P, Burger JA. The importance of B cell receptor isotypes and stereotypes in chronic lymphocytic leukemia. Leukemia. 2019;33(2):287-98.
52. Stevenson FK, Krysov S, Davies AJ, Steele AJ, Packham G. B-cell receptor signaling in chronic lymphocytic leukemia. Blood, The Journal of the American Society of Hematology. 2011;118(16):4313-20.
53. Hamblin TJ, Davis Z, Gardiner A, Oscier DG, Stevenson FK. Unmutated Ig VH genes are associated with a more aggressive form of chronic lymphocytic leukemia. Blood, The Journal of the American Society of Hematology. 1999;94(6):1848-54.
54. Morilla A, Gonzalez de Castro D, Del Giudice I, Osuji N, Else M, Morilla R, et al. Combinations of ZAP-70, CD38 and IGHV mutational status as predictors of time to first treatment in CLL. Leukemia & lymphoma. 2008;49(11):2108-15.
55. Ian Mockridge C, Potter KN, Wheatley I, Neville LA, Packham G, Stevenson FK. Reversible anergy of sIgM-mediated signaling in the two subsets of CLL defined by VH-gene mutational status. Blood. 2007;109(10):4424-31.
56. Jaramillo S, Agathangelidis A, Schneider C, Bahlo J, Robrecht S, Tausch E, et al. Prognostic impact of prevalent chronic lymphocytic leukemia stereotyped subsets: analysis within prospective clinical trials of the German CLL Study Group. Haematologica. 2020;105(11):2598.

57. Stamatopoulos K, Agathangelidis A, Rosenquist R, Ghia P. Antigen receptor stereotypy in chronic lymphocytic leukemia. Leukemia. 2017;31(2):282-91.
58. Agathangelidis A, Darzentas N, Hadzidimitriou A, Brochet X, Murray F, Yan X-J, et al. Stereotyped B-cell receptors in one-third of chronic lymphocytic leukemia: a molecular classification with implications for targeted therapies. Blood, The Journal of the American Society of Hematology. 2012;119(19):4467-75.
59. Agathangelidis A, Hadzidimitriou A, Minga E, Sutton L-A, Polychronidou E, Shanafelt TD, et al. Reappraising immunoglobulin repertoire restrictions in chronic lymphocytic leukemia: focus on major stereotyped subsets and closely related satellites. Blood. 2016;128(22):4376.
60. Stamatopoulos K, Belessi C, Moreno C, Boudjograh M, Guida G, Smilevska T, et al. Over 20% of patients with chronic lymphocytic leukemia carry stereotyped receptors: pathogenetic implications and clinical correlations. Blood. 2007;109(1):259-70.
61. Messmer BT, Albesiano E, Efremov DG, Ghiotto F, Allen SL, Kolitz J, et al. Multiple distinct sets of stereotyped antigen receptors indicate a role for antigen in promoting chronic lymphocytic leukemia. The Journal of experimental medicine. 2004;200(4):519-25.
62. Gounari M, Ntoufa S, Apollonio B, Papakonstantinou N, Ponzoni M, Chu CC, et al. Excessive antigen reactivity may underlie the clinical aggressiveness of chronic lymphocytic leukemia stereotyped subset# 8. Blood, The Journal of the American Society of Hematology. 2015;125(23):3580-7.
63. Del Giudice I, Chiaretti S, Santangelo S, Tavolaro S, Peragine N, Marinelli M, et al. Stereotyped subset# 1 chronic lymphocytic leukemia: a direct link between B-cell receptor structure, function, and patients' prognosis. American journal of hematology. 2014;89(1):74-82.
64. Baliakas P, Hadzidimitriou A, Sutton L-A, Minga E, Agathangelidis A, Nichelatti M, et al. Clinical effect of stereotyped B-cell receptor immunoglobulins in chronic lymphocytic leukaemia: a retrospective multicentre study. The lancet haematology. 2014;1(2):e74-e84.
65. Sutton L-A, Young E, Baliakas P, Hadzidimitriou A, Moysiadis T, Plevova K, et al. Different spectra of recurrent gene mutations in subsets of chronic lymphocytic leukemia harboring stereotyped B-cell receptors. haematologica. 2016;101(8):959.
66. Malek S. The biology and clinical significance of acquired genomic copy number aberrations and recurrent gene mutations in chronic lymphocytic leukemia. Oncogene. 2013;32(23):2805-17.
67. Puiggros A, Delgado J, Rodriguez-Vicente A, Collado R, Aventín A, Luño E, et al. Biallelic losses of 13q do not confer a poorer outcome in chronic lymphocytic leukaemia: analysis of 627 patients with isolated 13q deletion. British journal of haematology. 2013;163(1):47-54.
68. Calin GA, Dumitru CD, Shimizu M, Bichi R, Zupo S, Noch E, et al. Frequent deletions and down-regulation of micro-RNA genes miR15 and miR16 at 13q14 in chronic lymphocytic leukemia. Proceedings of the national academy of sciences. 2002;99(24):15524-9.
69. Abruzzo LV, Herling CD, Calin GA, Oakes C, Barron LL, Banks HE, et al. Trisomy 12 chronic lymphocytic leukemia expresses a unique set of activated and targetable pathways. Haematologica. 2018;103(12):2069.
70. Balatti V, Lerner S, Rizzotto L, Rassenti L, Bottoni A, Palamarchuk A, et al. Trisomy 12 CLLs progress through NOTCH1 mutations. Leukemia. 2013;27(3):740-3.
71. Sellmann L, Gesk S, Walter C, Ritgen M, Harder L, Martín-Subero JI, et al. Trisomy 19 is associated with trisomy 12 and mutated IGHV genes in B-chronic lymphocytic leukaemia. British journal of haematology. 2007;138(2):217-20.
72. Jiang Y, Chen H, Su X, Thompson P, Liu X, Do K, et al. ATM function and its relationship with ATM gene mutations in chronic lymphocytic leukemia with the recurrent deletion (11q22. 3-23.2). Blood cancer journal. 2016;6(9):e465-e.
73. Marasca R, Maffei R, Martinelli S, Fiorcari S, Bulgarelli J, Debbia G, et al. Clinical heterogeneity of de novo 11q deletion chronic lymphocytic leukaemia: prognostic relevance of extent of 11q deleted nuclei inside leukemic clone. Hematological Oncology. 2013;31(2):88-95.
74. Skowronska A, Parker A, Ahmed G, Oldreive C, Davis Z, Richards S, et al. Biallelic ATM inactivation significantly reduces survival in patients treated on the United Kingdom Leukemia Research Fund Chronic Lymphocytic Leukemia 4 trial. Journal of Clinical Oncology. 2012;30(36):4524-32.

75. Wattel E, Preudhomme C, Hecquet B, Vanrumbeke M, Quesnel B, Dervite I, et al. p53 mutations are associated with resistance to chemotherapy and short survival in hematologic malignancies. 1994.
76. Guarini A, Peragine N, Messina M, Marinelli M, Ilari C, Cafforio L, et al. Unravelling the suboptimal response of TP 53-mutated chronic lymphocytic leukaemia to ibrutinib. British Journal of Haematology. 2019;184(3):392-6.
77. Brown J, Hillmen P, O'brien S, Barrientos J, Reddy N, Coutre S, et al. Extended follow-up and impact of high-risk prognostic factors from the phase 3 RESONATE study in patients with previously treated CLL/SLL. Leukemia. 2018;32(1):83-91.
78. Stilgenbauer S, Zenz T, Winkler D, Buehler A, Schlenk RF, Groner S, et al. Subcutaneous alemtuzumab in fludarabine-refractory chronic lymphocytic leukemia: clinical results and prognostic marker analyses from the CLL2H study of the German Chronic Lymphocytic Leukemia Study Group. Journal of Clinical Oncology. 2009;27(24):3994-4001.
79. Rossi D, Rasi S, Spina V, Bruscaggin A, Monti S, Ciardullo C, et al. Integrated mutational and cytogenetic analysis identifies new prognostic subgroups in chronic lymphocytic leukemia. Blood, The Journal of the American Society of Hematology. 2013;121(8):1403-12.
80. Hallek M, Fischer K, Fingerle-Rowson G, Fink AM, Busch R, Mayer J, et al. Addition of rituximab to fludarabine and cyclophosphamide in patients with chronic lymphocytic leukaemia: a randomised, open-label, phase 3 trial. The Lancet. 2010;376(9747):1164-74.
81. Rossi D, Khiabanian H, Spina V, Ciardullo C, Bruscaggin A, Famà R, et al. Clinical impact of small TP53 mutated subclones in chronic lymphocytic leukemia. Blood, The Journal of the American Society of Hematology. 2014;123(14):2139-47.
82. Asslaber D, Piñón JD, Seyfried I, Desch P, Stöcher M, Tinhofer I, et al. microRNA-34a expression correlates with MDM2 SNP309 polymorphism and treatment-free survival in chronic lymphocytic leukemia. Blood, The Journal of the American Society of Hematology. 2010;115(21):4191-7.
83. Rassenti LZ, Jain S, Keating MJ, Wierda WG, Grever MR, Byrd JC, et al. Relative value of ZAP-70, CD38, and immunoglobulin mutation status in predicting aggressive disease in chronic lymphocytic leukemia. Blood, The Journal of the American Society of Hematology. 2008;112(5):1923-30.
84. Kröber A, Bloehdorn J, Hafner S, Bühler A, Seiler T, Kienle D, et al. Additional genetic high-risk features such as 11q deletion, 17p deletion, and V3-21 usage characterize discordance of ZAP-70 and VH mutation status in chronic lymphocytic leukemia. Journal of Clinical Oncology. 2006;24(6):969-75.
85. Quijano S, López A, Rasillo A, Sayagués JM, Barrena S, Sánchez ML, et al. Impact of trisomy 12, del (13q), del (17p), and del (11q) on the immunophenotype, DNA ploidy status, and proliferative rate of leukemic B-cells in chronic lymphocytic leukemia. Cytometry Part B: Clinical Cytometry: The Journal of the International Society for Analytical Cytology. 2008;74(3):139-49.
86. Baliakas P, Jeromin S, Iskas M, Puiggros A, Plevova K, Nguyen-Khac F, et al. Cytogenetic complexity in chronic lymphocytic leukemia: definitions, associations, and clinical impact. Blood, The Journal of the American Society of Hematology. 2019;133(11):1205-16.
87. Knisbacher BA, Lin Z, Hahn CK, Nadeu F, Duran-Ferrer M, Stevenson KE, et al. Molecular map of chronic lymphocytic leukemia and its impact on outcome. Nature genetics. 2022;54(11):1664-74.
88. Landau DA, Carter SL, Stojanov P, McKenna A, Stevenson K, Lawrence MS, et al. Evolution and impact of subclonal mutations in chronic lymphocytic leukemia. Cell. 2013;152(4):714-26.
89. Landau DA, Sun C, Rosebrock D, Herman SE, Fein J, Sivina M, et al. The evolutionary landscape of chronic lymphocytic leukemia treated with ibrutinib targeted therapy. Nature communications. 2017;8(1):2185.
90. Murali I, Kasar S, Naeem A, Tyekucheva S, Khalsa JK, Thrash EM, et al. Activation of the MAPK pathway mediates resistance to PI3K inhibitors in chronic lymphocytic leukemia. Blood, The Journal of the American Society of Hematology. 2021;138(1):44-56.
91. Elich M, Sauer K. Regulation of hematopoietic cell development and function through phosphoinositides. Frontiers in immunology. 2018;9:931.

92. Rossi D, Rasi S, Fabbri G, Spina V, Fangazio M, Forconi F, et al. Mutations of NOTCH1 are an independent predictor of survival in chronic lymphocytic leukemia. Blood, The Journal of the American Society of Hematology. 2012;119(2):521-9.
93. Arruga F, Gizdic B, Serra S, Vaisitti T, Ciardullo C, Coscia M, et al. Functional impact of NOTCH1 mutations in chronic lymphocytic leukemia. Leukemia. 2014;28(5):1060-70.
94. Hajdu M, Sebestyén A, Barna G, Reiniger L, Jánosi J, Sréter L, et al. Activity of the notch-signalling pathway in circulating human chronic lymphocytic leukaemia cells. Scandinavian journal of immunology. 2007;65(3):271-5.
95. Woods DB, Vousden KH. Regulation of p53 function. Experimental cell research. 2001;264(1):56-66.
96. El-Deiry WS, editor Regulation ofp53downstream genes. Seminars in cancer biology; 1998: Elsevier.
97. Lane DP. p53, guardian of the genome. Nature. 1992;358(6381).
98. Hollstein M, Rice K, Greenblatt M, Soussi T, Fuchs R, Sørlie T, et al. Database of p53 gene somatic mutations in human tumors and cell lines. Nucleic acids research. 1994;22(17):3551.
99. Muller PA, Vousden KH. p53 mutations in cancer. Nature cell biology. 2013;15(1):2-8.
100. Pettitt AR, Sherrington PD, Stewart G, Cawley JC, Taylor AMR, Stankovic T. p53 dysfunction in B-cell chronic lymphocytic leukemia: inactivation of ATM as an alternative to TP53 mutation. Blood, The Journal of the American Society of Hematology. 2001;98(3):814-22.
101. Starostik P, Manshouri T, O'Brien S, Freireich E, Kantarjian H, Haidar M, et al. Deficiency of the ATM protein expression defines an aggressive subgroup of B-cell chronic lymphocytic leukemia. Cancer research. 1998;58(20):4552-7.
102. Taylor A. What has the cloning of the ATM gene told us about ataxia telangiectasia? International journal of radiation biology. 1998;73(4):365-71.
103. Bai L, Zhu W-G. p53: structure, function and therapeutic applications. J Cancer Mol. 2006;2(4):141-53.
104. Nadeu F, Delgado J, Royo C, Baumann T, Stankovic T, Pinyol M, et al. Clinical impact of clonal and subclonal TP53, SF3B1, BIRC3, NOTCH1, and ATM mutations in chronic lymphocytic leukemia. Blood, The Journal of the American Society of Hematology. 2016;127(17):2122-30.
105. Guièze R, Robbe P, Clifford R, De Guibert S, Pereira B, Timbs A, et al. Presence of multiple recurrent mutations confers poor trial outcome of relapsed/refractory CLL. Blood, The Journal of the American Society of Hematology. 2015;126(18):2110-7.
106. Messina M, Del Giudice I, Khiabanian H, Rossi D, Chiaretti S, Rasi S, et al. Genetic lesions associated with chronic lymphocytic leukemia chemo-refractoriness. Blood, The Journal of the American Society of Hematology. 2014;123(15):2378-88.
107. Fischer K, Bahlo J, Fink AM, Goede V, Herling CD, Cramer P, et al. Long-term remissions after FCR chemoimmunotherapy in previously untreated patients with CLL: updated results of the CLL8 trial. Blood, The Journal of the American Society of Hematology. 2016;127(2):208-15.
108. Beà S, López-Guillermo A, Ribas M, Puig X, Pinyol M, Carrió A, et al. Genetic imbalances in progressed B-cell chronic lymphocytic leukemia and transformed large-cell lymphoma (Richter's syndrome). The American journal of pathology. 2002;161(3):957-68.
109. Orchard JA, Ibbotson RE, Davis Z, Wiestner A, Rosenwald A, Thomas PW, et al. ZAP-70 expression and prognosis in chronic lymphocytic leukaemia. The Lancet. 2004;363(9403):105-11.
110. Boonstra JG, van Lom K, Langerak AW, Graveland WJ, Valk PJ, Kraan J, et al. CD38 as a prognostic factor in B cell chronic lymphocytic leukaemia (B-CLL): Comparison of three approaches to analyze its expression. Cytometry Part B: Clinical Cytometry: The Journal of the International Society for Analytical Cytology. 2006;70(3):136-41.
111. Crespo M, Bosch F, Villamor N, Bellosillo B, Colomer D, Rozman M, et al. ZAP-70 expression as a surrogate for immunoglobulin-variable-region mutations in chronic lymphocytic leukemia. New England Journal of Medicine. 2003;348(18):1764-75.
112. Chen L, Apgar J, Huynh L, Dicker F, Giago-McGahan T, Rassenti L, et al. ZAP-70 directly enhances IgM signaling in chronic lymphocytic leukemia. Blood. 2005;105(5):2036-41.
113. Kong G-H, Bu J-Y, Kurosaki T, Shaw AS, Chant AC. Reconstitution of Syk function by the ZAP-70 protein tyrosine kinase. Immunity. 1995;2(5):485-92.

114. Dürig J, Nückel H, Cremer M, Führer A, Halfmeyer K, Fandrey J, et al. ZAP-70 expression is a prognostic factor in chronic lymphocytic leukemia. Leukemia. 2003;17(12):2426-34.
115. Deaglio S, Vaisitti T, Aydin S, Bergui L, D'Arena G, Bonello L, et al. CD38 and ZAP-70 are functionally linked and mark CLL cells with high migratory potential. Blood, The Journal of the American Society of Hematology. 2007;110(12):4012-21.
116. Deaglio S, Vaisitti T, Bergui L, Bonello L, Horenstein AL, Tamagnone L, et al. CD38 and CD100 lead a network of surface receptors relaying positive signals for B-CLL growth and survival. Blood. 2005;105(8):3042-50.
117. Tanaka Y, Albelda SM, Horgan KJ, Van Seventer GA, Shimizu Y, Newman W, et al. CD31 expressed on distinctive T cell subsets is a preferential amplifier of beta 1 integrin-mediated adhesion. The Journal of experimental medicine. 1992;176(1):245-53.
118. Hallek M, Langenmayer I, Nerl C, Knauf W, Dietzfelbinger H, Adorf D, et al. Elevated serum thymidine kinase levels identify a subgroup at high risk of disease progression in early, nonsmoldering chronic lymphocytic leukemia. Blood, The Journal of the American Society of Hematology. 1999;93(5):1732-7.
119. Wierda WG, O'Brien S, Wang X, Faderl S, Ferrajoli A, Do K-A, et al. Prognostic nomogram and index for overall survival in previously untreated patients with chronic lymphocytic leukemia. Blood, The Journal of the American Society of Hematology. 2007;109(11):4679-85.
120. Pflug N, Bahlo J, Shanafelt TD, Eichhorst BF, Bergmann MA, Elter T, et al. Development of a comprehensive prognostic index for patients with chronic lymphocytic leukemia. Blood, The Journal of the American Society of Hematology. 2014;124(1):49-62.
121. Thompson PA, O'Brien SM, Xiao L, Wang X, Burger JA, Jain N, et al. β2-microglobulin normalization within 6 months of ibrutinib-based treatment is associated with superior progression-free survival in patients with chronic lymphocytic leukemia. Cancer. 2016;122(4):565-73.
122. Herishanu Y, Pérez-Galán P, Liu D, Biancotto A, Pittaluga S, Vire B, et al. The lymph node microenvironment promotes B-cell receptor signaling, NF-κB activation, and tumor proliferation in chronic lymphocytic leukemia. Blood, The Journal of the American Society of Hematology. 2011;117(2):563-74.
123. Shadman M. Diagnosis and treatment of chronic lymphocytic leukemia: a review. Jama. 2023;329(11):918-32.
124. Liu W, Tolar P, Song W, Kim TJ. Bcr signaling and b cell activation. Frontiers Media SA; 2020. p. 45.
125. Lam K-P, Kühn R, Rajewsky K. In vivo ablation of surface immunoglobulin on mature B cells by inducible gene targeting results in rapid cell death. Cell. 1997;90(6):1073-83.
126. Kraus M, Alimzhanov MB, Rajewsky N, Rajewsky K. Survival of resting mature B lymphocytes depends on BCR signaling via the Igα/β heterodimer. Cell. 2004;117(6):787-800.
127. Minden MD-v, Übelhart R, Schneider D, Wossning T, Bach MP, Buchner M, et al. Chronic lymphocytic leukaemia is driven by antigen-independent cell-autonomous signalling. Nature. 2012;489(7415):309-12.
128. Pieper K, Grimbacher B, Eibel H. B-cell biology and development. Journal of Allergy and Clinical Immunology. 2013;131(4):959-71.
129. Ghia P, ten Boekel E, Sanz E, de la Hera A, Rolink A, Melchers F. Ordering of human bone marrow B lymphocyte precursors by single-cell polymerase chain reaction analyses of the rearrangement status of the immunoglobulin H and L chain gene loci. The Journal of experimental medicine. 1996;184(6):2217-30.
130. Xu JL, Davis MM. Diversity in the CDR3 region of VH is sufficient for most antibody specificities. Immunity. 2000;13(1):37-45.
131. Shapiro-Shelef M, Calame K. Regulation of plasma-cell development. Nature Reviews Immunology. 2005;5(3):230-42.
132. Oppezzo P, Dighiero G. Role of the B-cell receptor and the microenvironment in chronic lymphocytic leukemia'. Blood cancer journal. 2013;3(9):e149-e.
133. Ternynck Trs, Dighiero G, Follezou J, Binet J-L. Comparison of normal and CLL lymphocyte surface Ig determinants using peroxidase-labeled antibodies. I. Detection and quantitation of light chain determinants. Blood. 1974;43(6):789-95.

134. Woyach JA, Johnson AJ, Byrd JC. The B-cell receptor signaling pathway as a therapeutic target in CLL. Blood, The Journal of the American Society of Hematology. 2012;120(6):1175-84.
135. Friess MD, Pluhackova K, Böckmann RA. Structural model of the mIgM B-cell receptor transmembrane domain from self-association molecular dynamics simulations. Frontiers in immunology. 2018;9:2947.
136. Suljagic M, Laurenti L, Tarnani M, Alam M, Malek S, Efremov D. Reduced expression of the tumor suppressor PHLPP1 enhances the antiapoptotic B-cell receptor signal in chronic lymphocytic leukemia B-cells. Leukemia. 2010;24(12):2063-71.
137. Engels N, Wollscheid B, Wienands J. Association of SLP-65/BLNK with the B cell antigen receptor through a non-ITAM tyrosine of Ig-α. European journal of immunology. 2001;31(7):2126-34.
138. Kabak S, Skaggs BJ, Gold MR, Affolter M, West KL, Foster MS, et al. The direct recruitment of BLNK to immunoglobulin α couples the B-cell antigen receptor to distal signaling pathways. Molecular and cellular biology. 2002.
139. Alsadeq A, Hobeika E, Medgyesi D, Kläsener K, Reth M. The role of the Syk/Shp-1 kinase-phosphatase equilibrium in B cell development and signaling. The Journal of Immunology. 2014;193(1):268-76.
140. Tkachenko A, Kupcova K, Havranek O. B-cell receptor signaling and beyond: the role of Igα (CD79a)/Igβ (CD79b) in normal and malignant B cells. International Journal of Molecular Sciences. 2023;25(1):10.
141. Kalimuthu S, Se-Kwon K. Cell survival and apoptosis signaling as therapeutic target for cancer: marine bioactive compounds. International journal of molecular sciences. 2013;14(2):2334-54.
142. Manning BD, Toker A. AKT/PKB signaling: navigating the network. Cell. 2017;169(3):381-405.
143. Hoxhaj G, Manning BD. The PI3K–AKT network at the interface of oncogenic signalling and cancer metabolism. Nature Reviews Cancer. 2020;20(2):74-88.
144. Koehrer S, Burger JA. Chronic lymphocytic leukemia: Disease biology. Acta Haematol. 2024;147(1):8-21.
145. Iacovelli S, Hug E, Bennardo S, Duehren-von Minden M, Gobessi S, Rinaldi A, et al. Two types of BCR interactions are positively selected during leukemia development in the Eμ-TCL1 transgenic mouse model of CLL. Blood, The Journal of the American Society of Hematology. 2015;125(10):1578-88.
146. Chakraborty S, Martines C, Porro F, Fortunati I, Bonato A, Dimishkovska M, et al. B-cell receptor signaling and genetic lesions in TP53 and CDKN2A/CDKN2B cooperate in Richter transformation. Blood, The Journal of the American Society of Hematology. 2021;138(12):1053-66.
147. Seda V, Mraz M. B-cell receptor signalling and its crosstalk with other pathways in normal and malignant cells. European journal of haematology. 2015;94(3):193-205.
148. Binder M, Müller F, Frick M, Wehr C, Simon F, Leistler B, et al. CLL B-cell receptors can recognize themselves: alternative epitopes and structural clues for autostimulatory mechanisms in CLL. Blood, The Journal of the American Society of Hematology. 2013;121(1):239-41.
149. Ziegler CG, Kim J, Piersanti K, Oyler-Yaniv A, Argyropoulos KV, van den Brink MR, et al. Constitutive activation of the B cell receptor underlies dysfunctional signaling in chronic lymphocytic leukemia. Cell reports. 2019;28(4):923-37. e3.
150. Muzio M, Apollonio B, Scielzo C, Frenquelli M, Vandoni I, Boussiotis V, et al. Constitutive activation of distinct BCR-signaling pathways in a subset of CLL patients: a molecular signature of anergy. Blood, The Journal of the American Society of Hematology. 2008;112(1):188-95.
151. Contri A, Brunati AM, Trentin L, Cabrelle A, Miorin M, Cesaro L, et al. Chronic lymphocytic leukemia B cells contain anomalous Lyn tyrosine kinase, a putative contribution to defective apoptosis. The Journal of clinical investigation. 2005;115(2):369-78.
152. Gobessi S, Laurenti L, Longo P, Carsetti L, Berno V, Sica S, et al. Inhibition of constitutive and BCR-induced Syk activation downregulates Mcl-1 and induces apoptosis in chronic lymphocytic leukemia B cells. Leukemia. 2009;23(4):686-97.

153. Ringshausen I, Schneller F, Bogner C, Hipp S, Duyster J, Peschel C, et al. Constitutively activated phosphatidylinositol-3 kinase (PI-3K) is involved in the defect of apoptosis in B-CLL: association with protein kinase Cδ. Blood, The Journal of the American Society of Hematology. 2002;100(10):3741-8.
154. Muggen A, Pillai S, Kil L, Van Zelm M, Van Dongen J, Hendriks R, et al. Basal Ca2+ signaling is particularly increased in mutated chronic lymphocytic leukemia. Leukemia. 2015;29(2):321-8.
155. Schmid VK, Khadour A, Ahmed N, Brandl C, Nitschke L, Rajewsky K, et al. B cell antigen receptor expression and phosphatidylinositol 3-kinase signaling regulate genesis and maintenance of mouse chronic lymphocytic leukemia. Haematologica. 2022;107(8):1796-814.
156. Maity PC, Bilal M, Koning MT, Young M, van Bergen CA, Renna V, et al. IGLV3-21* 01 is an inherited risk factor for CLL through the acquisition of a single-point mutation enabling autonomous BCR signaling. Proceedings of the National Academy of Sciences. 2020;117(8):4320-7.
157. Mazzarello AN, Gentner-Göbel E, Dühren-von Minden M, Tarasenko TN, Nicolò A, Ferrer G, et al. B cell receptor isotypes differentially associate with cell signaling, kinetics, and outcome in chronic lymphocytic leukemia. The Journal of clinical investigation. 2022;132(2).
158. Chen J, Sathiaseelan V, Reddy Chilamakuri CS, Roamio Franklin VN, Jakwerth CA, D'Santos C, et al. ZAP-70 augments tonic B-cell receptor and CCR7 signaling in IGHV–unmutated chronic lymphocytic leukemia. Blood Advances. 2024;8(5):1167-78.
159. Packham G, Krysov S, Allen A, Savelyeva N, Steele AJ, Forconi F, et al. The outcome of B-cell receptor signaling in chronic lymphocytic leukemia: proliferation or anergy. haematologica. 2014;99(7):1138.
160. Sadras T, Martin M, Kume K, Robinson ME, Saravanakumar S, Lenz G, et al. Developmental partitioning of SYK and ZAP70 prevents autoimmunity and cancer. Molecular cell. 2021;81(10):2094-111. e9.
161. Schmid VK, Hobeika E. B cell receptor signaling and associated pathways in the pathogenesis of chronic lymphocytic leukemia. Frontiers in Oncology. 2024;14:1339620.
162. Hanahan D, Weinberg RA. The hallmarks of cancer. cell. 2000;100(1):57-70.
163. Fruman DA, Rommel C. PI3K and cancer: lessons, challenges and opportunities. Nature reviews Drug discovery. 2014;13(2):140-56.
164. Wen Y, Jing Y, Yang L, Kang D, Jiang P, Li N, et al. The regulators of BCR signaling during B cell activation. Blood Science. 2019;1(02):119-29.
165. Abdelrasoul H, Werner M, Setz CS, Okkenhaug K, Jumaa H. PI3K induces B-cell development and regulates B cell identity. Scientific reports. 2018;8(1):1327.
166. Vadas O, Burke JE, Zhang X, Berndt A, Williams RL. Structural basis for activation and inhibition of class I phosphoinositide 3-kinases. Science signaling. 2011;4(195):re2-re.
167. Jia S, Liu Z, Zhang S, Liu P, Zhang L, Lee SH, et al. Essential roles of PI (3) K–p110β in cell growth, metabolism and tumorigenesis. Nature. 2008;454(7205):776-9.
168. Ortiz-Maldonado V, García-Morillo M, Delgado J. The biology behind PI3K inhibition in chronic lymphocytic leukaemia. Therapeutic advances in hematology. 2015;6(1):25-36.
169. Marshall AJ, Niiro H, Yun TJ, Clark EA. Regulation of B-cell acitvation and differentiation by the phosphatidyllinositol 3-kinase and phospholipase Cγ pathways. Immunological reviews. 2000;176(1).
170. Davies CC, Mason J, Wakelam MJ, Young LS, Eliopoulos AG. Inhibition of phosphatidylinositol 3-kinase-and ERK MAPK-regulated protein synthesis reveals the pro-apoptotic properties of CD40 ligation in carcinoma cells. Journal of Biological Chemistry. 2004;279(2):1010-9.
171. Bilancio A, Okkenhaug K, Camps M, Emery JL, Ruckle T, Rommel C, et al. Key role of the p110δ isoform of PI3K in B-cell antigen and IL-4 receptor signaling: comparative analysis of genetic and pharmacologic interference with p110δ function in B cells. Blood. 2006;107(2):642-50.
172. Henley T, Kovesdi D, Turner M. B-cell responses to B-cell activation factor of the TNF family (BAFF) are impaired in the absence of PI3K delta. European journal of immunology. 2008;38(12):3543-8.
173. Herman SE, Gordon AL, Wagner AJ, Heerema NA, Zhao W, Flynn JM, et al. Phosphatidylinositol 3-kinase-δ inhibitor CAL-101 shows promising preclinical activity in chronic

lymphocytic leukemia by antagonizing intrinsic and extrinsic cellular survival signals. Blood, The Journal of the American Society of Hematology. 2010;116(12):2078-88.
174. Liu L, Puri KD, Penninger JM, Kubes P. Leukocyte PI3Kγ and PI3Kδ have temporally distinct roles for leukocyte recruitment in vivo. Blood, The Journal of the American Society of Hematology. 2007;110(4):1191-8.
175. Konrad S, Ali SR, Wiege K, Syed SN, Engling L, Piekorz RP, et al. Phosphoinositide 3-kinases γ and δ, linkers of coordinate C5a receptor-Fcγ receptor activation and immune complex-induced inflammation. Journal of Biological Chemistry. 2008;283(48):33296-303.
176. Donahue TR, Tran LM, Hill R, Li Y, Kovochich A, Calvopina JH, et al. Integrative survival-based molecular profiling of human pancreatic cancer. Clinical Cancer Research. 2012;18(5):1352-63.
177. Limon JJ, Fruman DA. Akt and mTOR in B cell activation and differentiation. Frontiers in immunology. 2012;3:228.
178. Fruman DA, Chiu H, Hopkins BD, Bagrodia S, Cantley LC, Abraham RT. The PI3K pathway in human disease. Cell. 2017;170(4):605-35.
179. Manning BD, Cantley LC. AKT/PKB signaling: navigating downstream. Cell. 2007;129(7):1261-74.
180. Yang J, Nie J, Ma X, Wei Y, Peng Y, Wei X. Targeting PI3K in cancer: mechanisms and advances in clinical trials. Molecular cancer. 2019;18(1):26.
181. Sarbassov DD, Guertin DA, Ali SM, Sabatini DM. Phosphorylation and regulation of Akt/PKB by the rictor-mTOR complex. Science. 2005;307(5712):1098-101.
182. Jacinto E, Facchinetti V, Liu D, Soto N, Wei S, Jung SY, et al. SIN1/MIP1 maintains rictor-mTOR complex integrity and regulates Akt phosphorylation and substrate specificity. Cell. 2006;127(1):125-37.
183. Hennessy BT, Smith DL, Ram PT, Lu Y, Mills GB. Exploiting the PI3K/AKT pathway for cancer drug discovery. Nature reviews Drug discovery. 2005;4(12):988-1004.
184. Lindhurst MJ, Sapp JC, Teer JK, Johnston JJ, Finn EM, Peters K, et al. A mosaic activating mutation in AKT1 associated with the Proteus syndrome. New England Journal of Medicine. 2011;365(7):611-9.
185. Burgering B. A brief introduction to FOXOlogy. Oncogene. 2008;27(16).
186. Paradis S, Ruvkun G. Caenorhabditis elegans Akt/PKB transduces insulin receptor-like signals from AGE-1 PI3 kinase to the DAF-16 transcription factor. Genes & development. 1998;12(16):2488-98.
187. Calamito M, Juntilla MM, Thomas M, Northrup DL, Rathmell J, Birnbaum MJ, et al. Akt1 and Akt2 promote peripheral B-cell maturation and survival. Blood, The Journal of the American Society of Hematology. 2010;115(20):4043-50.
188. Chen J, Limon JJ, Blanc C, Peng SL, Fruman DA. Foxo1 regulates marginal zone B-cell development. European journal of immunology. 2010;40(7):1890-6.
189. Dengler HS, Baracho GV, Omori SA, Bruckner S, Arden KC, Castrillon DH, et al. Distinct functions for the transcription factor Foxo1 at various stages of B cell differentiation. Nature immunology. 2008;9(12):1388-98.
190. Omori SA, Cato MH, Anzelon-Mills A, Puri KD, Shapiro-Shelef M, Calame K, et al. Regulation of class-switch recombination and plasma cell differentiation by phosphatidylinositol 3-kinase signaling. Immunity. 2006;25(4):545-57.
191. Limon JJ, So L, Jellbauer S, Chiu H, Corado J, Sykes SM, et al. mTOR kinase inhibitors promote antibody class switching via mTORC2 inhibition. Proceedings of the National Academy of Sciences. 2014;111(47):E5076-E85.
192. Zhuang J, Hawkins SF, Glenn MA, Lin K, Johnson GG, Carter A, et al. Akt is activated in chronic lymphocytic leukemia cells and delivers a pro-survival signal: the therapeutic potential of Akt inhibition. haematologica. 2010;95(1):110.
193. Ticchioni M, Essafi M, Jeandel P, Davi F, Cassuto J, Deckert M, et al. Homeostatic chemokines increase survival of B-chronic lymphocytic leukemia cells through inactivation of transcription factor FOXO3a. Oncogene. 2007;26(50):7081-91.

194. Lin A, Piao H-l, Zhuang L, Sarbassov DD, Ma L, Gan B. FoxO transcription factors promote AKT Ser473 phosphorylation and renal tumor growth in response to pharmacologic inhibition of the PI3K–AKT pathway. Cancer research. 2014;74(6):1682-93.
195. Hendriks RW, Yuvaraj S, Kil LP. Targeting Bruton's tyrosine kinase in B cell malignancies. Nature Reviews Cancer. 2014;14(4):219-32.
196. Profitós-Pelejà N, Santos JC, Marín-Niebla A, Roué G, Ribeiro ML. Regulation of B-cell receptor signaling and its therapeutic relevance in aggressive B-cell lymphomas. Cancers. 2022;14(4):860.
197. Bojarczuk K, Sasi BK, Gobessi S, Innocenti I, Pozzato G, Laurenti L, et al. BCR signaling inhibitors differ in their ability to overcome Mcl-1–mediated resistance of CLL B cells to ABT-199. Blood, The Journal of the American Society of Hematology. 2016;127(25):3192-201.
198. Compagno M, Wang Q, Pighi C, Cheong T-C, Meng F-L, Poggio T, et al. Phosphatidylinositol 3-kinase δ blockade increases genomic instability in B cells. Nature. 2017;542(7642):489-93.
199. Zhang K, Husami A, Marsh R, Jordan MB. Identification of a phosphoinositide 3-kinase (PI-3K) p110δ (PIK3CD) deficient individual. J Clin Immunol. 2013;33(3):673-4.
200. Fruman DA, Cantley LC. Idelalisib—a PI3Kδ inhibitor for B-cell cancers. Mass Medical Soc; 2014. p. 1061-2.
201. Burger JA, Ghia P, Rosenwald A, Caligaris-Cappio F. The microenvironment in mature B-cell malignancies: a target for new treatment strategies. Blood, The Journal of the American Society of Hematology. 2009;114(16):3367-75.
202. Stein H, Bonk A, Tolksdorf G, Lennert K, Rodt H, Gerdes J. Immunohistologic analysis of the organization of normal lymphoid tissue and non-Hodgkin's lymphomas. Journal of Histochemistry & Cytochemistry. 1980;28(8):746-60.
203. Burger JA, Tsukada N, Burger M, Zvaifler NJ, Dell'Aquila M, Kipps TJ. Blood-derived nurse-like cells protect chronic lymphocytic leukemia B cells from spontaneous apoptosis through stromal cell–derived factor-1. Blood, The Journal of the American Society of Hematology. 2000;96(8):2655-63.
204. Bürkle A, Niedermeier M, Schmitt-Gräff A, Wierda WG, Keating MJ, Burger JA. Overexpression of the CXCR5 chemokine receptor, and its ligand, CXCL13 in B-cell chronic lymphocytic leukemia. Blood, The Journal of the American Society of Hematology. 2007;110(9):3316-25.
205. Patten PE, Buggins AG, Richards J, Wotherspoon A, Salisbury J, Mufti GJ, et al. CD38 expression in chronic lymphocytic leukemia is regulated by the tumor microenvironment. Blood, The Journal of the American Society of Hematology. 2008;111(10):5173-81.
206. Burger JA, Chiorazzi N. B cell receptor signaling in chronic lymphocytic leukemia. Trends in immunology. 2013;34(12):592-601.
207. Baudino TA, Maclean KH, Brennan J, Parganas E, Yang C, Aslanian A, et al. Myc-mediated proliferation and lymphomagenesis, but not apoptosis, are compromised by E2f1 loss. Molecular cell. 2003;11(4):905-14.
208. Kostareli E, Gounari M, Janus A, Murray F, Brochet X, Giudicelli V, et al. Antigen receptor stereotypy across B-cell lymphoproliferations: the case of IGHV4-59/IGKV3-20 receptors with rheumatoid factor activity. Leukemia. 2012;26(5):1127-31.
209. Burger JA, Quiroga MP, Hartmann E, Bürkle A, Wierda WG, Keating MJ, et al. High-level expression of the T-cell chemokines CCL3 and CCL4 by chronic lymphocytic leukemia B cells in nurselike cell cocultures and after BCR stimulation. Blood, The Journal of the American Society of Hematology. 2009;113(13):3050-8.
210. Deaglio S, Morra M, Mallone R, Ausiello CM, Prager E, Garbarino G, et al. Human CD38 (ADP-ribosyl cyclase) is a counter-receptor of CD31, an Ig superfamily member. The Journal of Immunology. 1998;160(1):395-402.
211. Nishio M, Endo T, Tsukada N, Ohata J, Kitada S, Reed JC, et al. Nurselike cells express BAFF and APRIL, which can promote survival of chronic lymphocytic leukemia cells via a paracrine pathway distinct from that of SDF-1α. Blood. 2005;106(3):1012-20.

212. Costinean S, Zanesi N, Pekarsky Y, Tili E, Volinia S, Heerema N, et al. Pre-B cell proliferation and lymphoblastic leukemia/high-grade lymphoma in Eμ-miR155 transgenic mice. Proceedings of the National Academy of Sciences. 2006;103(18):7024-9.
213. Cui B, Chen L, Zhang S, Mraz M, Fecteau J-F, Yu J, et al. MicroRNA-155 influences B-cell receptor signaling and associates with aggressive disease in chronic lymphocytic leukemia. Blood, The Journal of the American Society of Hematology. 2014;124(4):546-54.
214. Ramsay AD, Rodriguez-Justo M. Chronic lymphocytic leukaemia–the role of the microenvironment pathogenesis and therapy. British journal of haematology. 2013;162(1):15-24.
215. Buske C, Gogowski G, Schreiber K, Rave-Fränk M, Hiddemann W, Wörmann B. Stimulation of B-chronic lymphocytic leukemia cells by murine fibroblasts, IL-4, anti-CD40 antibodies, and the soluble CD40 ligand. Experimental hematology. 1997;25(4):329-37.
216. Lagneaux L, Delforge A, Bron D, De Bruyn C, Stryckmans P. Chronic lymphocytic leukemic B cells but not normal B cells are rescued from apoptosis by contact with normal bone marrow stromal cells. Blood, The Journal of the American Society of Hematology. 1998;91(7):2387-96.
217. Aguilar-Hernandez MM, Blunt MD, Dobson R, Yeomans A, Thirdborough S, Larrayoz M, et al. IL-4 enhances expression and function of surface IgM in CLL cells. Blood, The Journal of the American Society of Hematology. 2016;127(24):3015-25.
218. de Totero D, Meazza R, Zupo S, Cutrona G, Matis S, Colombo M, et al. Interleukin-21 receptor (IL-21R) is up-regulated by CD40 triggering and mediates proapoptotic signals in chronic lymphocytic leukemia B cells. Blood. 2006;107(9):3708-15.
219. Shachar I, Haran M. The secret second life of an innocent chaperone: the story of CD74 and B cell/chronic lymphocytic leukemia cell survival. Leukemia & lymphoma. 2011;52(8):1446-54.
220. Vaisitti T, Aydin S, Rossi D, Cottino F, Bergui L, D'arena G, et al. CD38 increases CXCL12-mediated signals and homing of chronic lymphocytic leukemia cells. Leukemia. 2010;24(5):958-69.
221. Burger JA, Montserrat E. Coming full circle: 70 years of chronic lymphocytic leukemia cell redistribution, from glucocorticoids to inhibitors of B-cell receptor signaling. Blood, The Journal of the American Society of Hematology. 2013;121(9):1501-9.
222. Herman SE, Gordon AL, Hertlein E, Ramanunni A, Zhang X, Jaglowski S, et al. Bruton tyrosine kinase represents a promising therapeutic target for treatment of chronic lymphocytic leukemia and is effectively targeted by PCI-32765. Blood, The Journal of the American Society of Hematology. 2011;117(23):6287-96.
223. Ponader S, Chen S-S, Buggy JJ, Balakrishnan K, Gandhi V, Wierda WG, et al. The Bruton tyrosine kinase inhibitor PCI-32765 thwarts chronic lymphocytic leukemia cell survival and tissue homing in vitro and in vivo. Blood, The Journal of the American Society of Hematology. 2012;119(5):1182-9.
224. de Rooij MF, Kuil A, Geest CR, Eldering E, Chang BY, Buggy JJ, et al. The clinically active BTK inhibitor PCI-32765 targets B-cell receptor–and chemokine-controlled adhesion and migration in chronic lymphocytic leukemia. Blood, The Journal of the American Society of Hematology. 2012;119(11):2590-4.
225. Hoellenriegel J, Meadows SA, Sivina M, Wierda WG, Kantarjian H, Keating MJ, et al. The phosphoinositide 3'-kinase delta inhibitor, CAL-101, inhibits B-cell receptor signaling and chemokine networks in chronic lymphocytic leukemia. Blood, The Journal of the American Society of Hematology. 2011;118(13):3603-12.
226. Chen L, Huynh L, Apgar J, Tang L, Rassenti L, Weiss A, et al. ZAP-70 enhances IgM signaling independent of its kinase activity in chronic lymphocytic leukemia. Blood, The Journal of the American Society of Hematology. 2008;111(5):2685-92.
227. Stevenson FK, Caligaris-Cappio F. Chronic lymphocytic leukemia: revelations from the B-cell receptor. Blood. 2004;103(12):4389-95.
228. Ruuskanen O, Pittard 3rd W, Miller K, Pierce G, Sorensen RU, Polmar SH. Staphylococcus aureus Cowan I-induced immunoglobulin production in human cord blood lymphocytes. Journal of immunology (Baltimore, Md: 1950). 1980;125(1):411-3.
229. Bernal A, Pastore RD, Asgary Z, Keller SA, Cesarman E, Liou H-C, et al. Survival of leukemic B cells promoted by engagement of the antigen receptor. Blood, The Journal of the American Society of Hematology. 2001;98(10):3050-7.

230. Nédellec S, Renaudineau Y, Bordron A, Berthou C, Porakishvili N, Lydyard PM, et al. B cell response to surface IgM cross-linking identifies different prognostic groups of B-chronic lymphocytic leukemia patients. The Journal of Immunology. 2005;174(6):3749-56.
231. Binder M, Léchenne B, Ummanni R, Scharf C, Balabanov S, Trusch M, et al. Stereotypical chronic lymphocytic leukemia B-cell receptors recognize survival promoting antigens on stromal cells. PloS one. 2010;5(12):e15992.
232. Crassini K, Shen Y, Mulligan S, Giles Best O. Modeling the chronic lymphocytic leukemia microenvironment in vitro. Leukemia & lymphoma. 2017;58(2):266-79.
233. Barbaglio F, Belloni D, Scarfò L, Sbrana FV, Ponzoni M, Bongiovanni L, et al. Three-dimensional co-culture model of chronic lymphocytic leukemia bone marrow microenvironment predicts patient-specific response to mobilizing agents. Haematologica. 2021;106(9):2334.
234. Abrisqueta P, Pereira A, Rozman C, Aymerich M, Giné E, Moreno C, et al. Improving survival in patients with chronic lymphocytic leukemia (1980-2008): the Hospital Clinic of Barcelona experience. Blood, The Journal of the American Society of Hematology. 2009;114(10):2044-50.
235. Herling CD, Cymbalista F, Groß-Ophoff-Müller C, Bahlo J, Robrecht S, Langerbeins P, et al. Early treatment with FCR versus watch and wait in patients with stage Binet A high-risk chronic lymphocytic leukemia (CLL): a randomized phase 3 trial. Leukemia. 2020;34(8):2038-50.
236. Langerbeins P, Zhang C, Robrecht S, Cramer P, Fürstenau M, Al-Sawaf O, et al. The CLL12 trial: ibrutinib vs placebo in treatment-naïve, early-stage chronic lymphocytic leukemia. Blood, The Journal of the American Society of Hematology. 2022;139(2):177-87.
237. Catovsky D, Richards S, Matutes E, Oscier D, Dyer M, Bezares R, et al. Assessment of fludarabine plus cyclophosphamide for patients with chronic lymphocytic leukaemia (the LRF CLL4 Trial): a randomised controlled trial. The Lancet. 2007;370(9583):230-9.
238. Eichhorst B, Fink A-M, Bahlo J, Busch R, Kovacs G, Maurer C, et al. First-line chemoimmunotherapy with bendamustine and rituximab versus fludarabine, cyclophosphamide, and rituximab in patients with advanced chronic lymphocytic leukaemia (CLL10): an international, open-label, randomised, phase 3, non-inferiority trial. The lancet oncology. 2016;17(7):928-42.
239. Goede V, Fischer K, Busch R, Engelke A, Eichhorst B, Wendtner CM, et al. Obinutuzumab plus chlorambucil in patients with CLL and coexisting conditions. New England Journal of Medicine. 2014;370(12):1101-10.
240. Robak T. Therapy of chronic lymphocytic leukaemia with purine nucleoside analogues: facts and controversies. Drugs & aging. 2005;22:983-1012.
241. Chang JE, Kahl BS. Bendamustine for treatment of chronic lymphocytic leukemia. Expert opinion on pharmacotherapy. 2012;13(10):1495-505.
242. Lukenbill J, Kalaycio M. Fludarabine: a review of the clear benefits and potential harms. Leukemia research. 2013;37(9):986-94.
243. Anaissie EJ, Kontoyiannis DP, O'Brien S, Kantarjian H, Robertson L, Lerner S, et al. Infections in patients with chronic lymphocytic leukemia treated with fludarabine. Annals of internal medicine. 1998;129(7):559-66.
244. Plunkett W, Gandhi V, Huang P, Robertson L, Yang L, Gregoire V, et al., editors. Fludarabine: pharmacokinetics, mechanisms of action, and rationales for combination therapies. Seminars in oncology; 1993.
245. Rai KR, Peterson BL, Appelbaum FR, Kolitz J, Elias L, Shepherd L, et al. Fludarabine compared with chlorambucil as primary therapy for chronic lymphocytic leukemia. New England Journal of Medicine. 2000;343(24):1750-7.
246. Hillmen P, Robak T, Janssens A, Babu KG, Kloczko J, Grosicki S, et al. Chlorambucil plus ofatumumab versus chlorambucil alone in previously untreated patients with chronic lymphocytic leukaemia (COMPLEMENT 1): a randomised, multicentre, open-label phase 3 trial. The Lancet. 2015;385(9980):1873-83.
247. Hallek M. Signaling the end of chronic lymphocytic leukemia: new frontline treatment strategies. Blood, The Journal of the American Society of Hematology. 2013;122(23):3723-34.
248. Jain N, O'Brien S. Initial treatment of CLL: integrating biology and functional status. Blood, The Journal of the American Society of Hematology. 2015;126(4):463-70.

249. Keating MJ, O'Brien S, Albitar M, Lerner S, Plunkett W, Giles F, et al. Early results of a chemoimmunotherapy regimen of fludarabine, cyclophosphamide, and rituximab as initial therapy for chronic lymphocytic leukemia. Journal of clinical oncology. 2005;23(18):4079-88.
250. Fischer K, Cramer P, Busch R, Stilgenbauer S, Bahlo J, Schweighofer CD, et al. Bendamustine combined with rituximab in patients with relapsed and/or refractory chronic lymphocytic leukemia: a multicenter phase II trial of the German Chronic Lymphocytic Leukemia Study Group. Journal of clinical oncology. 2011;29(26):3559-66.
251. Thompson PA, Tam CS, O'Brien SM, Wierda WG, Stingo F, Plunkett W, et al. Fludarabine, cyclophosphamide, and rituximab treatment achieves long-term disease-free survival in IGHV-mutated chronic lymphocytic leukemia. Blood, The Journal of the American Society of Hematology. 2016;127(3):303-9.
252. Kutsch N, Bahlo J, Robrecht S, Franklin J, Zhang C, Maurer C, et al. Long term follow-up data and health-related quality of life in frontline therapy of fit patients treated with FCR versus BR (CLL10 trial of the GCLLSG). Hemasphere. 2020;4(1):e336.
253. Byrd JC, Jones JJ, Woyach JA, Johnson AJ, Flynn JM. Entering the era of targeted therapy for chronic lymphocytic leukemia: impact on the practicing clinician. Journal of Clinical Oncology. 2014;32(27):3039-47.
254. Wiestner A. Emerging role of kinase-targeted strategies in chronic lymphocytic leukemia. Blood, The Journal of the American Society of Hematology. 2012;120(24):4684-91.
255. Nguyen P-H, Fedorchenko O, Rosen N, Koch M, Barthel R, Winarski T, et al. LYN kinase in the tumor microenvironment is essential for the progression of chronic lymphocytic leukemia. Cancer Cell. 2016;30(4):610-22.
256. Nguyen P-H, Niesen E, Hallek M. New roles for B cell receptor associated kinases: when the B cell is not the target. Leukemia. 2019;33(3):576-87.
257. Honigberg LA, Smith AM, Sirisawad M, Verner E, Loury D, Chang B, et al. The Bruton tyrosine kinase inhibitor PCI-32765 blocks B-cell activation and is efficacious in models of autoimmune disease and B-cell malignancy. Proceedings of the National Academy of Sciences. 2010;107(29):13075-80.
258. Pan Z, Scheerens H, Li S-J, Schultz BE, Sprengeler PA, Burrill LC, et al. Discovery of selective irreversible inhibitors for Bruton's tyrosine kinase. ChemMedChem. 2007;2(1):58-61.
259. Rey-Barroso J, Munaretto A, Rouquié N, Mougel A, Chassan M, Gadat S, et al. Lymphocyte migration and retention properties affected by ibrutinib in chronic lymphocytic leukemia. Haematologica. 2024;109(3):809.
260. Herman SE, Mustafa RZ, Gyamfi JA, Pittaluga S, Chang S, Chang B, et al. Ibrutinib inhibits BCR and NF-κB signaling and reduces tumor proliferation in tissue-resident cells of patients with CLL. Blood, The Journal of the American Society of Hematology. 2014;123(21):3286-95.
261. Ishdorj G, Nugent Z, Squires M, Kost S, Banerji V, Davidson L, et al. Rapid improvement in symptoms and physical function following ibrutinib initiation in chronic lymphocytic leukemia and the associated changes in plasma cytokines. Leukemia Research. 2021;109:106628.
262. Davids MS, Brown JR. Ibrutinib: a first in class covalent inhibitor of Bruton's tyrosine kinase. Future oncology. 2014;10(6):957-67.
263. Byrd JC, Furman RR, Coutre SE, Flinn IW, Burger JA, Blum KA, et al. Targeting BTK with ibrutinib in relapsed chronic lymphocytic leukemia. New England Journal of Medicine. 2013;369(1):32-42.
264. Byrd JC, Furman RR, Coutre SE, Flinn IW, Burger JA, Blum K, et al. Ibrutinib treatment for first-line and relapsed/refractory chronic lymphocytic leukemia: final analysis of the pivotal phase Ib/II PCYC-1102 study. Clinical Cancer Research. 2020;26(15):3918-27.
265. Munir T, Brown JR, O'Brien S, Barrientos JC, Barr PM, Reddy NM, et al. Final analysis from RESONATE: Up to six years of follow-up on ibrutinib in patients with previously treated chronic lymphocytic leukemia or small lymphocytic lymphoma. American journal of hematology. 2019;94(12):1353-63.
266. Burger JA, Barr PM, Robak T, Owen C, Ghia P, Tedeschi A, et al. Long-term efficacy and safety of first-line ibrutinib treatment for patients with CLL/SLL: 5 years of follow-up from the phase 3 RESONATE-2 study. Leukemia. 2020;34(3):787-98.

267. Barr PM, Owen C, Robak T, Tedeschi A, Bairey O, Burger JA, et al. Up to 8-year follow-up from RESONATE-2: first-line ibrutinib treatment for patients with chronic lymphocytic leukemia. Blood advances. 2022;6(11):3440-50.
268. Woyach JA, Ruppert AS, Heerema NA, Zhao W, Booth AM, Ding W, et al. Ibrutinib regimens versus chemoimmunotherapy in older patients with untreated CLL. New England Journal of Medicine. 2018;379(26):2517-28.
269. Moreno C, Greil R, Demirkan F, Tedeschi A, Anz B, Larratt L, et al. Ibrutinib plus obinutuzumab versus chlorambucil plus obinutuzumab in first-line treatment of chronic lymphocytic leukaemia (iLLUMINATE): a multicentre, randomised, open-label, phase 3 trial. The Lancet Oncology. 2019;20(1):43-56.
270. Shanafelt TD, Wang XV, Kay NE, Hanson CA, O'Brien S, Barrientos J, et al. Ibrutinib–rituximab or chemoimmunotherapy for chronic lymphocytic leukemia. New England Journal of Medicine. 2019;381(5):432-43.
271. Tam CS, Brown JR, Kahl BS, Ghia P, Giannopoulos K, Jurczak W, et al. Zanubrutinib versus bendamustine and rituximab in untreated chronic lymphocytic leukaemia and small lymphocytic lymphoma (SEQUOIA): a randomised, controlled, phase 3 trial. The Lancet Oncology. 2022;23(8):1031-43.
272. Sharman JP, Egyed M, Jurczak W, Skarbnik A, Pagel JM, Flinn IW, et al. Efficacy and safety in a 4-year follow-up of the ELEVATE-TN study comparing acalabrutinib with or without obinutuzumab versus obinutuzumab plus chlorambucil in treatment-naïve chronic lymphocytic leukemia. Leukemia. 2022;36(4):1171-5.
273. Mato AR, Nabhan C, Thompson MC, Lamanna N, Brander DM, Hill B, et al. Toxicities and outcomes of 616 ibrutinib-treated patients in the United States: a real-world analysis. Haematologica. 2018;103(5):874.
274. Byrd JC, Hillmen P, Ghia P, Kater AP, Chanan-Khan A, Furman RR, et al. Acalabrutinib versus ibrutinib in previously treated chronic lymphocytic leukemia: results of the first randomized phase III trial. Journal of clinical oncology. 2021;39(31):3441-52.
275. Barf T, Covey T, Izumi R, van de Kar B, Gulrajani M, van Lith B, et al. Acalabrutinib (ACP-196): a covalent Bruton tyrosine kinase inhibitor with a differentiated selectivity and in vivo potency profile. Journal of Pharmacology and Experimental Therapeutics. 2017;363(2):240-52.
276. Byrd JC, Harrington B, O'Brien S, Jones JA, Schuh A, Devereux S, et al. Acalabrutinib (ACP-196) in relapsed chronic lymphocytic leukemia. New England Journal of Medicine. 2016;374(4):323-32.
277. Woyach JA, Ruppert AS, Guinn D, Lehman A, Blachly JS, Lozanski A, et al. BTK C481S-mediated resistance to ibrutinib in chronic lymphocytic leukemia. Journal of Clinical Oncology. 2017;35(13):1437-43.
278. Bonfiglio S, Sutton L-A, Ljungström V, Capasso A, Pandzic T, Weström S, et al. BTK and PLCG2 remain unmutated in one-third of patients with CLL relapsing on ibrutinib. Blood advances. 2023;7(12):2794-806.
279. Gomez EB, Ebata K, Randeria HS, Rosendahl MS, Cedervall EP, Morales TH, et al. Preclinical characterization of pirtobrutinib, a highly selective, noncovalent (reversible) BTK inhibitor. Blood, The Journal of the American Society of Hematology. 2023;142(1):62-72.
280. Mato AR, Shah NN, Jurczak W, Cheah CY, Pagel JM, Woyach JA, et al. Pirtobrutinib in relapsed or refractory B-cell malignancies (BRUIN): a phase 1/2 study. The Lancet. 2021;397(10277):892-901.
281. Mato AR, Woyach JA, Brown JR, Ghia P, Patel K, Eyre TA, et al. Pirtobrutinib after a covalent BTK inhibitor in chronic lymphocytic leukemia. New England Journal of Medicine. 2023;389(1):33-44.
282. Courtney KD, Corcoran RB, Engelman JA. The PI3K pathway as drug target in human cancer. Journal of clinical oncology. 2010;28(6):1075-83.
283. Lannutti BJ, Meadows SA, Herman SE, Kashishian A, Steiner B, Johnson AJ, et al. CAL-101, a p110δ selective phosphatidylinositol-3-kinase inhibitor for the treatment of B-cell malignancies, inhibits PI3K signaling and cellular viability. Blood, The Journal of the American Society of Hematology. 2011;117(2):591-4.

284. von Keudell G, Moskowitz AJ. The role of PI3K inhibition in lymphoid malignancies. Current hematologic malignancy reports. 2019;14:405-13.
285. Longo PG, Laurenti L, Gobessi S, Sica S, Leone G, Efremov DG. The Akt/Mcl-1 pathway plays a prominent role in mediating antiapoptotic signals downstream of the B-cell receptor in chronic lymphocytic leukemia B cells. Blood, The Journal of the American Society of Hematology. 2008;111(2):846-55.
286. Ikeda H, Hideshima T, Fulciniti M, Perrone G, Miura N, Yasui H, et al. PI3K/p110δ is a novel therapeutic target in multiple myeloma. Blood, The Journal of the American Society of Hematology. 2010;116(9):1460-8.
287. Patel K, Danilov AV, Pagel JM. Duvelisib for CLL/SLL and follicular non-Hodgkin lymphoma. Blood, The Journal of the American Society of Hematology. 2019;134(19):1573-7.
288. Sharman JP, Coutre SE, Furman RR, Cheson BD, Pagel JM, Hillmen P, et al. Final results of a randomized, phase III study of rituximab with or without idelalisib followed by open-label idelalisib in patients with relapsed chronic lymphocytic leukemia. Journal of Clinical Oncology. 2019;37(16):1391-402.
289. Scheffold A, Stilgenbauer S. Revolution of chronic lymphocytic leukemia therapy: the chemo-free treatment paradigm. Current oncology reports. 2020;22:1-10.
290. Lampson BL, Kasar SN, Matos TR, Morgan EA, Rassenti L, Davids MS, et al. Idelalisib given front-line for treatment of chronic lymphocytic leukemia causes frequent immune-mediated hepatotoxicity. Blood, The Journal of the American Society of Hematology. 2016;128(2):195-203.
291. Lampson BL, Brown JR. The evolving use of phosphatidylinositol 3-kinase inhibitors for the treatment of chronic lymphocytic leukemia. Hematology/Oncology Clinics. 2021;35(4):807-26.
292. Flinn IW, Hillmen P, Montillo M, Nagy Z, Illés Á, Etienne G, et al. The phase 3 DUO trial: duvelisib vs ofatumumab in relapsed and refractory CLL/SLL. Blood, The Journal of the American Society of Hematology. 2018;132(23):2446-55.
293. Lunning M, Vose J, Nastoupil L, Fowler N, Burger JA, Wierda WG, et al. Ublituximab and umbralisib in relapsed/refractory B-cell non-Hodgkin lymphoma and chronic lymphocytic leukemia. Blood, The Journal of the American Society of Hematology. 2019;134(21):1811-20.
294. Davids MS, Kim HT, Nicotra A, Savell A, Francoeur K, Hellman JM, et al. Umbralisib in combination with ibrutinib in patients with relapsed or refractory chronic lymphocytic leukaemia or mantle cell lymphoma: a multicentre phase 1–1b study. The Lancet Haematology. 2019;6(1):e38-e47.
295. Gribben JG, Jurczak W, Jacobs RW, Grosicki S, Giannopoulos K, Wrobel T, et al. Umbralisib plus ublituximab (U2) is superior to obinutuzumab plus chlorambucil (O+ Chl) in patients with treatment naïve (TN) and relapsed/refractory (R/R) chronic lymphocytic leukemia (CLL): results from the phase 3 Unity-CLL study. Blood. 2020;136:37-9.
296. Johnson SA, Pleiman CM, Pao L, Schneringer J, Hippen K, Cambier JC. Phosphorylated immunoreceptor signaling motifs (ITAMs) exhibit unique abilities to bind and activate Lyn and Syk tyrosine kinases. Journal of immunology (Baltimore, Md: 1950). 1995;155(10):4596-603.
297. Currie KS, Kropf JE, Lee T, Blomgren P, Xu J, Zhao Z, et al. Discovery of GS-9973, a selective and orally efficacious inhibitor of spleen tyrosine kinase. Journal of medicinal chemistry. 2014;57(9):3856-73.
298. Danilov AV, Lam V, Thurlow B, Spurgeon SE, Park B, Orand K, et al. Final Results of a Phase 1/2 Study of Syk Inhibitor Entospletinib in Combination with Obinutuzumab in Patients with Relapsed/Refractory (R/R) Chronic Lymphocytic Leukemia (Cll). Blood. 2021;138:2643.
299. Sharman J, Hawkins M, Kolibaba K, Boxer M, Klein L, Wu M, et al. An open-label phase 2 trial of entospletinib (GS-9973), a selective spleen tyrosine kinase inhibitor, in chronic lymphocytic leukemia. Blood, The Journal of the American Society of Hematology. 2015;125(15):2336-43.
300. Zhang L, Ming L, Yu J. BH3 mimetics to improve cancer therapy; mechanisms and examples. Drug Resistance Updates. 2007;10(6):207-17.
301. Vogler M, Walter HS, Dyer MJ. Targeting anti-apoptotic BCL 2 family proteins in haematological malignancies–from pathogenesis to treatment. British journal of haematology. 2017;178(3):364-79.
302. Danial NN, Korsmeyer SJ. Cell death: critical control points. Cell. 2004;116(2):205-19.

303. Petros AM, Nettesheim DG, Wang Y, Olejniczak ET, Meadows RP, Mack J, et al. Rationale for Bcl-xL/Bad peptide complex formation from structure, mutagenesis, and biophysical studies. Protein Science. 2000;9(12):2528-34.
304. Moore VDG, Brown JR, Certo M, Love TM, Novina CD, Letai A. Chronic lymphocytic leukemia requires BCL2 to sequester prodeath BIM, explaining sensitivity to BCL2 antagonist ABT-737. The Journal of clinical investigation. 2007;117(1):112-21.
305. Majid A, Tsoulakis O, Walewska R, Gesk S, Siebert R, Kennedy DBJ, et al. BCL2 expression in chronic lymphocytic leukemia: lack of association with the BCL2− 938A> C promoter single nucleotide polymorphism. Blood, The Journal of the American Society of Hematology. 2008;111(2):874-7.
306. Souers AJ, Leverson JD, Boghaert ER, Ackler SL, Catron ND, Chen J, et al. ABT-199, a potent and selective BCL-2 inhibitor, achieves antitumor activity while sparing platelets. Nature medicine. 2013;19(2):202-8.
307. Roberts AW, Ma S, Kipps TJ, Coutre SE, Davids MS, Eichhorst B, et al. Efficacy of venetoclax in relapsed chronic lymphocytic leukemia is influenced by disease and response variables. Blood, The Journal of the American Society of Hematology. 2019;134(2):111-22.
308. Harrup RA, Kater AP, Eichhorst BF, Owen C, Chyla B, Jin HY, et al. Response to Subsequent Novel Therapies and Time to Second Progression-Free Survival Event in the MURANO Trial in Patients with Relapsed/Refractory Chronic Lymphocytic Leukemia Previously Treated with Fixed-Dose Venetoclax Plus Rituximab. Blood. 2023;142:1898.
309. Al-Sawaf O, Zhang C, Lu T, Liao MZ, Panchal A, Robrecht S, et al. Minimal residual disease dynamics after venetoclax-obinutuzumab treatment: extended off-treatment follow-up from the randomized CLL14 study. Journal of Clinical Oncology. 2021;39(36):4049-60.
310. Wierda WG, Allan JN, Siddiqi T, Kipps TJ, Opat S, Tedeschi A, et al. Ibrutinib plus venetoclax for first-line treatment of chronic lymphocytic leukemia: primary analysis results from the minimal residual disease cohort of the randomized phase II CAPTIVATE study. Journal of Clinical Oncology. 2021;39(34):3853-65.
311. Jain N, Keating M, Thompson P, Ferrajoli A, Burger JA, Borthakur G, et al. Ibrutinib plus venetoclax for first-line treatment of chronic lymphocytic leukemia: a nonrandomized phase 2 trial. JAMA oncology. 2021;7(8):1213-9.
312. Blombery P, Thompson ER, Nguyen T, Birkinshaw RW, Gong J-n, Chen X, et al. Multiple BCL2 mutations cooccurring with Gly101Val emerge in chronic lymphocytic leukemia progression on venetoclax. Blood, The Journal of the American Society of Hematology. 2020;135(10):773-7.
313. Thijssen R, Roberts AW. Venetoclax in lymphoid malignancies: new insights, more to learn. Cancer Cell. 2019;36(4):341-3.
314. Dreger P, Schnaiter A, Zenz T, Böttcher S, Rossi M, Paschka P, et al. TP53, SF3B1, and NOTCH1 mutations and outcome of allotransplantation for chronic lymphocytic leukemia: six-year follow-up of the GCLLSG CLL3X trial. Blood, The Journal of the American Society of Hematology. 2013;121(16):3284-8.
315. Turtle CJ, Hanafi L-A, Berger C, Gooley TA, Cherian S, Hudecek M, et al. CD19 CAR–T cells of defined CD4+: CD8+ composition in adult B cell ALL patients. The Journal of clinical investigation. 2016;126(6):2123-38.
316. Turtle CJ, Hanafi L-A, Berger C, Hudecek M, Pender B, Robinson E, et al. Immunotherapy of non-Hodgkin's lymphoma with a defined ratio of CD8+ and CD4+ CD19-specific chimeric antigen receptor–modified T cells. Science translational medicine. 2016;8(355):355ra116-355ra116.
317. Maude SL, Laetsch TW, Buechner J, Rives S, Boyer M, Bittencourt H, et al. Tisagenlecleucel in children and young adults with B-cell lymphoblastic leukemia. New England Journal of Medicine. 2018;378(5):439-48.
318. Fraietta JA, Lacey SF, Orlando EJ, Pruteanu-Malinici I, Gohil M, Lundh S, et al. Determinants of response and resistance to CD19 chimeric antigen receptor (CAR) T cell therapy of chronic lymphocytic leukemia. Nature medicine. 2018;24(5):563-71.
319. Mancikova V, Smida M. Current state of CAR T-cell therapy in chronic lymphocytic leukemia. International Journal of Molecular Sciences. 2021;22(11):5536.

320. Gauthier J, Hirayama AV, Purushe J, Hay KA, Lymp J, Li DH, et al. Feasibility and efficacy of CD19-targeted CAR T cells with concurrent ibrutinib for CLL after ibrutinib failure. Blood, The Journal of the American Society of Hematology. 2020;135(19):1650-60.
321. Siddiqi T, Maloney DG, Kenderian SS, Brander DM, Dorritie K, Soumerai J, et al. Lisocabtagene maraleucel in chronic lymphocytic leukaemia and small lymphocytic lymphoma (TRANSCEND CLL 004): a multicentre, open-label, single-arm, phase 1–2 study. The Lancet. 2023;402(10402):641-54.
322. Siddiqi T, Maloney DG, Kenderian S, Brander DM, Dorritie K, Soumerai J, et al. LISOCABTAGENE MARALEUCEL (LISO-CEL) IN R/R CHRONIC LYMPHOCYTIC LEUKEMIA (CLL)/SMALL LYMPHOCYTIC LYMPHOMA (SLL): PRIMARY ANALYSIS OF TRANSCEND CLL 004. Hematological Oncology. 2023;41.
323. U.S. FOOD & DRUG ADMINISTRATION. BREYANZI (lisocabtagene maraleucel) 2024 [13/06/2024]. Available from: https://www.fda.gov/vaccines-blood-biologics/cellular-gene-therapy-products/breyanzi-lisocabtagene-maraleucel.
324. Hanahan D, Weinberg RA. Hallmarks of cancer: the next generation. cell. 2011;144(5):646-74.
325. Vanhaesebroeck B, Stephens L, Hawkins P. PI3K signalling: the path to discovery and understanding. Nature reviews Molecular cell biology. 2012;13(3):195-203.
326. Eijkelenboom A, Burgering BM. FOXOs: signalling integrators for homeostasis maintenance. Nature reviews Molecular cell biology. 2013;14(2):83-97.
327. Benayoun BA, Caburet S, Veitia RA. Forkhead transcription factors: key players in health and disease. Trends in Genetics. 2011;27(6):224-32.
328. Yusuf D, Butland SL, Swanson MI, Bolotin E, Ticoll A, Cheung WA, et al. The transcription factor encyclopedia. Genome biology. 2012;13:1-25.
329. Furuyama T, Nakazawa T, Nakano I, Mori N. Identification of the differential distribution patterns of mRNAs and consensus binding sequences for mouse DAF-16 homologues. Biochemical Journal. 2000;349(2):629-34.
330. Fu Z, Tindall D. FOXOs, cancer and regulation of apoptosis. Oncogene. 2008;27(16):2312-9.
331. Bullock M. FOXO factors and breast cancer: outfoxing endocrine resistance. Endocrine-related cancer. 2016;23(2):R113-R30.
332. van der Horst A, Burgering BM. Stressing the role of FoxO proteins in lifespan and disease. Nature reviews Molecular cell biology. 2007;8(6):440-50.
333. Storz P. Forkhead homeobox type O transcription factors in the responses to oxidative stress. Antioxidants & redox signaling. 2011;14(4):593-605.
334. Yao S, Fan LY-N, Lam EW-F, editors. The FOXO3-FOXM1 axis: A key cancer drug target and a modulator of cancer drug resistance. Seminars in cancer biology; 2018: Elsevier.
335. Brown AK, Webb AE. Regulation of FOXO factors in mammalian cells. Current topics in developmental biology. 2018;127:165-92.
336. Calissi G, Lam EW-F, Link W. Therapeutic strategies targeting FOXO transcription factors. Nature reviews Drug discovery. 2021;20(1):21-38.
337. Janku F, Yap TA, Meric-Bernstam F. Targeting the PI3K pathway in cancer: are we making headway? Nature reviews Clinical oncology. 2018;15(5):273-91.
338. Van Der Heide LP, Hoekman MF, Smidt MP. The ins and outs of FoxO shuttling: mechanisms of FoxO translocation and transcriptional regulation. Biochemical Journal. 2004;380(2):297-309.
339. Calnan D, Brunet A. The foxo code. Oncogene. 2008;27(16):2276-88.
340. Obata T, Yaffe MB, Leparc GG, Piro ET, Maegawa H, Kashiwagi A, et al. Peptide and protein library screening defines optimal substrate motifs for AKT/PKB. Journal of Biological Chemistry. 2000;275(46):36108-15.
341. Zhang X, Gan L, Pan H, Guo S, He X, Olson ST, et al. Phosphorylation of serine 256 suppresses transactivation by FKHR (FOXO1) by multiple mechanisms: direct and indirect effects on nuclear/cytoplasmic shuttling and DNA binding. Journal of Biological Chemistry. 2002;277(47):45276-84.
342. Hornsveld M, Dansen T, Derksen P, Burgering B, editors. Re-evaluating the role of FOXOs in cancer. Seminars in cancer biology; 2018: Elsevier.

343. Yan L, Lavin VA, Moser LR, Cui Q, Kanies C, Yang E. PP2A regulates the pro-apoptotic activity of FOXO1. Journal of Biological Chemistry. 2008;283(12):7411-20.
344. Tzivion G, Dobson M, Ramakrishnan G. FoxO transcription factors; Regulation by AKT and 14-3-3 proteins. Biochimica et Biophysica Acta (BBA)-Molecular Cell Research. 2011;1813(11):1938-45.
345. Lehtinen MK, Yuan Z, Boag PR, Yang Y, Villén J, Becker EB, et al. A conserved MST-FOXO signaling pathway mediates oxidative-stress responses and extends life span. Cell. 2006;125(5):987-1001.
346. Greer EL, Oskoui PR, Banko MR, Maniar JM, Gygi MP, Gygi SP, et al. The energy sensor AMP-activated protein kinase directly regulates the mammalian FOXO3 transcription factor. Journal of Biological Chemistry. 2007;282(41):30107-19.
347. Plas DR, Thompson CB. Akt activation promotes degradation of tuberin and FOXO3a via the proteasome. Journal of Biological Chemistry. 2003;278(14):12361-6.
348. Welchman RL, Gordon C, Mayer RJ. Ubiquitin and ubiquitin-like proteins as multifunctional signals. Nature reviews Molecular cell biology. 2005;6(8):599-609.
349. Buus R, Faronato M, Hammond DE, Urbé S, Clague MJ. Deubiquitinase activities required for hepatocyte growth factor-induced scattering of epithelial cells. Current Biology. 2009;19(17):1463-6.
350. Matsuzaki H, Daitoku H, Hatta M, Tanaka K, Fukamizu A. Insulin-induced phosphorylation of FKHR (Foxo1) targets to proteasomal degradation. Proceedings of the National Academy of Sciences. 2003;100(20):11285-90.
351. Huang H, Tindall DJ. Regulation of FOXO protein stability via ubiquitination and proteasome degradation. Biochimica et Biophysica Acta (BBA)-Molecular Cell Research. 2011;1813(11):1961-4.
352. Aoki M, Jiang H, Vogt PK. Proteasomal degradation of the FoxO1 transcriptional regulator in cells transformed by the P3k and Akt oncoproteins. Proceedings of the National Academy of Sciences. 2004;101(37):13613-7.
353. Hu MC-T, Lee D-F, Xia W, Golfman LS, Ou-Yang F, Yang J-Y, et al. IκB kinase promotes tumorigenesis through inhibition of forkhead FOXO3a. Cell. 2004;117(2):225-37.
354. Yang J-Y, Zong CS, Xia W, Yamaguchi H, Ding Q, Xie X, et al. ERK promotes tumorigenesis by inhibiting FOXO3a via MDM2-mediated degradation. Nature cell biology. 2008;10(2):138-48.
355. Huang H, Regan KM, Wang F, Wang D, Smith DI, Van Deursen JM, et al. Skp2 inhibits FOXO1 in tumor suppression through ubiquitin-mediated degradation. Proceedings of the National Academy of Sciences. 2005;102(5):1649-54.
356. Lin H-K, Wang G, Chen Z, Teruya-Feldstein J, Liu Y, Chan C-H, et al. Phosphorylation-dependent regulation of cytosolic localization and oncogenic function of Skp2 by Akt/PKB. Nature cell biology. 2009;11(4):420-32.
357. Mamillapalli R, Gavrilova N, Mihaylova VT, Tsvetkov LM, Wu H, Zhang H, et al. PTEN regulates the ubiquitin-dependent degradation of the CDK inhibitor p27KIP1 through the ubiquitin E3 ligase SCFSKP2. Current Biology. 2001;11(4):263-7.
358. Kang-Decker N, Tong C, Boussouar F, Baker DJ, Xu W, Leontovich AA, et al. Loss of CBP causes T cell lymphomagenesis in synergy with p27Kip1 insufficiency. Cancer cell. 2004;5(2):177-89.
359. Fu W, Ma Q, Chen L, Li P, Zhang M, Ramamoorthy S, et al. MDM2 acts downstream of p53 as an E3 ligase to promote FOXO ubiquitination and degradation. Journal of Biological Chemistry. 2009;284(21):13987-4000.
360. Van der Horst A, de Vries-Smits AM, Brenkman AB, van Triest MH, van den Broek N, Colland F, et al. FOXO4 transcriptional activity is regulated by monoubiquitination and USP7/HAUSP. Nature cell biology. 2006;8(10):1064-73.
361. Jiramongkol Y, Lam EW-F. FOXO transcription factor family in cancer and metastasis. Cancer and Metastasis Reviews. 2020;39(3):681-709.
362. Kato S, Ding J, Pisck E, Jhala US, Du K. COP1 functions as a FoxO1 ubiquitin E3 ligase to regulate FoxO1-mediated gene expression. Journal of Biological Chemistry. 2008;283(51):35464-73.
363. Song MS, Salmena L, Carracedo A, Egia A, Lo-Coco F, Teruya-Feldstein J, et al. The deubiquitinylation and localization of PTEN are regulated by a HAUSP–PML network. Nature. 2008;455(7214):813-7.

364. Nakamura N, Ramaswamy S, Vazquez F, Signoretti S, Loda M, Sellers WR. Forkhead transcription factors are critical effectors of cell death and cell cycle arrest downstream of PTEN. Molecular and cellular biology. 2000.
365. Burgering BM, Medema RH. Decisions on life and death: FOXO Forkhead transcription factors are in command when PKB/Akt is off duty. Journal of Leucocyte Biology. 2003;73(6):689-701.
366. Zhang B, Tomita Y, Ch'ng E, Qiu Y, He J, Jin Y-F, et al. Prognostic significance of phosphorylated FOXO1 expression in soft tissue sarcoma. Annals of surgical oncology. 2009;16:1925-37.
367. Zhang H, Pan Y, Zheng L, Choe C, Lindgren B, Jensen ED, et al. FOXO1 inhibits Runx2 transcriptional activity and prostate cancer cell migration and invasion. Cancer research. 2011;71(9):3257-67.
368. Cheong J-W, Eom JI, Maeng H-Y, Lee ST, Hahn JS, Ko YW, et al. Constitutive phosphorylation of FKHR transcription factor as a prognostic variable in acute myeloid leukemia. Leukemia research. 2003;27(12):1159-62.
369. Bullock M, Bruce A, Sreekumar R, Curtis N, Cheung T, Reading I, et al. FOXO3 expression during colorectal cancer progression: biomarker potential reflects a tumour suppressor role. British journal of cancer. 2013;109(2):387-94.
370. Shiota M, Song Y, Yokomizo A, Kiyoshima K, Tada Y, Uchino H, et al. Foxo3a suppression of urothelial cancer invasiveness through Twist1, Y-box–binding protein 1, and E-cadherin regulation. Clinical Cancer Research. 2010;16(23):5654-63.
371. Santo EE, Stroeken P, Sluis PV, Koster J, Versteeg R, Westerhout EM. FOXO3a is a major target of inactivation by PI3K/AKT signaling in aggressive neuroblastoma. Cancer research. 2013;73(7):2189-98.
372. Sisci D, Maris P, Grazia Cesario M, Anselmo W, Coroniti R, Elvi Trombino G, et al. The estrogen receptor α is the key regulator of the bifunctional role of FoxO3a transcription factor in breast cancer motility and invasiveness. Cell cycle. 2013;12(21):3405-20.
373. Brunet A, Bonni A, Zigmond MJ, Lin MZ, Juo P, Hu LS, et al. Akt promotes cell survival by phosphorylating and inhibiting a Forkhead transcription factor. cell. 1999;96(6):857-68.
374. Kops GJ, Ruiter NDd, De Vries-Smits AM, Powell DR, Bos JL, Burgering BMT. Direct control of the Forkhead transcription factor AFX by protein kinase B. Nature. 1999;398(6728):630-4.
375. Medema RH, Kops GJ, Bos JL, Burgering BM. AFX-like Forkhead transcription factors mediate cell-cycle regulation by Ras and PKB through p27kip1. Nature. 2000;404(6779):782-7.
376. Kops GJ, Medema RH, Glassford J, Essers MA, Dijkers PF, Coffer PJ, et al. Control of cell cycle exit and entry by protein kinase B-regulated forkhead transcription factors. Molecular and cellular biology. 2002;22(7):2025-36.
377. Liu P, Kao T, Huang H. CDK1 promotes cell proliferation and survival via phosphorylation and inhibition of FOXO1 transcription factor. Oncogene. 2008;27(34):4733-44.
378. Schmidt M, de Mattos SF, van der Horst A, Klompmaker R, Kops GJL, Lam EW-F, et al. Cell cycle inhibition by FoxO forkhead transcription factors involves downregulation of cyclin D. Molecular and cellular biology. 2002.
379. de Keizer PL, Packer LM, Szypowska AA, Riedl-Polderman PE, van den Broek NJ, de Bruin A, et al. Activation of forkhead box O transcription factors by oncogenic BRAF promotes p21cip1-dependent senescence. Cancer research. 2010;70(21):8526-36.
380. Alvarez B, Martínez-A C, Burgering BM, Carrera AC. Forkhead transcription factors contribute to execution of the mitotic programme in mammals. Nature. 2001;413(6857):744-7.
381. Courtois-Cox S, Williams SMG, Reczek EE, Johnson BW, McGillicuddy LT, Johannessen CM, et al. A negative feedback signaling network underlies oncogene-induced senescence. Cancer cell. 2006;10(6):459-72.
382. Zhang X, Tang N, Hadden TJ, Rishi AK. Akt, FoxO and regulation of apoptosis. Biochimica et Biophysica Acta (BBA)-Molecular Cell Research. 2011;1813(11):1978-86.
383. Strasser A, Cory S, Adams JM. Deciphering the rules of programmed cell death to improve therapy of cancer and other diseases. The EMBO journal. 2011;30(18):3667-83.
384. Xie L, Ritz O, Leithäuser F, Guan H, Färbinger J, Weitzer CD, et al. FOXO1 downregulation contributes to the oncogenic program of primary mediastinal B-cell lymphoma. Oncotarget. 2014;5(14):5392.

385. Strasser A, Jost PJ, Nagata S. The many roles of FAS receptor signaling in the immune system. Immunity. 2009;30(2):180-92.
386. Ryter SW, Kim HP, Hoetzel A, Park JW, Nakahira K, Wang X, et al. Mechanisms of cell death in oxidative stress. Antioxidants & redox signaling. 2007;9(1):49-89.
387. Jan R. Understanding apoptosis and apoptotic pathways targeted cancer therapeutics. Advanced pharmaceutical bulletin. 2019;9(2):205.
388. Ushmorov A, Wirth T, editors. FOXO in B-cell lymphopoiesis and B cell neoplasia. Seminars in cancer biology; 2018: Elsevier.
389. Welinder E, Mansson R, Mercer EM, Bryder D, Sigvardsson M, Murre C. The transcription factors E2A and HEB act in concert to induce the expression of FOXO1 in the common lymphoid progenitor. Proceedings of the National Academy of Sciences. 2011;108(42):17402-7.
390. Mansson R, Welinder E, Åhsberg J, Lin YC, Benner C, Glass CK, et al. Positive intergenic feedback circuitry, involving EBF1 and FOXO1, orchestrates B-cell fate. Proceedings of the National Academy of Sciences. 2012;109(51):21028-33.
391. Lin YC, Jhunjhunwala S, Benner C, Heinz S, Welinder E, Mansson R, et al. A global network of transcription factors, involving E2A, EBF1 and Foxo1, that orchestrates B cell fate. Nature immunology. 2010;11(7):635-43.
392. Amin RH, Schlissel MS. Foxo1 directly regulates the transcription of recombination-activating genes during B cell development. Nature immunology. 2008;9(6):613-22.
393. Werner M, Hobeika E, Jumaa H. Role of PI3K in the generation and survival of B cells. Immunological reviews. 2010;237(1):55-71.
394. Nahar R, Ramezani-Rad P, Mossner M, Duy C, Cerchietti L, Geng H, et al. Pre-B cell receptor–mediated activation of BCL6 induces pre-B cell quiescence through transcriptional repression of MYC. Blood, The Journal of the American Society of Hematology. 2011;118(15):4174-8.
395. Venigalla RK, McGuire VA, Clarke R, Patterson-Kane JC, Najafov A, Toth R, et al. PDK1 regulates VDJ recombination, cell-cycle exit and survival during B-cell development. The EMBO journal. 2013;32(7):1008-22.
396. Duy C, Yu JJ, Nahar R, Swaminathan S, Kweon S-M, Polo JM, et al. BCL6 is critical for the development of a diverse primary B cell repertoire. The Journal of experimental medicine. 2010;207(6):1209.
397. Yusuf I, Zhu X, Kharas MG, Chen J, Fruman DA. Optimal B-cell proliferation requires phosphoinositide 3-kinase–dependent inactivation of FOXO transcription factors. Blood. 2004;104(3):784-7.
398. Hinman RM, Bushanam JN, Nichols WA, Satterthwaite AB. B cell receptor signaling down-regulates forkhead box transcription factor class O 1 mRNA expression via phosphatidylinositol 3-kinase and Bruton's tyrosine kinase. The Journal of Immunology. 2007;178(2):740-7.
399. Dansen TB, Burgering BM. Unravelling the tumor-suppressive functions of FOXO proteins. Trends in cell biology. 2008;18(9):421-9.
400. Srinivasan L, Sasaki Y, Calado DP, Zhang B, Paik JH, DePinho RA, et al. PI3 kinase signals BCR-dependent mature B cell survival. Cell. 2009;139(3):573-86.
401. Dominguez-Sola D, Kung J, Holmes AB, Wells VA, Mo T, Basso K, et al. The FOXO1 transcription factor instructs the germinal center dark zone program. Immunity. 2015;43(6):1064-74.
402. Rickert RC. New insights into pre-BCR and BCR signalling with relevance to B cell malignancies. Nature Reviews Immunology. 2013;13(8):578-91.
403. De Silva NS, Klein U. Dynamics of B cells in germinal centres. Nature reviews immunology. 2015;15(3):137-48.
404. Paik J-H, Kollipara R, Chu G, Ji H, Xiao Y, Ding Z, et al. FoxOs are lineage-restricted redundant tumor suppressors and regulate endothelial cell homeostasis. Cell. 2007;128(2):309-23.
405. Trinh DL, Scott DW, Morin RD, Mendez-Lago M, An J, Jones SJ, et al. Analysis of FOXO1 mutations in diffuse large B-cell lymphoma. Blood, The Journal of the American Society of Hematology. 2013;121(18):3666-74.

406. Kabrani E, Chu VT, Tasouri E, Sommermann T, Baßler K, Ulas T, et al. Nuclear FOXO1 promotes lymphomagenesis in germinal center B cells. Blood, The Journal of the American Society of Hematology. 2018;132(25):2670-83.
407. Xie L, Ushmorov A, Leithäuser F, Guan H, Steidl C, Färbinger J, et al. FOXO1 is a tumor suppressor in classical Hodgkin lymphoma. Blood, The Journal of the American Society of Hematology. 2012;119(15):3503-11.
408. Szydlowski M, Kiliszek P, Sewastianik T, Jablonska E, Bialopiotrowicz E, Gorniak P, et al. FOXO1 activation is an effector of SYK and AKT inhibition in tonic BCR signal-dependent diffuse large B-cell lymphomas. Blood, The Journal of the American Society of Hematology. 2016;127(6):739-48.
409. Köhrer S, Havranek O, Seyfried F, Hurtz C, Coffey GP, Kim E, et al. Pre-BCR signaling in precursor B-cell acute lymphoblastic leukemia regulates PI3K/AKT, FOXO1 and MYC, and can be targeted by SYK inhibition. Leukemia. 2016;30(6):1246-54.
410. Bloedjes TA, de Wilde G, Maas C, Eldering E, Bende RJ, van Noesel CJ, et al. AKT signaling restrains tumor suppressive functions of FOXO transcription factors and GSK3 kinase in multiple myeloma. Blood advances. 2020;4(17):4151-64.
411. Palacios F, Abreu C, Prieto D, Morande P, Ruiz S, Fernández-Calero T, et al. Activation of the PI3K/AKT pathway by microRNA-22 results in CLL B-cell proliferation. Leukemia. 2015;29(1):115-25.
412. Cosimo E, Tarafdar A, Moles MW, Holroyd AK, Malik N, Catherwood MA, et al. AKT/mTORC2 inhibition activates FOXO1 function in CLL cells reducing B-cell receptor-mediated survival. Clinical Cancer Research. 2019;25(5):1574-87.
413. Seda V, Vojackova E, Ondrisova L, Kostalova L, Sharma S, Loja T, et al. FoxO1-GAB1 axis regulates homing capacity and tonic AKT activity in chronic lymphocytic leukemia. Blood, The Journal of the American Society of Hematology. 2021;138(9):758-72.
414. Lees J, Hay J, Moles MW, Michie AM. The discrete roles of individual FOXO transcription factor family members in B-cell malignancies. Frontiers in Immunology. 2023;14:2557.
415. Swatek KN, Komander D. Ubiquitin modifications. Cell research. 2016;26(4):399-422.
416. French ME, Koehler CF, Hunter T. Emerging functions of branched ubiquitin chains. Cell discovery. 2021;7(1):6.
417. D'Arcy P, Wang X, Linder S. Deubiquitinase inhibition as a cancer therapeutic strategy. Pharmacology & therapeutics. 2015;147:32-54.
418. Karin M, Ben-Neriah Y. Phosphorylation meets ubiquitination: the control of NF-κB activity. Annual review of immunology. 2000;18(1):621-63.
419. Jin J, He J, Li X, Xiaoqi N, Jin X. The role of ubiquitination and deubiquitination in PI3K/AKT/mTOR pathway: A potential target for cancer therapy. Gene. 2023:147807.
420. Sun X-X, Li Y, Sears RC, Dai M-S. Targeting the MYC ubiquitination-proteasome degradation pathway for cancer therapy. Frontiers in oncology. 2021;11:679445.
421. Dutta D, Sharma V, Mutsuddi M, Mukherjee A. Regulation of Notch signaling by E3 ubiquitin ligases. The FEBS journal. 2022;289(4):937-54.
422. Clague MJ, Urbé S, Komander D. Breaking the chains: deubiquitylating enzyme specificity begets function. Nature reviews Molecular cell biology. 2019;20(6):338-52.
423. Harrigan JA, Jacq X, Martin NM, Jackson SP. Deubiquitylating enzymes and drug discovery: emerging opportunities. Nature reviews Drug discovery. 2018;17(1):57-78.
424. Turnbull AP, Ioannidis S, Krajewski WW, Pinto-Fernandez A, Heride C, Martin AC, et al. Molecular basis of USP7 inhibition by selective small-molecule inhibitors. Nature. 2017;550(7677):481-6.
425. Dewson G, Eichhorn PJ, Komander D. Deubiquitinases in cancer. Nature Reviews Cancer. 2023;23(12):842-62.
426. Madiraju C, Novack JP, Reed JC, Matsuzawa S-i. K63 ubiquitination in immune signaling. Trends in Immunology. 2022;43(2):148-62.
427. Sun L, Chen ZJ. The novel functions of ubiquitination in signaling. Current opinion in cell biology. 2004;16(2):119-26.
428. Chen Y, Zhou D, Yao Y, Sun Y, Yao F, Ma L. Monoubiquitination in homeostasis and cancer. International journal of molecular sciences. 2022;23(11):5925.

429. Farshi P, Deshmukh RR, Nwankwo JO, Arkwright RT, Cvek B, Liu J, et al. Deubiquitinases (DUBs) and DUB inhibitors: a patent review. Expert opinion on therapeutic patents. 2015;25(10):1191-208.
430. Nguyen LK, Kolch W, Kholodenko BN. When ubiquitination meets phosphorylation: a systems biology perspective of EGFR/MAPK signalling. Cell Communication and Signaling. 2013;11:1-15.
431. Adams J. The proteasome: a suitable antineoplastic target. Nature Reviews Cancer. 2004;4(5):349-60.
432. Fhu CW, Ali A. Dysregulation of the ubiquitin proteasome system in human malignancies: a window for therapeutic intervention. Cancers. 2021;13(7):1513.
433. Lub S, Maes K, Menu E, De Bruyne E, Vanderkerken K, Van Valckenborgh E. Novel strategies to target the ubiquitin proteasome system in multiple myeloma. Oncotarget. 2016;7(6):6521.
434. Tanguturi P, Kim K-S, Ramakrishna S. The role of deubiquitinating enzymes in cancer drug resistance. Cancer chemotherapy and pharmacology. 2020;85(4):627-39.
435. Chauhan D, Catley L, Li G, Podar K, Hideshima T, Velankar M, et al. A novel orally active proteasome inhibitor induces apoptosis in multiple myeloma cells with mechanisms distinct from Bortezomib. Cancer cell. 2005;8(5):407-19.
436. Bonacci T, Emanuele MJ, editors. Dissenting degradation: Deubiquitinases in cell cycle and cancer. Seminars in cancer biology; 2020: Elsevier.
437. Reyes-Turcu FE, Ventii KH, Wilkinson KD. Regulation and cellular roles of ubiquitin-specific deubiquitinating enzymes. Annual review of biochemistry. 2009;78(1):363-97.
438. Nakagawa T, Kajitani T, Togo S, Masuko N, Ohdan H, Hishikawa Y, et al. Deubiquitylation of histone H2A activates transcriptional initiation via trans-histone cross-talk with H3K4 di-and trimethylation. Genes & development. 2008;22(1):37-49.
439. Wang Y, Wang F. Post-translational modifications of deubiquitinating enzymes: expanding the ubiquitin code. Frontiers in pharmacology. 2021;12:685011.
440. Das T, Shin SC, Song EJ, Kim EE. Regulation of deubiquitinating enzymes by post-translational modifications. International journal of molecular sciences. 2020;21(11):4028.
441. Jiang S, Wang X, He Y, Huang H, Cao B, Zhang Z, et al. Suppression of USP7 induces BCR-ABL degradation and chronic myelogenous leukemia cell apoptosis. Cell Death & Disease. 2021;12(5):456.
442. Cartel M, Mouchel P-L, Gotanègre M, David L, Bertoli S, Mansat-De Mas V, et al. Inhibition of ubiquitin-specific protease 7 sensitizes acute myeloid leukemia to chemotherapy. Leukemia. 2021;35(2):417-32.
443. Druker BJ. Translation of the Philadelphia chromosome into therapy for CML. Blood, The Journal of the American Society of Hematology. 2008;112(13):4808-17.
444. Cilloni D, Saglio G. Molecular pathways: Bcr-abl. Clinical Cancer Research. 2012;18(4):930-7.
445. David L, Fernandez-Vidal A, Bertoli S, Grgurevic S, Lepage B, Deshaies D, et al. CHK1 as a therapeutic target to bypass chemoresistance in AML. Science signaling. 2016;9(445):ra90-ra.
446. Neizer-Ashun F, Bhattacharya R. Reality CHEK: Understanding the biology and clinical potential of CHK1. Cancer letters. 2021;497:202-11.
447. Schauer NJ, Liu X, Magin RS, Doherty LM, Chan WC, Ficarro SB, et al. Selective USP7 inhibition elicits cancer cell killing through a p53-dependent mechanism. Scientific reports. 2020;10(1):5324.
448. Liu Y, Xu J, Wang Y, Gan M, Hu Q, Wang J, et al. USP14 regulates cell cycle progression through deubiquitinating CDK1 in breast cancer: USP14 deubiquitinates CDK1 in breast cancer. Acta biochimica et biophysica Sinica. 2022;54(11):1610.
449. Wang Z, Kang W, You Y, Pang J, Ren H, Suo Z, et al. USP7: novel drug target in cancer therapy. Frontiers in Pharmacology. 2019;10:427.
450. Li Z, Cheng Z, Raghothama C, Cui Z, Liu K, Li X, et al. USP9X controls translation efficiency via deubiquitination of eukaryotic translation initiation factor 4A1. Nucleic acids research. 2018;46(2):823-39.

451. Zhang J, Zhang D, Sun L. Knockdown of ubiquitin-specific protease 14 (USP14) inhibits the proliferation and tumorigenesis in esophageal squamous cell carcinoma cells. Oncology research. 2017;25(2):249.
452. Hsieh AC, Liu Y, Edlind MP, Ingolia NT, Janes MR, Sher A, et al. The translational landscape of mTOR signalling steers cancer initiation and metastasis. Nature. 2012;485(7396):55-61.
453. Zou Z, Tao T, Li H, Zhu X. mTOR signaling pathway and mTOR inhibitors in cancer: progress and challenges. Cell & bioscience. 2020;10(1):31.
454. Porta C, Paglino C, Mosca A. Targeting PI3K/Akt/mTOR signaling in cancer. Frontiers in oncology. 2014;4:64.
455. Wrobel L, Siddiqi FH, Hill SM, Son SM, Karabiyik C, Kim H, et al. mTORC2 assembly is regulated by USP9X-mediated deubiquitination of RICTOR. Cell Reports. 2020;33(13).
456. Kuang X, Xiong J, Lu T, Wang W, Zhang Z, Wang J. Inhibition of USP1 induces apoptosis via ID1/AKT pathway in B-cell acute lymphoblastic leukemia cells. International Journal of Medical Sciences. 2021;18(1):245.
457. Das DS, Das A, Ray A, Song Y, Samur MK, Munshi NC, et al. Blockade of deubiquitylating enzyme USP1 inhibits DNA repair and triggers apoptosis in multiple myeloma cells. Clinical Cancer Research. 2017;23(15):4280-9.
458. Davis MI, Pragani R, Fox JT, Shen M, Parmar K, Gaudiano EF, et al. Small molecule inhibition of the ubiquitin-specific protease USP2 accelerates cyclin D1 degradation and leads to cell cycle arrest in colorectal cancer and mantle cell lymphoma models. Journal of Biological Chemistry. 2016;291(47):24628-40.
459. Agathanggelou A, Smith E, Davies NJ, Kwok M, Zlatanou A, Oldreive CE, et al. USP7 inhibition alters homologous recombination repair and targets CLL cells independently of ATM/p53 functional status. Blood, The Journal of the American Society of Hematology. 2017;130(2):156-66.
460. Carrà G, Panuzzo C, Torti D, Parvis G, Crivellaro S, Familiari U, et al. Therapeutic inhibition of USP7-PTEN network in chronic lymphocytic leukemia: a strategy to overcome TP53 mutated/deleted clones. Oncotarget. 2017;8(22):35508.
461. He Y, Wang S, Tong J, Jiang S, Yang Y, Zhang Z, et al. The deubiquitinase USP7 stabilizes Maf proteins to promote myeloma cell survival. Journal of Biological Chemistry. 2020;295(7):2084-96.
462. Chauhan D, Tian Z, Nicholson B, Kumar KS, Zhou B, Carrasco R, et al. A small molecule inhibitor of ubiquitin-specific protease-7 induces apoptosis in multiple myeloma cells and overcomes bortezomib resistance. Cancer cell. 2012;22(3):345-58.
463. Gavory G, O'Dowd CR, Helm MD, Flasz J, Arkoudis E, Dossang A, et al. Discovery and characterization of highly potent and selective allosteric USP7 inhibitors. Nature chemical biology. 2018;14(2):118-25.
464. Peterson LF, Sun H, Liu Y, Potu H, Kandarpa M, Ermann M, et al. Targeting deubiquitinase activity with a novel small-molecule inhibitor as therapy for B-cell malignancies. Blood, The Journal of the American Society of Hematology. 2015;125(23):3588-97.
465. Pham LV, Tamayo AT, Li C, Bornmann W, Priebe W, Ford RJ. Degrasyn potentiates the antitumor effects of bortezomib in mantle cell lymphoma cells in vitro and in vivo: therapeutic implications. Molecular cancer therapeutics. 2010;9(7):2026-36.
466. Wang X, Mazurkiewicz M, Hillert E-K, Olofsson MH, Pierrou S, Hillertz P, et al. The proteasome deubiquitinase inhibitor VLX1570 shows selectivity for ubiquitin-specific protease-14 and induces apoptosis of multiple myeloma cells. Scientific reports. 2016;6(1):1-15.
467. Tian Z, D'Arcy P, Wang X, Ray A, Tai Y-T, Hu Y, et al. A novel small molecule inhibitor of deubiquitylating enzyme USP14 and UCHL5 induces apoptosis in multiple myeloma and overcomes bortezomib resistance. Blood, The Journal of the American Society of Hematology. 2014;123(5):706-16.
468. Jiang L, Sun Y, Wang J, He Q, Chen X, Lan X, et al. Proteasomal cysteine deubiquitinase inhibitor b-AP15 suppresses migration and induces apoptosis in diffuse large B cell lymphoma. Journal of Experimental & Clinical Cancer Research. 2019;38(1):1-14.
469. Kropp KN, Maurer S, Rothfelder K, Schmied BJ, Clar KL, Schmidt M, et al. The novel deubiquitinase inhibitor b-AP15 induces direct and NK cell-mediated antitumor effects in human mantle cell lymphoma. Cancer immunology, immunotherapy. 2018;67:935-47.

470. LaPlante G, Zhang W. Targeting the ubiquitin-proteasome system for cancer therapeutics by small-molecule inhibitors. Cancers. 2021;13(12):3079.
471. Lei H, Wang J, Hu J, Zhu Q, Wu Y. Deubiquitinases in hematological malignancies. Biomarker Research. 2021;9(1):66.
472. Lv X-Y, Duan T, Li J. The multiple roles of deubiquitinases in liver cancer. American Journal of Cancer Research. 2020;10(6):1647.
473. Ozaki T, Nakagawara A. Role of p53 in cell death and human cancers. Cancers. 2011;3(1):994-1013.
474. Jacq X, Kemp M, Martin NM, Jackson SP. Deubiquitylating enzymes and DNA damage response pathways. Cell biochemistry and biophysics. 2013;67(1):25-43.
475. Rowinsky EK, Paner A, Berdeja JG, Paba-Prada C, Venugopal P, Porkka K, et al. Phase 1 study of the protein deubiquitinase inhibitor VLX1570 in patients with relapsed and/or refractory multiple myeloma. Investigational new drugs. 2020;38:1448-53.
476. Zhao C, Feng Y, Zhou Y, Li N, Zhao L. Artesunate attenuates osteoarthritis in mice by promoting MTA1 transcription through a USP7/FoxO1 axis. Toxicology and Applied Pharmacology. 2024:117075.
477. Hall JA, Tabata M, Rodgers JT, Puigserver P. USP7 attenuates hepatic gluconeogenesis through modulation of FoxO1 gene promoter occupancy. Molecular endocrinology. 2014;28(6):912-24.
478. Gao L, Zhu D, Wang Q, Bao Z, Yin S, Qiang H, et al. Proteome analysis of USP7 substrates revealed its role in melanoma through PI3K/Akt/FOXO and AMPK pathways. Frontiers in Oncology. 2021;11:650165.
479. Bridges CR, Tan M-C, Premarathne S, Nanayakkara D, Bellette B, Zencak D, et al. USP9X deubiquitylating enzyme maintains RAPTOR protein levels, mTORC1 signalling and proliferation in neural progenitors. Scientific reports. 2017;7(1):391.
480. Agrawal P, Chen Y-T, Schilling B, Gibson BW, Hughes RE. Ubiquitin-specific peptidase 9, X-linked (USP9X) modulates activity of mammalian target of rapamycin (mTOR). Journal of Biological Chemistry. 2012;287(25):21164-75.
481. Hay J, Tarafdar A, Holroyd AK, Moka HA, Dunn KM, Alshayeb A, et al. PKCβ facilitates Leukemogenesis in Chronic Lymphocytic Leukaemia by promoting constitutive BCR-mediated signalling. Cancers. 2022;14(23):6006.
482. Naik E, Dixit VM. Usp9X is required for lymphocyte activation and homeostasis through its control of ZAP70 ubiquitination and PKCβ kinase activity. The Journal of Immunology. 2016;196(8):3438-51.
483. Malik N, Hay J, Almuhanna HN, Dunn KM, Lees J, Cassels J, et al. mTORC1-selective activation of translation elongation promotes disease progression in chronic lymphocytic leukemia. Leukemia. 2023;37(12):2414-25.
484. Hay J, Moles MW, Cassels J, Michie AM. Subcellular fractionation of primary chronic lymphocytic leukemia cells to monitor nuclear/cytoplasmic protein trafficking. JoVE (Journal of Visualized Experiments). 2019(152):e60426.
485. DSMZ. MEC1 (ACC 497): German Collection of Microorganisms and Cell Culture; 2022 [Available from: https://www.dsmz.de/collection/catalogue/details/culture/ACC-497.
486. Rasul E, Salamon D, Nagy N, Leveau B, Banati F, Szenthe K, et al. The MEC1 and MEC2 lines represent two CLL subclones in different stages of progression towards prolymphocytic leukemia. PloS one. 2014;9(8):e106008.
487. Stacchini A, Aragno M, Vallario A, Alfarano A, Circosta P, Gottardi D, et al. MEC1 and MEC2: two new cell lines derived from B-chronic lymphocytic leukaemia in prolymphocytoid transformation. Leukemia research. 1999;23(2):127-36.
488. DSMZ. HG-3 (ACC 765): German Collection of Microorganisms and Cell Culture; 2022 [Available from: https://www.dsmz.de/collection/catalogue/details/culture/ACC-765.
489. Rosén A, Bergh A-C, Gogok P, Evaldsson C, Myhrinder AL, Hellqvist E, et al. Lymphoblastoid cell line with B1 cell characteristics established from a chronic lymphocytic leukemia clone by in vitro EBV infection. Oncoimmunology. 2012;1(1):18-27.

490. DSMZ. 293 (ACC 305): German Collection of Microorganisms and Cell Culture; 2022 [Available from: https://www.dsmz.de/collection/catalogue/details/culture/ACC-305.
491. Byrd JC, Brown JR, O'Brien S, Barrientos JC, Kay NE, Reddy NM, et al. Ibrutinib versus ofatumumab in previously treated chronic lymphoid leukemia. New England Journal of Medicine. 2014;371(3):213-23.
492. Reverdy C, Conrath S, Lopez R, Planquette C, Atmanene C, Collura V, et al. Discovery of specific inhibitors of human USP7/HAUSP deubiquitinating enzyme. Chemistry & biology. 2012;19(4):467-77.
493. Altun M, Kramer HB, Willems LI, McDermott JL, Leach CA, Goldenberg SJ, et al. Activity-based chemical proteomics accelerates inhibitor development for deubiquitylating enzymes. Chemistry & biology. 2011;18(11):1401-12.
494. Kapuria V, Peterson LF, Fang D, Bornmann WG, Talpaz M, Donato NJ. Deubiquitinase inhibition by small-molecule WP1130 triggers aggresome formation and tumor cell apoptosis. Cancer research. 2010;70(22):9265-76.
495. BD Biosciences. Annexin V Staining Protocol 2024 [Available from: https://www.bdbiosciences.com/en-gb/resources/protocols/annexin-v-staining-protocol.
496. Filby A, Begum J, Jalal M, Day W. Appraising the suitability of succinimidyl and lipophilic fluorescent dyes to track proliferation in non-quiescent cells by dye dilution. Methods. 2015;82:29-37.
497. ThermoFisher Scientific. CellTrace™ Violet Cell Proliferation Kit, for flow cytometry 2024 [Available from: https://www.thermofisher.com/order/catalog/product/C34557.
498. Taxman DJ, Moore CB, Guthrie EH, Huang MT-H. Short hairpin RNA (shRNA): design, delivery, and assessment of gene knockdown. RNA Therapeutics: Function, Design, and Delivery. 2010:139-56.
499. Sigma. Vector Maps 2024 [Available from: https://www.sigmaaldrich.com/GB/en/technical-documents/technical-article/genomics/gene-expression-and-silencing/vector-map.
500. addgene. pLKO.1 - TRC Cloning Vector 2024 [Available from: https://www.addgene.org/protocols/plko/.
501. Cilloni D, Panuzzo C, Messa F, Arruga F, Nicoli P, Messa E, et al. FoxO transcription factor is delocalized and inactivated in acute myeloid leukaemia patients. American Society of Hematology; 2007.
502. Burger JA, Tedeschi A, Barr PM, Robak T, Owen C, Ghia P, et al. Ibrutinib as initial therapy for patients with chronic lymphocytic leukemia. New England Journal of Medicine. 2015;373(25):2425-37.
503. Furman RR, Sharman JP, Coutre SE, Cheson BD, Pagel JM, Hillmen P, et al. Idelalisib and rituximab in relapsed chronic lymphocytic leukemia. New England Journal of Medicine. 2014;370(11):997-1007.
504. Thijssen R, Geest CR, de Rooij MF, Liu N, Florea BI, Weller K, et al. Possible mechanisms of resistance to the novel BH3-mimetic ABT-199 in in vitro lymph node models of CLL–the role of Abl and Btk. American Society of Hematology Washington, DC; 2013.
505. Dreger P, Schetelig J, Andersen N, Corradini P, Van Gelder M, Gribben J, et al. Managing high-risk CLL during transition to a new treatment era: stem cell transplantation or novel agents? Blood, The Journal of the American Society of Hematology. 2014;124(26):3841-9.
506. Sharma S, Rai KR. Chronic lymphocytic leukemia (CLL) treatment: So many choices, such great options. Cancer. 2019;125(9):1432-40.
507. Zou Z-J, Fan L, Wang L, Xu J, Zhang R, Tian T, et al. miR-26a and miR-214 down-regulate expression of the PTEN gene in chronic lymphocytic leukemia, but not PTEN mutation or promoter methylation. Oncotarget. 2015;6(2):1276.
508. Krysov S, Potter KN, Mockridge CI, Coelho V, Wheatley I, Packham G, et al. Surface IgM of CLL cells displays unusual glycans indicative of engagement of antigen in vivo. Blood, The Journal of the American Society of Hematology. 2010;115(21):4198-205.

509. Messmer BT, Messmer D, Allen SL, Kolitz JE, Kudalkar P, Cesar D, et al. In vivo measurements document the dynamic cellular kinetics of chronic lymphocytic leukemia B cells. The Journal of clinical investigation. 2005;115(3):755-64.
510. Farhan M, Wang H, Gaur U, Little PJ, Xu J, Zheng W. FOXO signaling pathways as therapeutic targets in cancer. International journal of biological sciences. 2017;13(7):815.
511. Maltzman JS, Carman JA, Monroe JG. Role of EGR1 in regulation of stimulus-dependent CD44 transcription in B lymphocytes. Molecular and cellular biology. 1996.
512. Gururajan M, Simmons A, Dasu T, Spear BT, Calulot C, Robertson DA, et al. Early growth response genes regulate B cell development, proliferation, and immune response. The Journal of Immunology. 2008;181(7):4590-602.
513. Moriyama H, Yonehara S. Rapid up-regulation of c-FLIP expression by BCR signaling through the PI3K/Akt pathway inhibits simultaneously induced Fas-mediated apoptosis in murine B lymphocytes. Immunology letters. 2007;109(1):36-46.
514. Xing Y-q, Li A, Yang Y, Li X-x, Zhang L-n, Guo H-c. The regulation of FOXO1 and its role in disease progression. Life sciences. 2018;193:124-31.
515. Meyer C, Lopes BA, Caye-Eude A, Cavé H, Arfeuille C, Cuccuini W, et al. Human MLL/KMT2A gene exhibits a second breakpoint cluster region for recurrent MLL–USP2 fusions. Leukemia. 2019;33(9):2306-40.
516. Yu M, Fang Z-x, Wang W-w, Zhang Y, Bu Z-l, Liu M, et al. Wu-5, a novel USP10 inhibitor, enhances crenolanib-induced FLT3-ITD-positive AML cell death via inhibiting FLT3 and AMPK pathways. Acta pharmacologica Sinica. 2021;42(4):604-12.
517. Zhang H, Huang H, Feng X, Song H, Zhang Z, Shen A, et al. Deubiquitinase USP28 inhibits ubiquitin ligase KLHL2-mediated uridine-cytidine kinase 1 degradation and confers sensitivity to 5'-azacytidine-resistant human leukemia cells. Theranostics. 2020;10(3):1046.
518. Szklarczyk D, Gable AL, Nastou KC, Lyon D, Kirsch R, Pyysalo S, et al. The STRING database in 2021: customizable protein–protein networks, and functional characterization of user-uploaded gene/measurement sets. Nucleic acids research. 2021;49(D1):D605-D12.
519. Guttilla IK, White BA. Coordinate regulation of FOXO1 by miR-27a, miR-96, and miR-182 in breast cancer cells. Journal of Biological Chemistry. 2009;284(35):23204-16.
520. Bartel DP. MicroRNAs: target recognition and regulatory functions. cell. 2009;136(2):215-33.
521. Rossi S, Shimizu M, Barbarotto E, Nicoloso MS, Dimitri F, Sampath D, et al. microRNA fingerprinting of CLL patients with chromosome 17p deletion identify a miR-21 score that stratifies early survival. Blood, The Journal of the American Society of Hematology. 2010;116(6):945-52.
522. Le HH, Cinaroglu SS, Manalo EC, Ors A, Gomes MM, Sahbaz BD, et al. Molecular modelling of the FOXO4-TP53 interaction to design senolytic peptides for the elimination of senescent cancer cells. EBioMedicine. 2021;73.
523. Pepper C, Lin TT, Pratt G, Hewamana S, Brennan P, Hiller L, et al. Mcl-1 expression has in vitro and in vivo significance in chronic lymphocytic leukemia and is associated with other poor prognostic markers. Blood, The Journal of the American Society of Hematology. 2008;112(9):3807-17.
524. Smit LA, Hallaert DY, Spijker R, de Goeij B, Jaspers A, Kater AP, et al. Differential Noxa/Mcl-1 balance in peripheral versus lymph node chronic lymphocytic leukemia cells correlates with survival capacity. Blood. 2007;109(4):1660-8.
525. LeBien TW, Tedder TF. B lymphocytes: how they develop and function. Blood, The Journal of the American Society of Hematology. 2008;112(5):1570-80.
526. Efremov DG, Wiestner A, Laurenti L. Novel agents and emerging strategies for targeting the B-cell receptor pathway in CLL. Mediterranean Journal of Hematology and Infectious Diseases. 2012;4(1).
527. Davis RE, Ngo VN, Lenz G, Tolar P, Young RM, Romesser PB, et al. Chronic active B-cell-receptor signalling in diffuse large B-cell lymphoma. Nature. 2010;463(7277):88-92.
528. Thompson AA, Talley JA, Do HN, Kagan HL, Kunkel L, Berenson J, et al. Aberrations of the B-cell receptor B29 (CD79b) gene in chronic lymphocytic leukemia. Blood, The Journal of the American Society of Hematology. 1997;90(4):1387-94.

529. Myers DR, Zikherman J, Roose JP. Tonic signals: why do lymphocytes bother? Trends in immunology. 2017;38(11):844-57.
530. Rassenti LZ, Huynh L, Toy TL, Chen L, Keating MJ, Gribben JG, et al. ZAP-70 compared with immunoglobulin heavy-chain gene mutation status as a predictor of disease progression in chronic lymphocytic leukemia. New England Journal of Medicine. 2004;351(9):893-901.
531. Schmitz R, Young RM, Ceribelli M, Jhavar S, Xiao W, Zhang M, et al. Burkitt lymphoma pathogenesis and therapeutic targets from structural and functional genomics. Nature. 2012;490(7418):116-20.
532. Sander S, Calado DP, Srinivasan L, Köchert K, Zhang B, Rosolowski M, et al. Synergy between PI3K signaling and MYC in Burkitt lymphomagenesis. Cancer cell. 2012;22(2):167-79.
533. Coqueret O. New roles for p21 and p27 cell-cycle inhibitors: a function for each cell compartment? Trends in cell biology. 2003;13(2):65-70.
534. Seoane J, Le H-V, Shen L, Anderson SA, Massagué J. Integration of Smad and forkhead pathways in the control of neuroepithelial and glioblastoma cell proliferation. Cell. 2004;117(2):211-23.
535. Boreddy SR, Pramanik KC, Srivastava SK. Pancreatic tumor suppression by benzyl isothiocyanate is associated with inhibition of PI3K/AKT/FOXO pathway. Clinical Cancer Research. 2011;17(7):1784-95.
536. Zhou BP, Liao Y, Xia W, Spohn B, Lee M-H, Hung M-C. Cytoplasmic localization of p21Cip1/WAF1 by Akt-induced phosphorylation in HER-2/neu-overexpressing cells. Nature cell biology. 2001;3(3):245-52.
537. Wu M, Bellas RE, Shen J, Sonenshein GE. Roles of the tumor suppressor p53 and the cyclin-dependent kinase inhibitor p21WAF1/CIP1 in receptor-mediated apoptosis of WEHI 231 B lymphoma cells. The Journal of experimental medicine. 1998;187(10):1671-9.
538. Glassford J, Soeiro Is, Skarell SM, Banerji L, Holman M, Klaus GG, et al. BCR targets cyclin D2 via Btk and the p85α subunit of PI3-K to induce cell cycle progression in primary mouse B cells. Oncogene. 2003;22(15):2248-59.
539. Carnero A, Blanco-Aparicio C, Renner O, Link W, Leal JF. The PTEN/PI3K/AKT signalling pathway in cancer, therapeutic implications. Current cancer drug targets. 2008;8(3):187-98.
540. Cancer, Research, UK. First treatment for chronic lymphocytic leukaemia (CLL): Cancer Research UK; 2023 [Available from: https://www.cancerresearchuk.org/about-cancer/chronic-lymphocytic-leukaemia-cll/treatment/first-treatment.
541. Advani RH, Buggy JJ, Sharman JP, Smith SM, Boyd TE, Grant B, et al. Bruton tyrosine kinase inhibitor ibrutinib (PCI-32765) has significant activity in patients with relapsed/refractory B-cell malignancies. Journal of Clinical Oncology. 2013;31(1):88.
542. Kapoor I, Li Y, Sharma A, Zhu H, Bodo J, Xu W, et al. Resistance to BTK inhibition by ibrutinib can be overcome by preventing FOXO3a nuclear export and PI3K/AKT activation in B-cell lymphoid malignancies. Cell death & disease. 2019;10(12):924.
543. Nakamura N, Ramaswamy S, Vazquez F, Signoretti S, Loda M, Sellers WR. Forkhead transcription factors are critical effectors of cell death and cell cycle arrest downstream of PTEN. Molecular and cellular biology. 2000;20(23):8969-82.
544. Fraile J, Quesada V, Rodríguez D, Freije J, López-Otín C. Deubiquitinases in cancer: new functions and therapeutic options. Oncogene. 2012;31(19):2373-88.
545. Schwickart M, Huang X, Lill JR, Liu J, Ferrando R, French DM, et al. Deubiquitinase USP9X stabilizes MCL1 and promotes tumour cell survival. Nature. 2010;463(7277):103-7.
546. Liu Y, Xu X, Lin P, He Y, Zhang Y, Cao B, et al. Inhibition of the deubiquitinase USP9x induces pre-B cell homeobox 1 (PBX1) degradation and thereby stimulates prostate cancer cell apoptosis. Journal of Biological Chemistry. 2019;294(12):4572-82.
547. Hu H-J, Zhang L-G, Wang Z-H, Guo X-X. FoxO6 inhibits cell proliferation in lung carcinoma through up-regulation of USP7. Molecular medicine reports. 2015;12(1):575-80.
548. Naik E, Webster JD, DeVoss J, Liu J, Suriben R, Dixit VM. Regulation of proximal T cell receptor signaling and tolerance induction by deubiquitinase Usp9X. Journal of experimental medicine. 2014;211(10):1947-55.

549. Paulus A, Akhtar S, Caulfield T, Samuel K, Yousaf H, Bashir Y, et al. Coinhibition of the deubiquitinating enzymes, USP14 and UCHL5, with VLX1570 is lethal to ibrutinib-or bortezomib-resistant Waldenstrom macroglobulinemia tumor cells. Blood cancer journal. 2016;6(11):e492-e.
550. Yang J, Meng C, Weisberg E, Case A, Lamberto I, Magin RS, et al. Inhibition of the deubiquitinase USP10 induces degradation of SYK. British Journal of Cancer. 2020;122(8):1175-84.
551. Xu X, Liu J, Shen C, Ding L, Zhong F, Ouyang Y, et al. The role of ubiquitin-specific protease 14 (USP 14) in cell adhesion-mediated drug resistance (CAM-DR) of multiple myeloma cells. European journal of haematology. 2017;98(1):4-12.
552. Mistry H, Hsieh G, Buhrlage SJ, Huang M, Park E, Cuny GD, et al. Small-molecule inhibitors of USP1 target ID1 degradation in leukemic cells. Molecular cancer therapeutics. 2013;12(12):2651-62.
553. Mao H, Wang M, Cao B, Zhou H, Zhang Z, Mao X. Interferon-stimulated gene 15 induces cancer cell death by suppressing the NF-κB signaling pathway. Oncotarget. 2016;7(43):70143.
554. Mehra A, Lee KH, Hatzimanikatis V. Insights into the relation between mRNA and protein expression patterns: I. Theoretical considerations. Biotechnology and bioengineering. 2003;84(7):822-33.
555. Buccitelli C, Selbach M. mRNAs, proteins and the emerging principles of gene expression control. Nature Reviews Genetics. 2020;21(10):630-44.
556. Mauger DM, Cabral BJ, Presnyak V, Su SV, Reid DW, Goodman B, et al. mRNA structure regulates protein expression through changes in functional half-life. Proceedings of the National Academy of Sciences. 2019;116(48):24075-83.
557. Luo H, Jing B, Xia Y, Zhang Y, Hu M, Cai H, et al. WP1130 reveals USP24 as a novel target in T-cell acute lymphoblastic leukemia. Cancer cell international. 2019;19(1):1-14.
558. Lin W-C, Chiu Y-L, Kuo K-L, Chow P-M, Hsu C-H, Liao S-M, et al. Anti-tumor effects of deubiquitinating enzyme inhibitor PR-619 in human chondrosarcoma through reduced cell proliferation and endoplasmic reticulum stress-related apoptosis. American Journal of Cancer Research. 2023;13(7):3055.
559. Zelenetz AD, Gordon LI, Wierda WG, Abramson JS, Advani RH, Andreadis CB, et al. Chronic lymphocytic leukemia/small lymphocytic lymphoma, version 1.2015. Journal of the National Comprehensive Cancer Network. 2015;13(3):326-62.
560. St-Pierre F, Ma S. Use of BTK inhibitors in chronic lymphocytic leukemia/small lymphocytic lymphoma (CLL/SLL): a practical guidance. Blood and Lymphatic Cancer: Targets and Therapy. 2022:81-98.
561. Eichhorst B, Ghia P, Committee EG. EHA endorsement of ESMO Clinical Practice Guidelines for diagnosis, treatment, and follow-up of chronic lymphocytic leukemia. LWW; 2021. p. e520.
562. Kojima K, Burger JA. Treatment algorithm for Japanese patients with chronic lymphocytic leukemia in the era of novel targeted therapies. Journal of clinical and experimental hematopathology. 2020;60(4):130-7.
563. Tam CS, Trotman J, Opat S, Burger JA, Cull G, Gottlieb D, et al. Phase 1 study of the selective BTK inhibitor zanubrutinib in B-cell malignancies and safety and efficacy evaluation in CLL. Blood, The Journal of the American Society of Hematology. 2019;134(11):851-9.
564. van Loosdregt J, Fleskens V, Fu J, Brenkman AB, Bekker CP, Pals CE, et al. Stabilization of the transcription factor Foxp3 by the deubiquitinase USP7 increases Treg-cell-suppressive capacity. Immunity. 2013;39(2):259-71.
565. Sheng Y, Saridakis V, Sarkari F, Duan S, Wu T, Arrowsmith CH, et al. Molecular recognition of p53 and MDM2 by USP7/HAUSP. Nature structural & molecular biology. 2006;13(3):285-91.
566. Lu C, Ning Z, Wang A, Chen D, Liu X, Xia T, et al. USP10 suppresses tumor progression by inhibiting mTOR activation in hepatocellular carcinoma. Cancer letters. 2018;436:139-48.
567. Zhao X, Gan L, Pan H, Kan D, Majeski M, Adam SA, et al. Multiple elements regulate nuclear/cytoplasmic shuttling of FOXO1: characterization of phosphorylation-and 14-3-3-dependent and-independent mechanisms. Biochemical Journal. 2004;378(3):839-49.
568. Oh H-M, Yu C-R, Dambuza I, Marrero B, Egwuagu CE. STAT3 protein interacts with Class O Forkhead transcription factors in the cytoplasm and regulates nuclear/cytoplasmic localization of

FoxO1 and FoxO3a proteins in CD4+ T cells. Journal of Biological Chemistry. 2012;287(36):30436-43.
569. Carracedo A, Pandolfi P. The PTEN–PI3K pathway: of feedbacks and cross-talks. Oncogene. 2008;27(41):5527-41.
570. Luo W, Hawse W, Conter L, Trivedi N, Weisel F, Wikenheiser D, et al. The AKT kinase signaling network is rewired by PTEN to control proximal BCR signaling in germinal center B cells. Nature immunology. 2019;20(6):736-46.
571. Stahl M, Dijkers PF, Kops GJ, Lens S, Coffer PJ, Burgering BM, et al. The forkhead transcription factor FoxO regulates transcription of p27Kip1 and Bim in response to IL-2. The Journal of Immunology. 2002;168(10):5024-31.
572. Wu L, Li H, Jia CY, Cheng W, Yu M, Peng M, et al. MicroRNA-223 regulates FOXO1 expression and cell proliferation. FEBS letters. 2012;586(7):1038-43.
573. Chan C-H, Li C-F, Yang W-L, Gao Y, Lee S-W, Feng Z, et al. The Skp2-SCF E3 ligase regulates Akt ubiquitination, glycolysis, herceptin sensitivity, and tumorigenesis. Cell. 2012;149(5):1098-111.
574. Gilley J, Coffer PJ, Ham J. FOXO transcription factors directly activate bim gene expression and promote apoptosis in sympathetic neurons. The Journal of cell biology. 2003;162(4):613-22.
575. Yan J, Zhou L, Liu M, Zhu H, Zhang X, Cai E, et al. Single-cell analysis reveals insights into epithelial abnormalities in ovarian endometriosis. Cell Reports. 2024;43(3).
576. Song X, Yang W, Wu C, Han Y, Lu Y. USP9X promotes the proliferation, invasion and metastasis of liver cancer cells through regulating the JAK2/STAT3 signaling. Oncology Letters. 2020;20(3):2897-905.
577. Chen Z, Yan X, Miao C, Liu L, Liu S, Xia Y, et al. Targeting MYH9 represses USP14-mediated NAP1L1 deubiquitination and cell proliferation in glioma. Cancer Cell International. 2023;23(1):220.
578. Jia Y, Jin H, Gao L, Yang X, Wang F, Ding H, et al. A novel lncRNA PLK4 up-regulated by talazoparib represses hepatocellular carcinoma progression by promoting YAP-mediated cell senescence. Journal of Cellular and Molecular Medicine. 2020;24(9):5304-16.
579. Luo W, Weisel F, Shlomchik MJ. B cell receptor and CD40 signaling are rewired for synergistic induction of the c-Myc transcription factor in germinal center B cells. Immunity. 2018;48(2):313-26. e5.
580. Gross D, Van Den Heuvel A, Birnbaum M. The role of FoxO in the regulation of metabolism. Oncogene. 2008;27(16):2320-36.
581. Roy SK, Srivastava RK, Shankar S. Inhibition of PI3K/AKT and MAPK/ERK pathways causes activation of FOXO transcription factor, leading to cell cycle arrest and apoptosis in pancreatic cancer. Journal of molecular signaling. 2010;5:1-13.
582. Hagenbuchner J, Kuznetsov A, Hermann M, Hausott B, Obexer P, Ausserlechner MJ. FOXO3-induced reactive oxygen species are regulated by BCL2L11 (Bim) and SESN3. Journal of cell science. 2012;125(5):1191-203.
583. Li J, Wang R, Jin J, Han M, Chen Z, Gao Y, et al. USP7 negatively controls global DNA methylation by attenuating ubiquitinated histone-dependent DNMT1 recruitment. Cell discovery. 2020;6(1):58.
584. Meroni G, Diez-Roux G. TRIM/RBCC, a novel class of 'single protein RING finger'E3 ubiquitin ligases. Bioessays. 2005;27(11):1147-57.
585. Esposito D, Koliopoulos MG, Rittinger K. Structural determinants of TRIM protein function. Biochemical Society Transactions. 2017;45(1):183-91.
586. Ozato K, Shin D-M, Chang T-H, Morse III HC. TRIM family proteins and their emerging roles in innate immunity. Nature reviews immunology. 2008;8(11):849-60.
587. Short KM, Cox TC. Subclassification of the RBCC/TRIM superfamily reveals a novel motif necessary for microtubule binding. Journal of Biological Chemistry. 2006;281(13):8970-80.
588. Sabile A, Meyer AM, Wirbelauer C, Hess D, Kogel U, Scheffner M, et al. Regulation of p27 degradation and S-phase progression by Ro52 RING finger protein. Molecular and cellular biology. 2006;26(16):5994-6004.
589. Barr SD, Smiley JR, Bushman FD. The interferon response inhibits HIV particle production by induction of TRIM22. PLoS pathogens. 2008;4(2):e1000007.

590. Jauharoh SNA, Saegusa J, Sugimoto T, Ardianto B, Kasagi S, Sugiyama D, et al. SS-A/Ro52 promotes apoptosis by regulating Bcl-2 production. Biochemical and biophysical research communications. 2012;417(1):582-7.
591. Yang Y-S, Yang M-CW, Wang B, Weissler JC. Autoantigen Ro52 directly interacts with human IgG heavy chain in vivo in mammalian cells. Molecular immunology. 2000;37(10):591-602.
592. James LC, Keeble AH, Khan Z, Rhodes DA, Trowsdale J. Structural basis for PRYSPRY-mediated tripartite motif (TRIM) protein function. Proceedings of the National Academy of Sciences. 2007;104(15):6200-5.
593. Mallery DL, McEwan WA, Bidgood SR, Towers GJ, Johnson CM, James LC. Antibodies mediate intracellular immunity through tripartite motif-containing 21 (TRIM21). Proceedings of the National Academy of Sciences. 2010;107(46):19985-90.
594. Espinosa A, Dardalhon V, Brauner S, Ambrosi A, Higgs R, Quintana FJ, et al. Loss of the lupus autoantigen Ro52/Trim21 induces tissue inflammation and systemic autoimmunity by disregulating the IL-23–Th17 pathway. Journal of experimental medicine. 2009;206(8):1661-71.
595. Yang K, Shi H-X, Liu X-Y, Shan Y-F, Wei B, Chen S, et al. TRIM21 is essential to sustain IFN regulatory factor 3 activation during antiviral response. The journal of immunology. 2009;182(6):3782-92.
596. Lazzari E, Korczeniewska J, Ní Gabhann J, Smith S, Barnes BJ, Jefferies CA. TRIpartite motif 21 (TRIM21) differentially regulates the stability of interferon regulatory factor 5 (IRF5) isoforms. PloS one. 2014;9(8):e103609.
597. McEwan WA, Tam JC, Watkinson RE, Bidgood SR, Mallery DL, James LC. Intracellular antibody-bound pathogens stimulate immune signaling via the Fc receptor TRIM21. Nature immunology. 2013;14(4):327-36.
598. Wada K, Niida M, Tanaka M, Kamitani T. Ro52-mediated monoubiquitination of IKKβ down-regulates NF-κB signalling. Journal of biochemistry. 2009;146(6):821-32.
599. Zhang J, Fang L, Zhu X, Qiao Y, Yu M, Wang L, et al. Ro52/SSA sensitizes cells to death receptor-induced apoptosis by down-regulating c-FLIP (L). Cell Biology International. 2012;36(5):463-8.
600. Brauner S, Zhou W, Backlin C, Green T, Folkersen L, Ivanchenko M, et al. Reduced expression of TRIM 21/Ro52 predicts poor prognosis in diffuse large B-cell lymphoma patients with and without rheumatic disease. Journal of internal medicine. 2015;278(3):323-32.
601. Chen X, Li Z, Yong H, Wang W, Wang D, Chu S, et al. Trim21-mediated HIF-1α degradation attenuates aerobic glycolysis to inhibit renal cancer tumorigenesis and metastasis. Cancer Letters. 2021;508:115-26.
602. Sun J, Chen X, Ji X, Meng S, Wang W, Wang P, et al. TRIM21 deficiency promotes cell proliferation and tumorigenesis via regulating p21 expression in ovarian cancer. Bioengineered. 2022;13(3):6024-35.
603. Ping M, Wang S, Guo Y, Jia J. TRIM21 improves apatinib treatment in gastric cancer through suppressing EZH1 stability. Biochemical and Biophysical Research Communications. 2022;586:177-84.
604. Jin Y, Zhang Y, Li B, Zhang J, Dong Z, Hu X, et al. TRIM21 mediates ubiquitination of Snail and modulates epithelial to mesenchymal transition in breast cancer cells. International journal of biological macromolecules. 2019;124:846-53.
605. Si W, Zhou J, Zhao Y, Zheng J, Cui L. SET7/9 promotes multiple malignant processes in breast cancer development via RUNX2 activation and is negatively regulated by TRIM21. Cell Death & Disease. 2020;11(2):151.
606. Itou J, Li W, Ito S, Tanaka S, Matsumoto Y, Sato F, et al. Sal-like 4 protein levels in breast cancer cells are post-translationally down-regulated by tripartite motif–containing 21. Journal of Biological Chemistry. 2018;293(17):6556-64.
607. Nguyen JQ, Irby RB. TRIM21 is a novel regulator of Par-4 in colon and pancreatic cancer cells. Cancer biology & therapy. 2017;18(1):16-25.
608. Zhao Z, Wang Y, Yun D, Huang Q, Meng D, Li Q, et al. TRIM21 overexpression promotes tumor progression by regulating cell proliferation, cell migration and cell senescence in human glioma. American journal of cancer research. 2020;10(1):114.

609. Wu Z, Wang Y, Yu Z, Meng Z, Duan W, Zhang W, et al. TRIM21-a potential biomarker for the prognosis of thyroid cancer. Experimental and Therapeutic Medicine. 2022;24(6):1-9.
610. Shu B, Zhou Y, Lei G, Peng Y, Ding C, Li Z, et al. TRIM21 is critical in regulating hepatocellular carcinoma growth and response to therapy by altering the MST1/YAP pathway. Cancer Science. 2024.
611. Zhang P, Li X, He Q, Zhang L, Song K, Yang X, et al. TRIM21–SERPINB5 aids GMPS repression to protect nasopharyngeal carcinoma cells from radiation-induced apoptosis. Journal of biomedical science. 2020;27:1-11.
612. Sarri N, Papadopoulos N, Lennartsson J, Heldin C-H. The E3 Ubiquitin Ligase TRIM21 Regulates Basal Levels of PDGFRβ. International Journal of Molecular Sciences. 2023;24(9):7782.
613. Cui Z, Sun H, Gao Z, Li C, Xiao T, Bian Y, et al. TRIM21/USP15 balances ACSL4 stability and the imatinib resistance of gastrointestinal stromal tumors. British Journal of Cancer. 2024:1-16.
614. Yang L, Zhang T, Zhang C, Xiao C, Bai X, Wang G. Upregulated E3 ligase tripartite motif-containing protein 21 in psoriatic epidermis ubiquitylates nuclear factor-κB p65 subunit and promotes inflammation in keratinocytes. British Journal of Dermatology. 2021;184(1):111-22.
615. Li Y, Bao L, Zheng H, Geng M, Chen T, Dai X, et al. E3 ubiquitin ligase TRIM21 targets TIF1γ to regulate β-catenin signaling in glioblastoma. Theranostics. 2023;13(14):4919.
616. Signorile A, Sgaramella G, Bellomo F, De Rasmo D. Prohibitins: a critical role in mitochondrial functions and implication in diseases. Cells. 2019;8(1):71.
617. Bavelloni A, Piazzi M, Raffini M, Faenza I, Blalock WL. Prohibitin 2: At a communications crossroads. IUBMB life. 2015;67(4):239-54.
618. Labriet A, Lévesque É, Cecchin E, De Mattia E, Villeneuve L, Rouleau M, et al. Germline variability and tumor expression level of ribosomal protein gene RPL28 are associated with survival of metastatic colorectal cancer patients. Scientific Reports. 2019;9(1):13008.
619. Raudvere U, Kolberg L, Kuzmin I, Arak T, Adler P, Peterson H, et al. g: Profiler: a web server for functional enrichment analysis and conversions of gene lists (2019 update). Nucleic acids research. 2019;47(W1):W191-W8.
620. Yeasmin Khusbu F, Chen FZ, Chen HC. Targeting ubiquitin specific protease 7 in cancer: a deubiquitinase with great prospects. Cell Biochemistry and Function. 2018;36(5):244-54.
621. Cheng J, Huang Y, Zhang X, Yu Y, Wu S, Jiao J, et al. TRIM21 and PHLDA3 negatively regulate the crosstalk between the PI3K/AKT pathway and PPP metabolism. Nature communications. 2020;11(1):1880.
622. Keeble AH, Khan Z, Forster A, James LC. TRIM21 is an IgG receptor that is structurally, thermodynamically, and kinetically conserved. Proceedings of the National Academy of Sciences. 2008;105(16):6045-50.
623. Hsu C-H, Yu Y-L. The interconnected roles of TRIM21/Ro52 in systemic lupus erythematosus, primary Sjögren's syndrome, cancers, and cancer metabolism. Cancer Cell International. 2023;23(1):289.
624. James LC. Intracellular antibody immunity and the cytosolic Fc receptor TRIM21. Fc Receptors: Springer; 2014. p. 51-66.
625. Ohtake F, Saeki Y, Ishido S, Kanno J, Tanaka K. The K48-K63 branched ubiquitin chain regulates NF-κB signaling. Molecular cell. 2016;64(2):251-66.
626. Jiang Z, Xing B, Feng Z, Ma J, Ma X, Hua X. Menin upregulates FOXO1 protein stability by repressing Skp2-mediated degradation in β cells. Pancreas. 2019;48(2):267-74.
627. Guièze R, Wu CJ. Genomic and epigenomic heterogeneity in chronic lymphocytic leukemia. Blood, The Journal of the American Society of Hematology. 2015;126(4):445-53.
628. Brenkman AB, de Keizer PL, van den Broek NJ, Jochemsen A, Burgering BM. Mdm2 induces mono-ubiquitination of FOXO4. PloS one. 2008;3(7):e2819.
629. Sun J, Shen D, Zheng Y, Ren H, Liu H, Chen X, et al. USP8 inhibitor suppresses HER-2 positive gastric cancer cell proliferation and metastasis via the PI3K/AKT signaling pathway. OncoTargets and therapy. 2020:9941-52.
630. Ruiz-Saenz A, Dreyer C, Campbell MR, Steri V, Gulizia N, Moasser MM. HER2 amplification in tumors activates PI3K/Akt signaling independent of HER3. Cancer research. 2018;78(13):3645-58.

631. Byun S, Lee S-Y, Lee J, Jeong C-H, Farrand L, Lim S, et al. USP8 is a novel target for overcoming gefitinib resistance in lung cancer. Clinical cancer research. 2013;19(14):3894-904.
632. Kang JJ, Ko A, Kil SH, Clair JM-S, Shin DS, Wang MB, et al. EGFR pathway targeting drugs in head and neck cancer in the era of immunotherapy. Biochimica et Biophysica Acta (BBA)-Reviews on Cancer. 2023;1878(1):188827.
633. Jing X, Chen Y, Chen Y, Shi G, Lv S, Cheng N, et al. Down-regulation of USP8 inhibits cholangiocarcinoma cell proliferation and invasion. Cancer management and research. 2020:2185-94.
634. Tao L, Liu X, Jiang X, Zhang K, Wang Y, Li X, et al. USP10 as a potential therapeutic target in human cancers. Genes. 2022;13(5):831.
635. He Y, Jiang S, Mao C, Zheng H, Cao B, Zhang Z, et al. The deubiquitinase USP10 restores PTEN activity and inhibits non–small cell lung cancer cell proliferation. Journal of Biological Chemistry. 2021;297(3).
636. Liao Y, Liu N, Xia X, Guo Z, Li Y, Jiang L, et al. USP10 modulates the SKP2/Bcr-Abl axis via stabilizing SKP2 in chronic myeloid leukemia. Cell discovery. 2019;5(1):24.
637. Weisberg EL, Schauer NJ, Yang J, Lamberto I, Doherty L, Bhatt S, et al. Inhibition of USP10 induces degradation of oncogenic FLT3. Nature chemical biology. 2017;13(12):1207-15.
638. Carnevale J, Ross L, Puissant A, Banerji V, Stone RM, DeAngelo DJ, et al. SYK regulates mTOR signaling in AML. Leukemia. 2013;27(11):2118-28.
639. Wang Q, Ma S, Song N, Li X, Liu L, Yang S, et al. Stabilization of histone demethylase PHF8 by USP7 promotes breast carcinogenesis. The Journal of clinical investigation. 2016;126(6):2205-20.
640. Su D, Ma S, Shan L, Wang Y, Wang Y, Cao C, et al. Ubiquitin-specific protease 7 sustains DNA damage response and promotes cervical carcinogenesis. The Journal of clinical investigation. 2018;128(10):4280-96.
641. Qin D, Wang W, Lei H, Luo H, Cai H, Tang C, et al. CDDO-Me reveals USP7 as a novel target in ovarian cancer cells. Oncotarget. 2016;7(47):77096.
642. Oliveira RI, Guedes RA, Salvador JA. Highlights in USP7 inhibitors for cancer treatment. Frontiers in Chemistry. 2022;10:1005727.
643. Zhang W, Sartori MA, Makhnevych T, Federowicz KE, Dong X, Liu L, et al. Generation and validation of intracellular ubiquitin variant inhibitors for USP7 and USP10. Journal of molecular biology. 2017;429(22):3546-60.
644. Futran AS, Lu T, Amberg-Johnson K, Xu J, Yang X, He S, et al. Ubiquitin-specific protease 7 inhibitors reveal a differentiated mechanism of p53-driven anti-cancer activity. Iscience. 2024;27(5).
645. Nakagawa R, Soh JW, Michie AM. Subversion of Protein Kinase Cα Signaling in Hematopoietic Progenitor Cells Results in the Generation of a B-Cell Chronic Lymphocytic Leukemia–Like Population In vivo. Cancer Research. 2006;66(1):527-34.
646. Garwood K, McLaughlin T, Garwood C, Joens S, Morrison N, Taylor CF, et al. PEDRo: a database for storing, searching and disseminating experimental proteomics data. Bmc Genomics. 2004;5:1-11.